Modelling nucleophilic substitution at main group elements by NMR spectroscopy and X-ray crystallography

Thesis

UNRESTRICTED

Modelling nucleophilic substitution at main group elements by NMR spectroscopy and X-ray crystallography

A thesis submitted for the degree of

Doctor of Philosophy in Chemistry

To

The Open University

Milton Keynes

David J. Parker

1997

Date of submission: 18th September 1997
Date of award : 19th November 1997

Department of Chemistry
The Open University
Walton Hall
Milton Keynes
MK7 6AA
UNITED KINGDOM

ProQuest LLC.
789 East Eisenhower Parkway
P.O. Box 1346
Ann Arbor, MI 48106 – 1346

Statement

The work constituting this thesis was carried out by the author between October 1993 and April 1997 in the laboratories of the Chemistry Department of the Open University in Milton Keynes and on placement at Humboldt Universität zu Berlin, Germany under the supervision of Professor Alan Bassindale and Dr Peter Taylor.

Parts of the work have been presented or published as listed below:

- *RSC Silicon, Germanium, Tin and Lead Discussion Group*, Kings College, London, April 1994.
- In: *Organosilicon Chemistry II: From Molecules to Materials*; N. Auner, J. Weiss (eds), Weinheim, 1996; pages 411-425.
- *XIth International Symposium on Organosilicon Chemistry*, Montpellier, France, September 1996.
- *RSC Blocks 13-15 Discussion Group*, Kings College, London, April 1997.
- Article 041, *Electronic Conference on Trends in Organometallic Chemistry*, H. S. Rzepa and C. Leach, (Eds), Royal Society of Chemistry, to be published in 1998. ISBN 0-85404-889-8. See also http://www.ch.ic.ac.uk/ectoc/ectoc-3/

David J. Parker

September 1997

Acknowledgements

- I would like to express my thanks to my supervisors, Professor Alan Bassindale and Dr Peter Taylor. For their continual encouragement, enthusiasm and guidance during the project I am particularly grateful.

- I thank Professor Dr N. Auner of Humbolt Universität zu Berlin for allowing me to visit his laboratories in Germany. I thank all the members of his research group for their help and making me welcome during my stay. I particularly wish to thank Dr Bernhard Herrschaft for his hard work over an extended period in obtaining the crystal structures presented here. I would also like to thank Herr Michael Becker for the solid state NMR work and Dr Thomas Müller for useful discussion.

- I thank the departments technical staff for their assistance, particularly Mr Gordon Howell for invaluable help with obtaining the numerous NMR spectra.

- I extend my thanks to the Engineering and Physical Sciences Research Council (EPSRC) for my studentship and to the Open University for funding my visit to Germany.

- Finally, to my family and friends both near and far for their all-important moral support; thank you for believing.

Another Cockcroft Communication (1997)

Abstract

The structures of intramolecularly pentacoordinated silicon and tin complexes are reminiscent of structures that occur on an S_N2 reaction profile. The technique of NMR solution-phase mapping, whereby the degree of nucleophile-silicon bond formation and the coordination state of the silicon in such complexes is inferred from their ^{13}C and ^{29}Si NMR spectra, is extended to 2-thiopyridones (**1**) and (**2**).

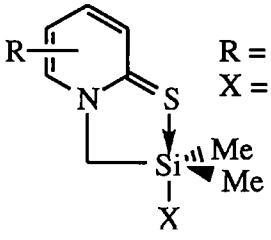

R = 6-Me
X = F, Cl, Br, OTf

(**1**)

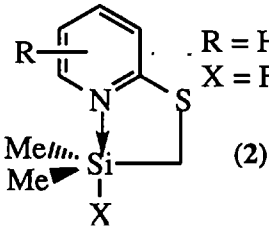

R = H, 4-Me, 5-CF_3
X = F, Cl, Br, OTf

(**2**)

The suitability and limitations of several classes of compound as models for zero substitution and 100% substitution is also investigated. An extensive variable temperature NMR study (-50 to +50°C) of compounds of type (**1**) and (**2**) has been performed and shows that different 'degrees of substitution' occur at different temperatures within a single complex.

The Dunitz solid-state *structural-correlation* approach to reaction pathway modelling is combined with a solution phase NMR study of the structure of the quinoline complexes (**3**). This is the first time that a joint investigation of such compounds in the solid-state and in solution has been undertaken. We have also isolated the first pentacoordinated protonated silanol complex (**4**). Its structure provides an insight into the species that might occur during the hydrolysis reactions of chlorosilanes.

(**3**)

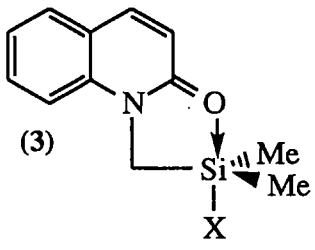

X = F, Cl, Br, OTf

(**4**)

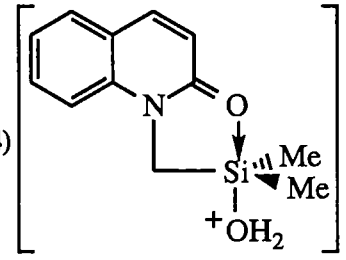

$Cl^-.H_2O$

(**5**)

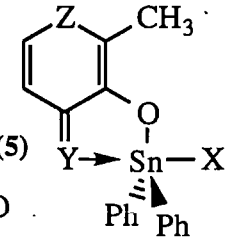

X = Ph, Cl, Br, I
Y = O, S
Z = O, NMe, NAr

To expand the scope of the NMR solution-phase mapping technique, we attempt to model S_N2 substitution at tin in solution using complexes based on the natural product 'maltol' (**5**). NMR spectroscopy shows a high 'degree of substitution' occurs in each complex which is largely independent of leaving group or ligand substituent. These structures are investigated by X-ray crystallography.

The affect of nucleophile N-methyl imidazole on a five coordinate silicon complex is studied and compared to the reaction of its tin analogue. Preliminary work on identifying complexes suitable for modelling substitution at boron and carbon centres is undertaken using maltol and related ligands.

Contents

Chapter 3: Modelling nucleophilic substitution at silicon using 2-thiopyridone-based ligands

Chapter 4: 5-Coordinate complexes stabilised by maltol-based ligands

Chapter 5: Experimental

Part A: Compounds from Chapters 2 and 3.

Part B: Compounds from Chapter 4

Abbreviations

α-Np	α-naphthyl	NMR	Nuclear Magnetic Resonance
acac	acetyl acetonato	^{n}Bu/Bu	normal-butyl
Ac	acetyl	^{n}Hept	normal-heptyl
Ar	aromatic (ring)	^{n}Oct	normal-octyl
ax	axial	^{n}Pr	normal-propyl
br	broad	Nu	nucleophile
d	doublet	OTf	triflate, OSO_2CF_3
DME	1,2-dimethoxyethane	ppm	parts per million
DMF	dimethylformamide	py	pyridine
eq	equatorial	q	quartet
equiv.	equivalents	s	singlet
Hz	hertz	^{s}Bu	secondary-butyl
^{i}Pr	iso-propyl	^{t}Bu	tertiary-butyl
^{i}Oct	iso-octyl	TBAF	tetrabutylammonium fluoride
J	coupling constant	TBP	trigonal bipyramidal
m	multiplet	THF	tetrahydrofuran
M	metal	TMS-OTf	trimethylsilyl triflate
n/c	not calculated	VT	variable temperature
NMI	N-methyl imidazole	X	leaving group/substituent

Chapter 1: Introduction

Part A: Silicon

1.1: Overview

Relative to carbon, silicon has a much smaller tendency to form compounds of coordination number less than four, such as silenes, silanones or silicenium ions, but a pronounced capacity for the enlargement of its coordination sphere. Complex formation was first observed early in the 19th century by Lussac and Davy[1] when they reported the $SiF_4.NH_3$ adduct. Later, in 1903, the hexacoordinate cationic complex $[Si(acac)_3]^+ HCl_2^-$ was reported by Dilthey[2] and represented a new structural type for the element.

Isolable organosilicon compounds with a coordination number greater than four generally contain halogen, oxygen or nitrogen ligands. The first notable exception[3] came in 1981 with the reported formation of the $[CH_2=CH\text{-}CH_2(CH_3)_2\overline{SiCH_2CH_2CH_2}]^-$ ion in the gas phase.

In the last 25 years the interest in hypervalent silicon compounds has grown considerably as the scope for additional coordination has been explored. New structural types, particularly those in which intramolecular coordination is favoured, have been developed and studies of permutational isomerization in pentacoordinate species have been vigorously pursued. Such studies are particularly relevant to the understanding of the stereospecificity generally observed in nucleophilic substitution reactions at silicon, in which pentacoordinated intermediates are usually involved.

1.2: Types of pentacoordinate silicon complex

Complexes of two main general types can be prepared, containing either inter- or intramolecularly coordinating ligands.

1.2.1: Intermolecular donation to an organosilane

Neutral complexes of silicon can be formed from coordination of an uncharged group V or VI donor to a tetravalent molecule; the first reported pentacoordinated complex being Lussac and Davy's $SiF_4.NH_3$ adduct.[1] Much of the work which established the readiness of silicon to expand its coordination sphere concerned the interaction of halotriorganosilanes with amines.[4] In these reactions nucleophilic

displacement of halide ion by amine often occurs with the formation of ionic adducts rather than hypervalent derivatives of silicon. Thus fluoro- and chloro-trimethylsilanes are coordinated only very weakly and reversibly by pyridine,[5] making characterisation considerably difficult. Bromo- and iodotrimethylsilanes give the salts $(CH_3)_3Si(py)^+X^-$ (X = Br, I).[6] More recently studies of this trimethylsilyl series confirmed that where X = halogen, perchlorate or triflate the reagents either reacted to form ionic tetracoordinate complexes or did not react at all.[7]

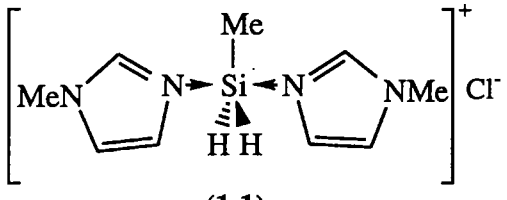

(1.1)

Isolable complexes in which the coordination number is increased to five at the silicon are formed only when there is more than one electronegative group bonded to the parent organosilicon compound as in $SiF_4.NH_3$,[1] or with two monodentate ligands (**1.1**).[8]

1.2.2: Intramolecular donation to an organosilane

The most common way of inducing pentacoordination at silicon is to place the donor which leads to extra-coordination, most commonly halogen, N, O or S, in the same molecule as the silicon centre. This results in the formation of at least one 4, 5 or 6-membered ring of which the silicon is a member, for example (**1.2**).[9] We will now consider ways in which such a large variety of complex types might be synthesised, and in so doing shed light on the range of structural types currently known.

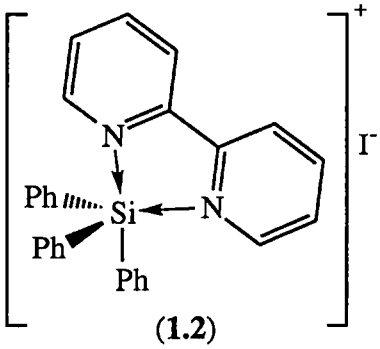

(1.2)

1.3: Synthesis of pentacoordinate complexes

The syntheses of pentacoordinate complexes fall into three broad classes.

1.3.1: Coordination of anions to tetracoordinate silicon compounds

A: Fluoride ion donation to an organosilane

Fluorosilanes SiF_4, $RSiF_3$ (R = Me, Ph) and Ph_2SiF_2 react with tetraalkylammonium fluorides in a 1:1 ratio to yield stable ionic compounds.[10] NMR[11] and vibrational[12] spectra confirm that these compounds (SiF_5^-, $RSiF_4^-$ and $Ph_2SiF_3^-$) are pentacoordinate at silicon.

Damrauer and Danahey have reported reactions of fluoride ion with cyclic silanes and uncovered a novel cleavage reaction which produces the α-silyl carbanion (**1.4**) as well as the expected pentacoordinate organofluorosilane anion (**1.3**) (Figure 1.1).[13]

Figure 1.1

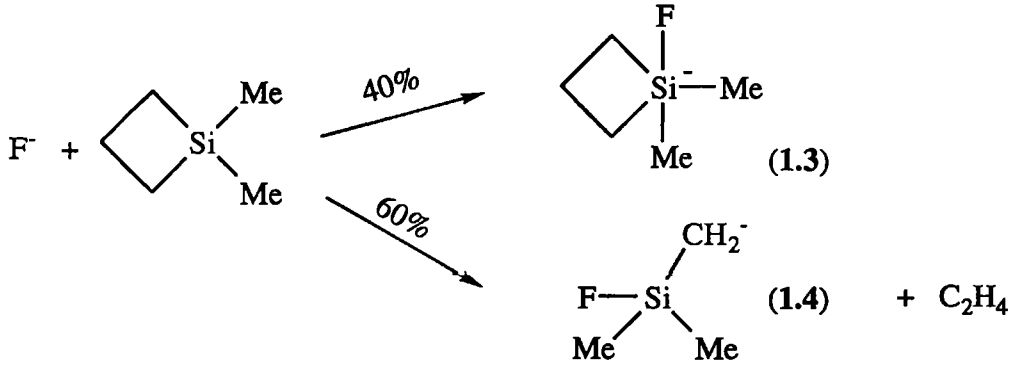

They also discovered that the presence of an 18-crown-6 ether greatly stabilises the formation of potassium salts of pentacoordinate fluorosilicates $[R_nSiF_{5-n}]^-$ (n=1-3).[14]

B: Alkoxide donation to an organosilane

Damrauer and Danaheys work using potassium ion 18-crown-6 ethers to complex pentacoordinate anionic silicates has since been extended to the preparation of alkoxy- and aryloxysilicates, for example (**1.5**).[15]

$Ph_nSi(OMe)_{4-n} + MeO^-[K, 18\text{-crown-6}]^+ \rightarrow [Ph_nSi(OMe)_{5-n}]^- [K, 18\text{-crown-6}]^+$ **(1.5)**

(n = 1-3)

The direct reaction of potassium alkoxide with trialkoxy- or aryloxysilane affords the anionic pentacoordinate silicon hydrides, (**1.6**), in good yield even without crown ether.[16]

$$HSi(OR)_3 + ROK \xrightarrow[DME]{THF\ or} [HSi(OR)_4]^-K^+ \quad \textbf{(1.6)}$$

R = Me, ^{n}Bu, ^{s}Bu,^{i}Pr, Ph.

C: Hydride ion donation to an organosilane

Potassium hydride reacts with trialkoxy- or triaryloxysilanes to produce the pentacoordinate anions (**1.7**) and (**1.8**).[17]

$$HSi(OR)_3 \xrightarrow{KH} [H_2Si(OR)_3]^-K^+ \ (\textbf{1.7}) + [HSi(OR)_4]^-K^+ \ (\textbf{1.8})$$

The formation of (**1.8**) was observed in all cases except when R = ^{i}Pr. This has been explained using the following disproportionation reaction.

$$4[H_2Si(OR)_3]^-K^+ \ (\textbf{1.7}) \longrightarrow 3[HSi(OR)_4]^-K^+ \ (\textbf{1.8}) + SiH_4 + KH$$

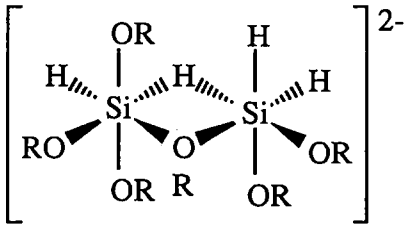

(**1.9**)

The proportion of the $[HSi(OR)_4]^-$ ion is found to decrease with increasing steric bulk of the OR group and also decrease with increasing solvating power of the solvent.[18] The migration of OR and H groups between pentacoordinate species is proposed to take place through a dimeric hexacoordinate intermediate (**1.9**).[18]

D: Coordination of an anion to a spirosilane

Müller and Heinrich[19] have demonstrated the preparation of two silicates (**1.10**) and (**1.11**) from their corresponding spirosilicates with lithium and sodium methoxide respectively.

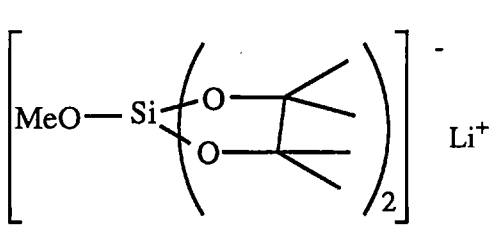

(1.10)

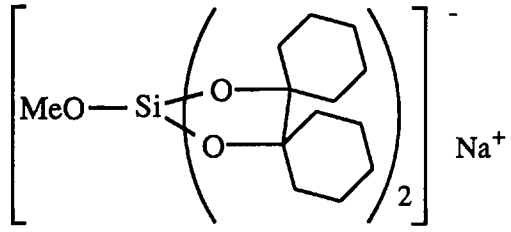

(1.11)

It has since been found[20] that simple amines are sufficiently basic to afford similar silicates (**1.12**) (Figure 1.2).

Figure 1.2

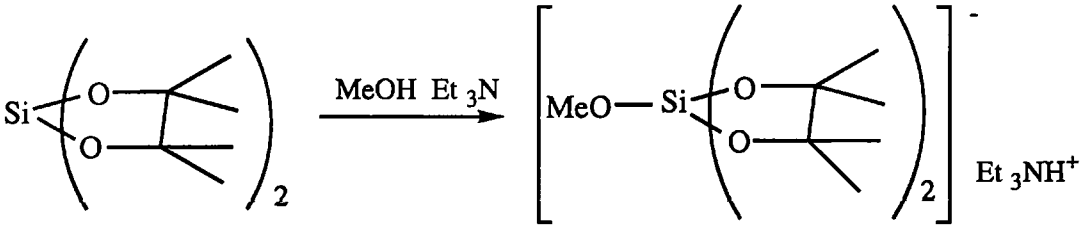

(1.12)

1.3.2: Substitution in a tri-functional organosilane

A: Substitution by a bi-dentate ligand

Cyclic compounds (**1.13**), complexed through oxygen atoms, have long been known (Figure 1.3).[21]

Figure 1.3

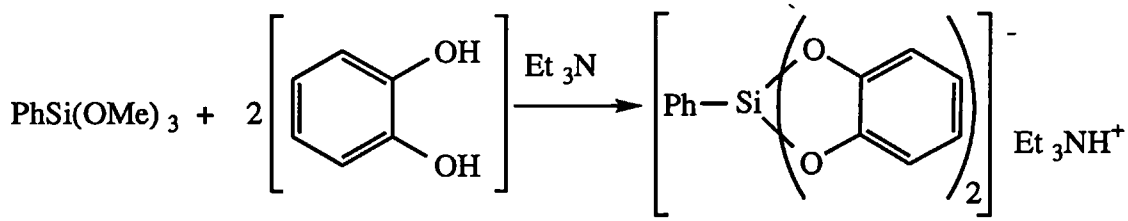

(1.13)

Similar complexes (**1.14**) can also be prepared from trichlorosilanes and alkali metal catecholates (Figure 1.4).[22]

Figure 1.4

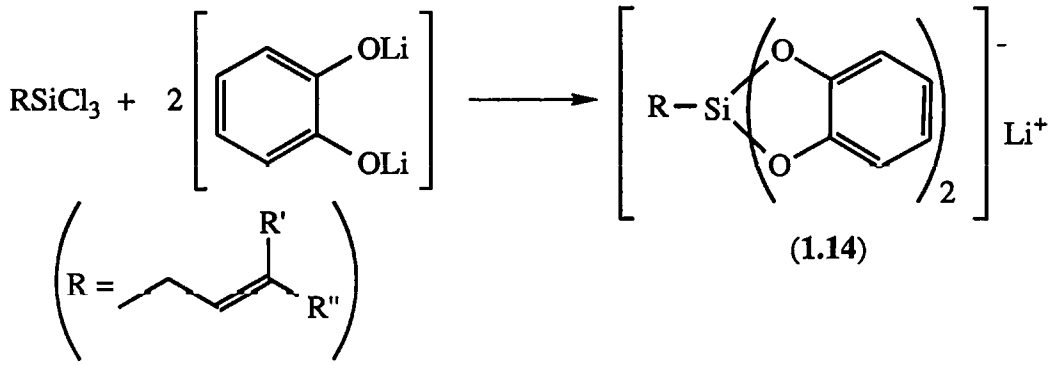

(1.14)

Aliphatic 1,2-diols react readily with tetra-alkoxysilanes to give pentacoordinate anionic complexes (**1.15**) (Figure 1.5).[23]

Figure 1.5

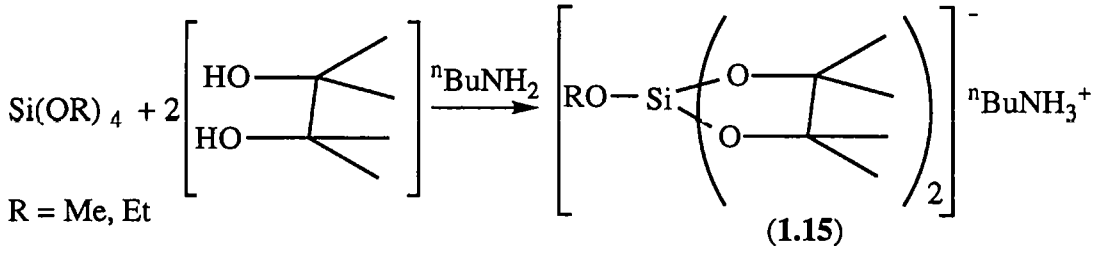

(**1.15**)

Pentacoordinate cationic complexes (**1.16**) and (**1.17**) are formed by reaction of a 1,3-diketone[24] or tropolone[25] with a monoorganosilicon halide.

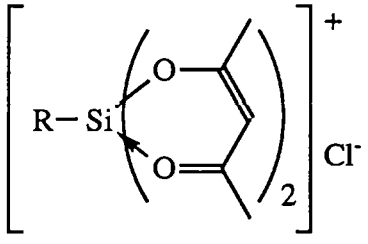

(**1.16**)

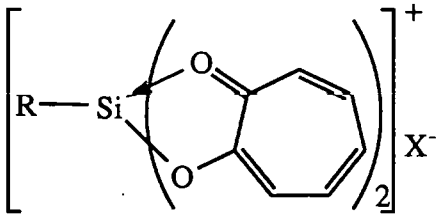

(**1.17**)

B: Substitution by trialkanolamines and tris(2-aminoethyl)amines

Frye *et al*[26] were the first to report the 1:1 reaction of triethanolamine with a variety of tri-functional silicon substrates yielding monomeric silanes, (**1.18**), now commonly termed *silatranes* (Figure 1.6).

Figure 1.6

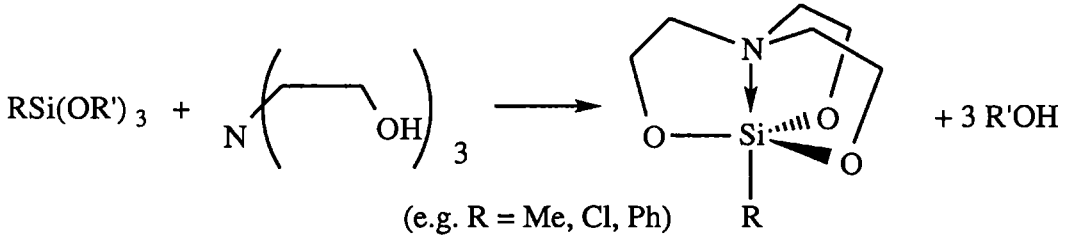

(**1.18**)

Frye and co-workers later prepared a variety of silicon substituted halo-, acyloxy-, siloxy- and hydroxy- complexes which resulted in further studies of their chemical and biological properties. Azasilatranes (**1.19**) (Figure 1.7) are similarly prepared by heating tris(dimethylamino)silanes with tris(2-aminoethyl)amine.[27]

Figure 1.7

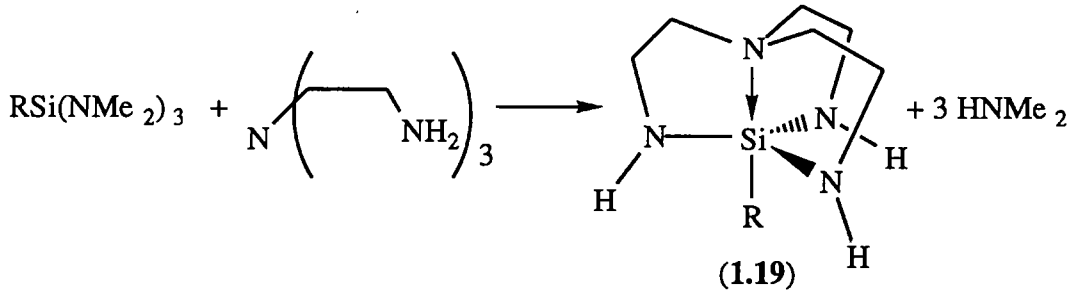

(1.19)

Spectroscopic and structural data suggest a strong similarity in structure with silatranes but with an even stronger interaction between the silicon and the axial nitrogen atom.

1.3.3: Intramolecular donation by a neutral donor to an organosilane

As already mentioned, one of the simplest ways of inducing pentacoordination at silicon is to place a coordinating group in a different part of the molecule containing the silicon centre, commonly four or five bonds from the silicon atom. Coordination of the donor group results in cyclisation and formation usually of a new five- or six-membered ring. Coordination can be achieved in two ways.

A: Use of a 'rigid ligand' framework

Figure 1.8

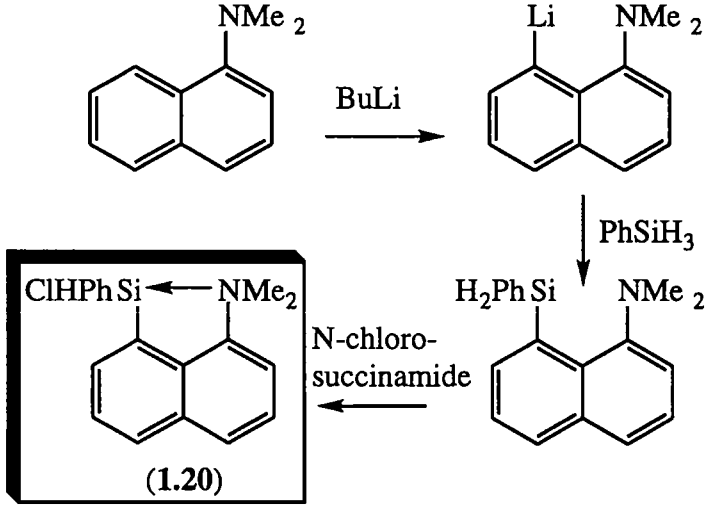

(1.20)

The neutral donor and silicon centre can be constrained into residing in within potential bonding proximity of each other by using a rigid ligand framework such as an aromatic ring. Complex **(1.20)**[28] (Figure 1.8) is such an example.

B: Use of an 'open chain' framework

Open chain donors have a greater number of degrees of freedom for possible coordinating interactions than rigid ligand donors. This allows a donor group the

possibility of residing in positions other than the optimal bonding distance from the silicon atom. This opens up a wider range of possibilities for donor-silicon interaction. In these cases the degree of interaction is much more dependant on the nature of the substituents attached to the silicon atom.

Structures (**1.21**)[29], (**1.22**)[30] and (**1.23**)[31] are examples of such complexes (Figure 1.9). Compound (**1.21**) is made by the same method as (**1.20**) but from the corresponding amine.

Figure 1.9

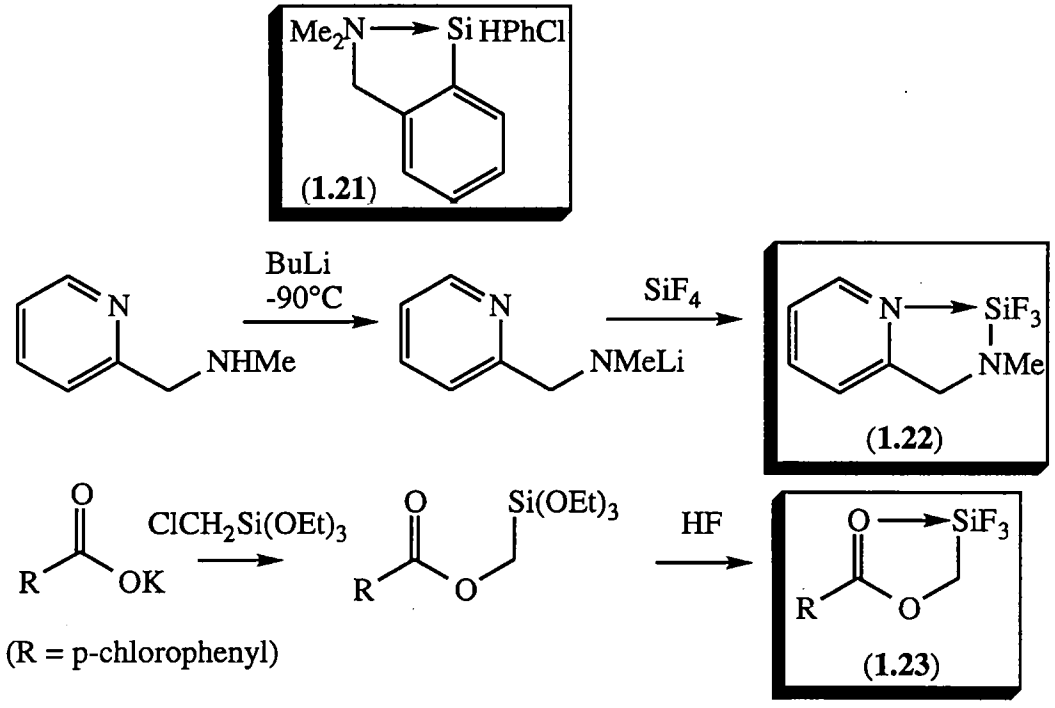

The extent of donor-acceptor interaction may be determined in the solid state by X-ray crystallography, giving the donor atom-silicon distance, or in solution using IR and especially NMR data. These techniques will be discussed later in this introduction.

1.4: Fluxionality of pentacoordinate silicon

Early work by Klanberg and Muetterties[32] on dynamic ^{19}F NMR spectroscopy of pentacoordinate fluorosilicates suggested that these trigonal-bipyramidal complexes underwent rapid intramolecular exchange of fluorine ligands. However, impurity-catalysed intermolecular exchange of fluorine ligands cast doubt on the intramolecular exchange mechanism. Later studies[33] showed that in the series of ions $[R_nSiF_{5-n}]^-$ where n=1 (R = ^{n}Pr, ^{t}Bu, mesityl, benzyl and o/m/p-tolyl), the exchange process is so rapid on the NMR time scale across the temperature range -100 to +30°C that only a

single ^{19}F resonance is observed. The persistence of ^{29}Si-^{19}F coupling verifies the intramolecular nature of site exchange. However ions where n=2 provide limiting low temperature spectra in which axial (low field) and equatorial (high field) fluorine atoms may be distinguished. Free energies for activation of intramolecular rearrangement could be calculated in the region of 9-12 kcal mol^{-1}. The precise value depends on the steric bulk of the R groups which hinder the rearrangement.

VT ^1H NMR studies[34] of monofunctional derivatives (**1.24**) and bifunctional derivatives (**1.25**) (X≠H) reveal increasing intramolecular pentacoordination on temperature reduction. This is demonstrated by the splitting of the diastereotopic N-methyl groups into two discrete signals. They become diastereotopic as a result of complexation with the chiral silicon centre.

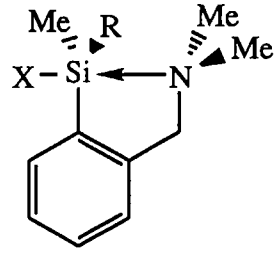

(R = H, α-Np)
(X = F, Cl, Br, OR, SR)

(1.24)

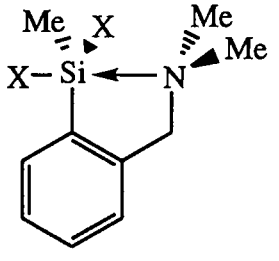

(X = OEt, SEt , F, Cl)

(1.25)

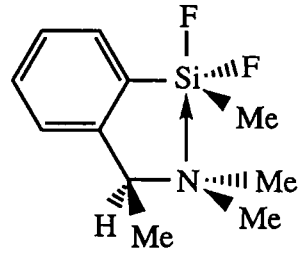

(1.26)

Such VT studies allow the evaluation of the free energy of activation for ring opening, and values in the region of 8-15 kcal mol^{-1} have been calculated. This demonstrates the greater stability of the chelated form over the ring-opened form. The order of increasing activation energy for ring opening was found to depend on X in the order X = R < OR < H < F < SR < OAc < Cl < Br.

It can be concluded that the extent of nitrogen coordination is not a function of the electronegativity of X, but depends on the polarisability of the Si-X bond under the influence of the coordinating donor atom. Corriu has proposed[35] that the stability of extra-coordinate silicon complexes is controlled largely by the tendency of the Si-X bond to be stretched under the influence of an incoming 'nucleophile'.

As the activation energies for ring opening of chelates (**1.24**) and (**1.25**) and the free energies of intramolecular rearrangement for the $[R_2SiF_3]^-$ ions discussed above, are very similar, it can sometimes be unclear as to the mechanism that the rearrangement

might take. There are two possibilities, a regular site exchange mechanism for the pentacoordinate silane, where the coordination remains unchanged or an alternative mechanism whereby the silicon momentarily, at least, becomes tetracoordinate.

Incorporation of a chiral centre at the position α to the dimethylamino group can be used as an independent probe for its decoordination and inversion, allowing the two processes to be monitored independently. Compound (**1.26**) has been used as such a model.[36] The limiting low temperature (-90°C) ^{1}H NMR spectrum of (**1.26**) displays four separate resonances for the dimethylamino group due to the chirality of both the benzylic carbon atom and the pentacoordinate silicon atom. As the temperature is raised (-45°C) the four resonances collapse to two (calculated activation energy ΔG = 9.4 kcal mol^{-1}). This arises because the intramolecular ligand exchange process occurs rapidly on the NMR time scale, thus rapidly *scrambling* the chiral environment about the silicon while the Si-N bond remains intact. This exchange process is confirmed from the ^{19}F DNMR spectrum which shows the coalescence of the axial and equatorial fluorines signals (calculated ΔG of 9.3 kcal mol^{-1}). On further warming (31°C) a second coalescence in the ^{1}H spectrum occurs at a ΔG of 11.8 kcal mol^{-1} corresponding to Si-N bond breaking accompanied by rotation and inversion at the nitrogen.

Recently Holmes *et al* have reported the preparation of diorganosilanes containing sulfinyl (**1.27**)[37] and sulfonyl (**1.28**)[38] groups.

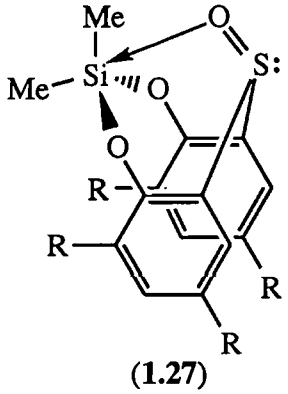

(1.27)

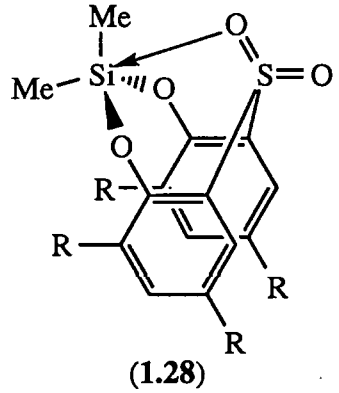

(1.28)

a: R = Me,
b: R = ^{t}Bu

The extent of oxygen coordination is found to depend on the steric bulk of R such that a ^{t}Bu group forces the bridging $SiMe_2$ moiety to reside closer to the sulfur group than does a methyl group. This results in stronger coordination. On cooling (**1.28a**) from -33°C to -88°C the singlet for the Si-Me groups collapsed to two signals, whereas even on warming (**1.27a**) from 23°C to 95°C the two signals of the inequivalent

methyl groups remained unchanged. The collapse of the signals for (**1.28a**) is consistent with ring flipping occurring at higher temperatures (Figure 1.10).

Figure 1.10

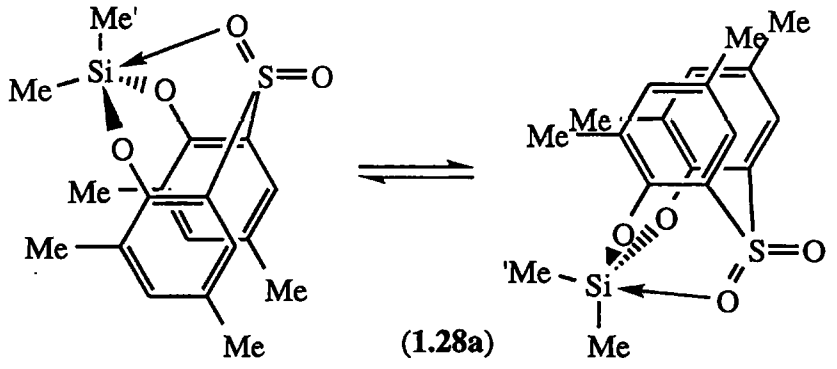

(**1.28a**)

The 'static' nature of the ^{1}H NMR VT spectra of (**1.27a**) is explained by the difference in structural stabilities of its two conformers. One conformer comprises a relatively weak S-Si interaction while the other a relatively stronger O-Si interaction.

Voronkov *et al*[39] studied the ^{29}Si variable temperature NMR spectra for a series of pentacoordinate amides and lactams, (**1.29**), (**1.30**) and (**1.31**).

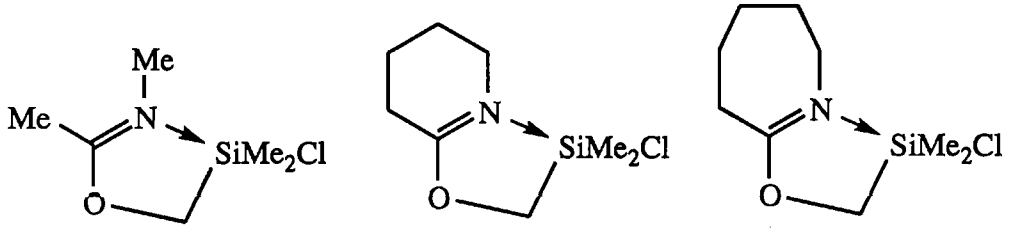

(**1.29**) (**1.30**) (**1.31**)

Cooling a solution of (**1.29**) from 0°C to -45°C causes a shift of the ^{29}Si NMR signal from δ -50.5 to δ -51.9. This is characteristic of compounds where the Si-N bond is the weaker coordinating component of the hypervalent X-Si-N bonding interaction. Cooling solutions of (**1.30**) and (**1.31**) results in the opposite temperature dependence of the ^{29}Si chemical shifts. Cooling from -40°C to -80°C is accompanied by a change in ^{29}Si chemical shift of δ -53.8 to δ -52.9 and δ -50 to δ -48 for (**1.30**) and (**1.31**) respectively. This is thought to be due to pentacoordinated silicon derivatives exhibiting a weak Si-Cl bond and a relatively stronger Si-N bond.

A similar temperature dependence to (**1.30**) and (**1.31**) was observed by Kummer *et al*[40] in complex (**1.32**), however the chemical shift change was larger.

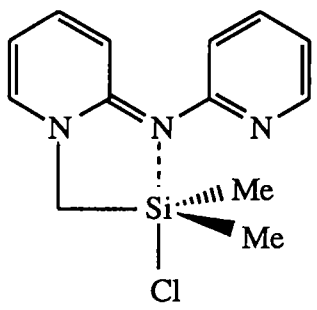

(**1.32**)

The crystal structure of compound (**1.32**) shows the silicon to be highly pentacoordinate. Solution ^{13}C NMR chemical shifts have been monitored over a temperature range from + 80°C to -70°C and show that the lower the temperature the more aminopyridinium in character the pyridone-imine ring becomes. The ^{29}Si NMR chemical shift has been measured over the range +100°C to -80°C in $CDCl_3$. The resonance moves down-field from δ -6.2 to δ +18.4, i.e. the silicon becomes more tetracoordinate in the process. The combined results reveal that the complex maintains structures of type (**II**) (Figure 1.11) where the N-Si bond is the stronger coordinative component. These structures are therefore more closely related to the model structure of complete 'substitution' (**III**) than the model of zero 'substitution' (**I**).

Figure 1.11

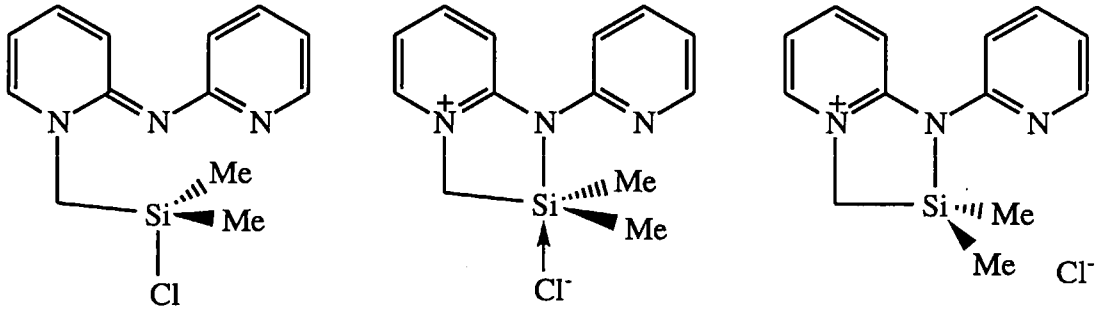

(**I**) (**II**) (**III**)

→ Decrease of temperature
← Increase of temperature

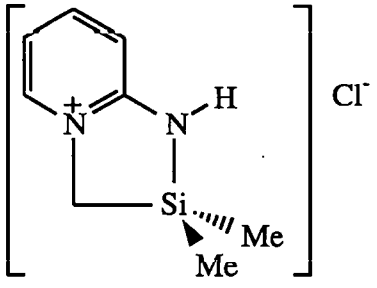

(**1.33**)

By contrast, complex (**1.33**)[41] has been shown by ^{29}Si and ^{13}C NMR to remain completely ionic throughout the temperature range +80°C to -80°C in $CDCl_3$. This is a consequence of the H-substituted amido nitrogen being significantly more 'nucleophilic' than the (2-pyridyl)-substituted amido nitrogen of (**1.32**).

1.5: Structures of pentacoordinate silicon complexes

1.5.1: Overview

The study of molecular structure involves both static and dynamic aspects. The dynamic aspects, which have already mentioned in Section 1.4, include variable temperature NMR which reveal the behaviour of molecules in motion. By monitoring complexes as they interconvert between structural forms, thermodynamic information may be obtained. For many years X-ray crystallography has been the major contributor to our understanding of the static aspects of molecular structure. There is now a considerable body of structural data for hypervalent silicon and comprehensive reviews have been published on this aspect by Voronkov *et al*[42] and Corriu *et al.*[43] This section will consider some of the significant structural features of pentacoordinate silicon complexes.

1.5.2: Site preferences of trigonal bipyramidal complexes

Complexes (**1.34**)-(**1.36**) help illustrate common structural characteristics (Table 1.1).

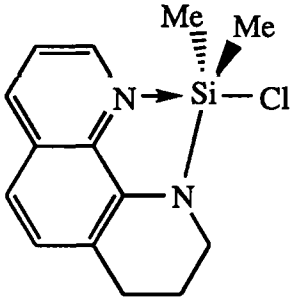

(**1.34**)

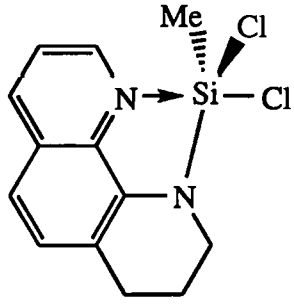

(**1.35**)

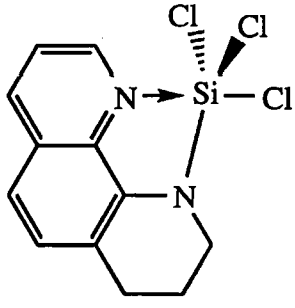

(**1.36**)

Table 1.1

Complex	Reference	N(ax)-Si (/Å)	Si-Cl(ax) (/Å)	Si-Cl(eq) (/Å)
(**1.34**)	44	2.028	2.269	-
(**1.35**)	44	2.027	2.207	2.049
(**1.36**)	45	1.984	2.150	2.094

(N(eq)–Si about 1.8 Å for all complexes, i.e. full covalent bonds)

In all these structures the geometry about the silicon is that of a somewhat distorted trigonal bipyramid in which the donor atom occupies an axial position. A distorted trigonal bipyramid is one in which the sum of the bond angles between the equatorial ligands is less than 360° and/or the diaxial bond angle is less than 180°.

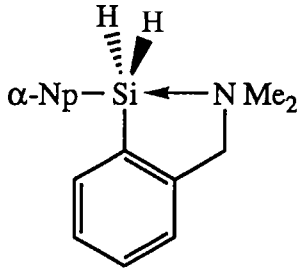

(**1.37**)

The rings formed in complexes (**1.34**)-(**1.36**) span axial and equatorial positions in a conformation which minimises ring strain. The second axial position is occupied by an electronegative atom (chlorine in the cases above). The common exception is that of silicon hydrides (for example (**1.37**)).[46]

Where there are identical electronegative groups (in our examples Si-Cl bonds) in both axial and equatorial positions, then the axial bond is appreciably lengthened over the equatorial bond(s). According to Corriu[35] this lengthening of the Si-Cl bond is induced by the donor atom interacting at the silicon centre. The progressive replacement of methyl groups on the silicon with chlorines in the sequence (**1.34**)-(**1.35**)-(**1.36**) increases the electrophilicity of the silicon. This is reflected by the shortening of the hypervalent N–Si bond. Donor-acceptor distances are significantly longer than normal single bond lengths but shorter than the sum of their van der Waals radii, in some instances indicating substantial coordination. For example, in the structure of compound (**1.34**), the equatorial covalently-bonded nitrogen is situated 1.77Å away from the silicon and the donor nitrogen 2.03Å away, while the sum of the van der Waals radii for nitrogen and silicon is 3.6Å.

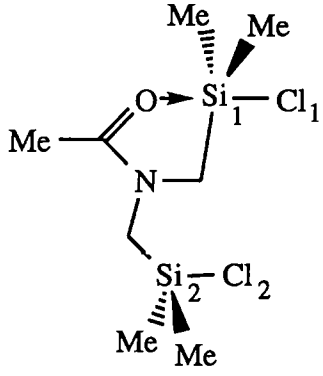

(**1.38**)
Si_1-Cl_1 = 2.35Å
Si_2-Cl_2 = 2.05Å

The geometry of (**1.38**) has been studied by X-ray crystallography[47] and it has been found that the pentacoordinate silicon centre is fully trigonal bipyramidal and the tetracoordinate silicon is fully tetrahedral. This allows a direct comparison of Si-Cl bond lengths of penta- and tetracoordinate silicon centres to be made. Dispite the considerable (0.3Å) lengthening of the Si-Cl bond upon extra-coordination, with the sum of the van der Waals radii for silicon and chlorine being 3.80Å, it is still classified as being covalent.[48]

1.6: Relating molecular geometry to reaction pathways by solid-state correlation techniques

Complexes in which an increase in the coordination number at silicon is achieved by intramolecular ring closure of chelating groups are particularly interesting in relation to the stereochemistry of nucleophilic substitution at silicon. In these compounds the donor atom may play the role of *captive nucleophile* and the nature and behaviour of the intramolecularly coordinated species serve as models for the properties of the intermediates or transition states participating in the substitution process.

What is less well known is that crystallography can provide important information about the dynamics of substitution. It might at first seem surprising that a static structure may provide dynamic information, however, by collecting as many structures as possible containing the molecule or structural environment of interest and comparing appropriate structural parameters (usually bond lengths and/or bond angles), considerable insight into the 'substitution' can be gained. The technique is known as *structural correlation.*

The structure of a molecule in the crystal environment is not necessarily identical to that of its equilibrium structure as an isolated molecule. The forces exerted by the crystal environment can deform its structure to a greater or lesser extent.

The technique of structural correlation is concerned more with the deformation of the molecule than the forces exerted on it. As many structures as possible containing the centre of interest are collected and sequenced so that a gradual transformation is observed. Each of the ordered structures represents a *snapshot* of a modelled molecular transformation at a particular point of progress. Each structure is thus regarded as a *frozen* point in the transformation induced by its particular crystal environment.

Bürgi[49] in 1975 was the first to map the reaction pathway of S_N2 nucleophilic substitution at a tetrahedrally coordinated atom centre on the basis of X-ray data. He considered complexes (**1.39**) with the local geometries which model substitution with inversion at Cd (II) in the Figure 1.12 shown below.

Figure 1.12

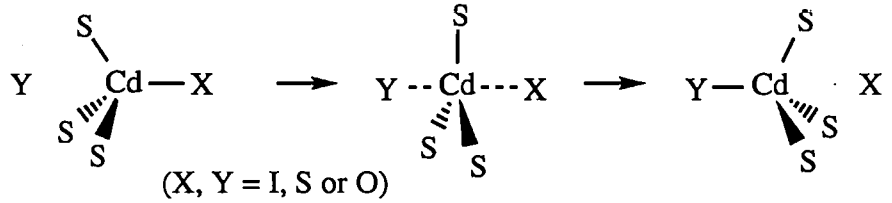

(1.39a) **(1.39b)** **(1.39c)**

The differences between the observed Cd-Y distances and the sum of the covalent radii for Cd and Y are calculated (Δy) and similarly for Cd and X (Δx). These are plotted (Figure 1.13) against (Δz), the distance that the cadmium atom resides out of the plane of the three equatorial sulfurs. Δz is thus a measure of how close the cadmium centre is to being completely trigonal bipyramidal.

Figure 1.13

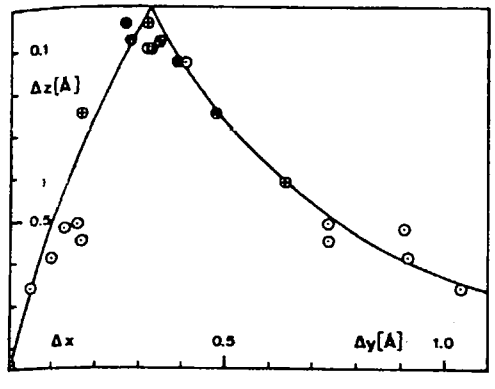

Nucleophilic substitution at Cd^{II}: Scatter plot of Δz versus the distance increments Δx, Δy

This plot illustrates the effect of an approaching Y-group lengthening the Cd-X distance. At the same time Δz tends to zero as the CdS_3 moiety becomes planar with a trigonal bipyramidal geometry at cadmium, (**1.39b**). Nucleophilic attack of a nitrogen lone pair on a carbonyl group was mapped from the crystal

structures of five natural products (**1.40A-E**) containing various degrees of intramolecular N-carbonyl carbon interaction.[50]

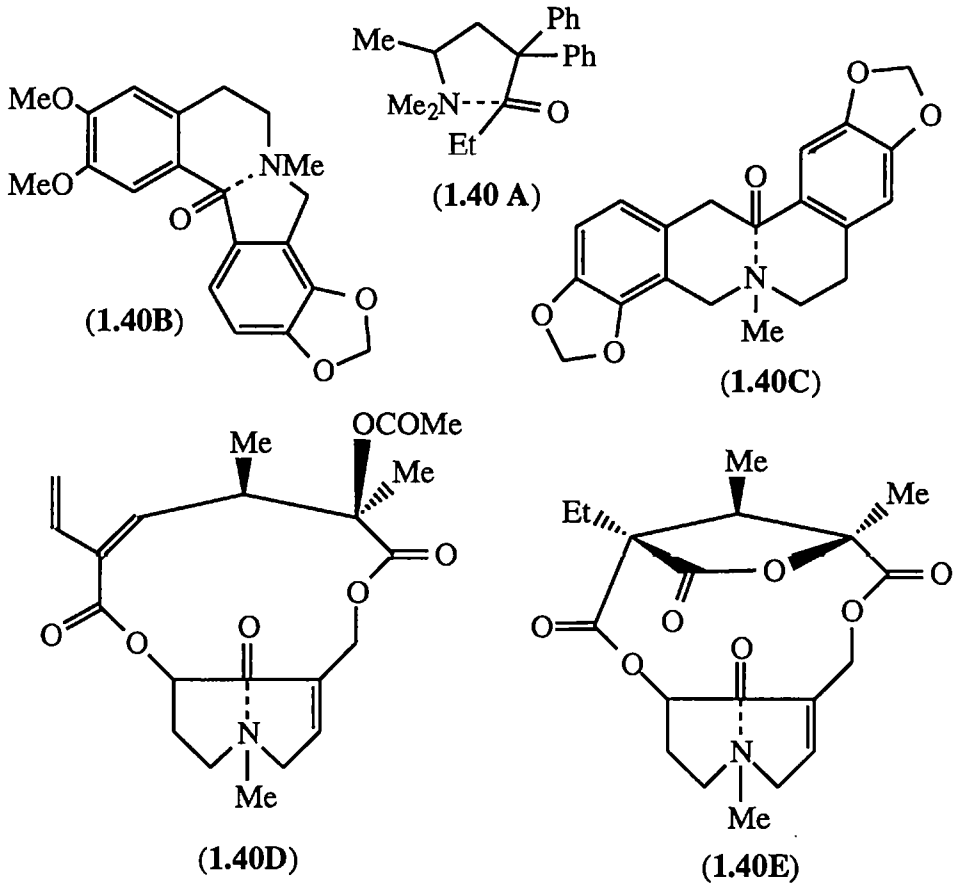

A combined diagrammatic representation showing the relative positions of the nitrogen, the carbon, the oxygen and the bisector of the R-C-R groups in each of the complexes could be drawn (Figure 1.14).

Figure 1.14

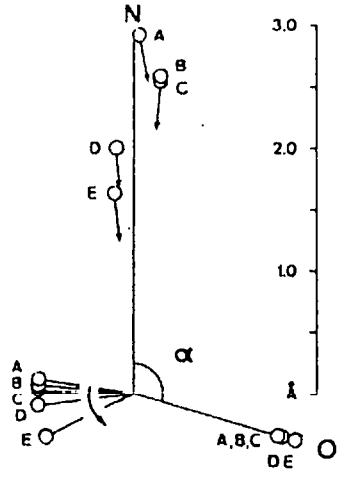

This illustrates the effect of the 'approaching nucleophile' on the geometry of the carbon and on the increasing length of the C=O bond as its single bond character increases. Through structures **A** → **E** the carbon becomes progressively more tetrahedral.

Later Britton and Dunitz applied the technique to model S_N2 substitution with inversion at Sn (IV)[51] based on a series of [R_3SnXY] complex crystal structures (**1.41**) (Figure 1.15).

Figure 1.15

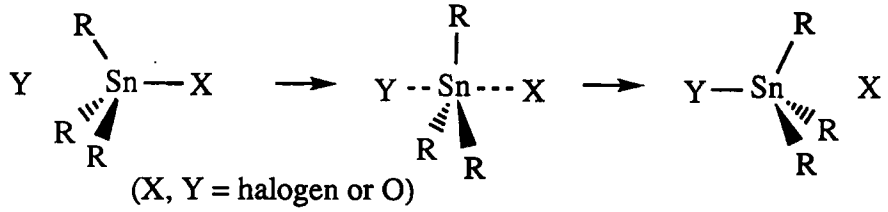

(X, Y = halogen or O)

(1.41a) **(1.41b)** **(1.41c)**

Figure 1.16

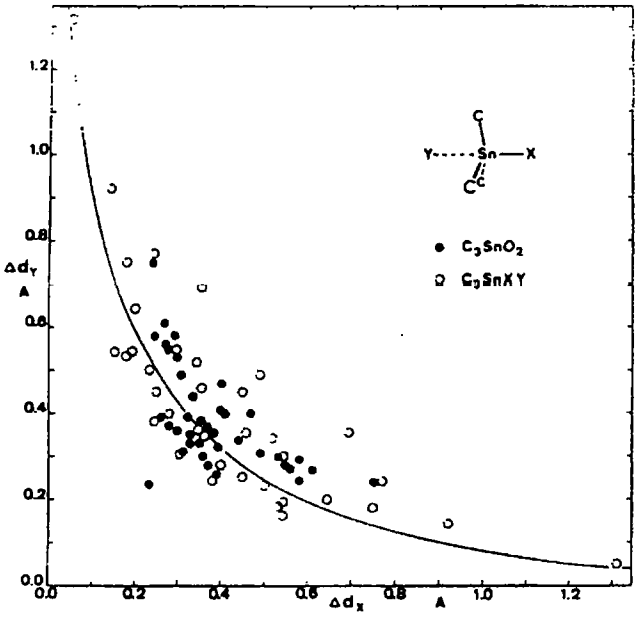

Δd_Y vs. Δd_X for SnC_3XY ensembles.

In Figure 1.16 Δd_y and Δd_X are the differences between the observed Sn-Y and Sn-X distances and the length of a standard Sn-Y and Sn-X bond respectively. It shows the concerted Sn-Y bond shortening and Sn-X bond lengthening as 'substitution' progresses.

More recently still[52] a general 3-D schematic representation has been generated of an X(2) nucleophile attacking at a metal centre M (M = Cd (II) or Sn (IV)) (Figure 1.17). d(X(2)) represents the extension of the M-X(2) distance beyond its typical length and d(X(1)) represents similarly the extension of the M-X(1) distance. The angle X(1)-M-R is represented on the diagram as α(X(1)MR). What is shown is that as X(2) approaches M, the M-X(1) bond is increasingly lengthened. Angle α(X(1)MR) is reduced as substitution inverts the configuration at M. Upon completion of the reaction d(X(2)) tends to zero with the formation of a full X(2)-M bond. At this point d(X(1)) is so large that X(1) is no longer within bonding distance of M.

Figure 1.17

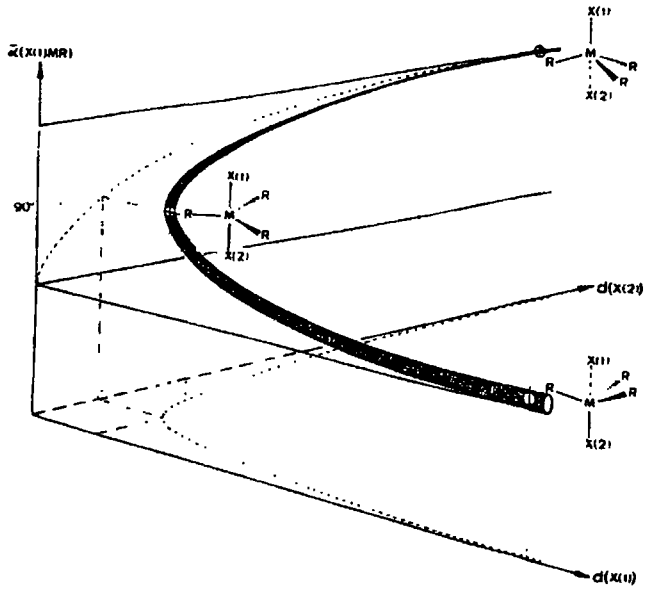

Schematic representation of reaction path for an S_N2-like process in the three-dimensional parameter space spanned by the two X–M distances and an X–M–R angle.

Leopold *et al*[53] modelled the attack of a nitrogen 'nucleophile' NR_3 on a BX_3 (X = H, F) Lewis acid centre (Figure 1.18). Key bond lengths and angles were obtained from X-ray crystallography (where possible) or else microwave spectroscopy. The progressive planar → tetrahedral change in boron geometry with strengthening B-N interaction was revealed by the following plot.

Figure 1.18

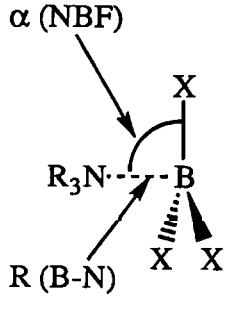

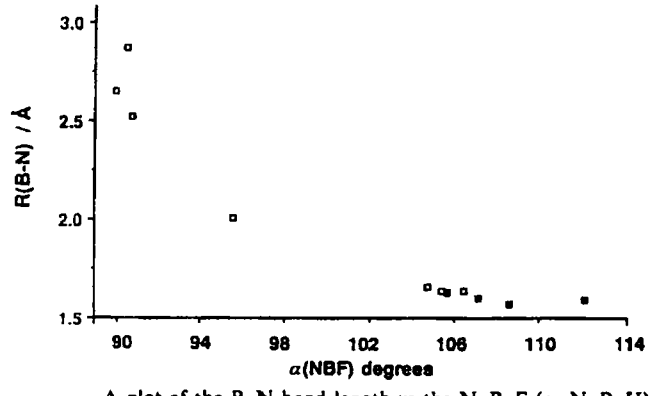

A plot of the B–N bond length vs the N–B–F (or N–B–H) angle for the addition complexes of BF_3 and BH_3 with nitrogen donors. Open squares represent gas-phase data, and solid squares correspond to crystallographic data.

Silatranes (**1.18**)[26] were among the first intramolecularly coordinated silicon complexes to be extensively studied by X-ray crystallography. Structural data for a variety of substituted complexes show that all have a distorted trigonal bipyramidal geometry at silicon and that the nitrogen and substituent group X on the silicon occupy the axial positions (Table 1.2).[54]

Table 1.2

X	NMe_2	$ClCH_2$	$3\text{-}NO_2C_6H_4$	C_6H_5	CH_3
$Si\text{-}N_{(donor)}$ (/Å)	2.02	2.12	2.12	2.15	2.17

Figure 1.19

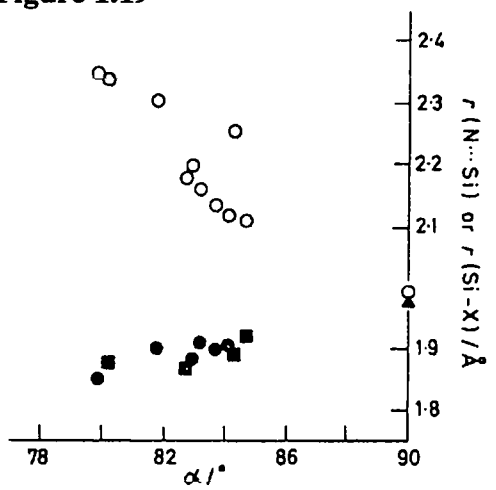

Scatter plot of $r(N \cdots Si)$, open circles, and $r(Si-X)$ [X = $C(sp^3)$ (●), $C(sp^2)$ (■), or N (▲)] against α

The stronger the electron withdrawing group at the silicon atom the shorter the $Si\text{-}N_{(donor)}$ interatomic distance becomes. Barrow *et al*[55] compiled data for 11 such complexes and plotted the mean $N_{(donor)}$-Si-O bond angle α against the interatomic $N_{(donor)}$-Si and Si-X distances (Figure 1.19). The data highlights how little the Si-X distance is perturbed by the varying $N_{(donor)}$-Si interaction. However, since the majority of X-groups are bound to the silicon through the same atom, carbon, it is perhaps not so surprising. When an NMe_2 leaving group is attached to the silicon, an appreciable shortening of the $Si\text{-}N_{(donor)}$ interatomic distance is observed.

Macharashvili *et al*[56] have used structure correlation to analyse a series of N-(halogenodimethylsilylmethyl) lactams, (**1.42**) (Table 1.3).

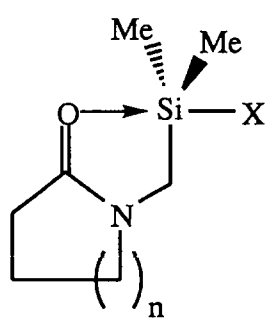

(**1.42**)

Table 1.3

Compound	n	X	O-Si (/Å)
(**1.42a**)	1	F	2.40
(**1.42b**)	2	Cl	1.95
(**1.42c**)	2	Br	1.80
(**1.42d**)	2	I	1.75

The Si-O interatomic distance was found to decrease in the order X = F > Cl > Br > I, the order of increasing leaving ability of group X. This was accompanied by a weakening of the C=O bond and strengthening of the C=N bond - visible from the IR spectra of the complexes. The geometry observed changes from distorted tetrahedral in

(**1.42a**) through to distorted trigonal bipyramidal in (**1.42b**) and (**1.42c**) then back to distorted tetrahedral in (**1.42d**), but with inverted configuration.

Pestunovich *et al*[57] have performed theoretical quantum chemical calculations on a series of pentacoordinated amides (**1.43**) and (**1.44**), allowing O-Si and Si-Cl bond distances to be predicted in each case.

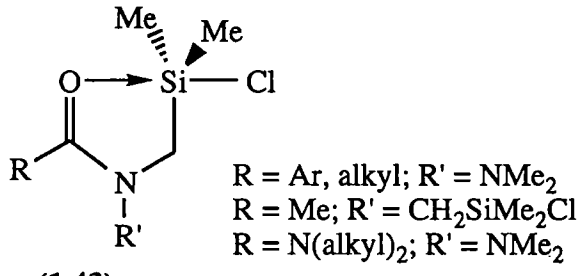

R = Ar, alkyl; R' = NMe_2
R = Me; R' = CH_2SiMe_2Cl
R = $N(alkyl)_2$; R' = NMe_2

(**1.43**)

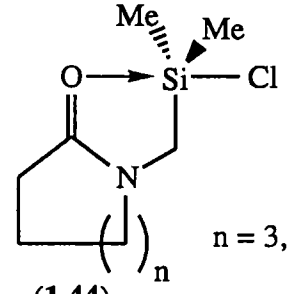

n = 3, 4, 5.

(**1.44**)

By plotting together the calculated and experimentally obtained O-Si and Si-Cl distances in each complex (l_{SiO} and l_{SiCl} respectively), good agreement between theory and practice was found with a characteristic hyperbolic curve being obtained (Figure 1.20).

Figure 1.20

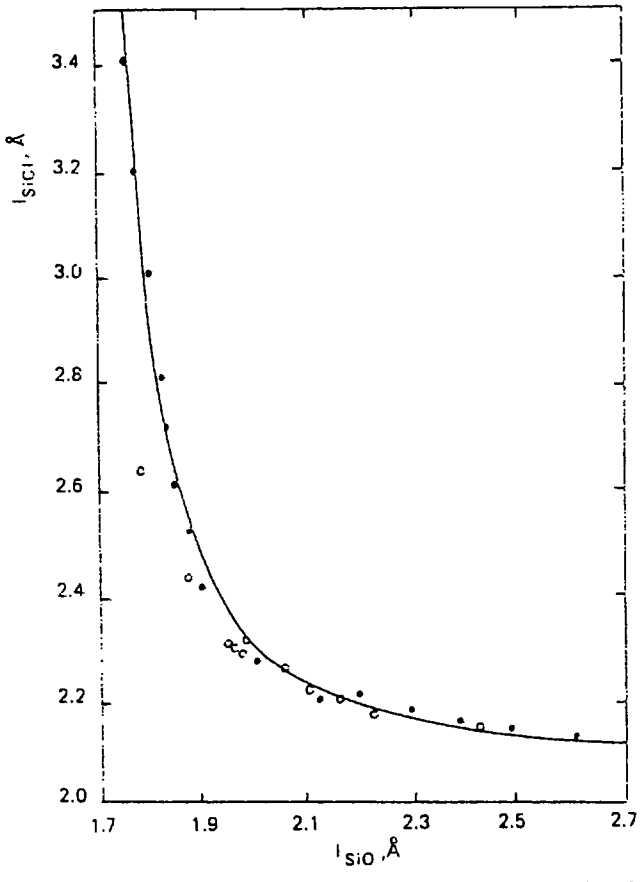

Relationship between the l_{SiCl} and l_{SiO} values calculated using MNDO (●) and those determined experimentally (○) for (O-Si)dimethyl(*N*-amidomethyl)chlorosilanes.

It is clear that structural correlation requires crystalline products for success and that there is considerable scope for a technique that is more widely applicable to include compounds where crystallisation is not possible, particularly one which is solution-based. It was with this aim in mind that Bassindale and Borbaruah developed the technique of *solution phase mapping*.[58] This is discussed fully in the introduction to Chapter 2.

So far we have concentrated on only five-coordinate silicon species, however it is important to note that silicon can expand its coordination number to six. Indeed six-coordinate complexes have been known for as long as five coordinate complexes. The first six-coordinate complex, the $[SiF_6]^{2-}$ anion, was independently reported by Gay Lussac[1] and Davy[59] in the early 1800's. Although hexacoordinate silicon complexes are largely beyond the scope of our work we will make mention of their preparation and structural characteristics.

1.7: Preparation of hexacoordinate silicon complexes

Hexacoordinate silicon complexes are mainly prepared by methods analogous to those used for the preparation of pentacoordinate silicon complexes:

- The addition of nucleophilic, anionic or neutral reagents to tetravalent silicon derivatives leading to respectively anionic or neutral complexes.
- The reaction of an organosilane containing two substitutable groups at the silicon with bi-dentate ligands.

1.7.1: Coordination to a tetracoordinate silicon compound

A: Fluoride ion donation to an organosilane

Kumada *et al*[60] developed a practical route for the preparation of organopentafluorosilicates (**1.45**) by reaction of excess potassium fluoride in aqueous or aqueous/alcoholic solution with organotrichlorosilanes.

$$RSiCl_3 \xrightarrow[H_2O/R'OH]{KF\ (excess)} \underset{\textbf{(1.45)}}{[RSiF_5]^{2-}}\ \ 2K^+ \quad (R = \text{long chain alkyl})$$

B: Intermolecular coordination to a silane

The series of stable hexacoordinate complexes $Me_2SiX_2.2py$, $MeSiX_3.2py$ and $SiX_4.2py$ (X = F, Cl or Br)[5, 61] provide a contrast to the reactions of the triorganosilanes and pyridine described earlier[7] where no stable hypervalent complexes could be isolated. Diamines such as 2,2'-bipyridine and 1,10-phenanthroline coordinate readily to halogenosilanes $SiCl_4$, $SiXYI_2$ and Si_2Br_6 to give mono (**1.46**),[62] bis (**1.47**)[63] and tris(chelate) (**1.48**)[64] complexes respectively.

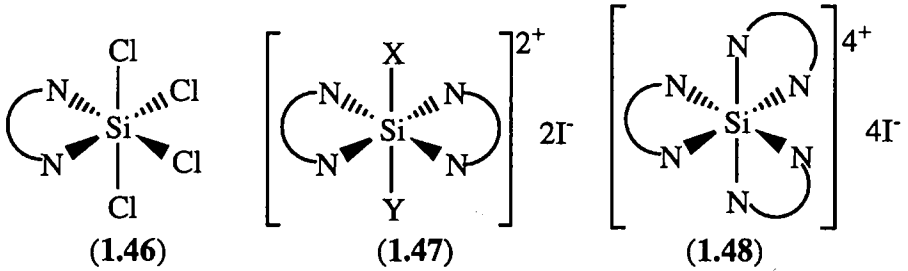

(1.46) **(1.47)** **(1.48)**

(X, Y = H, CH_3, Ph, OCH_3, Cl)

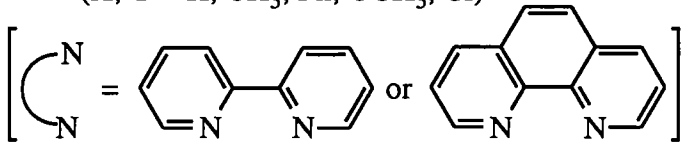

C: Intramolecular coordination to an organosilane

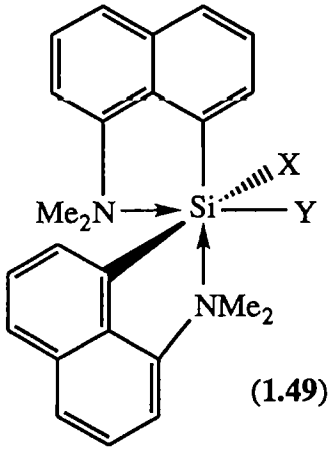

(1.49)

a: X, Y = H
b: X = H, Y = F
c: X, Y = F

Complexes of the type (**1.49**)[65] have been prepared using a similar method and ligands to those used with the corresponding pentacoordinate complexes (**1.20**)[28] and characterised by X-ray crystallography.

1.7.2: Substitution in a tetra-functional silane by a bi-dentate ligand

1,3-diketones can form, as well as pentavalent complexes such as (**1.16**), hexavalent complexes.[24] They react with either tetra-acetoxysilane to give a bis, neutral complex (**1.50**), or silicon tetrachloride to give a tris, cationic complex (**1.51**). A tropolone analogue of (**1.51**) can also be prepared, (**1.52**).[66]

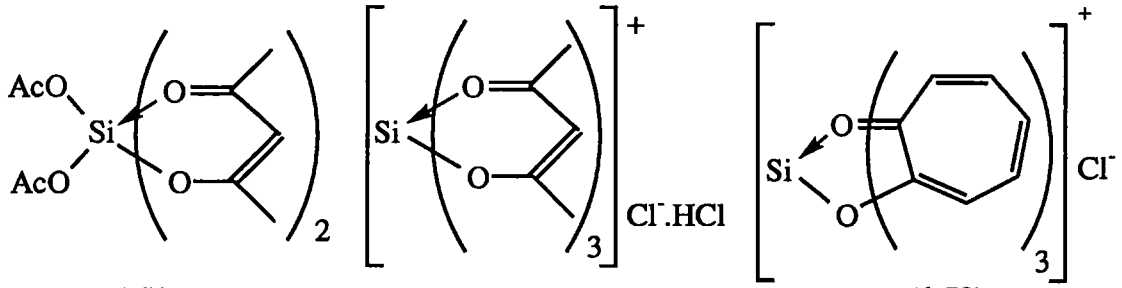

(1.50) (1.51) (1.52)

The tris(catechol) complex (**1.53**) is prepared from a tetraalkoxysilane and either sodium or potassium alkoxide (Figure 1.21).[21, 67]

Figure 1.21

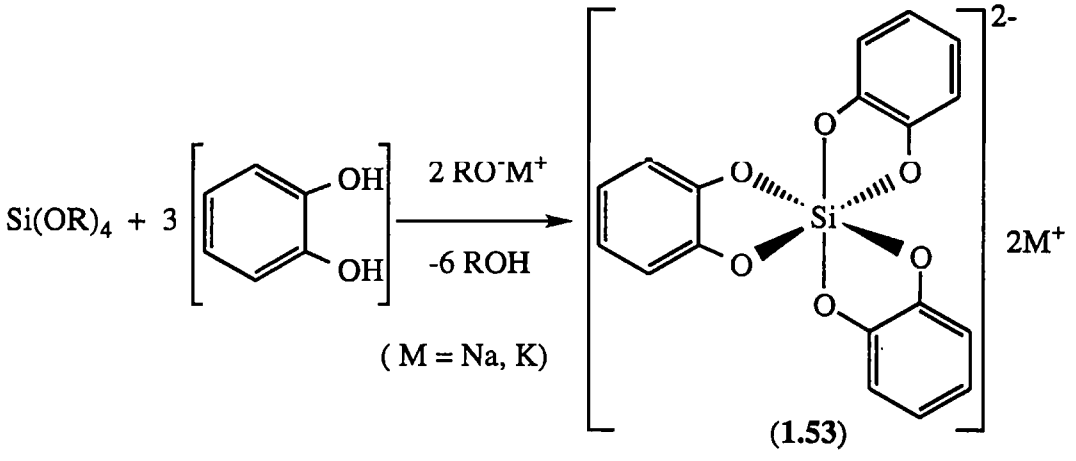

(1.53)

1,2-ethanediol forms an analogous complex (**1.54**) when reacted with silica and barium oxide (Figure 1.22).[68]

Figure 1.22

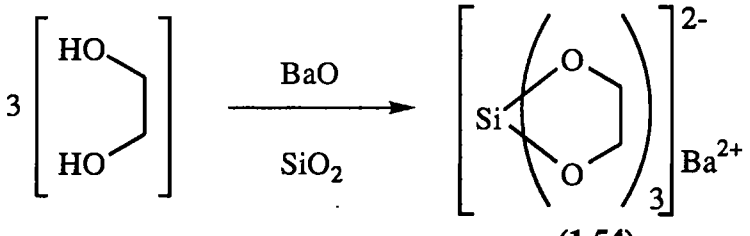

(1.54)

1.8: Structures of hexacoordinate silicon complexes

Many of the features of pentacoordinate silicon complexes previously discussed also apply to hexacoordinate silicon. This section will outline similarities and differences.

Hexacoordinate silicon complexes have an octahedral or distorted octahedral geometry. How close the geometry at the silicon is to octahedral is determined by the size of the attached groups and their steric interactions with each other. In the case of

multi-dentate ligands, another factor is the rigidity of the group, which restricts the donor atoms ability to occupy the precise octahedral positions. In contrast to pentacoordinate complexes, the axial and equatorial sites can be equivalent.

For example, the first identified hexacoordinate complex, the $[SiF_6]^{2-}$ dianion was reported in 1935 as having the expected octahedral geometry[69] with identical Si-F bond lengths (1.71Å). The bis pyridine adduct $SiF_4.2py$[61] also has also an octahedral geometry with the pyridine groups in a *trans* relationship.

Complex (**1.55**)[70] has been shown to have a somewhat distorted octahedral geometry with the Si-Cl bonds residing *trans* to the N–Si bonds. The Si-Cl bonds of the hexacoordinated silicon are longer than those of the tetracoordinated silicon, similar to the behaviour of axial donor-Si-Cl moieties in pentacoordinate complexes.

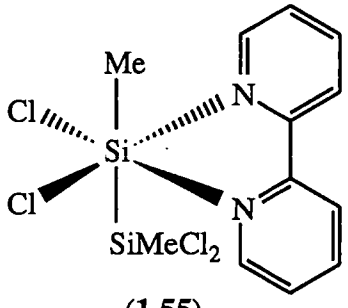

(**1.55**)

The use of rigid ligands such as 2,2'-bipyridyl to stabilise hexacoordinate silicon is more frequently necessary than for pentacoordinate silicon as the presence of six donor groups within the coordination sphere of more open-chain bidentate ligands has been shown to not always result in chelation of all potential donor groups. For example, complex (**1.56**)[71] in the solid state has only one of its dimethylaminomethyl groups within coordination distance of the silicon, the other being oriented away by rotation of the NMe_2 group about its Ar-CH_2NMe_2 bond.

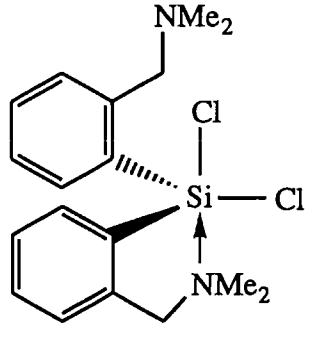

(**1.56**)

Part B: Tin

1.9: Overview

Since silicon has the ability to expand its coordination number beyond the conventional four, it is not unexpected that tin, being further down the same periodic group can also give rise to extra-coordination. In fact, tin does this far more readily than silicon and gives rise to an even more extensive range of structures. A multitude of hypervalent complexes of both Sn (II) and Sn (IV) have been reported.[72, 73, 74] As our work concerns only five- and six-coordinate Sn (IV) complexes, the introduction shall concentrate mainly on these.

Unlike silicon (IV), tin (IV) compounds rarely exist in four-coordinate, tetrahedral geometry. Only R_4Sn (R = simple organic e.g. alkyl or aryl group) and R_nSnX_{4-n} derivatives which are either sterically crowded (e.g. R = $(Me_3Si)_3C$),[75] or where the ligand is weakly electronegative (e.g. $Ph_3SnSnPh_3$)[76] have such a geometry in the solid state. Wherever possible, tin strives to expand its coordination number either through inter- or intramolecular coordination.

1.10: Intermolecular coordination

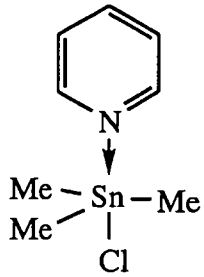

(**1.57**)

The earliest intermolecular complex was complex (**1.57**), established as a stable crystalline adduct of chlorotrimethyltin and pyridine.[77] This important discovery contrasts with the similar study of halogenotrimethylsilanes and their interaction with pyridine,[7] where no stable five-coordinate complex is observed.

Tin (IV) halides provide a wealth of structures. Tin tetrahalides SnX_4 and organotin halides R_nSnX_{4-n} (n = 1-3) are tetrahedral in the vapour and liquid phases but in the solid state exhibit a preponderance for the formation of halogen-bridged lattices. Tin fluorides in particular form strong one and two-dimensional polymers. For example, tin (IV) fluoride forms a highly stable two-dimensional polymer (**1.58**) with octahedrally coordinated tin. Dimethyltin difluoride (**1.59**) has a similar structure with the non-bridging fluorine atoms being replaced by methyl groups.[78]

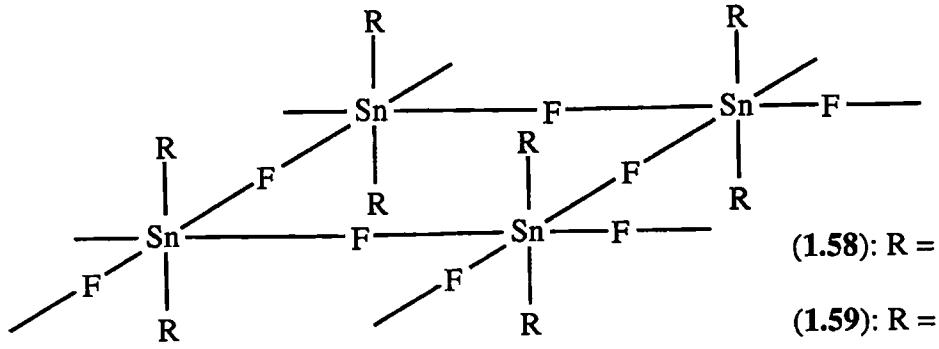

(**1.58**): R = F

(**1.59**): R = Me

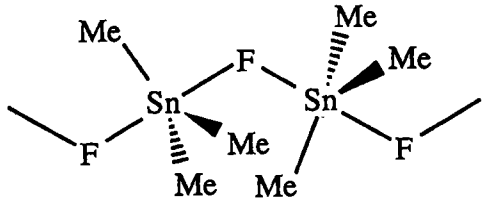

(**1.60**)

Fluorine bridging in trimethyltin fluoride (**1.60**) results in a one-dimensional polymer with a planar [Me_3Sn] moiety and trigonal bipyramidal coordination geometry at tin.[79] Consistent with their polymeric structures, these materials are infusible and insoluble. Only when the organic groups become large does steric hindrance preclude association.[75] In contrast, fluorotrimethylsilane is a liquid with a boiling point of 16°C. Bridging by other halogens is much weaker and reversible. A loosely associated one-dimensional chain is formed at low temperatures by chlorotrimethyltin[80] (Figure 1.23a) and trimethyltin hydroxide[81] (Figure 1.23b) similar to trimethyltin fluoride. Triphenyltin chloride[82] however has a tetrahedral structure about the tin with the crystal structure showing discrete, isolated molecules.

Figure 1.23

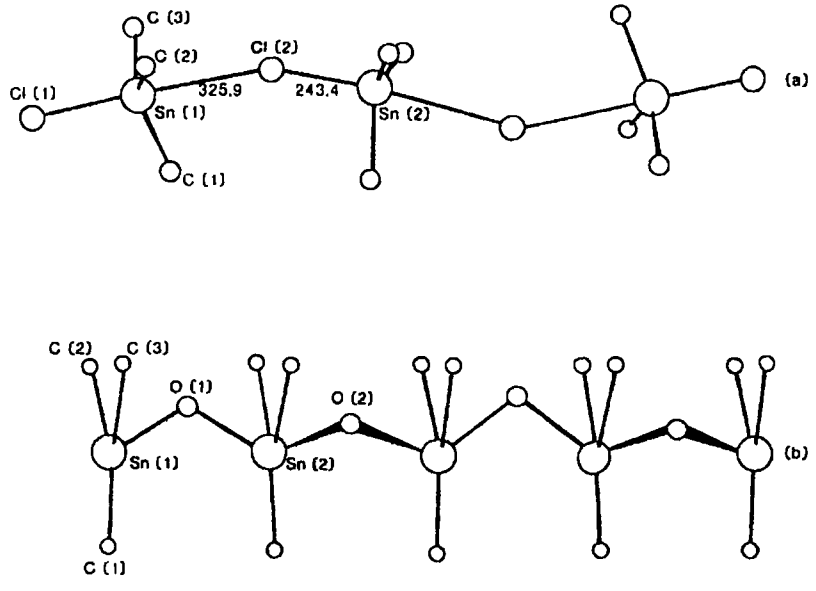

Distances in pm.

Dialkyltin dihalides, where the alkyl group is sterically small, also associate into one dimensional chain structures. In dimethyltin dichloride (**1.61**)[83] the covalently-bonded chlorines on each tin coordinate to different tin centres in the chain, while in bis(chloromethyl)tin dichloride (**1.62**)[84] the chlorines chelate to the same adjacent tin centre. In both cases the tin is hexacoordinate, but with a highly distorted octahedral geometry.

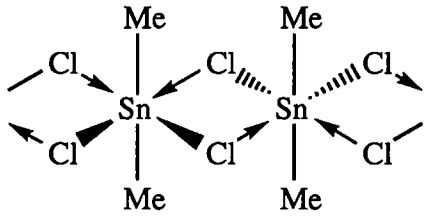

(1.61)

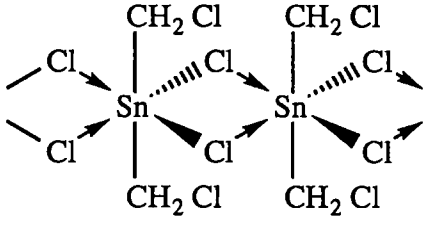

(1.62)

Neutral, non-polymeric intermolecular coordination complexes of tin involving a single donor-tin bond are relatively common compared to silicon. The Me_3SnCl.py adduct (**1.57**)[77] has already been mentioned. A further example, where triphenylphosphine oxide is the neutral donor, is (**1.63**). The crystal structure of this compound has recently been reported.[85]

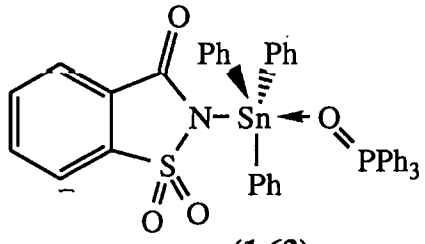

(1.63)

The geometry of the tin centre is trigonal bipyramidal with the oxygen and nitrogen groups in the axial positions. The O–Sn bond length of 2.34Å is markedly short (Sn-O typically 1.90Å). The same research group have reported the coordination of carbonyl[86] and sulfoxide[87] groups to this tin centre resulting in very similar tin structural geometries.

A 1:1 mixture of dimethyltin dichloride and diphenylcyclopropenone readily react to form an intermolecular complex. However, due to the low steric requirements of the donor, the crystal structure reveals a dimeric structure with one of the chlorines on each tin bridging with an adjacent tin, resulting in a hexacoordinate tin centre, (**1.64**).[88]

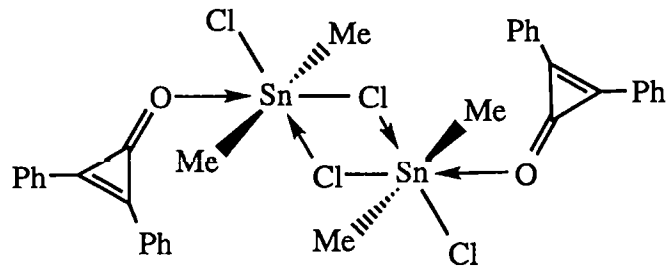

(1.64)

1.11: Intramolecular coordination

In the same way as silicon, hypercoordination can be generated by either rigid geometry or more open-chain ligands.

1.11.1: Rigid geometry ligands

As previously mentioned, simple tetraalkyl and aryl tin compounds are among the few tetrahedral, four-coordinate tin (IV) compounds. However with rigid geometry ligands, expansion to five (**1.65**)[89] or six (**1.66**)[90] coordination can be achieved.

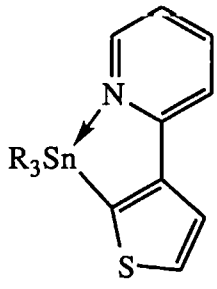

(**1.65**)

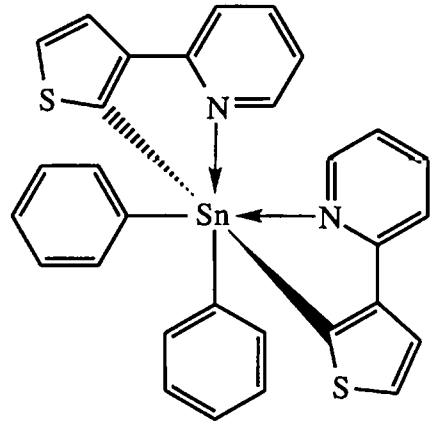

(**1.66**)

Compound (**1.67**)[91] has a structure reminiscent of the silatranes discussed earlier. Stannatranes themselves, (**1.68**), can be synthesised by dehydration of a mixture of the appropriate stannoic acid and triethanolamine.[92]

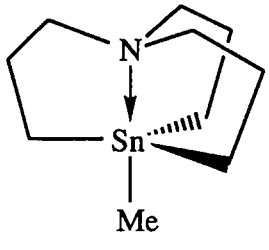

(**1.67**)

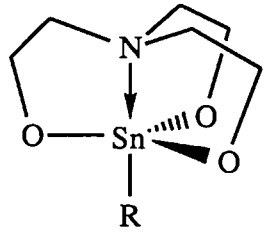

(R = Et, Bu, n-C_8H_{17})

(**1.68**)

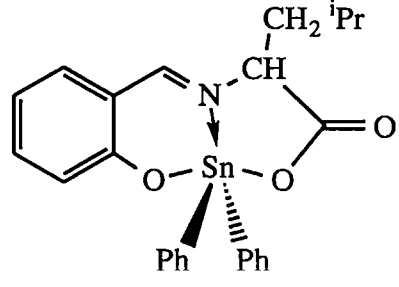

(**1.69**)

Wang *et al*[93] recently reported the crystal structure of a pentacoordinate biazostannoxide, (**1.69**). N–Sn bonding closes a nine-membered ring into fused five and six-membered rings. This ring closure results in a structure where the tin is pseudo-trigonal bipyramidal with the nitrogen donor forced to occupy an equatorial position with the phenyl groups, while the oxygens reside in the axial positions. With the tin atom being

at a ring junction, the O-Sn-O diaxial bond angle is distorted somewhat from linearity (157.6°).

2-Hydroxy and 2-mercaptopyridine-N-oxides (**1.70**) (Figure 1.24) readily stabilise hexa-coordinate tin.[94]

Figure 1.24

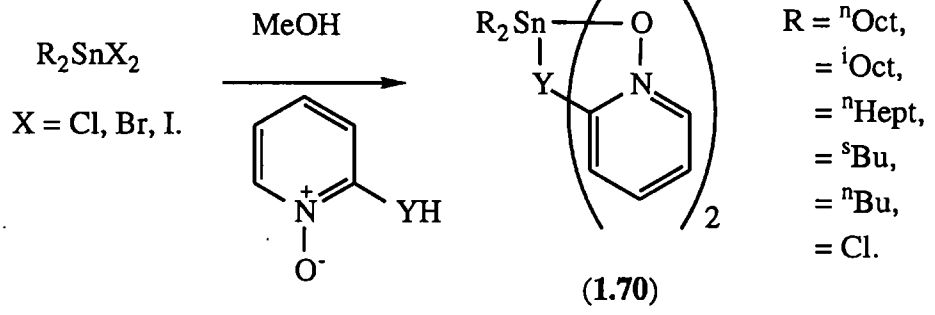

(1.70)

The tropolone ligand forms isostructural hexacoordinate complexes, (**1.71**) (Figure 1.25), to the silicon analogues previously described.[95]

Figure 1.25

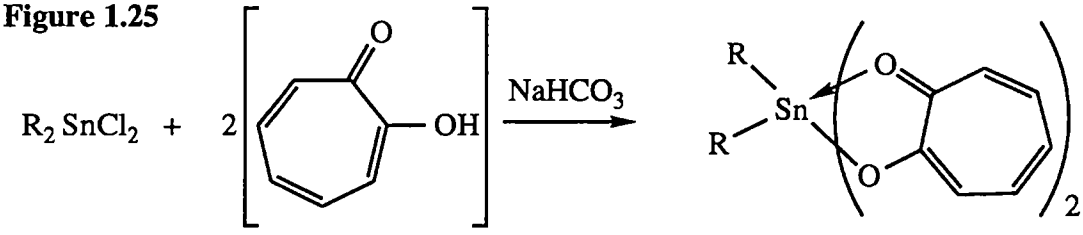

(R = Me, Et, Pr, ^{n}Bu, Ph, benzyl) **(1.71)**

Tris-tropolonato complexes have also been reported with heptacoordinate tin centres.[96]

1.11.2: Open-chain ligands

Such is tin's propensity to expand its coordination number to greater than four that chelation of less-*rigid* ligands occurs to tin centres, even with only low electronegative substituents. Complexes (**1.72**)[97] and (**1.73**)[98] are penta and hexacoordinate examples involving 1,3-diketone ligands. The silicon analogues of these compounds would be predicted to be fully tetracoordinate at silicon.

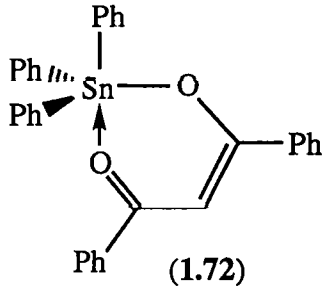

(1.72)

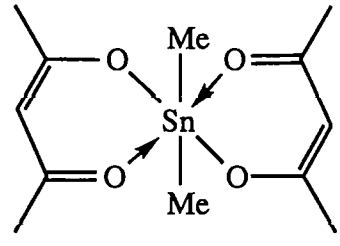

(1.73)

Tin carboxylates display interesting structural differences between solid and solution phases. Dialkyltin dicarboxylates (**1.74**)[99] exist in the solid state as intermolecularly coordinated bridged chain polymers (**1.74a**), while in solution they adopt intramolecularly coordinated monomeric structures containing two four-membered rings (**1.74b**). In both structures the R-groups are in a *trans* relationship at the tin.

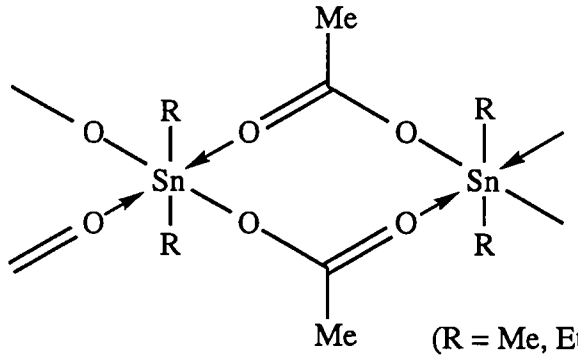

(R = Me, Et, ^{n}Pr, ^{n}Bu)

(1.74a)

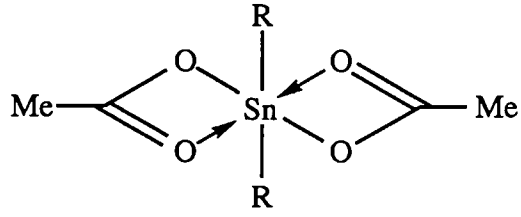

(1.74b)

A similar coordination switch between solid and solution phases occurs in compound (**1.75**).[100] In the solid state an infinite, single-bridge, intermolecularly pentacoordinated tin polymer, (**1.75a**), is favoured which contains oxygens in the axial positions. In solution the intramolecularly pentacoordinated tin monomer, (**1.75b**), is observed with axial chlorine and carbonyl-oxygen groups.

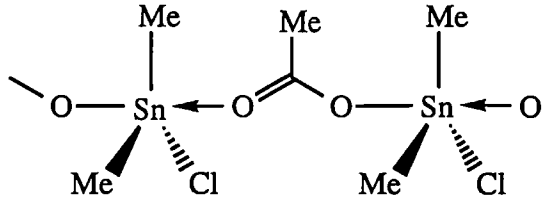

(1.75a)

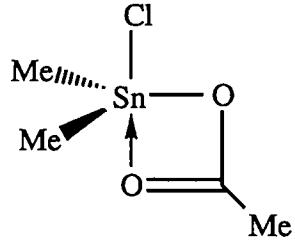

(1.75b)

The size of the ring formed by intramolecular donation to tin has also been found to play an important role in determining whether inter or intramolecular coordination is observed. ω-(Trichlorostannyl)alkyl acetates, (**1.76**),[101] have been found to exist as an equilibrium mixture of intra, (**1.76a**), and intermolecular, (**1.76b**), coordination structures where coordination to the tin can be through the alkoxy oxygen or the carbonyl oxygen (Figure 1.26).

Figure 1.26

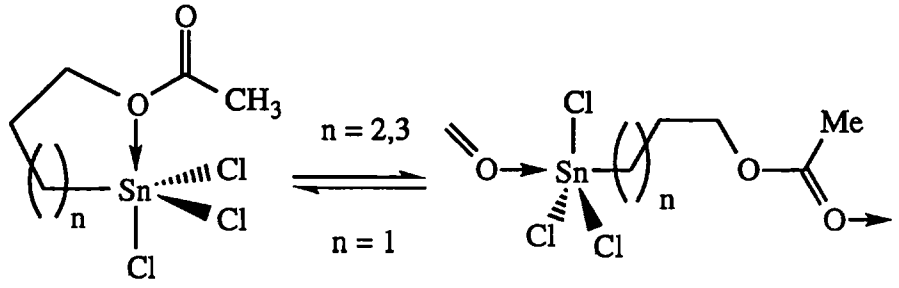

(1.76a) **(1.76b)**

When n = 1 there is a preference for structure (**1.76a**). This is thought to be due to the formation of a five-membered ring with relatively little strain. However when n = 2 or n = 3 the ring would be far more flexible and susceptible to ring opening due to thermal vibrations and hence an oligomeric species, (**1.76b**), based on intermolecular coordination is that which is preferred.

Molloy *et al*[102] have studied a number of triphenyltin benzoates (**1.77**) and found their choice of structure to be dependant on the nature of R, obtaining evidence for either oligomeric pentacoordinate, (**1.77a**), or monomeric tetracoordinate, (**1.77b**), structures.

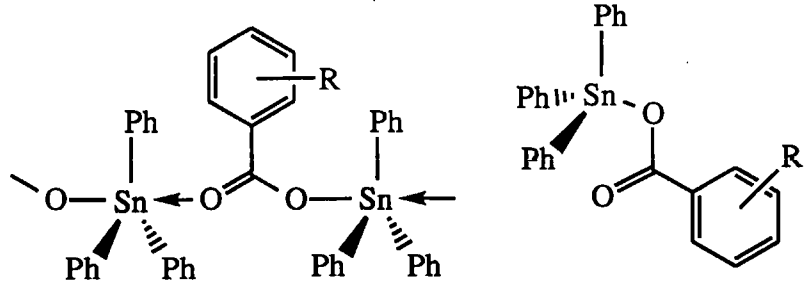

(1.77a) **(1.77b)**

The structural preference was found to depend on a complex interplay between the steric and electronic effect of the substituent(s) R and its (their) position on the aromatic ring. The pKa's of the corresponding benzoic acids reflect the electrophilicity of the tin centre such that it is more susceptible to pentacoordination when substituents are electron withdrawing. The size and position of R concurrently alters the steric environment about the tin making it more, or less easy for other molecules to get close enough to the tin to oligomerise.

1.12: Fluxionality of pentacoordinate tin complexes

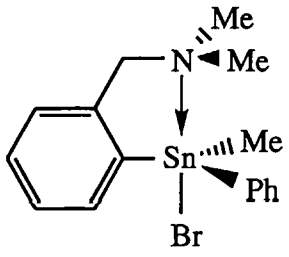

(1.78)

Van Koten *et al* have prepared a series of tin complexes to monitor the stereochemistry of substitution at tin. Complex (**1.78**)[103] is a similar model compound for substitution at tin as (**1.24**) is for substitution at silicon.[34] The ^{1}H NMR spectrum of (**1.78**) at 10°C displays the NMe_2 groups as a pair of diastereotopic singlets, consistent with the locked configuration of a pentacoordinate tin centre. As the sample is warmed to 123°C the signals collapse to a single sharp resonance as decoordination of the nitrogen atom and inversion at the tin centre takes place.

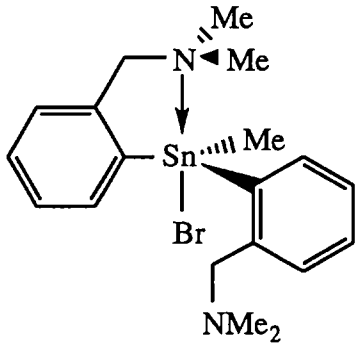

(1.79)

Complex (**1.79**)[103] allows the equilibrium between pentacoordinate and tetracoordinate tin states to be evaluated. At -50°C two pairs of diastereotopic NCH_2's are observed in the ^{1}H NMR spectrum, consistent with one tin-bound and one unbound NMe_2 group in the molecule. At room temperature only a pair of resonances is observed for both NCH_2 groups. This is caused by the fast, on the NMR time scale, intramolecular exchange between the NMe_2 groups coordinated to the tin. At 111°C the NCH_2 groups are observed in the spectrum as a single resonance as rapid inversion of the tin centre occurs.

Complex (**1.80**),[104] in contrast to (**1.81**), has dynamic NMR activity by virtue of it containing the donor group in a six-membered ring. This ring has two possible conformations leading to non equivalence of the NMe_2 groups.

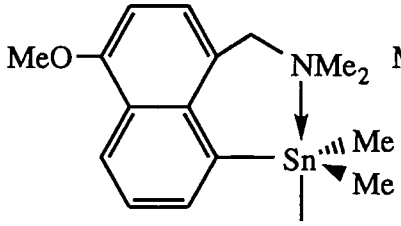

(1.80)

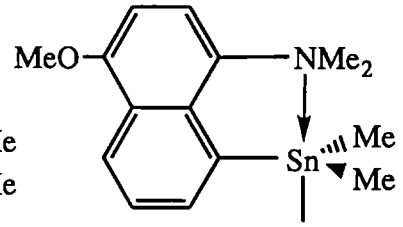

(1.81)

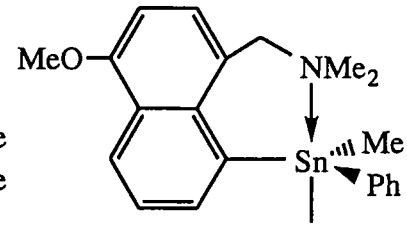

(1.82)

At room temperature complex (**1.80**) displays sharp ^{1}H NMR singlets for the NMe_2 and $SnMe_2$ groups as a result of rapid flipping between the conformations. At -30°C both of these groups exhibit pairs of resonances as flipping ceases. Decoordination of nitrogen and inversion of configuration at tin is invisible by NMR spectroscopy in this compound as the tin is achiral.

The chiral analogue (**1.82**)[104] allows both ring flipping and tin inversion to be observed. At -35°C separate ^{1}H NMR resonances for the NCH_2, NMe_2 and SnMe protons in both ring conformations are observed. Warming of the solution causes the collapse of the SnMe and NCH_2 resonances to single peaks as a result of fast ring flipping. With the nitrogen still coordinated to the tin atom, its chirality causes the NMe_2 groups to remain diastereotopic. However at 64°C, ring opening and rapid inversion of the tin centre gives rise to a single resonance for the NMe_2 group.

Intra and intermolecular site exchange in pentacoordinate tin has been studied[105] by the reaction of fluoride ion with dialkyl and diaryltin dichlorides and monitoring the ^{119}Sn and ^{19}F NMR spectra at different temperatures. A complex series of group exchange processes has been revealed by cooling solutions containing the appropriate mixture of diorganotin dichloride and fluoride ion to slow the otherwise rapid ligand migration and rearrangement processes. For example, the addition of fluoride ion to diphenyltin dichloride and phenyltin trichloride gives measurable quantities of the ions listed in Table 1.4.

The variable temperature behaviour of the ^{19}F NMR chemical shifts of the $[Ph_2SnF_3]^-$ ion highlight the intramolecular site exchange processes being studied (Figure 1.27).

Table 1.4

NMR Data for Species Formed from Reaction of Fluoride with Diphenyltin(IV) Dichloride or Phenyltin(IV) Trichloride in Dichloromethane Solution at −100 °C

species	$\delta(^{119}Sn)$, ppm	J(Sn–F), Hz	$\delta(^{19}F)$, ppm	J(F–F), Hz
$[Ph_2SnCl_3]^-$	−250			
$[Ph_2SnCl_4]^{2-}$	−425			
$[PhSnCl_4]^-$	−323			
$[PhSnCl_5]^{2-}$	−552			
$[Ph_2SnCl_2F]^-$	−291 (d)	2365	−139.7	
$[Ph_2SnCl_2F]^-$	−269 (d)	2410	−147.2	
$[Ph_2SnClF_2]^-$	−331 (d of d)	2420	−159.1 (d)	15
		2360	−159.7 (d)	15
$[Ph_2SnF_3]^-$	−402 (d of t)	2310 (d)	−173.8 (t)	28
		2250 (t)	−156.8 (d)	28
$[Ph_2SnCl_3F]^{2-}$	−464 (d)	2624	−140.3	
trans-$[Ph_2SnF_4]^{2-}$	−592 (quint)	2695	−125.0	
$[PhSnCl_2F_2]^-$	−503 (d of d)	2255	−79.4	
		2415	−55.6	
$[PhSnCl_3F_2]^{2-}$	−563 (d of d)	2560	−120.0 (d)	40
		1760	−74.0 (d)	40
trans-$[PhSnCl_4F]^{2-}$	−532 (d)	1825	−52.97	
$[PhSnF_5]^{2-}$	−692 (d of quint)	2430 (quint)	−140.0 (d)	20
		1180 (d)	−140.4 (quint)	20
$[SnF_6]^{2-}$	−803 (sept)	1625	−152.6	

Figure 1.27

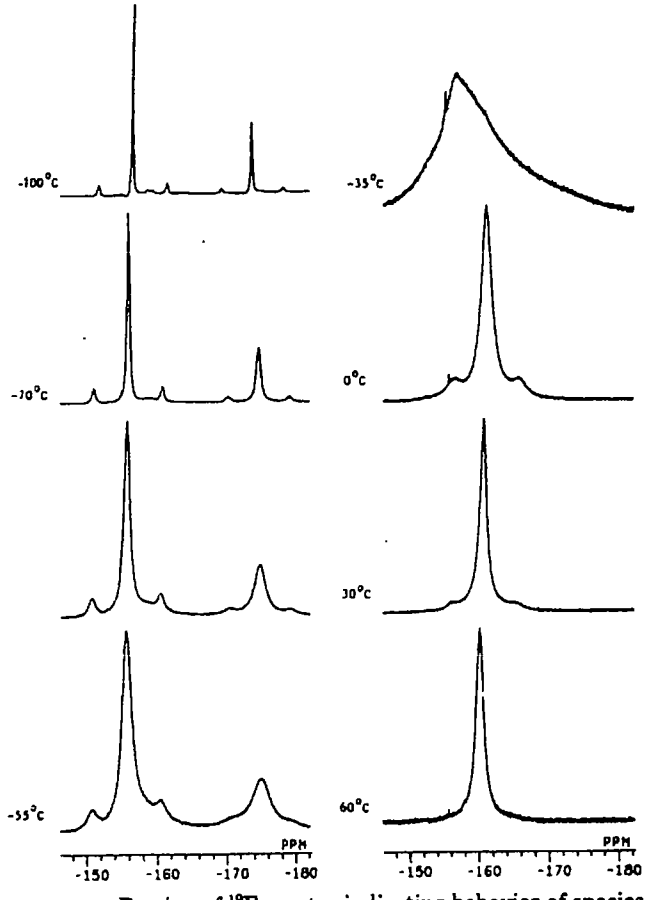

Portion of ^{19}F spectra indicating behavior of species $[Ph_2SnF_3]^-$ at various temperatures.

At -100°C separate sharp resonances for the axial and equatorial fluorines are observed. On warming to 60°C the signals broaden, collapse to one, then sharpen as rapid site exchange begins to take place. Cotton and Dakternieks[106] have studied the rates of intermolecular halogen exchange between 1:1 mixtures of diorganotin dihalides. The room temperature ^{119}Sn NMR spectrum of a mixture of diphenyltin dichloride and diphenyltin dibromide in dichloromethane displays three sharp resonances at δ -33, δ -52 and δ -75 for an equilibrium mixture of the dichloride, the bromide-chloride and the dibromide compounds respectively.

Resolution of a similar mixture of dimethyltin dichloride and dimethyltin dibromide into separate resonances is only achieved by cooling the solution to -100°C. This observation highlights the greater steric bulk of a phenyl group to a methyl group and the effect it has on lowering the rate of halogen exchange. In both cases the mixed halogen compounds disproportionate on attempts to isolate them.

^{119}Sn NMR chemical shifts are particularly sensitive to the electronic environment of the tin. In fact they are even more sensitive than ^{29}Si chemical shifts. Since we have already seen that extracoordination to tin is frequently temperature and phase dependant, then we can use ^{119}Sn NMR data to monitor how the coordination to a tin centre changes as its environment is manipulated.

1.13: ^{119}Sn NMR spectroscopy and factors that affect the chemical shift

There are a number of factors which influence the tin chemical shift, either individually or, as will become clear, more often in tandem.

1.13.1: Electronegativity

The more electron-donating is an R-group, the more shielded is the ^{119}Sn atom, as shown in Table 1.5.

Table 1.5: Effect of organic groups on the ^{119}Sn chemical shifts of R_3SnCl compounds. (Adapted from reference 107)

R	δ ^{119}Sn (/ppm)
Me	164
Et	155
Bu	141
$PhCH_2$	43
Ph	-48

For a series of compounds Me_3SnX, as the X-group becomes more inductively electron withdrawing, so the ^{119}Sn chemical shift moves increasingly down field. A plot of the Pauling electronegativity for various X groups against chemical shift results in a good linear correlation (Figure 1.28).

Figure 1.28

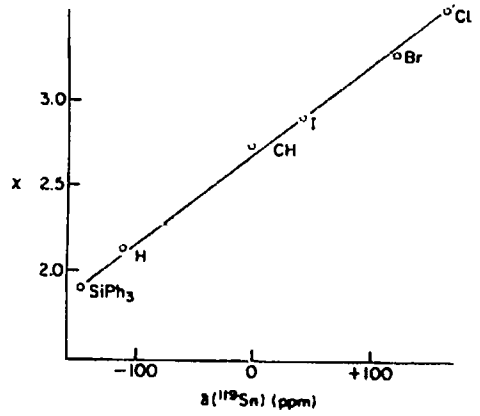

Dependence of ^{119}Sn chemical shifts (ppm) upon Pauling electronegativity χ of substituent for some Me_3SnX compounds.

Similarly, for a series of compounds $R_{4-n}SnX_n$ (n = 0-4), the more electron withdrawing groups placed around a tin the more de-shielded the centre would be expected to become. Between n = 0 and n = 1 this is usually true (e.g. Figure 1.29 for various $Bu_{4-n}SnX_n$ compounds).

Figure 1.29

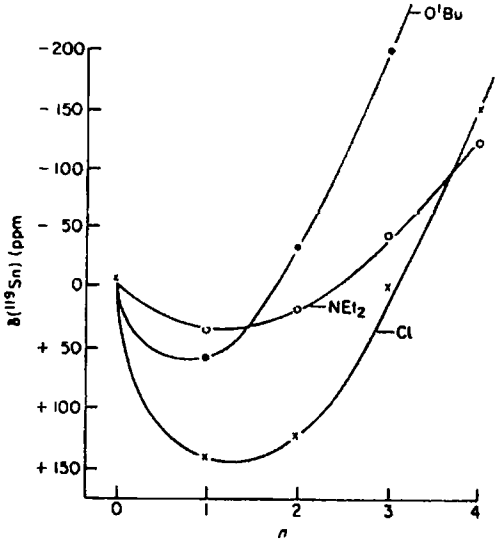

^{119}Sn chemical shifts (ppm) for unassociated butyltin compounds, $Bu_{4-n}SnX_n$ as a function of n.

However between n = 1 and n = 4 there is often an inverse dependence. The reason for this apparent discrepancy is not clearly understood. It has been suggested to arise from the X-groups inducing a p-electron imbalance in the other groups bonded to tin that results in a net shielding effect of the tin. As the number of X-groups increases so does the p-electron imbalance, which drowns the electron withdrawing effect.[108]

When X = vinyl, aryl, ethynyl or benzyl a linear relationship between n and chemical shift is observed throughout. For example Figure 1.30.

Figure 1.30

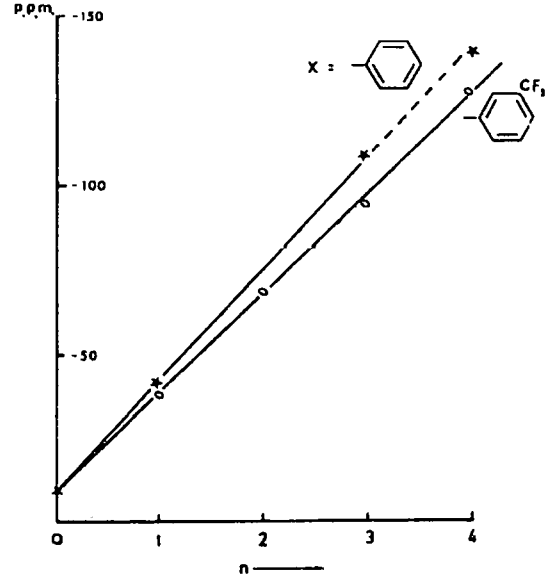

Tin chemical shifts for $Bu_{4-n}SnX_n$ compounds.

In this case the mechanism of shielding at the tin centre is different from that above but, once again, is not clearly defined. It may arise via some form of interaction between the π-electrons of the X group and the tin by either pπ-dπ orbital overlap and/or, with aromatic examples, a ring current effect.[109]

1.13.2: Concentration (solvent effects), coordination number and its dependence on temperature.

The choice of solvent when preparing samples for NMR measurement may affect the observed ^{119}Sn chemical shift. Non-coordinating organic solvents such as carbon tetrachloride, benzene or dichloromethane act essentially as dilutants and produce no marked change in shift as the concentration is varied.

Coordinating solvents however, such as acetone, DMSO or pyridine can produce large concentration dependant chemical shift changes. In these solvents formation of solvated species or adducts with the tin compound occurs. In the case of chlorotrimethyltin and pyridine in carbon tetrachloride the coordination is reversible and highly dependant on the concentration of pyridine. In the absence of pyridine a chemical shift as high as δ 165.8 has been reported.[77] A minimum value of δ -9.5 has been reported with 12.8 equivalents of pyridine. This is consistent with an increase in tin coordination number due to the pyridine. It is clear that the ^{119}Sn chemical shift is highly sensitive to changes in coordination state and so is equally useful in giving us an understanding of the chemical environment around the tin.

Tin species with a coordination number greater than four may be formed even in inert organic solvents if auto-association occurs. Many examples of such processes

occurring in the solid state have already been mentioned. The tendency for dimerisation in solutions of dibutyltin dialkoxides (**1.83**) (Figures 1.31 and 1.32) have been studied.[110]

Figure 1.31

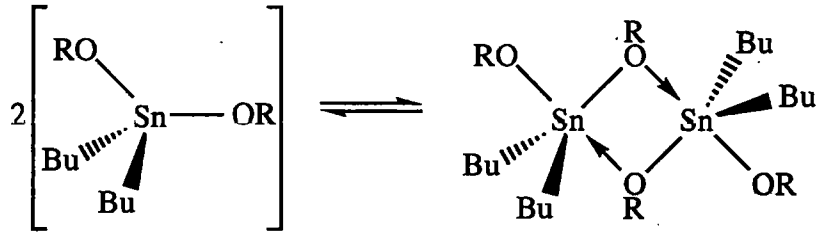

(1.83) R = Me, ^{i}Bu, ^{t}Bu, ^{i}Pr

Figure 1.32

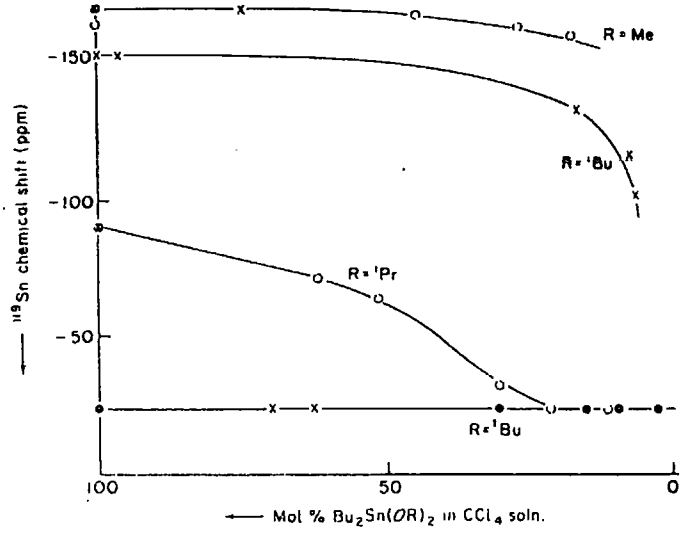

Effect of dilution on ^{119}Sn chemical shifts of $Bu_2Sn(OR)_2$ compounds.

Dimerisation is found to be greatest when R is small and dilution is found to increase the proportion of tetracoordinate monomer. Higher solution temperatures have also been shown to favour the monomeric state.

Davies *et al*[111] have reported that dilute solutions of dimethyltin methoxide chloride show two ^{119}Sn resonances at δ 126 and δ -90 corresponding to an equilibrium mixture of monomeric tetracoordinate and dimeric pentacoordinate tin centres respectively. The equilibrium proposed is analogous to the dibutyltin dialkoxide scheme above.

Solutions of trimethyltin formate (**1.84**) (Figure 1.33)[112] in deuterochloroform are believed to exist in equilibrium between monomeric four coordinate (^{119}Sn = δ 150 in 0.05M solution) and oligomeric, intermolecularly five-coordinated (^{119}Sn = δ 2.5 in 3M solution) tin species. The coordination number is higher in more concentrated solutions with only a single resonance observed -in contrast to Davies' result. The equilibrium in

trimethyltin formate is thus considerably faster on the NMR time scale at room temperature than for dimethyltinmethoxide chloride.

Figure 1.33

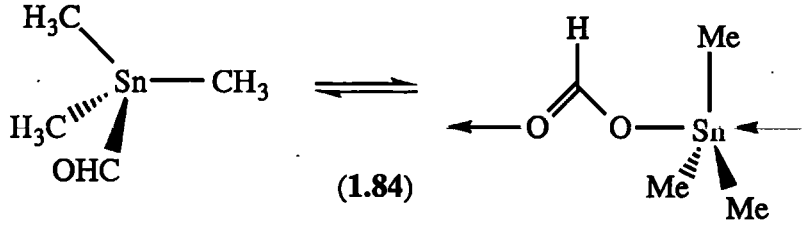

(1.84)

Recently, pentacoordinate diorganoyltin dithiolate complexes have been studied and the temperature dependant denticity of various classes of thiolate groups (**1.85**) (Table 1.6) analysed.[113]

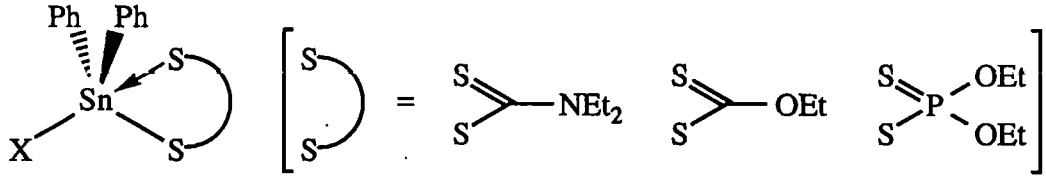

(1.85) **(1.85a)** **(1.85b)** **(1.85c)**

(X = Cl,Br)

Table 1.6

Compound type	X	δ ^{119}Sn (25°C)	δ ^{119}Sn (-100°C)
(1.85a)	Cl	-327	-330
(1.85a)	Br	-343	-345
(1.85b)	Cl	-275	-286
(1.85b)	Br	-285	-295
(1.85c)	Cl	-248	-279
(1.85c)	Br	-250	-282

The ^{119}Sn chemical shifts for complexes (**1.85a**) are virtually identical. This indicates a constant tin environment and hence the thiocarbamate ligand is strongly bidentate. However, dithiocarbonate complexes (**1.85b**) and dithiophosphate complexes (**1.85c**) show a marked shift to higher field at lower temperatures. This is indicative of a room temperature equilibrium between bidentate and monodentate coordination of the ligands. At lower temperatures the equilibrium favours bidentate binding and an effective higher coordination number results.

The work reported in Chapter 4 will attempt to model the S_N2 substitution at tin using the naturally occurring 4-pyrone, maltol, and several 4-pyridone derivatives. It describes the application of the previously described solution phase mapping and structural correlation techniques to tin complexes of these ligands. An introduction to the chemistry of these ligands is given at the beginning of the chapter.

Chapter 2: Modelling nucleophilic substitution at silicon using quinoline-based ligands.

2.1: Introduction to the modelling of molecular geometry in solution by NMR mapping

In solution as well as the solid state, intramolecularly-coordinated hypervalent complexes may adopt a structure reminiscent of an intermediate or transition state on an S_N2 reaction coordinate. The structure adopted is dependant on the steric and electronic characteristics of the groups around the reaction centre, the donor properties of the 'nucleophile' and the amount of strain in the ring being formed. The structures below represent those of a general S_N2 reaction at a tetracoordinate centre M. Thus a neutral nucleophile Nu displaces a leaving group X^- in a manner which may be modelled by a series of closely-related complexes (**2.2**).

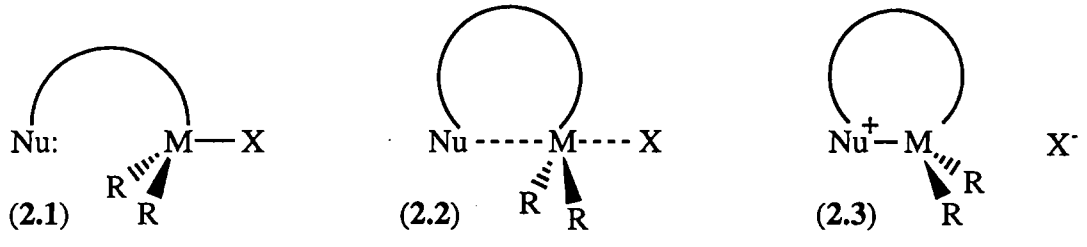

Each example of a complex of type (**2.2**) is a structure representing a different 'extent of reaction'. (**2.1**) and (**2.3**) are 'limiting' structures of the 'reaction', i.e. represent zero substitution and complete substitution respectively. For studies in solution these moieties must also be modelled.

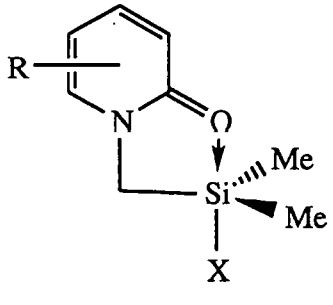

R = 6-Me, 6-Cl, 5-Cl, 3-OMe, 3-NO_2, H.
X = F, Cl, Br, OTf.

(**2.4**)

Nucleophilic attack at M affects the electronic environment of both M and of the ligand framework. In ligands where substitution is accompanied by a major structural change, such as aromatisation, then substitution can be quantitatively followed by NMR spectroscopy. This is achieved by monitoring how individual resonances of the carbons in the ligand and M itself, if an abundant NMR-active isotope, vary between related complexes. With this in mind, the 2-pyridone complexes

(**2.4**),[114] as specific examples of (**2.2**) above, were initially chosen to model S_N2 substitution at M = silicon by preceding co-workers in the group. The reaction being modelled is that of a carbonyl oxygen nucleophile substituting at a monofunctional trialkyl silane.

2.1.1: Preparation of model compounds

The major assumption is that as the modelled substitution progresses, the NMR chemical shifts in the pyridone ring can be closely approximated by the chemical shifts of an appropriate mixture of *model* compounds such as (**2.5**) and (**2.6**).[58]

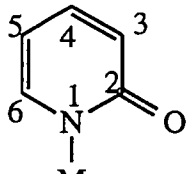

(**2.5**)

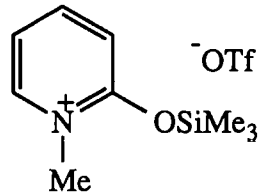

(**2.6**)

Compound (**2.5**) was converted into (**2.6**) by titration of a $CDCl_3$ solution with trimethylsilyl triflate (TMS-OTf). There is a fast equilibrium on the NMR time scale between (**2.5**) and (**2.6**) in the presence of TMS-OTf such that only one set of resonances in the ^{13}C NMR spectrum are observed. Successive fractions of TMS-OTf move the equilibrium further towards (**2.6**). The observed chemical shift of each carbon is dictated by the position of the equilibrium and is representative of the ratio of (**2.5**) and (**2.6**).

Figure 2.1

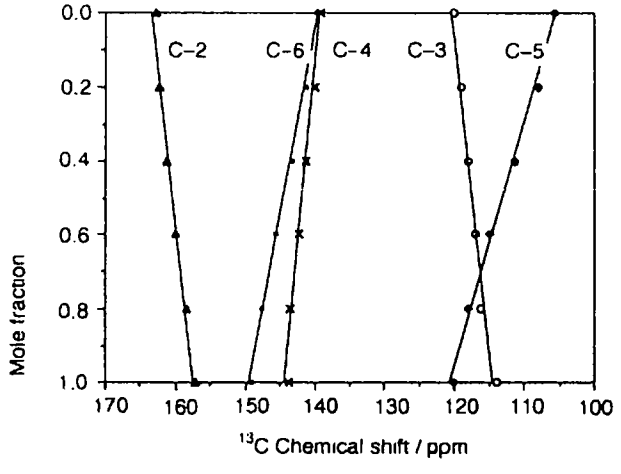

NMR chemical shift changes during the pyridone to pyridinium ion transformation

If the mole fraction of TMS-OTf is 0.x then the ratio of (**2.5**) and (**2.6**) is 1-(0.x) : 0.x. When a full equivalent of TMS-OTf has been added, the equilibrium has been displaced completely to the right and the ^{13}C resonances observed are that of (**2.6**). The ^{13}C data give a linear correlation when plotted against the mole fraction of TMS-OTf (Figure 2.1).

The overall assumption is therefore that an Si-O bond is *x* % formed when the ^{13}C NMR chemical shifts of the pyridone are equivalent to *x* % of (**2.6**) in the mixture, i.e. when a 0.*x* fraction of TMS-OTf has been added.

2.1.2: A map of substitution at silicon

The mapping technique was applied to a wide range of pyridone complexes (**2.4**). R-groups were chosen so as to modify the nucleophilicity of the carbonyl oxygen and the X-groups were chosen to have varying leaving-group ability. Disiloxane compounds (**2.7**) and (**2.8**) were synthesised as alternative models to (**2.5**) and (**2.6**). These alternative structures were used instead because they are more similar to the silyl-pyridone complexes (**2.4**) than are (**2.5**) or (**2.6**). Compounds (**2.5**)-(**2.8**) are all examples of the *limiting* structures (**2.1**) or (**2.3**). (**2.8**) was prepared by titration of disiloxane (**2.7**) with TMS-OTf in $CDCl_3$ solution. As TMS-OTf in this case was being titrated against a disiloxane, two equivalents of TMS-OTf were required to generate (**2.8**). So in the titration of (**2.7**), an Si-O bond is *x* % formed when the NMR chemical shifts of the disiloxane indicate *x* % (**2.8**) in the mixture, i.e. when a 0.(2*x*) fraction of TMS-OTf had been added. Similar linear plots of ^{13}C chemical shift against mole fraction TMS-OTf to those shown in Figure 2.1 were obtained for these compounds.

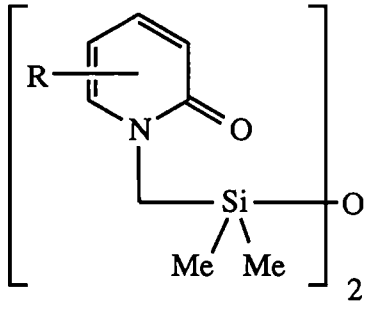

(**2.7**)

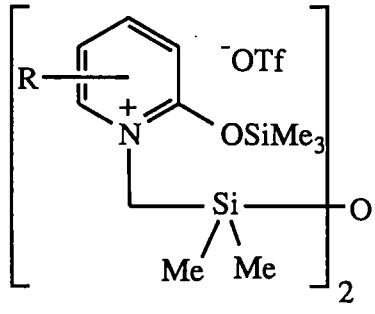

(**2.8**)

The ^{13}C NMR chemical shifts of the carbons in the aromatic ring of (**2.7**) (R=H) were compared with those of (**2.5**), another non silicon-containing model of zero substitution. A strong similarity between the data sets confirmed that the silicon in (**2.7**) is tetracoordinate. The series of unsubstituted pyridone complexes (**2.9**), along with their respective model complexes (**2.10**) and (**2.11**), shall be used to show how the calculations were performed.

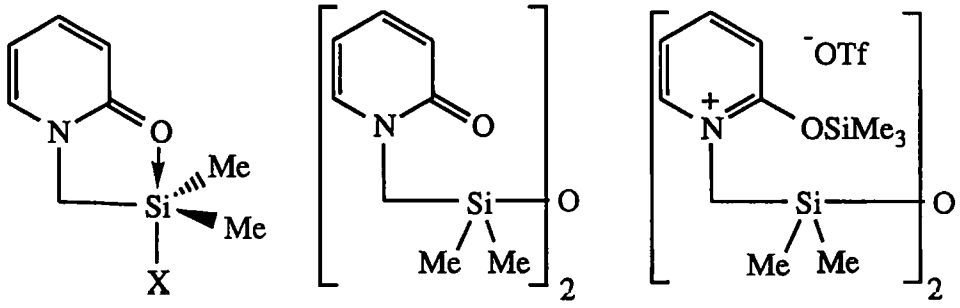

(2.9) (2.10) (2.11)

The chemical shift of each ring carbon in a complex (**2.9**) is compared with the *limiting* values that it holds in (**2.10**) and (**2.11**). The percentage silicon-oxygen bonding (extent of reaction) can be calculated for each carbon on the basis of its relative chemical shift position between (**2.10**) and (**2.11**). For example, if a particular ring carbon has a chemical shift of δ 143 in (**2.10**) and δ 138 in (**2.11**), then a chemical shift of δ 140 for that carbon in one of the complexes (**2.9**) represents 60% silicon-oxygen bonding (Figure 2.2). The mean of these values could then be calculated to give the overall value for each complex. The alternative method, which shall not be used, is to plot each complexes ring carbon chemical shifts onto the appropriate line of the titration graph and read off the percentage silicon-oxygen bond formation for each carbon.

Figure 2.2

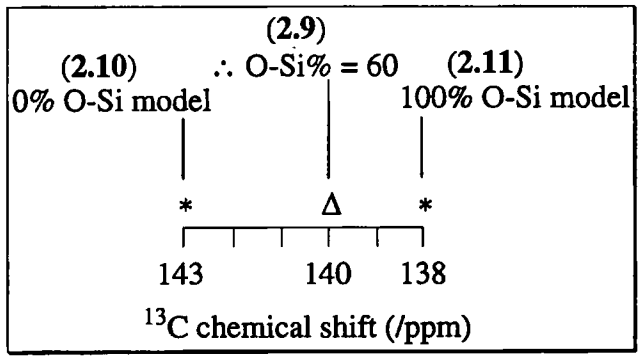

Figure 2.3

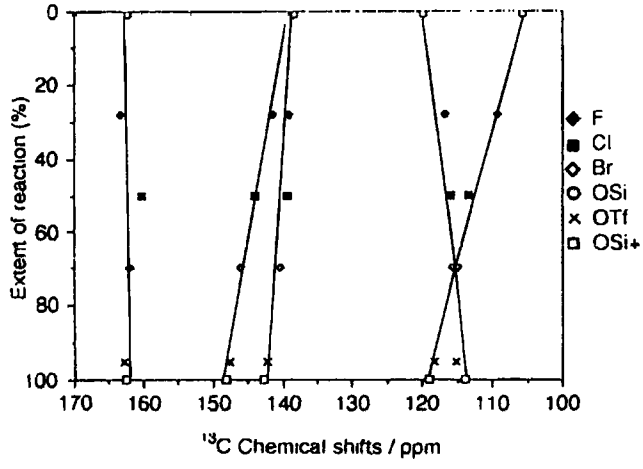

The values are plotted against the ^{13}C chemical shifts in Figure 2.3 and tabulated in Table 2.1 below.

Table 2.1

X	F	Cl	Br	OTf
% Si-O	27	50	70	96

Similar calculations were performed for the series of complexes where R = 6-Me, 6-Cl, 5-Cl, 3-OMe and 3-NO_2. For a given R-group the order of decreasing percentage of Si-O bond formation was found to be dependant on X in the order X = OTf > Br > Cl > F. For the series of fluoride complexes (i.e. X = F) the effect of substituents R was found to decrease the percentage of 'Si-O bond formation' in the order R = 6-Me > 6-Cl > H > 5-Cl > 3-OMe > 3-NO_2. This is the order of increasing electron-withdrawing character of the R group as experienced by the pyridone carbonyl group.

Having calculated the percentage O-Si bonding for each complex, the next step is to correlate it with the coordination state of the silicon. Pentacoordination at silicon has been found to cause a ^{29}Si NMR up-field chemical shift of as much as 70 ppm from four-coordinate silicon. The highest field shifts measured for complexes of type (**2.4**) have been for compounds (R = 6-Cl, X = Cl) and (R = H, X = Cl), both having values of approximately δ -40.

Compound (**1.38**)[47] is fully pentacoordinate at one of its silicon centres and fully tetracoordinate at the other, with solution ^{29}Si chemical shifts of δ -40 and δ +28 respectively. Therefore the limits of 100% (δ -40) and 0% (δ +28) pentacoordination are assigned to a fully pentacoordinate (**2.2**) structure and (**2.1**) respectively. The typical ^{29}Si chemical shift of (**2.3**) is taken to be the value measured for (**2.6**) (δ +40). Although the ^{29}Si chemical shift is affected by the nature of the substituent, for the leaving groups F, Cl, Br and OTf it is considerably smaller than the effect of coordination number. With these limits in mind, each complex's ^{29}Si chemical shift was assigned a percentage pentacoordination value. This could then be plotted against its respective percentage O-Si bond formation (i.e. extent of reaction) (Figure 2.4). The calculation, similar to that to determine percentage O-Si bond formation, compares the

measured chemical shift with appropriate limiting values and expresses its position in percentage terms. Which of the two 0% pentacoordination limits is used depends on the percentage O-Si bond formation value of each complex. For complexes with less than 50% O-Si bond formation, the value for model (**2.1**) is assumed. For complexes with greater than 50% O-Si bond formation, the value for model (**2.3**) is assumed. This approach is also applied in Chapter 3.

Figure 2.4

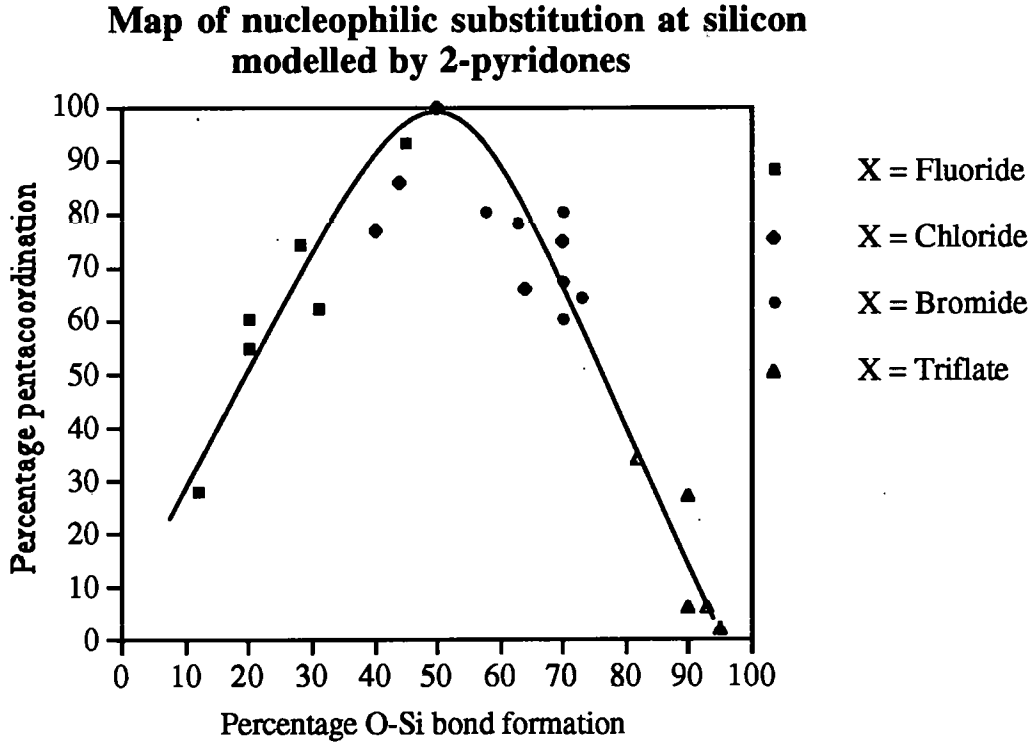

The inverted 'V' shape is characteristic of the transition from tetra, through penta to tetra coordination that occurs during conventional S_N2 substitution at silicon.

Although we have discussed compounds of type (**2.2**) as existing as single structures in solution, it is also possible that the chemical shifts measured are the time averaged result of fast equilibria between (**2.1**) and (**2.2**) and/or (**2.2**) and (**2.3**). In both cases (**2.2**) is a fully pentacoordinate structure (Figure 2.5).

Figure 2.5

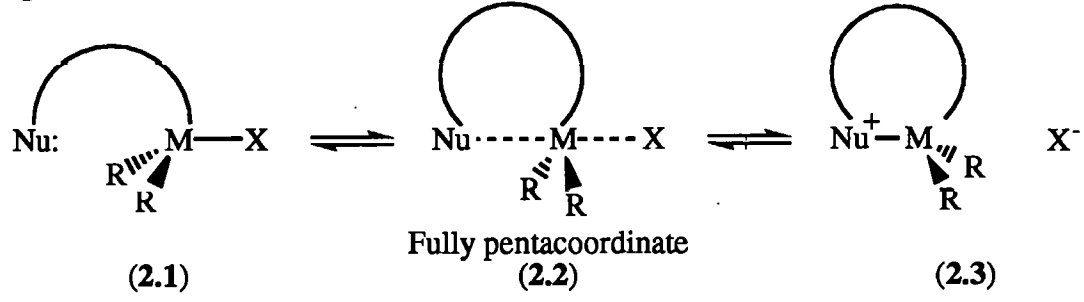

Therefore the differences in chemical shifts are caused by differences in the position of each equilibrium from compound to compound. Evidence that complexes (**2.9**) exist in isolation in solution rather than being artefacts of an equilibrium mixture came from conductivity measurements of complex (**2.12a**), which has a percentage O-Si bond formation of 70. Solutions of this complex do not conduct electricity.[114] If we were observing a fast equilibrium it would be between structures (**2.2**) and (**2.3**). An appreciable concentration of the ionic component (**2.3**) would therefore be expected to lead to a high conductivity.

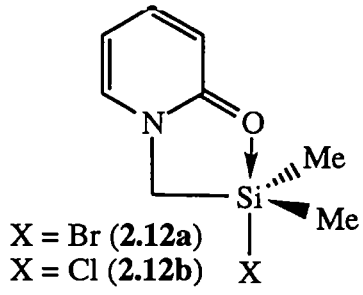

X = Br (**2.12a**)
X = Cl (**2.12b**)

2.1.3: Variable temperature NMR studies

Kummer[115] has recently undertaken a comprehensive variable temperature NMR study of complex (**2.12b**). As with his previous work with pyridone-imines (**1.32**),[40] it was noted that a decrease in $CDCl_3$ solution temperature led to increasing pyridinium ring character. This was shown by the ring ^{13}C NMR chemical shifts and confirmed the greater degree of substitution. At room temperature he observed a minima in the ^{29}Si chemical shift (δ -39) (Figure 2.6) assigned to a fully pentacoordinate structure. When the solution was either heated (maximum 100°C) or cooled (minimum -60°C) he observed a down field movement of the chemical shift.

Figure 2.6

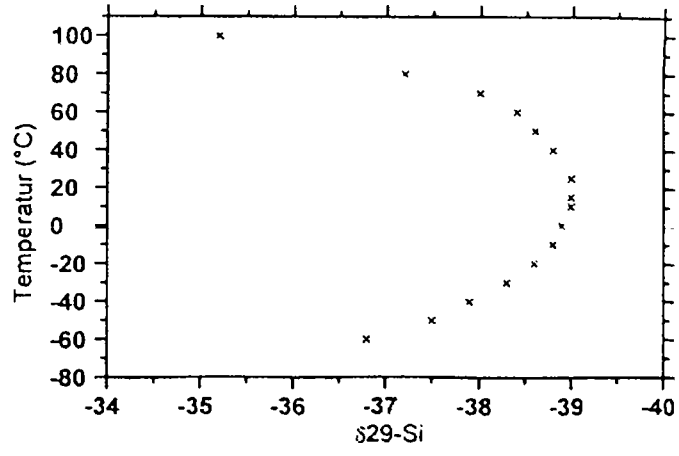

This was due to the structure reverting in character towards its tetracoordinated open-chain (**2.13**) and fully 'substituted' (**2.14**) structural forms respectively (Figure 2.7).

Figure 2.7

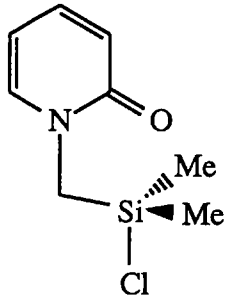

(2.13)

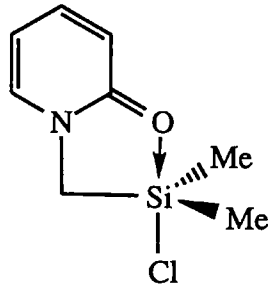

(2.12b)

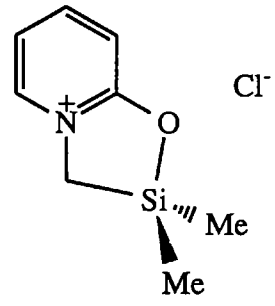

(2.14)

← Increase of temperature | Decrease of temperature→

2.2: Quinoline ligands and their coordination chemistry

8-Hydroxyquinoline (**2.15**) and 2-(1H)-quinolinone (**2.16**) can act as bidentate ligands, although not widely reported in the literature. Mason *et al*[116] have synthesised a series of pentacoordinate and hexacoordinate tin complexes (**2.17**) using 8-hydroxyquinoline.

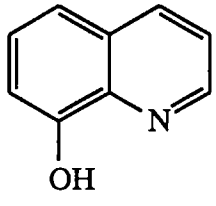

(2.15)

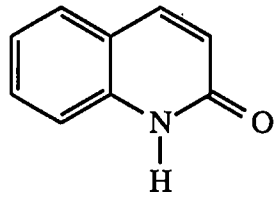

(2.16)

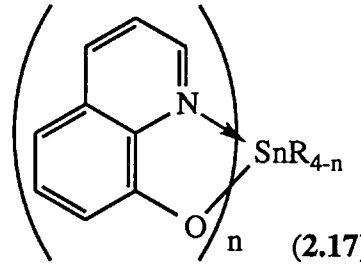

(2.17)

(n = 1, R = Ph_3, Me_3, Et_3, $^nBu_3$ Ph_2Cl, Et_2Cl, $^nOct_2Cl$)
(n = 2, R = Ph, ^nBu, Et, Me)

Two silicon analogues (**2.18**) and (**2.19**) have also been reported.[117]

(2.18)
$\delta\ ^{29}Si = -21.0$

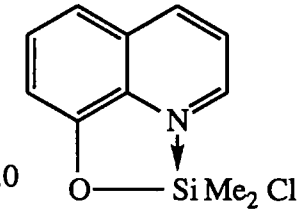

(2.19)
$\delta\ ^{29}Si = 19.6$

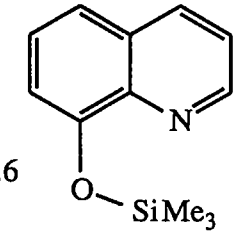

The ^{29}Si NMR shift of (**2.18**) indicates significant N–Si hypercoordination. However without the electronegative chlorine, compound (**2.19**) has a ^{29}Si chemical shift typical of a tetracoordinate species. Several antimony (V) complexes (**2.20**) and (**2.21**) have also been prepared.[118]

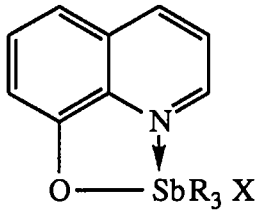

(2.20)

X = Cl, Br.
R = Me, Et, Ph

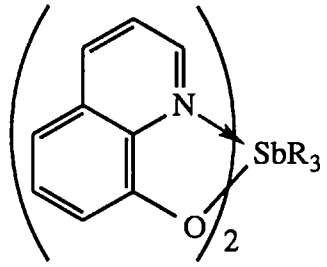

(2.21)

The complexes (**2.21**) are particularly fluxional in $CDCl_3$ solution due to the weakness of the N-Sb bonds. The antimony is regarded largely as a pentacoordinate centre where the quinoline acts as a mono dentate ligand.

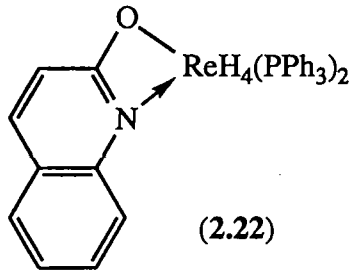

(2.22)

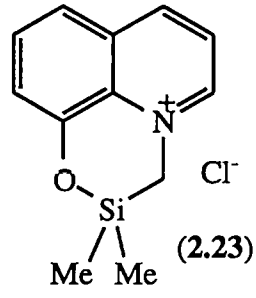

(2.23)

Figure 2.8

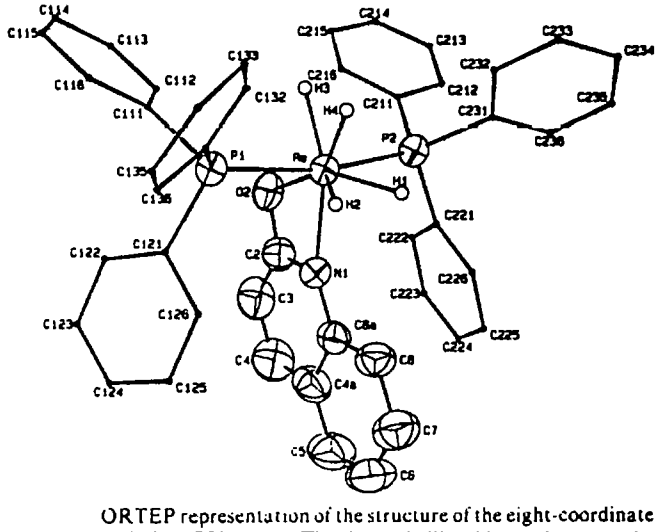

ORTEP representation of the structure of the eight-coordinate complex $ReH_4(hq)(PPh_3)_2$. The thermal ellipsoids are drawn at the 50% probability level, and the carbon atoms of the phenyl rings of the PPh_3 ligands and the four hydrido ligands are represented as circles of arbitrary radius.

The crystal structure of the eight-coordinate Rhenium (V) complex (**2.22**) has been reported by Walton *et al* and contains a single chelating 2-quinolinone ligand.[119] The environment of the rhenium atom is best described as a distorted dodecahedron (Figure 2.8). The complex (**2.23**) has been recently prepared.[120] The NMR spectra of (**2.23**) conclude that the silicon is completely tetracoordinate.

In this chapter we shall use (**2.16**) for the first time to stabilise five-coordinate silicon. (**2.16**), like its 2-pyridone analogues provides a suitable backbone for the study of nucleophilic substitution at silicon in solution using NMR spectroscopy. Since the same mode of intramolecular coordination is present we can directly re-apply the

solution-phase mapping methodology to this ligand. With the greater number of carbons in the extended aromatic ring system we can examine the sensitivity to change of the ^{13}C NMR chemical shifts of the carbons more remote from the substitution site. In practical terms it has proved easier to grow single crystals of the quinoline-based complexes than of the pyridones. For the first time we can therefore compare the structures of the complexes in solution and in the solid state.

2.3: Synthesis of complexes

2-Trimethylsiloxyquinoline (**2.24**) (Figure 2.9) is the precursor to all the quinoline complexes (**2.25a-d**). It is readily isolated by the silylation of 2-(1H)-quinolinone (**2.16**).

Figure 2.9

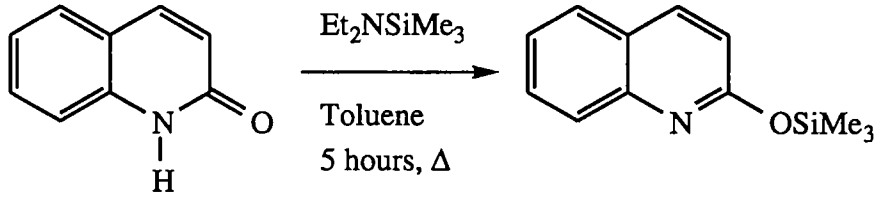

(**2.16**) (**2.24**)

The silyl chloride (**2.25b**) and silyl bromide (**2.25c**) complexes (Figure 2.10) are prepared quantitatively from the reaction of (**2.24**) with the appropriate chloro(halomethyl)dimethylsilane in dry benzene.

Figure 2.10

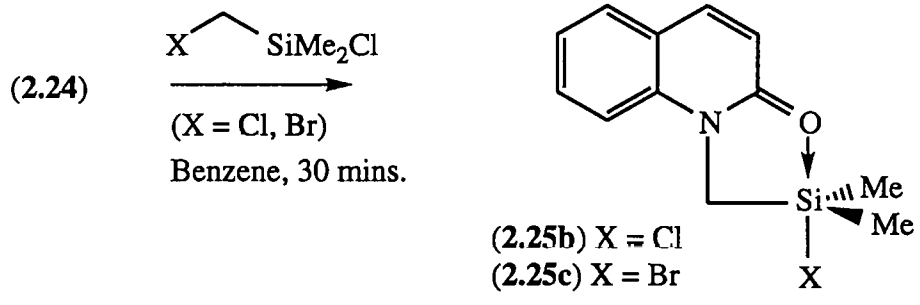

The fluoride (**2.25a**) and triflate (**2.25d**) derivatives are obtained from reactions of (**2.25b**) with antimony trifluoride and TMS-OTf respectively (Figure 2.11).

Figure 2.11

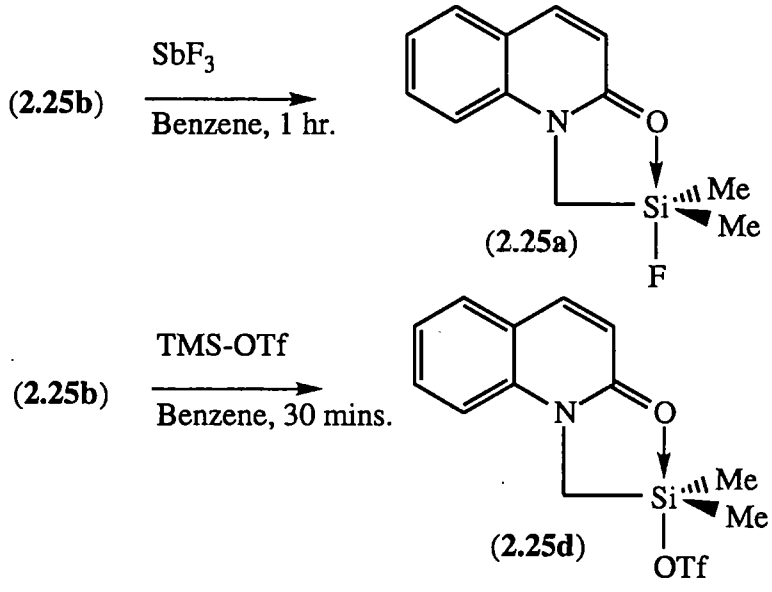

2.4: Synthesis of model complexes

The hydrolysis of (**2.25b**) and self-condensation of the transient silanol in an acetone-water mixture readily forms the parent disiloxane (**2.26**). By analogy with the pyridine work, this compound is a good model for the completely 'unsubstituted' silicon centre (0% nucleophile-Si bond) (Figure 2.12).

Figure 2.12

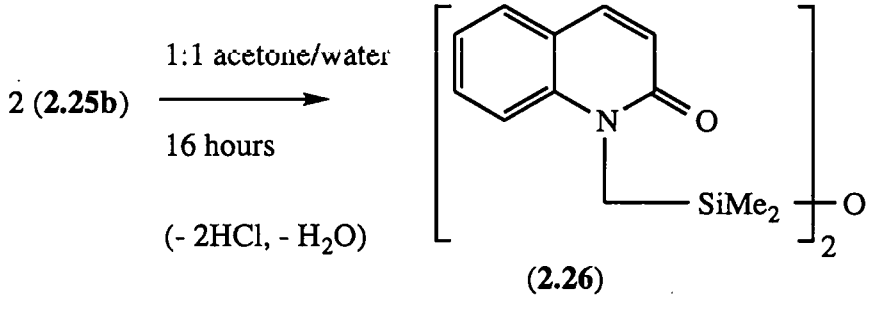

Titration of (**2.26**) with aliquots of TMS-OTf gave a linear relationship between the ring ^{13}C chemical shifts and the proportion of TMS-OTf added. After two equivalents of the triflate had been added, no further chemical shift changes occurred and the NMR data was consistent with structure (**2.27**). This is the model chosen for complete 'substitution' (100% nucleophile-Si bond) (Figure 2.13).

Figure 2.13

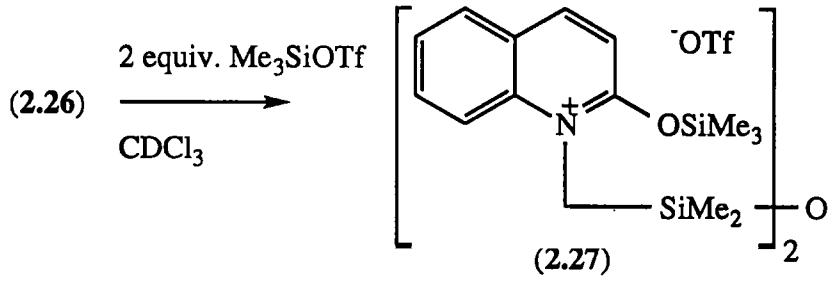

For solutions containing less than 2.0 equivalents TMS-OTf, fast (on the NMR time scale) exchange of the trimethylsilyl groups means only a single set of average resonances are observed. The positions of the resonances are representative of the appropriate ratio of **(2.26)** and **(2.27)**. The data is summarised in Table 2.2 and plotted, excluding the *4 equivalents* data set, in Figure 2.15. The numbering scheme used is shown in Figure 2.14.

Figure 2.14

(Numbering scheme for the ring carbons)

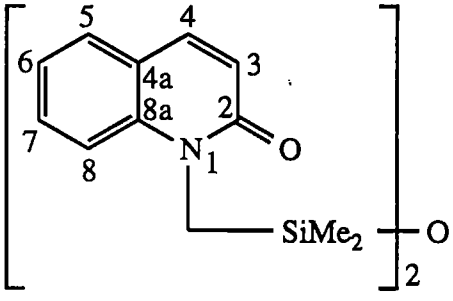

Table 2.2

Equiv. TMSOTf	^{13}C chemical shift of ring carbons (/ppm)								
	C-2	C-3	C-4	C-4a	C-5	C-6	C-7	C-8	C-8a
0	161.8	120.9	138.4	120.8	128.7	121.8	130.3	115.3	139.9
0.4	162.1	118.8	140.5	121.4	129.1	123.1	131.3	115.9	139.2
0.8	162.1	117.8	141.3	121.6	129.2	123.6	131.7	116.1	138.9
1.2	162.2	117.0	142.3	121.8	129.4	124.1	132.1	116.3	138.6
1.6	162.6	115.4	144.2	122.4	129.7	125.2	132.9	116.8	138.2
2	163.3	113.7	146.3	123.2	130.1	126.5	133.9	117.1	137.6
4	163.5	113.5	146.9	123.5	130.2	126.9	134.2	117.2	137.6

Figure 2.15

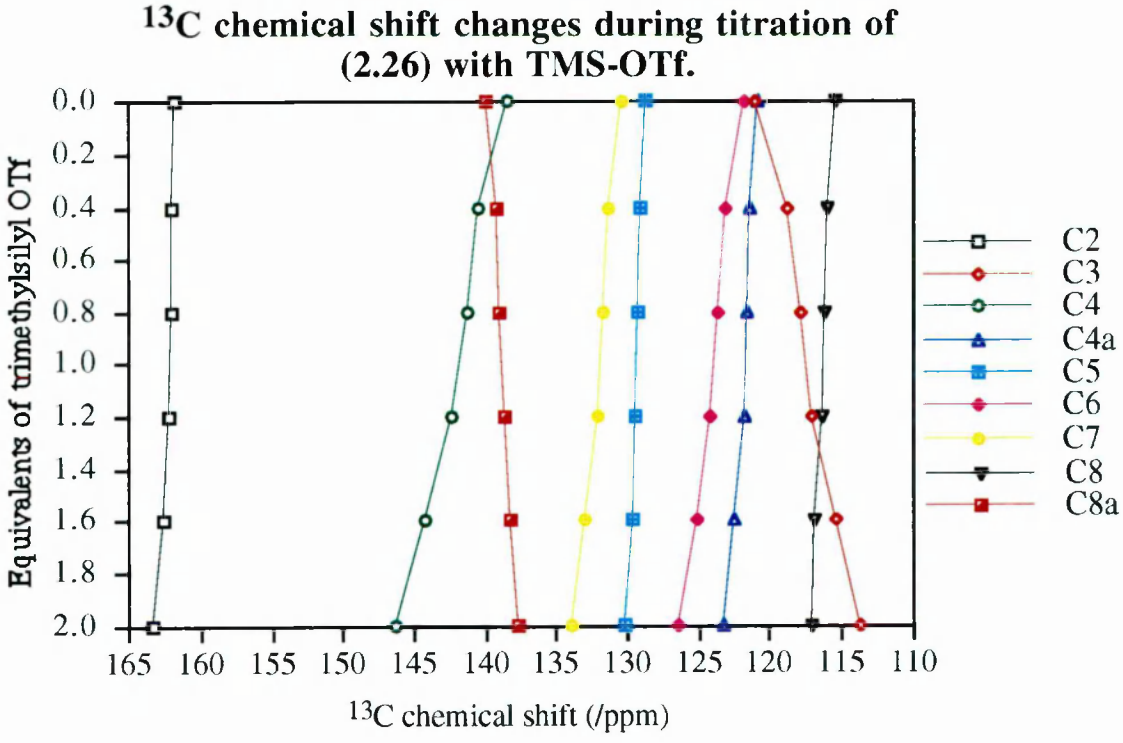

2.5: Solution calculations

Comparison of the ^{13}C chemical shifts of complexes (**2.25a-d**) with their respective values in complexes (**2.26**) and (**2.27**) enables the percentage O-Si bond formation of each complex to be obtained. The same type of calculations as previously applied to pyridones are used (Figure 2.2). The ring ^{13}C data is presented in Table 2.3. The percentage Si-O bond formation calculated for each carbon in each complex and as an overall (mean) value for each complex is shown in Table 2.4. The chemical shift changes of all ring carbons except C_2 were used in the calculations. This is because the C_2 chemical shift change is largely the same in each complex.

Table 2.3

Complex	^{13}C chemical shift of ring carbons (/ppm)								
	C-2	C-3	C-4	C-4a	C-5	C-6	C-7	C-8	C-8a
(**2.26**)	161.8	120.9	138.4	120.8	128.7	121.8	130.3	115.3	139.9
(**2.25a**)	162.9	117.1	141.4	121.4	129.0	123.6	131.8	115.9	139.3
(**2.25b**)	163.4	115.4	143.1	121.9	129.3	124.8	132.7	116.5	138.1
(**2.25c**)	163.4	114.6	144.1	122.3	129.4	125.5	133.3	117.1	137.8
(**2.25d**)	163.4	113.8	145.5	122.8	129.7	126.4	133.9	117.2	137.7
(**2.27**)	163.3	113.7	146.3	123.2	130.1	126.5	133.9	117.1	137.6

Table 2.4

Complex	Calculated % Si-O bond formation									Overall
	C-2*	C-3	C-4	C-4a	C-5	C-6	C-7	C-8	C-8a	% Si-O*
(2.26)	0	0	0	0	0	0	0	0	0	0
(2.25a)	73	53	38	25	21	38	42	33	26	35
(2.25b)	107	76	60	46	43	64	67	67	78	63
(2.25c)	107	88	72	63	50	78	83	100	91	78
(2.25d)	107	99	90	83	71	98	100	106	96	93
(2.27)	100	100	100	100	100	100	100	100	100	100

* The C_2 chemical shift change is largely constant during 'substitution'. This results in spurious percentage figures. These are ignored in the averaging calculations.

The accuracy to which a chemical shift can be measured sometimes results in percentage values greater than 100. These are carried through the calculations un-adjusted as inaccuracy in the measurement is equally likely to cause other percentages to be artificially reduced. The ^{13}C NMR chemical shifts are plotted against the percentage O-Si bond formation in Figure 2.16.

Figure 2.16

Ring ^{13}C chemical shift changes for complexes (2.25a-d), (2.26) & (2.27) as a function of percentage Si-O bond formation.

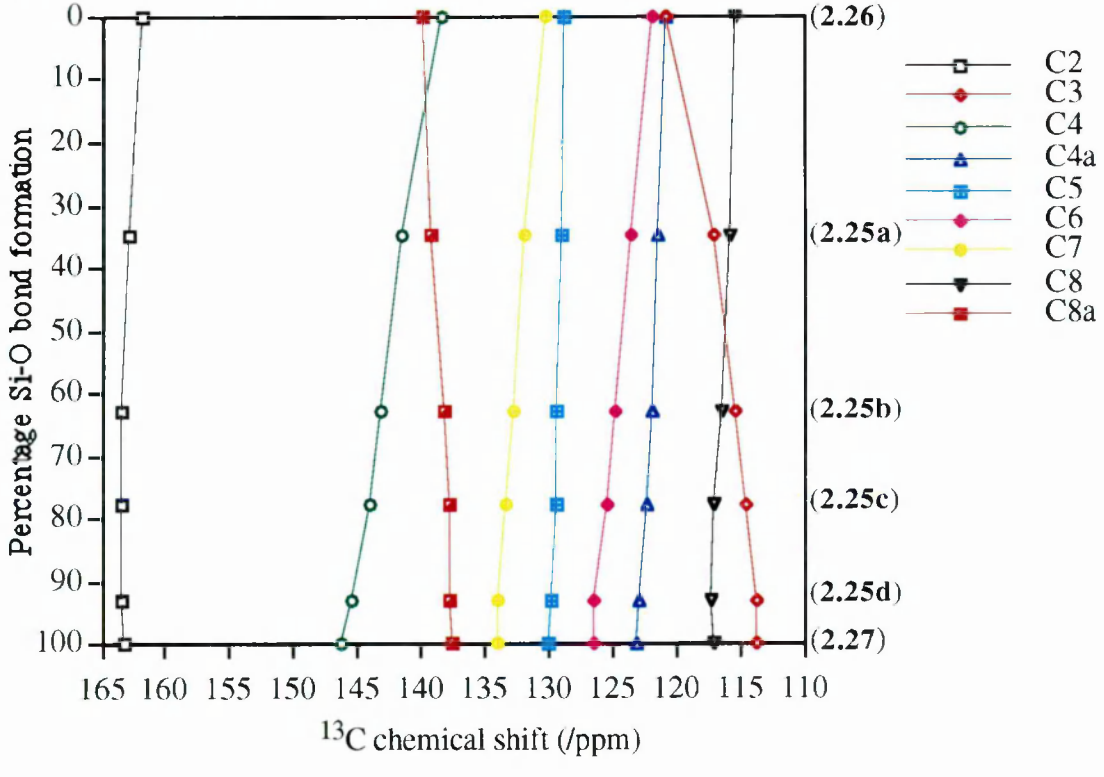

The chemical shifts of the complexes (**2.25a-d**), (**2.26**) and (**2.27**) closely mirror those obtained by the titration of (**2.26**) and TMS-OTf (Figure 2.17). To combine the data, the 'equivalents of TMS-OTf' values from the titration are converted into the percentage O-Si bond formation values they represent.

Figure 2.17

Comparison of the ^{13}C chemical shift changes measured in the (2.26) and TMS-OTf titration and the complexes (2.25a-d), (2.26) and (2.27).

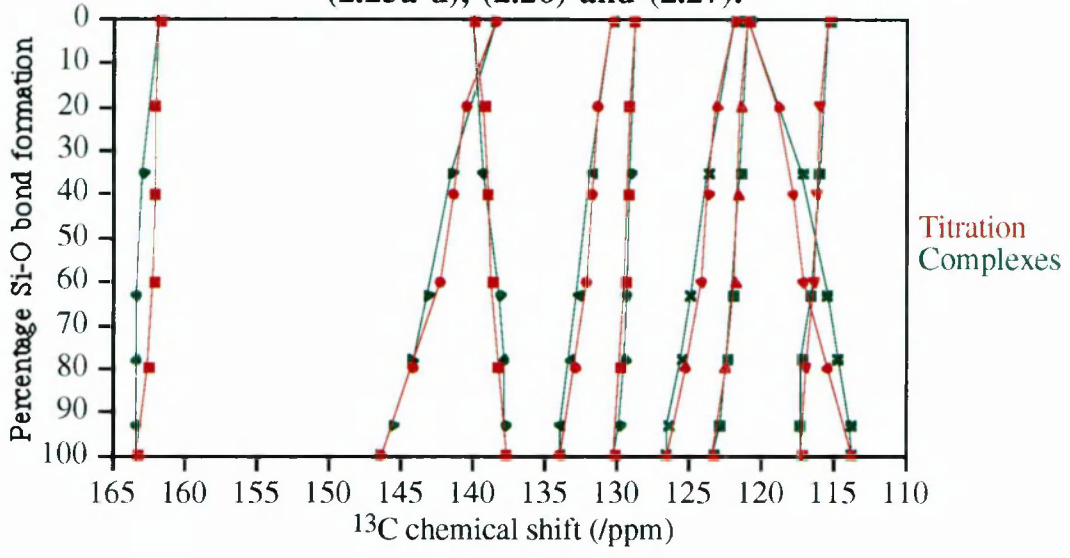

The previous work with pyridones has shown for complexes containing the 'leaving groups' X= F, Cl, Br and OTf, that the ^{29}Si NMR chemical shifts provide a very sensitive indicator of the coordination state of the silicon centre. Other environmental factors such as the substituent effect have been shown to be comparatively small for compounds with these good 'leaving groups'. We regard a chemical shift of δ -40 as indicating a wholly (100%) pentacoordinate silicon and values of δ +28 to suggest a completely 'unsubstituted' silicon (i.e. 0% pentacoordinate). The ^{29}Si chemical shift of (**2.28b**), (δ 12.2), is used as the typical value for a completely 'substituted' (0% pentacoordination) silicon centre. The pyridone analogue of (**2.28b**), (**2.6**) was used similarly in conjunction with complexes (**2.9**). (**2.28b**) is prepared in solution by treating (**2.28a**) with one equivalent of TMS-OTf in $CDCl_3$.

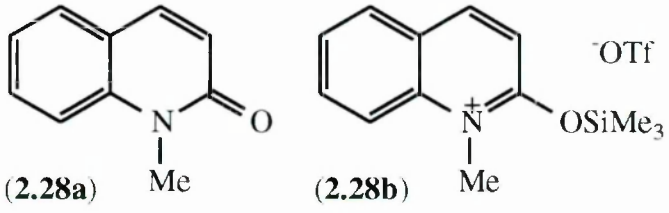

(**2.28a**) (**2.28b**)

By the application of these limits to complexes (**2.25a-d**), (**2.26**) and (**2.27**), a percentage pentacoordination may be calculated for each complex (Table 2.5). Complexes (**2.26**) and (**2.27**) are only suitable models of the extremes of substitution by ^{13}C NMR spectroscopy. This is because when the X-group at silicon is a relatively poor 'leaving group' (effectively an O-alkyl group) it has a significant substituent effect on the ^{29}Si chemical shift. Therefore to include complexes (**2.26**) and (**2.27**) in Table 2.5, these compounds must be set by default to 0% pentacoordination. The evidence that (**2.26**) contains tetracoordinate silicon comes instead from the similarity of its ring ^{13}C NMR spectrum to that of an alternative, non silicon-containing model of zero substitution, (**2.28a**) (Table 2.6).

Table 2.5

Complex	(**2.26**)	(**2.25a**)	(**2.25b**)	(**2.25c**)	(**2.25d**)	(**2.27**)
% O-Si	0	35	63	78	93	100
$\delta\ ^{29}Si$	(1.1)	-25.4	-38.4	-28.9	-8.0	(11.7 / -0.8)
% penta	0	79	97	79	38	0

Table 2.6

Complex	^{13}C chemical shift of ring carbons (/ppm)								
	C-2	C-3	C-4	C-4a	C-5	C-6	C-7	C-8	C-8a
(**2.26**)	161.8	120.9	138.4	120.8	128.7	121.8	130.3	115.3	139.9
(**2.28a**)	161.4	120.7	138.2	119.8	128.0	121.3	129.9	113.3	139.1

By plotting the percentage O-Si bond formation against the percentage pentacoordination, a two dimensional map of the development of coordination can be drawn (Figure 2.18).

Figure 2.18

A map of the development of pentacoordination in solution based on complexes (2.25a-d), (2.26) and (2.27)

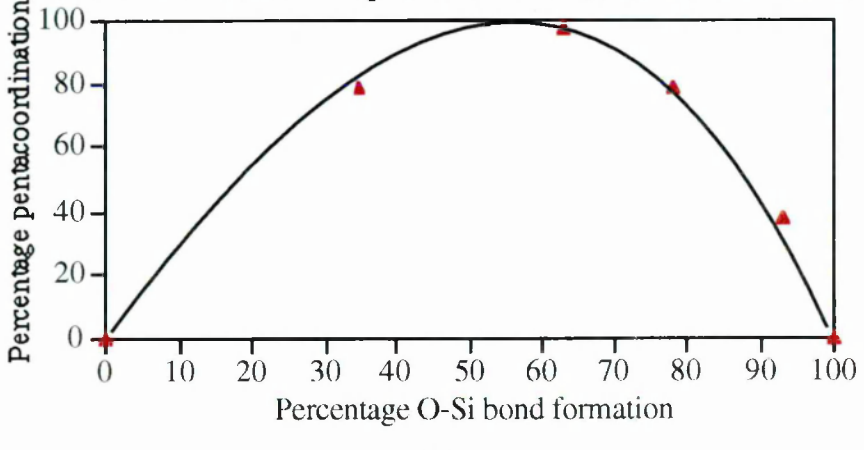

Data points for complexes (**2.25a-d**) may be added to Figure 2.4 as they model the same general substitution (Figure 2.19).

Figure 2.19

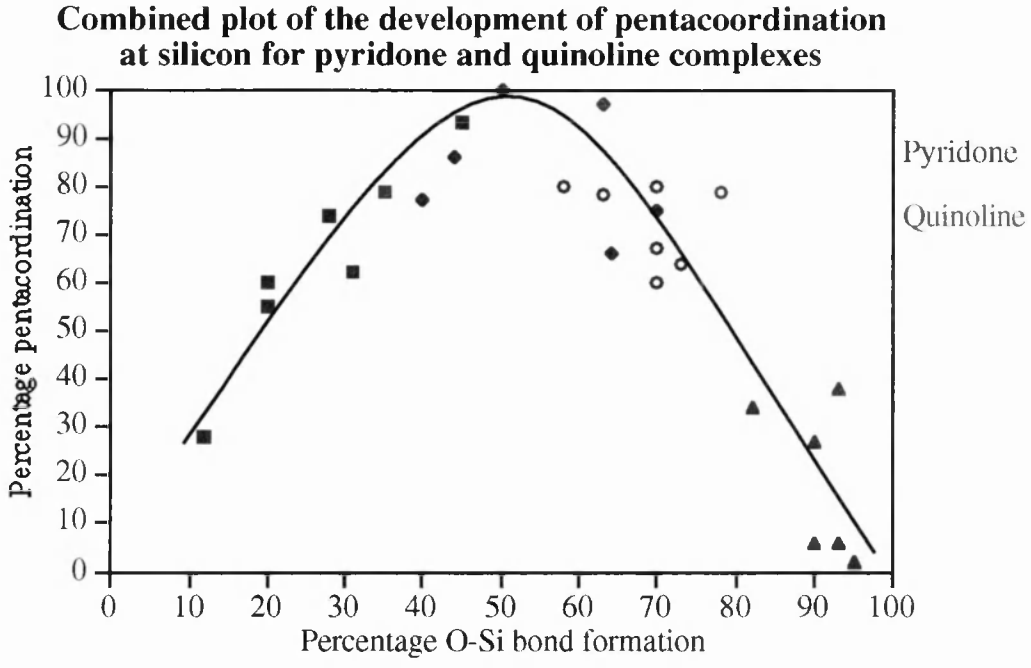

Figure 2.17 shows that in general the ^{13}C chemical shift changes during the titration experiment are linear and a good representation of the way they change in the modelled substitution. Table 2.4 shows how as the 'leaving group ability' is increased, so the percentage O-Si bond formation similarly increases.

Figure 2.18 displays the characteristic inverted 'V'-plot of Figure 2.4 showing the change in coordination number of the silicon from tetra, through penta to tetracoordination. When the pyridone and quinoline complexes data are combined in Figure 2.19 it can be seen that they overlap well. The percentage O-Si bond formation of each quinoline complex is calculated as being slightly higher than its unsubstituted pyridone analogue (Table 2.7).

Table 2.7

Ring system	Calculated percentage O-Si bond			
	F	Cl	Br	OTf
Quinoline (**2.25a-d**)	35	63	78	93
Pyridone (**2.9**)	28	50	70	90

To try to explain why the quinoline ligand is a stronger 'nucleophile' than the unsubstituted pyridone ligand we shall consider the resonance stabilisation of the fully 'substituted' silyl-quinoline (Figure 2.20) and pyridone (Figure 2.21) cations.

Figure 2.20

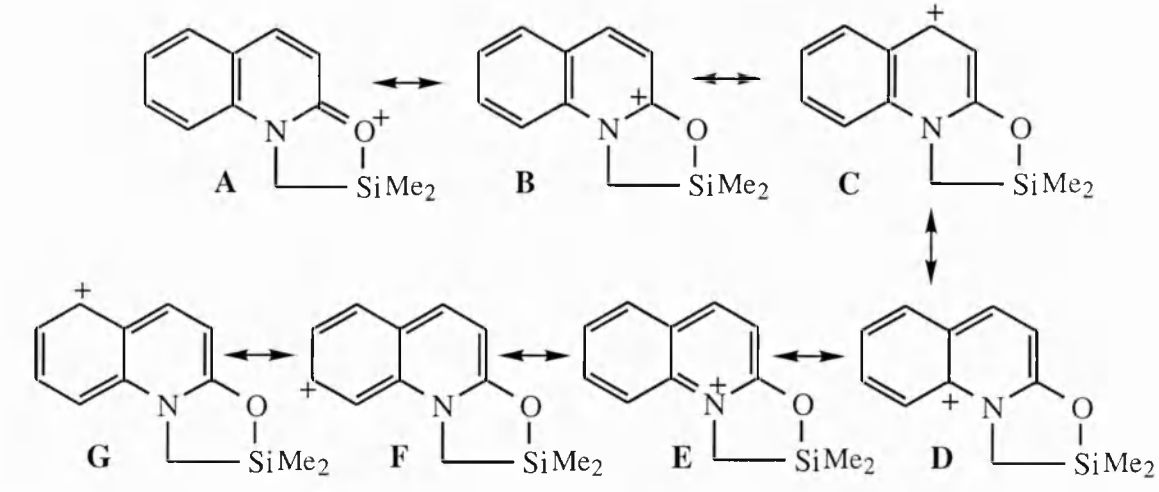

Figure 2.21

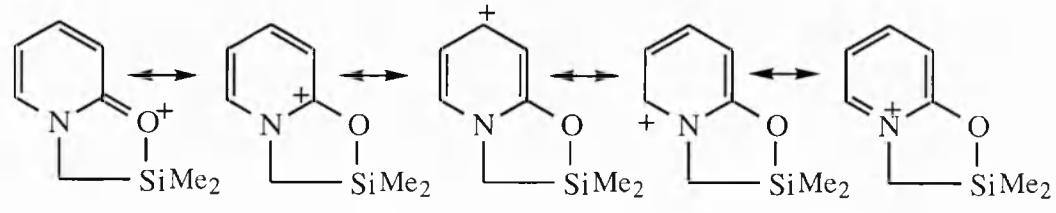

In addition, structures **A**, **B**, **C** and **E** each give rise to a further resonance hybrid due to the aromaticity of the fused benzene ring.

One simple justification for the increased nucleophilicity of the quinoline oxygen at silicon compared to the pyridone oxygen is that the quinoline ligand provides a greater number of resonance forms for the stabilisation of the positive charge and so is the more stable cation.

2.6: Solid state structures

The single crystal X-ray structures at 100K of complexes (**2.25a-d**) have been obtained to enable a comparison with their structures in solution. The ORTEP diagrams are presented in order of increasing 'leaving group' ability with the hydrogens omitted for clarity. Full structural data is presented in the appendix.

2.6.1: Fluoride complex (2.25a)

Figure 2.22

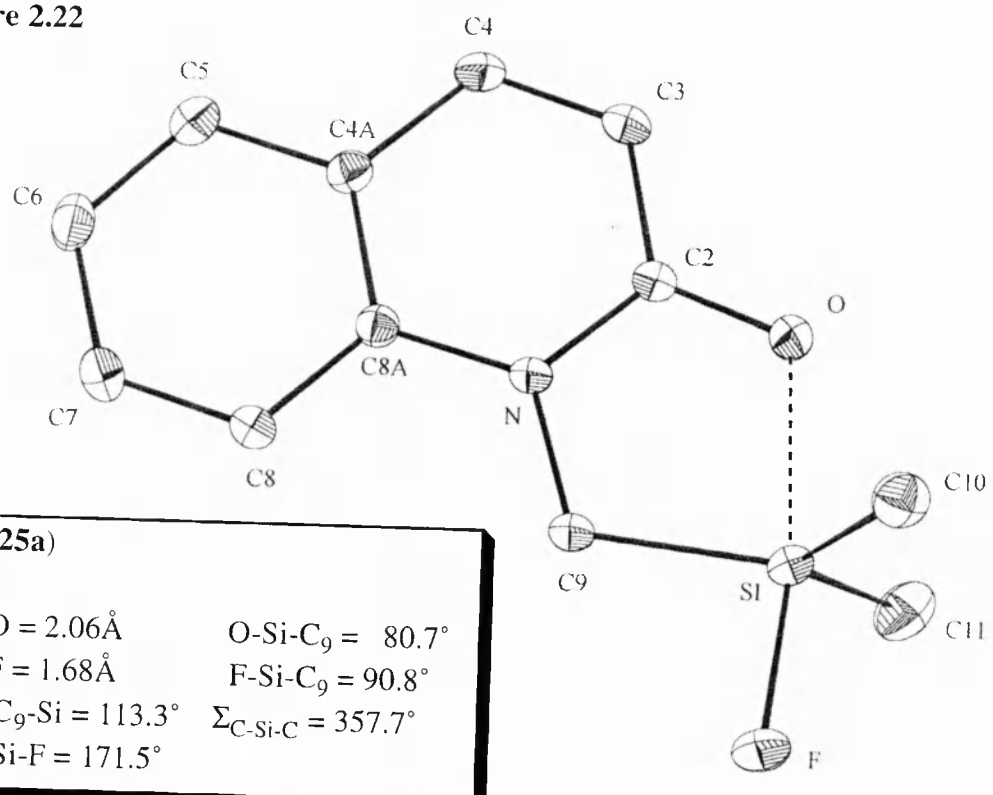

(**2.25a**)

SiO = 2.06Å	O-Si-C_9 = 80.7°
SiF = 1.68Å	F-Si-C_9 = 90.8°
N-C_9-Si = 113.3°	$\Sigma_{C\text{-}Si\text{-}C}$ = 357.7°
O-Si-F = 171.5°	

At 2.06Å the SiO distance represents the weakest 'nucleophilic' interaction with the silicon. The Si-F bond is elongated slightly by the relatively distant nucleophile and is about 0.1Å longer than a typical tetracoordinate Si-F bond. For a weak 'nucleophile' to silicon interaction it is surprising that the silicons geometry is so highly trigonal-bipyramidal. The sum of the equatorial groups bond angles at silicon is close to 360° and the C_9-Si-F angle is close to 90°.

2.6.2: Chloride complex (2.25b)

Figure 2.23

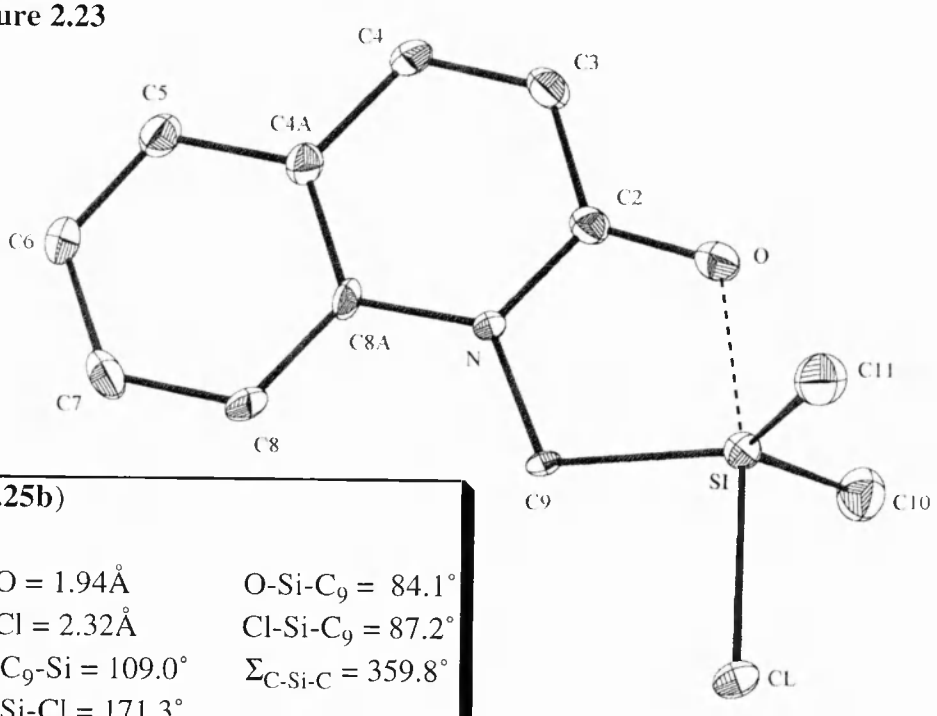

(2.25b)

SiO = 1.94Å	O-Si-C_9 = 84.1°
SiCl = 2.32Å	Cl-Si-C_9 = 87.2°
N-C_9-Si = 109.0°	$\Sigma_{C\text{-}Si\text{-}C}$ = 359.8°
O-Si-Cl = 171.3°	

In this complex the 'nucleophile' is about 0.1Å closer to the silicon centre than in (**2.25a**) (Figure 2.22). As a result, the extension occurring in the Si-X bond has increased. The Si-Cl bond length of 2.32Å is approximately 0.3Å longer than a conventional Si-Cl bond. The N-C_9-Si fragment bond angle has decreased slightly and the O-Si-C_9 bond angle increased slightly from (**2.25a**) as a result of 'ring closure' between the silicon and the oxygen; C_9 acting as a *hinge* between the nucleophilic and electrophilic centres. The sum of the equatorial bond angles at silicon, 359.8°, indicates that the [CH_2SiMe_2] moiety is virtually planar.

2.6.3: Bromide complex (2.25c)

The 'nucleophile' having approached the silicon centre by a further 0.11Å from (**2.25b**) is now causing considerable deformation of the Si-X bond (Figure 2.24). The observed Si-Br bond distance of 2.65Å is about 0.5Å longer than a common Si-Br bond. With this degree of elongation we cannot be certain of the precise nature of the Si-Br bond. That is whether it is best described as a stretched covalent bond, or an ionic bond between a bromide anion and a silyl-quinoline cation.

Figure 2.24

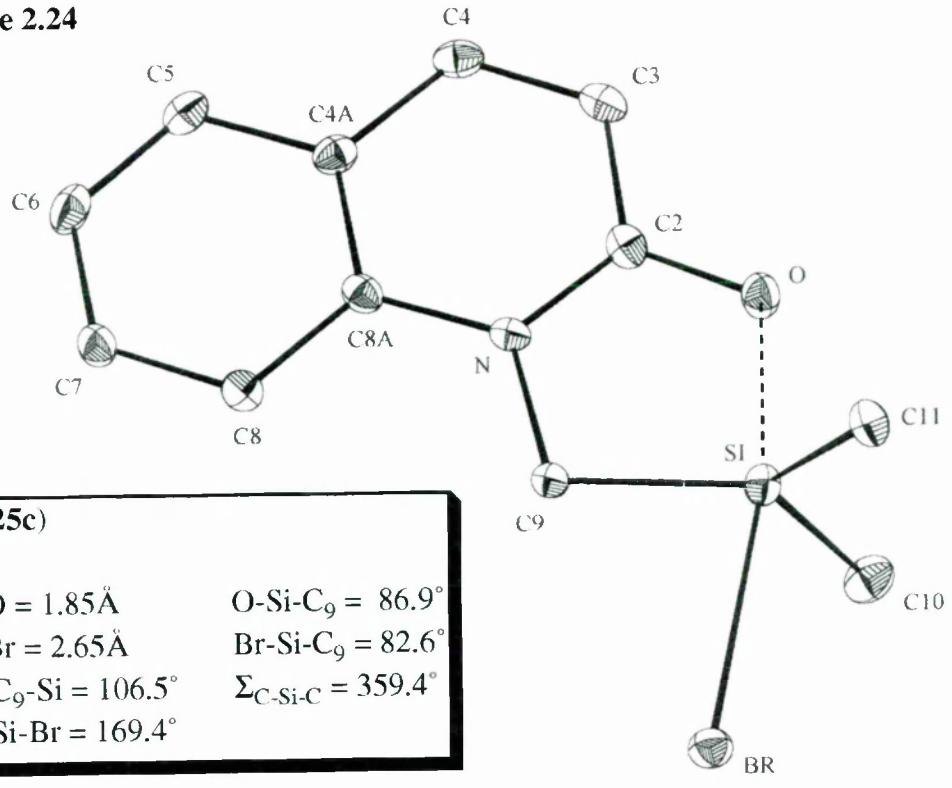

(2.25c)

SiO = 1.85Å	O-Si-C_9 = 86.9°
SiBr = 2.65Å	Br-Si-C_9 = 82.6°
N-C_9-Si = 106.5°	$\Sigma_{C\text{-}Si\text{-}C}$ = 359.4°
O-Si-Br = 169.4°	

2.6.4: Triflate complex (2.25d)

Figure 2.25: (2.25d) viewed in the x-y plane.

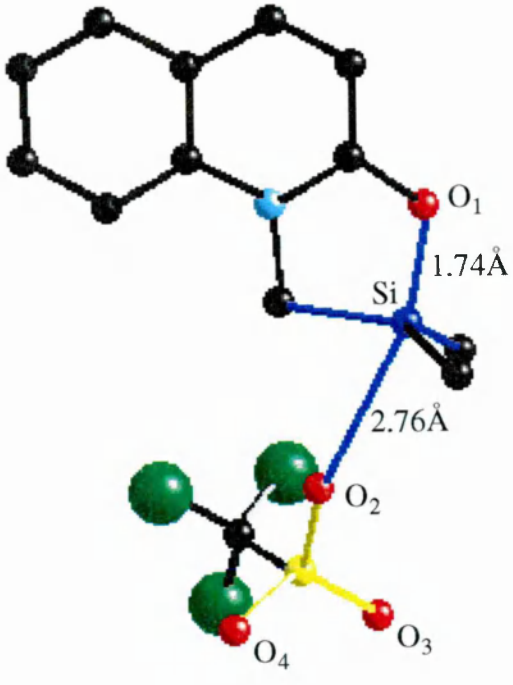

Figure 2.26: (2.25d) viewed along the y plane of the quinoline ring.

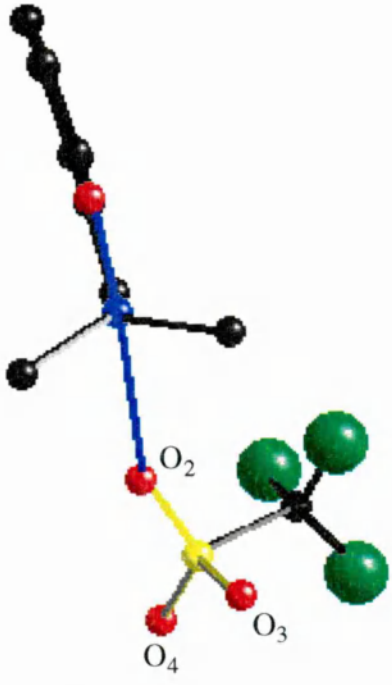

Two further drawings (Figures 2.25 and 2.26) are provided of (**2.25d**) in addition to the ORTEP diagram (Figure 2.27). This is because the ORTEP diagram is not the best representation of the shortest contact distance between the counter ions.

Figure 2.27

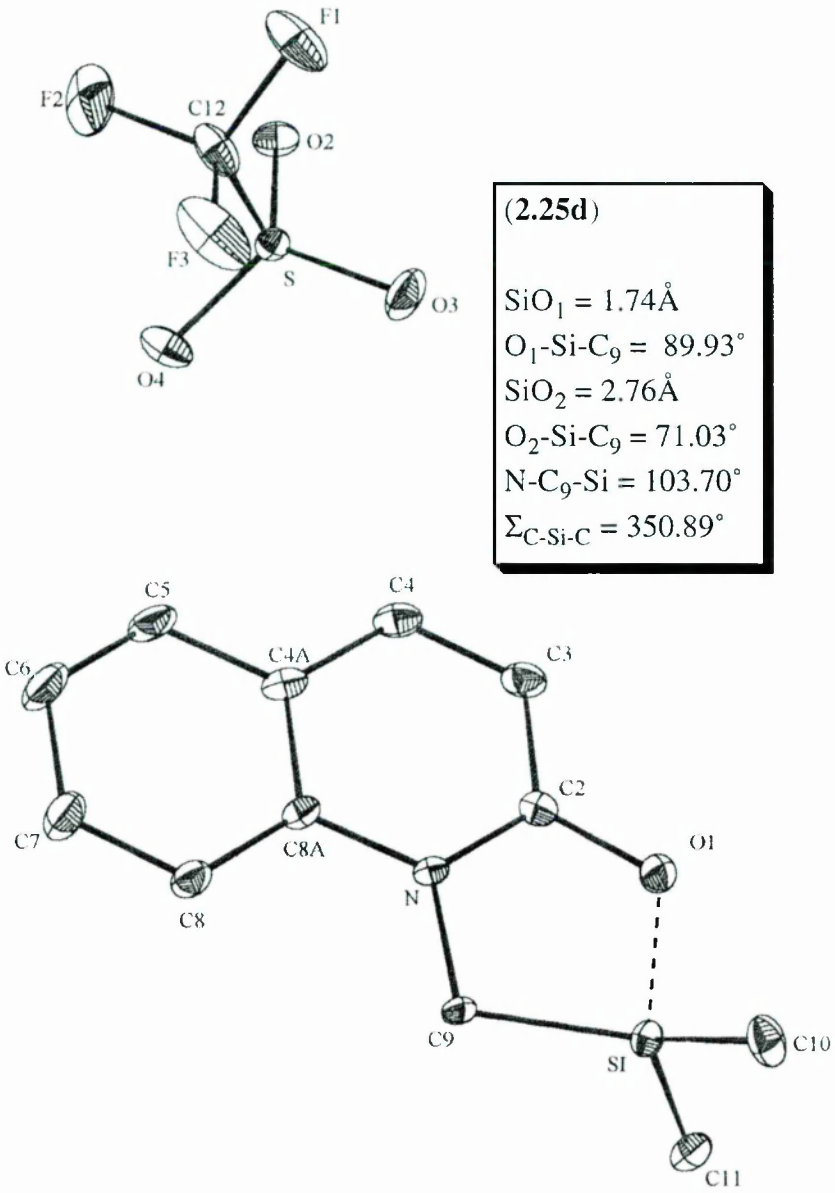

(2.25d)

SiO_1 = 1.74Å
O_1-Si-C_9 = 89.93°
SiO_2 = 2.76Å
O_2-Si-C_9 = 71.03°
N-C_9-Si = 103.70°
$\Sigma_{C\text{-}Si\text{-}C}$ = 350.89°

There is a single contact distance (O_2-Si) (2.76Å) between the counter ions within the sum of the van der Waals radii for silicon and oxygen (3.62Å). The Si-O_2 distance, some 1.25Å longer than a typical Si-O bond, is best described as an electrostatic interaction between the triflate anion and a silyl-quinoline cation. The next closest SiO contact distance is 3.90Å (between Si and O_4 in another adjacent triflate ion) and is too long for a chemical interaction.

This final complex of the series shows the greatest degree of 'substitution' and so the smallest N-C_9-Si angle of the four complexes, 103.7°. The 'leaving group' is only weakly bound to the silicon, which surprisingly still results in considerable trigonal-bipyramidal character. The geometry is best described as intermediate between

trigonal-bipyramidal and tetrahedral. This is reflected in the sum of the bond angles between the 'equatorial' groups at silicon (350.9°). For a tetrahedral silicon an angle sum of about 328° is expected while 360° is expected for a fully trigonal bipyramidal silicon. A view of the molecule along the Si-C_9 bond (Figure 2.26) shows that the packing requirements of the bulky triflate ion cause the O_1-O_2 axis to be distorted slightly out of the plain of the quinoline ring.

Unlike structures (**2.25a-c**), structure (**2.25d**) contains a molecule of recrystallisation solvent, benzene, in its lattice which was omitted from Figure 2.27. Calculations have suggested that the cavity in which the solvent molecule resides has an occupancy by a solvent molecule of approximately 50%, with filled sites being randomly distributed through the crystal. Figure 2.28 shows how the solvent molecule packs in the lattice, assuming a 100% site occupancy.

Figure 2.28

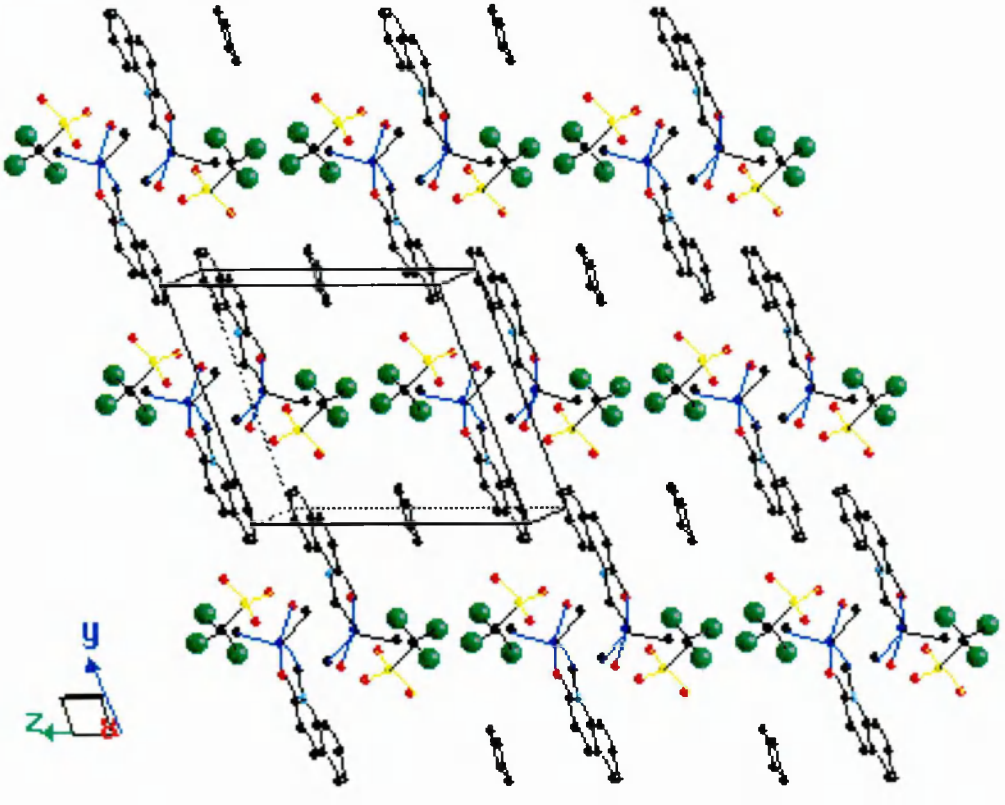

It is the ion packing requirements of the bulky triflate groups which are the probable reason for the crystal containing this cavity. There appear to be an unresolvable continuum of closely related orientations that the solvent molecule may adopt when occupying the cavity. This again varies randomly from occupied position to occupied position. X-ray crystallography views the average position of each atom

through the entire crystal and therefore produces large *thermal* ellipsoids in ORTEP diagrams for atoms whose positions vary considerably from unit cell to unit cell. This is why the solvent was not included in the ORTEP diagram. Table 2.8 summarises the key crystallographic data.

Table 2.8

Complex	(**2.25a**)	(**2.25b**)	(**2.25c**)	(**2.25d**)
X	F	Cl	Br	OTf
O-Si measured (/Å)	2.06	1.94	1.85	1.74
Si-X measured (/Å)	1.68	2.32	2.65	2.76
Sum of C-Si-C (/°)	357.7	359.8	359.4	350.9
N-C_9-Si (/°)	113.3	109.0	106.5	103.7
O_1-Si-C_9 (/°)	80.7	84.1	86.9	89.9
X-Si-C_9 (/°)	90.8	87.2	82.6	71.0
O_1-Si-X (/°)	171.5	171.3	169.4	160.4

The geometry around the silicon stays highly trigonal bipyramidal for the majority of the modelled 'reaction coordinate'. Only (**2.25d**), representing a structure close to the 100% substitution limit, has appreciable tetracoordinate character at the silicon. The O_1-Si-X axial group angle deviates increasingly from ideal linearity as the percentage O-Si bond formation increases because the 'nucleophile' is forced by the constraints of the ring to follow a somewhat distorted 'approach' to the silicon. This in turn affects the path by which the X-group 'leaves'. The carbonyl bond length remains largely unaffected (1.27Å in X = F, Cl, 1.30Å in X = Br and 1.31Å in X = OTf) by the 'substitution', maintaining a value between that expected for a single (typically 1.36Å) and double bond (1.24Å in the crystal structure of 2-(1H)-quinolinone (**2.16**).[121]).

Overall, the structures model convincingly the substitution pathway; the approaching 'nucleophile' causing increasing 'stretching' of the Si-X group while at the same time the five-membered 'ring closure' takes place which progressively reduces the N-C_9-Si angle. 'Inversion' at silicon is noted by $\Sigma_{C\text{-}Si\text{-}C}$ increasing from (**2.25a**) to a maxima for (**2.25b**) then decreasing through (**2.25c**) to (**2.25d**), while at the same time the C_9-Si-'nucleophile' bond angle gradually increases and the C_9-Si-X bond angle gradually decreases.

2.7: Related work

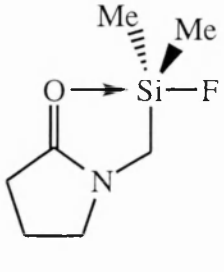

(**2.29a**)

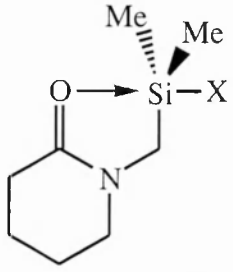

(**2.29b**) X = Cl
(**2.29c**) X = Br
(**2.29d**) X = OTf

Baukov and co-workers have performed a similar X-ray study on a series of pentacoordinated silyl 2-pyrrolidones and 2-piperidones (**2.29a-d**).[122-125] Table 2.9 summarises their crystallographic data and compares it to our own. Complexes (**2.29a-d**) are similar to (**2.25a-d**) in that they show a decreasing Si-O bond length with increasing X-group leaving ability. The 'inversion' of the silicon during the 'reaction' is also evident from the pattern of changing $\Sigma_{C\text{-}Si\text{-}C}$ with decreasing Si-O bond length.

In the solid state, the ligands of complexes (**2.29a-d**) would not appear to be consistently better or poorer 'nucleophiles' than quinolines for a given X-group. However, for a given leaving group, the complex type ((**2.25a-d**) or (**2.29a-d**)) that has the strongest O-Si bond, also has the most extended Si-X bond. Complexes (**2.25b**) and (**2.29b**) are largely similar in geometry, as are (**2.25d**) and (**2.29d**). The fluorosilylpyrrolidone complex (**2.29a**) has an Si-O bond 0.34Å longer than its quinoline analogue (**2.25a**) and its $\Sigma_{C\text{-}Si\text{-}C}$ is 4.7° less than in (**2.25a**). Therefore (**2.29a**) is the more tetracoordinate complex of the two. In contrast, the bromosilylpiperidone complex (**2.29c**) contains a stronger Si-O bond and a more elongated Si-Br bond than (**2.25c**). In terms of modelling S_N2 substitution, complexes (**2.29a-d**) comprise structures over a wider 'window' of the 'reaction' than complexes (**2.25a-d**). The range of measured Si-O bond lengths is 2.40-1.75Å for (**2.29a-d**) compared to 2.06-1.74Å for (**2.25a-d**).

Table 2.9

X	Ref'	Bond lengths (/Å)				Bond angles (/°)									
		O-Si		Si-X		$\Sigma_{C\text{-}Si\text{-}C}$		N-CH_2-Si		O-Si-CH_2		X-Si-CH_2		O-Si-X	
	(*)	(**2.25**)	(**2.29**)*	(**2.25**)	(**2.29**)*	(**2.25**)	(**2.29**)*	(**2.25**)	(**2.29**)*	(**2.25**)	(**2.29**)*	(**2.25**)	(**2.29**)*	(**2.25**)	(**2.29**)*
F (**a**)+	122	2.06	2.40	1.68	1.65	357.7	353.0	131.3	115.3	80.7	77.6	90.8	92.3	171.5	172.8
Cl (**b**)	123	1.94	1.95	2.32	2.31	359.8	359.7	109.0	109.6	84.1	83.2	87.2	88.0	171.3	171.2
Br (**c**)	124	1.85	1.80	2.65	3.12	359.4	355.9	106.5	106.0	86.9	87.9	82.6	74.7	169.4	162.6
OTf (**d**)	125	1.74	1.75	2.76	2.79	350.9	352.2	103.7	103.4	89.9	89.5	71.0	75.9	160.4	165.0

+ The crystal structure of (**2.29a**) contains four independant molecules. The data presented are therefore the mean values over all the molecules.

* Reference number for the appropriate (**2.29a-d**) crystal structure.

2.8: Structural correlation treatment of X-ray data

In order that the Si-X bond extensions be quantified and directly compared with each other, a term **percentage Si-X bond extension** shall be introduced. We shall define percentage Si-X bond extension as:

$$\text{Si-X extension} = \frac{\text{(Si-X(measured)) - (Si-X(typical))}}{\text{(}\Sigma\text{crystal ionic radii } Si^{+} \text{ \& } X^{-}\text{) - (Si-X(typical))}} \times 100$$

The crystal ionic radii used are those for Si^{+} and X^{-} since the breaking of the Si-X bond formally leads to the formation of these moieties. A crystal ionic radius is a typical value based on the analysis of large numbers of crystal structures of salts containing that ion. The sum of pairs of ionic radii represent the distance between ions if packed together in an ionic crystal lattice. The definition of 0% extension is of a covalent bond whose length is standard for its type. 100% extension is the minimum distance at which bonding between Si and X is essentially purely ionic, i.e. has negligible covalent component. Percentage Si-X bond extension values in excess of 100 represent weaker electrostatic interactions between the ions. Thus, on this scale, there is no upper limit to the distance of the chemical interaction between the ions. On this basis, a value of percentage Si-X extension can be calculated for each of the complex (**2.25a-d**) and (**2.29a-d**) (Table 2.10). The percentage Si-X extension can be plotted against the Si-O bond length (Figure 2.29). The plot comprises a parabolic curve, which in terms of the modelled substitution, shows that the stronger the 'nucleophile'-silicon interaction, the more 'extended' the Si-X bond becomes. The length of the Si-O bond in a structure modelling complete substitution may be extrapolated from the graph as about 1.7Å.

The $\Sigma_{C\text{-}Si\text{-}C}$ gives information about how trigonal bipyramidal the geometry at silicon is. We shall use a term **percentage trigonal-bipyramidal (%TBP)** to define this.

$$\%\ \text{TBP} = \frac{[\Sigma_{C\text{-}Si\text{-}C}(\text{observed}) - \Sigma_{C\text{-}Si\text{-}C}(\text{tetrahedral})]}{[\Sigma_{C\text{-}Si\text{-}C}(\text{TBP}) - \Sigma_{C\text{-}Si\text{-}C}(\text{tetrahedral})]} \times 100$$

$\Sigma_{C\text{-}Si\text{-}C}$(TBP) is 360.0° while $\Sigma_{C\text{-}Si\text{-}C}$(tetrahedral) is 328.4°. Therefore 0% TBP represents a fully tetracoordinate silicon centre and 100% TBP is completely trigonal bipyramidal silicon centre. The results of the above calculation for each complex of type (**2.25a-d**) and (**2.29a-d**) are shown in Table 2.11 and Figure 2.30.

Figure 2.29

The effect of nucleophilic attack on the Si-leaving group bond modelled by complexes (2.25a-d) and (2.29a-d).

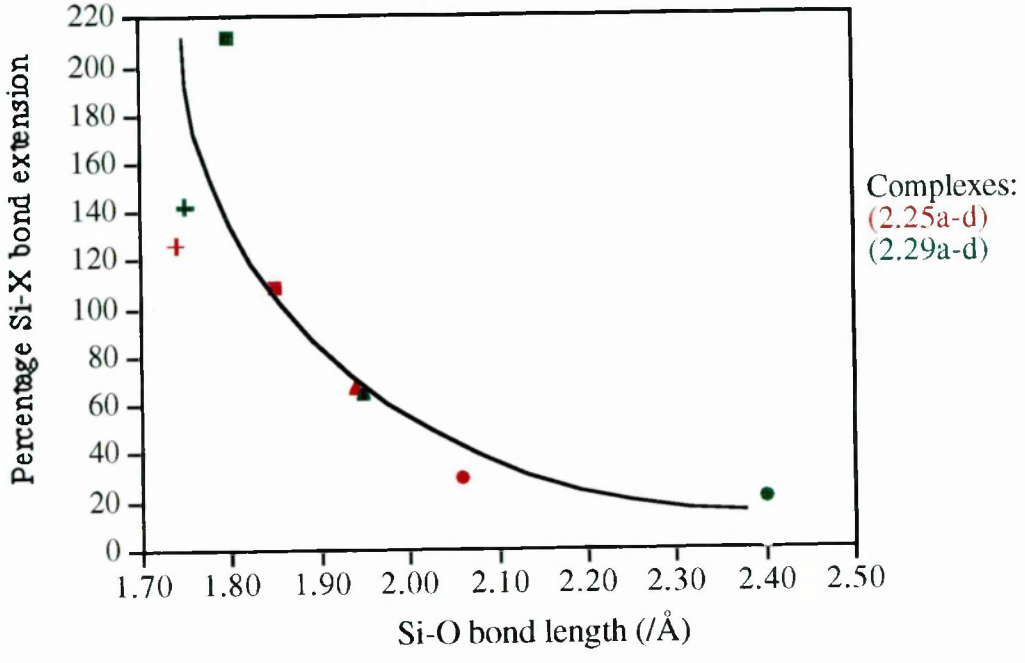

Figure 2.30

The effect of different degrees of Si-nucleophile interaction on the geometry of the silicon centre modelled by complexes (2.25a-d) and(2.29a-d).

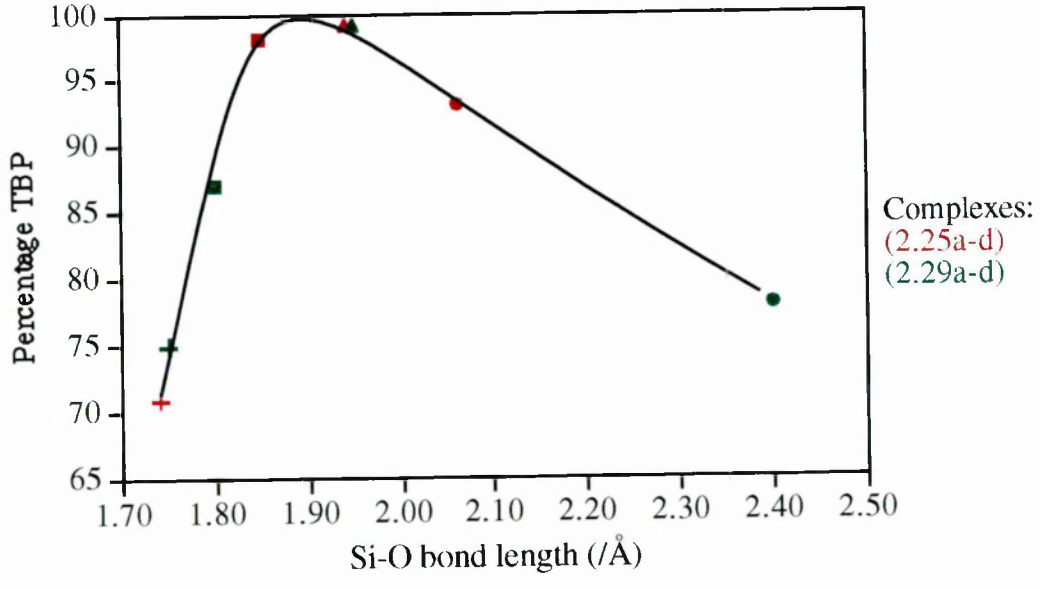

Table 2.10

X	O-Si measured /Å		Si-X measured /Å		Si-X typical /Å	Crystal ionic radii (Si^+) /Å	Crystal ionic radii (X^-) /Å	Σ Crystal ionic radii (Si^+X^-) /Å	% SiX bond ext'n	
	(2.25)	**(2.29)**	**(2.25)**	**(2.29)**					**(2.25)**	**(2.29)**
F (**a**)*	2.06	2.40	1.68	1.65	1.56	0.65	1.33	1.98	29	21
Cl (**b**)	1.94	1.95	2.32	2.31	2.03	0.65	1.81	2.46	67	65
Br (**c**)	1.85	1.80	2.65	3.12	2.15	0.65	1.96	2.61	109	211
OTf (**d**)	1.74	1.75	2.76	2.79	1.50	0.65	1.76	2.41	126	142

* The data presented for (**2.29a**) are mean values.

Table 2.11

X	Si-O (measured)		$\Sigma_{C\text{-}Si\text{-}C}$ (/°)		% TBP	
	(2.25)	**(2.29)**	**(2.25)**	**(2.29)**	**(2.25)**	**(2.29)**
F (**a**)*	2.06	2.40	357.7	353.0	93	78
Cl (**b**)	1.94	1.95	359.8	359.7	99	99
Br (**c**)	1.85	1.80	359.4	355.9	98	87
OTf (**d**)	1.74	1.75	350.9	352.2	71	75

* The data presented for (**2.29a**) are mean values.

The transition from tetrahedral, through fully trigonal bipyramidal and back towards tetrahedral geometry with decreasing Si-O bond length is seen. A fully trigonal bipyramidal complex is formed when the Si-O bond is approximately 1.90Å long.

Complexes (**2.25a-d**) may also be related to the crystal structures of pentacoordinated chlorosilyl amides (**1.43**) and (**1.44**) measured by Pestunovich *et al.*[57] The equation below can be used to convert values of 'percentage Si-X extension' of non-chloride derivatives into equivalent Si-Cl bond lengths. ie:

$$\text{Equivalent Si-Cl bond length} = \left[\frac{A(C-B)}{100}\right] + B$$

A = Percentage Si-X extension observed for non chloride complex
B = Length of a typical Si-Cl bond (2.03Å)
C = Sum of the crystal ionic radii for $Si^{+}Cl^{-}$ (2.46Å)

The results of the calculations are presented in Table 2.12 and included in Figure 2.31; a plot of the relationship between Si-Cl bond length and Si-O bond length for the amide complexes.

Table 2.12

	(2.25a)	**(2.26b)**	**(2.25c)**	**(2.25d)**
Si-X measured	1.68	2.32	2.65	2.76
% Si-X extension	29	67	109	126
Equv' Si-Cl length	2.15	2.32	2.50	2.57

Figure 2.31

Comparison of Si-O and equivalent Si-Cl bond lengths of complexes (2.25a-d) with those of amide structures of Pestunovich *et al.*

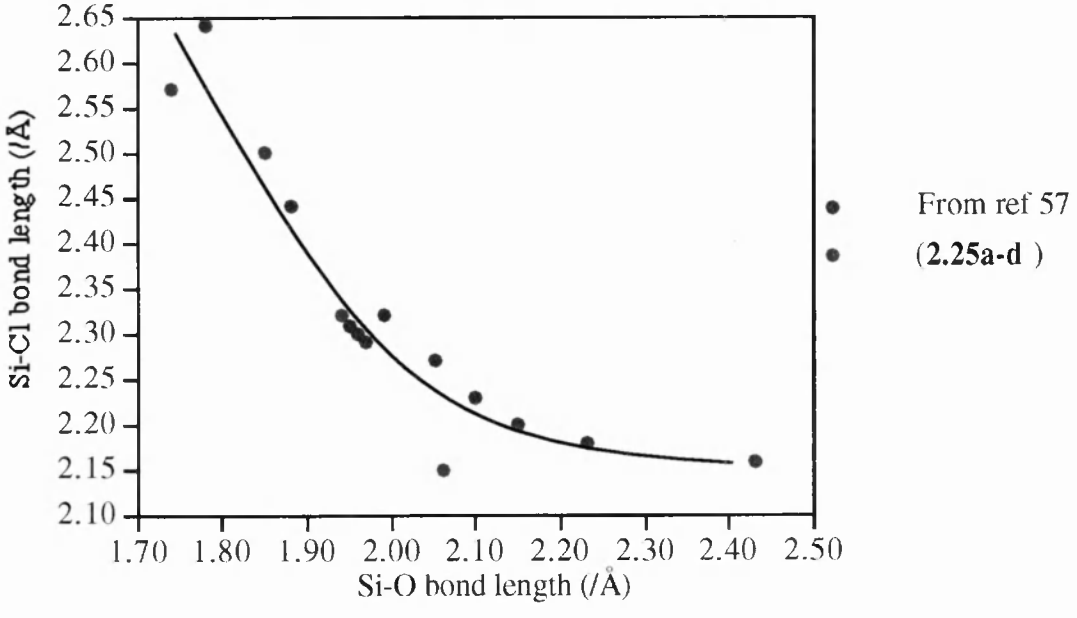

Only the 'fluoride' complex, (**2.25a**), deviates significantly from the curve. For the Si-O bond length measured, the calculated equivalent Si-Cl extension is about 1Å less than expected. This is because the actual Si-F bond in (**2.25a**) does not stretch so readily under the influence of the oxygen 'nucleophile' at silicon as do the other Si-X bonds. This is related to the strong pπ-dπ back bonding that occurs between fluorine and silicon that strengthens and reduces the *elasticity* of the Si-F bond.

2.9: A comparison of solid state and solution structures

Solid state NMR spectroscopy provides a link between the structure of a complex in the solid state and its structure in solution and allows us to determine whether the structure of a molecule in solution is comparable with its solid state structure. We have obtained a single isotropic solid-state ^{29}Si measurement for complex (**2.25b**) at room temperature. The solid state chemical shift is δ -39.6 compared to δ -38.4 in solution. This shows that, within experimental error, the structure of the complex in the solid state and in solution has the same degree of pentacoordination. We cannot conclude that the other complexes behave similarly, but this result suggests that they should. A plot of the percentage Si-O bond formation, as calculated by solution measurements, against the Si-nucleophile bond length from the solid state crystal structure, shows that the solid state and solution structures vary in a similar fashion. (Figure 2.32).

Figure 2.32

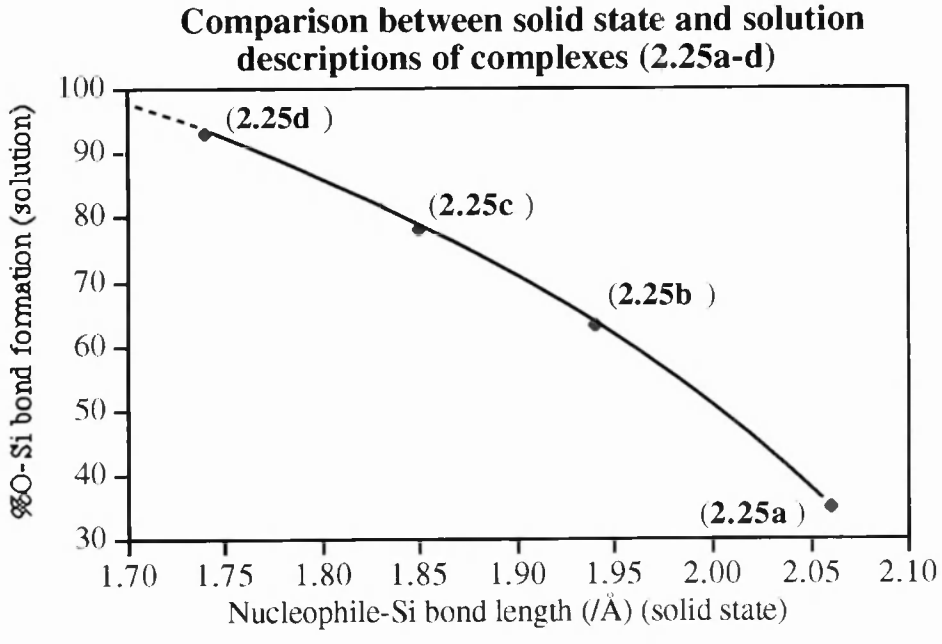

By extrapolation, the Si-O bond length representing complete substitution is about 1.7Å. This is the same value as extrapolated from Figure 2.29. Since it is neither practically convenient to perform NMR experiments at 100K or obtain a satisfactory single crystal X-ray structure at room temperature, we cannot measure the crystal structures and record NMR spectra at the same temperature.

2.10: An insight into the hydrolysis of chlorosilanes

During the preparation of single crystals of (**2.25b**) another material, (**2.30**), was found to co-crystallise when an acetonitrile solution was allowed to evaporate slowly in air for 3 days. The ORTEP diagram of the new compound is presented in Figure 2.33.

Figure 2.33

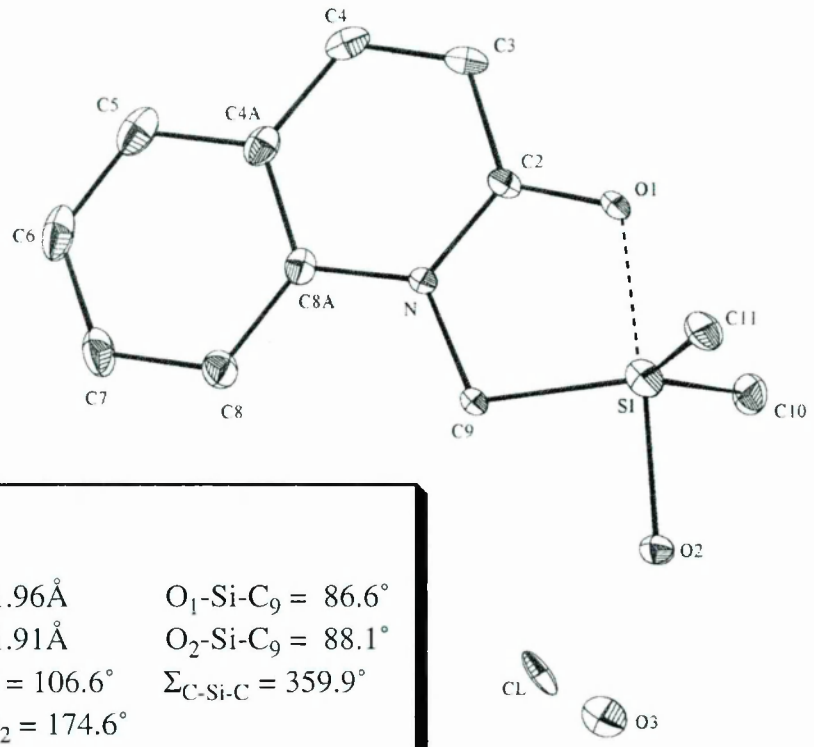

(**2.30**)

SiO_1 = 1.96Å	O_1-Si-C_9 = 86.6°
SiO_2 = 1.91Å	O_2-Si-C_9 = 88.1°
N-C_9-Si = 106.6°	$\Sigma_{C\text{-}Si\text{-}C}$ = 359.9°
O_1-Si-O_2 = 174.6°	

Initial inspection reveals that there is chlorine in the crystal, but not bonded directly to the silicon. The closest contact between silicon and chlorine atoms is 4.39Å. By comparison, a typical Si-Cl bond distance is 2.03Å and the sum of the van der Waals radii for Si and Cl is 3.85Å. In the place of the silicon chlorine bond is an Si-O bond of length 1.91Å (Si-O_2). A further oxygen atom (O_3) is also present in the structure. The closest silicon atom from O_3 is 3.97Å away while a typical Si-O distance is 1.50Å and the sum of the van der Waals radii for Si and O is 3.62Å. In order that the

structure is electrically neutral there must be four hydrogen atoms associated with O_2 and O_3. This presents two possibilities:

- **(2.30a)** O_2 is part of a water molecule bonded to the silicon (sometimes described as a *protonated silanol*) and O_3 is part of a further water molecule.

- **(2.30b)** O_2 is a silanol oxygen bonded to the silicon via a somewhat extended Si-O_2 bond and O_3 is a hydroxonium ion.

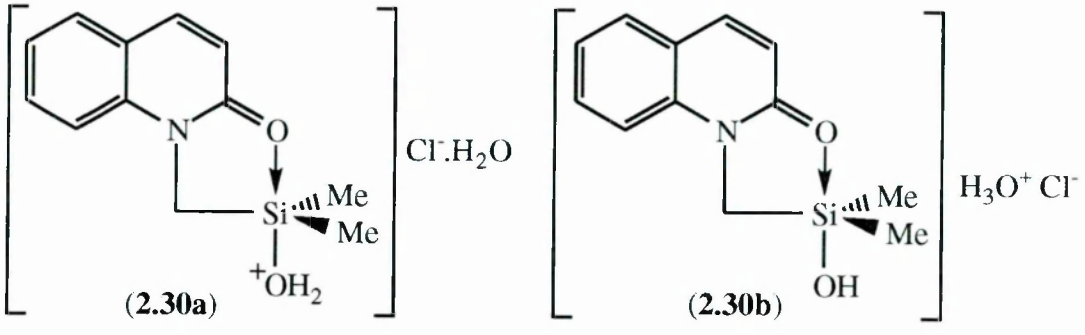

The infra red spectrum of (**2.30**) (KBr disc) contains an intense, broad band at 3307.0 cm^{-1}, indicating considerable hydrogen bonding in the crystal. Figure 2.34 shows an expanded unit cell view of the structure of (**2.30**). The view demonstrates how particularly O_2, O_3 and Cl (highlighted in red and green) reside in relative proximity to each other in vertical sheets.

Figure 2.34

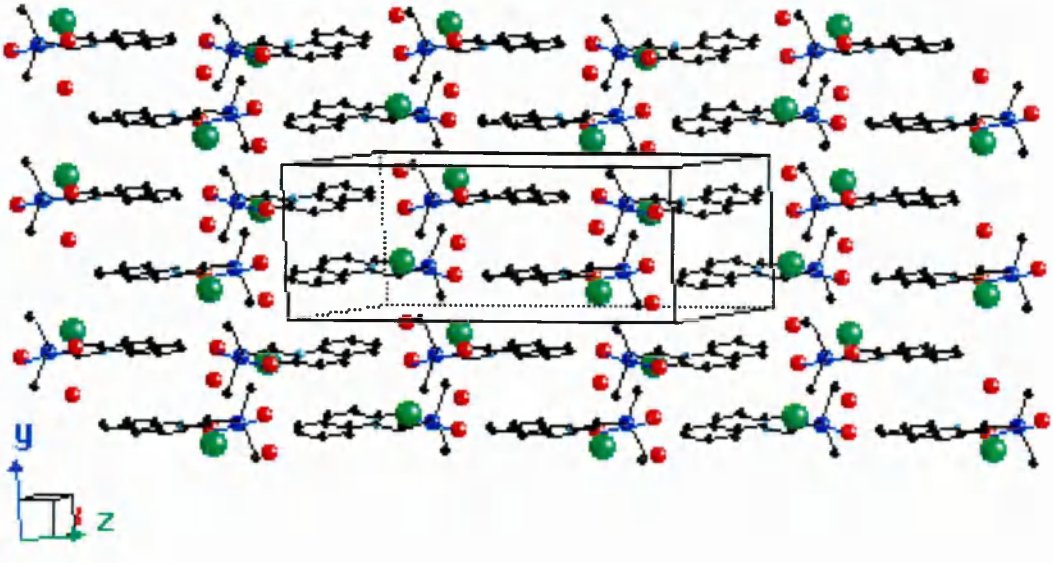

Analysis of the set of closest-contact distances between these three atoms reveals that many of the distances between them are of a suitable size for hydrogen bond bridging. Table 2.13 summarises the distances of such contacts in **bold**.

Table 2.13

Y-Z	Y-Z closest contact (/Å)	Y-Z 2nd closest contact (/Å)	Y-Z 3rd closest contact (/Å)	Typical Y-H-Z H-bond (/Å)
O_2-O_3	**2.59**	4.35	5.69	2.50
Cl-O_3	**3.05**	**3.06**	9.98	3.05
Cl-O_2	**3.02**	4.42	4.86	3.05

Since four suitable distances have been found and there are four protons whos positions need assigning, this suggests that all four protons are involved in an extensive network of hydrogen bonding. Figure 2.35, shows the same projection of the unit cell as Figure 2.34 but considers only the atoms Si, Cl, O_2 and O_3. The proposed hydrogen bond bridges are represented by standard bonds. The 'bond' angles range from 91.7° to 159.5° (both O_3-Cl-O_2) and are suitably large to support hydrogen bridging.

Figure 2.35

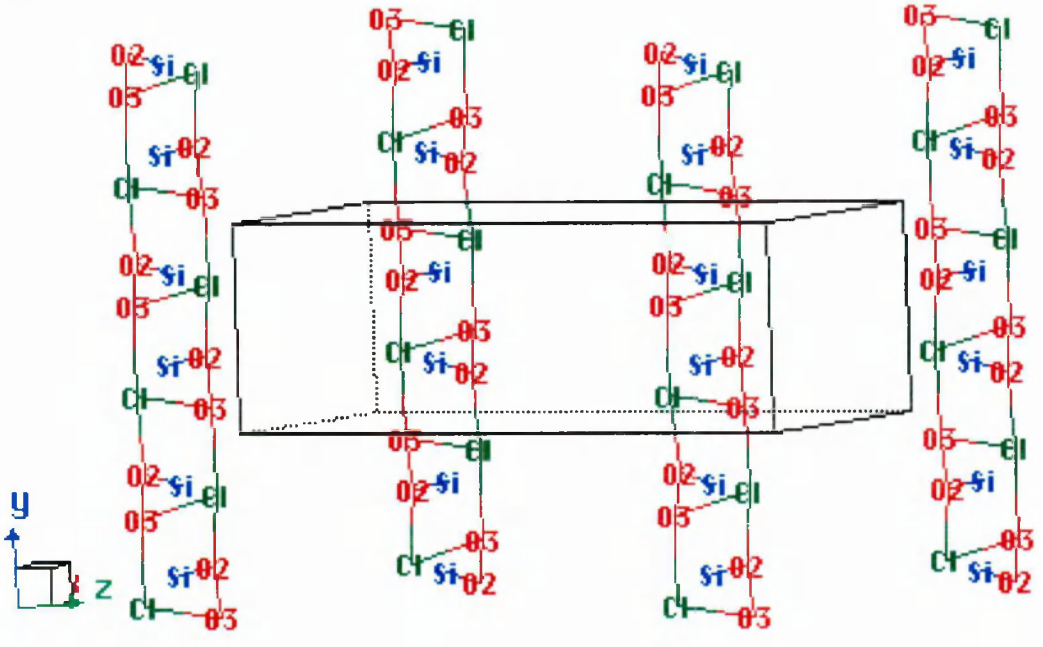

If we consider the structure as being similar to (**2.30b**) then the compound can be treated as though it were another member of the series (**2.25a-d**), with the 'leaving group' X being an OH. If this were the case, then, since OH is a far poorer 'leaving group' than Cl, it is difficult to explain why an O_1-Si interaction of almost the same magnitude (1.96Å) as that for the chloride complex (**2.25b**) (1.94Å) is observed. This apparent discrepancy is, however, explained if the compound resembles (**2.30a**) which

has the 'leaving group' $^{+}OH_2$ at silicon. $^{+}OH_2$ is a considerably better 'leaving group' than OH and explains the strong Si-O_1 bond and extended Si-O_2 bond. This combination of evidence strongly suggests that (**2.30a**) is the observed structure.

Aided by this information we were able to locate the remaining hydrogen atoms and confirm the structure to be that of (**2.30a**). Figure 2.36 shows the structure of the hydrogen bonded chains. Figure 2.37 shows how the quinoline rings interlock with each other between the hydrogen bond chains.

Figure 2.36

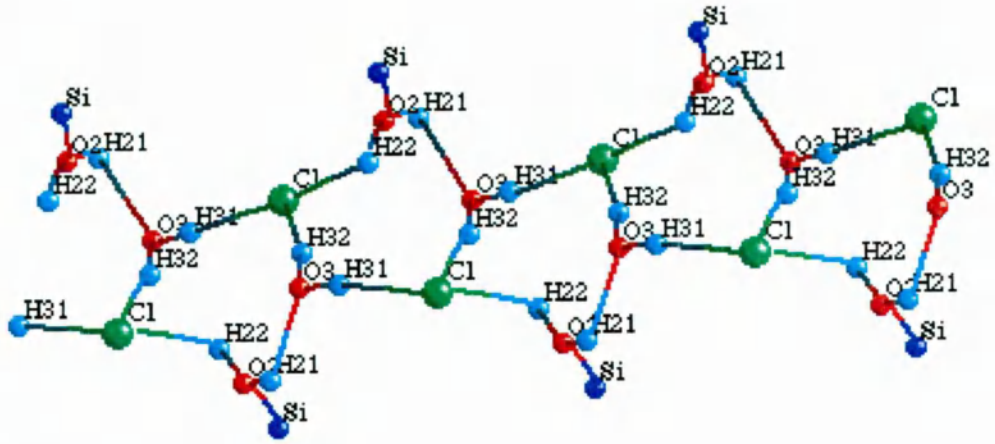

Figure 2.37

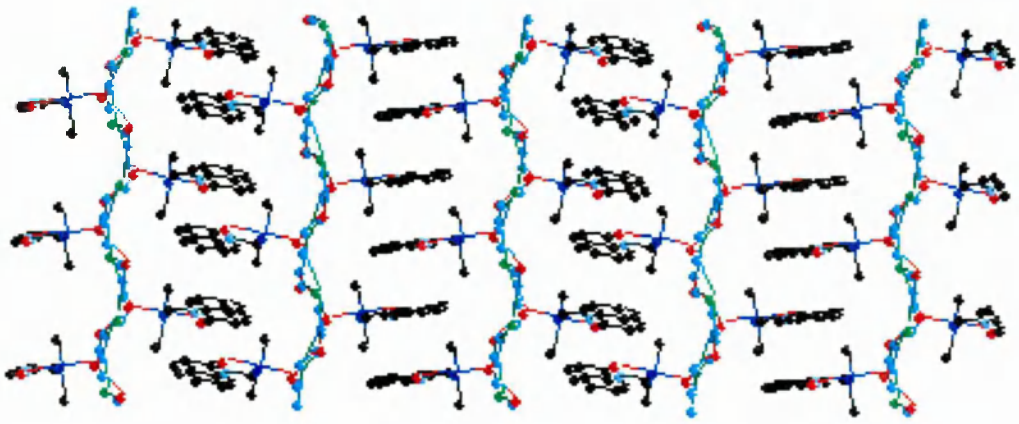

The chains are puckered and made up of fused, 10-membered rings with hydrogen atoms in alternate positions. All the hydrogen atoms associated with the two water molecules are involved in hydrogen bonding. The way the chains pack is shown in Figure 2.38. The chains extend indefinitely in parallel along the y-axis repeating every 7.22Å. Along the z axis the chains stack one above the other in an 'AB' fashion, repeating every 21.45Å. In the x direction the chains stack side by side in a repeating 'AA' manner every 9.13Å. Hydrogen bonding is limited to within each chain.

Figure 2.38

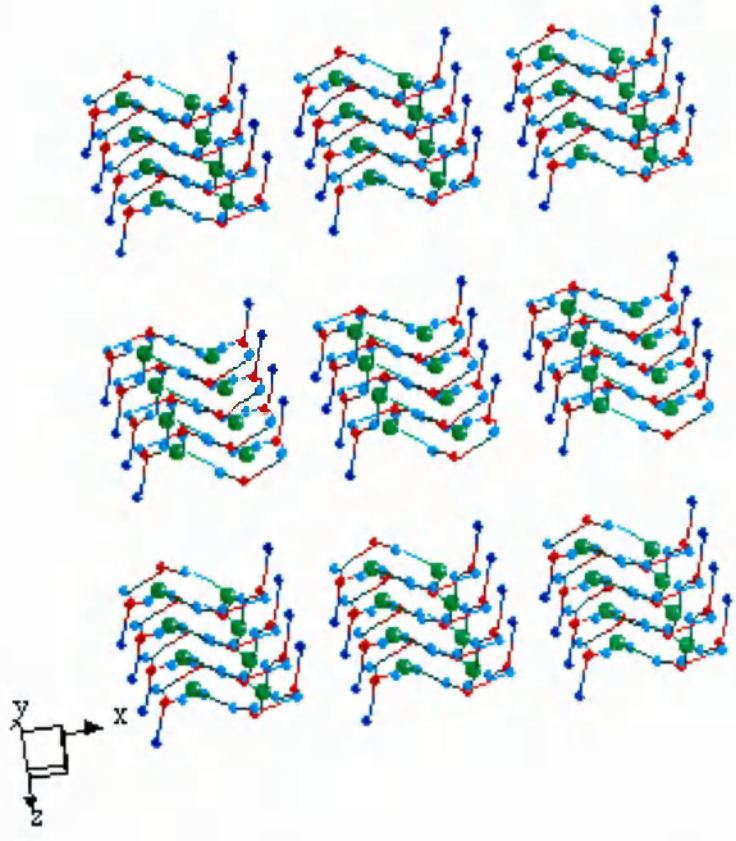

Only one other example of a protonated silanol complex has been reported in the literature by Reed *et al*[126] of $[^tBu_3Si(OH_2)]^+ [Br_6CB_{11}H_6]^-$ (**2.31**) (Figure 2.39).

Figure 2.39

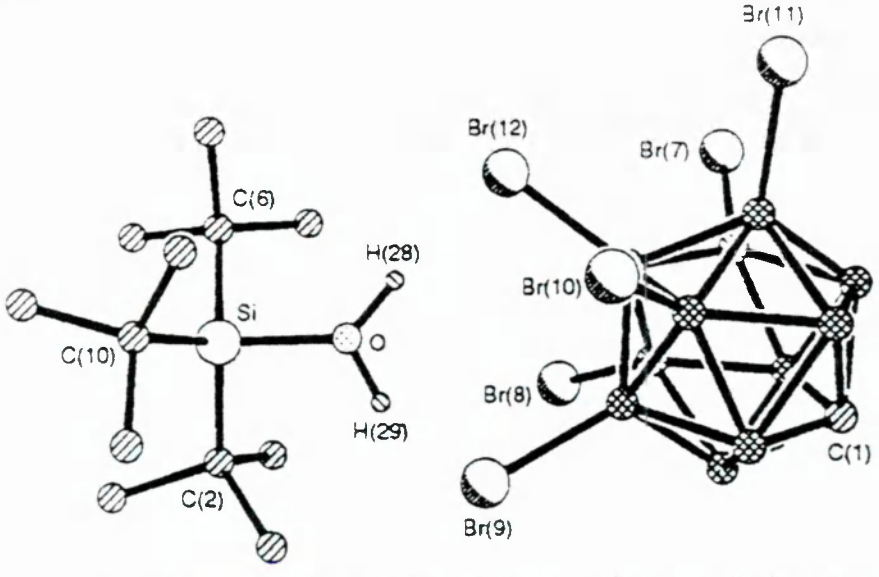

A perspective view of $[Bu^t_3Si(OH_2)]^+[Br_6CB_{11}H_6]^-$. Bond angles (°): C(2)–Si–C(6) 116.0(6), C(2)–Si–C(10) 116.1(6), C(6)–Si–C(10) 115.9(7), O–Si–C(2) 100.7(5). Bond distances (Å): Si–O 1.779(9), Si–C(2) 1.897(17), Si–C(6) 1.897(15), Si–C(10) 1.884(12). H(28) was found, H(29) is calculated.

The $Si-O_2$ distance we observe (1.91Å) is somewhat longer than Reeds equivalent distance (1.78Å). This is presumably because (**2.31**) is four coordinate whereas (**2.30a**) is five coordinate; the axial bond length distortion that commonly occurs in five-coordinate silicon complexes being well documented. The sole reported example of a pentacoordinated silanol is that of (**2.32**) by Karsch *et al* (Figure 2.40).[127] Here the silicon forms part of a four-membered ring

Figure 2.40

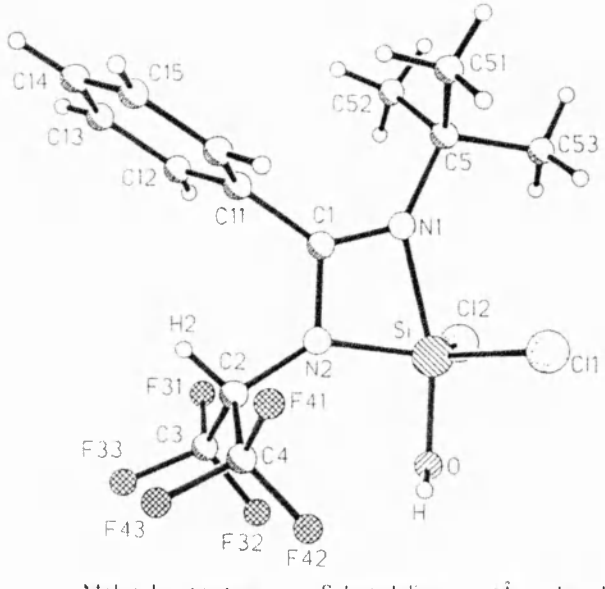

Molecular structure. Selected distances (Å) and angles (deg) are as follows: Si–Cl(1), 2.032(2); Si–Cl(2), 2.006(2); Si–O, 1.601(3); Si–N(1), 1.969(3); Si–N(2), 1.782(3); Cl(1)–Si–Cl(2), 117.3(1); Cl(1)–Si–O, 95.0(2); Cl(2)–Si–O, 93.9(2); N(2)–Si–O, 96.0(2); N(1)–Si–O, 164.5(2); N(1)–Si–N(2), 68.5(1).

Although the OH group is axial to a strong Si-N bond, the Si-O distance (1.60Å) is typical for that of a conventional tetracoordinate silanol Si-O bond.

Intermolecular hydrogen bonding in solid state silanol structures has been extensively studied. In fact, solid state silanol structures not exhibiting hydrogen bonding are comparatively rare. (**2.33**),[128] like (**2.32**) is a further example. Here the Si-O distance is 1.59Å.

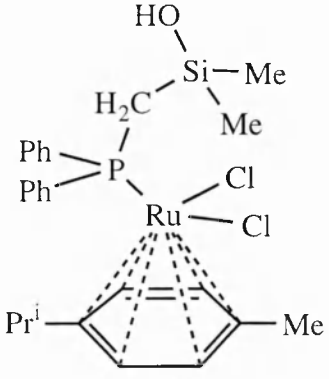

(**2.33**)

Hydrogen bonding may take many forms. For example, tetrameric molecular clusters form for bis(pentamethylcyclopentadienyl)silanediol (**2.34**)[129] (Figure 2.41) between which there is no hydrogen bonding. Other contrasting examples include di-iso-propylsilanediol (**2.35**)[130] (Figure 2.42), where hydrogen bonded dimers are linked together in ladder chains by further hydrogens, and tris(trimethylsilyl)silyl-silanetriol (**2.36**) (Figure 2.43)[131] which forms hexameric cages of hydrogen bonds.

Figure 2.41

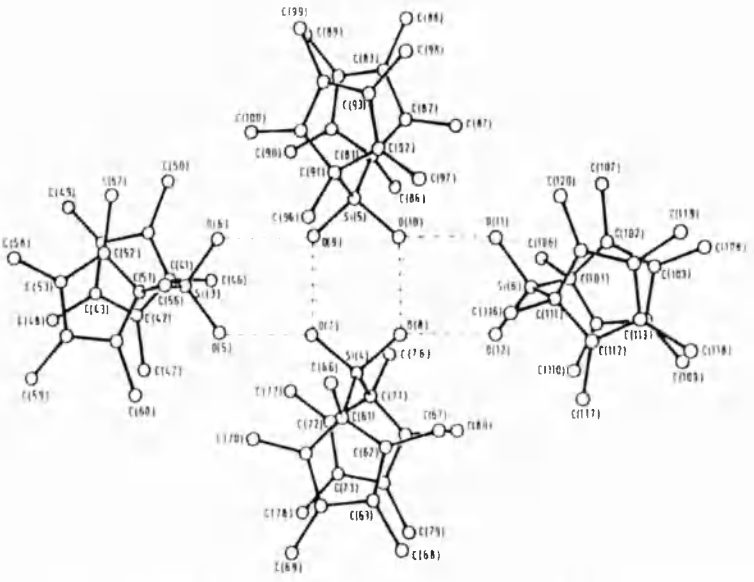

(2.34)

An ORTEP drawing of the molecular structure of and hydrogen bonding in the unsymmetrical tetramer of $(C_5Me_4)_2Si(OH)_2$, together with the atom numbering scheme.

Figure 2.42

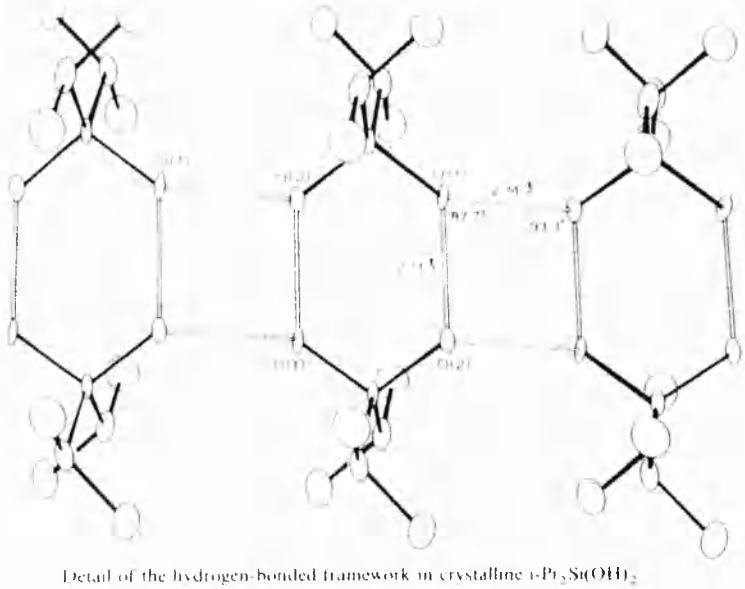

(2.35)

Detail of the hydrogen-bonded framework in crystalline $t\text{-Pr}_2Si(OH)_2$

Figure 2.43

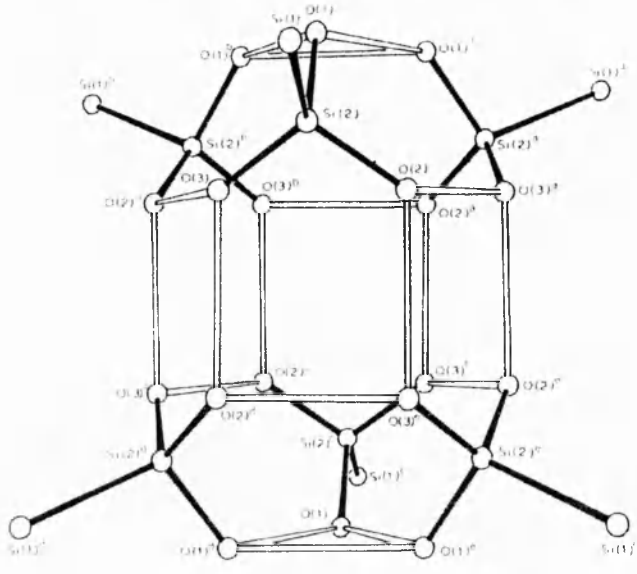

(2.36)

Detail of the hydrogen-bonded cage formed by $(Me_3Si)_3SiSi(OH)_3$

In terms of the hydrolysis of chlorosilanes, (**2.30a**) is a model of the stage where a chloride ion has been displaced by a water molecule and the resulting tetracoordinate cation is the subject of substitution of its the bound water molecule by another nucleophile (e.g. another water molecule).

2.11: Related 'pyridone' complexes

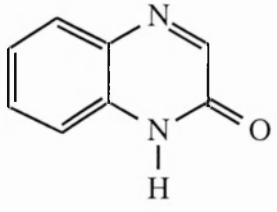

(**2.37**)

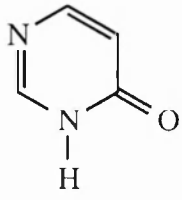

(**2.38**)

Two further ligands, 2-(1H)-quinoxalinone (**2.37**) and 4-(3H)-pyrimidone (**2.38**), have been examined and their 'nucleophilic' properties compared with those of the quinoline and pyridone ligands. (**2.37**) and (**2.38**) were silylated to give (**2.39**) and (**2.40**) respectively (Figure 2.44)

Figure 2.44

(**2.37**) $\xrightarrow[\text{Toluene, } \Delta \\ \text{5 hours.}]{Et_2NSiMe_3}$

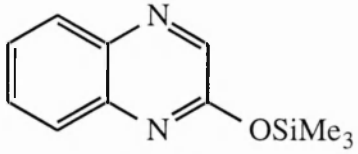

(**2.39**)

(**2.38**) $\xrightarrow[\text{Toluene, } \Delta \\ \text{5 hours.}]{Et_2NSiMe_3}$

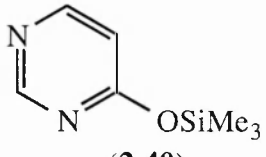

(**2.40**)

The 2-quinoxalinone (**2.41b**) and 4-pyrimidone (**2.42b**) derived silyl-chloride complexes were prepared by reaction of (**2.39**) and (**2.40**) precursors with chloro(chloromethyl)dimethylsilane (Figure 2.45).

Figure 2.45

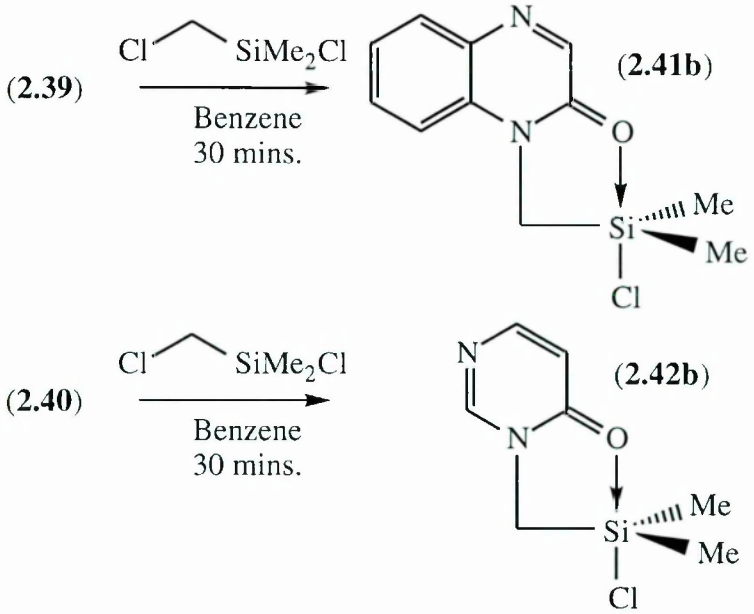

Fluoride derivatives (**2.41a**) and (**2.42a**) were isolated from the reactions of (**2.41b**) and (**2.42b**) with antimony trifluoride (Figure 2.46).

Figure 2.46

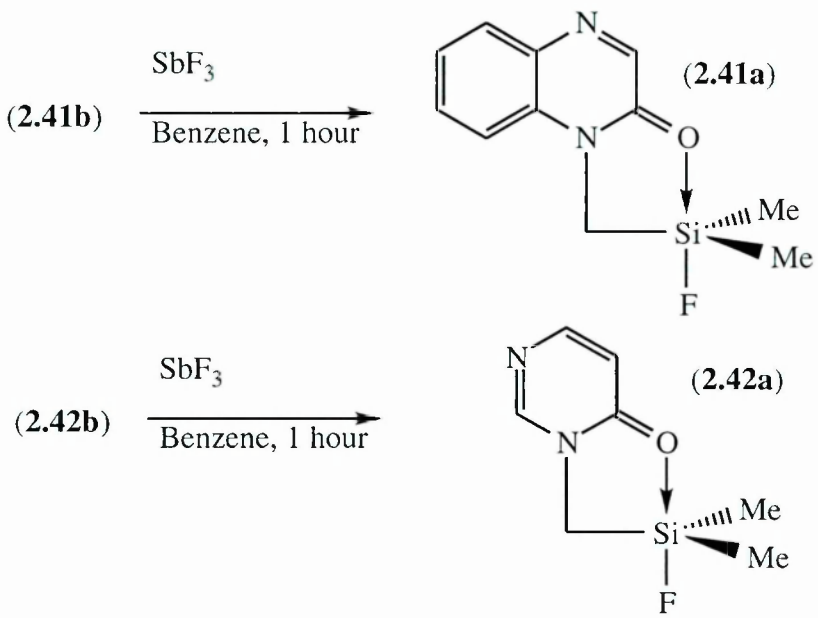

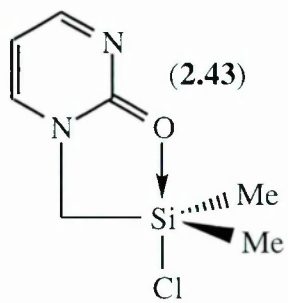

Although the local environment of the silicon is the same in each complex, the structures vary because of the differing electronic properties of the ligands and the use of two different 'leaving groups'. Table 2.14 summarises the ^{29}Si NMR chemical shift data for complexes (**2.41a/b**), (**2.42a/b**), (**2.25a/b**) and pyridones (**2.9**). A 2-pyrimidone analogue of (**2.42b**), (**2.43**), has also been prepared[132] and is also included in the table.

Table 2.14

Leaving group X →	^{29}Si NMR chemical shift (/ppm)	
	F (**a**)	Cl (**b**)
2-Pyridone (**2.9**)	-22.3	-41.1
2-Quinolinone (**2.25**)	-25.4	-38.3
2-Quinoxalinone (**2.41**)	-6.1	-27.1
4-Pyrimidone (**2.42**)	8.8	-16.7
2-Pyrimidone (**2.43**)	-	-33.7

Within each ring system the chloride complexes are more pentacoordinated than the fluoride complexes. This implies that all structures lie close to, or to the left of, a fully pentacoordinate structure. The second nitrogen in the aromatic ring acts as a strong electron withdrawing group, reducing the nucleophilicity of the oxygen lone pairs and thus lowering the extent of hypercoordination in complexes (**2.41a/b**) and (**2.42a/b**). In particular, a pyrimidone nitrogen in the 4-position acts as a stronger electron withdrawing group than when in the 2-position.

Mapping of the substitution was not possible for complexes (**2.41a/b**) or (**2.42a/b**) because of the interaction of the second ring nitrogen with TMS-OTf during titration experiments. Titration of the appropriate disiloxane, (**2.44**) or (**2.45**), gave ^{13}C NMR spectra consisting of an unresolvable multitude of resonances.

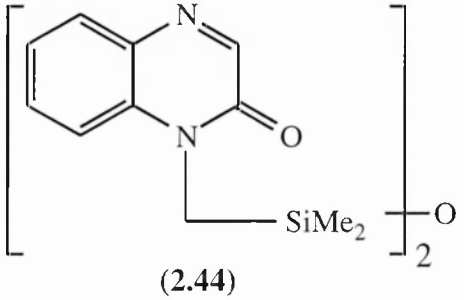

(2.44)

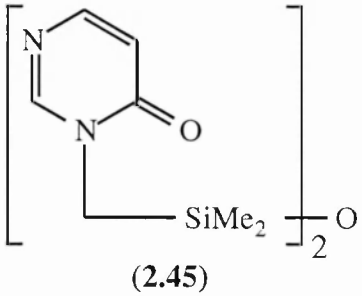

(2.45)

2.12: Desilylation reactions

The isolation and characterisation of (**2.42a**) was complicated by a desilylation reaction which caused the complete degradation of a sample allowed to stand under an inert atmosphere for 4 weeks at room temperature (Figure 2.47). The final product was shown to be 3-methyl-4-pyrimidone (**2.46**). Attempts to purify (**2.42a**) by distillation from traces of (**2.46**) only accelerated the formation of (**2.46**).

Figure 2.47

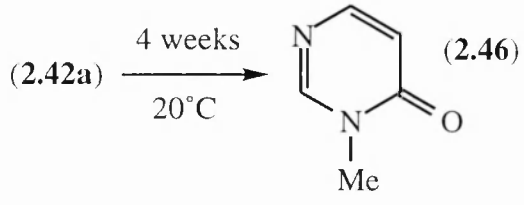

If, in the synthesis of (**2.42a**) from (**2.42b**), more than one equivalent of fluoride ion was used or if the reaction were worked-up under dilute, basic (NaOH), aqueous conditions, the only product isolable from the reaction was (**2.46**). The product is likely to be formed is via nucleophilic attack of either hydroxide or fluoride ion at the silicon, cleaving the Si-CH_2 bond. The resulting anion is then quenched by trace moisture in the reaction pot (Figure 2.48). It has not proved possible to characterise the silicon-containing product of this reaction.

Figure 2.48

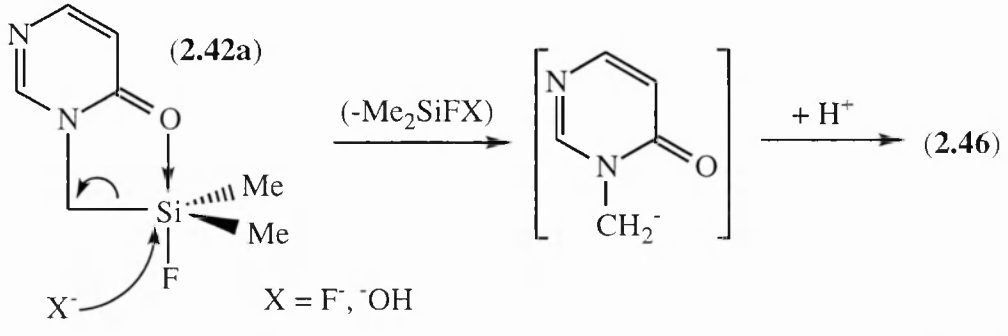

(**2.25a**) and (**2.41a**) are stable at room temperature but can be forced to undergo desilylation in concentrated (5M) aqueous sodium hydroxide over 18 hours. These reactions yield (**2.28a**) and (**2.47**) respectively.

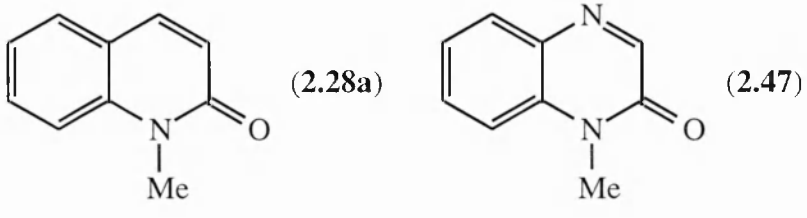

Desilylation reactions, particularly by fluoride ion, are frequently used synthetically. For example, the generation of oxazolium methyl ylides (**2.48**) by caesium fluoride (Figure 2.49).[133]

Allylsilanes react with dichlorocarbene to form dichlorocyclopropanes. These, in turn, ring open to form 2-chloro-1,3-dienes (**2.49**) when treated with caesium fluoride in DMF under reflux[134] (for example Figure 2.50).

Tetrabutylammonium fluoride (TBAF) is another common desilylating reagent. For example it can be used to desilylate 2,4,6-tris(trimethylsilyl)-1,3,5-trithianes (**2.50**)[135] as shown in Figure 2.51.

Figure 2.49

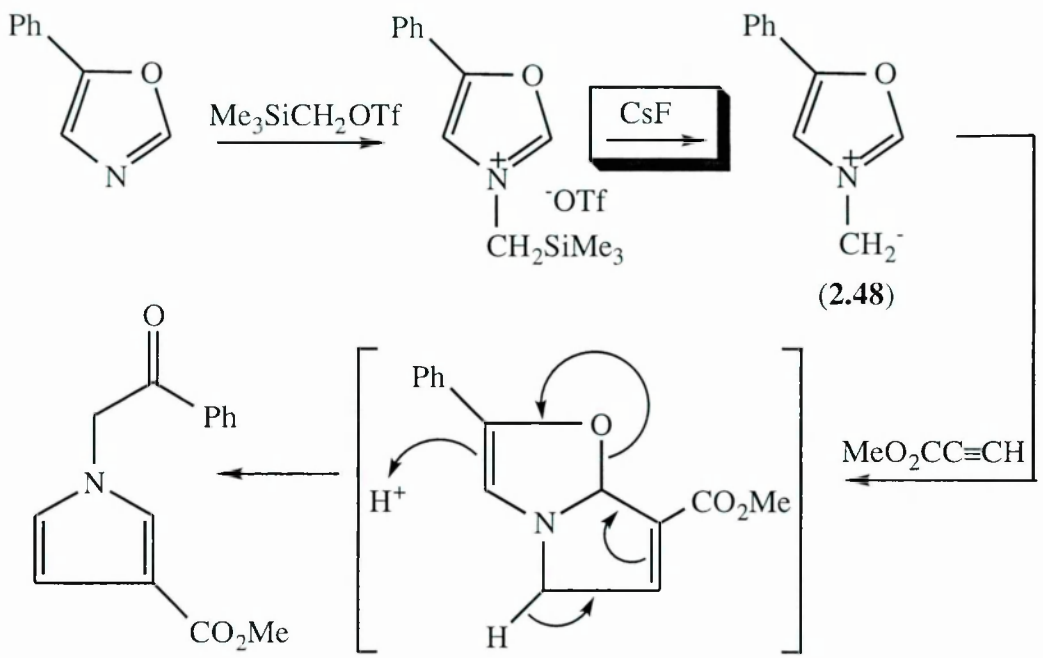

Figure 2.50

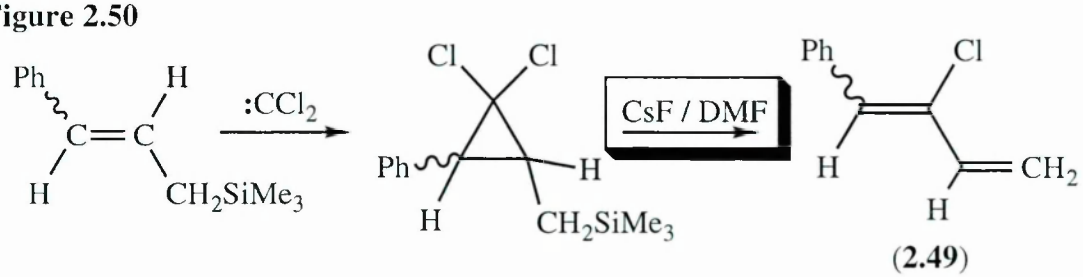

Figure 2.51

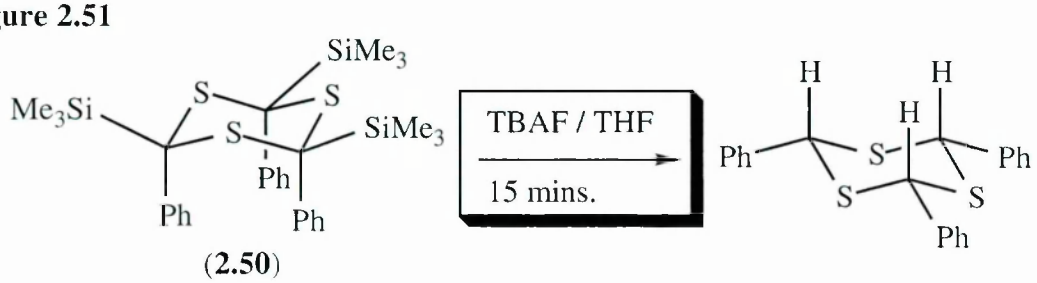

Chapter 3: Modelling nucleophilic substitution at silicon using 2-thiopyridone-based ligands.

3.1: Introduction

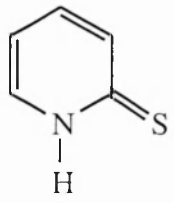

(**3.1**)

The 2-(1H)-thiopyridone ligand, (**3.1**), has a rich coordination chemistry. We will describe a variety of complexes and structural types to show the range of modes and geometries in which it coordinates to metal centres. Nickel (II) forms a particularly stable tris(2-thiopyridonato) complex (**3.2**) when tetraethylammonium tetrachloronickel (II) is reacted with (**3.1**) and sodium methoxide (Figure 3.1).[136]

Figure 3.1

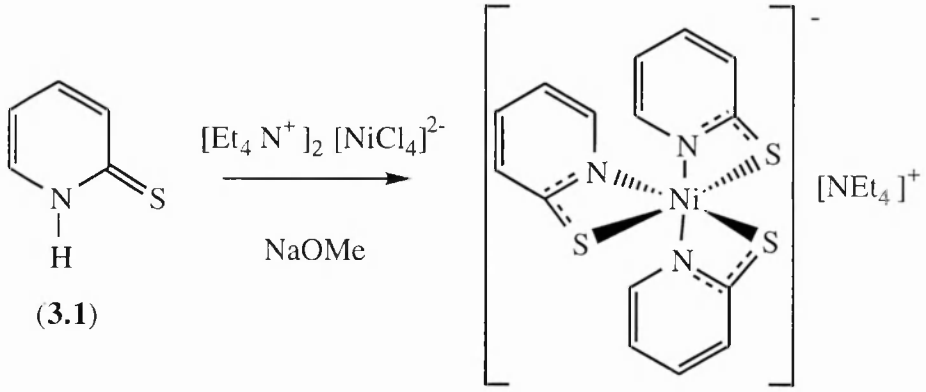

(**3.1**) (**3.2**)

The distorted octahedral nickel is isolated as its *mer* isomer and contains three four-membered rings. Each ligand has a particularly small N-Ni-S *bite* angle of about 68°. The crystal structure of the bis-chelate complex phenylbis(2-thio-pyridonato)antimony (III) (**3.3**) has been reported (Figure 3.2).[137] The pentacoordinated antimony centre has a distorted tetragonal pyramidal geometry with the phenyl group in the axial position.

Figure 3.2

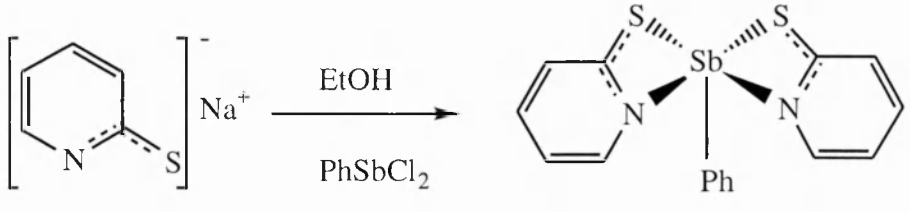

(**3.3**)

The novel bis-platinum complex (**3.4**), bridged by four 2-thiopyridone ligands is characterised by an X-ray structure by Ooi and co-workers.[138] Oxidation of Pt^{II} to Pt^{III} occurs in chloroform over several hours and complex (**3.5**) can be isolated.

(3.4)

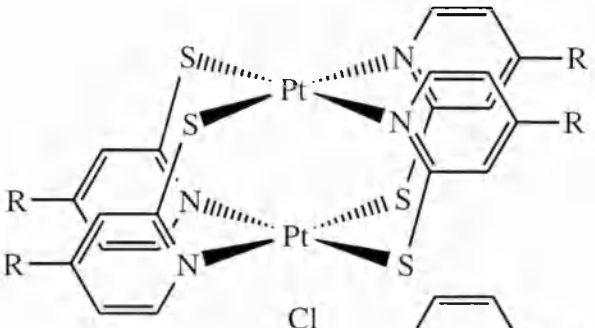

(R = H, Me)

(3.5)

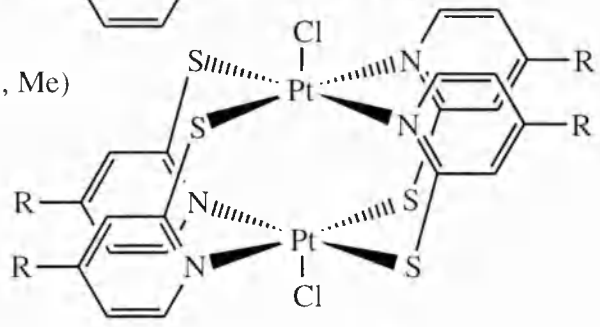

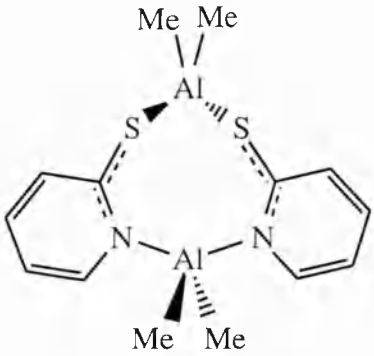

(3.6)

Complex (**3.6**) is prepared from the reaction of (**3.1**) and trimethylaluminium.[139] The unusual 'head-to-head' complex contains an eight-membered ring containing two tetracoordinate aluminiums.

Figure 3.3

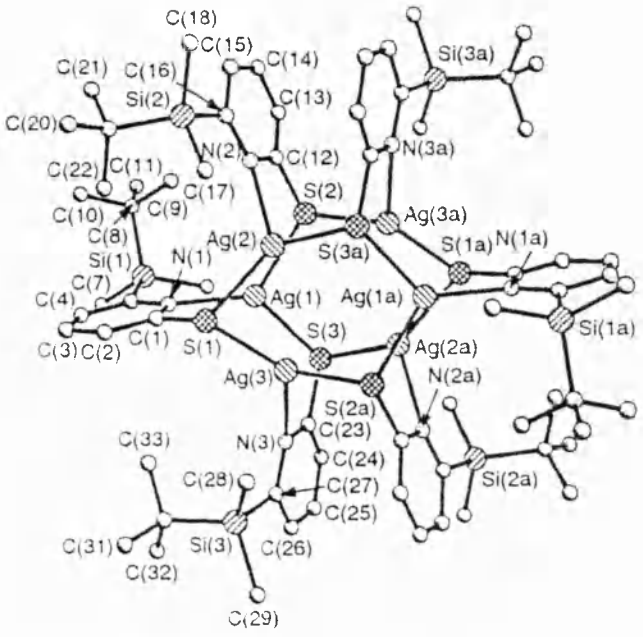

An ORTEP view of the structure of $[_{\infty}Ag(SR^{1})_{6}]$ I viewed parallel to the pseudo-three-fold axis passing through the centroids of the Ag_3S_3 rings

Compound (**3.7**) (Figure 3.3) can be obtained from the product of the electrochemical reaction of 6-(t-butyldimethylsilyl)-2-thiopyridone) in acetonitrile with a silver sacrificial anode.[140] The structure is characterised by two six-membered rings alternating between silver and sulphur, bridged by six thiopyridone ligands. Masaki *et al*[141] have reported the synthesis of (**3.8**) (Figure 3.4). The crystal structure reveals a highly distorted octahedral tin centre with two *trans* N–Sn-Cl moieties and a *cis* relationship between the chlorines.

Figure 3.4

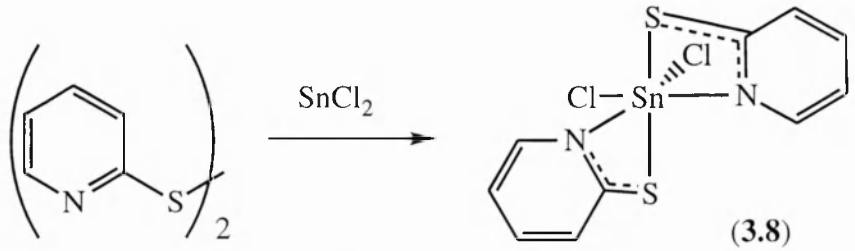

Pentacoordinated complexes (**3.9**) containing a single bidentate 2-thiopyridone ligand have been reported recently by Couce *et al* (Figure 3.5).[142] Formation of a four membered ring complex leads to considerable distortion of the trigonal bipyramidal geometry of the tin.

Figure 3.5

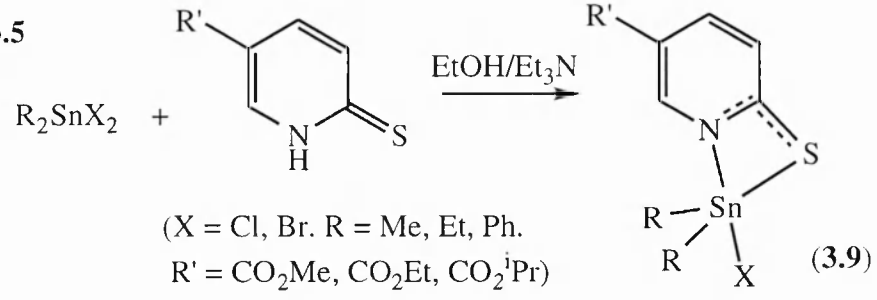

The work in this chapter focuses on the use of 2-thiopyridones as alternative ligands for modelling nucleophilic substitution at silicon in solution by NMR spectroscopy. A variety of substituted thiopyridone complexes have been synthesised in order to explore the effect of different substituents and leaving groups on the substitution being modelled.

3.2: Unsubstituted 2-thiopyridone complexes

3.2.1: Synthesis of complexes

The 2-(1H)-thiopyridone ligand (**3.1**) is a cheap, commercially available reagent and is readily converted into 2-(trimethylsilylthio)pyridine (**3.10**), the precursor for the synthesis of hypervalent silicon complexes (**3.11a-d**) (Figure 3.6).

Figure 3.6

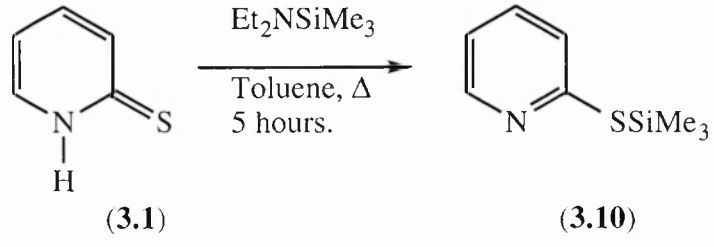

Silyl chloride (**3.11b**) and silyl bromide (**3.11c**) complexes (Figure 3.7) were prepared from the reaction of (**3.10**) with the appropriate chloro(halomethyl)dimethylsilane in dry benzene.

Figure 3.7

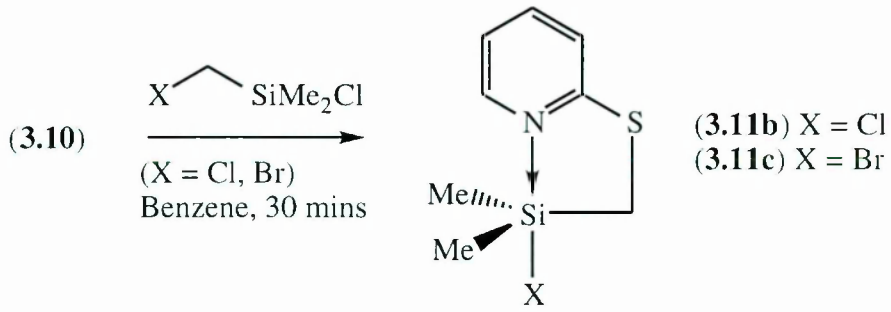

The fluoride (**3.11a**) and triflate (**3.11d**) derivatives (Figure 3.8) were obtained by reaction of (**3.11b**) with antimony trifluoride and TMS-OTf respectively.

Figure 3.8

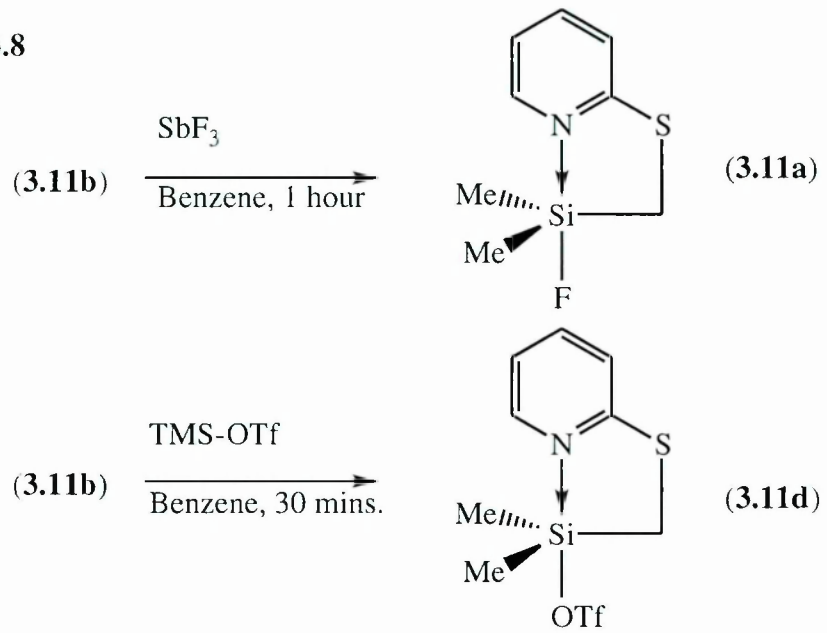

The structures of (**3.11a-d**) were found to be different from those of the pyridone complexes previously studied. All contain an S-CH_2 linkage with the pyridine nitrogen coordinating to the silicon. The NMR data for 1-methyl-2-thiopyridone (**3.12**) and 2-(methylthio)pyridine (**3.13**)[143] enable us to differentiate between N-CH_2 and S-CH_2 bonded isomers. Comparison with the observed data (for example (**3.11a**)) confirms that the structure is more like that of a *thiopyridine* than a *thiopyridone* (Figure 3.9 and Table 3.1).

Figure 3.9 **Table 3.1**

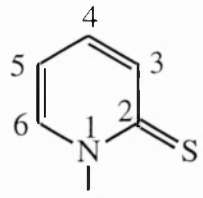

(**3.12**)

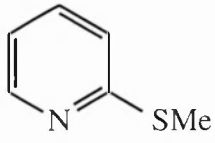

(**3.13**)

Complex	^{13}C chemical shift (/ppm)					
	C_2	C_3	C_4	C_5	C_6	CH_3
(**3.12**)	181.1	134.6	135.7	113.3	142.5	45.7
(**3.11a**)	159.2	121.5	136.1	119.3	147.7	14.0*
(**3.13**)	160.4	121.8	136.5	119.7	150.0	12.9

(* = CH_2)

Complexes (**3.11a-d**) are stable to re-arrangement to their N-CH_2 bonded isomers. For example, a $CDCl_3$ solution of (**3.11b**) remained unchanged after heating at 50°C for 5 days.

3.2.2: Synthesis of model compounds

To map the substitution of a 2-thiopyridine nitrogen at a monofunctionalised trialkyl silane we must also model *limiting* species (**3.14**) and (**3.15**). Having extensively used disiloxane-based materials as model compounds, it was decided to investigate the scope of other types of compounds for their suitability as models. In particular, the aim was to synthesise isolable, stable compounds that model 100% substitution. So far, such complexes have been species only observable in solution.

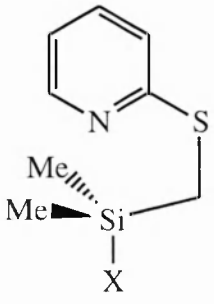

(**3.14**)

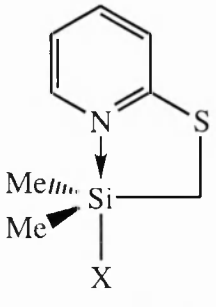

(**3.11a-d**)

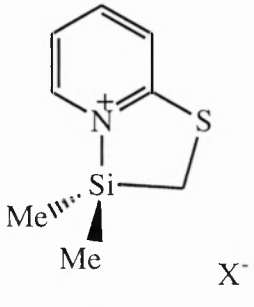

(**3.15**)

(**3.16**) was prepared as an example of (**3.14**), modelling 0% N-Si bond formation (Figure 3.10). By making X an exceptionally poor leaving group (i.e. a methyl group), it is assumed that no N–Si bonding occurs. The ^{29}Si NMR chemical shift of (**3.16**) is δ +1.9, which is consistent for a tetracoordinate silicon in a -CH_2-$SiMe_3$ environment.

Figure 3.10

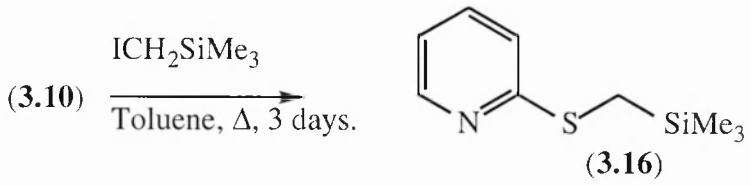

(**3.10**) (**3.16**)

Titration of (**3.16**) in $CDCl_3$ solution with equivalents of TMS-OTf did not produce any appreciable changes in either the ^1H or ^{13}C NMR spectra. Thus the alternative methyl quaternised analogue (**3.17**) was prepared (Figure 3.11). This compound is an example of (**3.15**) and is a model for 100% N-Si bond formation. It is assumed that quaternisation using a methyl group is a suitable mimic for a trimethylsilyl group in the same position.

Figure 3.11

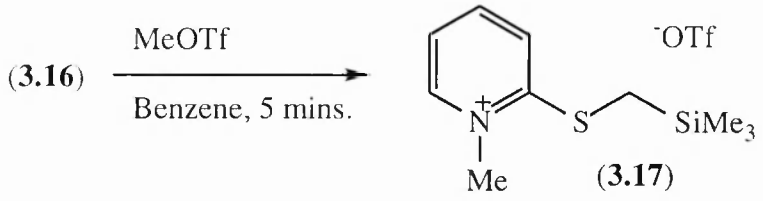

(**3.16**) (**3.17**)

Based on previous experience, it is also assumed that there is a linear relationship between the percentage N-Si bond formation and the change in the chemical shifts in ^{13}C NMR spectra during 'substitution'.

3.2.3: Solution calculations

The ^{29}Si and relevant ^{13}C NMR chemical shifts for the models (**3.16**) and (**3.17**) and complexes (**3.11a-d**) are displayed in Table 3.2. The chemical shifts of C_2 and C_6, being adjacent to the nitrogen, are those most likely to be affected by the use of the N-Me derivative, (**3.17**), rather than the preferred N-$SiMe_3$ species. Therefore only C_3, C_4 and C_5 ring carbon data are used to calculate the percentage N-Si bond formation of each complex; the method of calculation used is otherwise identical to that detailed in Chapter 2. On the basis of the calculated percentage N-Si bond formation, the change in ^{13}C shifts is plotted in Figure 3.12.

Unfortunately complex (**3.17**) is not the most ideal choice of model. This is exacerbated by the fact that the series of compounds do not give rise to large changes in ring ^{13}C chemical shifts, thus also amplifying experimental errors. For example, small temperature changes cause significant variation to the positions of individual resonances (see Section 3.7).

Table 3.2

Compound	^{13}C chemical shift (/ppm)					$\delta\ ^{29}Si$ (/ppm)	% N-Si*
	C_2	C_3	C_4	C_5	C_6		
(**3.16**)	161.4	121.3	135.6	118.9	149.2	(1.9)	0
(**3.11a**)	159.2	121.5	136.1	119.3	147.7	17.0	8
(**3.11b**)	159.6	122.3	138.6	120.1	144.5	-19.4	36
(**3.11c**)	162.7	123.3	141.2	121.2	143.6	-0.8	69
(**3.11d**)	164.4	123.6	143.3	122.3	143.9	40.6	92
(**3.17**)	163.1	124.6	143.5	122.0	146.7	(3.5)	100

(* Based on C_3, C_4 and C_5 only)

Figure 3.12

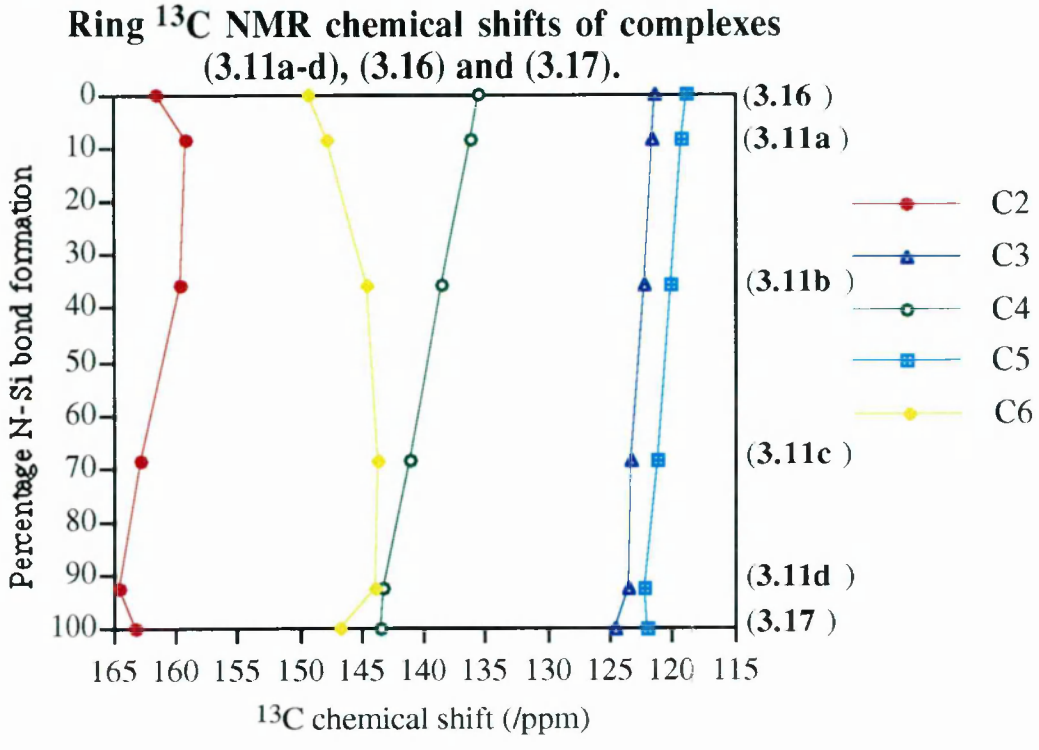

3.3: 5-Trifluoromethyl substituted 2-thiopyridone complexes

3.3.1: Synthesis of complexes

A series of 5-trifluoromethyl substituted complexes (**3.20a-d**) were prepared to make a direct comparison with the series (**3.11a-d**). The trimethylsilyl derivative, (**3.19**), was prepared from 5-trifluoromethyl-2-(1H)-thiopyridone (**3.18**), a commercially available material. Fluoride (**3.20a**), chloride (**3.20b**), bromide (**3.20c**) and triflate (**3.20d**) complexes were prepared in an identical manner to their unsubstituted analogues (**3.11a-d**).

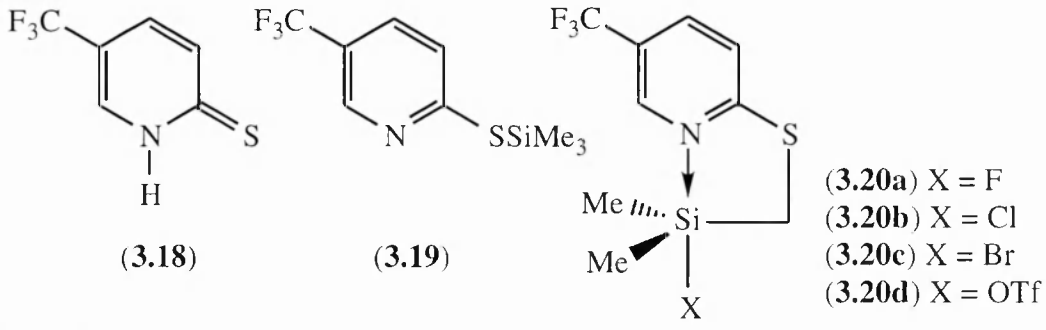

(**3.18**) (**3.19**)

3.3.2: Synthesis of model compounds

Compounds (**3.21**) and (**3.22**), the 5-trifluoromethyl analogues of (**3.16**) and (**3.17**) respectively, were used as models of the *limiting* structures. They were prepared from (**3.19**) as before.

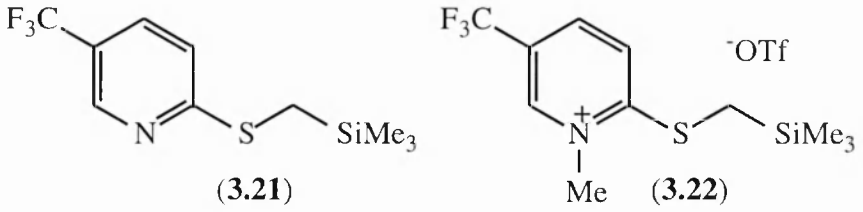

(**3.21**) (**3.22**)

3.3.3: Solution calculations

The important ^{13}C and ^{29}Si NMR data for (**3.20a-d**), (**3.21**) and (**3.22**) are presented in Table 3.3. On the basis of the C_3, C_4 and C_5 ring carbon chemical shifts, the percentage N-Si bond formation was calculated for each of the compounds (**3.20a-d**). This data is plotted in Figure 3.13 against the ^{13}C chemical shifts.

Table 3.3

Compound	^{13}C chemical shift (/ppm)					$\delta\ ^{29}Si$ (/ppm)	% N-Si*
	C_2	C_3	C_4	C_5	C_6		
(**3.21**)	166.5	120.9	132.2	122.0	146.2	(2.1)	0
(**3.20a**)	164.5	121.3	132.5	122.3	145.6	26.0	7
(**3.20b**)	164.3	121.6	132.9	122.6	145.2	19.2	16
(**3.20c**)	164.5	122.0	133.7	122.7	143.5	7.3	24
(**3.20d**)	167.2	123.7	137.3	124.6	140.5	7.6	77
(**3.22**)	168.3	125.8	139.1	124.6	144.5	(3.7)	100

(* Based on C_3, C_4 and C_5 only)

Figure 3.13

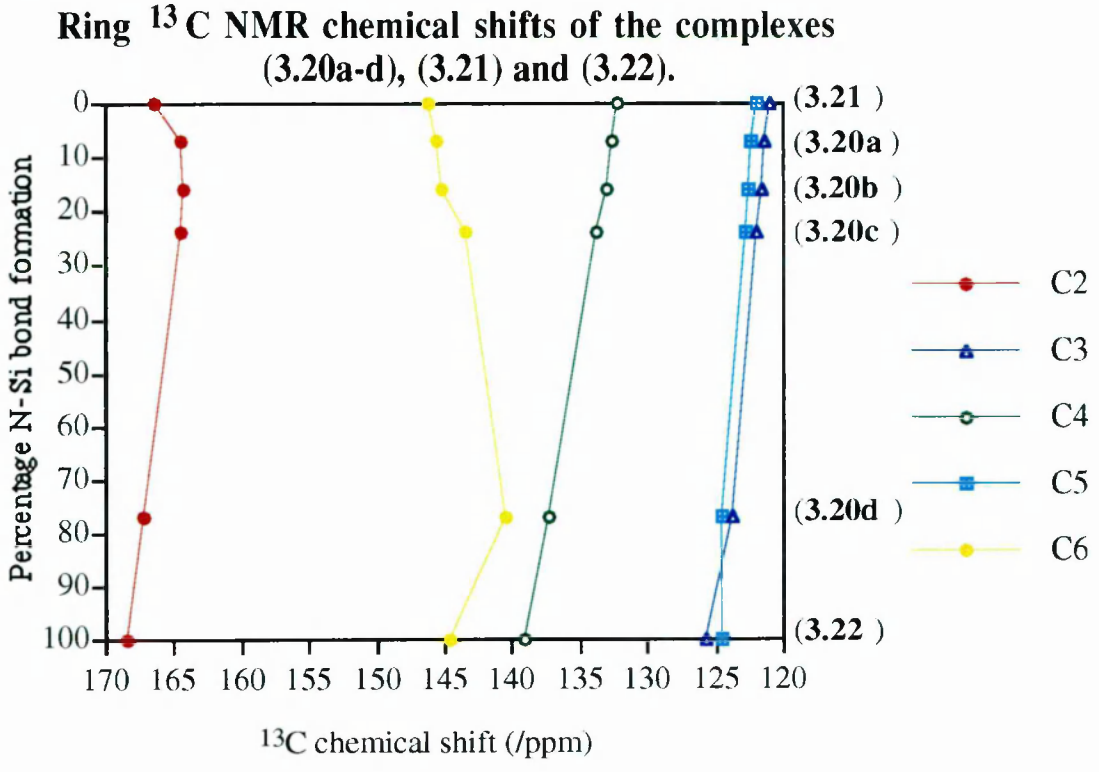

3.4: A two-dimensional map of nucleophilic substitution at silicon as modelled by 2-thiopyridone complexes (3.11a-d) and (3.20a-d)

Complexes (**3.11a-d**) and (**3.20a-d**), although containing different ring substituents, relate to the same basic model of substitution - that of a pyridine nitrogen at an R_3SiX organosilane. By converting the ^{29}Si chemical shifts into values of *percentage pentacoordination*, a plot of how the coordination state of the silicon changes with percentage N-Si bond formation can be drawn (Table 3.4 and Figure 3.14). The limit of 100% (δ -35) pentacoordination is based on the variable-temperature NMR study on complex (**3.11b**) reported in Sections 3.7.1 and 3.7.4. The limit of 0% pentacoordination for a completely 'unsubstituted' silicon, (**3.14**), is chosen by the chemical shift of the tetracoordinate silicon of (**1.38**) (δ 28). Since we do not have a suitable silicon-containing model of (**3.15**), the thiopyridine complex with the most down-field ^{29}Si chemical shift, that of complex (**3.11d**) (δ 40.6), shall be used instead as the limiting value. Compounds (**3.16**) / (**3.21**) and (**3.17**) / (**3.22**) are included in the plot by setting their percentage pentacoordination values to 0%. For (**3.16**) / (**3.21**) this must be done because of the substituent effect on the ^{29}Si NMR chemical shift. For (**3.17**) / (**3.22**) it is because a silicon atom is not involved in the quaternisation of the pyridine nitrogen. Which 0%

pentacoordination limit is used in a calculation depends on the percentage nucleophile-silicon bond formation of the given complex (See Chapter 2, page 47).

Table 3.4

Complex	% N-Si	δ ^{29}Si (/ppm)	% pentacoordination
(3.16) / (3.21)	0	(1.9 / 2.1)	0
(3.20a)	7	26.0	3
(3.11a)	8	17.0	17
(3.20b)	16	19.2	14
(3.20c)	24	7.3	33
(3.11b)	36	-19.4	75
(3.11c)	69	-0.8	55
(3.20d)	77	7.6	44
(3.11d)	92	40.6	0
(3.17) / (3.22)	100	(3.5 / 3.7)	0

Figure 3.14

A two-dimensional map of extent of pentacoordination as a function of N-Si bond formation for complexes (3.11a-d) and (3.20).

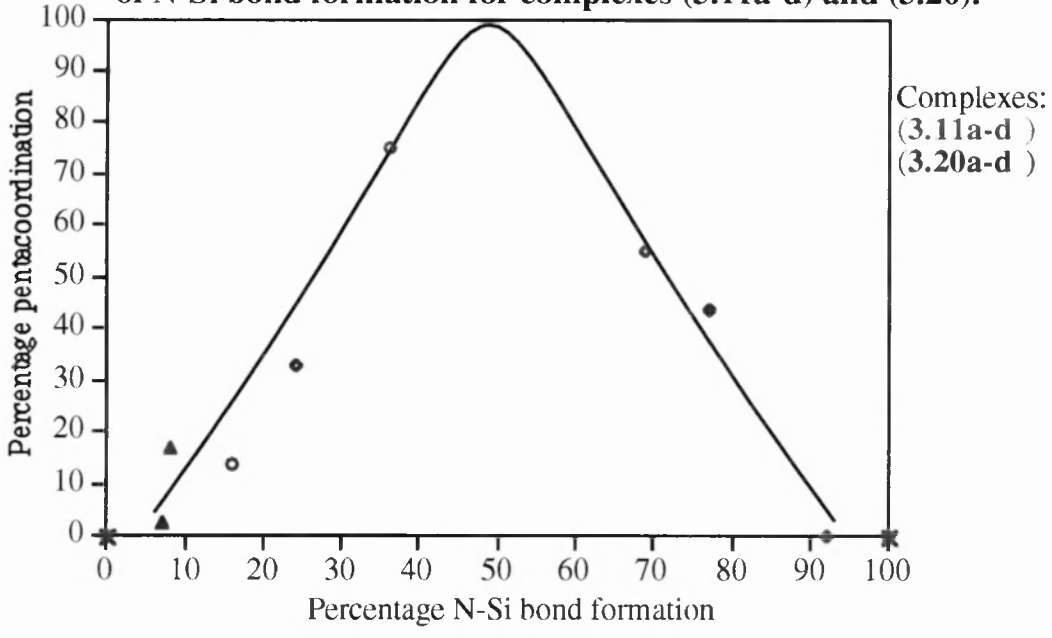

The plot outlines the characteristic transition from tetracoordination, through penta, then back to tetracoordination. The maximum of pentacoordination is predicted to occur around 50% N-Si bond formation. For both series, the order of measured N-Si bond formation mirrors the order of increasing leaving group ability of X. The effect of the strong inductively electron-withdrawing 5-trifluoromethyl group on the nucleophilicity of the pyridine nitrogen is readily apparent from a comparison (Table 3.5) of the percentage N-Si bond formation for complexes (**3.20a-d**) with those of unsubstituted ring complexes

(**3.11a-d**). In each case, for a given leaving group, the strength of the N-Si bond is less in (**3.20**) than in (**3.11**).

Table 3.5

Ring type	Percentage N-Si bond formation			
	Fluoride (**a**)	Chloride (**b**)	Bromide (**c**)	Triflate (**d**)
Unsubstituted (**3.11**)	8	36	69	92
5-CF_3 (**3.20**)	7	16	24	77

Such is the electron-withdrawing strength of the 5-CF_3 group on the nitrogen, that in the sequence (**3.20a**) - (**3.20b**) - (**3.20c**) there is little increase in N-Si bond formation with improving leaving group. Only in triflate complex (**3.20d**) does strong N-Si bonding occur. The shape of Figure 3.14 is very similar in outline to that found for the oxygen 'nucleophiles' pyridone and quinolines 'substituting' at silicon (Figure 2.19). Figure 3.15 is a combination of these plots.

Figure 3.15

A combined plot of the relationship between nucleophile-silicon bonding and percentage pentacoordination for thiopyridine, pyridone and quinoline complexes.

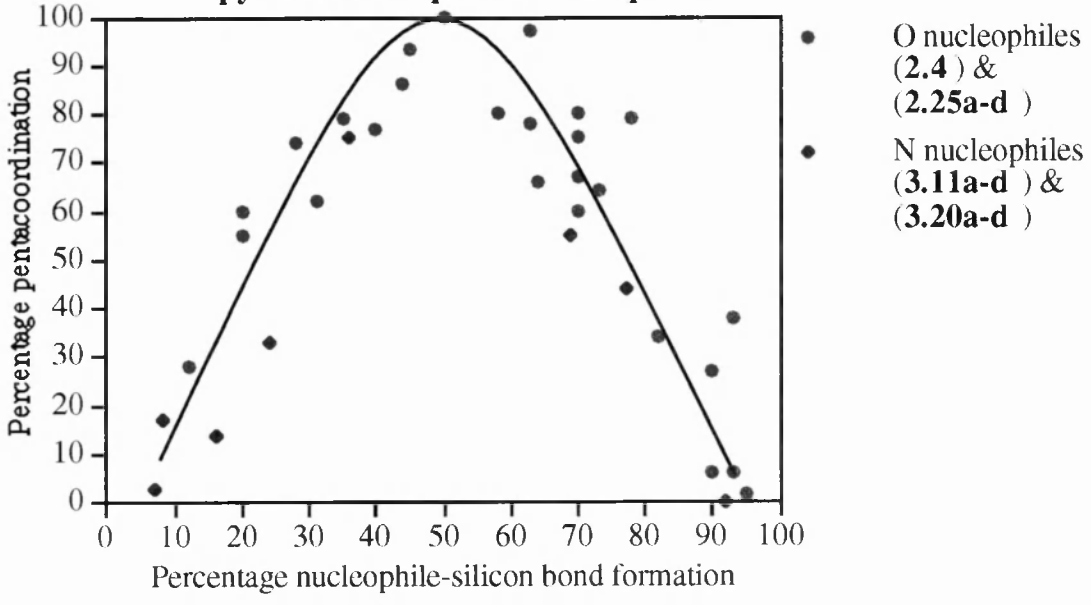

The data points for the thiopyridine complexes fit well on the curve. Deviations from the line are related to the formation of 'loose' or 'tight' hypervalent complexes. The concept is discussed later (Figure 3.25).

3.5: Di- and tri-chloro-silyl complexes

The 'electrophilicity' of the silicon may be increased progressively in thiopyridine complexes by the step-wise replacement of methyl groups by chlorines. This will affect the percentage of N–Si bond formation observed, the change in which may be observed by ^{13}C NMR spectroscopy. Di- (**3.23**) and tri- (**3.24**) chloro-complexes are synthesised from (**3.10**) using the appropriate chloro(chloromethyl)silane (Figure 3.16).

Figure 3.16

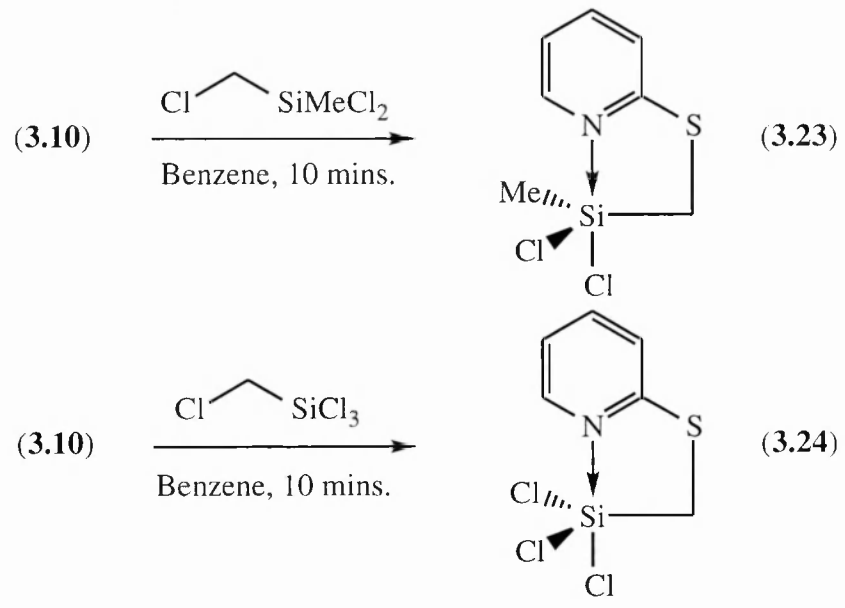

If the replacement of methyl groups by chlorines only affects the ring ^{13}C NMR chemical shifts through a change in the degree of N–Si bond formation, then we may calculate the degree of N-Si bond formation for each complex as before. We then have the series (**3.16**)-(**3.11b**)-(**3.23**)-(**3.24**) in which (**3.16**) is assigned as the lower limit of 0% N-Si bond formation. (**3.17**) remains a valid model for 100% N-Si bond formation. Table 3.6 shows the key NMR data and calculated percentage N-Si bond formation for each complex. C_2 and C_6 data are ignored in the calculations for the reason previously noted.

Table 3.6

Compound	^{13}C chemical shift (/ppm)					$\delta\ ^{29}Si$ (/ppm)	% N-Si*
	C_2	C_3	C_4	C_5	C_6		
(**3.16**)	161.4	121.3	135.6	118.9	149.2	(1.9)	0
(**3.11b**)	159.6	122.3	138.6	120.1	144.5	-19.4	36
(**3.23**)	157.5	122.8	139.9	120.5	144.3	-45.8	51
(**3.24**)	155.8	122.8	140.5	120.5	144.8	-59.1	53
(**3.17**)	163.1	124.6	143.5	122.0	146.7	(3.5)	100

(* Based on C_3, C_4 and C_5 only)

The pattern of increasing N-Si bond formation mirrors the increase in 'electrophilicity' of the silicon as more chlorines are attached. The change in the ^{29}Si NMR shifts are less quantifiable since the observed values are the combination of different degrees of hypercoordination and the differing shielding effects of the methyl and chlorine groups. Complex (**3.24**) unexpectedly shows little additional N-Si bonding over (**3.23**). Therefore, presumably, the 'electrophilicity' of silicon in these complexes is relatively similar.

3.6: 6-methyl substituted 2-thiopyridone complexes

3.6.1: Synthesis of complexes

Unlike (**3.1**) and (**3.18**), the 6-methyl analogue, (**3.26**), is not commercially available. It may instead be prepared from 6-methyl-2-(1H)-pyridone (**3.25**) and phosphorous pentasulfide. Trimethylsilylation of (**3.26**) yields (**3.27**) (Figure 3.17).

Figure 3.17

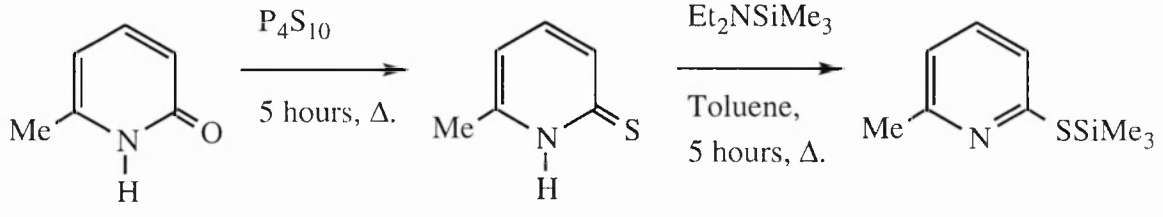

(**3.25**) (**3.26**) (**3.27**)

A series of 6-methyl substituted complexes (**3.28a-d**) were prepared using analogous routes and reagents to those previously described. The NMR spectra reveal a return to the 'pyridone' type structure characterised by an N-CH_2 linkage and S-Si intramolecular coordination. The ^{13}C NMR spectra display a resonance in the range δ 46.4 to 50.4, which is more typical of an N-CH_2 than an S-CH_2 (approximately δ 15). The

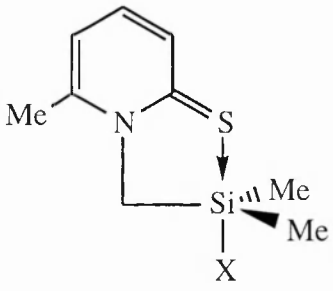

(**3.28a**) X = F
(**3.28b**) X = Cl
(**3.28c**) X = Br
(**3.28d**) X = OTf

spectra often also show a particularly low field C_2 resonance (δ 179.1 for (**3.28a**)). This is more characteristic of a C=S rather than a C-S (about δ 158) in this ring system.[143] The ^1H spectra similarly show a resonance at approximately δ 4.4 (N-CH_2) whereas δ 2.7 would be more typical for an S-CH_2 in this environment. Attempts to promote rearrangement of (**3.28b**) to the S-CH_2 form were unsuccessful after 6 days warming at 50°C in $CDCl_3$ solution. Hypervalent complexes containing S-Si intramolecular coordination are relatively rare. (**3.29**) is a dithiocarbamate example prepared by Voronkov *et al.*[144]

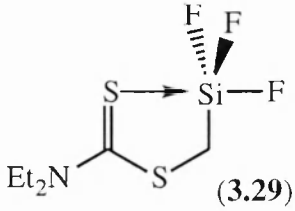

(**3.29**)

For comparison, a 4-methyl-2-(1H)-thiopyridone, (**3.30**), based complex was synthesised. (**3.30**) was prepared by a similar reaction to that used to prepare (**3.26**). Silylation of (**3.30**) allowed (**3.31**) to be isolated quantitatively and reaction of (**3.31**) with chloro(chloromethyl)dimethylsilane afforded the single complex (**3.32**). The S-CH_2 bound structural type was assigned from ^1H and ^{13}C NMR evidence.

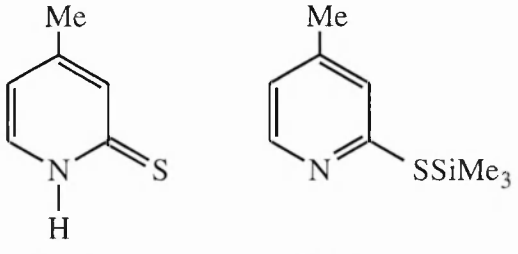

(**3.30**)

(**3.31**)

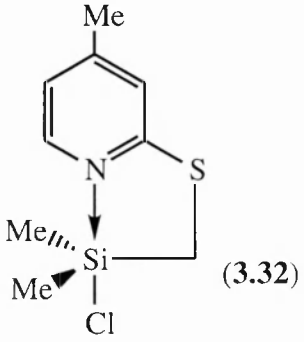

(**3.32**)

The possible mechanisms and reasons for the choice of structure adopted by each ligand shall be developed in Section 3.6.2.

3.6.2: Mechanistic routes for the formation of pyridone and thiopyridone complexes

Kalikhman *et al*[145] have studied the mechanism of the reaction of N-trimethylsilyl-amides and lactams (**3.33**) with chloro(chloromethyl)dimethylsilane and proposed the following scheme for their formation (Figure 3.18). The N-trans-silylation species (**3.34**) and O-alkylation products (**3.35**) were observed under kinetic (low temperature) conditions

by NMR spectroscopy. Under thermodynamic (room temperature) conditions, only the isomerised product (**3.36**) was observed.[146] Compound (**3.36**), was the only species isolable from the reactions.

Figure 3.18

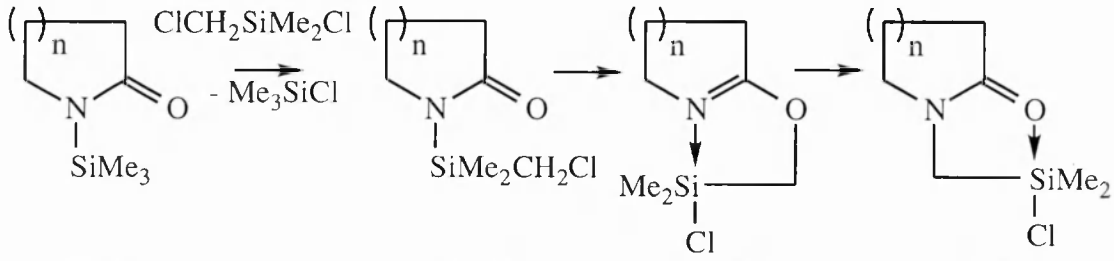

(**3.33**) (**3.34**) (**3.35**) (**3.36**)

A similar investigation of the reaction of chloro(chloromethyl)dimethylsilane with N-trimethylsilylthiolactams (**3.37**)[147] gave only N-trans-silylated, (**3.38**), and S-silylmethylated products (**3.39**). Of these only the latter was isolable (Figure 3.19). Attempts to isomerise (**3.39**) to the N-silylmethyl form were unsuccessful.

Figure 3.19

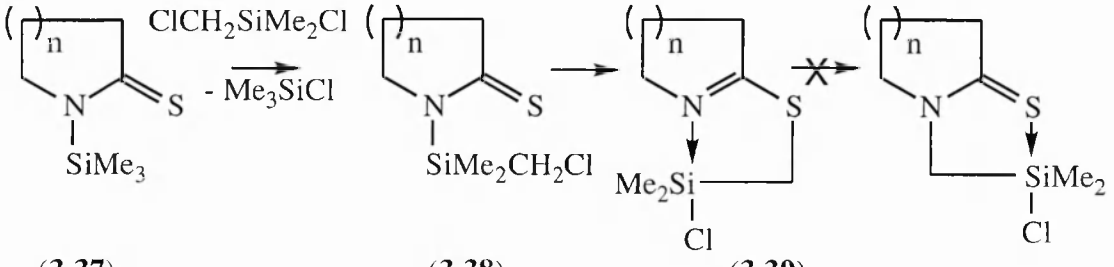

(**3.37**) (**3.38**) (**3.39**)

Figure 3.20 summarises the possible routes for the formation of pyridone and thiopyridone complexes. When Y = O it is known that species of type **A** and **B** exist in equilibrium.[148] However for thiopyridones, not enough is known about the nature of any equilibria or transition state structures to be able to fully describe the interplay of the different mechanisms involved.

As 4-methyl and 6-methyl substituted pyridine rings are electronically similar, it is unlikely that the distinction between mechanisms leading to either N-CH_2 or S-CH_2 structures is electronically controlled. The more likely factor controlling the mechanism is that of the steric effect of the methyl group. The steric argument for a switch in mechanism is based on the methyl group in the 6-position inhibiting the approach of the chlorosilane moiety to the pyridine nitrogen more than a hydrogen. This allows what might otherwise be a minor reaction pathway to take prominence and so lead to the alternative isomer.

Figure 3.20

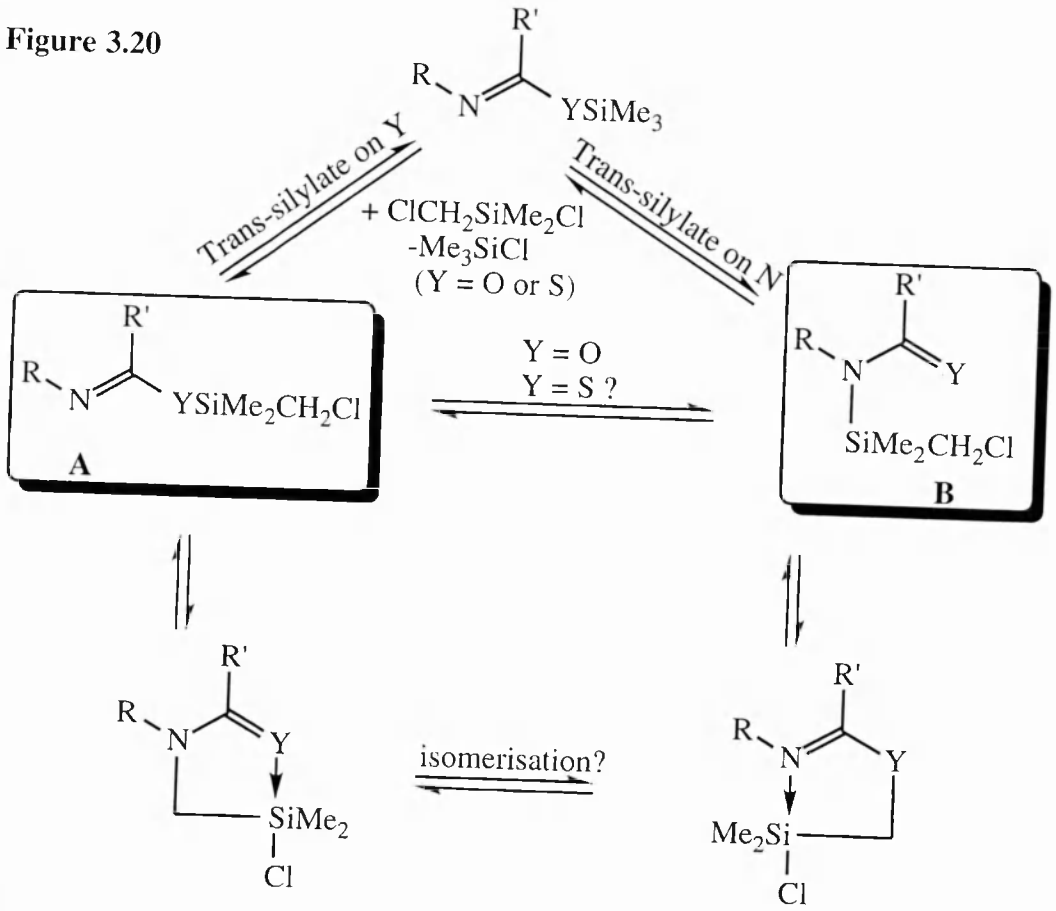

3.6.3: The desilylation of (3.28a)

Figure 3.21

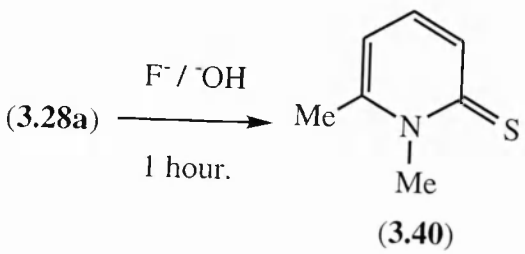

(3.40)

(**3.28a**) is susceptible to desilylation by either fluoride ion or aqueous hydroxide ion attack, similar to the silyl-fluoride complexes of the quinoline and related ligands (**2.25a**), (**2.41a**) and (**2.42a**) (Chapter 2). This results in the isolation of 1,6-dimethyl-2-thiopyridone (**3.40**) (Figure 3.21). This product was obtained if (**3.28a**) was deliberately exposed to either ion in solution during the reaction or work-up. The silicon-containing co-product was not isolated.

3.6.4: Preparation of model complexes and mapping

Initially, the isolation of (**3.40**) was an unwanted side reaction in the preparation of (**3.28a**), however, (**3.40**) was found later to be a suitable model compound for 0% S-Si bond formation. This was subsequently prepared quantitatively by deliberate decomposition of (**3.28a**) in aqueous sodium hydroxide. By treatment of (**3.40**) with methyl triflate, compound (**3.41**) was obtained. The ring ^{13}C NMR chemical shifts of (**3.41**) are a suitably characteristic model of 100% S-Si bond formation (Figure 3.22).

Figure 3.22

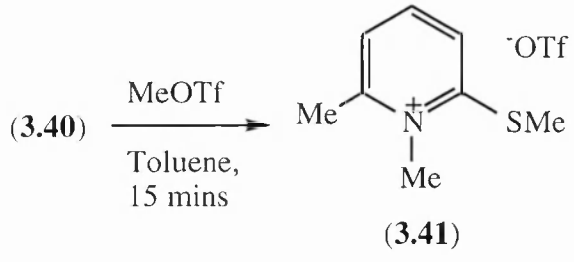

The key NMR data for complexes (**3.28a-d**) and models (**3.40**) and (**3.41**) are presented in Table 3.7 along with the calculated values of percentage S-Si bond formation.

Table 3.7

Compound	^{13}C chemical shift (/ppm)					$\delta\ ^{29}Si$	% S-Si*
	C_2	C_3	C_4	C_5	C_6		
(**3.40**)	181.4	133.6	133.4	115.1	149.4	-	0
(**3.28a**)	179.1	132.7	133.0	115.5	148.7	27.0	5
(**3.28b**)	176.4	130.5	134.6	116.6	149.9	-0.1	21
(**3.28c**)#	174.8	131.5	136.7	119.4	153.1	? +	34
(**3.28d**)§	163.9	126.4	143.4	124.6	158.4	26.7	91
(**3.41**)	161.7	122.2	142.8	124.1	156.4	-	100

(**Notes:** * Based on all ring carbons except C_6. # Sample in CD_3OD. + Attempts to observe a ^{29}Si resonance for this compound failed despite varying the solvent (CD_3CN / $CDCl_3$ / CD_3OD) and using different pulse delays (10-60 sec). It was therefore assumed that the signal was significantly broadened into the baseline. § Sample in CD_3CN.)

The chemical shift changes are much larger than for either (**3.11a-d**) or (**3.20a-d**) series of complexes. This allows all ring carbons, except C_6, to be used for the percentage S-Si bond formation calculations. Two of the complexes have C_6 chemical shifts outside the range defined for the chemical shift of C_6 in the models (**3.40**) and (**3.41**). The inclusion of the C_6 data in the calculations would lead to distortion of the figures and thus have been ignored. The ^{13}C data are plotted (Figure 3.23) against the percentage S-Si bond formation. Values of percentage pentacoordination were calculated for (**3.28a/b/d**)

(Table 3.8) on the basis of the previously defined limiting values (Section 3.4). Since the effect of a donor sulfur in a 100% pentacoordination complex is not known, a value of δ -35 shall be assumed as a good approximation.

Figure 3.23

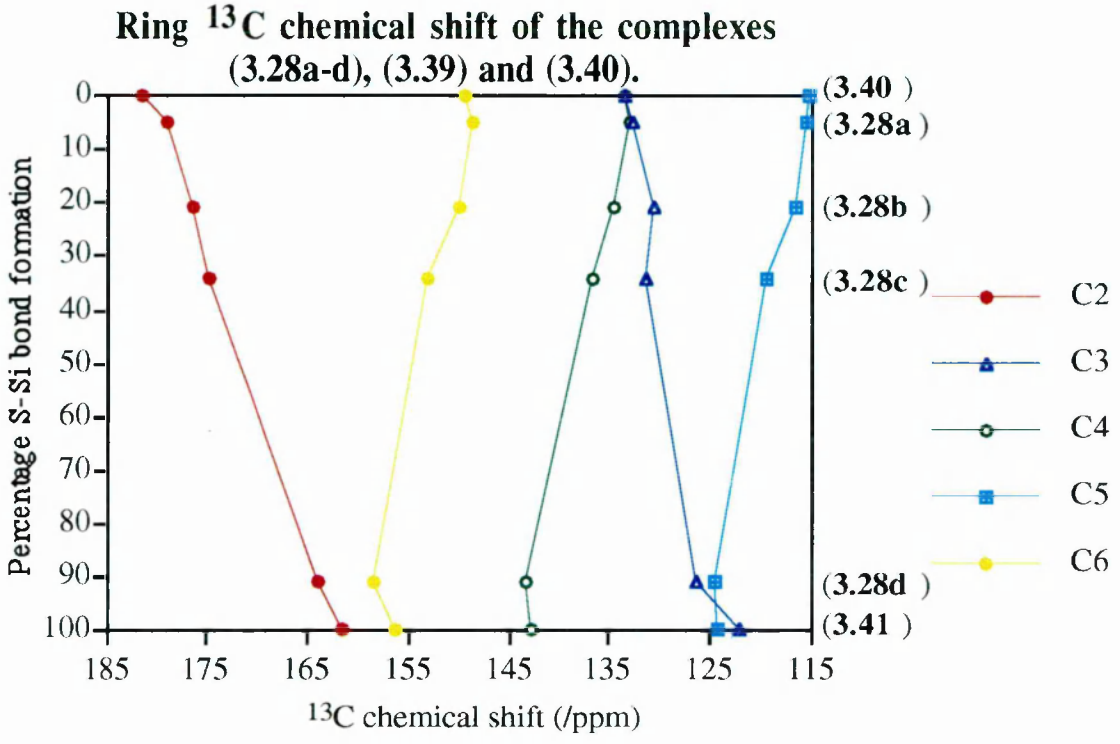

Table 3.8

Percentage pentacoordination		
(3.28a)	**(3.28b)**	**(3.28d)**
2	45	19

The fact that we have not been able to observe the ^{29}Si resonance for (**3.28c**) may be related to the NMR solvent in which the compound is soluble, methanol-d_4. The compound is not appreciably soluble in any other common NMR solvent and is the only complex analysed in methanol-d_4. It is likely that there is some interaction of the silicon with the methanol that broadens the ^{29}Si resonance. However, if the solvent were hydrolysing the complex, a resonance for the hydrolysis product would be expected, which was not observed.

We can directly compare (**3.28a-d**) with their analogous 6-methyl-2-pyridone complexes (Table 3.9).[149]

Table 3.9

Complex type	Percentage nucleophile-Si bond			
	Fluoride (**a**)	Chloride (**b**)	Bromide (**c**)	Triflate (**d**)
6-Me pyridone	40	70	72	90
6-Me thiopyridone (**3.28**)	5	21	34	91
5-CF_3 thiopyridone (**3.20**)	7	16	24	77

The data generally confirm that oxygen is a harder 'nucleophile' than sulfur, giving rise to stronger nucleophile-silicon bonds for a given leaving group. With the best 'leaving group' (triflate), the formation of a strong nucleophile-silicon bond depends less on the nature of the 'nucleophile' and more on the high 'electrophilicity' of the silicon centre. The change of percentage nucleophile-silicon bond formation with changing leaving group for compounds (**3.28a-d**) has a similar pattern to compounds (**3.20a-d**). The nucleophilicity of the sulfur in (**3.28a-d**) and nitrogen in (**3.20a-d**) are therefore comparable.

The percentage nucleophile silicon bond formation for all the complexes we have synthesised (thiopyridine (**3.11a-d**), (**3.20a-d**), (**3.28a/b/d**) and quinoline (**2.25a-d**)) and their respective percentage pentacoordinations are plotted in Figure 3.24 together with the data for the pyridones (**2.4**).

Figure 3.24

A combined two dimensional map of the extent of pentacoordination as a function of nucleophile-silicon bond formation for quinoline, pyridone (O nucleophile) and thiopyridone (N and S nucleophiles) complexes.

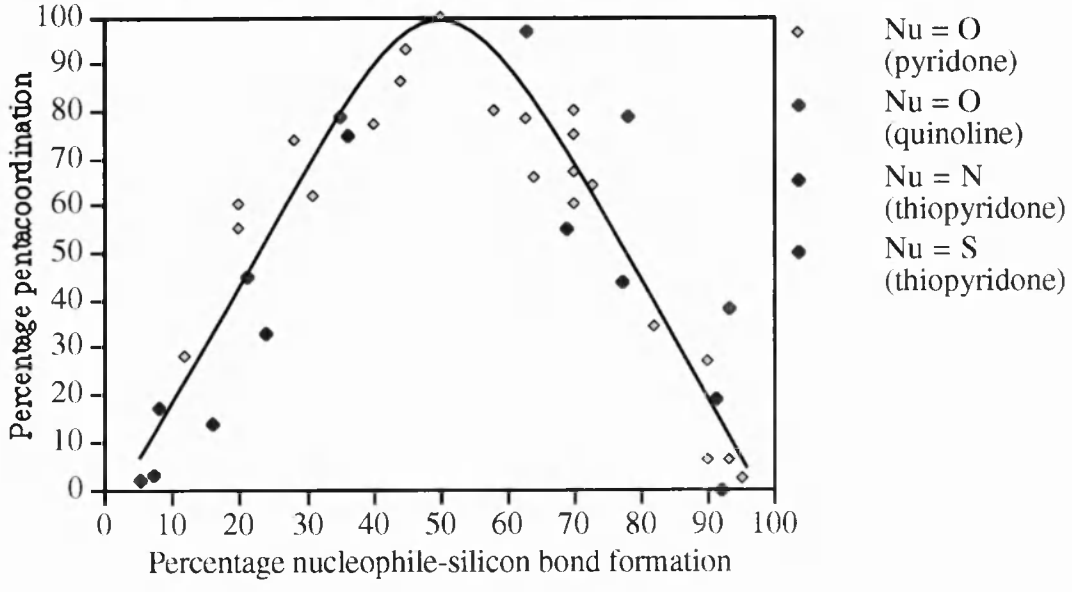

Deviations from the line are the result of using a variety of 'nucleophiles' and 'leaving groups' used to model the generalised S_N2 substitution. The deviations relate to the formation of 'loose' or 'tight' hypervalent structures. For example (Figure 3.25) a trigonal-bipyramidal complex may have the two axial groups relatively close to (*tight*, **A**) or relatively far away (*loose*, **B**) from the silicon. This means that complexes representing the same stage of 'substitution', e.g. maximum pentacoordination, can give rise to different extents of nucleophile-silicon bond formation. Otherwise, the data for the complexes fit together well on a single curve. The maximum extent of pentacoordination occurs, regardless of the specific 'nucleophile', at 50% ± 10% nucleophile-silicon bond formation. The 'rate' of *fall-off* of pentacoordination with percentage nucleophile-Si bond formation is the same either side of the maxima of pentacoordination.

Figure 3.25

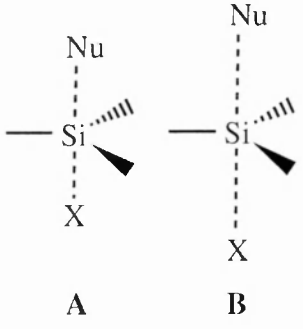

The 'nucleophilicity' of the ligands we have used in Chapters 2 and 3 may be compared using percentage pentacoordination data, and, where available, percentage nucleophile-silicon bond formation data (Table 3.10). The ligands are ordered for the silyl-chloride complexes by decreasing 'nucleophilicity'. The ordering was decided firstly from % nucleophile-Si bond formation data and secondly from % pentacoordination data.

Table 3.10

Chloro- complex...	$\delta\ ^{29}Si$ (/ppm)	% Nu-Si bond f'n	% Pentacoord'n
Quinoline (**2.25b**)	-38.3	63	97
2-Pyridone (**2.12b**)	-41.1	50	100
2-Pyrimidone (**2.43**)	-33.7	n/c	91
2-Quinoxalinone (**2.41b**)	-27.1	n/c	81
2-Thiopyridine (**3.11b**)	-19.4	36	75
4-Pyrimidone (**2.42b**)	-16.7	n/c	66
6-Me Thiopyridine (**3.28b**)	-0.1	21	45
5-CF_3 Thiopyridine (**3.20b**)	19.2	16	14

(n/c = Not calculated)

Oxygen donor ligands are generally more 'nucleophilic' than nitrogen or sulfur ones. The 'nucleophilicity' of both O and N donor ligands is significantly curtailed when strong electron withdrawing groups or atoms on the aromatic ring.

3.7: Variable-temperature NMR studies of 5-coordinate thiopyridine complexes

The expansion of the coordination sphere of silicon is often thermodynamically favourable. In contrast, 5-coordinate carbon transition states are potential energy maxima and are rarely observed. The variable-temperature NMR study by Kummer *et al*[115] of silyl-pyridone complex (**2.12b**) showed that the lower the temperature, the greater the percentage of Si-O bond formation in the complex. On this basis, nucleophilic substitution may be modelled by variable-temperature, multi-nuclear NMR spectroscopy of single compounds, giving a slightly different structure at each temperature.

3.7.1: Unsubstituted 2-thiopyridine complex (3.11b)

A deuterochloroform solution of the chloride complex (**3.11b**) was analysed by ^{13}C and ^{29}Si NMR spectroscopy at temperatures from -50°C to +50°C in 10°C intervals. It was assumed that the ^{13}C NMR shifts of the models (**3.16**) and (**3.17**) are not significantly temperature dependant (as later assumed for the other series'). The percentage N-Si bond formation at each temperature was calculated in the same way as for the series (**3.11a-d**) (using C_3, C_4 and C_5 data sets). Selected NMR data and results of the calculations are presented in Table 3.11.

Table 3.11

Temperature (/°C)	^{13}C chemical shift (/ppm)					$\delta\ ^{29}Si$ (/ppm)	% N-Si*
	C_2	C_3	C_4	C_5	C_6		
50	159.6	122.3	137.9	119.9	145.6	-8.7	30
40	159.6	122.3	138.1	120.0	145.2	-12.6	33
30	159.6	122.3	138.3	120.0	144.9	-16.4	33
20	159.6	122.3	138.6	120.0	144.5	-19.4	36
10	159.6	122.3	138.8	120.1	144.3	-22.4	37
0	159.6	122.3	138.9	120.2	144.0	-24.8	38
-10	159.6	122.4	139.1	120.2	143.8	-27.0	40
-20	159.6	122.4	139.3	120.3	143.6	-28.9	42
-30	159.7	122.4	139.3	120.3	143.5	-30.1	42
-40	159.7	122.4	139.4	120.3	143.4	-30.8	43
-50	159.7	122.4	139.5	120.4	143.3	-31.0	44

(* Based on C_3, C_4 and C_5 data only)

The percentage pentacoordination at each temperature can be calculated from the ^{29}Si NMR chemical shifts, (Table 3.12), and the change in coordination of the silicon followed as a function of the percentage N-Si bond formation. The limiting values of percentage pentacoordination are the same as those used in the mapping exercise (Section 3.4).

Table 3.12

Temp /°C	50	40	30	20	10	0	-10	-20	-30	-40	-50
δ ^{29}Si (/ppm)	-8.7	-12.6	-16.4	-19.4	-22.4	-24.8	-27.0	-28.1	-30.1	-30.8	-31.0
% penta	58	64	70	75	80	84	87	90	92	93	94
% N-Si	30	33	34	36	37	38	40	42	42	43	44

3.7.2: 5-Trifluoromethyl 2-thiopyridine complex (3.20d)

Identical variable-temperature ^{13}C and ^{29}Si NMR experiments were performed over the temperature range -50°C to +50°C on triflate complex (**3.20d**) in deuterochloroform. A summary of the key NMR data is given in Table 3.13. The percentage pentacoordination can also be calculated at each temperature (Table 3.14).

Table 3.13

Temperature (/°C)	^{13}C chemical shift (/ppm)					δ ^{29}Si (/ppm)	% N-Si*
	C_2	C_3	C_4	C_5	C_6		
50	167.0	123.7	137.1	124.7	140.7	5.2	76
40	167.1	123.7	137.2	124.7	140.7	5.8	77
30	167.1	123.7	137.2	124.7	140.6	6.7	77
20	167.2	123.7	137.3	124.6	140.5	7.6	77
10	167.2	123.8	137.4	124.6	140.5	9.1	78
0	167.3	123.8	137.4	124.6	140.5	10.5	78
-10	167.3	123.8	137.5	124.5	140.4	11.9	77
-20	167.4	123.8	137.6	124.5	140.4	13.5	78
-30	167.5	123.8	137.7	124.5	140.4	15.2	78
-40	167.5	123.8	137.8	124.4	140.4	17.1	78
-50	167.6	123.8	137.8	124.4	140.4	19.0	78

(* Based on C_3, C_4 and C_5 data only)

Table 3.14

Temp /°C	50	40	30	20	10	0	-10	-20	-30	-40	-50
δ ^{29}Si (/ppm)	5.2	5.8	6.7	7.6	9.1	10.5	11.9	13.5	15.2	17.1	19.0
% penta'	47	46	45	44	42	40	38	36	34	31	29
% N-Si	76	77	77	77	78	78	77	78	78	78	78

3.7.3: 6-Methyl-2-thiopyridone complex (3.28b)

The ^{13}C and ^{29}Si NMR spectra of a deuterochloroform solution of complex (**3.28b**) were measured over the temperature range -50°C to 50°C in 10-20°C intervals. The important NMR data is presented in Table 3.15, along with the calculated percentage S-Si bond formation at each temperature. From the ^{29}Si NMR chemical shifts, the percentage pentacoordination at each temperature is calculated (Table 3.16).

Table 3.15

Temperature (/°C)	^{13}C chemical shift (/ppm)					δ ^{29}Si (/ppm)	% S-Si*
	C_2	C_3	C_4	C_5	C_6		
50	177.7	131.2	133.9	116.1	149.5	4.2	14
40	177.3	131.0	134.1	116.2	149.6	2.9	16
30	176.9	130.8	134.3	116.4	149.8	1.6	18
20	176.4	130.5	134.6	116.6	149.9	-0.1	21
0	175.7	130.1	135.0	117.0	150.1	-4.0	25
-15	175.1	129.7	135.4	117.2	150.3	-7.7	28
-25	174.7	129.5	135.7	117.4	150.5	-10.6	30
-35	174.2	129.1	136.0	117.6	150.6	-13.8	33
-50	173.3	128.5	136.5	118.0	151.0	-18.7	38

(* Based on C_2, C_3, C_4 and C_5 data only)

Table 3.16

Temp' (/°C)	50	40	30	20	0	-15	-25	-35	-50
δ ^{29}Si (/ppm)	4.2	2.9	1.6	-0.1	-4.0	-7.7	-10.6	-13.8	-18.7
% penta'	38	40	42	45	51	57	61	66	74
% S-Si	14	16	18	21	25	28	30	33	38

3.7.4: Analysis of the data

Complexes (**3.11b**) and (**3.28b**) display a marked increase in nucleophile-silicon bonding as the temperature is lowered (Figure 3.26). This is in line with the observations by Kummer *et al* of the silyl-pyridone complex (**2.12b**).[115]

Figure 3.26

Variation of percentage nucleophile silicon bond formation with temperature for complexes (3.11b) and (3.28b).

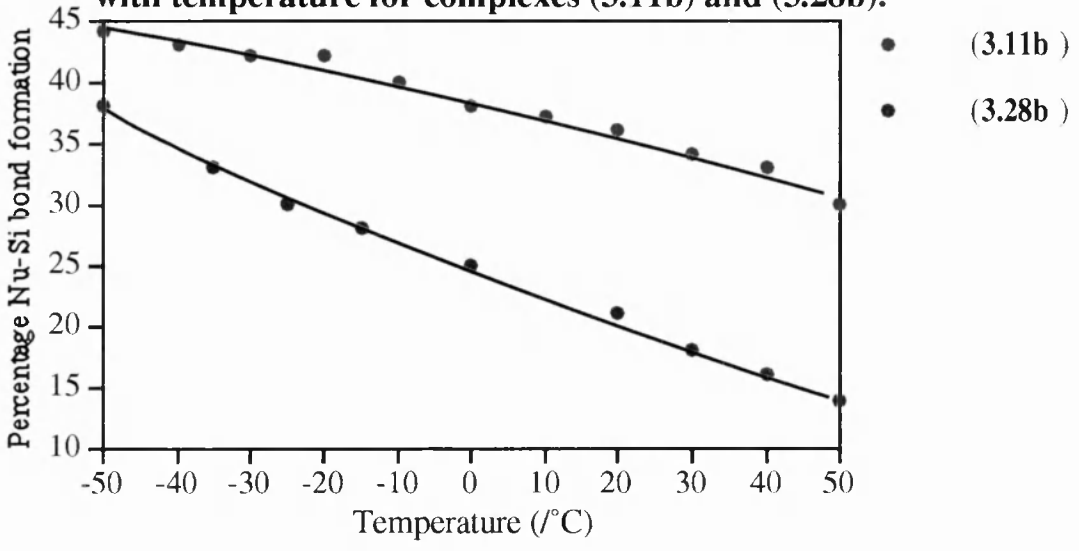

(**3.20d**), by contrast, maintains a constant level of N-Si bond formation. The small variation that is seen is within the bounds of experimental error. The percentage pentacoordination of (**3.20d**), however, changes considerably across this temperature range (Figure 3.27). As the percentage N-Si bond is greater than 50%, a decrease in temperature is expected to be accompanied by a decrease in percentage pentacoordination, i.e. to resemble a structure with a greater degree of 'substitution'. This is indeed what is observed. Complex (**1.32**), with a structure at silicon similar to (**3.20d**), displays the same ^{29}Si NMR temperature dependence.[40] For the ^{29}Si chemical shift to be affected by temperature and the percentage N-Si bond formation not to be, the degree of Si-leaving group bond formation must be that which is changing with temperature. At lower temperatures the percentage Si-leaving group bond formation is lower and so the silicon is less pentacoordinate.

Complexes (**3.11b**) and (**3.28b**) maintain structures with less than 50% nucleophile-silicon bond formation. At lower temperatures both compounds show higher extents of nucleophile-silicon bond formation. Therefore we expect (and observe) an increase in percentage pentacoordination as the temperature is lowered.

Figure 3.27

A comparison of the effect of temperature on the coordination state of the silicon for complexes (3.11b), (3.20d) and (3.28b).

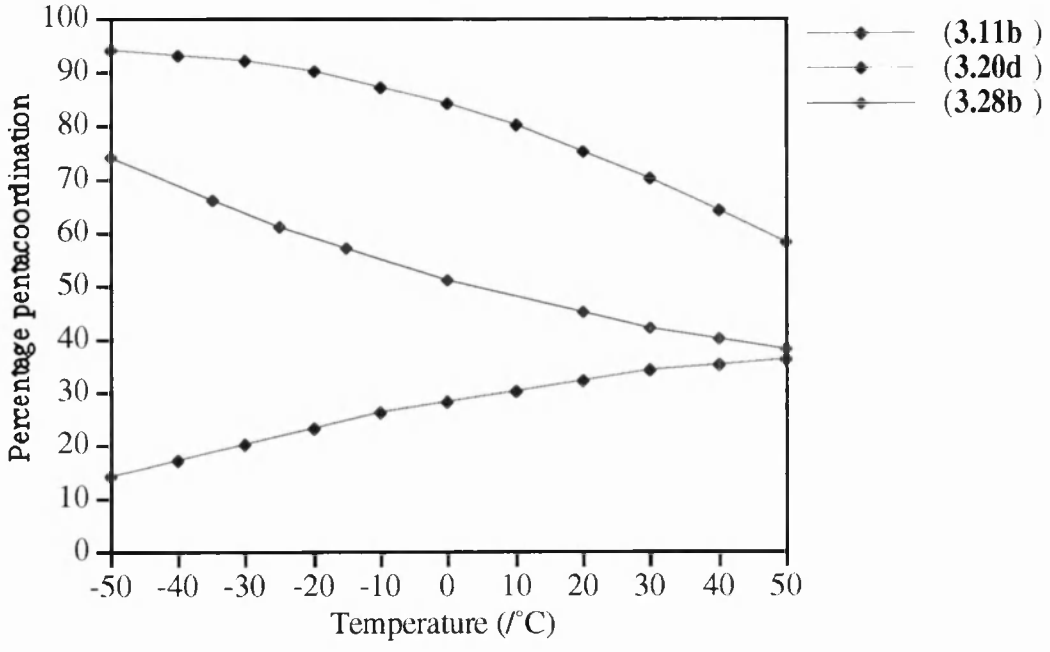

The flattening-out of the plot for (**3.11b**) at lower temperatures occurs as the percentage nucleophile-silicon bond formation approaches 50% as shown in Figure 3.28. At the same time, the structure is approaching 100% pentacoordination at silicon. The flattening-off occurs at ^{29}Si NMR chemical shift values of around δ -31 to δ -35. Thus δ -35 is chosen to define 100% pentacoordination for the percentage pentacoordination calculations above and in Sections 3.4 and 3.6.4.

Figure 3.28

A plot of the relationship between percentage N-Si bond formation and the coordination of the silicon in complex (3.11b).

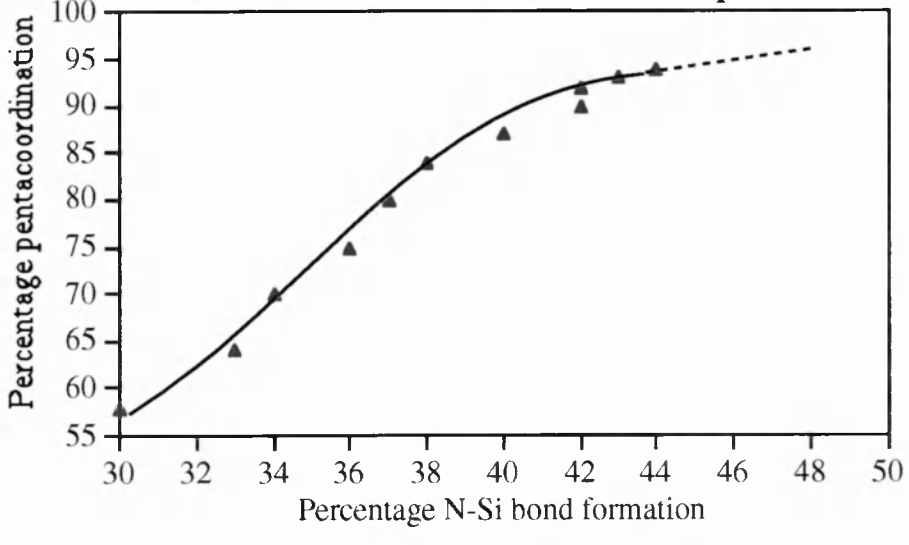

Following the high and low temperature measurements, the solutions were returned to room temperature and the ^{29}Si NMR spectra re-recorded. On each occasion the resonance reverted to the original chemical shift. This shows that nucleophile-silicon and leaving group-silicon bonding is reversible with temperature.

Kummer *et al*'s variable temperature study[115] of pentacoordinate silicon focused on the complex (**2.12b**). Its structure is centred on the fully pentacoordinate intermediate or transition state of the 'reaction'. They therefore were able to observe the reversal of temperature dependence of the ^{29}Si chemical shift across the temperature range 100°C to -50°C (Figure 2.6 in Chapter 2). They also performed a similar experiment on the bromide analogue (**2.12a**). Using ^{13}C and ^{29}Si VT data for (**2.12a**) and (**2.12b**)[115] and ^{13}C chemical shifts for compounds (**2.10**) and (**2.11**),[149] we have calculated percentage pentacoordination and percentage O-Si bond formation values for (**2.12b**) at 100, 25 and -50°C and (**2.12a**) at 80, 25 and -60°C (Table 3.17). It is apparent that differences occur in the room temperature ^{13}C and ^{29}Si NMR chemical shifts of Kummer *et al* and those reported by Borbaruah.[149] However, the deviations are small and lie within experimental error.

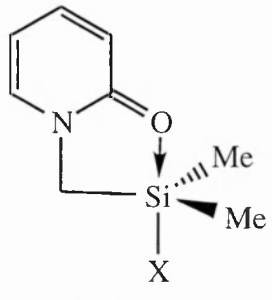

(**2.12a**) X = Br
(**2.12b**) X = Cl

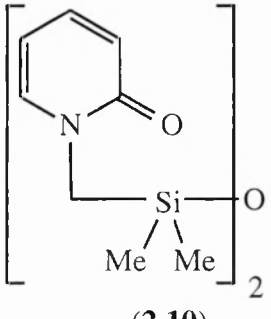

(**2.10**)

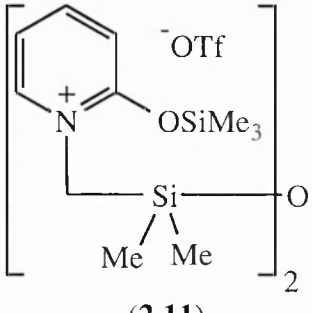

(**2.11**)

Table 3.17

Complex	Temp' (/°C)	% O-Si bond form'n	δ ^{29}Si (/ppm)	% pentacoord'n
(**2.12a**)	80	55	-27.3	84
	25	62	-19.0	74
	-60	74	-2.1	53
(**2.12b**)	100	44	-35.2	93
	25	45	-39.0	99
	-50	48	-37.5	96

Over the temperature range studied it has been only possible to observe limited changes to the degree of substitution in each complex. For example, (**3.11b**) increases its percentage N-Si bond formation only 14% between 50°C and -50°C. Therefore, instead of obtaining representative structures from across the complete 'reaction coordinate', variable temperature studies focus on narrow *windows* in which series of closely related structures are observed. It is the specific characteristics of the 'nucleophile' and 'leaving group' which control the position and size of the window over a given temperature range. Therefore, substitution at silicon may be mapped by collecting variable temperature NMR data for several related complexes, each having an appreciably different isothermic structure.

To map a general substitution by VT NMR spectroscopy, percentage nucleophile-silicon bond formation and percentage pentacoordination data for complexes (**2.12a**), (**2.12b**), (**3.11b**), (**3.20d**) and (**3.28b**) are plotted on a single graph (Figure 3.29). The plot is similar and characteristic in outline to that of Figure 3.24.

Figure 3.29

A plot showing the relationship between percentage pentacoordination and percentage nucleophile-silicon bond formation for complexes analysed by variable temperature, multi-nuclear NMR spectroscopy.

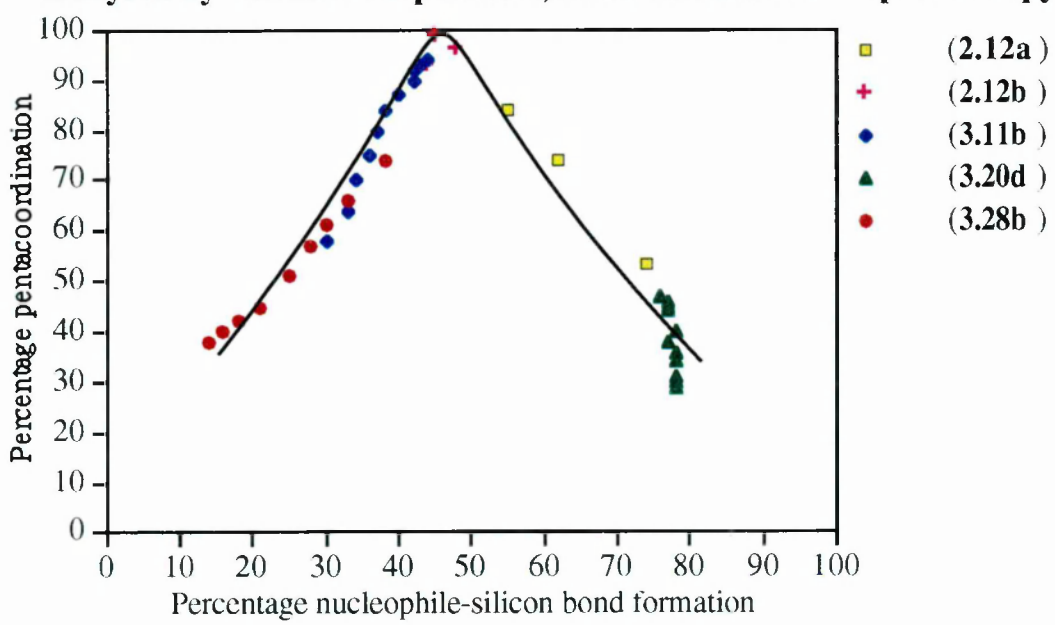

We have not been able to explain the reason for the anomalous behaviour of (**3.20d**), whose percentage N-Si bond formation remains essentially constant with temperature.

The complexes thus far have been considered as single structures which change reversibly into each other by changing the temperature. However, another interpretation based on equilibria can be envisaged. In this case, fast equilibria occur as shown for (**3.11b**) in Figure 3.30, between 'unsubstituted' (**A**), fully pentacoordinate (**B**) and fully 'substituted' (**C**) structures.

Figure 3.30

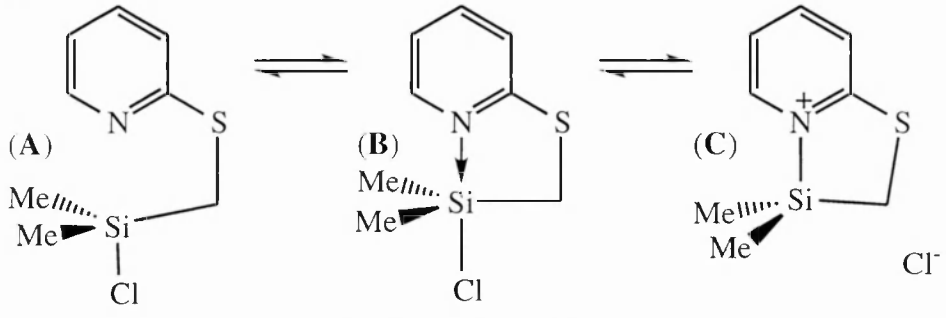

fully pentacoordinate

Changing the temperature thus changes the position of each equilibrium, with an average, single set of NMR resonances being observed at any given temperature. The previously described conductivity measurements of hypervalent complexes (Chapter 2, page 48)[114] however has shown that the structures exist in isolation in solution rather than as an equilibrium mixture.

3.8: A novel hexacoordinate thiopyridine complex

The reaction of (**3.10**) with dichloro(dichloromethyl)methylsilane gives only a single isolable product, (**3.42**), if reacted in the ratio 3:1. A single sharp δ ^{29}Si resonance of δ -104.2 ppm indicates a hexacoordinate silicon centre and the ^{13}C NMR spectrum in the aromatic region shows two sets of aromatic ring carbon resonances in an approximate intensity ratio of 2:1 (Figure 3.31). Table 3.18 compares the ^{13}C resonances of the aromatic rings in (**3.42**) with those of (**3.28b**) and (**3.11b**), which are representative of coordinating 2-thiopyridone and 2-thiopyridine ligands respectively.

Table 3.18

	Thiopyridine ring ^{13}C chemical shift (/ppm)					*Thiopyridone* ring ^{13}C chemical shift (/ppm)				
	C_2	C_3	C_4	C_5	C_6	$C_{2'}$	$C_{3'}$	$C_{4'}$	$C_{5'}$	$C_{6'}$
(**3.1**)	-	-	-	-	-	180.2	134.4	138.0	113.1	137.7
(**3.28b**)	-	-	-	-	-	176.4	130.5	134.6	116.6	149.9
(**3.11b**)	159.6	122.3	138.6	120.1	144.5	-	-	-	-	-
(**3.42**)	158.1	123.3	141.4	122.2	143.5	171.8	126.8	142.3	118.9	145.4

Figure 3.31

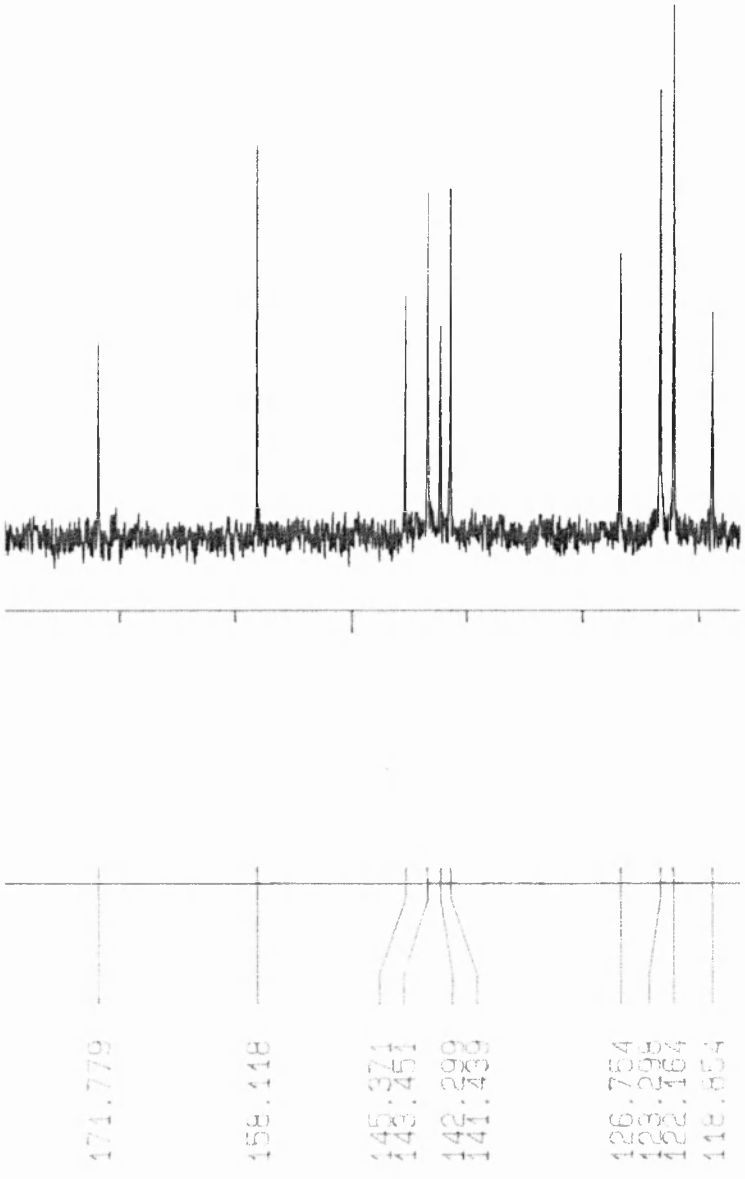

None of the peaks are assignable to (**3.1**), a possible hydrolysis product from (**3.10**) or (**3.42**). ^{1}H-^{1}H and ^{1}H-^{13}C COSY spectra were used to help assign the peaks. The resonances of (**3.42**) are grouped under the name *thiopyridine* or *thiopyridone* to reflect the rings more predominant form. The *thiopyridone* ring is better described as having intermediate character between '-ine' and '-one' tautomers. The ratio of *thiopyridine* carbons to *thiopyridone* carbons is 2:1 on the basis of the relative ^{13}C NMR peak intensities. A single tertiary carbon at δ 35.4 is also found.

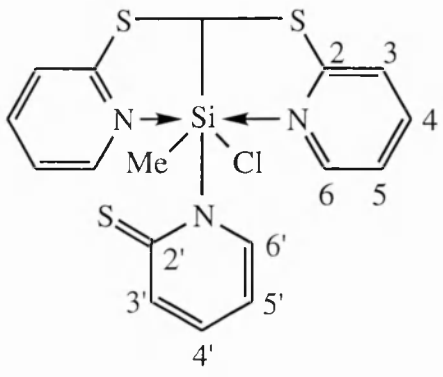

(**3.42**)

The most probable structure for (**3.42**), on the basis of the NMR information, is shown here. It consists of a silicon with two intramolecularly coordinating *thiopyridine* rings. There is also a conventional, covalently bonded third *thiopyridone* ring attached to the silicon, probably bound through nitrogen. However, from the intermediacy of the ^{13}C data for the *thiopyridone* ring between the '-ine' and '-one' forms, we cannot rule out the alternative S-Si binding mode. Further evidence for the structure of (**3.42**) comes from its hydrolysis. This yields the desilylated bis-thiopyridine fragment (**3.43**) (Figure 3.32).

Figure 3.32

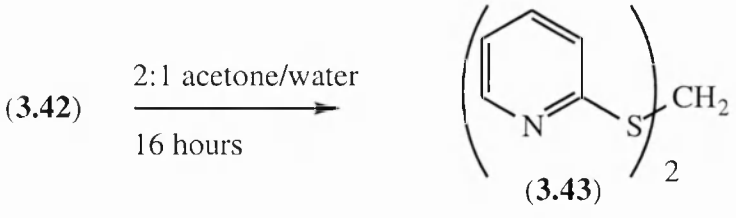

(**3.43**)

By contrast, the reaction of a 2-trimethylsiloxypyridine and dichloro(dichloromethyl)-methylsilane occurs in a 2:1 ratio and gives a dichloro-substituted hexacoordinate complex (**3.44**) (Figure 3.33).[149]

Figure 3.33

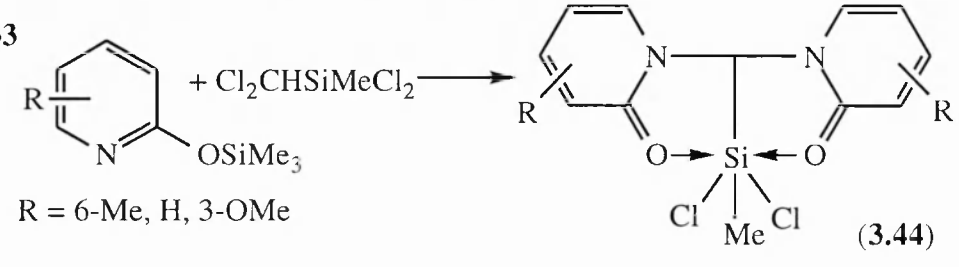

R = 6-Me, H, 3-OMe

(**3.44**)

When R= 6-Me or H, a single set of ^{13}C NMR chemical shifts and a single ^{29}Si shift are observed. When R = 3-OMe, two sets of peaks are observed in the NMR spectra corresponding to two isomers of the complex. Hexacoordinate silicon is characterised by ^{29}Si chemical shifts in the range δ -120.4 to -128.5.

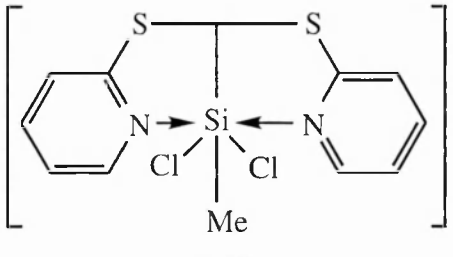

(**3.45**)

A thiopyridone analogue of (**3.44**), (**3.45**), is presumably an intermediate in the formation of (**3.42**); (**3.45**) reacting with a third equivalent of (**3.10**) to form the final product.

Chapter 4: 5-Coordinate complexes stabilised by maltol-based ligands.

4.1: Introduction

The bidentate ligand 3-hydroxy-2-methyl-4-pyrone (**4.1**) (maltol) is a natural product and was first isolated from larch bark. It is a permitted food additive (E636) and is widely used in the baking industry.

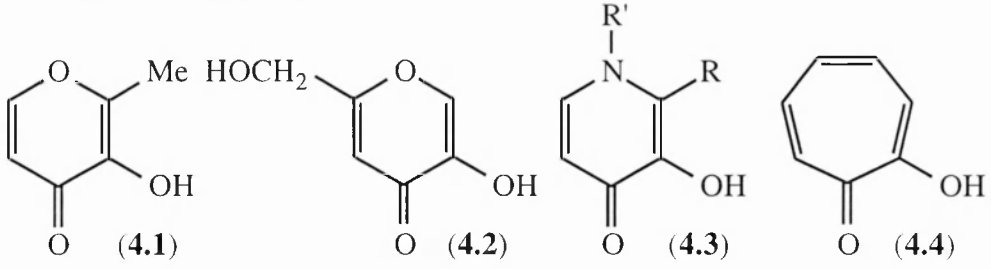

Maltol and structurally similar 5-hydroxy-2-(hydroxymethyl)-4-pyrone (kojic acid) (**4.2**), which is also naturally occurring, are thought to be important chelates in nature. (**4.1**) and its 4-pyridone analogues (**4.3**) have become attractive ligands in the medical field, for example, as a means of controlling metal ion concentrations in the human body and for the introduction of appropriate isotopes for diagnosis. It is also of interest to note the similarity of (**4.1**), (**4.2**) and (**4.3**) to that of tropolone (**4.4**).

In practice the 4-pyridone ligands have proved more suitable to practical applications since they form the significantly more stable complexes and two variable groups, R and R', may be tailored for a particular application. Although the emphasis in this chapter is to highlight the chemistry of these ligands, it is their potential biological and physiological applications that have been the driving force for their investigation.

The crystal structure of ethyl maltol (**4.5**)[150] has recently been compared with that of maltol hydrochloride (**4.6**) (Figure 4.1).[151] Protonation of the carbonyl-oxygen causes

Figure 4.1

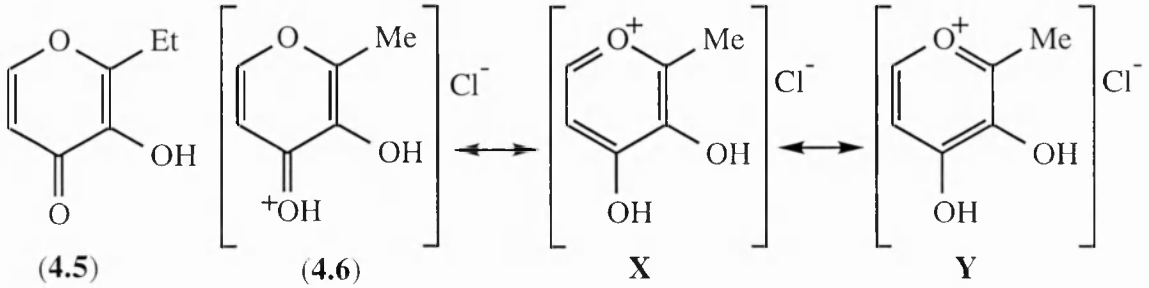

the C=O bond to lengthen by an average of 0.02Å, the ring C=C bonds to lengthen by an average of 0.02Å and the ring C-C bonds to shorten by an average of 0.02-0.03Å. This is consistent with increased contribution from the resonance forms **X** and **Y** of (**4.6**).

4.1.1: Tris(chelate) complexes

To date it has been the tris-complexes which have proved to have the greatest applications. For example, iron (III) complexes of (**4.3**) are used for the treatment of anaemia and complexes of ligand type (**4.3**) used to control aluminium levels in water supplies. These compounds are models of ion transport complexes found in nature.

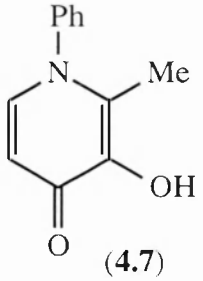

(**4.7**)

Much of the early work which established the versatility of these ligands to complex a wide variety of metal ions was carried out by Herak and Tamhina. They focused on the ability of 3-hydroxy-2-methyl-1-phenyl-4-pyridone, (**4.7**), to complex metal ions from aqueous solutions over a range of pH's. A typical experiment involved the mechanical shaking of a standardised aqueous solution of the metal ion at a precisely known pH with a chloroform solution containing the ligand in excess, for a fixed time. The organic phase would then be separated and the extent of metal ion extraction into the organic phase (i.e. percentage complexation) calculated from the UV absorption of the aqueous solution before and after mixing. A wide variety of metals have been shown to be extracted by (**4.7**) including iron (III),[152] molybdenum (IV),[153] gallium (III),[154] vanadium (V),[155] niobium (V),[156] titanium (IV),[157] hafnium (IV),[158] and indium (III).[159]

The selective extraction of metal ions from mixtures is possible, since different metal complexes are stable over different pH ranges. Thus, by careful choice of pH, quantitative separation of a particular metal ion is possible. For example, thorium (IV) and protactinium (V) can be separated in aqueous hydrochloric acid (Figure 4.2).[160] Thorium (IV) can be extracted quantitatively at pH's > 4. However, if the pH is maintained in the region 0.0-0.5 then protactinium (V) is extracted qualitatively. A similar methodology was applied to the separation of zinc (II) and copper (II) ions.[161] The ligand 3-hydroxy-2-methyl-4-thiopyrone, (**4.8**), has also been used to extract metal ions, but so far, to a more limited extent.[162]

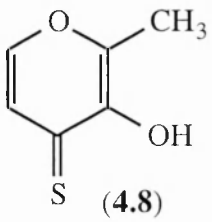

(**4.8**)

Figure 4.2

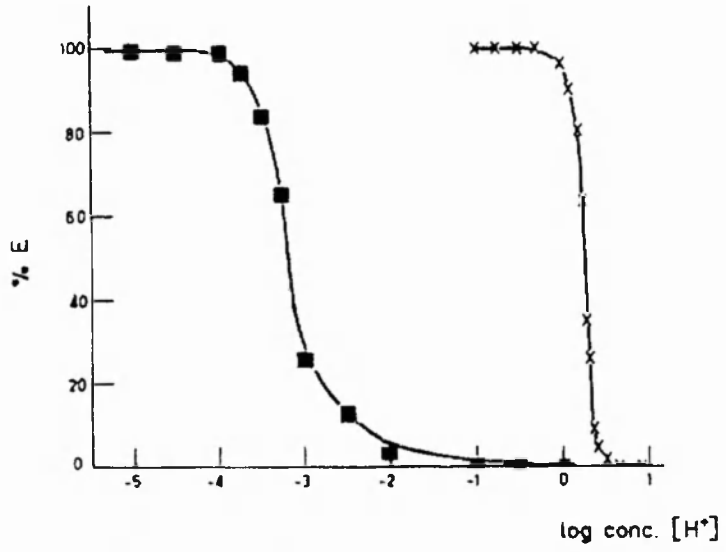

A plot of percentage extraction against log [H^+] for Thorium (IV) (squares) and Protactinium (V) (crosses) in aqueous hydrochloric acid by (**4.7**).

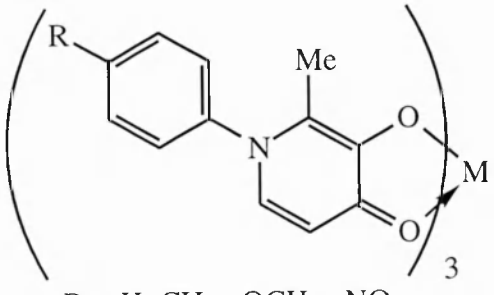

R = H, CH_3 , OCH_3 , NO_2
M = Al, Ga, In

(**4.9**)

Recent work has placed more emphasis on the structures of the complexes themselves. Orvig and co-workers[163] have isolated, and in some cases have obtained crystal structures of a variety of neutral tris(1-aryl-3-hydroxy-2-methyl-4-pyridonato)metal (III) complexes (**4.9**). The complexes are stable to > 200°C and either sparingly water-soluble or insoluble. Since they are very hygroscopic, they were isolated as reproducibly analysable hydrates. The crystal structure of the gallium complex, (**4.9**) (R = Me) (Figure 4.3), shows the metal to be in an octahedral environment with three *trans* $O_{(carbonyl)}$-Ga-O moieties with diaxial bond angles of 171.6°. The structurally similar aluminium (tris)maltolate complex has also been reported.[164]

Figure 4.3

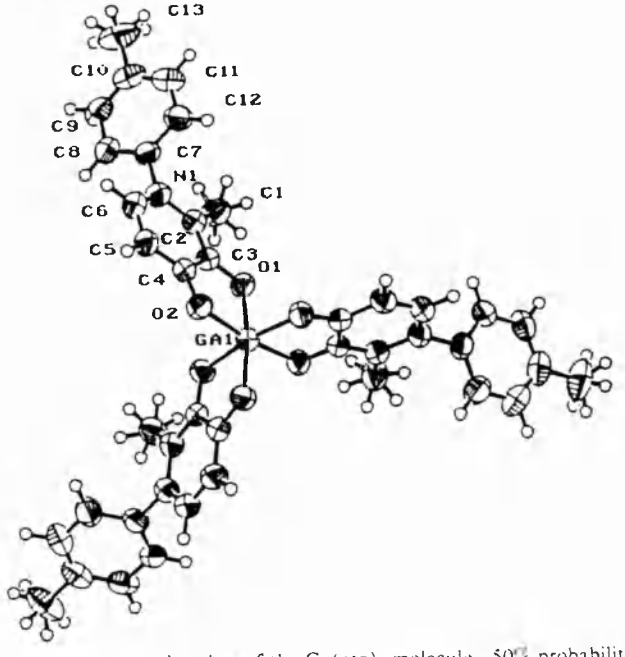

Perspective view of the $Ga(ptp)_3$ molecule. 50% probability thermal ellipsoids are shown for the non-hydrogen atoms. Labeled non-hydrogen atoms comprise the asymmetric unit.

Another pair of neutral M (III) complexes are the iron (III) tris(maltolate) complex (**4.10**) (R = Me),[165] and its ethylmaltol analogue (**4.11**) (R = Et).[166] Although, generally less well studied than maltolates and 4-pyridonates, several tris-kojate complexes have been prepared, such as iron (III) tris(kojate) (**4.12**).[167]

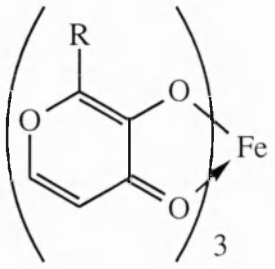

(**4.10**) R = Me
(**4.11**) R = Et

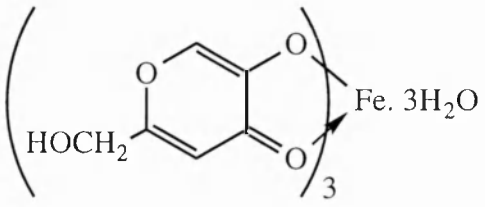

(**4.12**)

Charged, water-soluble complexes have also been synthesised. For example, it has long been suggested that the silicon tris(catecholate) dianion, (**1.53**), may act as a solublising transporter of silicon in nature. This compound and derivatives of it have been prepared by several groups.[21, 67] Silicon complexes (**4.13**)[168] of ligand (**4.3**) (R = Me) have been prepared by the following route (Figure 4.4).

Figure 4.4

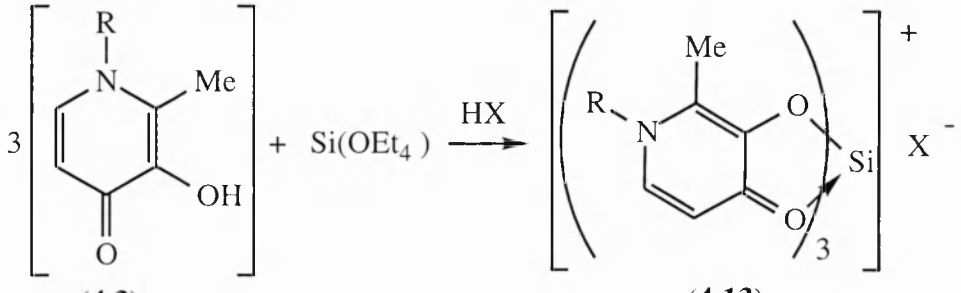

(**4.3**) (**4.13**)

(R = H, Me, Et. $X = HSO_4^-, Cl^-, {}^-OSO_2CF_3, CF_3CO_2^-$)

The non-equivalence of the two oxygens on each ligand gives rise to a mixture of meridonal and facial isomers in the solid state. When dissolved in DMSO, the interconversion of these isomers to an eventual statistical distribution can be observed over time (Figure 4.5).

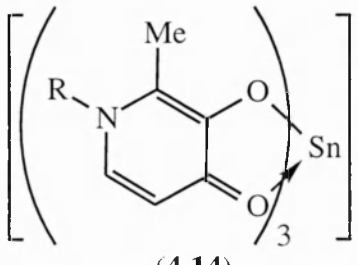

(**4.14**)

R = H, Me, Et
X = Cl, Br, I

A number of tin analogues (**4.14**)[169] of these complexes have been prepared from a hot aqueous medium of tetrahalotin and the appropriate free ligand to give the hydrate. The ^{119}Sn NMR chemical shifts in DMSO

are in the range δ -450 to δ -460, indicating the presence of hexacoordinate tin species in solution.

Figure 4.5

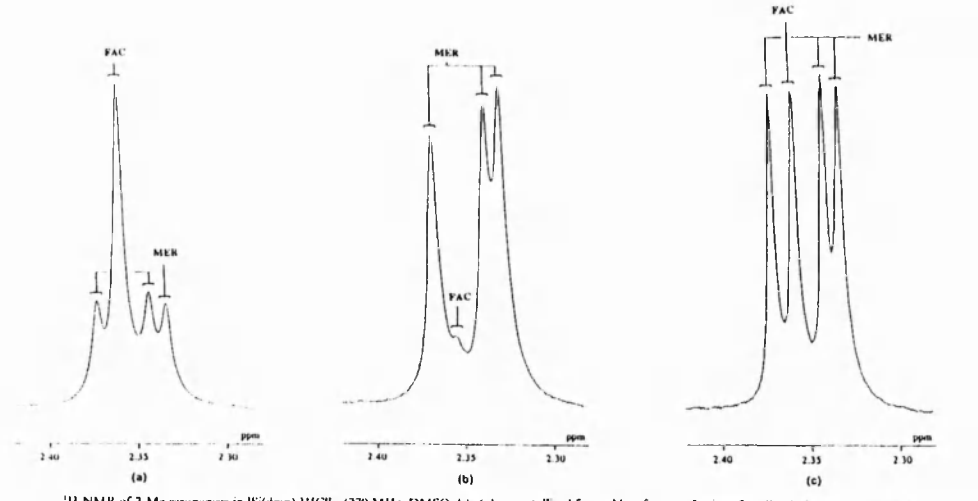

^{1}H NMR of 2-Me resonances in $[Si(dmp)_3]^+[Cl]$ (270 MHz, DMSO-d_6): (a) recrystallized from chloroform ~ 5 mins after dissolution; (b) recrystallized from ethanol/ether ~ 5 mins after dissolution; (c) solution (a) after 2 days at room temperature.

To date the tris(maltolato)tin (IV) cation has not been reported, however the neutral seven-coordinate butyltin tris(maltolate) (**4.15**) (Figure 4.6) has been isolated.[170]

Figure 4.6

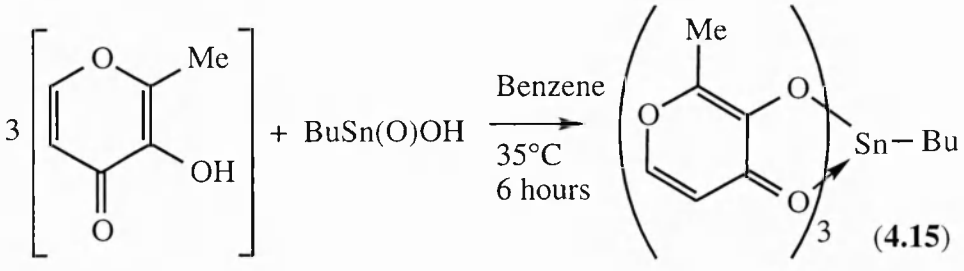

4.1.2: Bis(chelate) complexes

Gupta *et al*[170] have reported the synthesis of a variety of five and six coordinate (maltolato)tin complexes (**4.16**)-(**4.20**) (Figure 4.7).

Figure 4.7

$R_n SnCl_{4-n}$ + (4-n)NaL (LH = maltol) —CH_2Cl_2, 4 hours→ $R_n SnL_{4-n}$

(**4.16**) R = Me, n = 2
(**4.17**) R = Bu, n = 2
(**4.18**) R = Bu, n = 3

$Ph_3 SnCl$ + 2LH —NaOAc, CH_2Cl_2 4 hours→ $Ph_2 SnL_2$ (**4.19**)

$PhSnCl_3$ + 2LH —Benzene, Δ, 3 hours→ $Cl_2 SnL_2$ (**4.20**)

The bis(kojate) complex (**4.21**), first reported by Otera *et al*,[171] has a similar structure to (**4.19**) and (**4.20**).

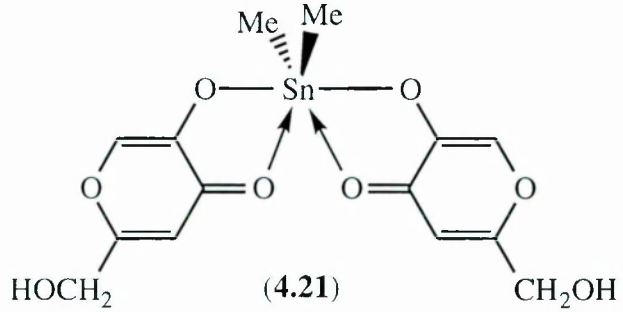

(**4.21**)

Burgess and Parsons[172] have prepared the bis(ethylmaltolato) tin analogue (**4.22**) and three 4-pyridone analogues (**4.23**)-(**4.25**).

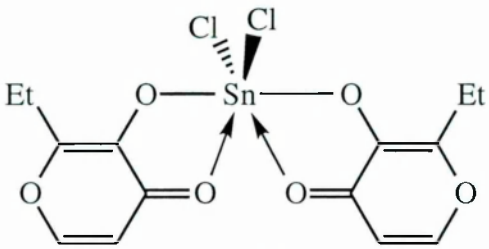

(**4.22**)

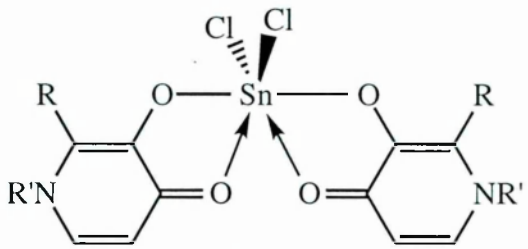

(**4.23**) R = R' = Me
(**4.24**) R = Et, R' = Me
(**4.25**) R = R' = Et

Sitran *et al*[173] have contrasted the reactions of MCl_4 (M = Sn, Ge) with excess free maltol in benzene and methanol. The solvent is found to play a vital role in the stoichiometry of the product (Figure 4.8). They also have shown that tin (II) chloride reacts with potassium maltolate to produce bis(maltolato)tin (II) quantitatively.

Figure 4.8

$$MCl_4 + LH \text{ (excess)} \xrightarrow[\text{2: Dry, vacuum}]{\text{1: Benzene (dry)}} M(LH)_4Cl_4 \quad (\mathbf{4.26})$$

$$MCl_4 + LH \text{ (excess)} \xrightarrow{MeOH} M(L)_2Cl_2 \quad (\mathbf{4.27})$$

(M = Sn, Ge; LH = maltol)

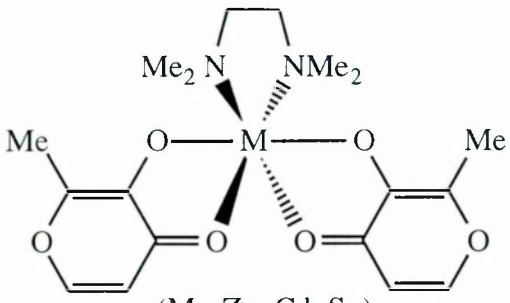

(M= Zn, Cd, Sn)
(**4.28**)

Electrochemical synthesis using a sacrificial metallic anode (M = Zn, Cd, Cu, Sn, In) and an acetonitrile solution of maltol (LH), has allowed the preparation of complexes $M(L)_2$ (M = Zn, Sn, Cd, Cu) and $In(L)_3$.[174] Further reaction of the maltolate complexes $M(L)_2$

(M = Zn, Cd and Sn) with N,N,N',N'-tetramethylethylenediamine yields the hexacoordinate M^{II} complexes (**4.28**).

The ligand 3-hydroxyflavone, (**4.29**), bears a strong resemblance to maltol and has been shown to be as good a chelate to tin as maltol itself. For example, bis(flavonato) complexes, (**4.30**), containing hexacoordinate tin have been prepared.[175]

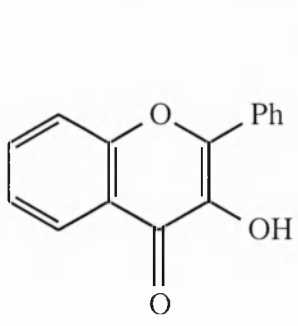

(**4.29**)

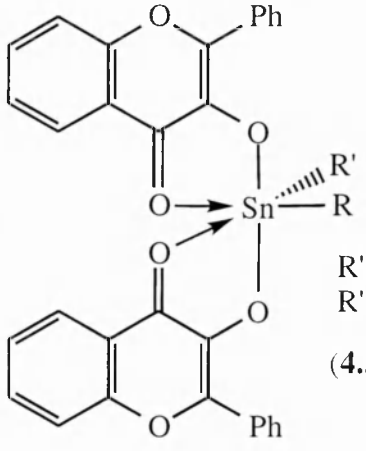

R' = R = Ph, Me, Bu.
R' = Me, R = Cl

(**4.30**)

4.1.3: Mono(chelate) complexes

During a study on the antibacterial effects of organomercury compounds, a number of tricoordinate maltolatomercury, (**4.31**), and kojatomercury, (**4.32**), complexes (Figure 4.9) were synthesised.[176]

Figure 4.9

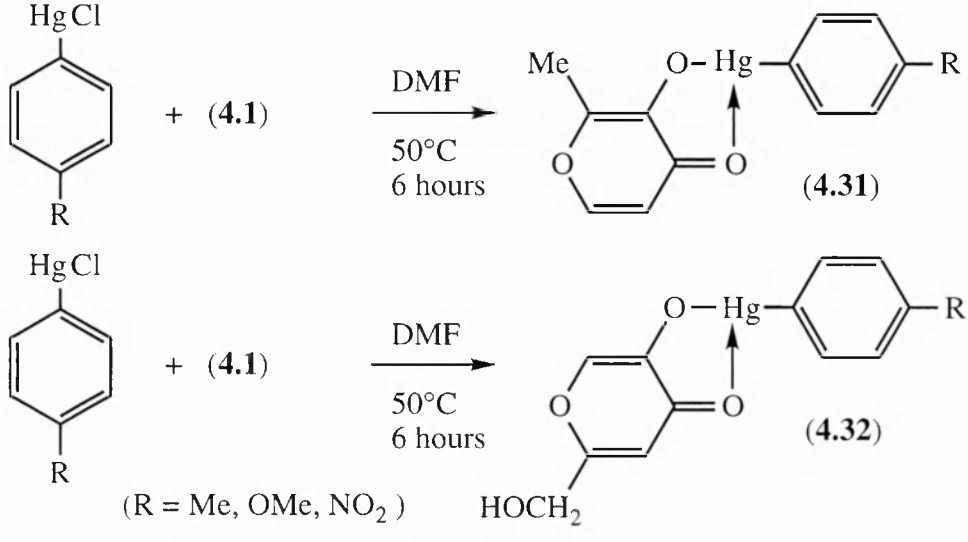

Sitran *et al*[177] have published the syntheses of a series of dimethyltin, (**4.33**) (Figure 4.10), and phenyltin, (**4.34**) (Figure 4.11), substituted pentacoordinate complexes, stabilised by a single maltol ligand, from the appropriate diorganotin dihalide and potassium maltolate. Blunden and Smith[175] have prepared several flavone analogues, (**4.35**), by refluxing the appropriate tin hydroxide with a stoichiometric quantity of (**4.29**) (Figure 4.12).

Figure 4.10

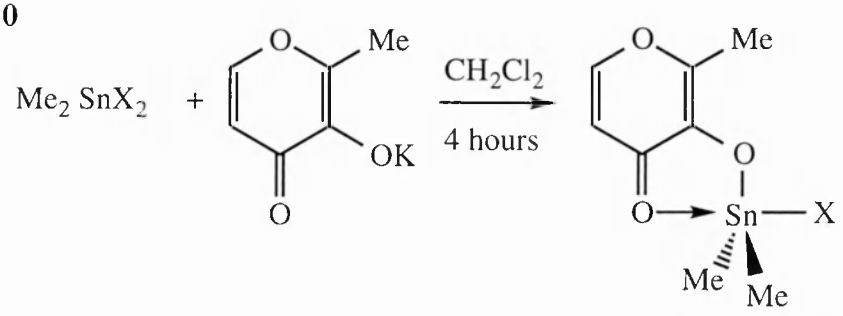

(**4.33**) (X = Cl, Br)

Figure 4.11

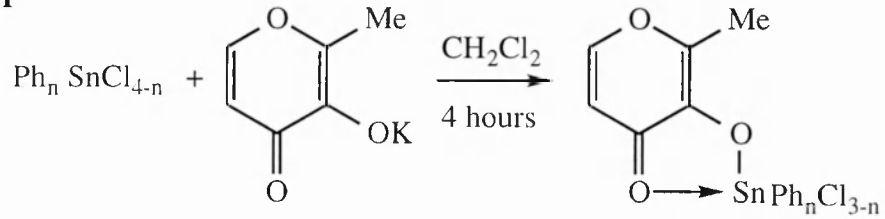

(**4.34**) (n = 2, 3)

Figure 4.12

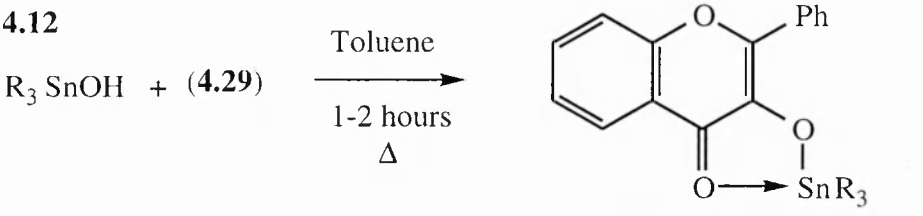

(R = Bu, Ph, c-C_6H_{11} , $PhMe_2CCH_2$)

(**4.35**)

Alternatively, complexes (**4.36**)[178] and (**4.37**)[175] (Figure 4.13) were prepared at room temperature in methanol. The ^{119}Sn NMR spectra of the flavone complexes are consistently about 100ppm up-field of shifts for related tetracoordinate compounds. This indicates pentacoordinated tin in each case.

Figure 4.13

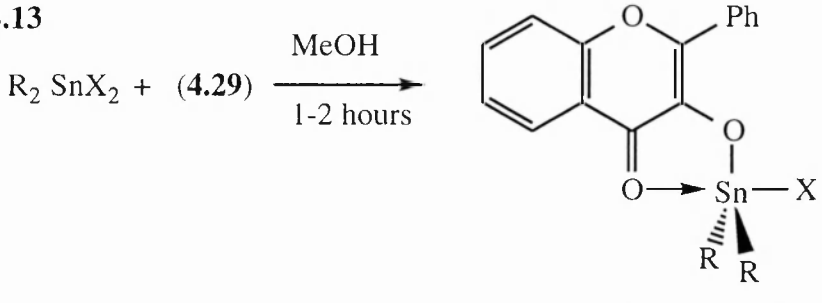

(**4.36**) R = Me, ^{n}Bu, Et, ^{n}Oct. X = Cl, Br

(**4.37**) R = Ph, X = Cl

To extend the NMR solution phase mapping of nucleophilic substitution to new ligands and new substitution centres we have synthesised a series of compounds having structures reminiscent to those of (**4.33**)-(**4.37**).

4.2: Tin complexes of maltol

On the basis of Britton and Dunitz's structural correlation work with tin[51] and by analogy with our previous methodology, the following scheme - modelling nucleophilic substitution at tin was envisaged.

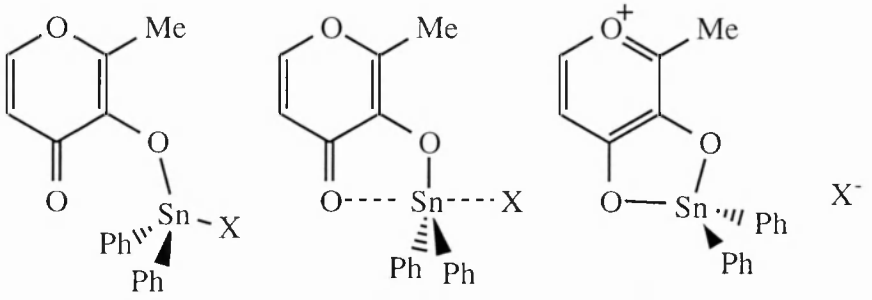

(**4.38**) (**4.39a-d**) (**4.40**)

A series of complexes (**4.39a-d**) were synthesised with X-groups of different 'leaving ability'. Complexes which model the zero substitution structure (**4.38**) and completed substitution structure (**4.40**) were also prepared (Section 4.2.2).

4.2.1: Synthesis of complexes (4.39a-d) and their precursors

The triphenyl derivative (**4.39a**) (i.e. X = Ph) was produced by the reaction of the sodium salt of maltol, (**4.41**), with chlorotriphenyltin (**4.42a**) (Figure 4.14). Crystals of (**4.39a**) for X-ray analysis were prepared by recrystallisation from a hot acetonitrile solution.

Figure 4.14

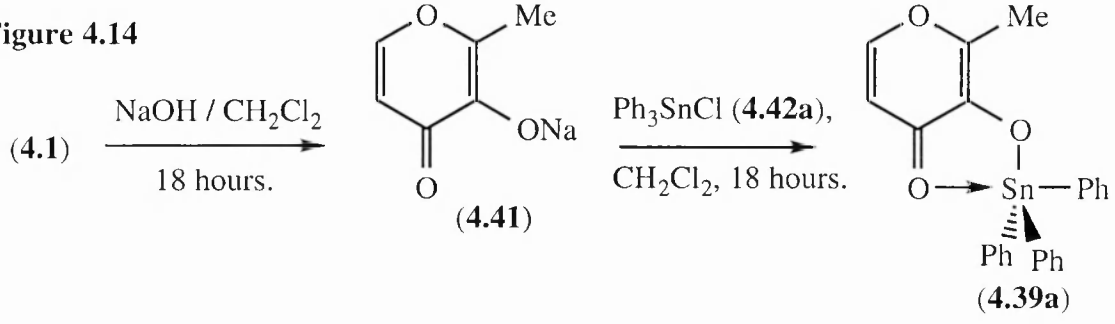

(**4.1**) $NaOH / CH_2Cl_2$, 18 hours. (**4.41**) Ph_3SnCl (**4.42a**), CH_2Cl_2, 18 hours. (**4.39a**)

Where X = halogen, complexes (**4.39b-d**) were prepared from methanolic solutions of (**4.1**) and the appropriate dihalodiphenyltin compound (**4.42b-d**) at room temperature (Figure 4.15). Suitable crystals for single-crystal X-ray analysis were grown from dilute solutions at room temperature. Although (**4.42a**) and (**4.42b**) are commercial reagents, (**4.42c**) and (**4.42d**) must be prepared from (**4.42b**). Hydrolysis of (**4.42b**) with hot, concentrated, aqueous sodium hydroxide solution yields diphenyltin oxide (**4.43**). Treatment of (**4.43**) with a concentrated aqueous solution of the appropriate hydrohalic acid affords the required dihalodiphenyltin (**4.42c**) or (**4.42d**) (Figure 4.16).

Figure 4.15

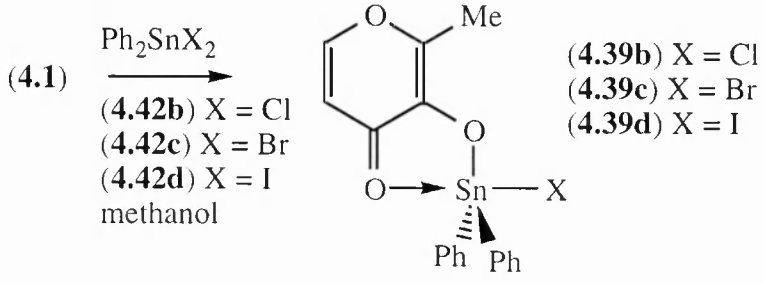

Figure 4.16

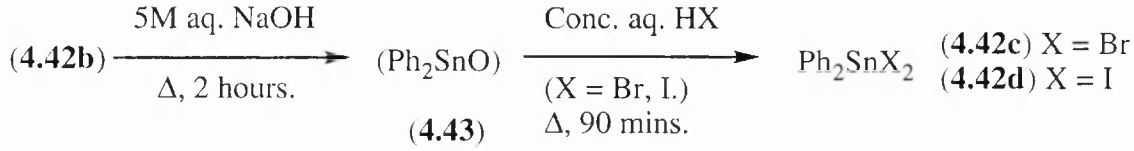

4.2.2: Synthesis of compounds for use as models for 0% and 100% substitution

Models for *limiting* species (**4.38**) and (**4.40**) were prepared ((**4.44**) and (**4.45**) respectively) (Figure 4.17). A methyl group was used in place of the tin substituent at the carbonyl oxygen.

Figure 4.17

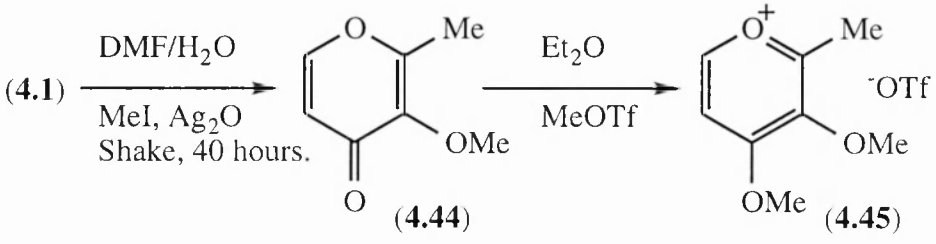

4.2.3: A map of nucleophilic substitution at tin?

Figure 4.18

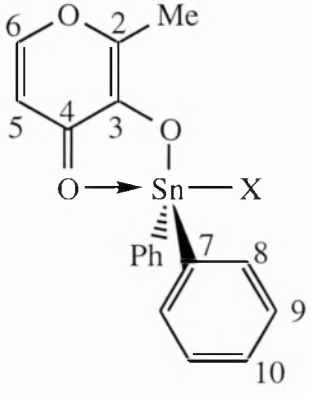

Table 4.1 shows the key ^{13}C NMR data for the complexes, including, where appropriate, the phenyl ring carbon and ^{119}Sn NMR chemical shifts. The numbering system used is shown in Figure 4.18. The ^{119}Sn chemical shift is particularly prone to change with concentration (See Section 4.6). Thus the concentration of NMR solutions were standardised at 0.52M for all tin complexes unless noted otherwise. The NMR solvent in this study was d_3-acetonitrile unless stated otherwise. There is very little pattern discernible for the change of chemical shifts with increasing leaving group ability through the series (**4.44**)-(**4.39a-d**)-(**4.45**). In general there is little difference between the data sets between complexes (**4.39a-d**). The ^{119}Sn chemical shifts all indicate significant

Table 4.1

Complex	^{13}C chemical shift (/ppm)									$\delta\ ^{119}Sn$
	C_2	C_3	C_4	C_5	C_6	C_7	C_8	C_9	C_{10}	
(**4.44**)	160.2	146.3	175.3	118.2	155.3	-	-	-	-	-
(**4.39a**)	156.3	145.7	175.9	111.1	153.4	136.3	137.5	129.3	130.0	-166.6
(**4.39b**)	158.9	145.7	172.5	112.6	158.3	143.8	136.3	129.6	131.1	-201.5
(**4.39c**)	158.5	144.2	172.3	112.5	158.2	143.7	135.8	129.7	131.3	-196.0
(**4.39d**)	156.8	144.0	173.4	113.0	153.6	139.4	135.5	129.9	131.8	-271.4
(**4.45**)	174.6	144.7	173.7	110.2	163.8	-	-	-	-	-

pentacoordination in each compound. The ^{119}Sn shift of (**4.39d**) is also influenced by the heavy atom iodine, to which it is attached. The ^{119}Sn shift of (**4.39b**) was not reported when first prepared,[177] but the value we have measured is very similar to that reported for its flavone analogue (**4.36**) (δ -196.0).[175]

It may be concluded that these complexes, instead of adopting a variety of structures at different points along the substitution pathway, are instead *frozen* at the same point. A calculation to determine the 'percentage Sn-O bond formation' at which the complexes are *frozen* was performed in a similar way to the silicon complexes of Chapters 2 and 3. This calculation compared the mean ^{13}C chemical shift of each ring carbon in complexes (**4.39a-d**) to its value in (**4.44**) and (**4.45**) (Table 4.2). C_2 is most adversely affected by the use of a methyl group in place of a tin substituent in complex (**4.45**) and so its values were discounted from the calculation. From the other ring carbon data, a value of approximately 70% 'Sn-O bond formation' was determined. All the complexes thus contain strong $Sn\text{-}O_{(carbonyl)}$ bonds. To investigate this deduction further, single crystal X-ray structures of each of the tin complexes were obtained. The ORTEP diagrams are presented in Figures 4.19-4.22. The hydrogens have been omitted for clarity.

Table 4.2

Complex	^{13}C chemical shift (/ppm)				
	C_2	C_3	C_4	C_5	C_6
(**4.44**)	160.2	146.3	175.3	118.2	155.3
(**4.39a-d**) (mean)	157.6	144.9	173.5	112.3	155.9
(**4.45**)	174.6	144.7	173.7	110.2	163.8

4.2.4: Crystal structures of tin-maltol complexes (4.39a-d).

Figure 4.19: Triphenyltin complex (4.39a)

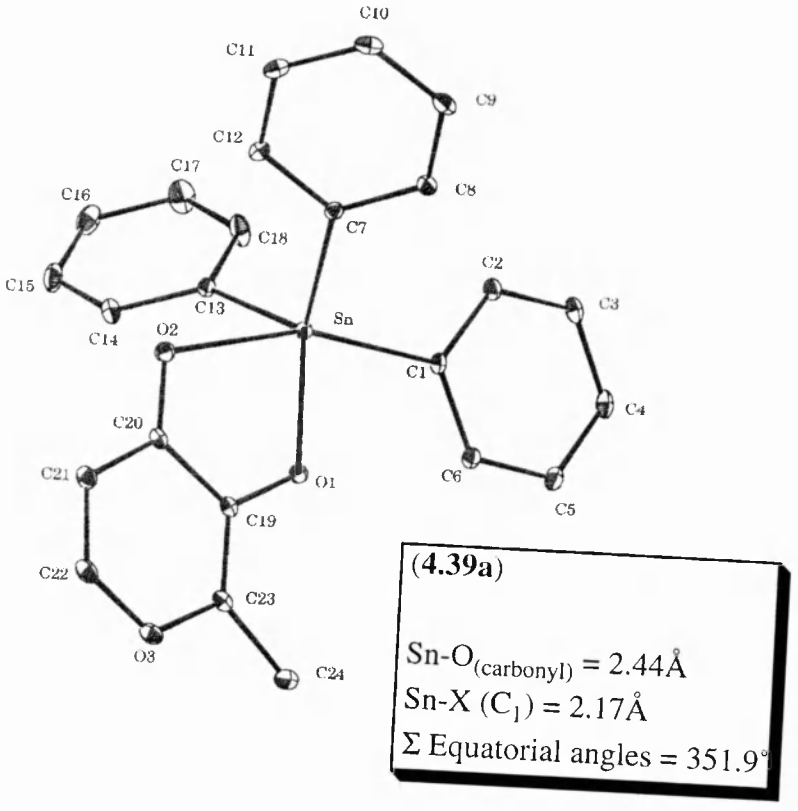

Figure 4.20: Chloride complex (4.39b)

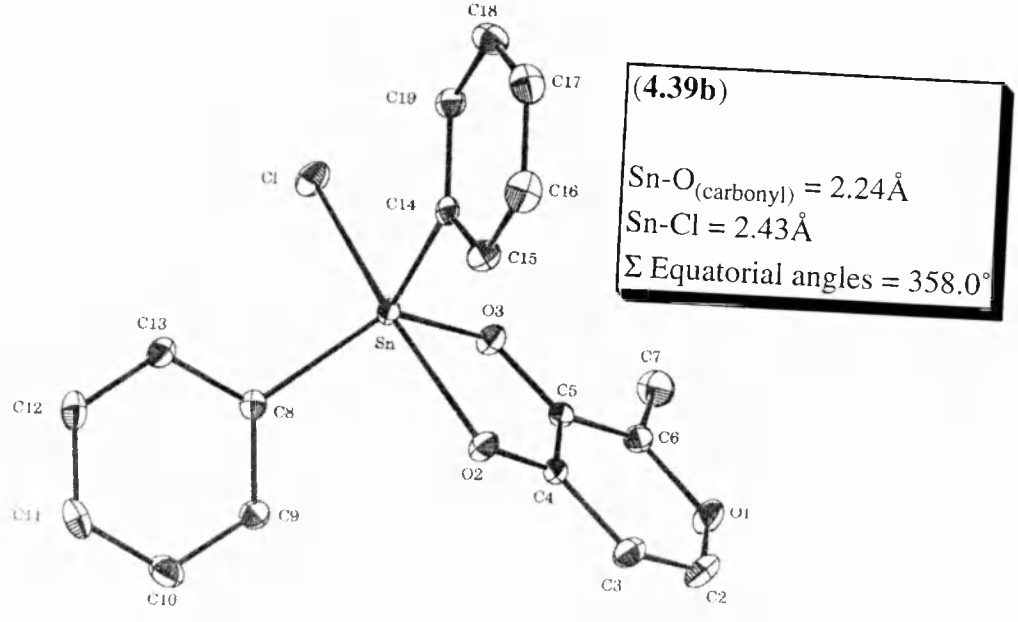

Figure 4.21: Bromide complex (4.39c)

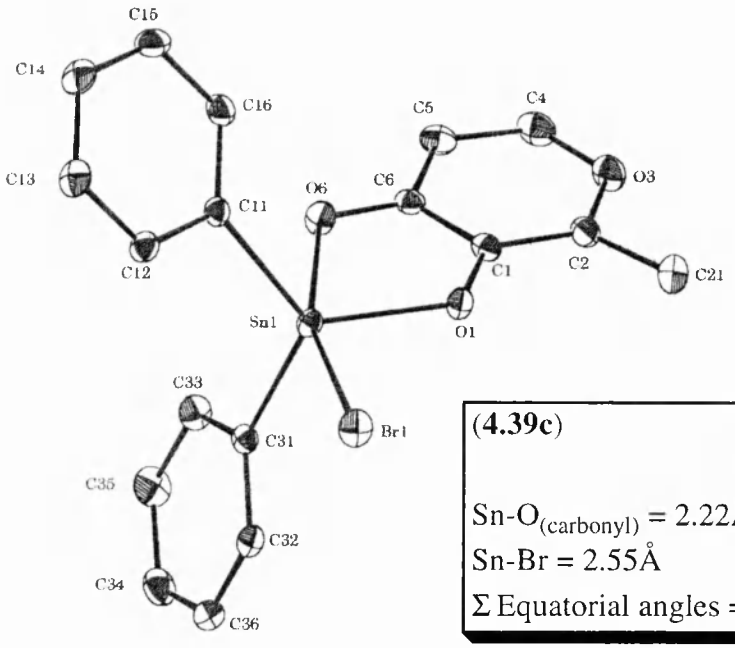

(4.39c)

$Sn\text{-}O_{(carbonyl)}$ = 2.22Å
Sn-Br = 2.55Å
Σ Equatorial angles = 357.8°

Figure 4.22: Iodide complex (4.39d)

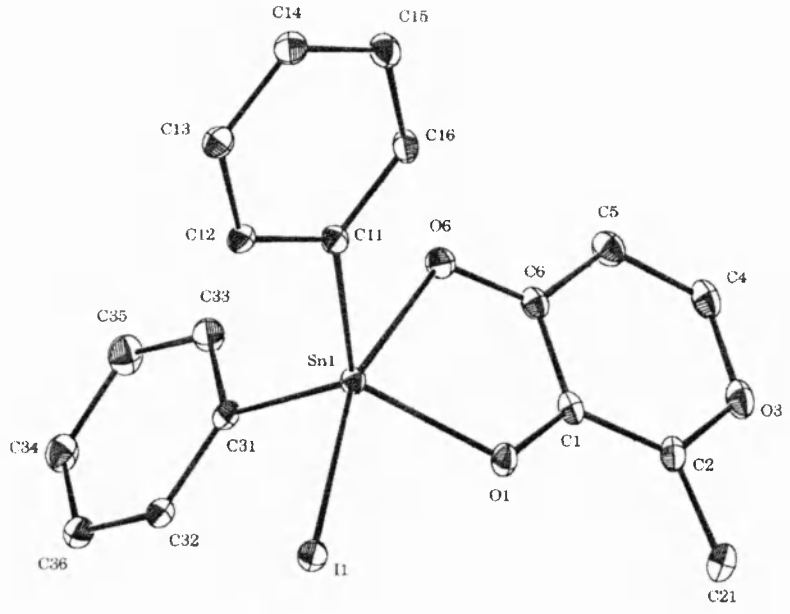

(4.39d)

$Sn\text{-}O_{(carbonyl)}$ = 2.23Å
Sn-I = 2.80Å
Σ Equatorial angles = 357.8°

The key crystallographic data are summarised in Table 4.3.

Table 4.3

X	Ph (**4.39a**)	Cl (**4.39b**)	Br (**4.39c**)	I (**4.39d**)
Sn-X (/Å)	2.17	2.43	2.55	2.80
$Sn\text{-}O_{(carbonyl)}$ (/Å)	2.44	2.24	2.22	2.23
Sn-O (/Å)	2.05	2.05	2.03	2.06
C=O (/Å)	1.25	1.28	1.25	1.28
O-Sn-X (/°)	159.3	163.1	162.0	161.9
Sum of equatorial angles (/°)	351.9	358.0	357.8	357.8

The data reveals that the configuration of the tin remains locked as a trigonal-bipyramidal structure with the only major difference between the structures being the length of the Sn-X bond. The $Sn\text{-}O_{(carbonyl)}$ bond length in each case is largely independent of the 'leaving group'. Only in the case of (**4.39a**) which has a very poor 'leaving group', a phenyl group, is this bond any longer. The $Sn\text{-}O_{(carbonyl)}$ bond length for this compound is about 0.2Å longer and the sum of the equatorial bond angles about 6° less than (**4.39b-d**). This tin complex is therefore the most tetracoordinate structure of the series (**4.39a-d**). The $Sn\text{-}O_{(carbonyl)}$ bond of each complex is 0.2-0.4Å longer than the other Sn-O covalent bond. Therefore, all the $Sn\text{-}O_{(carbonyl)}$ bonds are of considerable strength. This is in agreement with the percentage Sn-O bond formation of approximately 70% calculated for the complexes from the ^{13}C NMR data.

In all structures the diaxial bond angle is distorted from linearity because of the intramolecular nature of the 'nucleophilic attack'. The next-nearest intermolecular tin-halogen distances in the crystals are 6.40Å (**4.39b**), 6.34Å (**4.39c**) and 6.35Å (**4.39d**). These lengths are too great for halogen bridging to be occurring between adjacent tin atoms.

The next step was to modify the 'nucleophilicity' of the ligand. The choice of 3-hydroxy-2-methyl-4-pyridone analogues of (**4.1**) ensured the same local coordination environment at the tin but enabled the electronic structure of the ligand to be changed using different substituents at nitrogen.

4.3: Tin complexes of 4-pyridones

4.3.1: Synthesis of 3-hydroxy-2-methyl-1-phenyl-4-pyridone complexes

Figure 4.23

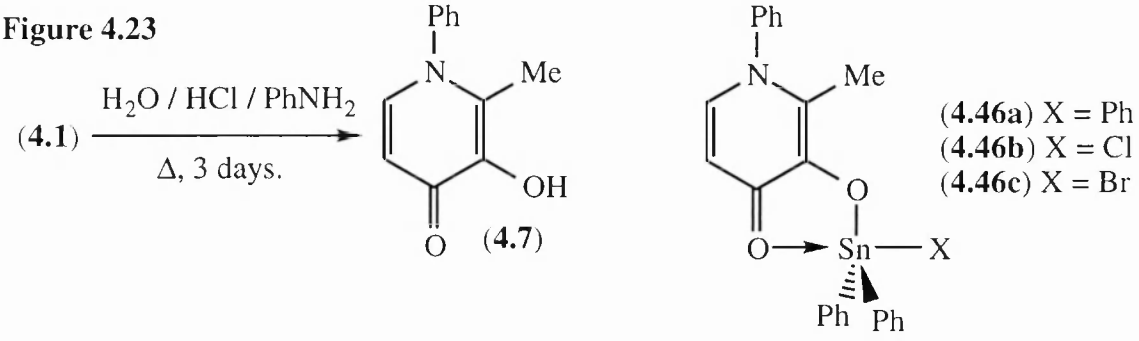

(**4.1**) can be converted into a variety of substituted 4-pyridones in a single step reaction with primary amines.[163] The 3-hydroxy-2-methyl-1-phenyl-4-pyridone ligand (**4.7**) can therefore be prepared from aniline (Figure 4.23). A series of complexes (**4.46a-c**) were prepared via identical routes to the preparation of complexes (**4.39a-d**). We were unable to isolate the iodide analogue of (**4.46a-c**), (**4.46d**), by crystallisation and no further work on this compound was carried out. 3-Hydroxy-1,2-dimethyl-4-pyridone, (**4.47**), is a commercial reagent and was reacted with (**4.42b**) in methanol to produce the 1-methyl substituted complex (**4.48**) (Figure 4.24).

Figure 4.24

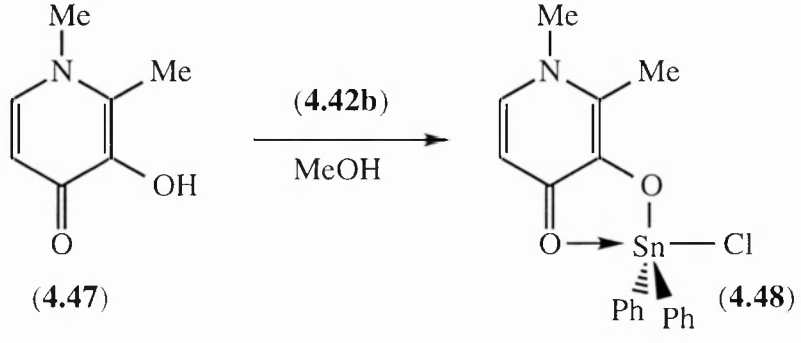

Key spectral data for the complexes (**4.46a-c**) and (**4.48**) are displayed in Table 4.4 with the atom numbering scheme shown in Figure 4.25. The general similarity between the ^{13}C and ^{119}Sn NMR spectra of the four complexes indicates a similar degree of extensive pentacoordination at the tin centre in each case. In d_3-acetonitrile, the least polar solvent in which the compounds were reasonably soluble, the ^{119}Sn chemical shifts are both sensitive to concentration and temperature. Although extensive efforts were made to standardise the measurement conditions, it was not possible to compare reliably the relative extents of hypercoordination between the complexes in solution.

Figure 4.25

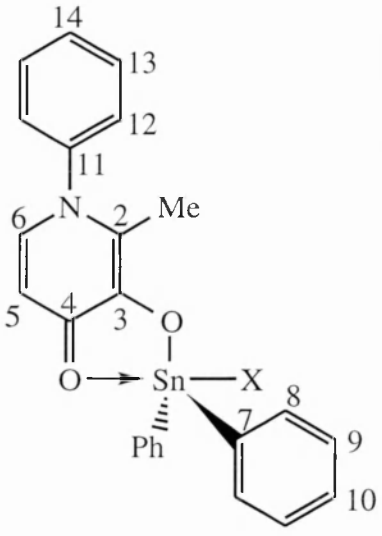

Table 4.4

Compound		(**4.46a**)*	(**4.48**)	(**4.46b**)	(**4.46c**)
^{13}C chemical shift (/ppm)	C_2	158.4	151.3	146.2	151.2
	C_3	150.0	144.2	141.8	142.8
	C_4	169.1	167.4	168.7	168.8
	C_5	108.5	109.7	111.7	109.8
	C_6	146.5	136.1	139.7	137.6
	C_7	134.2	131.9	131.4	130.7
	C_8	137.1	137.0	136.3	136.9
	C_9	127.9	129.6	129.5	129.4
	C_{10}	128.3	131.1	131.2	131.1
	C_{11}	131.4	$(44.1)^+$	130.6	130.8
	C_{12}	129.8	-	131.0	130.9
	C_{13}	126.3	-	127.0	127.4
	C_{14}	129.5	-	131.8	131.0
$\delta\ ^{119}Sn$ (/ppm)		-193.9	-218.8	-198.9	-215.0

(* = Sample in $CDCl_3$, $^+$ = N-Me)

To examine the structures in more detail, single crystals of complexes (**4.46a-c**) were grown and their X-ray structures determined. ORTEP diagrams are presented in Figures 4.26 - 4.28. Table 4.5 is a summary of the key crystallographic data.

4.3.2: Crystal structures of 3-hydroxy-2-methyl-1-phenyl-4-pyridone complexes (4.46a-c).

Figure 4.26: Triphenyltin complex (4.46a)

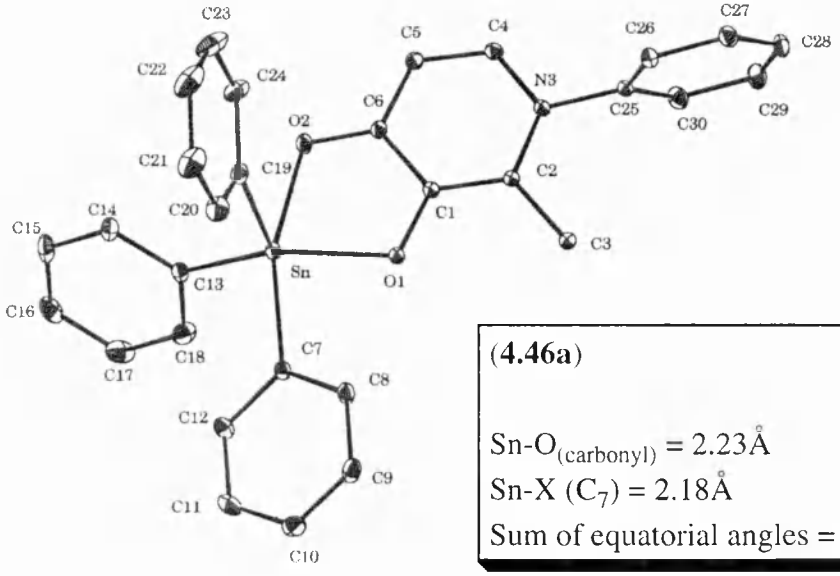

(**4.46a**)

$Sn\text{-}O_{(carbonyl)}$ = 2.23Å
Sn-X (C_7) = 2.18Å
Sum of equatorial angles = 355.9°

Figure 4.27: Chloride complex (4.46b)

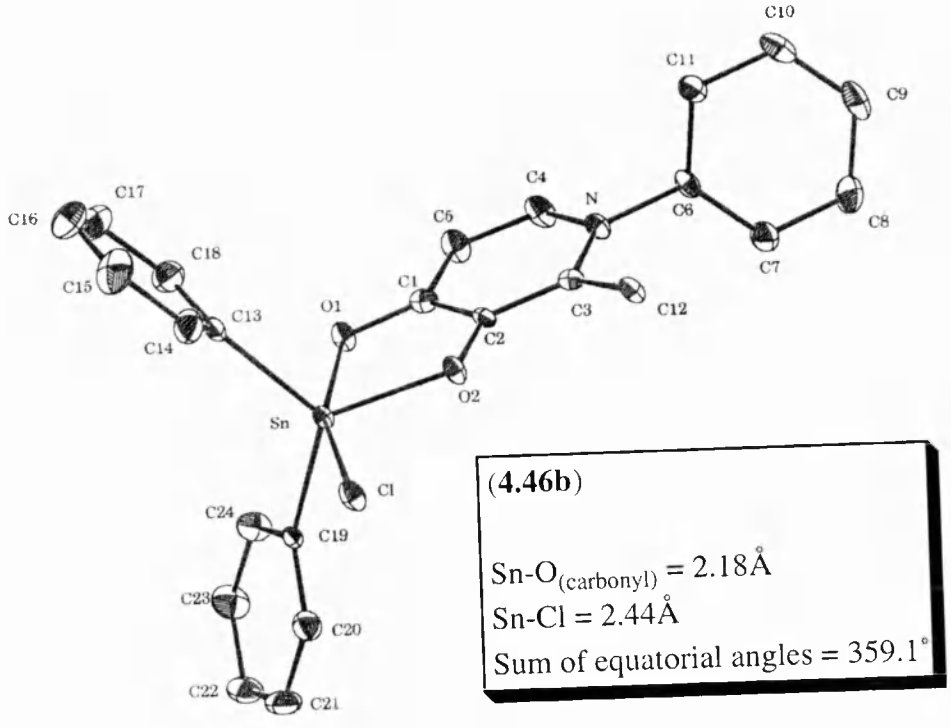

(4.46b)

$Sn\text{-}O_{(carbonyl)}$ = 2.18Å
Sn-Cl = 2.44Å
Sum of equatorial angles = 359.1°

Figure 4.28: Bromide complex (4.46c)

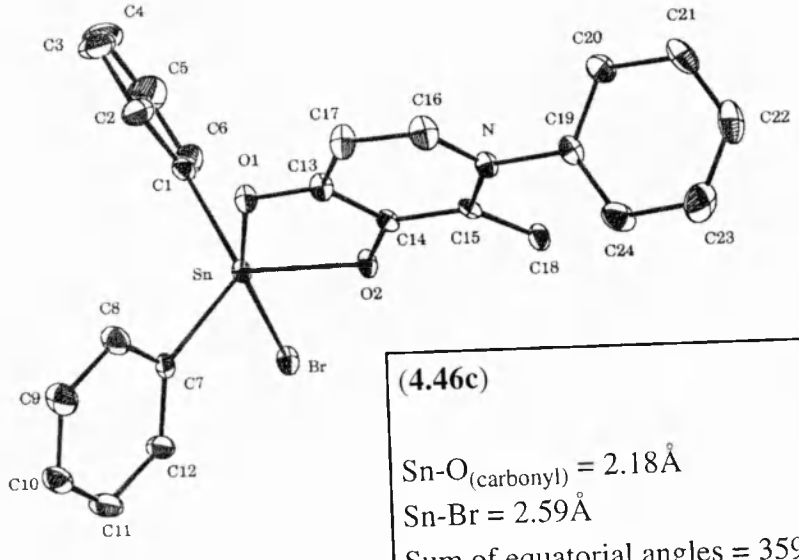

(4.46c)

$Sn\text{-}O_{(carbonyl)}$ = 2.18Å
Sn-Br = 2.59Å
Sum of equatorial angles = 359.0°

Table 4.5

Leaving group X	Ph (**4.46a**)	Cl (**4.46b**)	Br (**4.46c**)
Sn-X (/Å)	2.18	2.44	2.59
$Sn\text{-}O_{(carbonyl)}$ (/Å)	2.23	2.18	2.18
Sn-O (/Å)	2.10	2.06	2.06
C=O (/Å)	1.29	1.28	1.30
O-Sn-X (/°)	159.1	161.6	161.3
Sum of equatorial angles (/°)	355.9	359.1	359.0

As was found for complexes (**4.39a-d**) in Section 4.2.4, the only significant difference between the structures is the Sn-X bond length. Each complex has a distorted, trigonal bipyramidal geometry at tin. When X is the very poor 'leaving group', phenyl, (**4.46a**), a slight increase in the $Sn\text{-}O_{(carbonyl)}$ bond length is observable. The next-nearest tin-halogen distances indicate no bridging between adjacent tin atoms (6.23Å in (**4.46b**) and 6.36Å in (**4.46c**)).

4.3.3: Analysis of the combined crystal data

Table 4.6 compares selected solid state data for complexes (**4.46a-c**) and (**4.39a-c**).

Table 4.6

Leaving group X		Ph (**a**)	Cl (**b**)	Br (**c**)
Sn-X (/Å)	(**4.39**)	2.17	2.43	2.55
	(**4.46**)	2.18	2.44	2.59
$Sn\text{-}O_{(carbonyl)}$ (/Å)	(**4.39**)	2.44	2.24	2.22
	(**4.46**)	2.23	2.18	2.18
Sum of equatorial angles (/°)	(**4.39**)	351.9	358.0	357.8
	(**4.46**)	355.9	359.1	359.0

In summary:

- The Sn-X bond lengths are fractionally longer in complexes (**4.46**) than their (**4.39**) analogues.
- The $Sn\text{-}O_{(carbonyl)}$ distances are slightly shorter in complexes (**4.46**) than their (**4.39**) analogues.
- The sum of the equatorial angles are closer to 360° (ideal trigonal bipyramidal) in complexes (**4.46**) than their (**4.39**) analogues.

The data show that for a given X group, the degree of 'substitution' modelled by the pyridone complexes (**4.46a-c**) is fractionally further along the 'reaction coordinate' for substitution than their maltol analogues (**4.39a-c**). This implies that the pyridone ligand is a marginally better 'nucleophile' than maltol. Changing the 'nucleophilicity' of the 'nucleophile' in hypervalent silicon complexes has a considerable effect on the percentage of nucleophile-silicon bond formation. By contrast for tin, a high 'percentage of nucleophile-tin bond formation' occurs which is much less dependent on the electronic structure of the ligand or the 'leaving group' attached to tin.

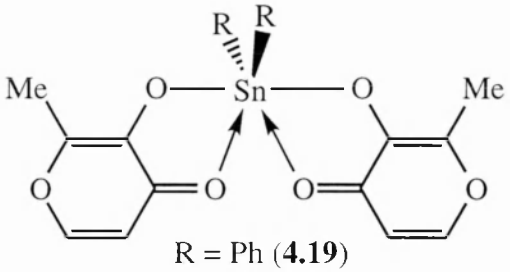

R = Ph (**4.19**)
R = Cl (**4.20**)

As far as we are aware, no crystal structures of pentacoordinate tin complexes of maltol or the related 3-hydroxy-2-methyl-4-pyridones have been published to date, however, the crystal structures of hexacoordinate (**4.19**) and (**4.20**) are known[170] and can be compared to (**4.39a**)/(**4.46a**) and (**4.39b**)/(**4.46b**) respectively (Table 4.7).

Table 4.7

	(**4.39a**)	(**4.46a**)	(**4.19**)*	(**4.39b**)	(**4.46b**)	(**4.20**)
Sn-X (/Å)	2.17	2.18	2.14	2.43	2.44	2.37
$Sn\text{-}O_{(carbonyl)}$ (/Å)	2.44	2.23	2.25	2.24	2.18	2.13
Sn-O (/Å)	2.05	2.10	2.10	2.05	2.06	2.06
C=O (/Å)	1.25	1.29	1.27	1.28	1.28	1.30
$O_{(carbonyl)}$-Sn-X (/°)	159.3	159.1	162.9	163.1	161.6	168.0

* Mean values over the two independent molecules in the crystal

The strength of the ligand-tin binding in (**4.39a**) and (**4.46a**) is comparable with that of (**4.19**) dispite the difference in tin coordination number. The diaxial bond angle of (**4.19**) is closer to being linear than those of (**4.39a**) and (**4.46a**). This is primarily because the greater crowding around tin in a hexacoordinate complex requires the groups around it to more closely occupy their ideal sites. The same applies to (**4.20**) compared to (**4.39b**) and (**4.46b**).

The crystal structures of a number of intramolecularly pentacoordinated triphenyltin complexes have been reported, for example (**1.72**),[97] (**4.49**)[179] and (**4.50**).[180]

Table 4.8 below summarises the important crystal data. The ordering of the complexes is that of decreasing 'Sn-$O_{(carbonyl)}$' bond length.

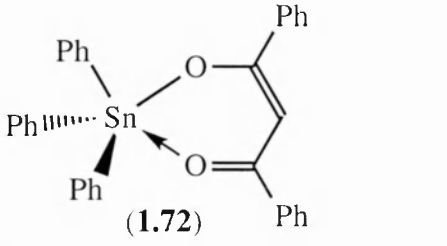

(**1.72**)

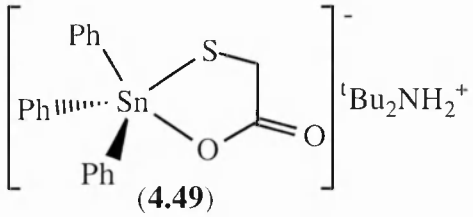

(**4.49**)

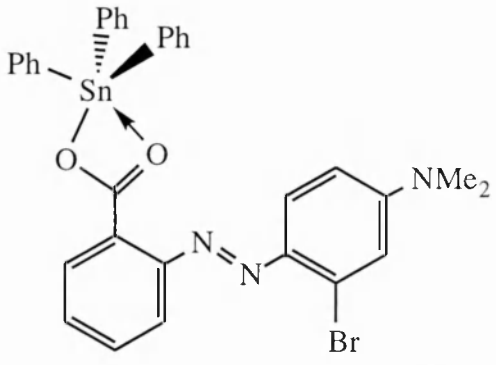

(**4.50**)

Table 4.8

	(**4.50**)	(**4.49**)	(**4.39a**)	(**1.72**)	(**4.46a**)
Sn-$Ph_{(axial)}$ (/Å)	2.15	2.17	2.17	2.18	2.18
Sn-$O_{(carbonyl)}$ (/Å)	2.66	2.61*	2.44	2.28	2.23
$O_{(carbonyl)}$-Sn-$Ph_{(axial)}$ (/°)	148.0	166.8	159.3	163.7	159.1
Σ Equatorial angles (/°)	339.6	350.0	351.9	355.2	355.9
C=O (/Å)	1.25	$(1.24)^+$	1.25	1.26	1.29

(* = Sn-OCOR, $^+$ = carbonyl not involved in chelation to tin)

In summary:

- The shorter the Sn-$O_{(carbonyl)}$ bond, the more trigonal bipyramidal is the tin. The sum of the equatorial angles for (**4.50**) is particularly small because the chelate forms a four-membered ring. This causes considerable distortion to the geometry of the tin.
- Strong pentacoordination does not lead to appreciable Sn-$Ph_{(axial)}$ bond extension.
- The C=O bond lengthens slightly with increasing Sn-$O_{(carbonyl)}$ bond strength.
- The $O_{(carbonyl)}$-Sn-$Ph_{(axial)}$ diaxial angle changes erratically with increasing Sn-$O_{(carbonyl)}$ bonding because it is also affected by the size of the ring formed on chelation.

By comparing the crystal structures of complexes (**4.39a**) and (**4.39c**), the effect of chelation on the pyrone ring can be judged. (**4.39c**) has a Sn-$O_{(carbonyl)}$ bond 0.20Å shorter than (**4.39a**). In (**4.39c**) the pyrone ring C=C bonds are about 0.01Å longer and the C-C bonds about 0.02Å shorter, on average, than (**4.39a**). This corresponds to there being

greater ring π electron delocalisation in the complex containing the stronger Sn-$O_{(carbonyl)}$ bond. This is in agreement with the observations made on the effect of protonation of the pyrone carbonyl-oxygen in Section 4.1.

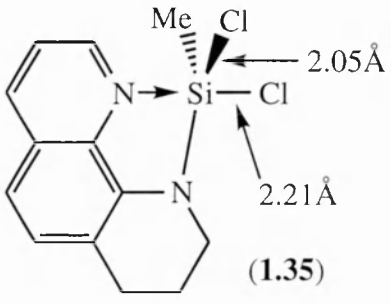

(**1.35**)

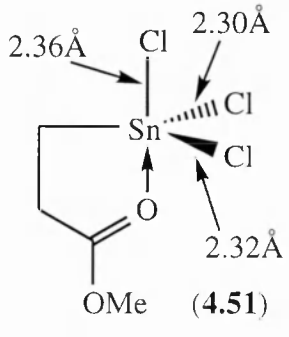

(**4.51**)

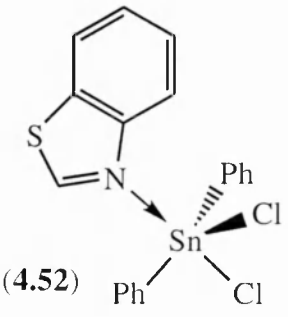

(**4.52**)

Axial silicon-chlorine bonds are often considerably longer than when in equatorial positions in pentacoordinate compounds (for example (**1.35**)

[44]) or in tetra-coordinate silicon compounds. In contrast, tin-chlorine bonds are affected relatively little by their axial/equatorial position, for example (**4.51**).[181] Tin-chlorine bonds in general are affected little by increase in coordination number. By our own calculation, complex (**4.39b**) contains an Sn-$O_{(carbonyl)}$ bond which is approximately 70% formed, yet the Sn-Cl bond length of 2.43Å is only about 0.1Å longer than the Sn-Cl distance in tetracoordinate triphenyltin chloride, 2.32Å.[182] The 2.43Å Sn-Cl bond in (**4.39b**) is a typical pentacoordinate Sn-Cl bond length. For example (**4.52**)[183] has an axial Sn-Cl bond of 2.45Å and an equatorial Sn-Cl bond of 2.34Å.

The Sn-Br bond lengths in complexes (**4.39c**) and (**4.46c**) are 2.55Å and 2.59Å respectively. These lengths are of a similar dimension to examples of both pentacoordinate (**4.53**)[184] and tetracoordinate (**4.54**)[185] tin-bromide complex crystal structures in the literature.

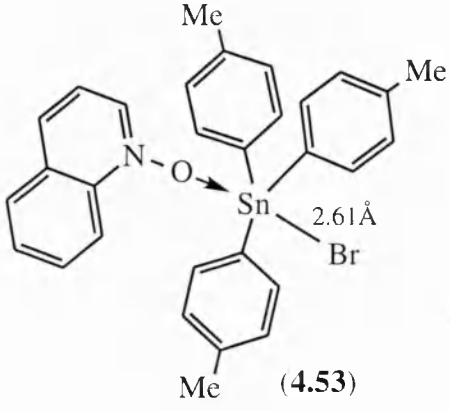

(**4.53**)

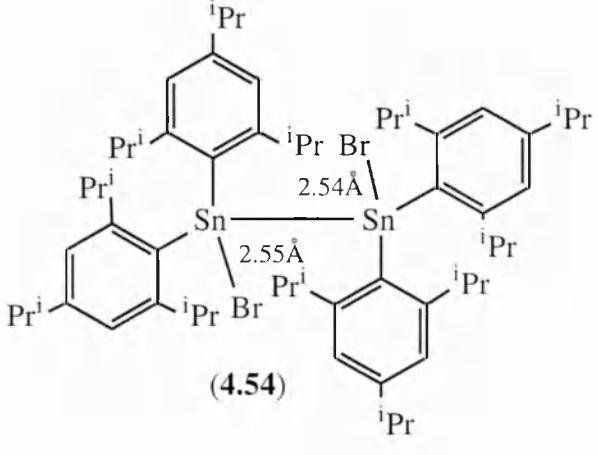

(**4.54**)

The Sn-I bond length in complex (**4.39d**) is 2.80Å. This distance is relatively large compared to examples of tetracoordinate (**4.55**)[186] and even hexacoordinate (**4.56**)[187] iodide complex crystal structures reported in the literature.

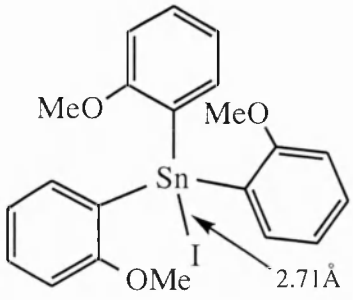

(**4.55**)

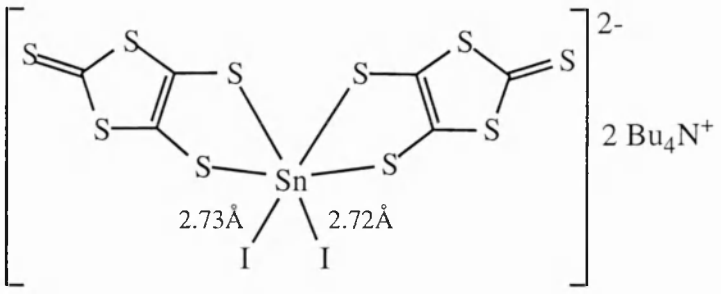

(**4.56**)

The data for our structures can be plotted onto the map of nucleophilic substitution at tin produced by Dunitz[51] (Table 4.9 and Figure 4.29). The lower limits of bond length used to determine Δd_y and Δd_x are Sn-O 1.90Å, Sn-C 2.10Å, Sn-Cl 2.29Å, Sn-Br 2.45Å and Sn-I 2.69Å, as used by Dunitz. The data points lie close together and are all positioned beneath the curve. Therefore the structures are models of the same small region of the 'reaction' profile are particularly *tight* in having shorter Sn-'nucleophile' and Sn-'leaving group' bond lengths than those typical of Dunitz's study. Although Dunitz's paper does not name the specific compounds, he considered approximately fifty complexes of very varied types. The fact that our data do not fit exactly the trend of the plot is related to the specific chelating characteristics of the maltol and pyridone ligands and the small number of relatively similar compounds we prepared, rather than a breakdown of the structural correlation method.

Table 4.9

	Sn-O (/Å)	Δ Sn-O (Δd_y) (/Å)	Sn-X (/Å)	Δ Sn-X (Δd_x) (/Å)
(**4.39a**)	2.44	0.54	2.17	0.07
(**4.39b**)	2.24	0.34	2.43	0.14
(**4.39c**)	2.22	0.32	2.55	0.10
(**4.39d**)	2.23	0.33	2.80	0.11
(**4.46a**)	2.23	0.33	2.18	0.08
(**4.46b**)	2.18	0.28	2.44	0.15
(**4.46c**)	2.18	0.28	2.59	0.14

Figure 4.29

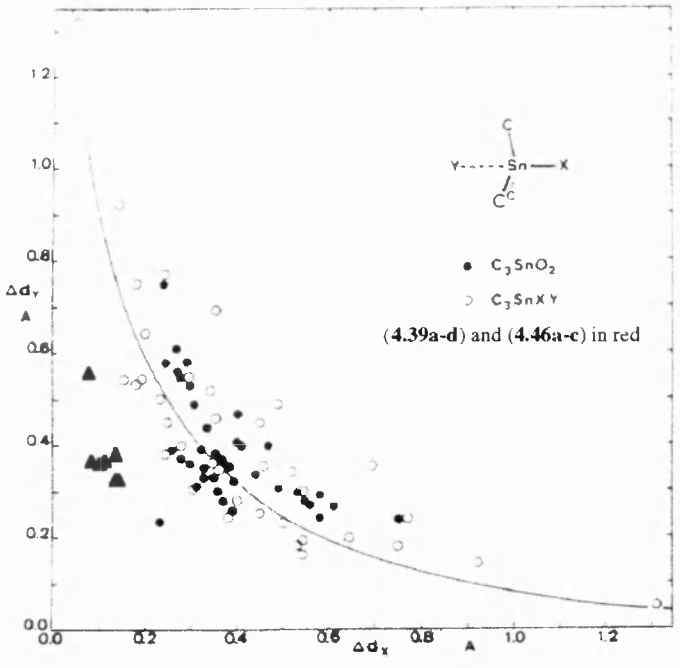

4.3.4: Synthesis of 3-hydroxy-1-(4-methoxyphenyl)-2-methyl-4-pyridone complexes

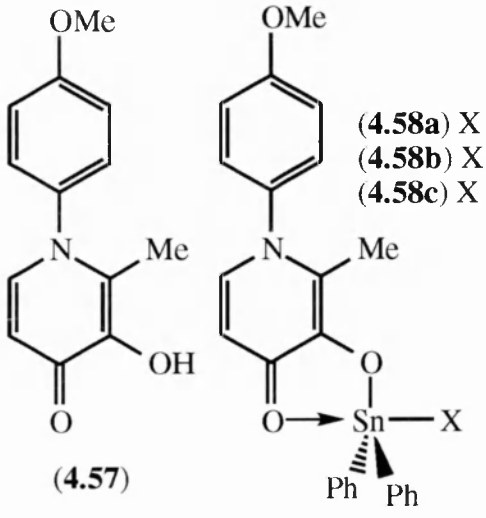

(**4.58a**) X = Ph
(**4.58b**) X = Cl
(**4.58c**) X = Br

Since ligand modification caused a small geometric change to the extent of substitution, further electronic adjustment was attempted by substituting the 1-phenyl ring in the *para* position with a 4-methoxy group (an electron donor relative to hydrogen). The ligand (**4.57**) was prepared from (**4.1**) and 4-methoxyaniline as before. A series of complexes (**4.58a-c**) were prepared via the routes discussed previously for (**4.39a-d**) and (**4.46a-c**). It was not possible to grow crystals suitable for X-ray analysis, however, the ^{119}Sn NMR resonances indicate strong pentacoordination in all complexes (Table 4.10).

Table 4.10

X	Ph (**a**)	Cl (**b**)	Br (**c**)
(**4.58**)	-195.8	-215.4	-213.6

4.4: Tin complexes of 3-hydroxy-2-methyl-4-thiopyrones

A final attempt to perturb the geometry of the tin/maltol complex system was made by softening the 'nucleophilicity' of the 'nucleophile'. This was achieved by the use of 3-hydroxy-2-methyl-4-thiopyrone (**4.8**) as the chelating ligand. (**4.8**) was prepared by the thiolation of (**4.1**) with phosphorous pentasulfide (Figure 4.30). The chloride (**4.59b**) and bromide (**4.59c**) complexes were prepared in the same manner to (**4.39b**) and (**4.39c**) (Figure 4.15).

Figure 4.30

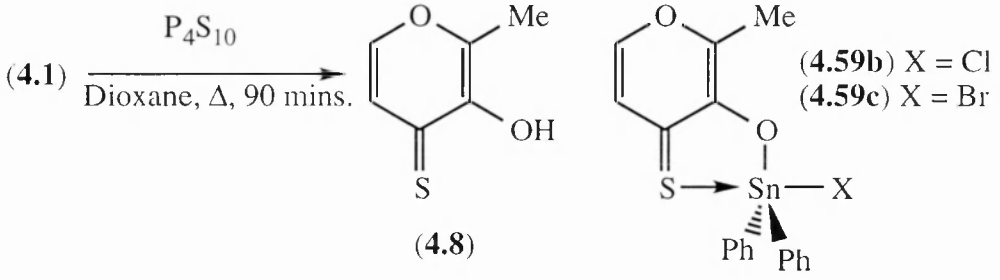

The ^{119}Sn NMR spectra of complexes (**4.59b/c**) display resonances characteristic of highly pentacoordinated tin (about δ -210) with no clear differences from the spectra of complexes (**4.39a-d**). The ^{119}Sn chemical shifts of all the tin complexes are summarised in Table 4.11.

Table 4.11

Complex type	^{119}Sn chemical shift (/ppm)			
	Ph (**a**)	Cl (**b**)	Br (**c**)	I (**d**)
Maltol (**4.39**)	-166.6	-201.5	-196.0	-271.4
1-Ph 4-pyridone (**4.46**)	-193.9*	-198.9	-215.0	-
1-Me 4-pyridone (**4.48**)	-	-218.8	-	-
1-(4-OMe)-Ph-4-pyridone (**4.58**)	-195.8	-215.4	-213.6	-
4-Thiopyrone (**4.59**)	-	-208.8*	-212.0*	-

(* sample in $CDCl_3$)

Excluding (**4.39d**), which shows a *heavy atom* effect, the only complex which deviates significantly from the δ -200 region is (**4.39a**). This may be the only compound where the degree of substitution measurably affects the ^{119}Sn chemical shift. (**4.39a**) involves the poorest 'nucleophile' coordinating to the least 'electrophilic' tin centre and so contains the weakest nucleophilic attack at tin. This gives rise to the least shielded ^{119}Sn resonance of all the tin complexes. This is in agreement with the crystal

structure data (assuming the same structure in the solid-state and solution). The $Sn\text{-}O_{(carbonyl)}$ distance observed in complex (**4.39a**) (2.44Å) is 0.20Å longer than the next-longest such measured distance (2.24Å in complex (**4.39b**)). The remaining $Sn\text{-}O_{(carbonyl)}$ distances are relatively similar - occurring in a narrow range from 2.23 to 2.18Å.

Throughout the series of complexes synthesised ((**4.39a-d**), (**4.46a-c**) (**4.48**), (**4.58a-c**) and (**4.59b/c**)), broadly similar, highly pentacoordinate structures have been observed, largely independent of 'leaving group', ligand 'nucleophilicity' or the softness of the 'nucleophilic' atom. This confirms that tin (IV)'s preference for the formation and stabilisation of coordination states higher than four is much greater than is the case for silicon. In this sense tin (IV) acts far more like a transition metal than silicon. The particular geometry of the ligand appears particularly suited, in combination with the other substituents at tin, to the formation of strong 5-coordinate complexes. It is this characteristic which causes our complexes to deviate from the trend of Figure 4.29. Therefore instead of modelling substitution, we are largely modelling tin coordination number expansion.

4.5: A pentacoordinate silicon complex of maltol

Figure 4.31

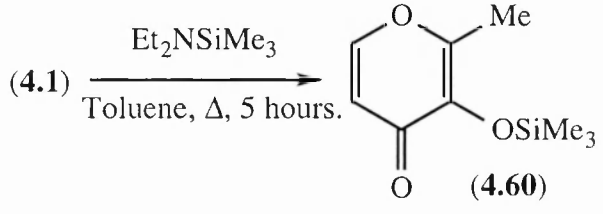

The preparation of a silicon analogue of the tin/maltol compounds will allow a direct comparison of the ability of the two metals to form hypercoordinate complexes. (**4.60**), the trimethylsilylated form of (**4.1**), was prepared from (**4.1**) using trimethylsilyldiethylamine (Figure 4.31). The chlorodiphenylsilyl complex, (**4.61**), was then isolated from a dry acetonitrile solution of dichlorodiphenylsilane and (**4.60**) (Figure 4.32).

Figure 4.32

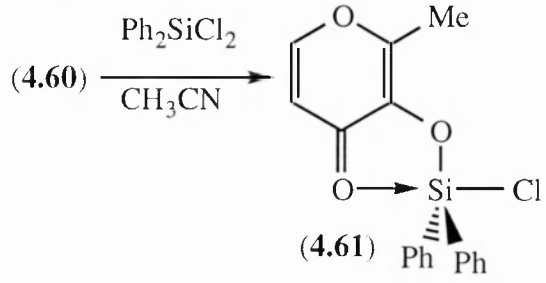

Single crystals suitable for X-ray structure analysis were prepared by cooling a concentrated acetonitrile solution in a refrigerator at 3°C for 2 days. The ORTEP diagram is presented in Figure 4.33. Two molecules are pictured as the unit cell contains two independent molecules. The geometry of the silicon complex (M = Si) is visually compared to its tin analogue (**4.39b**) (M = Sn) in Figure 4.34 and by their key crystallographic data in Table 4.12.

Table 4.12

	M-X (/Å)	M-$O_{(C=O)}$ (/Å)	M-O (/Å)	O-M-$O_{(C=O)}$ (/°)	$O_{(C=O)}$ M-X (/°)	Sum of equatorial angles (/°)
(**4.61**)*	2.21	1.97	1.73	84.2	169.4	359.3
(**4.39b**)	2.43	2.24	2.05	76.8	163.1	358.0

* Mean values

Figure 4.33

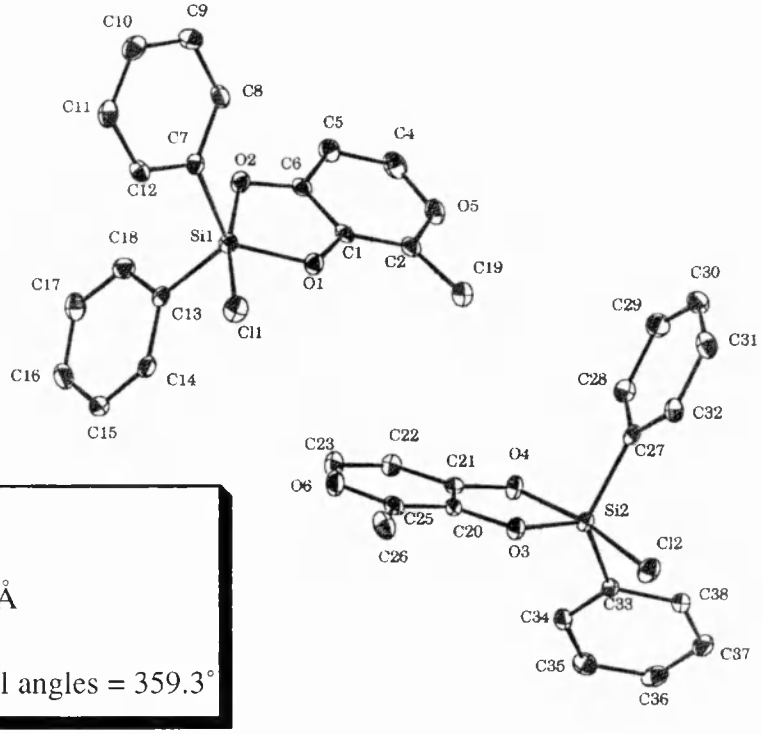

(**4.61**)

Si-$O_{(C=O)}$ = 1.97Å
Si-Cl = 2.21Å
Sum of equatorial angles = 359.3°

Figure 4.34

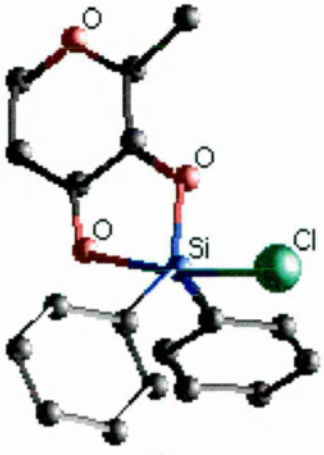

(**4.61**)

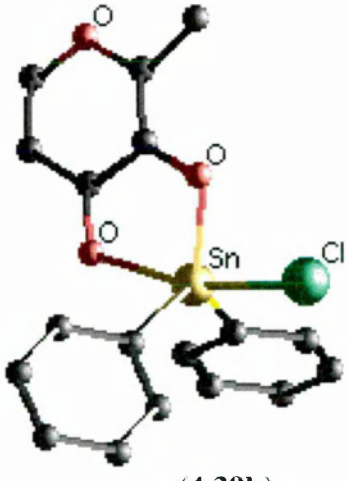

(**4.39b**)

The rigid nature of the ligand backbone and the greater covalent radius of tin compared to silicon causes (**4.39b**) to have a more distorted pentacoordinate trigonal bipyramidal geometry than (**4.61**). This is shown in the $O_{(carbonyl)}$-M-X diaxial bond angle which is more distorted from the ideal 180° and the sum of the equatorial bond angles which is more distorted from the ideal 360°. As the tin is situated further away from the maltol ligand, its O-M-O 'bite' angle is smaller. The Sn-$O_{(carbonyl)}$ distance is considerably closer to a full Sn-O bond (about 2Å) than the Si-$O_{(carbonyl)}$ bond is to a full Si-O bond (about 1.5Å). Therefore, as expected, tin is the better 'electrophile'.

In order to compare the extension of different Si-X bonds in Chapter 2, a 'percentage Si-X bond extension' term was used. The calculations relied on values of the crystal ionic radii for Si^+ and X^- for success. However, we are unaware that a value for Sn^+ is available in the literature. Instead, a more general **percentage length** term shall be used for a comparison of hypervalent bonding in silicon and tin. We define this as:

$$\text{Percentage length} = \frac{\text{Found bond length}}{\text{Typical bond length}} \times 100$$

Values of typical bond lengths involving tin are those used by Dunitz[51] (page 136). Typical bond lengths involving silicon are those quoted in Table 2.10. Therefore if the percentage length of M-O and M-X bonds in complexes (**4.61**) and (**4.39b**) were calculated and summed, values in excess of 200% would be expected. Summed values close to 200% represent complexes containing strong M-O and M-X bonds where M prefers to increase its coordination number when a 'nucleophile

attacks'. The larger the sum of the percentages the more M favours a *loose* pentacoordinate state. In terms of our nucleophilic attack model, the extent of bond formation matches that of bond breaking. Totals of 250% for (**4.61**) and 228% for (**4.39b**) are obtained. This confirms tins greater ability to expand its coordination number from four to five.

The structure of (**4.61**) can also be compared to that of the quinoline silyl-chloride complex (**2.25b**) (Table 4.13).

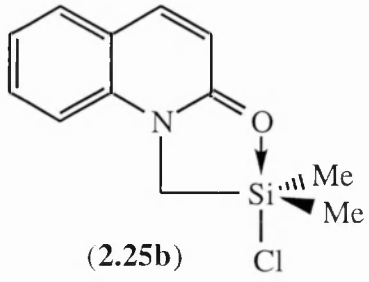

(**2.25b**)

Table 4.13

Complex	Si-$O_{(carbonyl)}$ (/Å)	Si-Cl (/Å)
(**4.61**)	1.97	2.21
(**2.25b**)	1.94	2.32

Complex (**2.25b**) contains a shorter $O_{(carbonyl)}$-Si interaction and a longer Si-Cl bond which represents 'substitution' *frozen* marginally further towards completion. The maltol ligand is therefore the slightly poorer 'nucleophile'.

4.6: Temperature, concentration and solvent dependence of the ^{119}Sn chemical shift

In practice it has proved difficult to obtain consistent ^{119}Sn NMR chemical shifts for the tin complexes in CD_3CN. Since X-ray data has shown that the intramolecular coordination is largely identical in all the complexes, fluctuations in the ^{119}Sn chemical shift in solution are almost certainly derived from independent processes related to the interaction, **1**, between the solvent and the pentacoordinate Sn (IV) centre or, **2**, between complex molecules themselves.

The first effect arises because acetonitrile contains a nitrogen lone pair capable of coordination to the tin. Since tin can readily expand its coordination number to six, it is possible that, for example, a hexacoordinate solvent complex ([**4.62**]) may exist in fast equilibrium with (**4.39c**) and free solvent (Figure 4.35). The higher the concentration of this hexacoordinate species, the lower the ^{119}Sn chemical shift. This 'reaction' is exothermic such that the 6-coordinate state is favoured over the five-coordinate state at lower temperatures. The process is solvent dependant and so less 'nucleophilic' solvents are unlikely to promote it.

Figure 4.35

$(maltol)Ph_2SnBr \quad CH_3CN \rightleftharpoons [(maltol)Ph_2BrSn{\leftarrow}NCCH_3]$

(**4.39c**) ([**4.62**])

The second effect arises from halogen-bridging interactions. This may lead to, for example, a dimer species ([**4.63**]) containing two hexacoordinate tin atoms in fast equilibrium with pentacoordinate complex monomers (Figure 4.36).

Figure 4.36

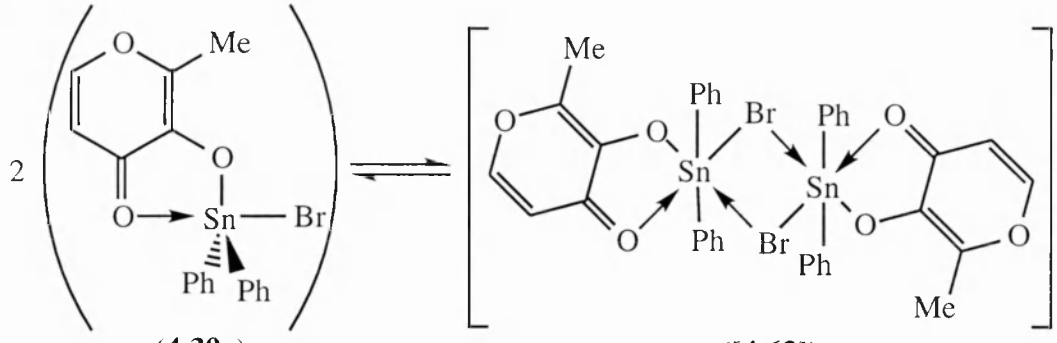

(**4.39c**) ([**4.63**])

Dilution reduces the relative concentration of the hexacoordinate dimer with respect to the pentacoordinate monomer leading to ^{119}Sn chemical shifts of lower field. Stable dimer complexes containing pairs of halogen bridges can sometimes be isolated in the solid state, for example, (**1.64**).[88]

4.6.1: Variable temperature ^{119}Sn NMR studies on complex (4.39c)

Two solutions of (**4.39c**) were prepared of identical concentration (0.4M), one in deuterochloroform, the other in d_3-acetonitrile. The ^{119}Sn chemical shift was measured at a range of temperatures above and below room temperature. The data is presented in Table 4.14 and Figure 4.37.

When the complex solutions were returned to room temperature after the experiment, the chemical shifts reverted to their original room temperature values. Changes to the chemical shifts were thus caused by a temperature-dependant equilibria. Since changing the solvent drastically reduces the effect of temperature on the ^{119}Sn chemical shifts, reversible solvent complexation is the probable cause of the dependency of the ^{119}Sn chemical shift on temperature. If dimerisation were the key process for the temperature effect, then changing the solvent from CD_3CN (a polar organic solvent) to $CDCl_3$ (a moderately polar organic solvent) should not significantly change its dependence on temperature. The fact that the plots cross implies that both

Table 4.14

Temperature (/°C)	^{119}Sn chemical shift of (**4.39c**) (/ppm)	
	$CDCl_3$	CD_3CN
65	-	-144.7
55	-	-154.3
45	-195.5	-166.5
35	-195.0	-177.6
25	-194.4	-187.0
20	-194.1	-191.5
10	-193.5	-199.5
0	-193.1	-208.1
-10	-192.6	-217.3
-20	-192.2	-226.3
-30	-191.7	-234.7
-40	-191.3	-
-50	-191.9	-
-55	-190.7	-

Figure 4.37

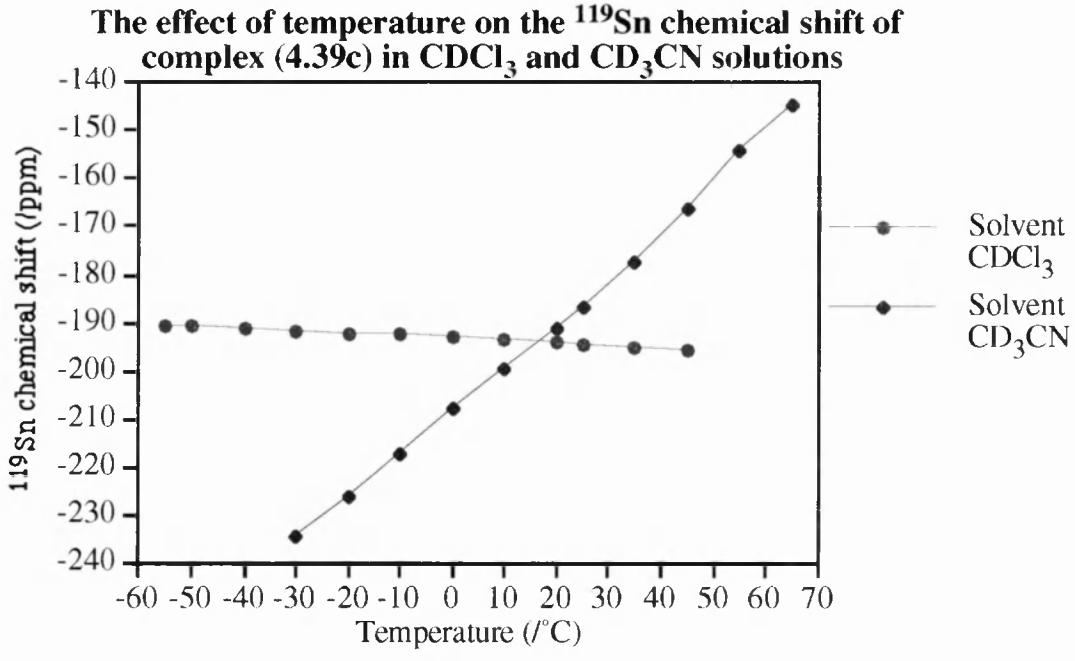

solvents have the same degree of interaction with the complex at that particular temperature (about 20°C). It also implies that the $CDCl_3$ must interact with (**4.39c**), but that the interaction remains constant with temperature. We cannot explain why the plots cross in this fashion.

4.6.2: Variable concentration studies

The ^{119}Sn NMR chemical shift of (**4.39c**) was measured in 25°C CD_3CN solutions at a variety of concentrations. The results are shown in Table 4.15 and plotted in Figure 4.38.

Table 4.15

Solution concentration (/M)	0.41	0.34	0.30	0.26	0.21	0.17	0.15
δ ^{119}Sn (/ppm)	-201.7	-198.9	-197.0	-196.3	-192.6	-189.5	-186.5

Figure 4.38

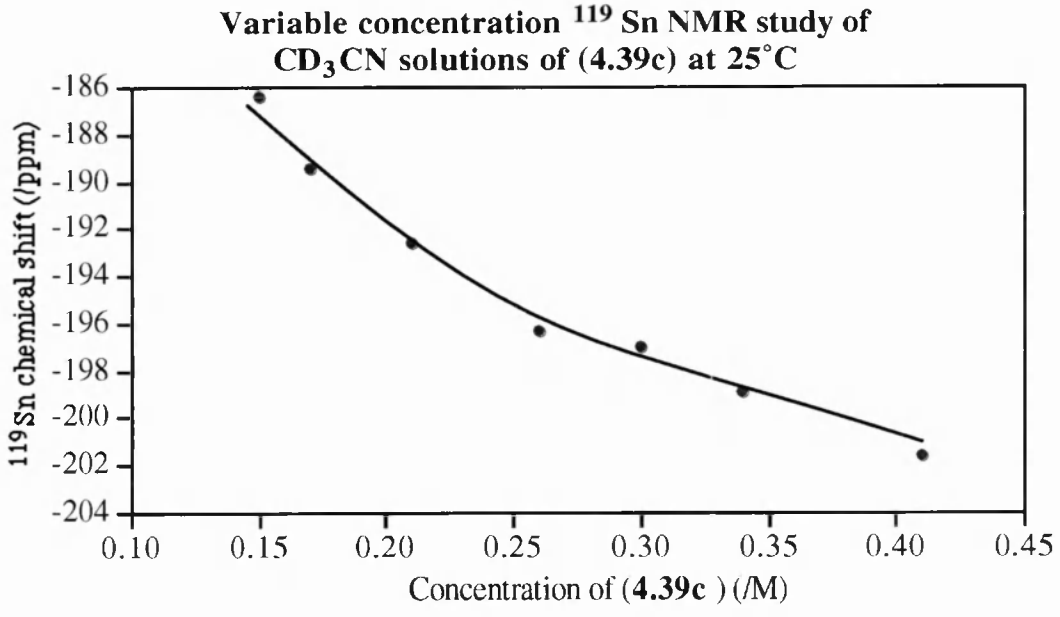

The down field movement of the observed ^{119}Sn shift with increased dilution is in agreement with the reversible formation of dimer complexes. We would expect that any solvent interaction would not be affected by increased dilution unless there is a large change in dielectric constant and thus would have little effect on the chemical shift. These studies thus suggest that in acetonitrile both dimerisation and solvent interaction are present.

A CD_3CN solution containing a 1:1 mixture of the chloride (**4.39b**) and the bromide (**4.39c**) (both approximately 0.2M) complexes gives rise to only a single ^{119}Sn NMR peak in the temperature range 20°C to -50°C. This suggests that, unless the resonances are accidentally equivalent, there is a fast (on the NMR timescale) intermolecular exchange of halogen atoms giving rise to an average tin signal. On cooling the resonance moves more up field (Table 4.16). This again suggests that in

CD_3CN solutions both solvent coordination and halogen bridging occurs, and that the equilibrium constant for the solvent-tin complexation is affected by temperature much more than dimerisation.

Table 4.16

Temp' (/°C)	20	10	0	-10	-20	-30	-40	-50
δ ^{119}Sn 1:1 (**4.39b/c**)	- 206.4	- 216.7	- 228.2	- 238.3	- 246.9	- 254.1	- 260.7	- 266.5

Figure 4.39

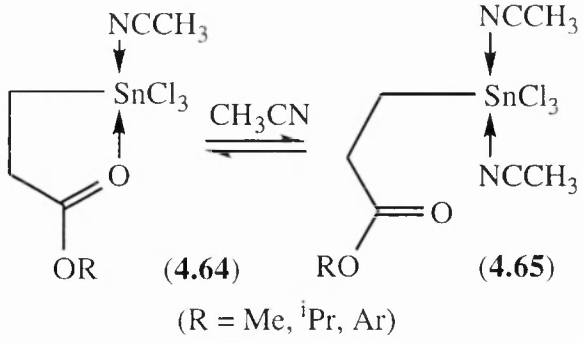

(**4.64**) (**4.65**)

(R = Me, ^{i}Pr, Ar)

Coordination of acetonitrile to tin is already well known and indeed a stable 2:1 complex of CH_3CN and $SnCl_4$ has been characterised in the solid state.[188] In acetonitrile solution, structures of type (**4.64**) are stable and studies of their interconversion to ring opened form (**4.65**) by attack of a second solvent molecule have been performed (Figure 4.39).[189] The position of the IR bands for the coordinated and uncoordinated carbonyl groups distinguish the structures apart.

4.7: The effect of added nucleophile on five coordinate silicon and tin centres

4.7.1: Silicon complex (4.61)

Aliquots of the nucleophile N-methyl imidazole (NMI) were added to a $CDCl_3$ solution of complex (**4.61**) and the ^{29}Si NMR spectra recorded. A solution of (**4.61**) gave a ^{29}Si resonance at δ -85.3 for the pentacoordinated silicon. Upon addition of one equivalent of NMI, a single sharp resonance at δ -72.2 appeared, while the original, and still the major, peak broadened slightly and moved to δ -87.6. With a second equivalent of NMI, the resonance at δ -72.2 remained unchanged while the second peak broadened significantly into the baseline at about δ -89. In comparison, a study of the interaction of complex (**1.38**) with NMI in solution has been reported.[190] A solution of

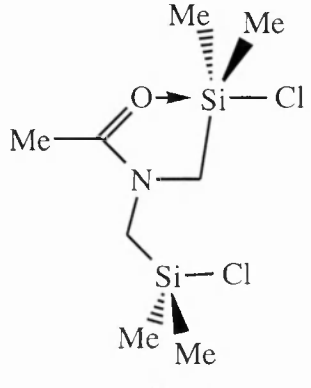

(**1.38**)

(**1.38**) gave a ^{29}Si NMR chemical shift of δ -39 for the pentacoordinate silicon and δ 26.8 for the tetracoordinate silicon. When half an equivalent of NMI was present, the signal at δ -39 broadened almost completely into the base line. When an equivalent of NMI had been added, it sharpened slightly with a chemical shift of δ -54. Finally, with two equivalents of NMI this peak had sharpened to a normal line width and retained the same chemical shift. Meanwhile the tetracoordinate silicons chemical shift remained largely unaffected. This revealed that substitution was taking place exclusively at the pentacoordinate silicon centre yielding a species ([**4.66**]) (Figure 4.40).

Our observations of complex (**4.61**) are that its ^{29}Si NMR peak broadens and becomes more shielded the more NMI added. This is consistent with exchange of NMI and chloride ion taking place to give ([**4.67**]). Attempts to isolate ([**4.67**]) yielded only (**4.61**) and NMI. In contrast to the study of (**1.38**), we do not observe a sharpening of the ^{29}Si resonance in the solution containing two equivalents of NMI. This suggests that the equilibrium between (**4.61**) and ([**4.67**]) is slower on the NMR timescale than between (**1.38**) and ([**4.66**]). We are unable to explain the appearance of the sharp peak at δ -72.2; though it is only a minor component of the solution.

Figure 4.40

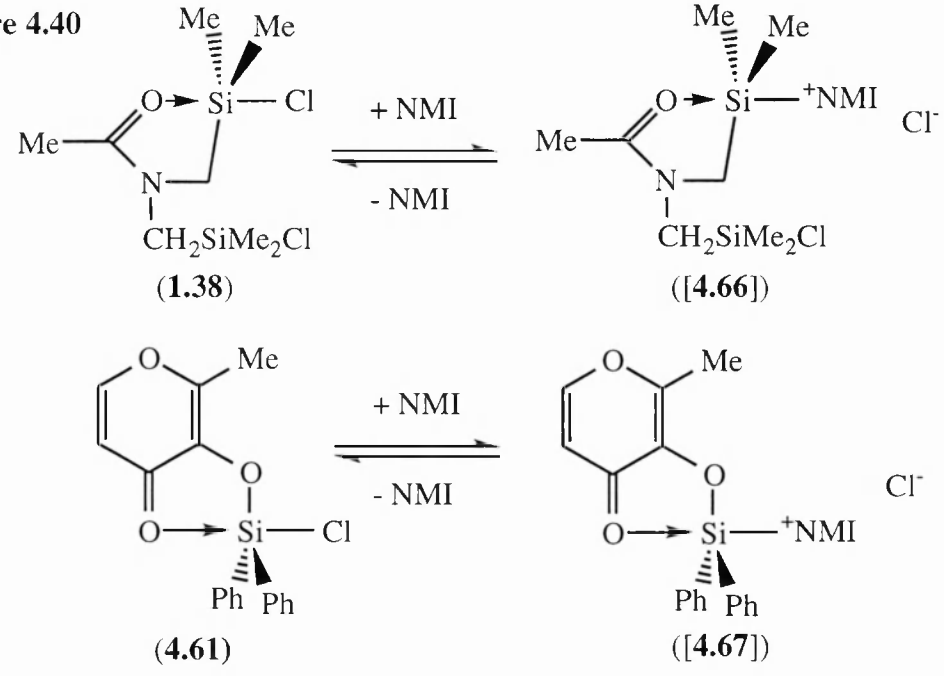

The fact that the addition of NMI to (**1.38**) led initially to peak broadening but a sharp peak was obtained with two equivalents of NMI, yet addition of two equivalents of NMI to (**4.61**) led only to a broadened signal, suggests that the equilibrium for the formation of (**4.66**) lies further to the right than that of (**4.67**).

4.7.2 : Tin complex (4.39b)

The addition of one equivalent of NMI to a solution of complex (**4.39b**) saw the disappearance of the ^{119}Sn peak for the pentacoordinate tin at δ -205.0 and the appearance of a sharp resonance of δ -352.4. This shifted to δ -352.7 with a second equivalent of NMI. This is consistent with the expansion of the coordination sphere of tin taking place to give a hexacoordinate species (**4.68**) in solution (Figure 4.41).

Figure 4.41

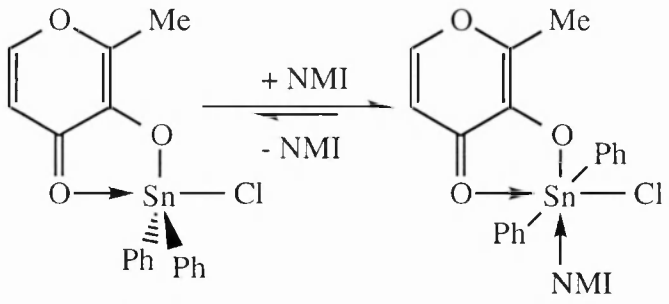

(**4.39b**) (**4.68**)

On standing for 30 minutes, colourless crystals formed from the solution. The crystals were not sufficiently soluble in common NMR solvents to be analysed by NMR spectroscopy. The EI mass spectrum of the crystals failed to show any fragments containing the maltol ligand. Also, microanalyses (carbon, hydrogen and nitrogen) of the crystal (Table 4.17) were inconsistent with (**4.68**). Crystals suitable for X-ray analysis were grown from a preparative scale reaction of (**4.39b**) with one equivalent of NMI in acetonitrile. The X-ray structure (Figure 4.42) (with hydrogens omitted) of a single crystal of the material revealed the product to be dichlorobis(N-methylimidazole)diphenyltin, (**4.69**). The microanalysis results are in agreement with (**4.69**)'s theoretical composition.

Table 4.17

	% C	% H	% N
(**4.68**)	51.25	4.11	5.43
Found 1	47.63	4.50	10.84
Found 2	47.46	4.67	11.21
(**4.69**)	47.22	4.36	11.02

Each pair of the three types of tin substituent exist in a *trans* relationship with the three diaxial bond angles being exactly 180°. The phenyl groups rings lie in the same plane, as do the NMI five-membered rings; though one NMI group is rotated 180° about its N-Sn bond with respect to the other (Figure 4.43). The tin is therefore

Figure 4.42 (distances in picometers)

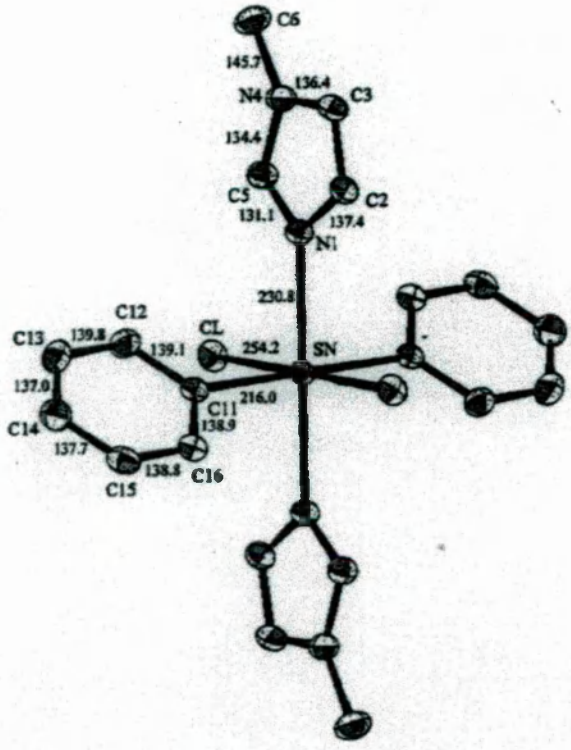

Figure 4.43

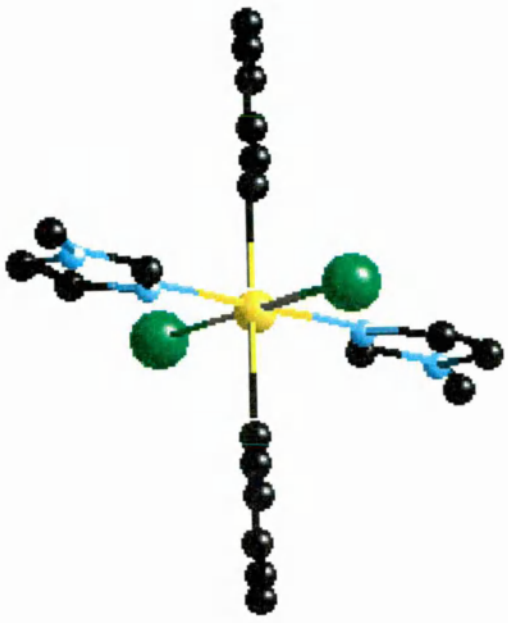

centrosymmetric and thus a centre of inversion. The *cis* bond angles between the different groups range from 91.2° to 88.8° and mean that the in has a highly octahedral geometry. (**4.69**) is probably one of the products of a disproportionation equilibrium of (**4.68**); (**4.68**) being soluble in acetonitrile and initially observed in solution. However, the insolubility of (**4.69**) in acetonitrile drives the equilibrium far over to the right and leads quantitatively to (**4.69**) with presumably the co-product, (**4.19**), remaining in solution (Figure 4.44). We have not investigated the composition of the solution after (**4.69**) has been crystallised and separated.

Figure 4.44

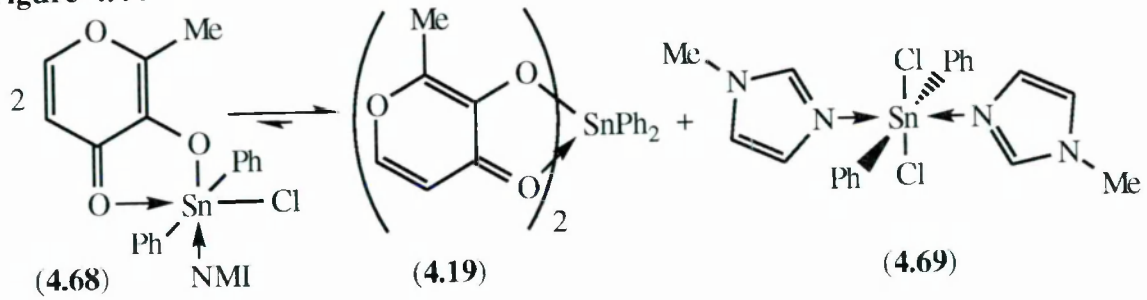

Disproportionation reactions of tin are well established. For example, dilute toluene solutions of triphenyl(4-acetylpyrazol-5-onato)tin (Ph_3Sn(PMAP)), (**4.70**), disproportionate over several days giving a solution of (**4.71**) and crystals of (**4.72**) (Figure 4.45).[191]

Figure 4.45

$$2\ Ph_3Sn(PMAP) \rightleftharpoons Ph_2Sn(PMAP)_2 + Ph_4Sn$$

(**4.70**) (**4.71**) (**4.72**)

Neat samples often require higher temperatures for disproportion to be initiated. Triorganotin halides (R_3SnX) heated to 200°C undergo some degree of disproportionation according to Figure 4.46.[192]

Figure 4.46

$$2\ R_3SnX \rightleftharpoons R_2SnX_2 + R_4Sn$$

The structure of (**4.69**) is similar to other known complexes of this type. Both molecules of dibromodicyclohexylbis(imidazole)tin, (**4.73**), found in its crystal structure have an identical, all-*trans*, centrosymmetric structure at tin as (**4.69**). The three diaxial bond angles are therefore exactly 180° while the axial-equatorial bond angles range from 91.6° to 88.2° (Figure 4.47).[193]

Figure 4.47

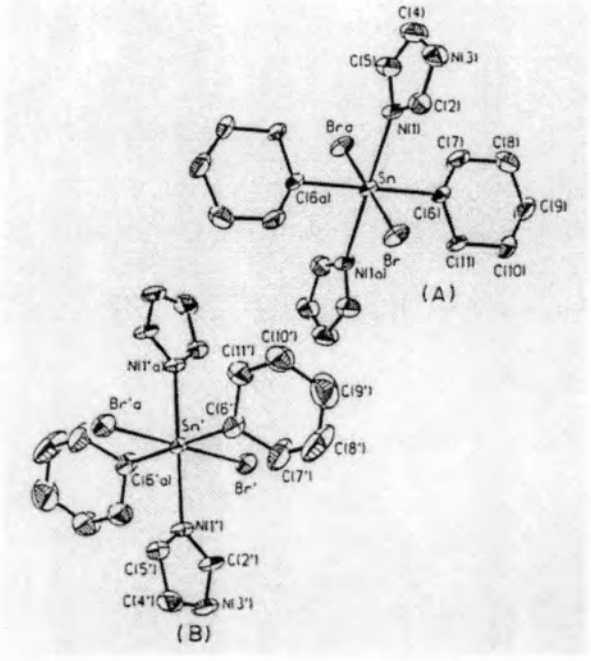

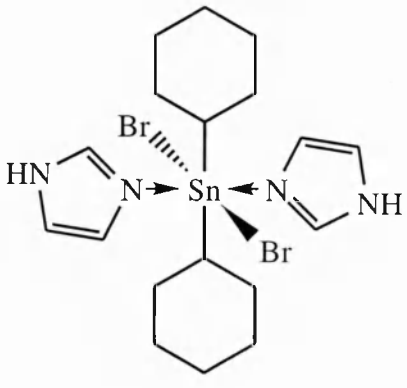

(**4.73**)
Sn-Br = 2.76Å / 2.76Å
Sn-N = 2.39Å / 2.39Å

The crystal structure of related dichlorodiphenylbis(pyrazole)tin (**4.74**) is non centrosymmetric, though retaining the all-*trans* arrangement of each group at tin. The tin remains highly octahedral with diaxial bond angles of 178.2-179.5° and axial-equatorial bond angles in the range 89.2-90.9° (Figure 4.48).[194] The Sn-Cl and Sn-N bonds are slightly shorter than those of (**4.69**) (2.54Å and 2.30Å, see Figure 4.42).

Figure 4.48

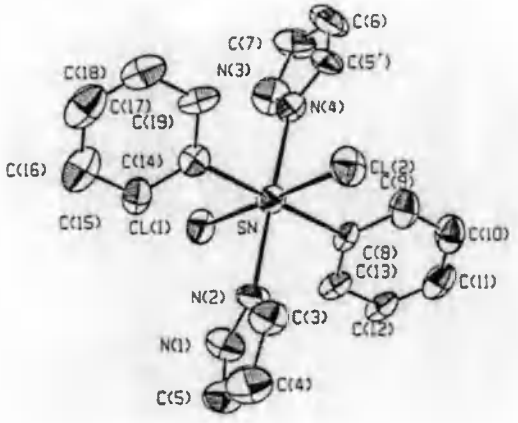

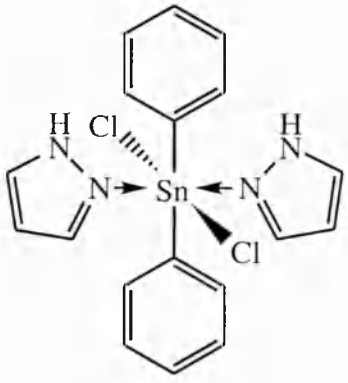

(**4.74**)
Sn-Cl = 2.42 / 2.45Å
Sn-N = 2.28 / 2.22Å

The crystal structure of dichlorodiphenylbis(thiazole)tin (**4.75**) is similar to that of (**4.74**) with a slightly distorted octahedral geometry at tin (Figure 4.49).[195]

Figure 4.49

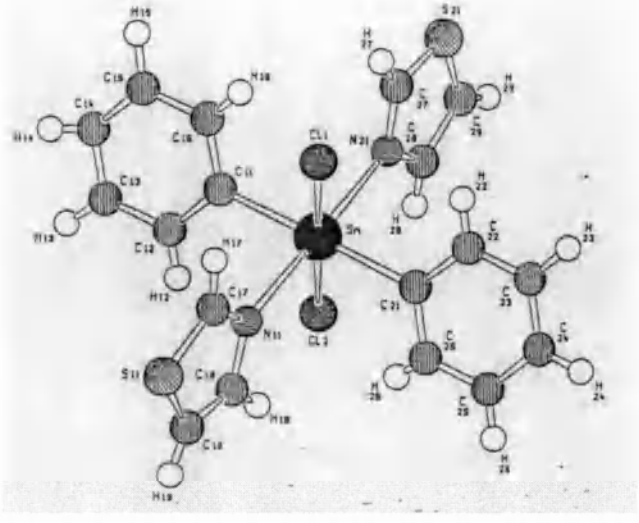

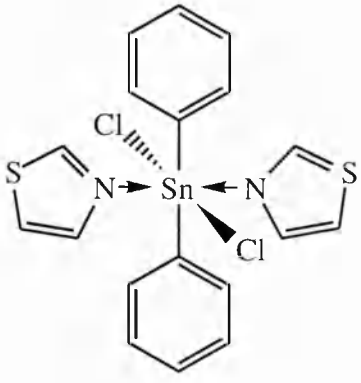

(**4.75**)
Sn-Cl = 2.51 / 2.57Å
Sn-N = 2.37 / 2.37Å

4.8: Boron complexes of maltol and 3-hydroxy-2-methyl-1-phenyl-4-pyridone

The maltol complex (**4.77**) and its 4-pyridone analogue (**4.78**) were synthesised from diphenylboronic acid (**4.76**) (Figure 4.50) and (**4.1**) and (**4.7**) respectively (Figure 4.51).

Figure 4.50

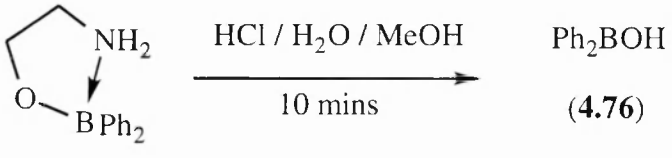

(**4.76**)

Figure 4.51

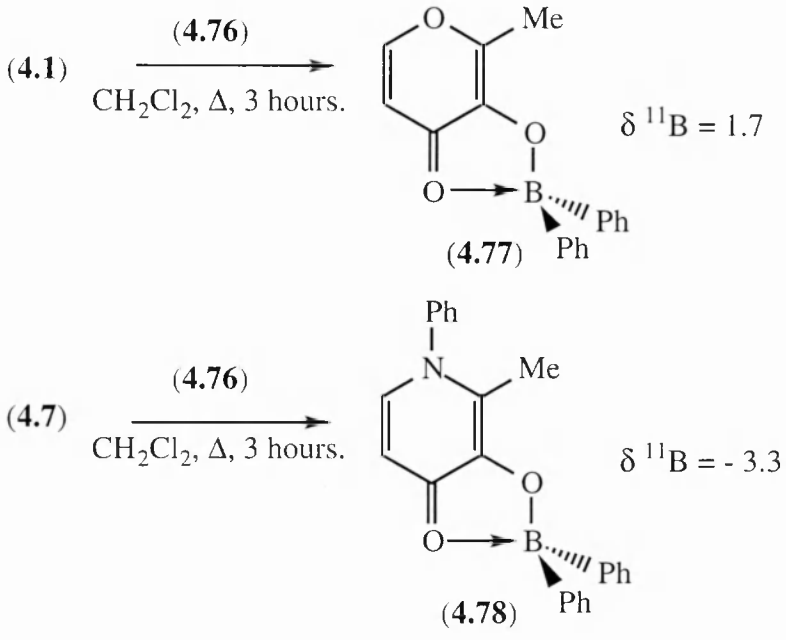

The greater shielding of the ^{11}B nucleus in (**4.78**) indicates a stronger $O_{(carbonyl)}$-B interaction than with (**4.77**). This is in agreement with the previous comparisons drawn between the relative 'nucleophilicities' of the two ligands. Attempts to prepare the bis (maltolato)phenylboron complex (**4.79**) (Figure 4.52) were unsuccessful.

Figure 4.52

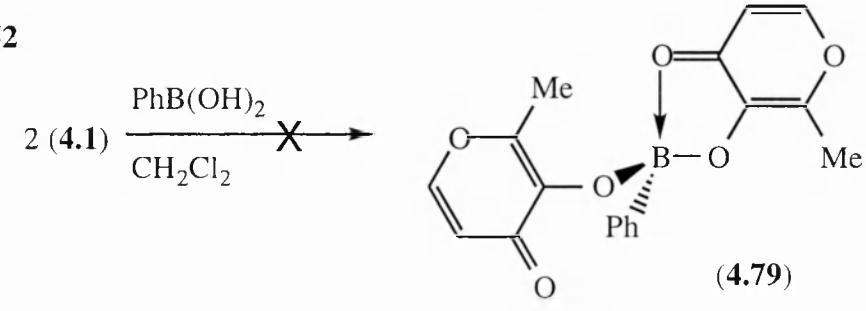

The crystal structure of (**4.77**) (Figure 4.53) has been reported by Orvig *et al*[196] and contains a strong $O_{(carbonyl)}$–B hypervalent bond of 1.60Å length.

Figure 4.53

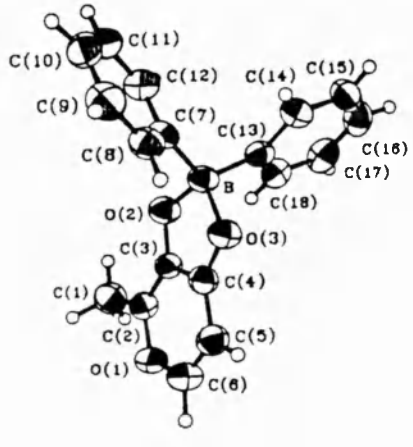

(**4.77**) is one of a class of tetracoordinate diphenylboron complexes. Complexes (**4.80**)[197] and (**4.81**)[198] are other such examples whos crystal structures are reported in the literature. The degree of tetracoordination varies slightly from complex to complex.

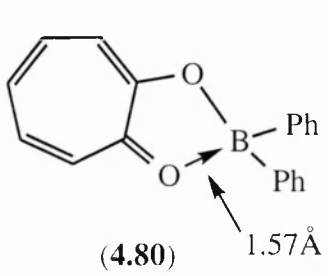

(**4.80**)

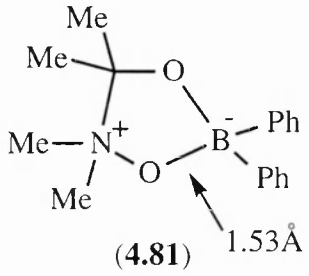

(**4.81**)

4.9: A carbon 'complex'?

The preparation of 3-acetyl-2-methyl-4-pyrone (**4.82**) enables us to investigate whether reversible intramolecular substitution involving carbon can be observed, as shown in Figure 4.54. Two solvents, CD_3CN and CD_3OD, were used to compare whether the degree of 'substitution' might be solvent specific. There is a strong similarity in the ring ^{13}C NMR data between solutions of (**4.82**) in the two solvents. Since both data sets are more similar to (**4.44**) than (**4.45**), and there is strong carbonyl character to the acetyl C=O carbon, we can confirm that there is no appreciable tetrahedral 'substituted product' formation takes place in either CD_3CN or CD_3OD (Table 4.18). If the carbonyl group were more activated, such as if a more electronegative group were to replace the COMe group, then 'substitution' maybe more likely to be observed.

Figure 4.54

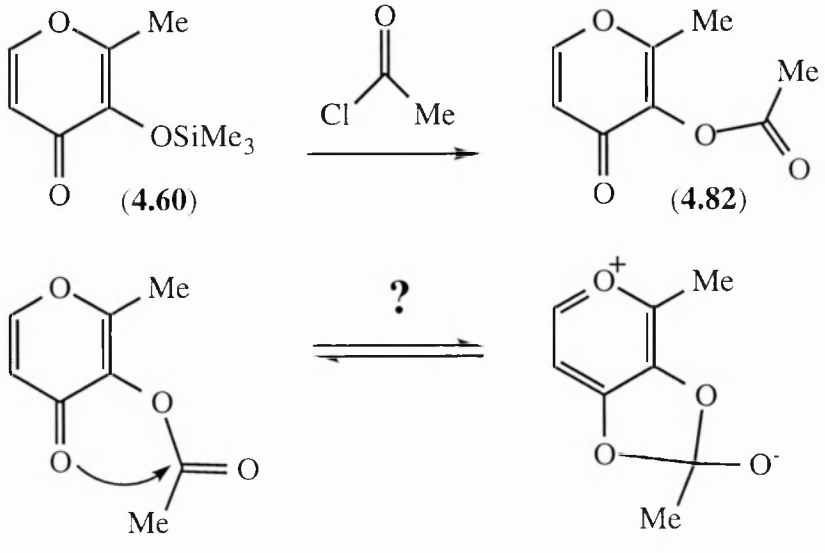

Table 4.18

Compound	^{13}C chemical shift (/ppm)							
	C_2	C_3	C_4	C_5	C_6	2-CH_3	acetyl C=O	acetyl CH_3
(**4.44**)	160.2	146.3	175.3	118.2	155.3	14.8	-	-
(**4.82**) (CD_3CN)	160.2	139.2	168.3	116.8	156.1	15.0	172.3	20.4
(**4.82**) (CD_3OD)	162.1	139.3	169.0	117.0	157.4	14.9	174.5	20.1
(**4.45**)	174.6	144.7	173.7	110.2	163.8	16.9	-	-

Chapter 5: Experimental.

5.1: General notes

a: NMR spectroscopy

All NMR measurements were made on either a Jeol FX90Q or an EX400 FT machine fitted with a multinuclear probe. ^{13}C spectra were broad band decoupled. The pulse delay for ^{29}Si spectra was standardised at 15 seconds. Extensive use of ^{1}H-^{1}H COSY, ^{1}H-^{13}C COSY and ^{13}C DEPT programs was made to help assign the peaks of spectra.

Unless stated otherwise all spectra were recorded at room temperature (20°C) using deuterochloroform ($CDCl_3$) dried over 4A molecular sieves as solvent. The internal NMR reference compound for ^{1}H, ^{13}C and ^{29}Si spectra, tetramethylsilane, was present in all samples. The external reference compounds for ^{19}F and ^{119}Sn spectra were $CFCl_3$ and tetramethyltin respectively. The external reference compound for ^{11}B spectra was H_3BO_3 in D_2O. The spectral data point positions of these compounds were accurately located beforehand. The concentration of tin complex solutions was standardised at 0.52M (unless otherwise stated) due to the dependence of the NMR shift on complex concentration.

Although great effort was made to eliminate moisture from solvents, reagents and reaction vessels, small traces of hydrolysis products from the highly moisture sensitive materials prepared cannot be discounted. As much coupling information as could be reliably observed is presented. On occasions due to peak overlap, broadening or simply a coupling not being seen, it has not been possible to quote a full set of coupling constants.

b: Micro-analyses

Microanalyses were performed by MEDAC Limited (Brunel University) and Butterworth Laboratories Limited (Teddington, Middlesex) with acceptable C and H compositions (+/- 0.5 % theoretical value) being the standard analyses. Usually a third element was also measured, either B, N, Cl, Br or I. If an acceptable microanalysis could not be obtained then high resolution mass spectrometry was normally used instead. Compounds already reported in the literature require less comprehensive characterisation and are individually referenced.

c: Mass spectrometry

Low resolution mass spectra were recorded on a VG20-250 mass spectrometer. The simple peak isotope patterns for complexes not containing tin are quoted with approximate intensity ratios. The more complex patterns produced by the larger numbers of abundant tin isotopes (often in combination with Cl or Br) were observed as expected in each case but only the mass of the most intense peak is quoted.

d: High resolution mass spectrometry

High resolution mass spectrometry was performed by the National Mass Spectrometry Service Centre based at the University of Wales, Swansea. EI measurements were made on a VG ZAB-E instrument using PFK peaks as mass standards. FAB measurements were made on a VG Autospec instrument using PEG peaks as mass standards. Additional accurate-mass EI spectra were provided by Hoechst Roussel Limited, Milton Keynes using a Kratos MS80RFA instrument with PFK as the standard.

e: Melting points

These were determined on an Electrothermal Digital melting point apparatus and are uncorrected. The high moisture sensitivity of many of the compounds often prevented melting point determinations from being carried out.

f: X-ray crystallography

Measurements were made on either a STOE STADI4 (Structures in Chapter 4 except (**4.69**)) or a STOE IPDS25 (Structures in Chapter 2 and (**4.69**)) diffractometer using Mo K_α, 71.069 pm (graphite monochromator) radiation. Full details are given in the crystallographic appendix.

g: Solvents

The following solvents were dried before use:

Benzene	- dried over sodium wire.
Toluene	- dried over sodium wire.
Diethyl ether	- dried over sodium wire.
Chloroform	- dried over 4A molecular sieves.
Dichloromethane	- dried over 4A molecular sieves.
Acetonitrile	- dried over calcium hydride.

h: Chemicals / handling / storage

All chemical handling, reactions and work-up were performed in an efficient fume cupboard. Reagents were obtained primarily from the Aldrich Chemical Company or from Fluorochem Limited and used as purchased. Many of the silanes are particularly moisture sensitive and so were distilled under a nitrogen atmosphere every 3-4 months to remove high boiling point siloxane hydrolysis products. These reagents and many of the trimethylsilylated materials were stored in *Reacti-flasks* with either PTFE-silicone rubber septa caps or septa (*Miniert*) valves to allow efficient transfer to syringe while preventing moisture from entering. The transfer of moisture sensitive liquid reagents was achieved by appropriately sized gas-tight syringes fitted with fine gauge needles with pointed tips to minimise damage to septa seals.

Extensive use was made of a combined high vacuum (ca 0.03 mmHg) and dry nitrogen line to maintain anhydrous, inert atmospheric conditions during reactions. 50 cm^3 round-bottomed flasks fitted with an inlet tap and septa adapter were used for the preparation of moisture sensitive complexes.

It was standard practice to transfer all new potentially moisture sensitive products to an argon purged and P_2O_5 dried glove box for storage to minimise their degradation. Samples sent to other laboratories for analysis were suitably packaged to prevent damage in transit. Small, air tight, screw-capped plastic or glass bottles charged in a glove box were found to be the most suitable.

Part A: Compounds from Chapters 2 and 3.

5.2: Synthesis of substituted 2-thiopyridones from 2-pyridones and phosphorous pentasulfide.

The 2-pyridone precursor and phosphorous pentasulfide (1:1 molar ratio) in the form of powders were shaken vigorously together in a 250 cm^3 stoppered, round-bottomed flask. Under a gentle flow of nitrogen the flask was heated in an oil bath at a carefully regulated temperature for 5 hours. The temperature chosen was close to the melting point of the 2-pyridone.

The fused mixture was allowed to cool to room temperature and hydrolysed by concentrated aqueous sodium hydroxide (about 150 cm^3). Initially this was drop-wise and then in larger aliquots as effervescence became less vigorous. The resulting suspension was stirred for a further 18 hours to allow hydrolysis to reach completion. The pH was corrected to approximately 8 with concentrated hydrochloric acid (5 cm^3).

The product was extracted into chloroform (4 x 50 cm^3) with the washings being combined and dried over magnesium sulfate. Removal of solvent by rotary evaporation afforded a solid brown residue. This was recrystallised from 3:1 ethyl acetate / chloroform giving yellow/orange plate-like crystals of the 2-thiopyridone compound.

a: 6-Methyl-2-(1H)-thiopyridone (3.26)[199]

6-Methyl-2-(1H)-pyridone (**3.25**)	15.12 g / 0.14 mol
Phosphorous pentasulfide	61.40 g / 0.14 mol
Oil bath temperature	155-165°C
Mass of recrystallised (**3.26**) isolated	12.03 g / 96.10 mmol (70%)

δ **^{1}H** (400 MHz) = 13.8 (b, 1H, NH), 7.37 (d, 1H, $^3J_{H3-H4}$ = 8.4 Hz), H_3), 7.31 (dd, 1H, $^3J_{H4-H5}$ = $^3J_{H4-H3}$ = 8.4 Hz, H_4), 6.55 (d, 1H, $^3J_{H5-H4}$ = 8.4 Hz, H_5), 2.48 (s, 3H, CH_3); δ **^{13}C** (400 MHz) = 176.4 (C_2), 148.8 (C_6), 138.7 (C_4), 130.7 (C_3), 114.1 (C_5), 18.9 (CH_3). **M/Z** (EI^+) = 125 (M^+), 110, 80. **Found %** C 57.31, H 5.59, N 11.07; requires C 57.57, H 5.64, N 11.19 (C_6H_7NS).

b: 4-Methyl-2-(1H)-thiopyridone (3.30)[199]

4-Methyl-2-(1H)-pyridone	8.00 g / 73.31 mmol
Phosphorous pentasulfide	32.71 g / 73.58 mmol
Oil bath temperature	130-140°C
Mass of recrystallised (**3.30**) isolated	5.76 g / 46.01 mmol (63%)

δ **^{1}H** (400 MHz) = 13.0 (b, 1H, NH), 7.53 (d, 1H, $^{3}J_{H6\text{-}H5}$ = 6.4 Hz), H_6), 7.41 (s, 1H, H_3), 6.64 (dd, 1H, $^{3}J_{H5\text{-}H6}$ = 6.4 Hz, $^{4}J_{H5\text{-}H3}$ = 2.0 Hz, H_5), 2.27 (s, 3H, CH_3); δ **^{13}C** (400 MHz) = 174.9 (C_2), 150.5 (C_4), 136.2 (C_6), 132.9 (C_3), 116.3 (C_5), 21.4 (CH_3). **M/Z** (EI^+) = 125 (M^+), 110, 80. **Found %** C 57.46, H 5.61, N 11.13; requires C 57.57, H 5.64, N 11.19 (C_6H_7NS).

5.3: Synthesis of trimethylsilylated 2-thiopyridines from 2-thiopyridones.

To a solution of the appropriate 2-thiopyridone compound in toluene was added trimethylsilyldiethylamine (about 1.1 equivalents). The solution was refluxed under nitrogen for 5 hours. The solvent was removed by distillation under nitrogen leaving a dark brown liquid. This liquid was distilled under high vacuum conditions and yielded the silylated derivative as a bright yellow distillate.

a: 2-(Trimethylsilylmercapto)pyridine (3.10)[200]

2-(1H)-Thiopyridone (**3.1**)	6.20 g / 55.77 mmol
Toluene	40 cm^3
Trimethylsilyldiethylamine	9.01 g / 62.00 mmol
Mass of distilled (**3.10**) obtained	9.21 g / 50.23 mmol (90%)
Boiling point	35°C (0.03 mmHg)

δ **^{1}H** (400 MHz) = 8.21 (d, 1H, $^{3}J_{H6\text{-}H5}$ = 4.8 Hz, H_6), 7.26 (ddd, 1H, $^{3}J_{H4\text{-}H3}$ = $^{3}J_{H4\text{-}H5}$ = 7.6 Hz, $^{4}J_{H4\text{-}H6}$ = 2.0 Hz, H_4), 7.14 (ddd, 1H, $^{3}J_{H3\text{-}H4}$ = 7.6 Hz, $^{4}J_{H3\text{-}H5}$ = $^{5}J_{H3\text{-}H6}$ = 0.8 Hz, H_3), 6.80 (ddd, 1H, $^{3}J_{H5\text{-}H4}$ = 7.6 Hz, $^{3}J_{H5\text{-}H6}$ = 4.8 Hz, $^{4}J_{H5\text{-}H3}$ = 0.8 Hz, H_5), 0.36 (s, 9H, $Si(CH_3)_3$); δ **^{13}C** (400 MHz) = 158.4 (C_2), 148.5 (C_6), 135.5 (C_4), 125.8 (C_3), 119.0 (C_5), 1.1 ($Si(CH_3)_3$); δ **^{29}Si** (400 MHz) = 16.6. **M/Z** (EI^+) = 183 (M^+), 168, 153, 138, 78.

b: 5-Trifluoromethyl-2-(trimethylsilylmercapto)pyridine (3.19)

5-Trifluoromethyl-2-(1H)-thiopyridone (**3.18**)	2.97 g / 16.58 mmol
Toluene	40 cm^3
Trimethylsilyldiethylamine	2.77 g / 19.06 mmol
Mass of distilled (**3.19**) obtained	3.13 g / 12.45 mmol (75%)
Boiling point	50°C (0.05 mmHg)

δ **^{1}H** (400 MHz) = 8.79 (d, 1H, $^4J_{H6-H4}$ = 2.4 Hz, H_6), 7.62 (dd, 1H, $^3J_{H4-H3}$ = 8.4 Hz, $^4J_{H4-H6}$ = 2.4 Hz, H_4), 7.36 (d, 1H, $^3J_{H3-H4}$ = 8.4 Hz, H_3), 0.48 (s, 9H, $Si(CH_3)_3$); δ **^{13}C** (400 MHz) = 164.5 (C_2), 145.8 (C_6), 132.7 (C_4), 125.2 (C_3), 124.0 (q, $^1J_{C-F}$ = 270.2 Hz, CF_3), 122.4 (q, $^2J_{C-F}$ = 33.1 Hz, C_5), 1.2 ($Si(CH_3)_3$); δ **^{19}F** (90 MHz) = - 64.1; δ **^{29}Si** (400 MHz) = 18.0. **M/Z** (EI^+) = 251 (M^+), 236, 232, 73. **Found %** C 42.77, H 4.80, N 5.71; requires C 43.01, H 4.81, N 5.57 ($C_9H_{12}F_3NSSi$).

c: 6-Methyl-2-(trimethylsilylmercapto)pyridine (3.27)

6-Methyl-2-(1H)-thiopyridone (**3.26**)	6.01 g / 47.93 mmol
Toluene	30 cm^3
Trimethylsilyldiethylamine	12.21 g / 84.02 mmol
Mass of distilled (**3.27**) obtained	8.89 g / 45.05 mmol (94%)
Boiling point	52°C (0.03 mmHg)

δ **^{1}H** (400 MHz) = 7.28 (dd, 1H, $^3J_{H4-H3}$ = $^3J_{H4-H5}$ = 7.8 Hz, H_4), 7.05 (d, 1H, $^3J_{H3-H4}$ = 7.8 Hz, H_3), 6.79 (d, 1H, $^3J_{H5-H4}$ = 7.8 Hz, H_5), 2.43 (s, 3H, 6-CH_3), 0.44 (s, 9H, $Si(CH_3)_3$); δ **^{13}C** (400 MHz) = 157.8 (C_2), 157.4 (C_6), 136.3 (C_4), 122.7 (C_3), 118.8 (C_5), 24.0 (6-CH_3), 1.4 ($Si(CH_3)_3$); δ ^{29}Si (400 MHz) = 16.2. **M/Z** (EI^+) = 197 (M^+) (measured 197.0694, requires 197.0695 for $C_9H_{15}NSSi$), 182, 167, 152, 92, 73.

d: 4-Methyl-2-(trimethylsilylmercapto)pyridine (3.31)

4-Methyl-2-(1H)-thiopyridone (**3.30**)	1.74 g / 13.90 mmol
Toluene	20 cm^3
Trimethylsilyldiethylamine	2.22 g / 15.29 mmol
Mass of distilled (**3.31**) obtained	2.26 g / 11.44 mmol (82%)
Boiling point	60°C (0.06 mmHg)

Over 5 days the liquid crystallised - giving yellow plate-like crystals (melting point 42°C).

δ **^{1}H** (90 MHz) = 8.14 (d, 1H, $^{3}J_{H6\text{-}H5}$ = 4.9 Hz, H_6), 7.14 (s, 1H, H_3), 6.77 (d, 1H, $^{3}J_{H5\text{-}H6}$ = 4.9 Hz, H_5), 2.22 (s, 3H, 4-CH_3), 0.44 (s, 9H, $Si(CH_3)_3$); δ **^{13}C** (90 MHz) = 158.7 (C_2), 148.2 (C_4), 147.1 (C_6), 127.6 (C_3), 120.6 (C_5), 20.7 (4-CH_3), 1.4 ($Si(CH_3)_3$); δ **^{29}Si** (400 MHz) = 17.0. **M/Z** (EI^+) = 197 (M^+) (measured 197.0694, requires 197.0695 for $C_9H_{15}NSSi$), 182, 92, 73.

5.4: Synthesis of O-trimethylsilylated ligands.

The appropriate unsilylated derivative was dissolved in either benzene or toluene. To this solution was added trimethylsilyldiethylamine (typically 1.1 equivalents) and the solution refluxed under nitrogen for 5 hours. Separating the solvent by careful distillation at atmospheric pressure under a flow of nitrogen left a brown liquid residue. Distillation of this residue as appropriate afforded the pure, silylated product as a colourless distillate.

a: 2-(Trimethylsiloxy)quinoline (2.24)[201]

Reaction solvent	Toluene (30 cm^3)
2-(1H)-Quinolinone (**2.16**)	2.12 g / 14.60 mmol
Trimethylsilyldiethylamine	2.40 g / 16.52 mmol
Mass of distilled (**2.24**) obtained	2.82 g / 12.96 mmol (89%)
Boiling point	50°C (0.05 mmHg)

Product vacuum distilled at 0.05 mmHg. Over 8 days at room temperature the liquid crystallised, giving colourless plate-like crystals (melting point 45°C).

δ **^{1}H** (90 MHz) = 7.80 (d, 1H, $^{3}J_{H4\text{-}H3}$ = 8.6 Hz, H_4), 7.59-7.13 (m, 4H, H_5/H_6/H_7/H_8), 6.81 (d, 1H, $^{3}J_{H3\text{-}H4}$ = 8.6 Hz, H_3), 0.45 (s, 9H, $Si(CH_3)_3$); δ **^{13}C** (90 MHz) = 161.0 (C_2), 146.8 (C_{8a}), 139.0 (C_4), 129.1 (C_7), 127.4 (C_5), 127.2 (C_6), 124.9 (C_{4a}), 123.8 (C_3), 114.6 (C_8), 0.6 ($Si(CH_3)_3$); δ **^{29}Si** (90 MHz) = 21.1. **M/Z** (EI^+) = 217 (M^+), 202, 128.

b: 2-(Trimethylsiloxy)quinoxaline (2.39)[202]

Reaction solvent	Toluene (30 cm^3)
2-(1H)-Quinoxalinone (**2.37**)	3.40 g / 23.26 mmol
Trimethylsilyldiethylamine	3.50 g / 24.10 mmol
Mass of distilled (**2.39**) obtained	3.79 g / 17.40 mmol (75%)
Boiling point	104°C (0.05 mmHg)

(**2.39**) 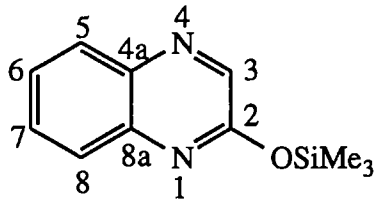

Product vacuum distilled at 0.05 mmHg. The liquid crystallised within minutes giving colourless plate-like crystals (melting point 49°C).

δ **^{1}H** (90 MHz) = 8.46 (s, 1H, H_3), 8.05-7.31 (m, 4H, H_5/H_6/H_7/H_8), 0.45 (s, 9H, $Si(CH_3)_3$); δ **^{13}C** (90 MHz) = 156.2 (C_2), 141.0 (C_3), 140.5 (C_{8a}), 138.9 (C_{4a}), 129.7 / 128.9 / 127.3 / 126.4 ($C_{5\text{-}8}$), 0.3 ($Si(CH_3)_3$); δ **^{29}Si** (90 MHz) = 24.4. **M/Z** (EI^+) = 218 (M^+), 203, 73.

c: 4-(Trimethylsiloxy)-3-pyrimidine (2.40)[203]

Reaction solvent	Benzene (20 cm^3)
4-(3H)-Pyrimidone (**2.38**)	5.35 g / 56.68 mmol
Trimethylsilyldiethylamine	9.05 g / 62.28 mmol
Mass of distilled (**2.40**) obtained	7.00 g / 41.55 mmol (73%)
Boiling point	120°C (1 atm.)

(**2.40**) 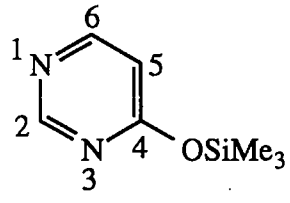

Product distilled at atmospheric pressure under a flow of nitrogen.

δ **^{1}H** (90 MHz) = 8.72 (s, 1H, H_2), 8.45 (d, 1H, $^3J_{H6\text{-}H5}$ = 5.8 Hz, H_6), 6.68 (d, 1H, $^3J_{H5\text{-}H6}$ = 5.8 Hz, H_5), 0.39 (s, 9H, $Si(CH_3)_3$); δ **^{13}C** (90 MHz) = 168.0 (C_4), 158.4/158.0 (C_2/C_6), 110.5 (C_5), 0.2 ($Si(CH_3)_3$); δ **^{29}Si** (90 MHz) = 24.4.

d: 2-Methyl-3-(trimethylsiloxy)-4-pyrone (4.60)[204]

Reaction solvent	Toluene (25 cm^3)
Maltol (**4.1**)	6.36 g / 50.43 mmol
Trimethylsilyldiethylamine	8.28 g / 56.98 mmol
Mass of distilled (**4.60**) obtained	8.41 g / 42.41 mmol (84%)
Boiling point	61°C (0.05 mmHg)

Product vacuum distilled at 0.05 mmHg pressure.

δ **^{1}H** (90 MHz) = 7.64 (d, 1H, $^3J_{H6\text{-}H5}$ = 5.6 Hz, H_6), 6.28 (d, 1H, $^3J_{H5\text{-}H6}$ = 5.6 Hz, H_5), 2.26 (s, 3H, 2-CH_3), 0.27 (s, 9H, $Si(CH_3)_3$); δ **^{13}C** (90 MHz) = 174.1 (C_4), 154.8 (C_2), 153.2 (C_6), 142.6 (C_3), 115.6 (C_5), 14.6 (2-CH_3), 1.3 ($Si(CH_3)_3$); δ **^{29}Si** (90 MHz) = 22.1. **M/Z** (EI^+) = 199 (MH^+), 183, 153, 109, 73.

5.5: Synthesis of stable 5-coordinate silyl fluoride complexes from their chloride analogues using antimony trifluoride.

The appropriate chlorosilane complex was either dissolved or suspended in benzene under a nitrogen atmosphere. Granular antimony trifluoride ($^1/_3$ equivalent) was introduced and the reagents stirred together for 1 hour at room temperature. The organic phase was decanted from the oily antimony containing by products and hydrolysed by shaking with distilled water (50 cm^3). The organic phase was extracted into dichloromethane (3 x 50 cm^3). The extracts were combined and dried over magnesium sulfate and the solvents removed by rotary evaporation. The remaining residue, either an oily liquid or crystalline solid, was either vacuum distilled or recrystallised from an appropriate solvent. This step afforded the pure title compound.

a: 1-(Fluorodimethylsilylmethyl)-2-quinolinone (2.25a)

Volume of solvent	4 cm^3
1-(Chlorodimethylsilylmethyl)-2-quinolinone (**2.25b**)	0.75 g / 2.98 mmol
Antimony trifluoride	0.18 g / 1.01 mmol
Mass of (**2.25a**) isolated	0.40 g / 1.70 mmol (57%)
State	Colourless crystals, recrystallised by evaporation of a chloroform solution.

δ **^{1}H** (400 MHz) = 7.95 (d, 1H, $^3J_{H4-H3}$ = 9.4 Hz, H_4), 7.73-7.64 (m, 3H, H_5/H_7/H_8), 7.38 (m, 1H, H_6), 6.82 (d, 1H, $^3J_{H3-H4}$ = 9.4 Hz, H_3), 3.18 (s, 2H, N-CH_2), 0.38 (d, 6H, $^3J_{H-F}$ = 6.4 Hz, Si(CH_3)$_2$); δ **^{13}C** (400 MHz) = 162.9 (C_2), 141.4 (C_4), 139.3 (C_{8a}), 131.8 (C_7), 129.0 (C_5), 123.6 (C_6), 121.4 (C_{4a}), 117.1 (C_3), 115.9 (C_8), 33.9 (d, $^2J_{C-F}$ = 47.5 Hz, N-CH_2), 2.0 (d, $^2J_{C-F}$ = 23.8 Hz, Si(CH_3)$_2$); δ **^{19}F** (90 MHz) = - 114.2; δ **^{29}Si** (400 MHz) = - 25.4 (d, $^1J_{Si-F}$ = 254.3 Hz). **M/Z** (EI^+) = 235 (M^+), 234 (M^+-H), 220. **Found %** C 60.83, H 5.98, N 5.86; requires C 61.25, H 6.00, N 5.95 ($C_{12}H_{14}FNOSi$).

b: 1-(Fluorodimethylsilylmethyl)-2-quinoxalinone (2.41a)

Volume of solvent	40 cm^3
1-(Chlorodimethylsilylmethyl)-2-quinoxalinone (**2.41b**)	11.02 g / 43.60 mmol
Antimony trifluoride	2.60 g / 14.55 mmol
Mass of (**2.41a**) isolated	5.43 g / 23.98 mmol (53%)
State	White crystalline solid, recrystallised from acetonitrile.

δ **^{1}H** (400 MHz) = 8.40 (s, 1H, H_3), 7.96 (d, 1H, $^3J_{H5-H6}$ = 8.0 Hz, H_5), 7.71 (m, 1H, H_7), 7.56 (d, 1H, $^3J_{H8-H7}$ = 8.4 Hz, H_8), 7.47 (m, 1H, H_6), 3.23 (s, 2H, N-CH_2), 0.43 (d, 6H, $^3J_{H-F}$ = 7.8 Hz, Si(CH_3)$_2$); δ **^{13}C** (400 MHz) = 155.5 (C_2), 146.9 (C_3), 134.4 (C_{8a}), 132.9 (C_{4a}), 131.9 (C_7), 130.6 (C_5), 124.8 (C_6), 115.1 (C_8), 33.4 (d, $^2J_{C-F}$ = 40.5 Hz, N-CH_2), 1.3 (d, $^2J_{C-F}$ = 22.1 Hz, Si(CH_3)$_2$); δ **^{19}F** (90 MHz) = - 128.7; δ **^{29}Si** (400 MHz) = - 6.1 (d, $^1J_{Si-F}$ = 260.3 Hz). **M/Z** (EI^+) = 236 (M^+), 235 (M^+-H), 221, 158, 77. **Found %** C 56.40, H 5.49, N 12.30; requires C 55.91, H 5.54, N 11.85 ($C_{11}H_{13}FN_2OSi$).

c: 2-(Fluorodimethylsilylmethylmercapto)pyridine (3.11a)

Volume of solvent	5 cm^3
2-(Chlorodimethylsilylmethylmercapto)pyridine (**3.11b**)	1.19 g / 5.45 mmol
Antimony trifluoride	0.33 g / 1.85 mmol
Mass of (**3.11a**) isolated from vacuum distillation	0.42 g / 2.10 mmol (39%)
State	Pale yellow oil. Boiling point 47°C (0.05 mmHg).

δ **^{1}H** (400 MHz) = 8.30 (d, 1H, $^{3}J_{H6\text{-}H5}$ = 5.6 Hz, H_6), 7.41 (ddd, 1H, $^{3}J_{H4\text{-}H3}$ = 8.4 Hz, $^{3}J_{H4\text{-}H5}$ = 7.2 Hz, $^{4}J_{H4\text{-}H6}$ = 2.0 Hz, H_4), 7.17 (d, 1H, $^{3}J_{H3\text{-}H4}$ = 8.4 Hz, H_3), 6.93 (ddd, 1H, $^{3}J_{H5\text{-}H4}$ = 7.2 Hz, $^{3}J_{H5\text{-}H6}$ = 5.6 Hz, $^{4}J_{H5\text{-}H3}$ = 0.8 Hz, H_5), 2.37 (d, 2H, $^{3}J_{H\text{-}F}$ = 4.8 Hz, S-CH_2), 0.33 (d, 6H, $^{3}J_{H\text{-}F}$ = 7.3 Hz, Si(CH_3)$_2$); δ **^{13}C** (400 MHz) = 159.2 (C_2), 147.7 (C_6), 136.1 (C_4), 121.5 (C_3), 119.3 (C_5), 14.0 (d, $^{2}J_{C\text{-}F}$ = 22.0 Hz, S-CH_2), - 0.4 (d, $^{2}J_{C\text{-}F}$ = 16.5 Hz, Si(CH_3)$_2$); δ **^{19}F** (400 MHz) = - 142.5; δ **^{29}Si** (400 MHz) = 17.0 (d, $^{1}J_{Si\text{-}F}$ = 275.8 Hz). **M/Z** (EI^+) = 202 (MH^+), 186, 182, 124, 78, 77. **Found %** C 48.15, H 6.10, N 6.93; requires C 47.73, H 6.01, N 6.96 ($C_8H_{12}FNSSi$).

d: 2-(Fluorodimethylsilylmethylmercapto)-5-trifluoromethylpyridine (3.20a)

Volume of solvent	5 cm^3
2-(Chlorodimethylsilylmethylmercapto)-5-trifluoromethylpyridine (**3.20b**)	0.50 g / 1.75 mmol
Antimony trifluoride	0.11 g / 0.62 mmol
Mass of (**3.20a**) isolated from vacuum distillation	0.11 g / 0.41 mmol (23%)
State	Pale yellow oil. Boiling point 52°C (0.06 mmHg).

δ **^{1}H** (400 MHz) = 8.63 (s, 1H, H_6), 7.67 (dd, 1H, $^{3}J_{H4\text{-}H3}$ = 8.4 Hz, $^{4}J_{H4\text{-}H6}$ = 2.4 Hz, H_4), 7.31 (d, 1H, $^{3}J_{H3\text{-}H4}$ = 8.4 Hz, H_3), 2.51 (d, 2H, $^{3}J_{H\text{-}F}$ = 5.2 Hz, S-CH_2), 0.36 (d, 6H, $^{3}J_{H\text{-}F}$ = 7.2 Hz, Si(CH_3)$_2$); δ **^{13}C** (400 MHz) = 164.5 (C_2), 145.6 (C_6), 132.5 (C_4), 123.8 (q, $^{1}J_{C\text{-}F}$ = 270.2 Hz, CF_3), 122.3 (q, $^{2}J_{C\text{-}F}$ = 33.1 Hz, C_5), 121.3 (C_3), 14.4 (d, $^{2}J_{C\text{-}F}$ = 18.4 Hz, S-CH_2), - 1.1 (d, $^{2}J_{C\text{-}F}$ = 14.7 Hz, Si(CH_3)$_2$); δ **^{19}F** (90 MHz) = - 63.9 (CF_3), - 155.5 (Si-F); δ **^{29}Si** (400 MHz) = 26.0 (d, $^{1}J_{Si\text{-}F}$ = 280.3 Hz). **M/Z** (EI^+) = 270 (MH^+), 254, 250, 192, 77. **Found %** C 40.42, H 4.29, N 5.38; requires C 40.14, H 4.12, N 5.20 ($C_9H_{11}F_4NSSi$).

5.6: Synthesis of unstable 5-coordinate silyl-fluoride complexes (2.42a) and (3.28a) from their chloride analogues using antimony trifluoride.

Complexes (**2.42a**) and (**3.28a**) efficiently undergo desilylation with traces of excess fluoride ion in the reaction pot or dilute aqueous hydroxide ion in the work-up. The synthetic method of Section 5.5 was therefore modified by reducing the proportion of antimony trifluoride to approximately $^1/_4$ equivalent. This led to a mixture of products being isolated at the end of the work-up with the title compound being the major component.

Attempts to separate the silyl-fluoride compounds from their co-products by vacuum distillation or column chromatography only accelerated the desilylation process. The compounds were therefore characterised in the crude product mixture by their molecular ion peaks in accurate-mass EI spectra.

a: 3-(Fluorodimethylsilylmethyl)-4-pyrimidone (2.42a)

Volume of solvent	20 cm^3
3-(Chlorodimethylsilylmethyl)-4-pyrimidone (**2.42b**)	4.95 g / 24.43 mmol
Antimony trifluoride	1.09 g / 6.10 mmol
Mass of crude (**2.42a**) isolated	1.90 g / 10.20 mmol (42%)
State	Pale yellow oil.

δ **^{1}H** (400 MHz) = 8.27 (s, 1H, H_2), 7.98 (d, 1H, $^3J_{H6\text{-}H5}$ = 7.2 Hz, H_6), 6.51 (d, 1H, $^3J_{H5\text{-}H6}$ = 7.2 Hz, H_5), 3.32 (s, 2H, N-CH_2), 0.37 (d, 6H, $^3J_{H\text{-}F}$ = 7.6 Hz, $Si(CH_3)_2$); δ **^{13}C** (400 MHz) = 162.3 (C_4), 154.6 (C_6), 151.8 (C_2), 114.0 (C_5), 37.3 (d, $^2J_{C\text{-}F}$ = 32.9 Hz, N-CH_2), - 0.2 (d, $^2J_{C\text{-}F}$ = 18.3 Hz, $Si(CH_3)_2$); δ **^{19}F** (90 MHz) = - 141.6; δ **^{29}Si** (400 MHz) = 8.8 (d, $^1J_{Si\text{-}F}$ = 269.0 Hz). **M/Z** (EI^+) = 187 (MH^+) (measured 187.0703, requires 187.0703 for $C_7H_{12}FN_2OSi$).

b: 1-(Fluorodimethylsilylmethyl)-6-methyl-2-thiopyridone (3.28a)

Volume of solvent	5 cm^3
1-(Chlorodimethylsilylmethyl)-6-methyl-2-thiopyridone (**3.28b**)	1.76 g / 7.59 mmol
Antimony trifluoride	0.34 g / 1.90 mmol
Mass of crude (**3.28b**) isolated	1.02 g / 4.74 mmol (62%)
State	Pale yellow oil.

δ **^{1}H** (90 MHz) = 7.63 (d, 1H, $^3J_{H3-H4}$ = 8.8 Hz, H_3), 7.10 (m, 1H, H_4), 6.60 (d, 1H, $^3J_{H5-H4}$ = 7.2 Hz, H_5), 4.38 (d, 2H, $^3J_{H-F}$ = 6.8 Hz, N-CH_2), 2.54 (s, 3H, 6-CH_3), 0.38 (d, 6H, $^3J_{H-F}$ = 8.0 Hz, Si(CH_3)$_2$); δ **^{13}C** (400 MHz) = 179.1 (C_2), 148.7 (C_6), 133.0 (C_4), 132.7 (C_3), 115.5 (C_5), 46.4 (d, $^2J_{C-F}$ = 23.7 Hz, N-CH_2), 22.8 (6-CH_3), - 1.0 (d, $^2J_{C-F}$ = 14.6 Hz, Si(CH_3)$_2$); δ **^{19}F** (90 MHz) = - 150.2; δ **^{29}Si** (90 MHz) = 27.0 (d, $^1J_{Si-F}$ = 281.3 Hz). **M/Z** (EI^+) = 215 (M^+) (measured 215.0600, requires 215.0600 for $C_9H_{14}FNSSi$), 200, 196, 138, 78.

5.7: Synthesis of 5-coordinate silyl mono-chloride complexes from silylated ligand precursors and chloro(chloromethyl)dimethylsilane.

A solution of the silylated ligand was prepared in benzene under a nitrogen atmosphere. Chloro(chloromethyl)dimethylsilane (1 equivalent) was added drop-wise with stirring and the solution allowed to stand for 30 minutes at room temperature. Where crystallisation or precipitation of the title product occurred, the solvent was decanted off, the material washed twice with diethyl ether and dried for 1 hour under high vacuum. No further purification was necessary. For the examples (**2.41b**) and (**3.20b**) the solution remained homogeneous. The work-up procedures for these compounds are detailed separately below.

a: 1-(Chlorodimethylsilylmethyl)-2-quinolinone (2.25b)

Volume of solvent	4 cm^3
2-(Trimethylsiloxy)quinoline (**2.24**)	0.65 g / 2.99 mmol
Chloro(chloromethyl)dimethylsilane	0.44 g / 3.08 mmol
Mass of (**2.25b**) isolated	0.67 g / 2.66 mmol (89%)

Compound was recrystallised from acetonitrile yielding colourless, needle-like, flat-ended crystals suitable for single crystal X-ray analysis.

δ **^{1}H** (400 MHz) = 8.09 (d, 1H, $^3J_{H4\text{-}H3}$ = 9.2 Hz, H_4), 7.83-7.77 (m, 3H, H_5/H_7/H_8), 7.49 (m, 1H, H_6), 6.93 (d, 1H, $^3J_{H3\text{-}H4}$ = 9.2 Hz, H_3), 3.65 (s, 2H, N-CH_2), 0.75 (s, 6H, Si(CH_3)$_2$); δ **^{13}C** (400 MHz) = 163.4 (C_2), 143.1 (C_4), 138.1 (C_{8a}), 132.7 (C_7), 129.3 (C_5), 124.8 (C_6), 121.9 (C_{4a}), 116.5 (C_8), 115.4 (C_3), 38.6 (N-CH_2), 7.4 (Si(CH_3)$_2$); δ **^{29}Si** (400 MHz) = - 38.4 (solution), - 39.6 (solid state). **Found %** C 57.15, H 5.86, N 5.35; requires C 57.24, H 5.60, N 5.56 ($C_{12}H_{14}ClNOSi$).

b: 1-(Chlorodimethylsilylmethyl)-2-quinoxalinone (2.41b)

The solvent was removed by distillation under nitrogen and latterly by high vacuum pumping and the resulting brown solid residue cooled to room temperature. By washing the residue with diethyl ether (2 x 2 cm^3) and drying the creamy white power obtained under high vacuum for 1 hour, the title compound was isolated.

Volume of solvent	10 cm^3
2-(Trimethylsiloxy)quinoxaline (**2.39**)	0.85 g / 3.89 mmol
Chloro(chloromethyl)dimethylsilane	0.56 g / 3.90 mmol
Mass of (**2.41b**) isolated	0.80 g / 3.16 mmol (81%)

δ **^{1}H** (400 MHz) = 8.53 (s, 1H, H_3), 8.05 (dd, 1H, $^3J_{H5\text{-}H6}$ = 8.4 Hz, $^4J_{H5\text{-}H7}$ = 1.6 Hz, H_5), 7.80 (ddd, 1H, $^3J_{H7\text{-}H8}$ = 8.8 Hz, $^3J_{H7\text{-}H6}$ = 7.6 Hz, $^4J_{H7\text{-}H5}$ = 1.6 Hz, H_7), 7.67 (dd, 1H, $^3J_{H8\text{-}H7}$ = 8.8 Hz, $^4J_{H8\text{-}H6}$ = 1.1 Hz, H_8), 7.58 (ddd, 1H, $^3J_{H6\text{-}H5}$ = 8.4 Hz, $^3J_{H6\text{-}H7}$ = 7.6 Hz, $^4J_{H6\text{-}H8}$ = 1.1 Hz, H_6), 3.54 (s, 2H, N-CH_2), 0.76 (s, 6H, Si(CH_3)$_2$); δ **^{13}C** (400 MHz) = 155.8 (C_2), 144.3 (C_3), 135.1 (C_{8a}), 132.7 (C_7), 131.5 (C_{4a}), 130.9 (C_5), 126.0 (C_6), 115.7 (C_8), 37.3 (N-CH_2), 6.9 (Si(CH_3)$_2$); δ **^{29}Si** (400 MHz) = - 27.1. **M/Z** (EI$^+$) = 252/254 (3:1) (M^+) (measured 252.0486 (M^+:^{35}Cl), requires 252.0486 for $C_{11}H_{13}{}^{35}ClN_2OSi$), 251/253 (3:1) ($M^+$-H) 237/239 (3:1) ($M^+$-Me), 217, 129.

c: 3-(Chlorodimethylsilylmethyl)-4-pyrimidone (2.42b)

Volume of solvent	5 cm^3
4-(Trimethylsiloxy)-3-pyrimidine (**2.40**)	1.74 g / 10.34 mmol
Chloro(chloromethyl)dimethylsilane	1.48 g / 10.35 mmol
Mass of (**2.42b**) isolated	1.81 g / 8.93 mmol (86%)
State	White crystalline solid

δ **^{1}H** (400 MHz) = 8.38 (s, 1H, H_2), 8.13 (d, 1H, $^3J_{H6\text{-}H5}$ = 6.4 Hz, H_6), 6.63 (d, 1H, $^3J_{H5\text{-}H6}$ = 6.4 Hz, H_5), 3.53 (s, 2H, N-CH_2), 0.68 (s, 6H, $Si(CH_3)_2$); δ **^{13}C** (90 MHz) = 163.3 (C_4), 156.0 (C_6), 150.9 (C_2), 112.7 (C_5), 39.4 (N-CH_2), 5.7 ($Si(CH_3)_2$); δ **^{29}Si** (400 MHz) = - 16.7. **M/Z** (EI^+) = 202/204 (3:1) (M^+) (measured 202.0329 (M^+:^{35}Cl), requires 202.0329 for $C_7H_{11}{}^{35}ClN_2OSi$), 167 (M^+-Cl) (measured 167.0641, requires 167.0641 for $C_7H_{11}N_2OSi$)

d: 2-(Chlorodimethylsilylmethylmercapto)pyridine (3.11b)

Volume of solvent	5 cm^3
2-(Trimethylsilylmercapto)pyridine (**3.10**)	1.00 g / 5.45 mmol
Chloro(chloromethyl)dimethylsilane	0.78 g / 5.45 mmol
Mass of (**3.11b**) isolated	0.98 g / 4.50 mmol (83%)
State	Yellow crystalline solid

δ **^{1}H** (400 MHz) = 8.28 (d, 1H, $^3J_{H6\text{-}H5}$ = 4.8 Hz, H_6), 7.70 (dd, 1H, $^3J_{H4\text{-}H3}$ = 8.4 Hz, $^3J_{H4\text{-}H5}$ = 7.6 Hz, H_4), 7.32 (d, 1H, $^3J_{H3\text{-}H4}$ = 8.4 Hz, H_3), 7.20 (dd, 1H, $^3J_{H5\text{-}H4}$ = 7.6 Hz, $^3J_{H5\text{-}H6}$ = 4.8 Hz, H_5), 2.65 (s, 2H, S-CH_2), 0.76 (s, 6H, $Si(CH_3)_2$); δ **^{13}C** (400 MHz) = 159.6 (C_2), 144.5 (C_6), 138.6 (C_4), 122.3 (C_3), 120.1 (C_5), 16.7 (S-CH_2), 8.8 ($Si(CH_3)_2$); δ **^{29}Si** (400 MHz) = - 19.4. **M/Z** (EI^+) = 217/219 (3:1) (M^+), 202/204 (3:1) (M^+-Me), 182, 124, 78. **Found %** C 44.12, H 5.52, N 6.34, Cl 14.30; requires C 44.12, H 5.55, N 6.43, Cl 14.72 ($C_8H_{12}ClNSSi$).

e: 2-(Chlorodimethylsilylmethylmercapto)-5-trifluoromethylpyridine (3.20b)

Removal of the reaction solvent by distillation under nitrogen afforded a highly moisture sensitive brown oil (about 0.7g). Vacuum distillation of the oil (60°C/0.03 mmHg) allowed the title compound to be isolated as a bright yellow liquid.

Volume of solvent	3 cm^3
5-Trifluoromethyl-2-(trimethylsilylmercapto)pyridine (**3.19**)	1.01 g / 3.50 mmol
Chloro(chloromethyl)dimethylsilane	0.51 g / 3.56 mmol
Mass of (**3.20b**) isolated	0.55 g / 1.92 mmol (55%)

δ **^{1}H** (400 MHz) = 8.61 (s, 1H, H_6), 7.69 (dd, 1H, $^3J_{H4-H3}$ = 8.8 Hz, $^4J_{H4-H6}$ = 2.4 Hz, H_4), 7.34 (d, 1H, $^3J_{H3-H4}$ = 8.8 Hz, H_3), 2.70 (s, 2H, S-CH_2), 0.58 (s, 6H, Si(CH_3)$_2$); δ **^{13}C** (400 MHz) = 164.3 (C_2), 145.2 (C_6), 132.9 (C_4), 123.7 (q, $^1J_{C-F}$ = 270.2 Hz, CF_3), 122.6 (q, $^2J_{C-F}$ = 33.0 Hz, C_5), 121.6 (C_3), 17.0 (S-CH_2), 2.7 (Si(CH_3)$_2$); δ **^{19}F** (90 MHz) = - 64.2; δ **^{29}Si** (400 MHz) = 19.2. **M/Z** (EI^+) = 285/287 (3:1) (M^+) (measured 285.0021 (M^+:^{35}Cl), requires 285.0022 for $C_9H_{11}{}^{35}ClF_3NSSi$), 270/272 (3:1) ($M^+$-Me), 250, 192, 93.

f: 1-(Chlorodimethylsilylmethyl)-6-methyl-2-thiopyridone (3.28b)

Volume of solvent	3 cm^3
6-Methyl-2-(trimethylsilylmercapto)pyridine (**3.27**)	1.50 g / 7.90 mmol
Chloro(chloromethyl)dimethylsilane	1.16 g / 8.11 mmol
Mass of (**3.28b**) isolated	1.47 g / 6.34 mmol (80%)
State	Pale yellow crystalline solid

δ **^{1}H** (400 MHz) = 7.57 (d, 1H, $^3J_{H3-H4}$ = 8.8 Hz, H_3), 7.22 (m, 1H, H_4), 6.70 (d, 1H, $^3J_{H5-H4}$ = 7.6 Hz, H_5), 4.34 (s, 2H, N-CH_2), 2.63 (s, 3H, 6-CH_3), 0.72 (s, 6H, Si(CH_3)$_2$); δ **^{13}C** (400 MHz) = 176.4 (C_2), 149.9 (C_6), 134.6 (C_4), 130.5 (C_3), 116.6 (C_5), 49.9 (N-CH_2), 23.0 (6-CH_3), 5.9 (Si(CH_3)$_2$); δ **^{29}Si** (400 MHz) = - 0.1. **M/Z** (EI^+) = 231/233 (3:1) (M^+) (measured 231.0305 (M^+:^{35}Cl), requires 231.0305 for $C_9H_{14}{}^{35}ClNSSi$), 216/218 (3:1) (M^+-Me), 196, 138.

g: 2-(Chlorodimethylsilylmethylmercapto)-4-methylpyridine (3.32)

Volume of solvent	4 cm^3
4-Methyl-2-(trimethylsilylmercapto)pyridine (**3.31**)	0.63 g / 3.19 mmol
Chloro(chloromethyl)dimethylsilane	0.46 g / 3.20 mmol
Mass of (**3.32**) isolated	0.58 g / 2.50 mmol (81%)
State	Yellow crystalline solid

δ **^{1}H** (400 MHz) = 8.08 (d, 1H, $^3J_{H6\text{-}H5}$ = 6.0 Hz, H_6), 7.12 (s, 1H, H_3), 7.00 (d, 1H, $^3J_{H5\text{-}H6}$ = 6.0 Hz, H_5), 2.70 (s, 2H, S-CH_2), 2.39 (s, 3H, 4-CH_3), 0.77 (s, 6H, Si(CH_3)$_2$); δ **^{13}C** (400 MHz) = 159.7 (C_2), 151.2 (C_4), 143.2 (C_6), 122.0 (C_3), 121.7 (C_5), 21.2 (4-CH_3), 16.6 (S-CH_2), 8.4 (Si(CH_3)$_2$); δ **^{29}Si** (400 MHz) = - 26.9. **M/Z** (EI^+) = 231/233 (3:1) (M^+) (measured 231.0305 (M^+:^{35}Cl), requires 231.0305 for $C_9H_{14}{}^{35}ClNSSi$), 216/218 (3:1) (M^+-Me), 196, 138.

5.8: Synthesis of bi- and tri-chlorosilyl complexes (3.23) and (3.24) from (3.10) and the appropriate chlorosilane.

a: 2-(Dichloromethylsilylmethylmercapto)pyridine (3.23)

To a solution of (**3.10**) (0.50 g / 2.73 mmol) in benzene (4 cm^3) under a nitrogen atmosphere was added (chloromethyl)dichloromethylsilane (0.45 g / 2.75 mmol) and the solution stirred briefly. The title compound, (**3.23**), precipitated from the solution as a yellow crystalline material within 30 minutes. The compound was isolated by decanting off the solvent, washing the residue with benzene (2 x 5 cm^3) and drying it under high vacuum for 90 minutes. Isolated (**3.23**) (0.52 g / 2.18 mmol) (80%).

δ **^{1}H** (400 MHz) = 8.67 (d, 1H, $^3J_{H6\text{-}H5}$ = 5.6 Hz, H_6), 7.80 (m, 1H, H_4), 7.39 (d, 1H, $^3J_{H3\text{-}H4}$ = 7.6 Hz, H_3), 7.29 (m, 1H, H_5), 2.91 (s, 2H, S-CH_2), 1.02 (s, 3H, Si-CH_3); δ **^{13}C** (400 MHz) = 157.5 (C_2), 144.3 (C_6), 139.9 (C_4), 122.8 (C_3), 120.5 (C_5), 18.5 (S-CH_2), 12.0 (Si-CH_3); δ **^{29}Si** (90 MHz) = - 45.8. **M/Z** (EI^+) 237/239/241 (9:6:1) (M^+), 222/224/226 (9:6:1) (M^+-Me), 202/204 (3:1) (M^+-Cl), 124, 78. **Found %** C 34.98, H 3.74, N 5.64; requires C 35.30, H 3.81, N 5.88 ($C_7H_9Cl_2NSSi$).

b: (Trichlorosilylmethylmercapto)pyridine (3.24)

To a solution of (**3.10**) (0.50 g / 2.73 mmol) in benzene (2 cm^3) under a nitrogen atmosphere was added (chloromethyl)trichlorosilane (0.51 g / 2.77 mmol) and the solution stirred briefly. The title compound, (**3.24**), precipitated from the solution as a bright yellow crystalline material within 20 minutes. The compound was isolated by decanting off the solvent, washing the residue with benzene (2 x 3 cm^3) and drying it under a high vacuum for 90 minutes. Isolated (**3.24**) (0.61 g / 2.36 mmol) (86%).

δ ^{1}**H** (400 MHz) = 8.68 (d, $^3J_{H6\text{-}H5}$ = 6.0 Hz, H_6), 7.81 (m, 1H, H_4), 7.38 (d, 1H, $^3J_{H3\text{-}H4}$ = 8.4 Hz, H_3), 7.30 (m, 1H, H_5), 3.13 (s, 2H, S-CH_2); δ ^{13}**C** (400 MHz) = 155.8 (C_2), 144.8 (C_6), 140.5 (C_4), 122.8 (C_3), 120.5 (C_5), 19.1 (S-CH_2); δ ^{29}**Si** (400 MHz) = - 59.1. **M/Z** (EI^+) = 257/259/261/263 (≃ 27:27:9:1) (M^+) (measured 256.9056 (M^+:$^{35}Cl_3$), requires 256.9056 for $C_6H_6{}^{35}Cl_3NSSi$), 222/224/226 (9:6:1) (M^+-Cl), 124, 78.

5.9: Synthesis of 5-coordinate silyl-bromide complexes from silylated ligand precursors and (bromomethyl)chlorodimethylsilane.

A solution of the silylated ligand was prepared in benzene under a nitrogen atmosphere. (Bromomethyl)chlorodimethylsilane (1 equivalent) was added drop-wise with stirring and the solution allowed to stand for 30 minutes at room temperature. During this time, crystallisation or precipitation of the title compound occurred. The solvent was decanted off, the material washed twice with diethyl ether and dried for 1 hour under high vacuum.

a: 1-(Bromodimethylsilylmethyl)-2-quinolinone (2.25c)

Volume of solvent	5 cm^3
2-(Trimethylsiloxy)quinoline (**2.24**)	0.65 g / 2.99 mmol
(Bromomethyl)chlorodimethylsilane	0.56 g / 2.99 mmol
Mass of (**2.25c**) isolated	0.74 g / 2.50 mmol (84%)

Compound recrystallised from acetonitrile yielding colourless, cubic-shaped crystals suitable for single crystal X-ray analysis.

δ **^{1}H** (400 MHz) = 8.22 (d, 1H, $^3J_{H4\text{-}H3}$ = 8.5 Hz, H_4), 7.91-7.84 (m, 3H, H_5/H_7/H_8), 7.55 (m, 1H, H_6), 7.04 (d, 1H, $^3J_{H3\text{-}H4}$ = 8.5 Hz, H_3), 3.94 (s, 2H, N-CH_2), 0.81 (s, 6H, Si(CH_3)$_2$); δ **^{13}C** (400 MHz) = 163.4 (C_2), 144.1 (C_4), 137.8 (C_{8a}), 133.3 (C_7), 129.4 (C_5), 125.5 (C_6), 122.3 (C_{4a}), 117.1 (C_8), 114.6 (C_3), 39.0 (N-CH_2), 6.1 (Si(CH_3)$_2$); δ **^{29}Si** (400 MHz) = - 28.9. **M/Z** (EI$^+$) = 295/297 (1:1) (M^+), 294/296 (1:1) (M^+-H), 280/282 (1:1) (M^+-Me), 216, 128. **Found %** C 49.37, H 4.88, N 4.79; requires C 48.65, H 4.76, N 4.73 ($C_{12}H_{14}BrNOSi$).

b: 2-(Bromodimethylsilylmethylmercapto)pyridine (3.11c)

Volume of solvent	5 cm^3
2-(Trimethylsilylmercapto)pyridine (**3.10**)	0.50 g / 2.72 mmol
(Bromomethyl)chlorodimethylsilane	0.52 g / 2.77 mmol
Mass of (**3.11c**) isolated	0.55 g / 2.53 mmol (93%)
State	White crystalline solid

δ **^{1}H** (400 MHz) = 8.49 (d, 1H, $^3J_{H6\text{-}H5}$ = 5.6 Hz, H_6), 7.96 (m, 1H, H_4), 7.51 (d, 1H, $^3J_{H3\text{-}H4}$ = 8.8 Hz, H_3), 7.44 (m, 1H, H_5), 3.01 (s, 2H, S-CH_2), 1.07 (s, 6H, Si(CH_3)$_2$); δ **^{13}C** (400 MHz) = 162.7 (C_2), 143.6 (C_6), 141.2 (C_4), 123.3 (C_3), 121.2 (C_5), 16.5 (S-CH_2), 7.9 (Si(CH_3)$_2$); δ **^{29}Si** (400 MHz) = - 0.8. **M/Z** (FAB$^+$) = 182 (M^+-Br); (FAB$^-$) = 79/81 (1:1) (Br^-). **Found %** C 36.22, H 4.74, N 5.34; requires C 36.64, H 4.61, N 5.34 ($C_8H_{12}BrNSSi$).

c: 2-(Bromodimethylsilylmethylmercapto)-5-trifluoromethylpyridine (3.20c)

Volume of solvent	6 cm^3
5-Trifluoromethyl-2-(trimethylsilylmercapto)pyridine (**3.19**)	0.85 g / 3.38 mmol
(Bromomethyl)chlorodimethylsilane	0.64 g / 3.41 mmol
Mass of (**3.20c**) isolated	0.70 g / 2.13 mmol (63%)
State	Yellow crystalline solid.

δ **^{1}H** (400 MHz) = 8.51 (s, 1H, H_6), 7.72 (d, 1H, $^3J_{H4-H3}$ = 7.8 Hz, H_4), 7.35 (d, 1H, $^3J_{H3-H4}$ = 7.8 Hz, H_3), 2.74 (s, 2H, S-CH_2), 0.66 (s, 6H, Si(CH_3)$_2$); δ **^{13}C** (400 MHz) = 164.5 (C_2), 143.5 (C_6), 133.7 (C_4), 123.0 (q, $^1J_{C-F}$ = 272.1 Hz, CF_3), 122.7 (q, $^2J_{C-F}$ = 34.9 Hz, C_5), 122.0 (C_3), 17.3 (S-CH_2), 4.7 (Si(CH_3)$_2$); δ **^{19}F** (90 MHz) = - 64.2; δ **^{29}Si** (400 MHz) = 7.3. **M/Z** (FAB$^+$) = 250 (M$^+$-Br); (FAB$^-$) = 79/81 (1:1) (Br^-). **Found %** C 32.51, H 3.33, N 4.21; requires C 32.73, H 3.36, N 4.24 ($C_9H_{11}BrF_3NSSi$).

d: 1-(Bromodimethylsilylmethyl)-6-methyl-2-thiopyridone (3.28c)

Volume of solvent	5 cm^3
6-Methyl-2-(trimethylsilylmercapto)pyridine (**3.27**)	1.23 g / 6.23 mmol
(Bromomethyl)chlorodimethylsilane	1.18 g / 6.29 mmol
Mass of (**3.28c**) isolated	1.66 g / 6.01 mmol (97%)
State	White crystalline solid

δ **^{1}H** (400 MHz / CD_3OD) = 7.65 (d, 1H, $^3J_{H3-H4}$ = 8.4 Hz, H_3), 7.40 (m, 1H, H_4), 6.99 (d, 1H, $^3J_{H5-H4}$ = 7.2 Hz, H_5), 4.47 (s, 2H, N-CH_2), 2.66 (s, 3H, 6-CH_3), 0.32 (s, 6H, Si(CH_3)$_2$); δ **^{13}C** (400 MHz / CD_3OD) = 174.8 (C_2), 153.1 (C_6), 136.7 (C_4), 131.5 (C_3), 119.4 (C_5), 47.4 (N-CH_2), 22.8 (6-CH_3), - 1.5 (Si(CH_3)$_2$); δ **^{29}Si** (unattainable, see Section 3.6.4). **M/Z** (EI$^+$) = 196 (M$^+$-Br) (measured 196.0616, requires 196.0616 for $C_9H_{14}NSSi$); (FAB$^-$) = 79/81 (1:1) (Br^-).

5.10: Synthesis of 5-coordinate silyl-triflate complexes from their chloride analogues using trimethylsilyl triflate.

To a solution or suspension of the appropriate silyl chloride complex (usually freshly prepared) under a nitrogen atmosphere, was added trimethylsilyl triflate (1 equivalent) by syringe, drop-wise, with stirring. Within 30 minutes the title product usually formed as a suspension in the solution. If this was the case, the solvent was decanted off. In the preparation of (**2.25d**), however, the solution remained homogeneous and the solvent was removed by a combination of distillation at atmospheric pressure under nitrogen and latterly by high vacuum pumping. The isolated material was washed with diethyl ether (2 x 5 cm^3) and dried under high vacuum for 2 hours.

a: 1-(Dimethyltriflatosilylmethyl)-2-quinolinone (2.25d)

Volume of solvent (benzene)	10 cm^3
1-(Chlorodimethylsilylmethyl)-2-quinolinone (**2.25b**)	0.37 g / 1.47 mmol
Trimethylsilyl triflate	0.34 g / 1.53 mmol
Mass of (**2.25d**) isolated	0.48 g / 1.31 mmol (89%)

Colourless, cubic-shaped crystals suitable for single-crystal X-ray analysis were grown by slowly cooling a hot, concentrated benzene solution.

δ **^{1}H** (400 MHz) = 8.36 (d, 1H, $^3J_{H4\text{-}H3}$ = 9.2 Hz, H_4), 7.95-7.88 (m, 3H, H_5/H_7/H_8), 7.64 (m, 1H, H_6), 7.11 (d, 1H, $^3J_{H3\text{-}H4}$ = 9.2 Hz, H_3), 3.88 (s, 2H, N-CH_2), 0.69 (s, 6H, $Si(CH_3)_2$); δ **^{13}C** (400 MHz) = 163.4 (C_2), 145.5 (C_4), 137.7 (C_{8a}), 133.9 (C_7), 129.7 (C_5), 126.4 (C_6), 122.8 (C_{4a}), 119.8 (q, $^1J_{C\text{-}F}$ = 316.4 Hz, $SO_3\underline{C}F_3$), 117.2 (C_8), 113.8 (C_3), 37.2 (N-CH_2), 2.7 ($Si(CH_3)_2$); δ **^{19}F** (90 MHz) = - 79.9; δ **^{29}Si** (400 MHz) = - 8.1. **M/Z** (EI^+) = 365 (M^+), 364 (M^+-H), 350, 216, 128. **Found %** C 42.24, H 3.99, N 3.77; requires C 42.73, H 3.86, N 3.83 ($C_{13}H_{14}F_3NO_4SSi$).

b: 2-(Dimethyltriflatosilylmethylmercapto)pyridine (3.11d)

Volume of solvent (diethyl ether)	3 cm^3
2-(Chlorodimethylsilylmethylmercapto)pyridine (**3.11b**)	0.24 g / 1.10 mmol
Trimethylsilyl triflate	0.20 g / 1.22 mmol
Mass of (**3.11d**) isolated	0.29 g / 0.88 mmol (80%)
State	White crystalline solid

δ **^{1}H** (400 MHz) = 8.61 (d, 1H, $^3J_{H6\text{-}H5}$ = 6.0 Hz, H_6), 8.07 (m, 1H, H_4), 7.63 (d, 1H, $^3J_{H3\text{-}H4}$ = 8.8 Hz, H_3), 7.55 (m, 1H, H_5), 2.80 (s, 2H, S-CH_2), 0.87 (s, 6H, $Si(CH_3)_2$); δ **^{13}C** (400 MHz) = 164.4 (C_2), 143.9 (C_6), 143.3 (C_4), 123.6 (C_3), 122.3 (C_5), 120.5 (q, $^1J_{C\text{-}F}$ = 327.3 Hz, $SO_3\underline{C}F_3$), 12.5 (S-CH_2), 0.8 ($Si(CH_3)_2$); δ **^{19}F** (90 MHz) = - 80.1; δ **^{29}Si** (400 MHz) = 40.6. **M/Z** (EI^+) = 182 (M^+-OTf) (measured 182.0459, requires 182.0459 for $C_8H_{12}NSSi$); (FAB^-) = 149 ($^-$OTf), 80, 69.

c: 2-(Dimethyltriflatosilylmethylmercapto)-5-trifluoromethylpyridine (3.20d)

Volume of solvent (diethyl ether)	2 cm^3
2-(Chlorodimethylsilylmethylmercapto)-5-trifluoromethylpyridine (**3.20b**)	0.50 g / 1.75 mmol
Trimethylsilyl triflate	0.40 g / 1.80 mmol
Mass of (**3.20d**) isolated	0.54 g / 1.35 mmol (77%)
State	Yellow crystalline solid

δ **^{1}H** (400 MHz) = 8.62 (s, 1H, H_6), 8.13 (dd, 1H, $^3J_{H4-H3}$ = 8.8 Hz, $^4J_{H4-H6}$ = 2.0 Hz, H_4), 7.77 (d, 1H, $^3J_{H3-H4}$ = 8.8 Hz, H_3), 2.77 (s, 2H, S-CH_2), 0.82 (s, 6H, $Si(CH_3)_2$); δ **^{13}C** (400 MHz) = 167.2 (C_2), 140.5 (C_6), 137.3 (C_4), 124.6 (q, $^2J_{C-F}$ = 34.8 Hz, C_5), 123.7 (C_3), 122.0 (q, $^1J_{C-F}$ = 270.6 Hz, 5-CF_3), 119.2 (q, $^1J_{C-F}$ = 316.3 Hz, $SO_3\underline{C}F_3$), 13.3 (S-CH_2), 3.2 ($Si(CH_3)_2$); δ **^{19}F** (90 MHz) = - 64.5 (5-CF_3), - 80.0 (SO_3CF_3); δ **^{29}Si** (400 MHz) = 7.6. **M/Z** (FAB^+) = 250 (M^+-OTf); (FAB^-) = 149 ($^-$OTf), 80, 69. **Found %** C 30.34, H 2.82, N 3.86; requires C 30.07, H 2.78, N 3.51 ($C_{10}H_{11}F_6NO_3S_2Si$).

d: 1-(Dimethyltriflatosilylmethyl)-6-methyl-2-thiopyridone (3.28d)

Volume of solvent (toluene)	10 cm^3
1-(Chlorodimethylsilylmethyl)-6-methylpyridine (**3.28b**)	0.17 g / 0.73 mmol
Trimethylsilyl triflate	0.16 g / 0.74 mmol
Mass of (**3.28d**) isolated	0.21 g / 0.61 mmol (84%)
State	White crystalline solid

δ **^{1}H** (400 MHz / CD_3CN) = 7.94 (m, 1H, H_4), 7.72 (d, 1H, $^3J_{H3-H4}$ = 8.4 Hz, H_3), 7.43 (d, 1H, $^3J_{H5-H4}$ = 8.0 Hz, H_5), 4.24 (s, 2H, N-CH_2), 2.70 (s, 3H, 6-CH_3), 0.75 (s, 6H, $Si(CH_3)_2$); δ **^{13}C** (400 MHz / CD_3CN) = 163.9 (C_2), 158.4 (C_6), 143.4 (C_4), 126.4 (C_3), 124.6 (C_5), 122.0 (q, $^1J_{C-F}$ = 318.2 Hz, $SO_3\underline{C}F_3$), 50.4 (N-CH_2), 22.9 (6-CH_3), 1.2 ($Si(CH_3)_2$); δ **^{19}F** (90 MHz / CD_3CN) = - 75.8; δ **^{29}Si** (400 MHz / CD_3CN) = 26.7. **M/Z** (EI^+) = 196 (M^+-OTf) (measured 196.0616, requires 196.0616 for $C_9H_{14}NSSi$); (FAB^-) = 149 ($^-$OTf), 80, 69.

5.11: Synthesis of '0%' models for mapping series (3.11a-d) and (3.20a-d).

To a solution of the appropriate silylated ligand in toluene (20 cm^3) was added (iodomethyl)trimethylsilane (1 equivalent). The mixture was refluxed for 3 days under a nitrogen atmosphere and allowed to cool to room temperature. The solution was hydrolysed by stirring vigorously with aqueous sodium hydroxide (0.1 M) (10 cm^3) overnight. The organic phase was extracted into dichloromethane (3 x 30 cm^3) and the extracts combined and dried over magnesium sulfate. Removal of the solvent on a rotary evaporator afforded about 1 g of a brown oil. By high vacuum distillation (0.05 mmHg) of this oil, the title compound was isolated as a pale yellow liquid.

a: 2-(Trimethylsilylmethylmercapto)pyridine (3.16)

2-(Trimethylsilylmercapto)pyridine (**3.10**)	0.85 g / 4.64 mmol
(Iodomethyl)trimethylsilane	1.00 g / 4.67 mmol
Mass of (**3.16**) obtained	0.83 g / 4.21 mmol (91%)
Boiling point	50°C (0.05 mmHg)

δ **^{1}H** (90 MHz) = 8.41 (ddd, 1H, $^3J_{H6\text{-}H5}$ = 4.9 Hz, $^4J_{H6\text{-}H4}$ = 1.8 Hz, $^5J_{H6\text{-}H3}$ = 0.9 Hz, H_6), 7.43 (ddd, 1H, $^3J_{H4\text{-}H3}$ = 8.2 Hz, $^3J_{H4\text{-}H5}$ = 7.2 Hz, $^4J_{H4\text{-}H6}$ = 1.8 Hz, H_4), 7.17 (ddd, 1H, $^3J_{H3\text{-}H4}$ = 8.2 Hz, $^4J_{H3\text{-}H5}$ = 1.2 Hz, $^5J_{H3\text{-}H6}$ = 0.9 Hz, H_3), 6.91 (ddd, 1H, $^3J_{H5\text{-}H4}$ = 7.2 Hz, $^3J_{H5\text{-}H6}$ = 4.9 Hz, $^4J_{H5\text{-}H3}$ = 1.2 Hz, H_5), 2.37 (s, 2H, S-CH_2), 0.15 (s, 9H, $Si(CH_3)_3$); δ **^{13}C** (90 MHz) = 161.4 (C_2), 149.2 (C_6), 135.6 (C_4), 121.3 (C_3), 118.9 (C_5), 15.4 (S-CH_2), - 1.6 ($Si(CH_3)_3$); δ **^{29}Si** (90 MHz) = 1.9. **M/Z** (EI^+) = 197 (M^+), 182, 167, 124, 78, 73. **Found %** C 54.35, H 7.48, N 6.98; requires C 54.77, H 7.66, N 7.10 ($C_9H_{15}NSSi$).

b: 5-Trifluoromethyl-2-(trimethylsilylmethylmercapto)pyridine (3.21)

5-Trifluoromethyl-2-(trimethylsilylmercapto)pyridine (**3.19**)	1.10 g / 4.39 mmol
(Iodomethyl)trimethylsilane	0.94 g / 4.39 mmol
Mass of (**3.21**) obtained	0.53 g / 2.00 mmol (46%)
Boiling point	52°C (0.05 mmHg)

δ **^{1}H** (90 MHz) = 8.67 (s, 1H, H_6), 7.63 (dd, 1H, $^3J_{H4-H3}$ = 8.5 Hz, $^4J_{H4-H6}$ = 2.5 Hz, H_4), 7.27 (d, 1H, $^3J_{H3-H4}$ = 8.5 Hz, H_3), 2.41 (s, 2H, S-CH_2), 0.16 (s, 9H, Si(CH_3)$_3$); δ **^{13}C** (90 MHz) = 166.5 (C_2), 146.2 (C_6), 132.2 (C_4), 124.1 (q, $^1J_{C-F}$ = 271.9 Hz, CF_3), 122.0 (q, $^2J_{C-F}$ = 33.6 Hz, C_5), 120.9 (C_3), 15.4 (S-CH_2), - 1.7 (Si(CH_3)$_3$); δ **^{19}F** (90 MHz) = - 64.0; δ **^{29}Si** (90 MHz) = 2.1. **M/Z** (EI$^+$) = 265 (M^+), 250, 246, 73. **Found %** C 45.43, H 5.02, N 5.44; requires C 45.26, H 5.32, N 5.28 ($C_{10}H_{14}F_3NSSi$).

5.12: Synthesis of '100%' models for mapping complex series (3.11a-d) and (3.20a-d).

A solution of the appropriate 2-(trimethylsilylmethylmercapto)pyridine compound in benzene (5 cm^3) was prepared and methyl triflate (1 equivalent) added drop-wise by syringe. A white precipitate of the title compound formed within 5 minutes and was isolated by decanting off the solvent and washing the residue with diethyl ether (2 x 1 cm^3) before drying it under high vacuum for 1 hour.

a: 1-Methyl-2-(trimethylsilylmethylmercapto)pyridinium triflate (3.17)

2-(Trimethylsilylmethylmercapto)pyridine (**3.16**)	0.26 g / 1.32 mmol
Methyl triflate	0.22 g / 1.32 mmol
Mass of (**3.17**) isolated	0.45 g / 1.23 mmol (93%)

δ **^{1}H** (400 MHz) = 8.88 (d, 1H, $^3J_{H6-H5}$ = 5.6 Hz, H_6), 8.33 (m, 1H, H_4), 8.07 (d, 1H, $^3J_{H3-H4}$ = 8.4 Hz, H_3), 7.61 (m, 1H, H_5), 4.25 (s, 3H, N-CH_3), 2.46 (s, 2H, S-CH_2), 0.27 (s, 9H, Si(CH_3)$_3$); δ **^{13}C** (400 MHz) = 163.1 (C_2), 146.7 (C_6), 143.5 (C_4), 124.6 (C_3), 122.0 (C_5), 120.7 (q, $^1J_{C-F}$ = 321.7 Hz, $SO_3\underline{C}F_3$), 45.8 (N-CH_3), 17.9 (S-CH_2), - 1.8 (Si(CH_3)$_3$); δ **^{19}F** (90 MHz) = - 80.1; δ **^{29}Si** (400 MHz) = 3.5. **M/Z** (FAB$^+$) = 212 (M^+-OTf), 73; (FAB$^-$) = 149 ($^-$OTf), 80, 69. **Found %** C 36.12, H 4.93, N 3.78; requires C 36.55, H 5.01, N 3.87 ($C_{11}H_{18}F_3NO_3S_2Si$).

b: 1-Methyl-5-trifluoromethyl-2-(trimethylsilylmethylmercapto)pyridinium triflate (3.22)

5-Trifluoromethyl-2-(trimethylsilylmethylmercapto)pyridine (**3.21**) 0.40 g / 1.51 mmol

Methyl triflate 0.25 g / 1.52 mmol

Mass of (**3.22**) isolated 0.63 g / 1.46 mmol (97%)

δ **^{1}H** (90 MHz) = 9.13 (s, 1H, H_6), 8.37-8.32 (m, 2H, H_3/H_4), 4.28 (s, 3H, N-CH_3), 2.53 (s, 2H, S-CH_2), 0.26 (s, 9H, $Si(CH_3)_3$); δ **^{13}C** (90 MHz) = 168.3 (C_2), 144.5 (C_6), 139.1 (C_4), 125.8 (C_3), 124.6 (q, $^{2}J_{C-F}$ = 37.5 Hz, C_5), 121.8 (q, $^{1}J_{C-F}$ = 270.1 Hz, 5-CF_3), 120.8 (q, $^{1}J_{C-F}$ = 323.3 Hz, $SO_3\underline{C}F_3$), 46.5 (N-CH_3), 18.2 (S-CH_2), - 1.9 ($Si(CH_3)_3$); δ **^{19}F** (90 MHz) = - 64.6 (5-CF_3), - 80.4 ($SO_3\underline{C}F_3$); δ **^{29}Si** (90 MHz) = 3.7. **M/Z** (FAB^+) = 280 (M^+-OTf), 73; (FAB^-) = 149 ($^-$OTf), 80, 69. **Found** % C 33.44, H 3.82, N 3.38; requires C 33.56, H 3.99, N 3.26 ($C_{12}H_{17}F_6NO_3S_2Si$).

5.13: Synthesis of 'model' compounds for the complex series (2.25a-d).

a: Disiloxane (2.26)

(**2.25b**) (4.54 g / 15.33 mmol) was dissolved in acetone (20 cm^3) with stirring. Distilled water (20 cm^3) was added and stirring continued for a further 16 hours at room temperature. The solution was extracted with chloroform (3 x 50 cm^3) and the aqueous phase discarded. The extracts were combined and dried over magnesium sulfate. Removal of the solvent initially by rotary evaporation and latterly by high vacuum pumping afforded the title compound as a colourless, highly viscous oil. Isolated (**2.26**) (5.21 g / 11.61 mmol) (76%).

δ **^{1}H** (400 MHz) = 7.66 (d, 2H, $^3J_{H4-H3}$ = 9.2 Hz, H_4), 7.57 (m, 4H, H_5/H_7), 7.39 (m, 2H, H_8), 7.20 (m, 2H, H_6), 6.72 (d, 2H, $^3J_{H3-H4}$ = 9.2 Hz, H_3), 3.66 (s, 4H, N-CH_2), 0.13 (s, 12H, Si(CH_3)$_2$); δ **^{13}C** (400 MHz) = 161.8 (C_2), 139.9 (C_{8a}), 138.4 (C_4), 130.3 (C_7), 128.7 (C_5), 121.8 (C_6), 120.9 (C_3), 120.8 (C_{4a}), 115.3 (C_8), 35.4 (N-CH_2), 1.1 (Si(CH_3)$_2$); δ **^{29}Si** (400 MHz) = 1.5. **M/Z** (EI^+) = 433 (M^+-Me) (measured 433.1404, requires 433.1404 for $C_{23}H_{25}N_2O_3Si_2$), 290 (measured 290.1033, requires 290.1033 for $C_{14}H_{20}NO_2Si_2$), 216.

b: (2.26)-trimethylsilyltriflate adduct, (2.27)

In a 10 mm NMR tube capped by a rubber septum was prepared a solution of (**2.26**) (0.45 g / 1.00 mmol) in deuterochloroform (2.5 cm^3). To the solution was added, by syringe, trimethylsilyl triflate (0.45 g / 2.02 mmol) and the reagents shaken briefly together. (**2.27**) could only be observed in solution and is characterised by its NMR spectra.

δ **^{1}H** (400 MHz) = 8.56 (d, 2H, $^3J_{H4-H3}$ = 9.4 Hz, H_4), 8.03 (m, 2H, H_5), 7.95 (m, 2H, H_7,), 7.88 (m, 2H, H_8), 7.67 (m, 2H, H_6), 7.22 (d, 2H, $^3J_{H3-H4}$ = 9.4 Hz, H_3), 3.96 (s, 4H, N-CH_2), 0.73 (s, 12H, Si(CH_3)$_2$), 0.08 (s, 18H, Si(CH_3)$_3$); δ **^{13}C** (400 MHz) = 163.3 (C_2), 146.3 (C_4), 137.6 (C_{8a}), 133.9 (C_7), 130.1 (C_5), 126.5 (C_6), 123.2 (C_{4a}), 120.9 (q, $^1J_{C-F}$ = 320.0 Hz, $SO_3\underline{C}F_3$), 117.1 (C_8), 113.7 (C_3), 37.1 (N-CH_2), 2.0 (Si(CH_3)$_3$), 1.6 (Si(CH_3)$_2$); δ **^{19}F** (90 MHz) = - 80.0; δ **^{29}Si** (90 MHz) = 11.7 (Si(CH_3)$_3$), - 0.8 (Si(CH_3)$_2$).

c: (2.28a)-trimethylsilyltriflate adduct, (2.28b)

In a 10mm NMR tube capped by a rubber septum was prepared a solution of (**2.28a**) (0.14 g / 0.89 mmol) in deuterochloroform (2.5cm^3). To the solution was added, by syringe, trimethylsilyl triflate (0.20 g / 0.89 mmol) and the reagents shaken together briefly. The structure (**2.28b**) could only be observed in solution and is characterised by its NMR spectra.

δ ^{1}**H** (400 MHz) = 8.75 (d, 1H, $^{3}J_{H4\text{-}H3}$ = 9.2 Hz, H_4), 8.07 (m, 1H, H_5), 8.01 (m, 1H, H_8), 7.95 (m, 1H, H_7), 7.64 (m, 1H, H_6), 7.39 (d, 1H, $^{3}J_{H3\text{-}H4}$ = 9.2 Hz, H_3), 4.17 (s, 3H, N-CH_3), 0.51 (s, 9H, Si(CH_3)$_3$); δ ^{13}**C** (90 MHz) = 157.9 (C_2), 147.6 (C_4), 137.1 (C_{8a}), 134.3 (C_7), 129.4 (C_5), 126.8 (C_6), 123.3 (C_{4a}), 120.8 (q, $^{1}J_{C\text{-}F}$ = 320.4 Hz, $SO_3\underline{C}F_3$), 117.0 (C_8), 113.0 (C_3), 33.6 (N-CH_3), - 0.9 (Si(CH_3)$_3$); δ ^{19}**F** (90 MHz) = - 80.2; δ ^{29}**Si** (90 MHz) = 12.2.

5:14: Desilylation reactions of silyl fluorides.

5.14.1: Desilylation by hydroxide ion attack.

The synthesis proceeded as though preparing a silyl-fluoride complex (Section 5.5) until the point of hydrolysis of the fluorinated reaction mixture. At this point, hydrolysis was performed with 5M sodium hydroxide (50 cm^3) rather than distilled water. The bi-phasic mixture was vigorously stirred for 18 hours before the organic fraction was extracted into dichloromethane (3 x 50 cm^3). The extracts were combined and dried over magnesium sulfate. Removal of the solvent left a residue of the desilylated product which was washed with diethyl ether (2 x 10 cm^3).

a: 3-Methyl-4-pyrimidone (2.46)[205]

Volume of benzene	5 cm^3
3-(Chlorodimethylsilylmethyl)-4-pyrimidone (**2.42b**)	2.10 g / 10.34 mmol
Antimony trifluoride	0.47 g / 2.63 mmol
Mass of (**2.46**) isolated	0.52 g / 4.72 mmol (46%)
State	White crystalline solid.

δ ^{1}**H** (400 MHz) = 8.14 (s, 1H, H_2), 7.90 (d, 1H, $^{3}J_{H6\text{-}H5}$ = 6.4 Hz, H_6), 6.47 (s, 1H, $^{3}J_{H5\text{-}H6}$ = 6.4 Hz, H_5), 3.53 (s, 3H, N-CH_3); δ ^{13}**C** (400 MHz) = 161.5 (C_4), 153.5 (C_6), 151.5 (C_2), 115.7 (C_5), 34.4 (N-CH_3). **M/Z** (EI^+) = 110 (M^+), 82, 42.

b: 1-Methyl-2-quinolinone (2.28a)[206]

Volume of benzene	15 cm^3
1-(Chlorodimethylsilylmethyl)-2-quinolinone (**2.25b**)	1.49 g / 6.16 mmol
Antimony trifluoride	0.37 g / 2.05 mmol
Mass of (**2.28a**) isolated	0.76 g / 4.77 mmol (77%)
State	Colourless oil, boiling point 110°C (0.07 mmHg).

δ ^{1}**H** (90 MHz) = 7.55 (d, 1H, $^3J_{H4\text{-}H3}$ = 9.5 Hz, H_4), 7.48-7.13 (m, 4H, $H_{5\text{-}8}$), 6.61 (d, 1H, $^3J_{H3\text{-}H4}$ = 9.5 Hz, H_3), 3.59 (s, 3H, N-CH_3); δ ^{13}**C** (90 MHz) = 161.4 (C_2), 139.1 (C_{8a}), 138.2 (C_4), 129.9 (C_7), 128.0 (C_5), 121.3 (C_6), 120.7 (C_3), 119.8 (C_{4a}), 113.3 (C_8), 28.5 (N-CH_3). **M/Z** (EI^+) = 159 (M^+), 130.

c: 1-Methyl-2-quinoxalinone (2.47)[207]

Volume of benzene	10 cm^3
1-(Chlorodimethylsilylmethyl)-2-quinoxalinone (**2.41b**)	1.09 g / 4.32 mmol
Antimony trifluoride	0.26 g / 1.44 mmol
Mass of (**2.47**) isolated	0.50 g / 3.12 mmol (72%)
State	White solid (melting point 59°C)

δ ^{1}**H** (400 MHz) = 8.30 (s, 1H, H_3), 7.87 (dd, 1H, $^3J_{H5\text{-}H6}$ = 8.4 Hz, $^4J_{H5\text{-}H7}$ = 1.3 Hz, H_5), 7.60 (m, 1H, H_7), 7.37 (m, 1H, H_6), 7.35 (d, 1H, $^3J_{H8\text{-}H7}$ = 8.4 Hz, H_8), 3.69 (s, 3H, N-CH_3). δ ^{13}**C** (400 MHz) = 155.0 (C_2), 150.1 (C_3), 133.3/133.2 (C_{4a}/C_{8a}), 131.1 (C_7), 130.4 (C_5), 123.8 (C_6), 113.8 (C_8), 28.7 (N-CH_3). **M/Z** (EI^+) = 160 (M^+).

5.14.2: Desilylation by fluoride ion attack.

1,6-Dimethyl-2-thiopyridone (3.40)

The synthesis proceeded as though preparing (**3.28a**) but using half an equivalent of antimony trifluoride. Work-up was performed as for (**3.28a**) except that the residue obtained following the removal of solvent was of (**3.40**). The product was purified by recrystallisation from 1:1 diethyl ether/ethyl acetate yielding a pale yellow crystalline solid.

Volume of benzene	5 cm^3
1-(Chlorodimethylsilylmethyl)-6-methyl-2-thiopyridone (**3.28b**)	2.39 g / 10.29 mmol
Antimony trifluoride	0.92 g / 5.15 mmol
Mass of recrystallised (**3.40**) isolated	1.17 g / 8.40 mmol (82%)

δ **^{1}H** (90 MHz) = 7.64 (d, 1H, $^3J_{H3\text{-}H4}$ = 8.6 Hz, H_3), 7.04 (m, 1H, H_4), 6.50 (d, 1H, $^3J_{H5\text{-}H4}$ = 6.8 Hz, H_5), 4.04 (s, 3H, N-CH_3), 2.47 (s, 3H, 6-CH_3); δ **^{13}C** (90 MHz) = 181.4 (C_2), 149.4 (C_6), 133.6 (C_3), 133.4 (C_4), 115.1 (C_5), 40.0 (N-CH_3), 22.5 (6-CH_3). **M/Z** (EI^+) = 139 (M^+), 124, 94. **Found %** C 59.97, H 6.47, N 9.93; requires C 60.39, H 6.52, N 10.06 (C_7H_9NS).

5.15: Miscellaneous reactions.

a: Protonated silanol complex (2.30a)

(**2.30a**) co-crystallised with (**2.25b**) (approximately 1:3) from a saturated acetonitrile solution of (**2.25b**) left to partially evaporate in air over 24 hours. It is characterised by its X-ray crystal structure (see appendix). The colourless, needle-like crystals have wedge-shaped ends, unlike those of (**2.25b**) whos needles are flat-ended.

b: 1,6-Dimethyl-2-(methylmercapto)pyridinium triflate (3.41)

(**3.40**) (0.18 g / 1.29 mmol) was dissolved in toluene (7 cm^3) under a nitrogen atmosphere. Methyl triflate (0.23 g / 1.40 mmol) was added drop-wise with stirring. The solution momentarily turned cloudy before the title compound, (**3.41**), precipitated as a yellow crystalline solid. The solvent was decanted off, the crystals washed with diethyl ether (3 x 5 cm^3) and dried on a high vacuum line for 2 hours. Isolated (**3.41**) (0.22 g / 0.73 mmol) (52%).

δ **^{1}H** (90 MHz) = 8.13 (m, 1H, H_4), 7.73 (d, 1H, $^3J_{H3\text{-}H4}$ = 8.6 Hz, H_3), 7.57 (d, 1H, $^3J_{H5\text{-}H4}$ = 8.1 Hz, H_5), 4.09 (s, 3H, N-CH_3), 2.81 (s, 3H, 6-CH_3), 2.78 (s, 3H, S-CH_3); δ **^{13}C** (90 MHz) = 161.7 (C_2), 156.4 (C_6), 142.8 (C_4), 124.1 (C_5), 122.4 (C_3), 120.8 (q, $^1J_{C\text{-}F}$ = 319.8 Hz, $SO_3\underline{C}F_3$), 40.7 (N-CH_3), 21.8 (6-CH_3), 16.4 (S-CH_3); δ **^{19}F** (90 MHz) = - 80.1. **M/Z** (FAB^+) = 154 (M^+-OTf), 139, 107, 92; (FAB^-) = 149 ($^-$OTf), 80, 69. **Found %** C 35.20, H 4.01, N 4.55; requires C 35.64, H 3.99, N 4.62 ($C_9H_{12}F_3NO_3S_2$).

c: Hexacoordinate complex (3.42)

A solution of (**3.10**) (0.99 g / 5.40 mmol) in dry benzene (10 cm^3) was prepared under a nitrogen atmosphere. Dichloro(dichloromethyl)methylsilane (0.54 g / 1.80 mmol) ($^1/_3$ equivalent) was added drop-wise with stirring. Within 30 minutes the title compound, (**3.42**), precipitated from the solution as bright yellow crystalline solid. The solvent was decanted away from the product and the precipitate washed with diethyl ether (2 x 5 cm^3). The material was isolated by high vacuum pumping for 1 hour. Isolated (**3.42**) (0.67 g / 1.59 mmol) (88%).

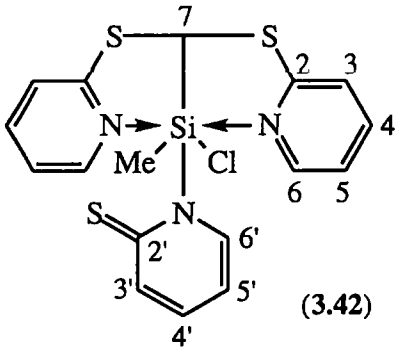

(**3.42**)

δ **^{1}H** (400 MHz) = 9.49 (d, 1H, $^3J_{H6'-H5'}$ = 6.4 Hz, $H_{6'}$), 8.36 (d, 2H, $^3J_{H6-H5}$ = 6.0 Hz, H_6), 7.99 (m, 2H, H_4), 7.75 (m, 1H, $H_{4'}$), 7.62 (d, 2H, $^3J_{H3-H4}$ = 7.6 Hz, H_3), 7.61 (m, 1H, $H_{5'}$), 7.39 (m, 2H, H_5), 7.16 (d, 1H, $^3J_{H3'-H4'}$ = 8.4 Hz, $H_{3'}$), 4.01 (s, 1H, H_7), 1.04 (s, 3H, Si-CH_3); δ **^{13}C** (400 MHz) = 171.8 ($C_{2'}$), 158.1 (C_2), 145.4 ($C_{6'}$), 143.5 (C_6), 142.3 ($C_{4'}$), 141.4 (C_4), 126.8 ($C_{3'}$), 123.3 (C_3), 122.5 (C_5), 118.9 ($C_{5'}$), 35.4 (C_7), 8.2 (Si-CH_3); δ **^{29}Si** (400 MHz) = - 104.2. **M/Z** (EI^+) = 387 (M^+- Cl), 234, 124, 111, 78. **Found %** C 48.09, H 4.23, N 10.02; requires C 48.38, H 3.82, N 9.95 ($C_{17}H_{16}ClN_3S_3Si$).

d: Bis(S-2-mercaptopyridinyl)methane (3.43)

(**3.42**) (0.27 g / 0.64 mmol) was dissolved in a 2:1 v/v acetone/water mixture (20 cm^3) and the solution stirred for 18 hours. The solution was extracted with toluene (2 x 20 cm^3) and the aqueous phase discarded. The organic extracts were combined and dried over magnesium sulfate and the solvent removed by rotary evaporation. The remaining pale yellow residue, being the title compound, was washed with diethyl ether (5 cm^3) and allowed to dry in air. Isolated (**3.43**) (0.07 g / 0.35 mmol) (55%).

δ **^{1}H** (90 MHz) = 8.48 (d, 2H, $^3J_{H6-H5}$ = 5.1 Hz, H_6), 7.50 (m, 2H, H_4), 7.16 (d, 2H, $^3J_{H3-H4}$ = 8.1 Hz, H_3), 6.99 (m, 2H, H_5), 1.26 (s, 2H, S-CH_2-S); δ **^{13}C** (90 MHz) = 157.7 (C_2), 149.5 (C_6), 136.0 (C_4), 122.5 (C_3), 119.7 (C_5), 29.7 (S-CH_2-S). **M/Z** (EI^+) = 234 (M^+), 124, 111, 78. **Found %** C 55.98, H 4.50, N 11.59; requires C 56.38, H 4.30, N 11.95 ($C_{11}H_{10}N_2S_2$).

Part B: Compounds from Chapter 4 .

5.16: Preparation of other dihalodiphenyltin compounds from dichlorodiphenyltin (4.42b).

(**4.42b**) was dissolved in aqueous sodium hydroxide (2M) (120 cm^3) and the solution stirred under reflux for 2 hours. After cooling the reaction to room temperature, the resulting white suspension, that of diphenyltin oxide (**4.43**), was filtered-off and washed with distilled water (40 cm^3) and acetone (2 x 40 cm^3). The product was dried in an oven (50°C) overnight and used without any further purification or characterisation.

To a stirred suspension of (**4.43**) in distilled water (60 cm^3) was added the appropriate concentrated aqueous hydrohalic acid and the solution refluxed gently for 90 minutes. The completion of the reaction was observed from the complete dissolution of the suspension and the formation of a brown, oily layer at the bottom of the reaction flask. The cooled two-phase solution was extracted with dichloromethane (3 x 40 cm^3) and the aqueous phase discarded. The organic extracts were combined and dried over magnesium sulfate. Removal of the solvent by rotary evaporation afforded a residue of the crude dihalodiphenyltin compound.

a: Dibromodiphenyltin (4.42c)[208]

Mass of dichlorodiphenyltin (**4.42b**)	8.03 g / 23.36 mmol
Volume of concentrated aqueous hydrobromic acid	18 cm^3

The brown residue was in the form of a viscous oil and was vacuum distilled (approximately 100°C, 0.07 mmHg) allowing pure (**4.42c**) to be collected as a colourless distillate. The liquid subsequently crystallised at room temperature over 2 days yielding hexagonal-shaped crystalline plates. Isolated (**4.42c**) (7.26 g / 16.78 mmol) (72%). Melting point 35-37°C.

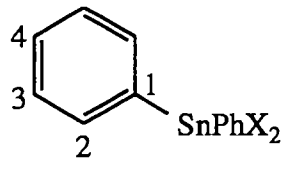

δ **^{1}H** (90 MHz) = 7.65-7.44 (m, 10H, H_{2-4}); δ **^{13}C** (90 MHz) = 137.2 (C_1), 134.8 (C_2), 131.6 (C_4), 129.5 (C_3); δ **^{119}Sn** (90 MHz) = - 73.1. **M/Z** (EI^+) = 432 (M^+), 353, 276, 199, 77.

b: Diiododiphenyltin (4.42d)[209]

Mass of dichlorodiphenyltin (**4.42b**)	11.71 g / 34.03 mmol
Volume of concentrated aqueous hydroiodic acid	40 cm^3

The oil quickly solidified at room temperature and was found to be sufficiently pure for analysis. Isolated (**4.42d**) (10.82 g / 20.54 mmol) (60%). Melting point 80-85°C.

δ **^{1}H** (90 MHz) = 7.70-7.41 (m, 10H, H_{2-4}); δ **^{13}C** (90 MHz) = 136.1 (C_1), 134.7 (C_2), 131.2 (C_4), 129.2 (C_3); δ **^{119}Sn** (90 MHz) = - 244.3. **M/Z** (EI^+) = 528 (M^+), 451, 401, 247, 197, 77.

5.17: Synthesis of N-aryl substituted 4-pyridone ligands (4.7) and (4.57) from maltol and primary amines.

Maltol (**4.1**) (12.09 g / 95.87 mmol) was suspended in water (300 cm^3). Concentrated hydrochloric acid (10 cm^3) was added with stirring followed by the appropriate aromatic primary amine (2 equivalents). The solution was refluxed for 3 days and allowed to cool to room temperature. Cooling caused the crystallisation of the title compound which could be separated from the solution by filtration. The residue was washed with diethyl ether (40 cm^3) and recrystallised from hot methanol. A second batch of crystals was obtained by evaporating half of the solvent from the filtrate and recrystallising the suspension thus formed.

a: 3-Hydroxy-2-methyl-1-phenyl-4-pyridone (4.7)[163]

Mass of aniline	19.02 g / 0.20 mol
Mass of product isolated (1st recrystallisation)	7.19 g
Mass of product isolated (2nd recrystallisation)	4.68 g
Total (**4.7**) isolated	11.87 g / 58.99 mmol (62%)
State	Creamy-white, needle-like crystals

δ ^{1}**H** (90 MHz / CD_3CN) = 7.60-7.39 (m, 6H, H_6/H_{12-14}), 6.30 (d, $^{1}J_{H5-H6}$ = 7.3 Hz, H_5), 5.9 (br, 1H, OH), 2.03 (s, 3H, CH_3); δ ^{13}**C** (90 MHz / CD_3CN) = 170.8 (C_4), 146.3 (C_2), 142.9 (C_3), 139.3 (C_6), 130.7 (C_{12}), 130.4 (C_{14}), 130.0 (C_{11}), 128.1 (C_{13}), 111.1 (C_5), 13.9 (CH_3). **M/Z** (EI^+) = 201 (M^+), 200 (M^+-H), 184, 77. **Found %** C 71.68, H 5.55, N 6.91; requires C 71.63, H 5.51, N 6.96 ($C_{12}H_{11}NO_2$).

b: 3-Hydroxy-1-(4-methoxyphenyl)-2-methyl-4-pyridone (4.57)[163]

Mass of 4-methoxyaniline	23.79 g / 0.19 mol
Mass of product isolated (1st recrystallisation)	8.55 g
Mass of product isolated (2nd recrystallisation)	5.34 g
Total (**4.57**) isolated	13.89 g / 64.53 mmol (67%)
State	Grey plate-like crystals

δ ^{1}**H** (90 MHz) = 7.29 (d, 1H, $^{3}J_{H6-H5}$ = 7.4 Hz, H_6), 7.20 (d, 2H, $^{3}J_{H12-H13}$ = 9.2 Hz, H_{12}), 6.99 (d, 2H, $^{3}J_{H13-H12}$ = 9.2 Hz, H_{13}), 6.45 (d, 1H, $^{3}J_{H5-H6}$ = 7.4 Hz, H_5), 5.4 (br, 1H, OH), 3.87 (s, 1H, O-CH_3), 2.10 (s, 3H, 2-CH_3); δ ^{13}**C** (90 MHz) = 170.0 (C_4), 160.1 (C_{14}), 145.6 (C_2), 137.7 (C_6), 134.6 (C_3), 129.1 (C_{11}), 127.8 (C_{12}), 114.8 (C_{13}), 110.8 (C_5), 55.6 (O-CH_3), 13.6 (2-CH_3). **M/Z** (EI^+) = 231 (M^+), 216.

5.18: Synthesis of 3-hydroxy-2-methyl-4-thiopyrone (4.8) from (4.1) and phosphorous pentasulfide.[210]

Maltol (**4.1**) (5.15 g / 40.84 mmol) and phosphorous pentasulfide (2.22 g / 5.00 mmol) were dissolved in dioxane (80 cm^3) and the solution stirred under reflux for 90 minutes. After cooling to room temperature the black suspension was removed by filtration. The filtrate was poured into water (150 cm^3) which caused the immediate precipitation of a brown solid. This material was isolated by filtration and dissolved in warm 95% ethanol (15 cm^3). Standing the solution in a fridge (0°C) for 5 hours yielded small yellow crystals of the title compound. The remaining solvent was decanted away, the crystals washed with diethyl ether (10 cm^3) and dried in the air. Isolated (**4.8**) (4.05 g / 28.49 mmol) (70%).

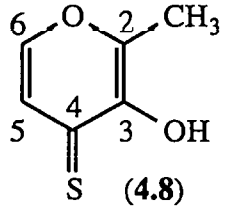

(**4.8**)

δ **^{1}H** (400 MHz) = 7.78 (s, 1H, OH), 7.58 (d, 1H, $^3J_{H6\text{-}H5}$ = 5.0 Hz, H_6), 7.32 (d, 1H, $^3J_{H5\text{-}H6}$ = 5.0 Hz, H_5), 2.45 (s, 3H, CH_3); δ **^{13}C** (400 MHz) = 185.9 (C_4), 150.6 (C_2), 147.0 (C_6), 145.3 (C_3), 124.2 (C_5), 15.1. **M/Z** (EI^+) = 142 (M^+).

5.19: Synthesis of pentacoordinated triphenyltin complexes from the ligands sodium salts and chlorotriphenyltin.

Part A

To a dichloromethane solution (50 cm^3) of the appropriate ligand was added a freshly ground powder of sodium hydroxide (1 equivalent) with stirring. After 18 hours of further stirring under a nitrogen atmosphere, a light brown suspension formed and was isolated by filtration. This residue was dried under high vacuum (0.05 mmHg) in an oil bath (120°C) for 2 hours. The product, a deep brown flaky solid, was that of the ligands sodium salt and was used immediately without further purification or characterisation.

Part B

A portion of this material was suspended in a dichloromethane solution (50 cm^3) of chlorotriphenyltin (**4.42a**) (1 equivalent) and stirred for 18 hours under a nitrogen atmosphere. At the end of the reaction the reaction mixture consisted of a brown solution and white suspension. The suspension was removed by filtration and discarded. The solvent was removed from the filtrate by rotary evaporation to leave a residue of the crude title complex as a brown crystalline solid.

a: 2-Methyl-3-(triphenylstannoxy)-4-pyrone (4.39a)[177]

A	Maltol (**4.1**)	4.40 g / 34.89 mmol
	Sodium hydroxide	1.40 g / 35.02 mmol
	Mass of crude sodium salt (**4.41**) isolated	3.35 g / 22.62 mmol (65%)
B	Mass of (**4.41**) used	0.88 g / 5.94 mmol
	Chlorotriphenyltin (**4.42a**)	2.29 g / 5.95 mmol

Compound was recrystallised from acetonitrile and colourless, plate-like crystals isolated.

Mass of recrystallised (**4.39a**) isolated	1.51 g / 3.18 mmol (54%)

δ **^{1}H** (90 MHz / CD_3CN) = 7.88 (d, 1H, $^3J_{H6-H5}$ = 5.2 Hz, H_6), 7.72-7.62 (m, 6H, H_8), 7.42-7.29 (m, 9H, H_9/H_{10}), 6.51 (d, 1H, $^3J_{H5-H6}$ = 5.2 Hz, H_5), 2.44 (s, 3H, CH_3); δ **^{13}C** (90 MHz / CD_3CN) = 175.9 (C_4), 156.3 (C_6), 153.4 (C_2), 145.7 (C_3), 137.5 (C_8), 136.3 (C_7), 130.0 (C_{10}), 129.3 (C_9), 111.1 (C_5), 15.2 (CH_3); δ **^{119}Sn** (90 MHz / CD_3CN) = - 166.6. **M/Z** (EI^+) = 399 (M^+-Ph), 351, 245, 197, 126. **Found %** C 60.50, H 4.26, N 25.10; requires C 60.67, H 4.24, N 24.99 ($C_{24}H_{20}O_3Sn$).

b: 2-Methyl-1-phenyl-3-(triphenylstannoxy)-4-pyridone (4.46a)

A	3-Hydroxy-2-methyl-1-phenyl-4-pyridone (**4.7**)	2.37 g / 11.78 mmol
	Sodium hydroxide	0.49 g / 12.26 mmol
	Mass of crude sodium salt isolated	2.14 g / 9.59 mmol (81%)
B	Mass of crude sodium salt used	1.08 g / 4.84 mmol
	Chlorotriphenyltin (**4.42a**)	1.87 g / 4.83 mmol

Compound recrystallised from acetonitrile and colourless, cubic-shaped crystals isolated.

	Mass of recrystallised (**4.46a**) isolated	1.42 g / 2.58 mmol (53%)

δ **^{1}H** (90 MHz) = 7.86-7.55/7.50-7.10 (m, 21H, $H_6/H_{8-10}/H_{12-14}$), 6.62 (d, 1H, $^3J_{H5-H6}$ = 6.9 Hz, H_5), 2.22 (s, 3H, CH_3); δ **^{13}C** (90 MHz) = 169.1 (C_4), 158.4 (C_2), 150.0 (C_3), 146.5 (C_6), 137.1 (C_8), 134.2 (C_7), 131.4 (C_{11}), 129.8 (C_{12}), 129.5 (C_{14}), 128.3 (C_{10}), 127.9 (C_9), 126.3 (C_{13}), 108.5 (C_5), 14.4 (CH_3); δ **^{119}Sn** (90 MHz) = - 193.9. **M/Z** (EI^+) = 474 (M^+-Ph), 351, 274, 197, 120, 77. **Found %** C 64.88, H 4.74, N 2.43; requires C 65.49, H 4.58, N 2.55 ($C_{30}H_{25}NO_2Sn$).

c: 1-(4-Methoxyphenyl)-2-methyl-3-(triphenylstannoxy)-4-pyridone (4.58a)

A	3-Hydroxy-1-(4-methoxyphenyl)-2-methyl-4-pyridone (**4.57**)	4.28 g / 18.51 mmol
	Sodium hydroxide	0.75 g / 18.75 mmol
	Mass of crude sodium salt isolated	4.05 g / 17.07 mmol (92%)
B	Mass of crude sodium salt used	3.62 g / 14.30 mmol
	Chlorotriphenyltin (**4.42a**)	5.51 g / 14.30 mmol

The product was washed with diethyl ether (2 x 5 cm^3) and dried under high vacuum for 30 minutes. State: White, crystalline solid. Mass of (**4.58a**) isolated 5.22 g / 9.25 mmol (65%).

δ **^{1}H** (90 MHz / CD_3CN) = 7.74-7.47/7.38-6.94 (m, 18H, $H_6/H_{8-10}/H_{12}$), 6.99 (d, 2H, $^3J_{H13-H12}$ = 9.2 Hz, H_{13}), 6.55 (d, 1H, $^3J_{H5-H6}$ = 6.8 Hz, H_5), 3.81 (s, 3H, O-CH_3), 2.17 (s, 3H, 2-CH_3); δ **^{13}C** (90 MHz / CD_3CN) = 169.4 (C_4), 161.2 (C_{14}), 147.8 (C_2), 141.7 (C_3), 137.5 (C_8), 136.7 (C_6), 136.4 (C_7), 130.6 (C_{10}), 129.7 (C_{12}), 128.8 (C_9), 128.5 (C_{11}), 115.6 (C_{13}), 108.6 (C_5), 56.4 (OCH_3), 14.6 (2-CH_3); δ **^{119}Sn** (90 MHz / CD_3CN) = - 195.8. **M/Z** (EI^+) = 580 (M^+-H), 504 (M^+-Ph) (measured 504.0620, requires 504.0621 for $C_{25}H_{22}NO_3Sn$), 351 ($SnPh_3^+$) (measured 351.0196, requires 351.0196 for $C_{18}H_{15}Sn$), 274, 197, 120, 77.

5.20: Synthesis of pentacoordinated tin halides by crystallisation from methanolic solutions of ligand (4.1), (4.7) or (4.8) and dihalodiphenyltin compound (4.42b-d).

The ligand of choice was dissolved in warm methanol. A methanolic solution (20 cm^3) of the dihalodiphenyltin compound (1 equivalent) was added with stirring. The solution was stoppered and allowed to stand until crystallisation of the title product occurred on the walls and base of the flask. The rate of crystallisation was controlled by solution concentration and optimised so that good quality, single crystals, suitable for X-ray analysis, were grown from dilute solutions. In order to obtain enhanced yields more quickly, but at the expense of crystal quality, the total volume of solvent could be halved. The crystals were separated by decanting off the solvent, washed with diethyl ether (2 x 30 cm^3) and dried in air for 30 minutes.

a: 3-(Chlorodiphenylstannoxy)-2-methyl-4-pyrone (4.39b)[177]

Total volume of methanol	80 cm^3
Maltol (**4.1**)	0.73 g / 5.82 mmol
Dichlorodiphenyltin (**4.42b**)	2.01 g / 5.85 mmol
Crystallisation time	3 hours (20°C)
Mass of (**4.39b**) isolated	1.91 g / 4.41 mmol (76%)
State	colourless, cubic-shaped crystals.

δ **^{1}H** (90 MHz / CD_3CN) = 8.18 (d, 1H, $^3J_{H6-H5}$ = 5.3 Hz, H_6), 8.03-7.92 (m, 4H, H_8), 7.52-7.35 (m, 6H, H_9/H_{10}), 6.88 (d, 1H, $^3J_{H5-H6}$ = 5.3 Hz, H_5), 2.45 (s, 3H, CH_3); δ **^{13}C** (90 MHz / CD_3CN) = 172.5 (C_4), 158.9 (C_2), 158.3 (C_6), 145.7 (C_3), 143.8 (C_7), 136.3 (C_8), 131.1 (C_{10}), 129.6 (C_9), 112.6 (C_5), 15.6 (CH_3); δ **^{119}Sn** (90 MHz / CD_3CN) = - 201.5. **M/Z** (EI^+) = 434 (M^+), 399, 357, 309, 245, 197, 126, 77. **Found %** C 49.32, H 3.51, Cl 8.19; requires C 49.88, H 3.49, Cl 8.18 ($C_{18}H_{15}ClO_3Sn$).

b: 3-(Bromodiphenylstannoxy)-2-methyl-4-pyrone (4.39c)

Total volume of methanol	30 cm^3
Maltol (**4.1**)	0.36 g / 2.90 mmol
Dibromodiphenyltin (**4.42c**)	1.25 g / 2.90 mmol
Crystallisation time	12 hours (20°C)
Mass of (**4.39c**) isolated	0.78 g / 1.63 mmol (56%)
State	colourless, cubic-shaped crystals.

δ **^{1}H** (90 MHz / CD_3CN) = 8.17 (d, 1H, $^3J_{H6-H5}$ = 5.1 Hz, H_6), 7.90-7.84 (m, 4H, H_8), 7.49-7.35 (m, 6H, H_9/H_{10}), 6.88 (d, 1H, $^3J_{H5-H6}$ = 5.1 Hz, H_5), 2.46 (s, 3H, CH_3); δ **^{13}C** (90 MHz / CD_3CN) = 172.3 (C_4), 158.5 (C_2), 158.2 (C_6), 144.2 (C_3), 143.7 (C_7), 135.8 (C_8), 131.3 (C_{10}), 129.7 (C_9), 112.5 (C_5), 15.6 (CH_3); δ **^{119}Sn** (90 MHz / CD_3CN) = - 196.0. **M/Z** (FAB^+) = 399 (M^+-Br); (FAB^-) = 79/81 (1:1) (Br^-), 77. **Found %** C 45.01, H 3.15, Br 16.51; requires C 45.24, H 3.16, Br 16.72 ($C_{18}H_{15}BrO_3Sn$).

c: 3-(Iododiphenylstannoxy)-2-methyl-4-pyrone (4.39d)

Total volume of methanol	70 cm^3
Maltol (**4.1**)	1.22 g / 9.67 mmol
Diiododiphenyltin (**4.42d**)	5.10 g / 9.68 mmol
Crystallisation time	7 days (20°C)
Mass of (**4.39d**) isolated	1.73 g / 3.30 mmol (34%)
State	colourless, cubic-shaped crystals.

δ **^{1}H** (90 MHz / CD_3CN) = 7.97 (d, 1H, $^3J_{H6-H5}$ = 5.4 Hz, H_6), 7.78-7.42 (m, 10H, $H_8/H_9/H_{10}$), 6.60 (d, 1H, $^3J_{H5-H6}$ = 5.4 Hz, H_5), 2.37 (s, 3H, CH_3); δ **^{13}C** (90 MHz / CD_3CN) = 173.4 (C_4), 156.8 (C_6), 153.6 (C_2), 144.0 (C_3), 139.4 (C_7), 135.5 (C_8), 131.8 (C_{10}), 129.9 (C_9), 113.0 (C_5), 14.9 (CH_3); δ **^{119}Sn** (90 MHz / CD_3CN) = - 271.4. **M/Z** (FAB^+) = 399 (M^+-I); (FAB^-) = 127 (I^-). **Found %** C 41.28, H 2.87, I 23.97; requires C 41.19, H 2.88, I 24.18 ($C_{18}H_{15}IO_3Sn$).

d: 3-(Chlorodiphenylstannoxy)-2-methyl-1-phenyl-4-pyridone (4.46b)

Total volume of methanol	320 cm^3
3-Hydroxy-2-methyl-1-phenyl-4-pyridone (**4.7**)	1.00 g / 4.97 mmol
Dichlorodiphenyltin (**4.42b**)	1.72 g / 5.00 mmol
Crystallisation time	1 week (2°C fridge)
Mass of (**4.46b**) isolated	1.15 g / 2.26 mmol (46%)
State	colourless, needle-like crystals.

δ **^{1}H** (90 MHz / CD_3CN) = 8.04-7.94/7.66-7.41 (m, 17H, $H_5/H_6/H_{8-10}/H_{12-14}$), 2.21 (s, 3H, CH_3); δ **^{13}C** (90 MHz / CD_3CN) = 168.7 (C_4), 146.2 (C_2), 141.8 (C_3), 139.7 (C_6), 136.3 (C_8), 131.8 (C_{14}), 131.4 (C_7), 131.2 (C_{10}), 131.0 (C_{12}), 130.6 (C_{11}), 129.5 (C_9), 127.0 (C_{13}), 111.7 (C_5), 15.2 (CH_3); δ **^{119}Sn** (90 MHz / CD_3CN) = - 198.9. **M/Z** (FAB^+) = 474 (M^+-Cl), 320; (FAB^-) = 35/37 (3:1) (Cl^-), 77. **Found %** C 56.59, H 4.06, N 2.78; requires C 56.68, H 3.96, N 2.75 ($C_{24}H_{20}ClNO_2Sn$).

e: 3-(Bromodiphenylstannoxy)-2-methyl-1-phenyl-4-pyridone (4.46c)

Total volume of methanol	95 cm^3
3-Hydroxy-2-methyl-1-phenyl-4-pyridone (**4.7**)	0.99 g / 4.92 mmol
Dibromodiphenyltin (**4.42c**)	2.15 g / 4.97 mmol
Crystallisation time	3 weeks (3°C fridge)
Mass of (**4.46c**) isolated	0.50 g / 0.90 mmol (18%)
State	colourless, needle-like crystals.

δ **^{1}H** (90 MHz / CD_3CN) = 8.03-7.91/7.61-7.33 (m, 16H, H_6/H_{8-10}/H_{12-14}), 6.85 (d, 1H, $^3J_{H5-H6}$ = 7.1 Hz, H_5), 2.19 (s, 3H, CH_3); δ **^{13}C** (90 MHz / CD_3CN) = 168.8 (C_4), 151.2 (C_2), 142.8 (C_3), 137.3 (C_6), 136.9 (C_8), 131.1 (C_{10}), 131.0 (C_{14}), 130.9 (C_{12}), 130.8 (C_{11}), 130.0 (C_7), 129.4 (C_9), 127.4 (C_{13}), 109.8 (C_5), 14.7 (CH_3); δ **^{119}Sn** (90 MHz / CD_3CN) = - 215.0. **M/Z** (FAB^+) = 474 (M^+-Br), 320; (FAB^-) = 79/81 (1:1) (Br^-), 77. **Found %** C 52.06, H 3.77, N 2.51; requires C 52.13, H 3.65, N 2.53 ($C_{24}H_{20}BrNO_2Sn$).

f: 3-(Chlorodiphenylstannoxy)-2-methyl-4-thiopyrone (4.59b)

Total volume of methanol	40 cm^3
3-Hydroxy-2-methyl-4-thiopyrone (**4.8**)	0.32 g / 2.25 mmol
Dichlorodiphenyltin (**4.42b**)	0.77 g / 2.25 mmol
Crystallisation time	2 hours (20°C)
Mass of (**4.59b**) isolated	0.62 g / 1.38 mmol (61%)
State	orange/brown, cubic shaped crystals.

δ **^{1}H** (400 MHz) = 8.01 (m, 4H, H_8), 7.74 (d, 1H, $^3J_{H6-H5}$ = 4.4 Hz, H_6), 7.40-7.34 (m, 7H, H_5/H_9/H_{10}), 2.70 (s, 3H, CH_3); δ **^{13}C** (400 MHz) = 168.1 (C_4), 157.5/157.3 (C_2/C_3), 147.2 (C_6), 143.3 (C_7), 136.0 (C_8), 129.9 (C_{10}), 128.5 (C_9), 120.1 (C_5), 16.9 (CH_3); δ **^{119}Sn** (400 MHz) = - 208.8. **M/Z** (EI^+) = 450 (M^+), 415, 373, 309, 232, 197, 154, 142, 77. **Found %** C 47.93, H 3.34, Cl 8.14; requires C 48.10, H 3.36, Cl 7.89 ($C_{18}H_{15}ClO_2SSn$).

g: 3-(Bromodiphenylstannoxy)-2-methyl-4-thiopyrone (4.59c)

Total volume of methanol	30 cm^3
3-Hydroxy-2-methyl-4-thiopyrone (**4.8**)	0.17 g / 1.20 mmol
Dibromodiphenyltin (**4.42c**)	0.54 g / 1.25 mmol
Crystallisation time	24 hours (20°C)
Mass of (**4.59c**) isolated	0.26 g / 0.53 mmol (44%)
State	orange/brown, cubic-shaped crystals.

δ ^{1}**H** (400 MHz) = 8.02 (m, 4H, H_8), 7.77 (d, 1H, $^3J_{H6-H5}$ = 4.4 Hz, H_6), 7.44-7.32 (m, 7H, $H_5/H_9/H_{10}$), 2.69 (s, 3H, CH_3); δ ^{13}**C** (400 MHz) = 167.8 (C_4), 157.7/157.3 (C_2/C_3), 147.4 (C_6), 143.3 (C_7), 135.9 (C_8), 129.8 (C_{10}), 128.5 (C_9), 119.8 (C_5), 16.9 (CH_3); δ ^{119}**Sn** (90 MHz) = - 212.0. **M/Z** (EI^+) = 417 (M^+-Ph), 415 (M^+-Br), 353, 142, 77. **Found %** C 43.59, H 3.04, Br 16.40; requires C 43.77, H 3.06, Br 16.18 ($C_{18}H_{15}BrO_2SSn$).

5.21: Synthesis of pentacoordinated tin halides from methanolic solutions of ligand (4.47) or (4.57) and dihalodiphenyltin compound (4.42b-c).

The appropriate ligand was dissolved in warm methanol. A methanolic solution (15 cm^3) containing the dihalodiphenyltin was added with stirring. The reaction was allowed to stand at room temperature for 5 hours, during which time the solution remained homogeneous. The solvent was removed by distillation and in the latter stages by high vacuum pumping. Washing the residue with diethyl ether (2 x 15 cm^3) and drying it under high vacuum for 2 hours afforded the title compound as a white crystalline solid.

a: 3-(Chlorodiphenylstannoxy)-1,2-dimethyl-4-pyridone (4.48)

Total volume of methanol	100 cm^3
3-Hydroxy-1,2-dimethyl-4-pyridone (**4.47**)	1.23 g / 8.84 mmol
Dichlorodiphenyltin (**4.42b**)	3.06 g / 8.90 mmol
Mass of (**4.48**) isolated	3.60 g / 8.06 mmol (91%)

δ **^{1}H** (90 MHz / CD_3CN) = 7.98-7.88/7.54-7.39 (m, 11H, H_6/H_{8-10}), 6.71 (d, 1H, $^3J_{H5-H6}$ = 7.3 Hz, H_5), 3.72 (s, 3H, N-CH_3), 2.45 (s, 3H, 2-CH_3); δ **^{13}C** (90 MHz / CD_3CN) = 167.4 (C_4), 151.3 (C_2), 144.2 (C_3), 137.0 (C_8), 136.1 (C_6), 131.9 (C_7), 131.1 (C_{10}), 129.6 (C_9), 109.7 (C_5), 44.1 (N-CH_3), 13.2 (2-CH_3); δ **^{119}Sn** (90 MHz / CD_3CN) = - 218.8. **M/Z** (FAB^+) = 412 (M^+-Cl) (measured 412.0379, requires 412.0360 for $C_{19}H_{18}NO_2Sn$); (FAB^-) = 35/37 (3:1) (Cl^-).

b: 3-(Chlorodiphenylstannoxy)-1-(4-methoxyphenyl)-2-methyl-4-pyridone (4.58b)

Total volume of methanol	100 cm^3
3-Hydroxy-1-(4-methoxyphenyl)-2-methyl-4-pyridone (**4.57**)	0.51 g / 2.21 mmol
Dichlorodiphenyltin (**4.42b**)	0.76 g / 2.21 mmol
Mass of (**4.58b**) isolated	1.01 g / 1.88 mmol (85%)

δ **^{1}H** (90 MHz / CD_3CN) = 8.01-7.91/7.58-7.26 (m, 12H, $H_5/H_6/H_{8-10}$), 7.24 (d, 2H, $^3J_{H12-H13}$ = 9.1 Hz, H_{12}), 7.02 (d, 2H, $^3J_{H13-H12}$ = 9.1 Hz, H_{13}), 3.81 (s, 3H, O-CH_3), 2.16 (s, 3H, 2-CH_3); δ **^{13}C** (90 MHz / CD_3CN) = 167.9 (C_4), 161.5 (C_{14}), 151.4 (C_2), 144.3/144.2 (C_3/C_7), 136.8 (C_8), 135.6 (C_6), 131.1 (C_{10}), 129.6 (C_9), 129.0 (C_{11}), 128.5 (C_{12}), 115.8 (C_{13}), 109.5 (C_5), 56.6 (O-CH_3), 14.9 (2-CH_3); δ **^{119}Sn** (90 MHz / CD_3CN) = - 215.4. **M/Z** (EI^+) = 309 ($SnPh_2Cl^+$) (measured 308.9493, requires 308.9493 for $C_{12}H_{10}ClSn$), 230 (M^+-$SnPh_2Cl$) (measured 230.0817, requires 230.0817 for $C_{13}H_{12}NO_3$).

c: 3-(Bromodiphenylstannoxy)-1-(4-methoxyphenyl)-2-methyl-4-pyridone (4.58c)

Total volume of methanol	50 cm^3
3-Hydroxy-1-(4-methoxyphenyl)-2-methyl-4-pyridone (**4.57**)	0.57 g / 2.46 mmol
Dibromodiphenyltin (**4.42c**)	1.07 g / 2.47 mmol
Mass of (**4.58c**) isolated	0.81 g / 1.43 mmol (58%)

δ **^{1}H** (90 MHz / CD_3CN) = 8.01-7.86/7.63-7.27 (m, 12H, $H_5/H_6/H_{8-10}$), 7.30 (d, 2H, $^{3}J_{H12-H13}$ = 9.1 Hz, H_{12}), 7.06 (d, 2H, $^{3}J_{H13-H12}$ = 9.1 Hz, H_{13}), 3.85 (s, 3H, O-CH_3), 2.19 (s, 3H, 2-CH_3); δ **^{13}C** (90 MHz / CD_3CN) = 168.4 (C_4), 160.7 (C_{14}), 150.1 (C_2), 144.8/144.7 (C_3/C_7), 136.9 (C_6), 135.6 (C_8), 130.7 (C_{10}), 129.0 (C_9), 128.2 (C_{11}), 127.8 (C_{12}), 115.0 (C_{13}), 109.0 (C_5), 55.7 (O-CH_3), 14.0 (2-CH_3); δ **^{119}Sn** (90 MHz / CD_3CN) = - 213.6. **M/Z** (EI^+) = 353 ($SnPh_2Br^+$) (measured 352.8986, requires 352.8988 for $C_{12}H_{10}BrSn$), 230 (M^+-$SnPh_2Br$) (measured 230.0817, requires 230.0817 for $C_{13}H_{12}NO_3$).

5.22: Synthesis of diphenylboron complexes of ligands (4.1) and (4.7).

Part A

Diphenylboronic acid - ethanolamine complex (1.01 g / 4.49 mmol) was dissolved in methanol (10 cm^3) at room temperature with stirring. The solution was hydrolysed with 1M hydrochloric acid (30 cm^3) with vigorous stirring for 10 minutes. Diphenylboronic acid, (**4.76**), formed as a gum at the bottom of the reaction vessel. The gum was extracted into diethyl ether (3 x 20 cm^3), dried over magnesium sulfate and the solvent removed by rotary evaporation. This yielded (**4.76**) as a colourless oil in an assumed 100% yield. The compound was immediately used in the second step to minimise degradation.

Part B

A solution of (**4.76**) was prepared in dichloromethane (30 cm^3). The appropriate powdered ligand (4.49 mmol) was added and the solution refluxed for 3 hours. The solvent was removed by distillation and final traces by high vacuum pumping. This left a white powdery residue. Recrystallisation of the residue from toluene yielded a white crystalline material of the target boron complex.

a: 3-(Diphenylboronato)-2-methyl-4-pyrone (4.77)[196]

Maltol (**4.1**)	0.56 g / 4.49 mmol
Mass of recrystallised (**4.77**) isolated	1.16 g / 4.00 mmol (89%)

δ **^{1}H** (400 MHz) = 7.80 (d, 1H, $^3J_{H6-H5}$ = 5.2 Hz, H_6), 7.51 (dd, 4H, $^3J_{H8-H9}$ = 7.6 Hz, $^4J_{H8-H10}$ = 1.6 Hz, H_8), 7.27 (m, 4H, H_9), 7.20 (m, 2H, H_{10}), 6.70 (d, 1H, $^3J_{H5-H6}$ = 5.2 Hz, H_5), 2.52 (s, 3H, CH_3); δ **^{13}C** (400 MHz) = 175.3 (C_4), 158.0 (C_6), 151.4/151.3 (C_2/C_3), 147.1 (C_7), 131.6 (C_8), 127.3 (C_9), 126.7 (C_{10}), 106.3 (C_5), 14.8 (CH_3); δ **^{11}B** (400 MHz) = 1.7. **M/Z** (EI$^+$) = 290 (M^+), 289 (M^+-H), 213. **Found %** C 74.54, H 5.13, B 3.76; requires C 74.52, H 5.21, B 3.73 ($C_{18}H_{15}O_3B$).

b: 3-(Diphenylboronato)-2-methyl-1-phenyl-4-pyridone (4.78)

3-Hydroxy-2-methyl-1-phenyl-4-pyridone (**4.7**)	0.90 g / 4.49 mmol
Mass of recrystallised (**4.78**) isolated	1.38 g / 3.79 mmol (84%)

δ **^{1}H** (400 MHz) = 7.57 (dd, 4H, $^3J_{H8-H9}$ = 8.0 Hz, $^4J_{H8-H10}$ = 1.6 Hz, H_8), 7.54-7.49 (m, 3H, H_{10}/H_{14}), 7.23 (m, 4H, H_9), 7.19-7.11 (m, 5H, H_6/H_{12}/H_{13}), 6.64 (d, 1H, $^3J_{H5-H6}$ = 6.4 Hz, H_5), 2.17 (s, 3H, CH_3); δ **^{13}C** (400 MHz) = 168.5, (C_4), 154.0 (C_2), 149.4 (C_7), 141.1 (C_3), 137.3 (C_6), 131.7 (C_8), 130.3 (C_{14}), 130.2 (C_{10}), 129.7 (C_{11}), 127.1 (C_9), 126.1/126.0 (C_{12}/C_{13}), 104.5 (C_5), 13.7 (CH_3); δ **^{11}B** (400 MHz) = - 3.3. **M/Z** (EI$^+$) = 365 (M^+), 364 (M^+-H), 288, 77. **Found %** C 78.96, H 5.51, N 3.92, B 3.02; requires C 78.93, H 5.52, N 3.83, B 2.96 ($C_{24}H_{20}NO_2B$).

5.23: Preparation and methylation of 3-methoxy-2-methyl-4-pyrone (methyl maltol) (4.44).

Maltol (**4.1**) (12.62 g / 0.10 mol) was dissolved in a solution of dimethylformamide (75 cm^3) water (2 cm^3) and methyl iodide (42.66 g / 0.30 mol). With vigorous stirring, powdered silver oxide (22.50 g / 97.09 mmol) was added slowly over 30 minutes. After addition was complete, the flask was securely stoppered and mechanically shaken for 40 hours.

The grey suspension which formed was removed by filtration to leave a clear brown filtrate. Water (200 cm^3) was poured in with stirring and caused an immediate solution colour change to cloudy white. Sodium cyanide (10 g) was added and after 15 minutes stirring the solution became clear brown again. The mixture was extracted with chloroform (3 x 100 cm^3) and the organic extracts combined and dried over magnesium

sulfate. Removal of solvent by rotary evaporation afforded a dark brown oil (about 8 cm^3). The oil was vacuum distilled (4 mmHg / 80°C) and the title compound, (**4.44**),[211] a colourless liquid, was isolated (6.17 g / 44.03 mmol) (44%).

δ **^1H** (90 MHz / CD_3CN) = 7.77 (d, 1H, $^3J_{H6-H5}$ = 5.7 Hz, H_6), 6.25 (d, 1H, $^3J_{H5-H6}$ = 5.7 Hz, H_5), 3.76 (s, 3H, O-CH_3), 2.27 (s, 3H, 2-CH_3); δ **^{13}C** (90 MHz / CD_3CN) = 175.3 (C_4), 160.2 (C_2), 155.3 (C_6), 146.3 (C_3), 118.2 (C_5), 60.1 (O-CH_3), 14.8 (2-CH_3). **M/Z** (EI^+) = 140 (M^+), 125, 122, 69.

Methyl maltol (**4.44**) (1.02 g / 7.28 mmol) was dissolved in diethyl ether under a nitrogen atmosphere. Methyl triflate (1.20 g / 7.31 mmol) was added by syringe, drop-wise, with stirring and the solution allowed to stand for 30 minutes at room temperature. During this time (**4.45**) precipitated from the solution. It was isolated by decanting off the solvent, washed with further diethyl ether (2 x 2 cm^3) and dried under high vacuum for 2 hours. Isolated (**4.45**) (1.89 g / 6.21 mmol) (85%).

δ **^1H** (90 MHz / CD_3CN) = 8.94 (d, 1H, $^3J_{H6-H5}$ = 5.4 Hz, H_6), 7.74 (d, 1H, $^3J_{H5-H6}$ = 5.4 Hz, H_5), 4.34 (s, 3H, 4-OCH_3), 3.94 (s, 3H, 3-OCH_3), 2.71 (s, 3H, 2-CH_3); δ **^{13}C** (90 MHz / CD_3CN) = 174.6 (C_2), 173.7 (C_4), 163.8 (C_6), 144.7 (C_3), 119.9 (q, $^1J_{C-F}$ = 316.9 Hz, $SO_3\underline{C}F_3$), 110.2 (C_5), 62.4 (4-OCH_3), 61.5 (3-OCH_3), 16.9 (2-CH_3); δ **^{19}F** (90 MHz / CD_3CN) = - 75.8. **M/Z** (FAB^+) = 155 (M^+-OTf), (FAB^-) = 149 ($^-$OTf), 80, 69. **Found %** C 34.71, H 3.78; requires C 35.53, H 3.64 ($C_9H_{11}F_3O_6S$).

5.24: Miscellaneous reactions.

a: 3-(Chlorodiphenylsiloxy)-2-methyl-4-pyrone (4.61)

To a solution of (**4.60**) (0.40 g / 2.02 mmol) in warm acetonitrile (2 cm^3) was added dichlorodiphenylsilane (0.51 g / 2.02 mmol). The solution was cooled in a refrigerator (3°C) for 3 hours. This promoted the growth of orange-coloured crystals of the title complex. The solvent was decanted off and the crystals pumped dry under high vacuum for 1 hour. Isolated (**4.61**) (0.38 g / 1.11 mmol) (55%). Higher quality crystals for single-crystal X-ray analysis were grown by recrystallisation from a dilute acetonitrile solution in a refrigerator (0°C) over 2 days.

δ **^{1}H** (400 MHz) = 7.77 (m, 4H, H_8), 7.57 (d, 1H, $^{3}J_{H6\text{-}H5}$ = 5.6 Hz, H_6), 7.34-7.13 (m, 6H, H_9/H_{10}), 6.31 (d, 1H, $^{3}J_{H5\text{-}H6}$ = 5.6 Hz, H_5), 2.47 (s, 3H, CH_3); δ **^{13}C** (400 MHz) = 173.2 (C_4), 154.8 (C_6), 152.7 (C_2), 145.0 (C_3), 134.6 (C_8), 129.6 (C_7), 127.4 (C_{10}), 126.9 (C_9), 110.8 (C_5), 14.9 (CH_3); δ **^{29}Si** (400 MHz) = - 85.3. **M/Z** (EI^+) = 343/345 (3:1) (M^++H) (measured 343.0557 (M^+:^{35}Cl+H), requires 343.0557 for $C_{18}H_{16}{}^{35}ClO_3Si$), 342/344 (3:1) ($M^+$) (measured 342.0479 ($M^+$:^{35}Cl), requires 342.0480 for $C_{18}H_{15}{}^{35}ClO_3Si$), 307 ($M^+$-Cl), 265/267 (3:1) ($M^+$-Ph), 154, 77.

b: (4.39b)-NMI complex, (4.68)

(**4.39b**) (0.09 g / 0.21 mmol) was dissolved in deuterochloroform (0.75 cm^3) in a 5 mm NMR tube and N-methyl imidazole (16.6 µl / 0.21 mmol) added. Compound (**4.68**) was only observed in freshly prepared solutions and was characterised by its ^{1}H, ^{13}C and ^{119}Sn NMR spectra. Its rapid disproportionation prevented this species from being isolated.

δ **^{1}H** (400 MHz) = 7.71-7.67 (m, 5H, H_6/H_8), 7.41 (s, 1H, NMI), 7.30-7.24 (m, 6H, H_9/H_{10}), 7.03 (s, 1H, NMI), 6.84 (s, 1H, NMI), 6.49 (d, 1H, $^{3}J_{H5\text{-}H6}$ = 5.4 Hz, H_5), 3.63 (s, 3H, NMI-CH_3), 2.52 (s, 3H, 2-CH_3); δ **^{13}C** (400 MHz) = 174.6 (C_4), 153.6 (C_3), 153.3 (C_6), 149.1/148.9 (C_2/C_7), 137.8 (NMI), 135.5 (C_8), 129.4 (NMI), 128.2 (C_{10}), 127.9 (C_9), 120.1 (NMI), 110.2 (C_5), 33.3 (NMI-CH_3), 15.4 (2-CH_3); δ **^{119}Sn** (400 MHz) = - 352.5.

c: Dichlorobis(N-methylimidazole)diphenyltin (4.69)

(**4.39b**) (0.48 g / 1.11 mmol) was dissolved in warm chloroform (50 cm^3). N-methyl imidazole (0.09 g / 1.10 mmol) was added by syringe and the solution stirred briefly. The stoppered reaction flask was allowed to stand for 24 hours at room temperature. Small, colourless, cubic-shaped crystals of (**4.69**) formed on the walls and base of the reaction vessel. The solution was decanted off, the crystals washed with diethyl ether (2 x 10 cm^3) and dried in air for 30 minutes. The crystals were characterised by microanalysis and mass spectrometry but were too insoluble in common NMR solvents for NMR spectra to be obtained. However, they were of suitable quality for their structure to be determined by X-ray crystallography (see appendix). Isolated (**4.69**) (0.25 g / 0.50 mmol) (89%).

M/Z (EI+) = 391 (M^+-Cl -NMI), 344 (M^+-2NMI), 309, 232, 82, 77. **Found %** C 47.63, H 4.50, N 10.84; requires C 47.22, H 4.36, N 11.02 ($C_{20}H_{22}Cl_2N_4Sn$).

d: 3-Acetyl-2-methyl-4-pyrone (4.82)

2-Methyl-3-(trimethylsiloxy)-4-pyrone (**4.60**) (0.22 g / 1.11 mmol) was dissolved in chloroform (5 cm^3) and acetyl chloride (0.09 g / 1.15 mmol) added with stirring. The solution remained homogeneous and after 15 minutes the solvent was removed under vacuum leaving a small quantity of brown oil. Distillation of the oil produced a colourless distillate of (**4.82**). Isolated (**4.82**) (0.10 g / 0.59 mmol) (53%).

δ **^{1}H** (90 MHz / CD_3CN) = 7.83 (d, 1H, $^3J_{H6\text{-}H5}$ = 5.9 Hz, H_6), 6.30 (d, 1H, $^3J_{H5\text{-}H6}$ = 5.9 Hz, H_5), 2.26/2.23 (2x (s, 3H), acetyl CH_3/2-CH_3)); δ **^{13}C** (90 MHz / CD_3CN) = 172.3 (acetyl C=O), 168.3 (C_4), 160.2 (C_2), 156.1 (C_6), 139.2 (C_3), 116.8 (C_5), 20.4 (acetyl CH_3), 15.0 (2-CH_3). **M/Z** (EI^+) = 168 (M^+), 126, 43. **Found %** C 56.91, H 4.90; requires C 57.14, H 4.80 ($C_8H_8O_4$).

Chapter 6: Conclusions

We have extended the modelling of S_N2 substitution in solution by NMR spectroscopy to 2-quinolinone and various 2-thiopyridone complexes. For the 2-quinolinone ligand, all the ^{13}C chemical shifts except for C_2 are sensitive enough to the change of degree of nucleophile-silicon bond formation to be included in the mapping calculations. The X-ray crystal structures of quinolinone complexes (**2.25a-d**) show that the shorter the 'nucleophile'-silicon distance the more 'extended' the silicon-'leaving group' bond becomes. By the *structural correlation* approach, our data could be combined with results from similar crystal structures in the literature and plotted on a single graph - a parabolic curve of increasing percentage silicon-'leaving group' bond 'extension' with decreasing 'nucleophile'-silicon bond length for a generalised S_N2 'reaction' at an R_3SiX centre. The solution NMR data for all the silicon complexes could also be combined on a single graph with the results of Bassindale and Borbaruah's study of 2-pyridone complexes (**2.4**). The graph of percentage 'nucleophile'-silicon bond formation versus percentage pentacoordination for the same general 'substitution' showed the characteristic tetra- to penta- then back to tetra-coordination transition with increasing percentage nucleophile-silicon bond formation.

Unlike the 2-quinolinone complexes, the 2-thiopyridone complexes adopted one of two structures, either an *N-CH*$_2$ or *S-CH*$_2$ structure. We did not investigate the interplay between the mechanisms involved so we cannot discuss exactly how each complex is formed. However, the steric effect of groups in the 6-position of the thiopyridone ring seems to be an important factor. The general order of 'nucleophilicity' of the three donor atoms contained in the various pentacoordinate silicon complexes prepared was found to be O>N>S.

The new types of compound investigated as model compounds for 0% and 100% 'nucleophile-M bond formation' in Chapters 3 and 4 were found to be acceptable alternatives to the disiloxane-based compounds used in Chapter 2 and in Bassindale and Borbaruah's study of 2-pyridone complexes. The models of 100% 'nucleophile-M bond formation' were the first isolated complexes representing these structures and relied on a methyl group to mimic the effect of a fully-formed 'nucleophile'-M bond on each ligand.

However, they were found not to be as suitable as the previous disiloxanes. This is probably because this methyl group is not the ideal substitute for the silicon or tin groups it represents. This sometimes resulted in ^{13}C chemical shifts that were outside the range predicted by the *limiting* compounds so that they had to be ignored in the mapping calculations.

For the silicon complexes, it was generally observed that the better the 'leaving group' at silicon, the stronger the 'nucleophile'-silicon bond. Also, the more electron donating the ligand substituent, the stronger the 'nucleophile'-Si bond. For our tin maltol/thiomaltol/4-pyridone complexes however, strong 'nucleophile'-tin coordination (approximately 70% O-Sn bond formation) occured independently of the 'leaving group' or ligand substituents. This observation was made from the similarity of the complexes' NMR spectra and X-ray crystal structures. We conclude therefore that the tin is acting as a transition metal. This tendancy was accentuated by the contrasting behaviour of the tin complex (**4.39b**) with its silicon analogue (**4.61**) in the presence of the 'nucleophile' N-methyl imidazole (NMI). The tin complex added NMI and expanded its coordination sphere to six while the silicon complex substituted a chloride ion for NMI and remained five-coordinate.

The effect of decreasing the temperature of $CDCl_3$ solutions of pentacoordinated silyl-2-thiopyridone complexes was found by ^{13}C and ^{29}Si NMR spectroscopy to increase the degree of 'substitution' modelled by the complexes. This is in agreement with the various studies by Kummer *et al* of closely related complexes. The effect of decreasing the temperature on the ^{29}Si NMR chemical shift is dependant on which side of the fully pentacoordinate structure the compounds structure *sits* in the 'reaction' profile. If the structure is to the left of the fully pentacoordinate species of the 'reaction' then the shift moves upfield with decreasing temperature. The opposite is the case if the structure is to the right. In contrast, for tin complexes in $CDCl_3$ solution, the degree of 'substitution' was unaffected by temperature. However, in the polar solvent CD_3CN, reversible solvent coordination to the tin occured and the ^{119}Sn NMR resonance moved to higher fields as the temperature was lowered.

Appendix of crystallographic data

This section summarises the key instrument parameters and crystal data for the single crystal X-ray structures presented in Chapters 2 and 4. The appendix is split into 14 parts, one for each structure.

Structures from Chapter 2

Structures from Chapter 4

The lay out of each part is as follows:

Section A: Summary of crystal parameters, instrument conditions and data refinement information. Layout varies slightly depending on the software used to prepare the data table.

Section B and C: Listing of atomic coordinates and thermal parameters for non-hydrogen and hydrogen atoms respectively. The units of the thermal parameters vary between structures depending on the software used to prepared the data table.

Section D: Structure diagram(s) (usually ORTEP). Hydrogens normally omitted for clarity.

Section E: Listing of key bond lengths and angles (data for C-H bonds omitted).

Section F: Listing of hydrogen bond lengths and angles (Part 5 only).

The structures were solved using *SHELXLS86*, *SHELXLS93* and *SHELXLS97* programs and plotted using *ORTEP*. Ellipsoids at their surface are of 30% probability level. The isotropic structures were drawn using *Crystalmaker 2*.

Part 1. A: Summary

Compound number	**(2.25a)**		
Empirical Formula	$C_{12}H_{14}FNOSi$		
Formula Weight	235.33		
Crystal System	triclinic		
Space group	P-1 (No. 2)		
a, b, c [Å]	7.091(1)	8.750(2)	9.872(2)
alpha, beta, gamma [°]	101.29(3)	92.06(3)	103.64(3)
V [Å^3]	581.6(2)		
Z	2		
D(obs), D(calc) [g/cm^3]	0.000, 1.344		
F(000) [Electrons]	248		
Mu(MoKa) [/cm]	1.9		
Crystal Size [mm]	0.27 x 0.27 x 0.58		

Data Collection

Temperature (K)	200
Radiation [Å]	MoKa 0.71073
Theta Min-Max [°]	2.9, 28.2
Scan,(Type & Range) [°]	phi-scan rotation images on STOE IPDS25
Dataset	-9: 9 ; -11: 11 ; 0: 13
Tot., Uniq. Data, R(int)	2617, 2617, 0.000
Observed data [I > 2.0 sigma(I)]	2152

Refinement

Nref, Npar	2617, 201
R, wR, S	0.0408, 0.1124, 1.01
w = 1/[\s^2(Fo^2)+(0.0728P)^2] where P=(Fo^2+2Fc^2)/3	
Max. and Av. Shift/Error	0.00, 0.00
Min. and Max. resd. dens. [e/Å^3]	-0.25, 0.37

B: Final Coordinates and Equivalent Isotropic Thermal Parameters of the non-Hydrogen atoms for (**2.25a**)

Atom	x	y	z	U(eq) [Å^2][a]
Si	0.18578(6)	0.27619(5)	0.40354(4)	0.0295(1)
F	0.2136(2)	0.3887(1)	0.5645(1)	0.0490(4)
O	0.1596(2)	0.1696(1)	0.1955(1)	0.0325(3)
N	0.2295(2)	0.4288(1)	0.1763(1)	0.0238(3)
C2	0.1891(2)	0.2700(2)	0.1166(2)	0.0255(4)
C3	0.1822(2)	0.2236(2)	- 0.0310(2)	0.0312(4)
C4	0.2155(2)	0.3363(2)	- 0.1085(2)	0.0312(4)
C4A	0.2556(2)	0.5038(2)	- 0.0456(2)	0.0263(4)
C5	0.2858(2)	0.6239(2)	- 0.1252(2)	0.0325(5)
C6	0.3185(3)	0.7838(2)	- 0.0608(2)	0.0368(5)
C7	0.3223(3)	0.8265(2)	0.0822(2)	0.0368(5)
C8	0.2956(2)	0.7115(2)	0.1630(2)	0.0310(4)
C8A	0.2611(2)	0.5488(2)	0.0987(2)	0.0237(4)
C9	0.2336(3)	0.4636(2)	0.3276(2)	0.0328(5)
C10	0.3848(3)	0.1749(2)	0.4250(2)	0.0406(6)
C11	- 0.0687(3)	0.1612(3)	0.4099(2)	0.0467(6)

[a] Equivalent isotropic *U* defined as one-third of the trace of the orthogonalised U_{ij} tensor

C: Hydrogen Atom Positions and Isotropic Thermal Parameters for (**2.25a**)

Atom	x	y	z	U(iso) [Å^2]
H3	0.148(3)	0.113(3)	- 0.067(2)	0.045(5)
H4	0.211(3)	0.308(2)	- 0.205(2)	0.040(5)
H5	0.282(3)	0.594(2)	- 0.222(2)	0.041(5)
H6	0.336(3)	0.860(3)	- 0.120(2)	0.043(5)
H7	0.341(3)	0.936(3)	0.123(2)	0.050(6)
H8	0.297(3)	0.741(2)	0.253(2)	0.039(5)
H91	0.357(4)	0.532(3)	0.368(3)	0.065(7)
H92	0.136(3)	0.525(3)	0.352(2)	0.048(5)
H101	0.404(4)	0.171(3)	0.516(3)	0.073(8)
H102	0.361(4)	0.071(3)	0.374(3)	0.071(8)
H103	0.507(4)	0.236(3)	0.394(3)	0.080(8)
H111	- 0.151(4)	0.223(4)	0.391(3)	0.088(9)
H112	- 0.090(4)	0.145(3)	0.497(3)	0.081(8)
H113	- 0.098(4)	0.058(3)	0.350(3)	0.069(8)

D: ORTEP diagram

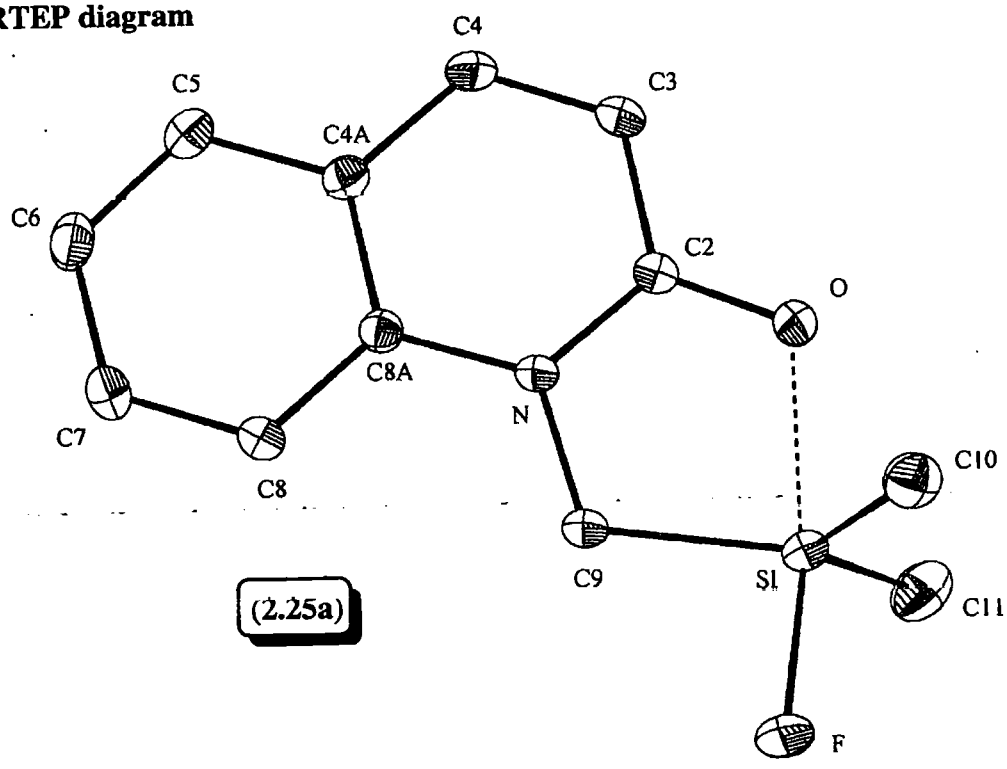

(2.25a)

E: Selected bond lengths (Å) and angles (°) for (**2.25a**)

Si-F	1.675(1)	C2-C3	1.430(3)
Si-O	2.065(1)	C3-C4	1.346(3)
Si-C9	1.898(2)	C4-C4A	1.431(3)
Si-C10	1.861(2)	C4A-C5	1.413(3)
Si-C11	1.857(2)	C4A-C8A	1.398(2)
O-C2	1.271(2)	C5-C6	1.380(3)
N-C2	1.356(2)	C6-C7	1.385(3)
N-C8A	1.398(2)	C7-C8	1.386(3)
N-C9	1.463(2)	C8-C8A	1.400(2)
F-Si-O	171.46(6)	O-C2-C3	123.25(16)
F-Si-C9	90.79(8)	N-C2-C3	118.79(16)
F-Si-C10	97.21(8)	C2-C3-C4	120.21(17)
F-Si-C11	96.97(9)	C3-C4-C4A	120.98(18)
O-Si-C9	80.66(7)	C4-C4A-C5	121.92(18)
O-Si-C10	87.18(8)	C4-C4A-C8A	118.69(17)
O-Si-C11	87.34(8)	C5-C4A-C8A	119.38(17)
C9-Si-C10	120.09(10)	C4A-C5-C6	120.12(18)

C9-Si-C11	119.72(11)	C5-C6-C7	119.86(17)
C10-Si-C11	117.96(10)	C6-C7-C8	121.28(17)
Si-O-C2	113.51(11)	C7-C8-C8A	119.36(17)
C2-N-C8A	122.47(14)	N-C8A-C4A	118.85(15)
C2-N-C9	114.54(14)	N-C8A-C8	121.15(14)
C8A-N-C9	122.98(13)	C4A-C8A-C8	120.00(16)
O-C2-N	117.96(16)	Si-C9-N	113.31(12)

Part 2. A: Summary

Compound number	**(2.25b)**		
Empirical Formula	$C_{12}H_{14}ClNOSi$		
Formula Weight	251.79		
Crystal System	triclinic		
Space group	P-1 (No. 2)		
a, b, c [Å]	6.932(1)	8.981(2)	10.621(2)
alpha, beta, gamma [°]	100.47(3)	91.04(3)	111.06(3)
V [$Å^3$]	604.3(2)		
Z	2		
D(obs), D(calc) [g/cm^3]	0.000, 1.384		
F(000) [Electrons]	264		
Mu(MoKa) [/cm]	3.9		
Crystal Size [mm]	0.154 x 0.154 x 0.962		

Data Collection

Temperature (K)	100
Radiation [Å]	MoKa 0.71073
Theta Min-Max [°]	2.8, 26.1
Scan,(Type & Range) [°]	phi-scan rotation images on STOE IPDS25
Dataset	-8: 8 ; -11: 10 ; 0: 13
Tot., Uniq. Data, R(int)	2168, 2168, 0.000
Observed data [I > 0.0 sigma(I)]	4

Refinement

Nref, Npar	2168, 154
R, wR, S	0.1002, 0.2932, 1.15

$w = 1/[\s^2(Fo^2)+(0.1876P)^2+2.1138P]$ where $P=(Fo^2+2Fc^2)/3$

Max. and Av. Shift/Error	0.00, 0.00
Min. and Max. resd. dens. [$e/Å^3$]	-0.69, 2.07

B: Final Coordinates and Equivalent Isotropic Thermal Parameters of the non Hydrogen atoms for (**2.25b**)

Atom	x	y	z	U(eq) [Å^2][a]
Cl	0.3162(2)	0.6246(2)	- 0.0798(1)	0.0231(5)
Si	0.3180(2)	0.7610(2)	0.1283(1)	0.0161(5)
O	0.3131(6)	0.8434(5)	0.3096(4)	0.0198(11)
N	0.2635(7)	0.5849(5)	0.3223(4)	0.0132(12)
C2	0.2915(8)	0.7402(6)	0.3814(5)	0.0148(14)
C3	0.2967(8)	0.7792(6)	0.5172(5)	0.0179(17)
C4	0.2755(8)	0.6645(7)	0.5881(5)	0.0174(17)
C4A	0.2449(8)	0.4999(6)	0.5259(5)	0.0158(17)
C5	0.2225(9)	0.3759(7)	0.5956(5)	0.0191(17)
C6	0.1948(9)	0.2208(7)	0.5321(5)	0.0207(17)
C7	0.1894(9)	0.1849(7)	0.3975(6)	0.0216(17)
C8	0.2127(9)	0.3036(7)	0.3268(5)	0.0178(16)
C8A	0.2396(8)	0.4617(6)	0.3904(5)	0.0142(14)
C9	0.2668(9)	0.5601(6)	0.1806(4)	0.0155(14)
C10	0.0951(9)	0.8187(7)	0.0871(5)	0.0220(17)
C11	0.5882(9)	0.9082(8)	0.1328(6)	0.0257(17)

[a] Equivalent isotropic *U* defined as one-third of the trace of the orthogonalised U_{ij} tensor

C: Hydrogen Atom Positions and Isotropic Thermal Parameters for (**2.25b**)

Atom	x	y	z	U(iso) [Å^2]
H3	0.315(2)	0.886(9)	0.559(3)	0.0220
H4	0.2804(9)	0.690(2)	0.673(7)	0.0210
H5	0.2266(9)	0.401(2)	0.690(7)	0.0230
H6	0.179(2)	0.137(7)	0.580(4)	0.0250
H7	0.173(2)	0.097(10)	0.362(4)	0.0260
H8	0.2107(9)	0.281(2)	0.246(7)	0.0210
H9A	0.142(7)	0.485(4)	0.142(2)	0.0180
H9B	0.368(5)	0.521(2)	0.156(1)	0.0180
H10A	- 0.028(6)	0.733(4)	0.0889(5)	0.0330
H10B	0.104(1)	0.842(1)	0.006(4)	0.0330
H10C	0.0990(9)	0.909(4)	0.146(3)	0.0330
H11A	0.684(5)	0.860(2)	0.156(1)	0.0380
H11B	0.608(1)	1.005(5)	0.196(3)	0.0380
H11C	0.613(2)	0.936(2)	0.050(4)	0.0380

D: ORTEP diagram

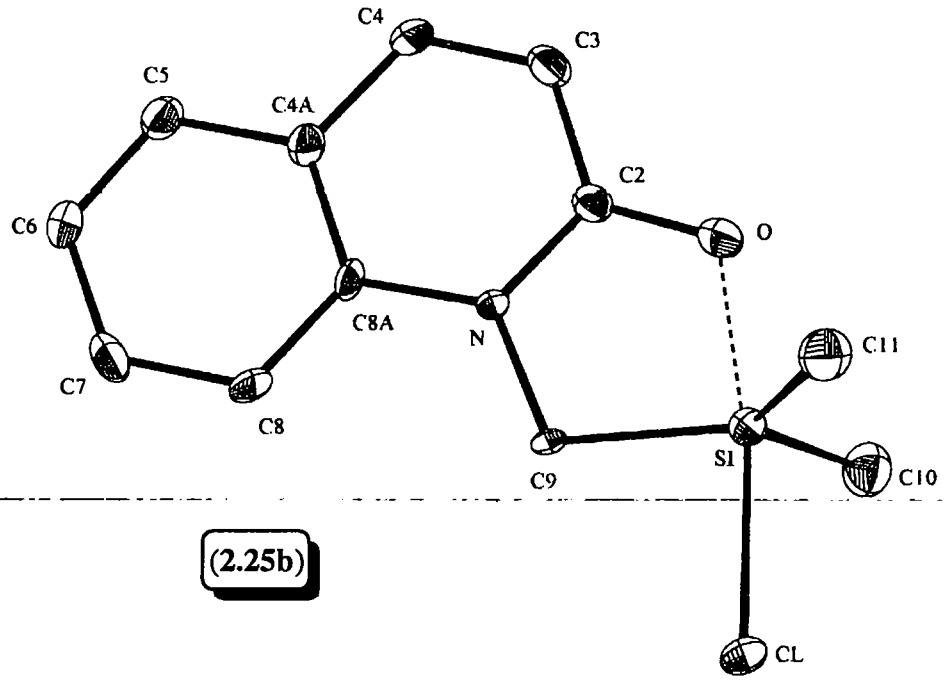

(2.25b)

E: Selected bond lengths (Å) and angles (°) for (**2.25b**)

Cl-Si	2.321(2)	C2-C3	1.418(7)
Si-O	1.939(1)	C3-C4	1.352(8)
Si-C9	1.898(5)	C4-C4A	1.443(8)
Si-C10	1.866(7)	C4A-C5	1.411(8)
Si-C11	1.858(7)	C4A-C8A	1.414(7)
O-C2	1.274(7)	C5-C6	1.376(8)
N-C2	1.364(7)	C6-C7	1.404(8)
N-C8A	1.392(7)	C7-C8	1.378(8)
N-C9	1.483(6)	C8-C8A	1.401(8)
Cl-Si-O	171.2(2)	O-C2-C3	123.6(5)
Cl-Si-C9	87.3(2)	N-C2-C3	119.3(5)
Cl-Si-C10	93.7(2)	C2-C3-C4	120.7(5)
Cl-Si-C11	94.0(2)	C3-C4-C4A	120.2(5)
O-Si-C9	83.9(2)	C4-C4A-C5	122.3(5)
O-Si-C10	90.9(2)	C4-C4A-C8A	118.9(5)
O-Si-C11	90.1(2)	C5-C4A-C8A	118.8(5)
C9-Si-C10	119.6(3)	C4A-C5-C6	120.3(5)
C9-Si-C11	120.3(3)	C5-C6-C7	120.2(5)
C10-Si-C11	119.9(3)	C6-C7-C8	120.9(6)

Si-O-C2	115.0(4)	C7-C8-C8A	119.3(5)
C2-N-C8A	122.5(4)	N-C8A-C4A	118.5(5)
C2-N-C9	114.4(4)	N-C8A-C8	121.0(5)
C8A-N-C9	123.1(4)	C4A-C8A-C8	120.5(5)
O-C2-N	117.1(5)	Si-C9-N	109.5(3)

Part 3. A: Summary

Compound number	**(2.25c)**		
Empirical Formula	$C_{12}H_{14}BrNOSi$		
Formula Weight	296.24		
Crystal System	monoclinic		
Space group	$P2_1/c$ (No. 14)		
a, b, c [Å]	10.005(2)	7.213(1)	17.692(4)
alpha, beta, gamma [°]	90	103.14(3)	90
V [$Å^3$]	1243.3(4)		
Z	4		
D(obs), D(calc) [g/cm^3]	0.000, 1.583		
F(000) [Electrons]	600		
Mu(MoKa) [/cm]	33.8		
Crystal Size [mm]	0.46 x 0.46 x 0.963		

Data Collection

Temperature (K)	100
Radiation [Å]	MoKa 0.71073
Theta Min-Max [°]	2.8, 25.0
Scan,(Type & Range) [°]	phi-rotation images on STOE IPDS25
Dataset	-11: 11 ; 0: 8 ; 0: 20
Tot., Uniq. Data, R(int)	2171, 2171, 0.000
Observed data [I > 0.0 sigma(I)]	0

Refinement

Nref, Npar	2171, 155
R, wR, S	00922, 0.2749, 1.13

$w = 1/[\backslash S^2(Fo^2)+(0.1270P)^2+20.2635P]$ where $P=(Fo^2+2Fc^2)/3$

Max. and Av. Shift/Error	0.00, 0.00
Min. and Max. resd. dens. [$e/Å^3$]	-1.00, 2.40

B: Final Coordinates and Equivalent Isotropic Thermal Parameters of the non Hydrogen atoms for (**2.25c**)

Atom	x	y	z	U(eq) [Å^2][a]
Br	- 0.14818(10)	0.18834(14)	0.68303(6)	0.0246(4)
Si	0.0973(3)	0.1575(4)	0.6517(2)	0.0188(8)
O	0.2807(7)	0.1343(11)	0.6495(4)	0.024(2)
N	0.3105(9)	0.1721(10)	0.7781(5)	0.019(2)
C2	0.3643(10)	0.1467(13)	0.7167(6)	0.020(3)
C3	0.5104(10)	0.1345(13)	0.7261(6)	0.022(3)
C4	0.5918(10)	0.1519(14)	0.7995(6)	0.023(3)
C4A	0.5331(11)	0.1814(12)	0.8643(6)	0.024(3)
C5	0.6149(12)	0.2052(14)	0.9396(6)	0.026(3)
C6	0.5574(11)	0.2404(14)	1.0005(6)	0.026(3)
C7	0.4172(11)	0.2512(16)	0.9896(6)	0.026(3)
C8	0.3318(12)	0.2273(15)	0.9167(6)	0.026(3)
C8A	0.3911(11)	0.1923(12)	0.8530(6)	0.020(3)
C9	0.1579(10)	0.1818(13)	0.7606(6)	0.019(3)
C10	0.0641(11)	0.3707(15)	0.5913(6)	0.028(3)
C11	0.0474(10)	- 0.0682(14)	0.6043(6)	0.023(3)

[a] Equivalent isotropic *U* defined as one-third of the trace of the orthogonalised U_{ij} tensor

C: Hydrogen Atom Positions and Isotropic Thermal Parameters for (**2.25c**)

Atom	x	y	z	U(iso) [Å^2]
H3	0.547(5)	0.116(3)	0.685(6)	0.0270
H4	0.684(14)	0.145(2)	0.807(1)	0.0290
H5	0.681(14)	0.199(2)	0.945(1)	0.0310
H6	0.619(8)	0.259(3)	1.055(7)	0.0320
H7	0.391(6)	0.267(4)	1.018(7)	0.0310
H8	0.230(14)	0.235(2)	0.909(1)	0.0310
H9A	0.127(3)	0.303(10)	0.778(2)	0.0220
H9B	0.120(3)	0.080(9)	0.788(2)	0.0220
H10A	0.092(3)	0.466(8)	0.620(2)	0.0420
H10B	- 0.023(7)	0.380(2)	0.572(2)	0.0420
H10C	0.108(4)	0.364(2)	0.555(3)	0.0420
H11A	0.068(2)	- 0.156(7)	0.638(3)	0.0340
H11B	0.091(3)	- 0.085(2)	0.568(3)	0.0340
H11C	- 0.040(7)	- 0.069(1)	0.585(2)	0.0340

D: ORTEP diagram

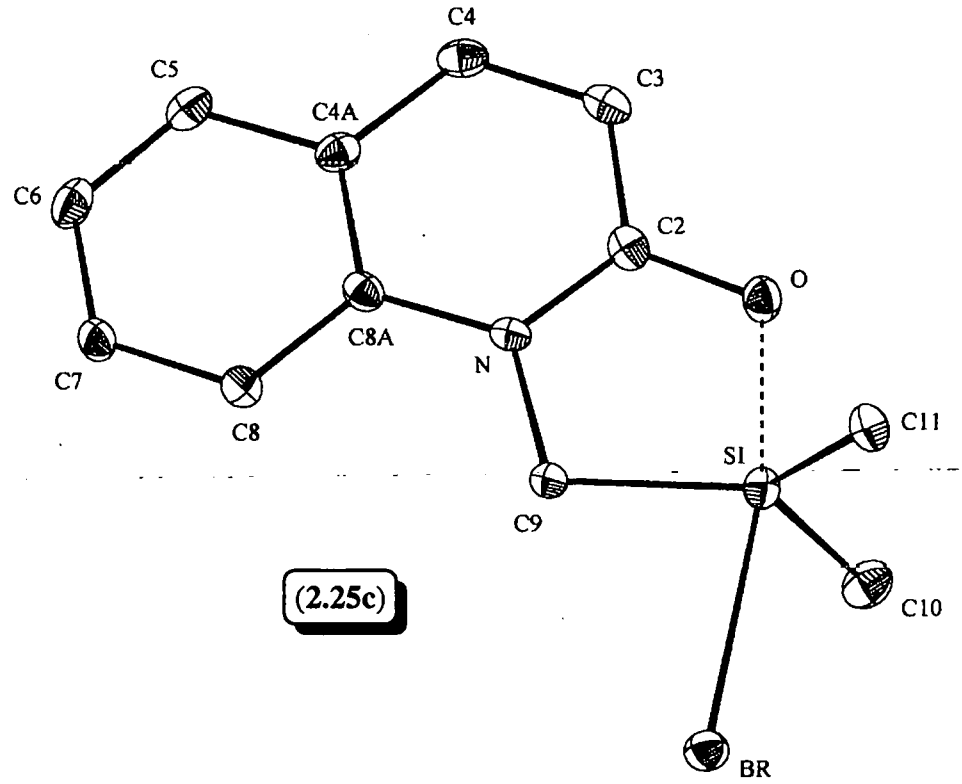

(2.25c)

E:	Selected bond lengths (Å) and angles (°) for (**2.25c**)		
Br-Si	2.648(3)	C2-C3	1.436(15)
Si-O	1.852(8)	C3-C4	1.373(15)
Si-C9	1.893(11)	C4-C4A	1.418(15)
Si-C10	1.859(11)	C4A-C5	1.407(15)
Si-C11	1.847(11)	C4A-C8A	1.391(16)
O-C2	1.292(12)	C5-C6	1.356(15)
N-C2	1.330(14)	C6-C7	1.374(16)
N-C8A	1.393(14)	C7-C8	1.386(15)
N-C9	1.489(14)	C8-C8A	1.411(15)
Br-Si-O	169.4(3)	O-C2-C3	122.1(9)
Br-Si-C9	82.9(3)	N-C2-C3	120.3(9)
Br-Si-C10	89.9(4)	C2-C3-C4	118.3(9)
Br-Si-C11	90.1(3)	C3-C4-C4A	120.9(10)
O-Si-C9	86.6(4)	C4-C4A-C5	121.7(10)
O-Si-C10	96.4(4)	C4-C4A-C8A	119.3(9)
O-Si-C11	94.5(4)	C5-C4A-C8A	119.0(10)
C9-Si-C10	118.9(5)	C4A-C5-C6	121.0(11)
C9-Si-C11	122.3(5)	C5-C6-C7	120.2(10)

C10-Si-C11	118.3(5)	C6-C7-C8	121.1(10)
Si-O-C2	114.3(6)	C7-C8-C8A	118.9(11)
C2-N-C8A	122.5(9)	N-C8A-C4A	118.8(9)
C2-N-C9	115.0(8)	N-C8A-C8	121.4(10)
C8A-N-C9	122.5(9)	C4A-C8A-C8	119.8(10)
O-C2-N	117.6(9)	Si-C9-N	106.5(7)

Part 4. A: Summary

Compound number	**(2.25d)**		
Empirical Formula	$[(C_{12}H_{14}NOSi)^+ (SO_3\text{-}CF_3)^-] + 0.53\ C_6H_6$		
Formula Weight	365.40 + (0.53 x 78.11)		
Crystal System	triclinic		
Space group	P-1 (No. 2)		
a, b, c [Å]	8.527(2)	11.056(2)	11.466(2)
alpha, beta, gamma [°]	68.96(3)	75.41(3)	77.02(3)
V [$Å^3$]	965.5(4)		
Z	1		
D(obs), D(calc) [g/cm^3]	0.000, 1.330		
F(000) [Electrons]	399		
Mu(MoKa) [/cm]	2.7		
Crystal Size [mm]	0.114 x 0.114 x 0.77		

Data Collection

Temperature (K)	123
Radiation [Å]	MoKa 0.71073
Theta Min-Max [°]	2.3, 25.0
Scan,(Type & Range) [°]	phi rotation images on STOE IPDS25
Dataset	-10: 10 ; -13: 13 ; -13: 13
Tot., Uniq. Data, R(int)	7931, 3168, 0.062
Observed data [I > 0.0 sigma(I)]	4

Refinement

Nref, Npar	3168, 221
R, wR, S	0.0767, 0.2314, 1.09
$w = 1/[\s^2(Fo^2)+(0.1851P)^2+0.1842P]$ where $P=(Fo^2+2Fc^2)/3$	
Max. and Av. Shift/Error	0.00, 0.00
Min. and Max. resd. dens. [$e/Å^3$]	-0.51, 1.53

B: Final Coordinates and Equivalent Isotropic Thermal Parameters of the non-Hydrogen atoms for (**2.25d**)

Atom	x	y	z	U(eq) [Å^2][a]
Silyl triflate molecule				
Si	0.78859(12)	- 0.45536(10)	0.81597(9)	0.0219(3)
O1	0.6177(3)	- 0.3336(3)	0.8015(3)	0.0280(8)
N	0.7903(4)	- 0.2161(3)	0.8179(3)	0.0198(8)
C2	0.6393(4)	- 0.2242(4)	0.8107(3)	0.0224(10)
C3	0.5113(5)	- 0.1185(4)	0.8123(4)	0.0297(11)
C4	0.5419(5)	- 0.0085(4)	0.8249(4)	0.0315(11)
C4A	0.6998(5)	0.0006(4)	0.8329(4)	0.0265(11)
C5	0.7386(5)	0.1153(4)	0.8420(4)	0.0366(14)
C6	0.8933(6)	0.1224(4)	0.8440(6)	0.0461(16)
C7	1.0186(6)	0.0139(4)	0.8434(6)	0.0467(16)
C8	0.9857(5)	- 0.0984(4)	0.8349(4)	0.0303(11)
C8A	0.8267(5)	- 0.1050(3)	0.8297(3)	0.0223(10)
C9	0.9103(4)	- 0.3366(3)	0.8228(3)	0.0206(10)
C10	0.8397(5)	- 0.4984(5)	0.6681(4)	0.0351(14)
C11	0.7232(5)	- 0.5847(4)	0.9638(4)	0.0279(11)
C12	0.3416(5)	0.4625(5)	0.6800(4)	0.0363(14)
S	0.24959(10)	0.34219(8)	0.82180(8)	0.0205(3)
F1	0.2460(3)	0.5136(3)	0.5928(2)	0.0549(9)
F2	0.3677(5)	0.5618(3)	0.7076(3)	0.0707(14)
F3	0.4843(3)	0.4075(4)	0.6288(3)	0.0689(12)
O2	0.0948(3)	0.4143(3)	0.8618(2)	0.0278(8)
O3	0.2379(4)	0.2420(3)	0.7749(4)	0.0452(10)
O4	0.3648(3)	0.3079(3)	0.9057(3)	0.0344(9)
Solvent of crystallisation, benzene (disordered)				
C30	0.340(2)	0.077(2)	0.535(2)	0.112(6)
C40	0.363(2)	- 0.049(2)	0.537(2)	0.129(8)
C50	0.509(2)	- 0.113(2)	0.498(2)	0.154(10)

[a] Equivalent isotropic *U* defined as one-third of the trace of the orthogonalised U_{ij} tensor

C: Hydrogen Atom Positions and Isotropic Thermal Parameters for (2.25d)

Atom	x	y	z	U(iso) [Å^2]
Silyl triflate molecule				
H3	0.4050(3)	- 0.1240(2)	0.8047(3)	0.036
H4	0.4558(3)	0.0622(2)	0.8283(4)	0.037
H5	0.6547(5)	0.1872(3)	0.8466(3)	0.044
H6	0.9188(2)	0.2009(3)	0.8460(2)	0.055
H7	1.1262(4)	0.0188(1)	0.8488(2)	0.056
H8	1.0702(3)	- 0.1705(1)	0.8326(2)	0.037
H9A	0.9541(2)	- 0.3699(2)	0.9026(5)	0.025
H9B	1.0027(3)	- 0.3203(4)	0.7496(7)	0.025
H10A	0.8724(6)	- 0.4224(2)	0.5956(2)	0.053
H10B	0.7436(3)	- 0.5241(2)	0.6560(5)	0.053
H10C	0.9302(4)	- 0.5715(5)	0.6740(3)	0.053
H11A	0.6990(6)	- 0.5511(3)	1.0357(2)	0.042
H11B	0.8109(4)	- 0.6598(2)	0.9765(2)	0.042
H11C	0.6246(4)	- 0.6122(4)	0.9581(5)	0.042
Solvent of crystallisation, benzene (disordered)				
H30	0.2386(2)	0.1295(4)	0.5529(6)	0.135
H40	0.2715(3)	- 0.0945(3)	0.5682(5)	0.155
H50	0.5064(4)	- 0.1962(2)	0.4924(1)	0.185

D: Isotropic structure diagram

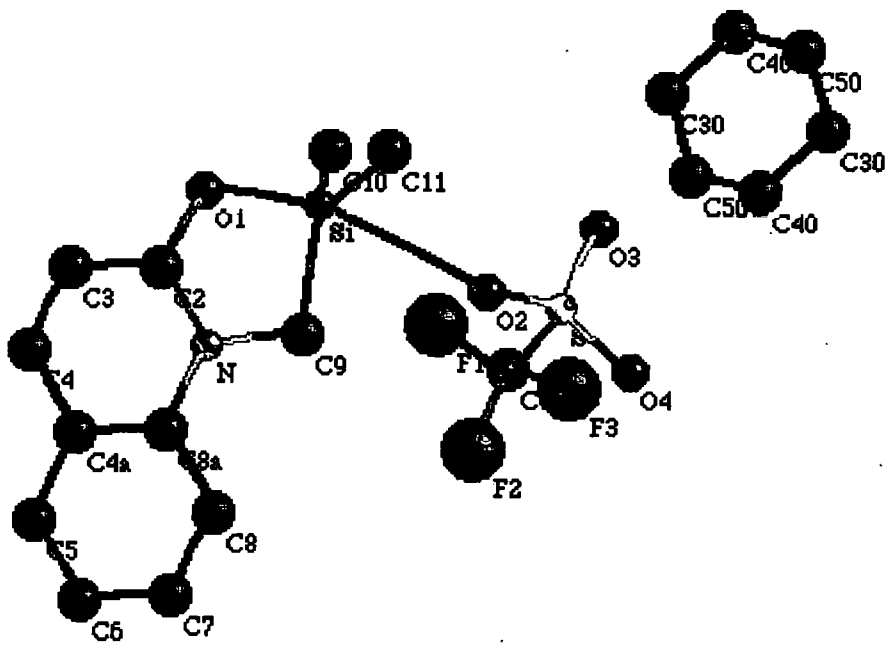

E: Selected bond lengths (Å) and angles (°) for (**2.25d**)

Silyl triflate molecule

Si-O1	1.745(3)	C4A-C8A	1.407(6)
Si-O2	2.762(3)	C5-C6	1.345(7)
Si-C9	1.880(4)	C6-C7	1.417(7)
Si-C10	1.845(5)	C7-C8	1.374(7)
Si-C11	1.836(4)	C8-C8A	1.391(6)
O1-C2	1.307(5)	S-O2	1.440(3)
N-C2	1.335(5)	S-O3	1.425(4)
N-C8A	1.391(5)	S-O4	1.443(3)
N-C9	1.479(5)	S-C12	1.817(5)
C2-C3	1.411(6)	F1-C12	1.335(5)
C3-C4	1.362(6)	F2-C12	1.323(6)
C4-C4A	1.400(6)	F3-C12	1.326(6)
C4A-C5	1.425(6)		

Solvent of crystallisation, benzene (disordered)

C30-C40	1.35(3)	C40-C50	1.34(3)
C30-C50#1	1.36(3)		

Silyl triflate molecule

O2-Si-O1	160.2(2)	C4A-C5-C6	120.4(4)
O2-Si-C9	71.0(2)	C5-C6-C7	120.7(5)
O2-Si-C10	87.3(2)	C6-C7-C8	120.5(5)
O2-Si-C11	81.7(2)	C7-C8-C8A	119.0(4)
O1-Si -C9	89.8(2)	N-C8A-C4A	118.2(4)
O1-Si-C10	106.1(2)	N-C8A-C8	120.4(4)
O1-Si-C11	104.3(2)	C4A-C8A-C8	121.4(4)
C9-Si-C10	116.3(2)	Si-C9-N	103.9(2)
C9-Si-C11	118.2(2)	O2-S-C12	103.0(2)
C10-Si-C11	116.5(2)	O3-S -O4	115.9(2)
Si-O1-C2	114.2(3)	O3-S-C12	102.9(2)
C2-N-C8A	121.6(4)	O4-S-C12	103.3(2)
C2-N-C9	115.2(3)	O2-S-O3	114.7(2)
C8A-N-C9	123.1(3)	O2-S-O4	114.5(2)
O1-C2-N	116.7(4)	S-C12-F1	112.4(3)
O1-C2-C3	122.5(4)	S-C12-F2	111.0(3)
N-C2-C3	120.8(4)	S-C12-F3	109.8(4)
C2-C3-C4	119.3(4)	S-O2-Si	149.3(3)
C3-C4-C4A	120.2(4)	F1-C12-F2	106.5(4)

C4-C4A-C5	122.2(4)	F1-C12-F3	108.8(4)
C4-C4A-C8A	119.8(4)	F2-C12-F3	108.2(4)
C5-C4A-C8A	118.0(4)		

Solvent of crystallisation, benzene (disordered)

C30-C40-C50	123.6(18)	C30#1-C50-C40	130(2)
C40-C30-C50#1	106.2(18)		

Symmetry transformations used to generate equivalent atoms

#1: -x+1, -y, -z+1

Part 5. A: Summary

Compound number	**(2.30a)**		
Empirical Formula	$C_{12}H_{16}NO_2Si.H_2O.Cl.$		
Formula Weight	287.82		
Crystal System	monoclinic		
Space group	$P2_1/c$ (No 14)		
a (x), b (y), c (z) [Å]	9.126(2)	7.223(1)	21.450(4)
alpha, beta, gamma [°]	90	91.54(3)	90
V [Å^3]	1413.4(5)		
Z	4		
D(obs), D(calc) [g/cm^3]	0.000, 1.353		
F(000) [Electrons]	608		
Mu(MoKa) [/cm]	3.5		
Crystal Size [mm]	0.154 x 0.154 x 0.924		

Data Collection

Temperature (K)	100
Radiation [Å]	MoKa 0.71073
Theta Min-Max [°]	2.2, 26.8
Scan,(Type & Range) [°]	phi rotation images on STOE IPDS25
Dataset	-11: 11 ; -8: 8 ; -26: 26
Tot., Uniq. Data, R(int)	9552, 2763, 0.000
Observed data [I > 0.0 sigma(I)]	4

Refinement

Nref, Npar	2763, 219
R, wR, S	0.0763, 0.2336, 1.13

w = 1/[\s2(Fo^2)+(0.1515P)^2+2.2368P] where P=(Fo^2+2Fc^2)/3

Max. and Av. Shift/Error	0.00, 0.00
Min. and Max. resd. dens. [e/Å^3]	-1.31, 1.72

B: Final Coordinates and Equivalent Isotropic Thermal Parameters of the non-Hydrogen atoms for (**2.30a**)

Atom	x	y	z	U(eq) [Å^2][a]
Si	0.86465(9)	0.24353(12)	0.65054(4)	0.0207(3)
O1	0.9117(2)	0.1990(4)	0.5633(1)	0.0179(7)
O2	0.7997(3)	0.2866(3)	0.7334(1)	0.0144(7)
O3	0.6200(3)	0.0650(4)	0.7885(1)	0.0213(8)
N	0.6692(3)	0.2443(3)	0.5544(1)	0.0112(8)
C2	0.8018(4)	0.2078(5)	0.5277(2)	0.0140(9)
C3	0.8162(4)	0.1807(5)	0.4617(2)	0.0202(10)
C4	0.6948(4)	0.1902(5)	0.4265(2)	0.0205(10)
C4A	0.5545(4)	0.2268(4)	0.4547(2)	0.0160(9)
C5	0.4259(5)	0.2356(5)	0.4192(2)	0.0228(11)
C6	0.2926(4)	0.2691(5)	0.4484(2)	0.0252(11)
C7	0.2822(4)	0.2955(6)	0.5134(2)	0.0235(11)
C8	0.4067(4)	0.2879(5)	0.5492(2)	0.0172(10)
C8A	0.5418(4)	0.2545(4)	0.5197(2)	0.0128(9)
C9	0.6696(3)	0.2695(4)	0.6226(2)	0.0124(9)
C10	0.9324(4)	0.0096(5)	0.6724(2)	0.0198(9)
C11	0.9885(4)	0.4495(5)	0.6513(2)	0.0196(10)
Cl	0.67071(9)	0.64335(12)	0.77734(4)	0.0163(3)

[a] Equivalent isotropic U defined as one-third of the trace of the orthogonalised U_{ij} tensor

C: Hydrogen Atom Positions and Isotropic Thermal Parameters for (**2.30a**)

Atom	x	y	z	U(iso) [Å^2]
H3	0.907(5)	0.142(6)	0.446(2)	0.025(11)
H4	0.689(6)	0.165(7)	0.381(3)	0.042(14)
H5	0.429(5)	0.220(7)	0.378(2)	0.030(12)
H6	0.204(6)	0.283(7)	0.423(2)	0.041(14)
H7	0.191(5)	0.305(6)	0.533(2)	0.024(11)
H8	0.399(5)	0.295(6)	0.591(2)	0.022(10)
H91	0.631(5)	0.402(7)	0.639(2)	0.029(12)
H92	0.612(4)	0.183(6)	0.646(2)	0.011(9)
H10A	0.8531(6)	- 0.0775(5)	0.6693(3)	0.034(11)
H10B	0.9710(6)	0.0119(7)	0.7145(2)	0.033(10)
H10C	1.0083(8)	- 0.0267(4)	0.6448(3)	0.030(12)
H111	1.017(6)	0.484(8)	0.612(3)	0.052(16)
H112	1.060(8)	0.395(9)	0.664(3)	0.062(19)

H113	0.978(10)	0.468(14)	0.715(4)	0.13(3)
H21	0.8190(5)	0.1961(9)	0.7552(3)	0.14(4)
H22	0.7090(6)	0.3538(4)	0.7420(2)	0.13(3)
H31	0.627(4)	- 0.056(7)	0.788(2)	0.015(10)
H32	0.518(6)	0.065(7)	0.771(2)	0.042(14)

D1: ORTEP diagram

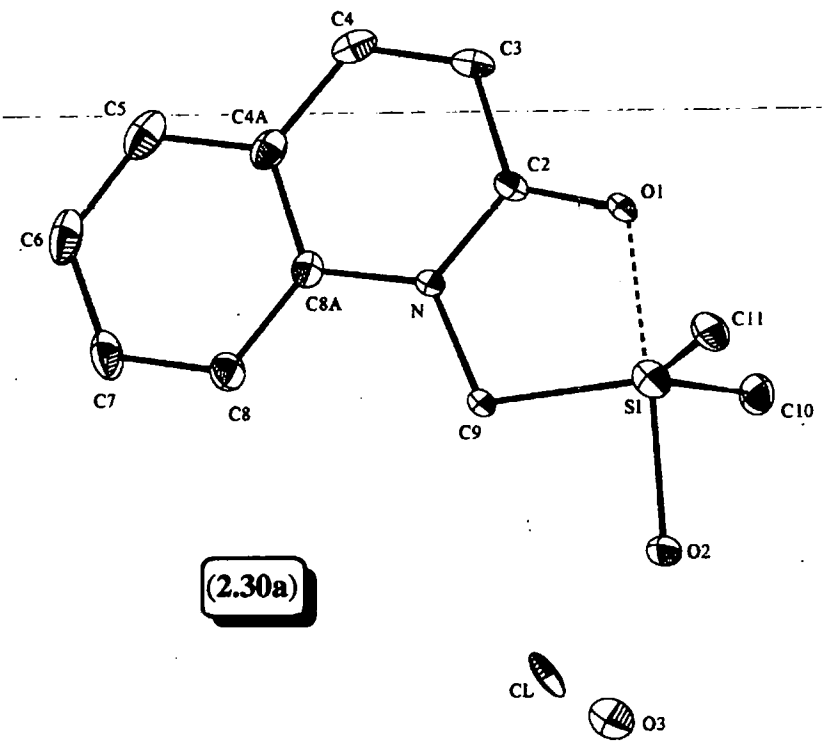

(2.30a)

D2: Structure of the hydrogen-bonded chains

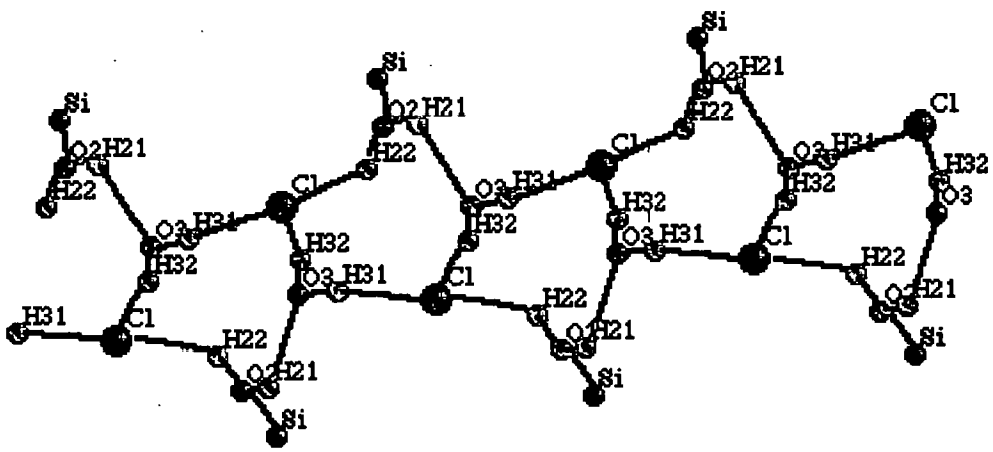

E:	Selected bond lengths (Å) and angles (°) for (**2.30a**)			
Si-O1	1.957(2)	C4-C4A	1.455(5)	
Si-O2	1.915(2)	C4A-C5	1.383(6)	
Si-C9	1.872(3)	C4A-C8A	1.416(5)	
Si-C10	1.855(4)	C5-C6	1.404(6)	
Si-C11	1.868(4)	C6-C7	1.413(6)	
O1-C2	1.247(4)	C7-C8	1.355(5)	
N-C2	1.379(4)	C8-C8A	1.421(5)	
N-C8A	1.366(4)	O2-H21	0.82(6)	
N-C9	1.474(4)	O2-H22	0.98(5)	
C2-C3	1.438(5)	O3-H32	0.99(5)	
C3-C4	1.326(5)	O3-H31	0.88(5)	
O1-Si-O2	174.6(1)	C2-C3-C4	117.2(3)	
O1-Si-C9	86.7(1)	C3-C4-C4A	120.2(3)	
O1-Si-C10	90.7(1)	C4-C4A-C5	121.4(3)	
O1-Si-C11	89.5(1)	C4-C4A-C8A	122.1(3)	
O2-Si-C9	88.0(1)	C5-C4A-C8A	116.4(3)	
O2-Si-C10	91.3(1)	C4A-C5-C6	119.7(4)	
O2-Si-C11	93.7(1)	C5-C6-C7	123.0(4)	
C9-Si-C10	118.7(2)	C6-C7-C8	118.4(3)	
C9-Si-C11	119.5(2)	C7-C8-C8A	118.7(3)	
C10-Si-C11	121.7(2)	N-C8A-C4A	116.0(3)	
Si-O1-C2	112.6(2)	N-C8A-C8	120.2(3)	
C2-N-C8A	121.8(3)	C4A-C8A-C8	123.8(3)	
C2-N-C9	117.3(3)	Si-C9-N	106.4(2)	
C8A-N-C9	120.9(3)	Si-O2-H21	109.4(3)	
O1-C2-N	117.1(3)	Si-O2-H22	122.5(4)	
O1-C2-C3	120.2(3)	H21-O2-H22	117(3)	
N-C2-C3	122.7(3)	H31-O3-H32	93(4)	

F:	Hydrogen bond lengths (Å) and angles (°) for (**2.30a**)			
O2-H21···O3	0.82(6)	2.18(4)	2.598(4)	111(4)
O2-H22···Cl	0.98(5)	2.26(6)	2.995(3)	131(3)
O3-H31···Cl	0.88(5)	2.22(5)	3.091(3)	172(3)
O3-H32···Cl	0.99(5)	2.07(5)	3.025(3)	162(4)

Part 6. A: Summary

Compound number	**(4.39a)**	
Empirical formula	$C_{24}H_{20}O_3Sn$	
Formula Weight	475.09	
Instrument	STOE STADI4	
Temperature (K)	293 (2)	
Wavelength (Å)	0.71073	
Crystal system	Orthorhombic, mmm	
Space group	Pbca (no 61)	
Unit cell dimensions	a = 11.519 (1) Å	$\alpha = 90°$
	b = 14.684 (1) Å	$\beta = 90°$
	c = 24.230 (3) Å	$\gamma = 90°$
Unit cell volume ($Å^3$)	4098.4 (7) $Å^3$	
Number of units (Z)	8	
Density (calculated) ($Mg\ m^{-3}$)	1.540	
Absorption coefficient (mm^{-1})	1.268	
F (000)	1904	
Crystal size (mm)	1.90 x 1.12 x 0.34	
Theta range for data collection (°)	1.68 to 25.96	
Index ranges	-2 <=h<= 14, 0 <=k<= 18, 0 <=l<= 29	
Reflections collected	4651	
Independent reflections	3993 [$R_{(int)}$ = 0.0187]	
Absorption correction	Psi-scan	
Max. and min transmission	0.4211 and 0.2164	
Refinement method on F^2	Full-matrix least-squares	
Data / restraints / parameters	3393 / 0 / 272	
G.O.F. on F^2	1.079	
Final R indices [I>2sigma(I)]	R1 = 0.0272, wR2 = 0.0693	
R indices (all data)	R1 = 0.0322, wR2 = 0.0724	
Extinction coefficient	0.0026 (2)	
Largest diff. peak and hole	0.697 and - 0.507 $e.Å^{-3}$	

B: Atomic coordinates and equivalent isotropic displacement parameters ($Å^2 \times 10^3$) for (**4.39a**)

Atom	x	y	z	U_{eq} [a]
C1	0.2380 (2)	0.0804 (2)	0.1540 (1)	44 (1)
C10	0.1333 (4)	0.3612 (2)	- 0.0128 (1)	79 (1)
C11	0.0229 (4)	0.3343 (2)	0.0023 (1)	74 (1)
C12	0.0076 (3)	0.2785 (2)	0.0473 (1)	55 (1)
C13	- 0.0472 (2)	0.0470 (2)	0.1166 (1)	47 (1)
C14	- 0.1616 (3)	0.0421 (3)	0.1326 (1)	71 (1)
C15	- 0.2338 (3)	- 0.0255 (3)	0.1125 (2)	87 (1)
C16	- 0.1944 (4)	- 0.0884 (3)	0.0763 (2)	88 (1)
C17	- 0.0835 (4)	- 0.0851 (3)	0.0604 (2)	109 (2)
C18	- 0.0104 (3)	- 0.0182 (3)	0.0805 (2)	89 (1)
C19	- 0.0058 (2)	0.2308 (2)	0.2480 (1)	45 (1)
C2	0.2979 (2)	0.0444 (2)	0.1089 (1)	55 (1)
C20	- 0.0958 (2)	0.2663 (2)	0.2128 (1)	48 (1)
C21	- 0.1803 (3)	0.3217 (2)	0.2393 (1)	60 (1)
C22	0.1741 (3)	0.3350 (2)	0.2935 (1)	69 (1)
C23	- 0.0075 (2)	0.2474 (2)	0.3028 (1)	53 (1)
C24	0.0746 (3)	0.2100 (3)	0.3441 (1)	74 (1)
C3	0.3976 (2)	- 0.0063 (2)	0.1160 (2)	65 (1)
C4	0.4409 (2)	- 0.0221 (2)	0.1679 (2)	67 (1)
C5	0.3846 (2)	0.0134 (2)	0.2133 (2)	63 (1)
C6	0.2838 (2)	0.0639 (2)	0.2060 (1)	52 (1)
C7	0.1021 (2)	0.2468 (2)	0.0778 (1)	45 (1)
C8	0.2124 (3)	0.2740 (2)	0.0615 (1)	57 (1)
C9	0.2279 (3)	0.3318 (2)	0.0169 (1)	72 (1)
O1	0.0760 (2)	0.1797 (2)	0.2251 (1)	55 (1)
O2	- 0.0938 (2)	0.2457 (2)	0.1626 (1)	60 (1)
O3	- 0.0921(2)	0.2997 (2)	0.3257 (1)	66 (1)
Sn	0.0735 (1)	0.1499 (1)	0.1423 (1)	41 (1)

[a] Equivalent isotropic U defined as one-third of the trace of the orthogonalised U_{ij} tensor.

C: Hydrogen coordinates and equivalent isotropic displacement parameters ($Å^2 \times 10^3$) for **(4.39a)**

Atom	x	y	z	U_{eq}
H2	0.2693 (10)	0.0550 (4)	0.0724 (12)	66
H3	0.4339 (15)	- 0.0286 (10)	0.0871 (13)	78
H4	0.5096 (27)	- 0.0576 (14)	0.1723 (3)	80
H5	0.4167 (12)	0.0028 (4)	0.2517 (14)	76
H6	0.2445 (13)	0.0883 (8)	0.2380 (10)	63
H8	0.2729 (24)	0.2544 (8)	0.0797 (7)	68
H9	0.3050 (32)	0.3153 (8)	0.0067 (4)	86
H10	0.1441 (6)	0.4006 (17)	- 0.0441 (13)	95
H11	- 0.0414 (30)	0.3540 (9)	- 0.0180 (9)	88
H12	- 0.0629 (25)	0.2625 (6)	0.0571 (4)	66
H14	- 0.1892 (12)	0.0824 (17)	0.1559 (10)	85
H15	- 0.3092 (36)	- 0.0277 (3)	0.1239 (6)	105
H16	- 0.2454 (25)	- 0.1347 (23)	0.0622 (7)	106
H17	- 0.0586 (17)	- 0.1229 (26)	0.0387 (15)	131
H18	0.0625 (33)	- 0.0176 (3)	0.0696 (5)	107
H21	- 0.2388 (2)	0.3483 (11)	0.2190 (8)	72
H22	- 0.2301 (23)	0.3708 (15)	0.3097 (7)	83
H24A	0.0574 (5)	0.2291 (5)	0.3750 (8)	111
H24B	0.1411 (18)	0.2263 (5)	0.3364 (2)	111
H24C	0.0711 (3)	0.1541 (15)	0.3439 (1)	111

D: ORTEP diagram

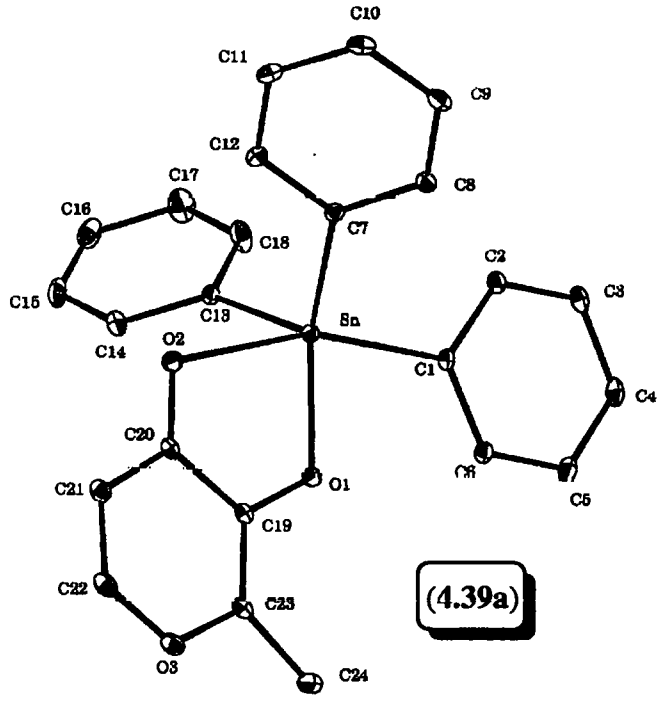

E: Selected bond lengths (Å) and angles (°) for (**4.39a**)

Sn-O(1)	2.054 (2)	C(11)-C(12)	1.377 (4)
Sn-C(7)	2.139 (3)	C(13)-C(18)	1.363 (4)
Sn-C(13)	2.146 (3)	C(13)-C(14)	1.376 (4)
Sn-C(1)	2.171 (2)	C(14)-C(15)	1.383 (5)
Sn-O(2)	2.436 (2)	C(15)-C(16)	1.353 (6)
C(1)-C(6)	1.387 (4)	C(16)-C(17)	1.336 (5)
C(1)-C(2)	1.395 (4)	C(17)-C(18)	1.382 (5)
C(2)-C(3)	1.380 (4)	O(1)-C(19)	1.327 (3)
C(3)-C(4)	1.372 (5)	O(2)-C(20)	1.253 (3)
C(4)-C(5)	1.378 (5)	O(3)-C(22)	1.330 (4)
C(5)-C(6)	1.390 (4)	O(3)-C(23)	1.359 (3)
C(7)-C(8)	1.389 (4)	C(19)-C(23)	1.350 (4)
C(7)-C(12)	1.395 (4)	C(19)-C(20)	1.440 (4)
C(8)-C(9)	1.385 (4)	C(20)-C(21)	1.422 (4)
C(9)-C(10)	1.376 (5)	C(21)-C(22)	1.329 (4)
C(10)-C(11)	1.382 (6)	C(23)-C(24)	1.483 (4)
O(1)-Sn-C(7)	124.73 (9)	C(12)-C(11)-C(10)	119.9 (3)
O(1)-Sn-C(13)	116.26 (9)	C(11)-C(12)-C(7)	121.2 (3)
C(7)-Sn-C(13)	110.88 (9)	C(18)-C(13)-C(14)	116.2 (3)
O(1)-Sn-C(1)	87.75 (8)	C(18)-C(13)-Sn	118.6 (2)

C(7)-Sn-C(1)	105.9 (1)	C(14)-C(13)-Sn	125.2 (2)
C(13)-Sn-C(1)	105.79 (9)	C(13)-C(14)-C(15)	121.0 (3)
O(1)-Sn-O(2)	71.97 (7)	C(16)-C(15)-C(14)	121.1 (3)
C(7)-Sn-O(2)	83.41 (8)	C(17)-C(16)-C(15)	118.8 (4)
C(13)-Sn-O(2)	87.29 (9)	C(16)-C(17)-C(18)	120.5 (4)
C(1)-Sn-O(2)	159.33 (8)	C(13)-C(18)-C(17)	122.4 (3)
C(6)-C(1)-C(2)	117.2 (2)	C(19)-O(1)-Sn	121.3 (2)
C(6)-C(1)-Sn	122.1 (2)	C(20)-O(2)-Sn	110.5 (2)
C(2)-C(1)-Sn	120.5 (2)	C(22)-O(3)-C(23)	119.4 (2)
C(3)-C(2)-C(1)	121.2 (3)	O(1)-C(19)-C(23)	121.6 (2)
C(4)-C(3)-C(2)	120.6 (3)	O(1)-C(19)-C(20)	117.9 (2)
C(3)-C(4)-C(5)	119.7 (3)	C(23)-C(19)-C(20)	120.5 (2)
C(4)-C(5)-C(6)	119.6 (3)	O(2)-C(20)-C(21)	126.1 (3)
C(1)-C(6)-C(5)	121.7 (3)	O(2)-C(20)-C(19)	118.3 (2)
C(8)-C(7)-C(12)	117.9 (3)	C(21)-C(20)-C(19)	115.6 (2)
C(8)-C(7)-Sn	122.6 (2)	C(22)-C(21)-C(20)	119.5 (3)
C(12)-C(7)-Sn	119.2 (2)	O(3)-C(22)-C(21)	124.1 (3)
C(9)-C(8)-C(7)	121.0 (3)	C(19)-C(23)-O(3)	120.8 (3)
C(10)-C(9)-C(8)	119.9 (3)	C(19)-C(23)-C(24)	126.0 (3)
C(9)-C(10)-C(11)	120.0 (3)	O(3)-C(23)-C(24)	113.1 (2)

Part 7. A: Summary

Compound number	**(4.39b)**	
Empirical formula	$C_{18}H_{15}ClO_3Sn$	
Formula Weight	433.47	
Instrument	STOE STADI4	
Temperature (K)	200 (2)	
Wavelength (Å)	0.71073	
Crystal system	Orthorhombic, 222	
Space group	$P2_12_12_1$ (no 19)	
Unit cell dimensions	a = 9.175 (2) Å	$\alpha = 90°$
	b = 11.165 (1) Å	$\beta = 90°$
	c = 16.586 (2) Å	$\gamma = 90°$
Unit cell volume ($Å^3$)	1699.1 (4)	
Number of units (Z)	4	
Density (calculated) ($Mg\ m^{-3}$)	1.695	
Absorption coefficient (mm^{-1})	1.533	
F (000)	856	
Crystal size (mm)	0.076 x 0.190 x 0.190	
Theta range for data collection (°)	2.46 to 28.12	
Index ranges	-12 <=h<= 12, -14 <=k<= 14, -21 <=l<= 21	
Reflections collected	14477	
Independent reflections	4066 [$R_{(int)}$ = 0.0338]	
Absorption correction	None	
Max. and min transmission	Neither recorded	
Refinement method on F^2	Full-matrix least-squares	
Data / restraints / parameters	4066 / 0 / 208	
G.O.F. on F^2	1.073	
Final R indices [I>2sigma(I)]	R1 = 0.0213, wR2 = 0.0472	
R indices (all data)	R1 = 0.0235, wR2 = 0.0477	
Absolute structure parameter	- 0.04 (2)	
Extinction coefficient	Dropped to zero on calculation	
Largest diff. peak and hole	0.901 and - 0.304 $e.Å^{-3}$	

B: Atomic coordinates and equivalent isotropic displacement parameters ($Å^2$ x 10^3) for (**4.39b**)

Atom	x	y	z	U_{eq} [a]
C10	0.2347 (3)	0.5883 (3)	0.1999 (2)	35 (1)
C11	0.1492 (3)	0.5481 (2)	0.1368 (2)	35 (1)
C12	0.2094 (3)	0.4810 (2)	0.0758 (2)	32 (1)
C13	0.3576 (3)	0.4518 (2)	0.0778 (1)	26 (1)
C14	0.7912 (2)	0.5336 (2)	0.0289 (2)	20 (1)
C15	0.7973 (3)	0.6577 (2)	0.0166 (2)	29 (1)
C16	0.8735 (3)	0.7038 (3)	- 0.0487 (2)	39 (1)
C17	0.9434 (3)	0.6285 (3)	- 0.1022 (2)	38 (1)
C18	0.9372 (3)	0.5053 (3)	- 0.0904 (1)	34 (1)
C19	0.8606 (2)	0.4590 (2)	- 0.0252 (1)	27 (1)
C2	0.9250 (3)	0.6962 (2)	0.3704 (2)	37 (1)
C3	0.8336 (3)	0.7211 (2)	0.3090 (1)	30 (1)
C4	0.7915 (2)	0.6263 (2)	0.2571 (1)	22 (1)
C5	0.8459 (2)	0.5088 (2)	0.2735 (1)	21 (1)
C6	0.9385 (3)	0.4922 (2)	0.3369 (1)	26 (1)
C7	0.0048 (3)	0.3786 (2)	0.3621 (2)	38 (1)
C8	0.4463 (2)	0.4937 (2)	0.1404 (1)	21 (1)
C9	0.3832 (3)	0.5626 (2)	0.2012 (1)	27 (1)
Cl	0.6743 (1)	0.2559 (1)	0.0946 (1)	34 (1)
O1	0.9772 (2)	0.5867 (2)	0.3846 (1)	35 (1)
O2	0.7064 (2)	0.6402 (1)	0.1964 (1)	26 (1)
O3	0.8046 (2)	0.4195 (1)	0.2257 (1)	25 (1)
Sn	0.6747 (1)	0.4668 (1)	0.1305 (1)	19 (1)

[a] Equivalent isotropic U defined as one-third of the trace of the orthogonalised U_{ij} tensor.

C: Hydrogen coordinates and equivalent isotropic displacement parameters ($Å^2 \times 10^3$) for (**4.39b**)

Atom	x	y	z	U_{eq}
H2	0.9535 (3)	0.7596 (2)	0.4052 (2)	44
H3	0.7984 (3)	0.8002 (2)	0.3006 (1)	36
H7A	1.0666 (3)	0.3922 (2)	0.4094 (2)	45
H7B	1.0640 (3)	0.3465 (2)	0.3179 (2)	45
H7C	0.9279 (3)	0.3212 (2)	0.3757 (2)	45
H9	0.4421 (3)	0.5922 (2)	0.2439 (1)	33
H10	0.1922 (3)	0.6335 (3)	0.2423 (2)	42
H11	0.0483 (3)	0.5670 (2)	0.1355 (2)	41
H12	0.1503 (3)	0.4545 (2)	0.0323 (2)	38
H13	0.3982 (3)	0.4032 (2)	0.0365 (1)	31
H15	0.7492 (3)	0.7103 (2)	0.0529 (2)	35
H16	0.8776 (3)	0.7879 (3)	- 0.0567 (2)	46
H17	0.9954 (3)	0.6606 (3)	- 0.1467 (2)	46
H18	0.9852 (3)	0.4529 (3)	- 0.1269 (1)	41
H19	0.8560 (2)	0.3747 (2)	- 0.0178 (1)	32

D: ORTEP diagram

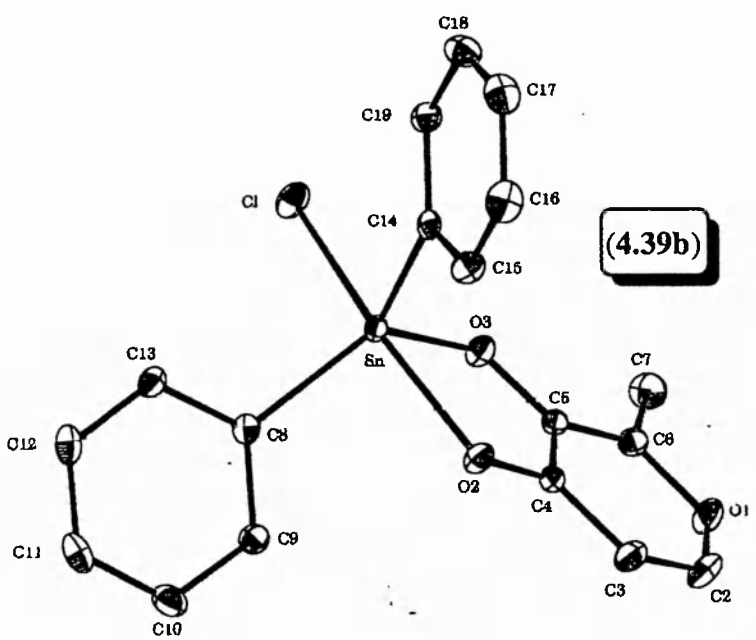

E: Selected bond lengths (Å) and angles (°) for (**4.39b**)

Sn-O(3)	2.047 (2)	C(6)-C(7)	1.466 (3)
Sn-C(8)	2.124 (2)	C(8)-C(9)	1.394 (3)
Sn-C(14)	2.130 (2)	C(8)-C(13)	1.400 (3)
Sn-O(2)	2.243 (2)	C(9)-C(10)	1.393 (4)
Sn-Cl	2.4280 (6)	C(10)-C(11)	1.383 (4)
O(1)-C(2)	1.333 (3)	C(11)-C(12)	1.375 (4)
O(1)-C(6)	1.366 (3)	C(12)-C(13)	1.399 (4)
C(2)-C(3)	1.349 (4)	C(14)-C(19)	1.381 (3)
O(2)-C(4)	1.283 (3)	C(14)-C(15)	1.401 (3)
C(3)-C(4)	1.417 (3)	C(15)-C(16)	1.388 (4)
O(3)-C(5)	1.329 (3)	C(16)-C(17)	1.379 (4)
C(4)-C(5)	1.429 (3)	C(17)-C(18)	1.390 (4)
C(5)-C(6)	1.366 (3)	C(18)-C(19)	1.390 (3)
O(3)-Sn-C(8)	123.46 (7)	C(6)-C(5)-C(4)	119.2 (2)
O(3)-Sn-C(14)	114.09 (8)	O(1)-C(6)-C(5)	120.2 (2)
C(8)-Sn-C(14)	120.44 (8)	O(1)-C(6)-C(7)	113.3 (2)
O(3)-Sn-O(2)	76.76 (6)	C(5)-C(6)-C(7)	126.5 (2)
C(8)-Sn-O(2)	88.15 (7)	C(9)-C(8)-C(13)	118.7 (2)
C(14)-Sn-O(2)	91.04 (8)	C(9)-C(8)-Sn	122.9 (2)
O(3)-Sn-Cl	86.57 (5)	C(13)-C(8)-Sn	118.0 (2)
C(8)-Sn-Cl	98.90 (6)	C(10)-C(9)-C(8)	120.6 (2)
C(14)-Sn-Cl	98.43 (7)	C(11)-C(10)-C(9)	120.0 (2)
O(2)-Sn-Cl	163.09 (4)	C(12)-C(11)-C(10)	120.4 (2)
C(2)-O(1)-C(6)	120.9 (2)	C(11)-C(12)-C(13)	120.0 (2)
O(1)-C(2)-C(3)	123.1 (2)	C(12)-C(13)-C(8)	120.3 (2)
C(4)-O(2)-Sn	110.9 (1)	C(19)-C(14)-C(15)	118.9 (2)
C(2)-C(3)-C(4)	118.3 (2)	C(19)-C(14)-Sn	122.3 (2)
C(5)-O(3)-Sn	115.6 (1)	C(15)-C(14)-Sn	118.8 (2)
O(2)-C(4)-C(3)	123.5 (2)	C(16)-C(15)-C(14)	120.0 (2)
O(2)-C(4)-C(5)	118.2 (2)	C(17)-C(16)-C(15)	120.6 (3)
C(3)-C(4)-C(5)	118.4 (2)	C(16)-C(17)-C(18)	119.6 (3)
O(3)-C(5)-C(6)	122.3 (2)	C(19)-C(18)-C(17)	119.9 (3)
O(3)-C(5)-C(4)	118.4 (2)	C(14)-C(19)-C(18)	120.9 (2)

Part 8. A: Summary

Compound number	**(4.39c)**	
Empirical formula	$C_{18}H_{15}BrO_3Sn$	
Formula Weight	477.90	
Instrument	STOE STADI4	
Temperature (K)	200 (2)	
Wavelength (Å)	0.71069	
Crystal system	'Orthorhombic, 222'	
Space group	'$P2_12_12_1$ (no 19)'	
Unit cell dimensions	a = 9.1250 (7) Å	$\alpha = 90°$
	b = 11.3350 (10) Å	$\beta = 90°$
	c = 16.6230 (10) Å	$\gamma = 90°$
Unit cell volume ($Å^3$)	1719.3 (2)	
Number of units (Z)	4	
Density (calculated) ($Mg\ m^{-3}$)	1.846	
Absorption coefficient (mm^{-1})	3.821	
F (000)	928	
Crystal size (mm)	0.38 x 0.38 x 0.38	
Theta range for data collection (°)	2.17 to 25.22	
Index ranges	-1 <=h<= 10, 0 <=k<= 13, 0 <=l<= 19	
Reflections collected	2191	
Independent reflections	1968 [$R_{(int)} = 0.0083$]	
Refinement method on F^2	Full-matrix least-squares	
Data / restraints / parameters	1968 / 0 / 222	
G.O.F. on F^2	1.057	
Final R indices [I>2sigma(I)]	R1 = 0.0256, wR2 = 0.0641	
R indices (all data)	R1 = 0.0296, wR2 = 0.0662	
Absolute structure parameter	0.02 (2)	
Extinction coefficient	0.0013 (3)	
Largest diff. peak and hole	0.455 and - 0.839 $e.Å^{-3}$	

B: Atomic coordinates and equivalent isotropic displacement parameters ($Å^2$ x 10^3) for (**4.39c**)

Atom	x	y	z	U_{eq} [a]
Br	0.1719 (1)	0.7543 (1)	0.0935 (1)	53 (1)
C1	0.3428 (6)	0.0137 (5)	0.2726 (3)	37 (1)
C11	- 0.0558 (6)	0.0002 (5)	0.1409 (3)	37 (1)
C12	- 0.1430 (7)	0.9573 (6)	0.0800 (4)	43 (1)
C13	- 0.2905 (6)	0.9846 (6)	0.0797 (4)	52 (2)
C14	- 0.3512 (7)	0.0501 (6)	0.1394 (4)	57 (2)
C15	- 0.2640 (7)	0.0896 (7)	0.2003 (4)	57 (2)
C16	- 0.1176 (7)	0.0655 (6)	0.2006 (4)	46 (2)
C2	0.4351 (7)	0.9961 (6)	0.3362 (3)	45 (1)
C21	0.5005 (9)	0.8837 (6)	0.3597 (4)	71 (2)
C31	0.2902 (6)	0.0403 (4)	0.0298 (3)	36 (1)
C32	0.3598 (6)	0.9696 (5)	- 0.0252 (3)	43 (1)
C33	0.2979 (8)	0.1607 (5)	0.0190 (4)	50 (2)
C34	0.4405 (9)	0.1344 (7)	- 0.0991 (4)	59 (2)
C35	0.3723 (9)	0.2065 (6)	- 0.0459 (4)	62 (2)
C36	0.4356 (7)	0.0154 (7)	- 0.0890 (4)	53 (2)
C4	0.4203 (8)	0.1952 (7)	0.3695 (4)	59 (2)
C5	0.3292 (8)	0.2192 (5)	0.3089 (3)	49 (2)
C6	0.2886 (6)	0.1274 (5)	0.2569 (3)	37 (1)
O1	0.3022 (4)	0.9264 (3)	0.2251 (2)	40 (1)
O3	0.4732 (5)	0.0881 (5)	0.3837 (2)	57 (1)
O6	0.2053 (5)	0.1408 (3)	0.1978 (2)	45 (1)
Sn	0.1741 (1)	0.9731 (1)	0.1304 (1)	33 (1)

[a] Equivalent isotropic U defined as one-third of the trace of the orthogonalised U_{ij} tensor.

C: Hydrogen coordinates and equivalent isotropic displacement parameters ($Å^2 \times 10^3$) for (**4.39c**)

Atom	x	y	z	U_{eq}
H21A	0.5517 (27)	0.8933 (8)	0.3993 (19)	106
H21B	0.5504 (26)	0.8584 (14)	0.3229 (19)	106
H21C	0.4358 (32)	0.8365 (24)	0.3701 (6)	106
H4	0.4513 (22)	1.2632 (44)	0.4072 (24)	70
H5	0.2938 (25)	1.2942 (50)	0.3015 (6)	59
H12	- 0.1052 (29)	0.9130 (33)	0.0417 (28)	52
H13	- 0.3438 (44)	0.9602 (21)	0.0417 (32)	62
H14	- 0.4361 (88)	1.0653 (17)	0.1389 (4)	69
H15	- 0.2986 (30)	1.1267 (32)	0.2358 (30)	68
H16	- 0.0676 (38)	1.0901 (19)	0.2361 (27)	55
H32	0.3552 (7)	0.8858 (57)	- 0.0187 (5)	51
H33	0.2498 (35)	1.2143 (37)	0.0580 (27)	61
H34	0.4900 (40)	1.1658 (26)	- 0.1419 (34)	71
H35	0.3757 (9)	1.2867 (65)	- 0.0533 (7)	75
H36	0.4821 (34)	0.9668 (36)	- 0.1243 (25)	64

D: ORTEP diagram

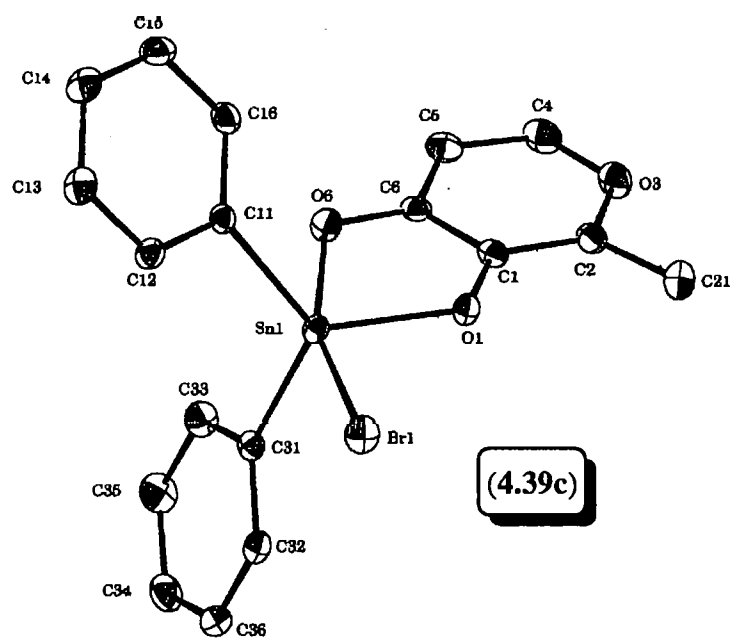

E: Selected bond lengths (Å) and angles (°) for **(4.39c)**

Sn-O(1)	2.032 (3)	C(6)-O(6)	1.252 (6)
Sn-C(31)	2.121 (5)	C(11)-C16)	1.360 (8)
Sn-C(11)	2.127 (6)	C(11)-C(12)	1.376 (8)
Sn-O(6)	2.224 (3)	C(12)-C(13)	1.381 (9)
Sn-Br	2.5549 (7)	C(13)-C(14)	1.358 (10)
O(1)-C(1)	1.319 (6)	C(14)-C(15)	1.363 (9)
C(1)-C(2)	1.366 (8)	C(15)-C(16)	1.364 (9)
C(1)-C(6)	1.405 (8)	C(31)-C(32)	1.372 (8)
C(2)-O(3)	1.353 (8)	C(31)-C(33)	1.378 (8)
C(2)-C(21)	1.461 (9)	C(32)-C(36)	1.370 (8)
O(3)-C(4)	1.327 (9)	C(33)-C(35)	1.378 (9)
C(4)-C(5)	1.334 (10)	C(34)-C(35)	1.356 (9)
C(5)-C(6)	1.403 (8)	C(34)-C(36)	1.359 (10)
O(1)-Sn-C(31)	114.7 (2)	O(6)-C(6)-C(5)	123.6 (6)
O(1)-Sn-C(11)	122.7 (2)	O(6)-C(6)-C(1)	118.2 (5)
C(31)-Sn-C(11)	120.4 (2)	C(5)-C(6)-C(1)	118.2 (5)
O(1)-Sn-O(6)	76.0 (1)	C(6)-O(6)-Sn	111.7 (4)
C(31)-Sn-O(6)	91.5 (2)	C(16)-C(11)-C(12)	119.3 (6)
C(11)-Sn-O(6)	87.8 (2)	C(16)-C(11)-Sn	123.2 (4)
O(1)-Sn-Br	86.4 (1)	C(12)-C(11)-Sn	117.3 (4)
C(31)-Sn-Br	99.4 (1)	C(11)-C(12)-C(13)	119.2 (6)
C(11)-Sn-Br	98.7 (2)	C(14)-C(13)-C(12)	121.1 (6)
O(6)-Sn-Br	162.0 (1)	C(13)-C(14)-C(15)	119.0 (6)
C(1)-O(1)-Sn	115.5 (3)	C(14)-C(15)-C(16)	120.6 (7)
O(1)-C(1)-C(2)	121.8 (5)	C(11)-C(16)-C(15)	120.9 (6)
O(1)-C(1)-C(6)	118.5 (5)	C(32)-C(31)-C(33)	118.0 (5)
C(2)-C(1)-C(6)	119.7 (5)	C(32)-C(31)-Sn	123.1 (4)
O(3)-C(2)-C(1)	119.8 (6)	C(33)-C(31)-Sn	118.9 (4)
O(3)-C(2)-C(21)	114.3 (5)	C(36)-C(32)-C(31)	121.9 (6)
C(1)-C(2)-C(21)	125.9 (6)	C(31)-C(33)-C(35)	120.0 (6)
C(4)-O(3)-C(2)	120.5 (5)	C(35)-C(34)-C(36)	120.2 (7)
O(3)-C(4)-C(5)	123.2 (6)	C(34)-C(35)-C(33)	120.6 (6)
C(4)-C(5)-C(6)	118.6 (6)	C(34)-C(36)-C(32)	119.3 (7)

Part 9. A: Summary

Compound number	**(4.39d)**	
Empirical formula	$C_{18}H_{15}IO_3Sn$	
Formula Weight	524.92	
Instrument	STOE STADI4	
Temperature (K)	160 (2)	
Wavelength (Å)	0.71073	
Crystal system	'Orthorhombic, 222'	
Space group	'$P2_12_12_1$ (no 19)'	
Unit cell dimensions	a = 9.0987 (8) Å	$\alpha = 90°$
	b = 11.6239 (6) Å	$\beta = 90°$
	c = 16.8720 (10) Å	$\gamma = 90°$
Unit cell volume ($Å^3$)	1784.4 (2)	
Number of units (Z)	4	
Density (calculated) ($Mg\ m^{-3}$)	1.954	
Absorption coefficient (mm^{-1})	2.942	
F (000)	1000	
Crystal size (mm)	1.200 x 0.700 x 0.500	
Theta range for data collection (°)	2.13 to 32.50	
Index ranges	-7 <=h<= 13, -17 <=k<= 17, -25 <=l<= 25	
Reflections collected	6164	
Independent reflections	5560 [$R_{(int)}$ = 0.0197]	
Absorption correction	Semi-empirical from psi-scans	
Max. and min transmission	0.9876 and 0.5533	
Refinement method on F^2	Full-matrix least-squares	
Data / restraints / parameters	5560 / 0 / 209	
G.O.F. on F^2	1.065	
Final R indices [I>2sigma(I)]	R1 = 0.0310, wR2 = 0.0859	
R indices (all data)	R1 = 0.0335, wR2 = 0.0874	
Absolute structure parameter	0.04 (3)	
Extinction coefficient	0.0023 (3)	
Largest diff. peak and hole	2.034 and - 0.854 $e.Å^{-3}$	

B: Atomic coordinates and equivalent isotropic displacement parameters ($Å^2 \times 10^3$) for **(4.39d)**

Atom	x	y	z	U_{eq} [a]
C1	0.3378 (5)	0.0197 (3)	0.2718 (2)	21 (1)
C11	- 0.0668 (4)	0.0057 (3)	0.1410 (2)	20 (1)
C12	- 0.1560 (5)	0.9624 (3)	0.0809 (2)	22 (1)
C13	- 0.3061 (4)	0.9891 (4)	0.0800 (2)	25 (1)
C14	- 0.3661 (5)	0.0565 (4)	0.1408 (2)	27 (1)
C15	- 0.2771 (5)	0.0970 (4)	0.2016 (3)	28 (1)
C16	- 0.1275 (5)	0.0726 (4)	0.2008 (2)	24 (1)
C2	0.4320 (5)	0.0025 (4)	0.3348 (2)	24 (1)
C21	0.4992 (6)	0.8918 (4)	0.3581(2)	35 (1)
C31	0.2804 (4)	0.0499 (3)	0.0308 (2)	20 (1)
C32	0.3477 (5)	0.9811 (3)	- 0.0262 (2)	23 (1)
C33	0.2883 (5)	0.1703 (3)	0.0225 (2)	26 (1)
C34	0.4288 (6)	0.1483 (4)	- 0.0977 (3)	31 (1)
C35	0.3615 (6)	0.2176 (4)	- 0.0424 (3)	34 (1)
C36	0.4217 (5)	0.0296 (4)	- 0.0902 (2)	27 (1)
C4	0.4179 (5)	0.1976 (4)	0.3677 (3)	30 (1)
C5	0.3264 (6)	0.2224 (4)	0.3080 (2)	29 (1)
C6	0.2828 (4)	0.1317 (4)	0.2560 (2)	22 (1)
I	0.1625 (1)	0.7470 (1)	0.0914 (1)	23 (1)
O1	0.2967 (3)	0.9338 (2)	0.2242 (2)	23 (1)
O3	0.4716 (4)	0.0919 (3)	0.3823 (2)	30 (1)
O6	0.1962 (4)	0.1448 (3)	0.1970 (2)	25 (1)
Sn	0.1656 (1)	0.9807 (1)	0.1304 (1)	17 (1)

[a] Equivalent isotropic U defined as one-third of the trace of the orthogonalised U_{ij} tensor.

C: Hydrogen coordinates and equivalent isotropic displacement parameters ($Å^2 \times 10^3$) for (**4.39d**)

Atom	x	y	z	U_{eq}
H21A	0.5614 (6)	0.9034 (4)	0.4048 (2)	42
H21B	0.5591 (6)	0.8623 (4)	0.3143 (2)	42
H21C	0.4216 (6)	0.8362 (4)	0.3706 (2)	42
H4	0.4467 (5)	1.2584 (4)	0.4019 (3)	36
H5	0.2913 (6)	1.2986 (4)	0.3004 (2)	34
H12	- 0.1151 (5)	0.9150 (3)	0.0407 (2)	26
H13	- 0.3670 (4)	0.9616 (4)	0.0383 (2)	30
H14	- 0.4680 (5)	1.0745 (4)	0.1404 (2)	32
H15	- 0.3182 (5)	1.1410 (4)	0.2436 (3)	34
H16	- 0.0661 (5)	1.1020 (4)	0.2415 (2)	29
H32	0.3430 (5)	0.8998 (3)	- 0.0214 (2)	27
H33	0.2441 (5)	1.2190 (3)	0.0609 (2)	31
H34	0.4800 (6)	1.1818 (4)	- 0.1411 (3)	37
H35	0.3649 (6)	1.2988 (4)	- 0.0486 (3)	41
H36	0.4672 (5)	0.9815 (4)	- 0.1285 (2)	32

D: ORTEP diagram

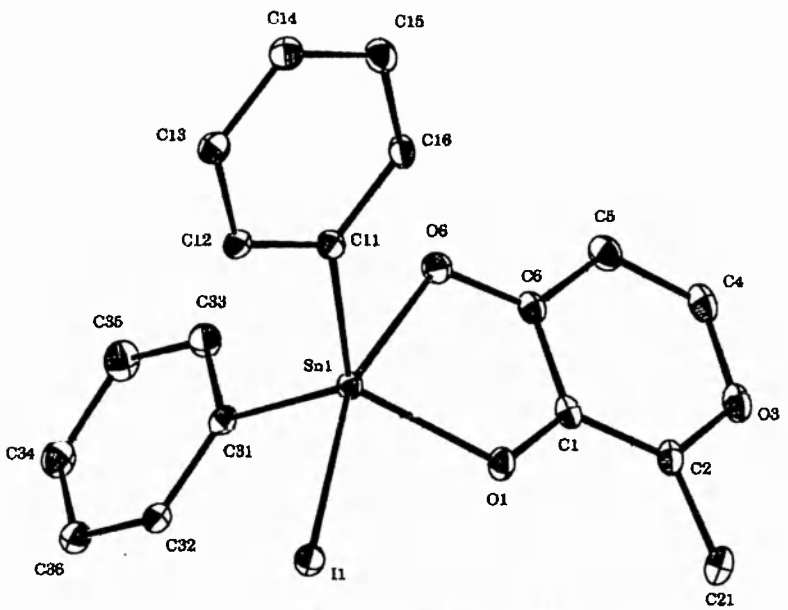

(4.39d)

E: Selected bond lengths (Å) and angles (°) for (**4.39d**)

Sn-O(1)	2.055 (3)	C(6)-O(6)	1.278 (5)
Sn-C(31)	2.135 (4)	C(11)-C16)	1.387 (5)
Sn-C(11)	2.142 (4)	C(11)-C(12)	1.393 (5)
Sn-O(6)	2.232 (3)	C(12)-C(13)	1.401 (6)
Sn-I	2.7953 (3)	C(13)-C(14)	1.401 (6)
O(1)-C(1)	1.337 (4)	C(14)-C(15)	1.390 (6)
C(1)-C(2)	1.379 (5)	C(15)-C(16)	1.391 (6)
C(1)-C(6)	1.420 (6)	C(31)-C(32)	1.394 (5)
C(2)-O(3)	1.362 (5)	C(31)-C(33)	1.408 (5)
C(2)-C(21)	1.479 (6)	C(32)-C(36)	1.390 (6)
O(3)-C(4)	1.345 (6)	C(33)-C(35)	1.396 (6)
C(4)-C(5)	1.338 (7)	C(34)-C(35)	1.376 (7)
C(5)-C(6)	1.428 (5)	C(34)-C(36)	1.388 (6)
O(1)-Sn-C(31)	115.0 (1)	O(6)-C(6)-C(5)	124.1 (4)
O(1)-Sn-C(11)	123.0 (1)	O(6)-C(6)-C(1)	118.2 (3)
C(31)-Sn-C(11)	119.9 (1)	C(5)-C(6)-C(1)	117.6 (4)
O(1)-Sn-O(6)	76.5 (1)	C(6)-O(6)-Sn	111.5 (3)
C(31)-Sn-O(6)	90.8 (1)	C(16)-C(11)-C(12)	120.0 (4)
C(11)-Sn-O(6)	88.0 (1)	C(16)-C(11)-Sn	122.0 (3)
O(1)-Sn-I	85.90 (8)	C(12)-C(11)-Sn	117.7 (3)
C(31)-Sn-I	100.7 (1)	C(11)-C(12)-C(13)	119.7 (4)
C(11)-Sn-I	98.1 (1)	C(14)-C(13)-C(12)	119.7 (4)
O(6)-Sn-I	161.88 (8)	C(13)-C(14)-C(15)	120.2 (4)
C(1)-O(1)-Sn	115.3 (2)	C(14)-C(15)-C(16)	119.6 (4)
O(1)-C(1)-C(2)	121.9 (4)	C(11)-C(16)-C(15)	120.8 (4)
O(1)-C(1)-C(6)	118.3 (3)	C(32)-C(31)-C(33)	118.6 (4)
C(2)-C(1)-C(6)	119.8 (3)	C(32)-C(31)-Sn	122.9 (3)
O(3)-C(2)-C(1)	120.5 (4)	C(33)-C(31)-Sn	118.5 (3)
O(3)-C(2)-C(21)	113.4 (3)	C(36)-C(32)-C(31)	121.1 (4)
C(1)-C(2)-C(21)	126.0 (4)	C(31)-C(33)-C(35)	119.7 (4)
C(4)-O(3)-C(2)	119.5 (3)	C(35)-C(34)-C(36)	119.9 (4)
O(3)-C(4)-C(5)	124.2 (4)	C(34)-C(35)-C(33)	120.9 (4)
C(4)-C(5)-C(6)	118.4 (4)	C(34)-C(36)-C(32)	119.8 (4)

Part 10. A: summary

Compound number	**(4.46a)**
Empirical formula	$C_{30}H_{25}NO_2Sn$
Formula Weight	550.20
Instrument	STOE STADI4
Temperature (K)	293 (2)
Wavelength (Å)	0.71073
Crystal system	Monoclinic, 2/m, 2nd setting
Space group	$P2_1/n$ (no 14), non-conventional $P2_1/c$
Unit cell dimensions	a = 13.077 (1) Å $\alpha = 90°$ b = 11.583 (1) Å $\beta = 105.43\ (1)°$ c = 17.374 (2) Å $\gamma = 90°$
Unit cell volume ($Å^3$)	2536.8 (4)
Number of units (Z)	4
Density (calculated) ($Mg\ m^{-3}$)	1.441
Absorption coefficient (mm^{-1})	1.034
F (000)	1112
Crystal size (mm)	1.33 x 1.045 x 0.76
Theta range for data collection (°)	1.74 to 27.48
Index ranges	-16 <=h<= 16, 0 <=k<= 15, -22 <=l<= 22
Reflections collected	6908
Independent reflections	5802 [$R_{(int)} = 0.0191$]
Absorption correction	Semi empirical from psi-scans
Max. and min transmission	0.9837 and 0.6464
Refinement method on F^2	Full-matrix least-squares
Data / restraints / parameters	5801 / 0 / 331
G.O.F. on F^2	1.136
Final R indices [I>2sigma(I)]	R1 = 0.0272, wR2 = 0.0721
R indices (all data)	R1 = 0.0324, wR2 = 0.0753
Extinction coefficient	0.0096 (4)
Largest diff. peak and hole	0.548 and - 0.353 $e.Å^{-3}$

B: Atomic coordinates and equivalent isotropic displacement parameters ($Å^2 \times 10^3$) for (**4.46a**)

Atom	x	y	z	U_{eq} [a]
C1	0.2380 (2)	0.1591 (2)	0.2010 (1)	40 (1)
C10	0.6307 (3)	- 0.1551 (3)	0.1401 (1)	79 (1)
C11	0.6805 (2)	- 0.1087 (3)	0.2119 (1)	76 (1)
C12	0.6362 (2)	- 0.0157 (2)	0.2415 (1)	59 (1)
C13	0.5635 (2)	0.1682 (2)	0.3715 (1)	47 (1)
C14	0.6247 (2)	0.2621 (3)	0.4056 (1)	60 (1)
C15	0.6945 (2)	0.2539 (4)	0.4813 (1)	78 (1)
C16	0.7041 (3)	0.1543 (4)	0.5237 (1)	90 (1)
C17	0.6430 (4)	0.0614 (3)	0.4919 (1)	95 (1)
C18	0.5739(3)	0.0685 (3)	0.4161 (1)	74 (1)
C19	0.5002 (2)	0.3255 (2)	0.1847 (1)	58 (1)
C2	0.1371 (2)	0.1319 (2)	0.1570 (1)	39 (1)
C20	0.5679 (3)	0.3151 (3)	0.1357 (2)	77 (1)
C21	0.5940 (4)	0.4092 (4)	0.0951 (2)	107 (1)
C22	0.5514 (5)	0.5143 (4)	0.1024 (3)	120 (2)
C23	0.4823 (5)	0.5275 (3)	0.1498 (3)	122 (2)
C24	0.4570 (3)	0.4331 (2)	0.1916 (2)	83 (1)
C25	- 0.0518 (2)	0.1843 (2)	0.1136 (1)	42 (1)
C26	- 0.0733 (2)	0.2354 (2)	0.0394 (1)	51 (1)
C27	- 0.1741 (2)	0.2264 (3)	- 0.0114 (2)	63 (1)
C28	- 0.2513 (2)	0.1671 (3)	0.0117 (2)	70 (1)
C29	- 0.2290 (2)	0.1159 (3)	0.0852 (2)	79 (1)
C3	0.1147 (2)	0.0328 (2)	0.0998 (1)	49 (1)
C30	- 0.1284 (2)	0.1244 (3)	0.1376 (2)	64 (1)
C4	0.0691 (2)	0.2864 (2)	0.2200 (1)	51 (1)
C5	0.1673 (2)	0.3143 (2)	0.2653 (2)	53 (1)
C6	0.2561 (2)	0.2532 (2)	0.2567 (1)	46 (1)
C7	0.5409 (2)	0.0331 (2)	0.1989 (1)	45 (1)
C8	0.4930 (2)	- 0.0142 (2)	0.1250 (2)	59 (1)
C9	0.5382 (2)	- 0.1072 (3)	0.0955 (2)	78 (1)
N3	0.0534 (1)	0.1979 (2)	0.1666 (1)	42 (1)
O1	0.3231 (1)	0.1016 (1)	0.1934 (1)	47 (1)
O2	0.3528 (1)	0.2747 (2)	0.2951 (1)	60 (1)
Sn	0.4708 (1)	0.1762 (1)	0.2488 (1)	42 (1)

[a] Equivalent isotropic U defined as one-third of the trace of the orthogonalised U_{ij} tensor.

C: Hydrogen coordinates and equivalent isotropic displacement parameters ($Å^2 \times 10^3$) for (**4.46a**)

Atom	x	y	z	U_{eq}
H4	0.0083 (19)	0.3307 (14)	0.2257 (2)	61
H5	0.1759 (3)	0.3746 (19)	0.3024 (12)	63
H3A	0.0543 (12)	0.0292 (2)	0.0800 (4)	73
H3B	0.1338 (4)	- 0.0241 (11)	0.1226 (4)	73
H3C	0.1445 (6)	0.0419 (2)	0.0672 (6)	73
H8	0.4256 (21)	0.0187 (11)	0.0926 (10)	70
H9	0.5061 (14)	- 0.1364 (13)	0.0463 (21)	93
H10	0.6575 (12)	- 0.2153 (26)	0.1224 (8)	95
H11	0.7434 (28)	- 0.1388 (14)	0.2408 (13)	92
H12	0.6724 (12)	0.0159 (11)	0.2929 (17)	71
H14	0.6188 (3)	0.3345 (22)	0.3762 (9)	72
H15	0.7324 (16)	0.3133 (26)	0.5017 (9)	94
H16	0.7530 (22)	0.1491 (5)	0.5752 (23)	108
H17	0.6479 (4)	- 0.0074 (31)	0.5215 (13)	113
H18	0.5335 (16)	0.0045 (26)	0.3950 (9)	89
H20	0.5952 (12)	0.2464 (31)	0.1301 (3)	92
H21	0.6451 (25)	0.3994 (6)	0.0599 (17)	128
H22	0.5680 (11)	0.5748 (36)	0.0766 (16)	144
H23	0.4565 (18)	0.5899 (41)	0.1533 (4)	146
H24	0.4114 (19)	0.4426 (5)	0.2240 (14)	99
H26	- 0.0233 (17)	0.2735 (13)	0.0246 (5)	61
H27	- 0.1894 (14)	0.2607 (13)	- 0.0613 (18)	76
H28	- 0.3178 (28)	0.1616 (3)	- 0.0220 (15)	85
H29	- 0.2778 (21)	0.0780 (17)	0.0991 (7)	95
H30	- 0.1135 (6)	0.0905 (13)	0.1874 (18)	76

D: ORTEP diagram

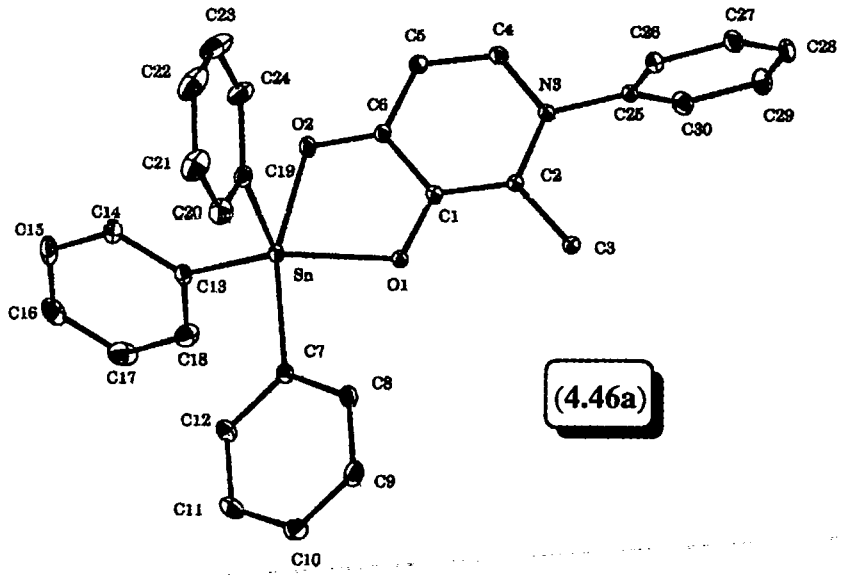

E: Selected bond lengths (Å) and angles (°) for (**4.46a**)

Sn-O(1)	2.100 (1)	C(11)-C(12)	1.385 (4)
Sn-C(19)	2.147 (3)	C(13)-C(18)	1.377 (4)
Sn-C(13)	2.156 (2)	C(13)-C(14)	1.386 (3)
Sn-C(7)	2.182 (2)	C(14)-C(15)	1.390 (4)
Sn-O(2)	2.233 (2)	C(15)-C(16)	1.356 (5)
O(1)-C(1)	1.332 (2)	C(16)-C(17)	1.365 (6)
O(2)-C(6)	1.287 (3)	C(17)-C(18)	1.388 (4)
C(1)-C(2)	1.374 (3)	C(19)-C(24)	1.387 (4)
C(1)-C(6)	1.435 (3)	C(19)-C(20)	1.387 (5)
C(2)-N	1.382 (3)	C(20)-C(21)	1.390 (5)
C(2)-C(3)	1.495 (3)	C(21)-C(22)	1.359 (7)
N-C(4)	1.360 (3)	C(22)-C(23)	1.383 (7)
N-C(25)	1.446 (3)	C(23)-C(24)	1.400 (5)
C(4)-C(5)	1.355 (3)	C(25)-C(30)	1.372 (3)
C(5)-C(6)	1.401 (3)	C(25)-C(26)	1.377 (3)
C(7)-C(8)	1.384 (3)	C(26)-C(27)	1.382 (3)
C(7)-C(12)	1.390 (3)	C(27)-C(28)	1.367 (4)
C(8)-C(9)	1.391 (4)	C(28)-C(29)	1.367 (5)
C(9)-C(10)	1.369 (5)	C(29)-C(30)	1.391 (4)
C(10)-C(11)	1.355 (5)		
O(1)-Sn-C(19)	111.30 (8)	C(7)-C(8)-C(9)	121.2 (3)
O(1)-Sn-C(13)	129.99 (8)	C(10)-C(9)-C(8)	120.2 (3)
C(19)-Sn-C(13)	114.56 (9)	C(11)-C(10)-C(9)	119.8 (3)

O(1)-Sn-C(7)	86.44 (7)	C(10)-C(11)-C(12)	120.3 (3)
C(19)-Sn-C(7)	104.7 (1)	C(11)-C(12)-C(7)	121.5 (3)
C(13)-Sn-C(7)	100.06 (8)	C(18)-C(13)-C(14)	117.2 (2)
O(1)-Sn-O(2)	74.70 (6)	C(18)-C(13)-Sn	122.5 (2)
C(19)-Sn-O(2)	90.6 (1)	C(14)-C(13)-Sn	119.9 (2)
C(13)-Sn-O(2)	85.82 (7)	C(13)-C(14)-C(15)	120.6 (3)
C(7)-Sn-O(2)	159.14 (7)	C(16)-C(15)-C(14)	120.9 (3)
C(1)-O(1)-Sn	116.1 (1)	C(15)-C(16)-C(17)	119.4 (3)
C(6)-O(2)-Sn	113.1 (1)	C(16)-C(17)-C(18)	120.0 (3)
O(1)-C(1)-C(2)	122.3 (2)	C(13)-C(18)-C(17)	121.7 (3)
O(1)-C(1)-C(6)	117.0 (2)	C(24)-C(19)-C(20)	118.2 (3)
C(2)-C(1)-C(6)	120.7 (2)	C(24)-C(19)-Sn	123.1 (3)
C(1)-C(2)-N	118.8 (2)	C(20)-C(19)-Sn	118.7 (2)
C(1)-C(2)-C(3)	122.3 (2)	C(19)-C(20)-C(21)	121.8 (4)
N-C(2)-C(3)	119.0 (2)	C(22) C(21) C(20)	119.5 (5)
C(4)-N-C(2)	121.2 (2)	C(21)-C(22)-C(23)	120.2 (4)
C(4)-N-C(25)	117.5 (2)	C(22)-C(23)-C(24)	120.3 (4)
C(2)-N-C(25)	120.8 (2)	C(19)-C(24)-C(23)	119.9 (4)
C(5)-C(4)-N	121.6 (2)	C(30)-C(25)-C(26)	121.3 (2)
C(4)-C(5)-C(6)	120.1 (2)	C(30)-C(25)-N	120.5 (2)
O(2)-C(6)-C(5)	125.1 (2)	C(26)-C(25)-N	118.2 (2)
O(2)-C(6)-C(1)	117.3 (2)	C(25)-C(26)-C(27)	119.2 (2)
C(5)-C(6)-C(1)	117.6 (2)	C(28)-C(27)-C(26)	120.2 (3)
C(8)-C(7)-C(12)	117.0 (2)	C(29)-C(28)-C(27)	120.2 (3)
C(8)-C(7)-Sn	122.4 (2)	C(28)-C(29)-C(30)	120.7 (3)
C(12)-C(7)-Sn	120.6 (2)	C(25)-C(30)-C(29)	118.4 (3)

Part 11. A: Summary

Compound number	**(4.46b)**
Empirical formula	$C_{24}H_{20}ClNO_2Sn$
Formula Weight	508.59
Instrument	STOE STADI4
Temperature (K)	200 (2)
Wavelength (Å)	0.71073
Crystal system	Monoclinic, 2/m, 2nd setting
Space group	$P2_1/n$ (no 14), non-conventional $P2_1/c$
Unit cell dimensions	a = 8.904 (1) Å $\quad \alpha = 90°$ b = 15.700 (2) Å $\quad \beta = 94.12\ (1)°$ c = 15.290 (2) Å $\quad \gamma = 90$
Unit cell volume ($Å^3$)	2132.0 (5)
Number of units (Z)	4
Density (calculated) ($Mg\ m^{-3}$)	1.585
Absorption coefficient (mm^{-1})	1.226
F (000)	1016
Crystal size (mm)	0.106 x 0.190 x 0.266
Theta range for data collection (°)	1.86 to 24.21
Index ranges	-10 <=h<= 10, -17 <=k<= 18, -17 <=l<= 17
Reflections collected	12160
Independent reflections	3362 [$R_{(int)}$ = 0.0214]
Absorption correction	None
Max. and min transmission	Not recorded
Refinement method on F^2	Full-matrix least-squares
Data / restraints / parameters	3362 / 0 / 262
G.O.F. on F^2	1.061
Final R indices [I>2sigma(I)]	R1 = 0.0473, wR2 = 0.1136
R indices (all data)	R1 = 0.0515, wR2 = 0.1159
Extinction coefficient	None
Largest diff. peak and hole	4.758 and - 0.620 $e.Å^{-3}$

B: Atomic coordinates and equivalent isotropic displacement parameters ($Å^2 \times 10^3$) for (**4.46b**)

Atom	x	y	z	U_{eq} [a]
C1	0.2113 (6)	0.2728 (4)	0.4541 (4)	24 (1)
C10	0.3712 (9)	0.5458 (5)	0.1687 (4)	43 (2)
C11	0.3126 (8)	0.4846 (4)	0.2213 (4)	31 (2)
C12	0.2261 (7)	0.5159 (4)	0.4588 (4)	26 (1)
C13	- 0.1628 (7)	0.2167 (4)	0.5717 (4)	27 (1)
C14	- 0.2919 (8)	0.2486 (5)	0.6032 (5)	41 (2)
C15	- 0.4311 (9)	0.2132 (6)	0.5768 (7)	60 (2)
C16	- 0.4424 (10)	0.1472 (7)	0.5196 (6)	64 (3)
C17	- 0.3139 (11)	0.1146 (6)	0.4880 (5)	60 (2)
C18	- 0.1736 (8)	0.1492 (5)	0.5134 (5)	42 (2)
C19	0.2000 (6)	0.1902 (4)	0.7003 (4)	20 (1)
C2	0.1985 (6)	0.3584 (4)	0.4819 (3)	18 (1)
C20	0.2405 (8)	0.2138 (4)	0.7862 (4)	35 (2)
C21	0.3337 (9)	0.1612 (5)	0.8400 (5)	44 (2)
C22	0.3819 (8)	0.0858 (5)	0.8086 (5)	42 (2)
C23	0.3433 (9)	0.0616 (5)	0.7233 (5)	46 (2)
C24	0.2524 (8)	0.1135 (4)	0.6697 (4)	37 (2)
C3	0.2510 (6)	0.4258 (4)	0.4341 (4)	22 (1)
C4	0.3370 (7)	0.3249 (4)	0.3328 (4)	32 (2)
C5	0.2844 (8)	0.2588 (4)	0.3771 (4)	34 (2)
C6	0.3787 (7)	0.4737 (4)	0.3051 (4)	25 (1)
C7	0.4992 (8)	0.5216 (5)	0.3354 (5)	40 (2)
C8	0.5552 (9)	0.5832 (5)	0.2823 (5)	48 (2)
C9	0.4894 (9)	0.5958 (5)	0.1990 (5)	45 (2)
Cl	- 0.0242 (2)	0.3640 (1)	0.7256 (1)	30 (1)
N	0.3209 (5)	0.4070 (3)	0.3592 (3)	25 (1)
O1	0.1563 (5)	0.2140 (2)	0.5005 (3)	25 (1)
O2	0.1295 (5)	0.3729 (2)	0.5553 (2)	24 (1)
Sn	0.0542 (1)	0.2651 (1)	0.6147 (1)	18 (1)

[a] Equivalent isotropic U defined as one-third of the trace of the orthogonalised U_{ij} tensor.

C: Hydrogen coordinates and equivalent isotropic displacement parameters ($Å^2 \times 10^3$) for **(4.46b)**

Atom	x	y	z	U_{eq}
H4	0.3872 (7)	0.3140 (4)	0.2812 (4)	38
H5	0.2968 (8)	0.2024 (4)	0.3564 (4)	40
H7	0.5443 (8)	0.5125 (5)	0.3928 (5)	48
H8	0.6390 (9)	0.6168 (5)	0.3031 (5)	58
H9	0.5261 (9)	0.6391 (5)	0.1628 (5)	54
H10	0.3287 (9)	0.5534 (5)	0.1104 (4)	51
H11	0.2291 (8)	0.4508 (4)	0.2005 (4)	38
H12A	0.2716 (7)	0.5536 (4)	0.4170 (4)	31
H12B	0.2726 (7)	0.5264 (4)	0.5179 (4)	31
H12C	0.1178 (7)	0.5272 (4)	0.4579 (4)	31
H14	- 0.2862 (8)	0.2950 (5)	0.6432 (5)	49
H15	- 0.5197 (9)	0.2356 (6)	0.5993 (7)	72
H16	- 0.5381 (10)	0.1239 (7)	0.5015 (6)	77
H17	- 0.3208 (11)	0.0679 (6)	0.4483 (5)	72
H18	- 0.0854 (8)	0.1265 (5)	0.4908 (5)	50
H20	0.2047 (8)	0.2659 (4)	0.8084 (4)	42
H21	0.3632 (9)	0.1780 (5)	0.8984 (5)	53
H22	0.4430 (8)	0.0494 (5)	0.8458 (5)	50
H23	0.3793 (9)	0.0093 (5)	0.7016 (5)	55
H24	0.2254 (8)	0.0964 (4)	0.6110 (4)	45

D: ORTEP diagram

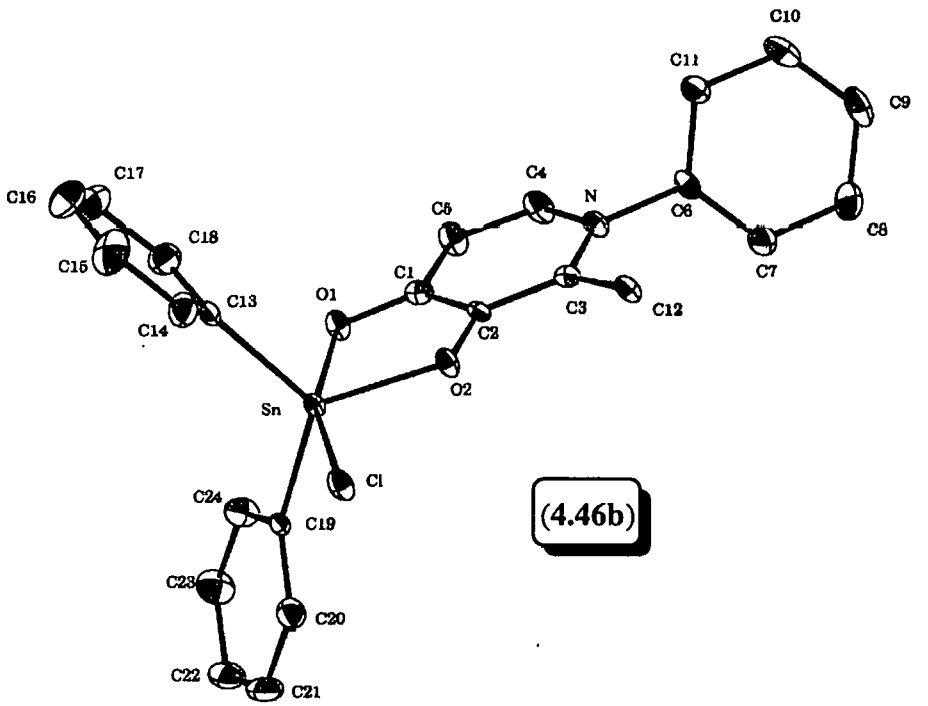

E:	Selected bond lengths (Å) and angles (°) for (**4.46b**)		

Sn-O(2)	2.055 (4)	C(7)-C(8)	1.379 (10)
Sn-C(19)	2.129 (5)	C(8)-C(9)	1.377 (11)
Sn-C(13)	2.136 (6)	C(9)-C(10)	1.367 (11)
Sn-O(1)	2.179 (4)	C(10)-C(11)	1.380 (10)
Sn-Cl	2.438 (2)	C(13)-C(14)	1.373 (10)
O(1)-C(1)	1.283 (7)	C(13)-C(18)	1.383 (10)
O(2)-C(2)	1.338 (7)	C(14)-C(15)	1.393 (11)
N-C(4)	1.360 (8)	C(15)-C(16)	1.354 (13)
N-C(3)	1.375 (7)	C(16)-C(17)	1.373 (13)
N-C(6)	1.452 (7)	C(17)-C(18)	1.392 (11)
C(1)-C(5)	1.403 (8)	C(19)-C(24)	1.386 (9)
C(1)-C(2)	1.415 (8)	C(19)-C(20)	1.387 (9)
C(2)-C(3)	1.386 (8)	C(20)-C(21)	1.397 (10)
C(3)-C(12)	1.485 (8)	C(21)-C(22)	1.358 (11)
C(4)-C(5)	1.342 (9)	C(22)-C(23)	1.377 (10)
C(6)-C(7)	1.363 (9)	C(23)-C(24)	1.377 (10)
C(6)-C(11)	1.381 (9)		

O(2)-Sn-C(19)	121.5 (2)	C(4)-C(5)-C(1)	120.1 (6)
O(2)-Sn-C(13)	118.2 (2)	C(7)-C(6)-C(11)	121.3 (6)
C(19)-Sn-C(13)	119.4 (2)	C(7)-C(6)-N	120.4 (5)
O(2)-Sn-O(1)	77.4 (1)	C(11)-C(6)-N	118.2 (6)

C(19)-Sn-O(1)	91.0 (2)	C(6)-C(7)-C(8)	119.7 (7)
C(13)-Sn-O(1)	92.4 (2)	C(9)-C(8)-C(7)	119.8 (7)
O(2)-Sn-Cl	84.4 (1)	C(10)-C(9)-C(8)	119.8 (7)
C(19)-Sn-Cl	96.7 (2)	C(9)-C(10)-C(11)	121.7 (7)
C(13)-Sn-Cl	98.2 (2)	C(10)-C(11)-C(6)	118.3 (6)
O(1)-Sn-Cl	161.6 (1)	C(14)-C(13)-C(18)	119.0 (6)
C(1)-O(1)-Sn	112.0 (3)	C(14)-C(13)-Sn	121.6 (5)
C(2)-O(2)-Sn	114.5 (3)	C(18)-C(13)-Sn	119.4 (5)
C(4)-N-C(3)	120.9 (5)	C(13)-C(14)-C(15)	120.1 (8)
C(4)-N-C(6)	117.8 (5)	C(16)-C(15)-C(14)	121.1 (8)
C(3)-N-C(6)	121.3 (5)	C(15)-C(16)-C(17)	119.2 (7)
O(1)-C(1)-C(5)	124.7 (6)	C(16)-C(17)-C(18)	120.6 (8)
O(1)-C(1)-C(2)	118.4 (5)	C(13)-C(18)-C(17)	119.9 (7)
C(5)-C(1)-C(2)	116.9 (5)	C(24)-C(19)-C(20)	118.7 (6)
O(2)-C(2)-C(3)	120.3 (5)	C(24)-C(19)-Sn	118.6 (4)
O(2)-C(2)-C(1)	117.7 (5)	C(20)-C(19)-Sn	122.7 (5)
C(3)-C(2)-C(1)	122.0 (5)	C(19)-C(20)-C(21)	120.2 (6)
N-C(3)-C(2)	117.7 (5)	C(22)-C(21)-C(20)	119.8 (7)
N-C(3)-C(12)	120.1 (5)	C(21)-C(22)-C(23)	120.8 (6)
C(2)-C(3)-C(12)	122.1 (5)	C(24)-C(23)-C(22)	119.8 (7)
C(5)-C(4)-N	122.4 (5)	C(23)-C(24)-C(19)	120.8 (6)

Part 12. A: Summary

Compound number	**(4.46c)**
Empirical formula	$C_{24}H_{20}BrNO_2Sn$
Formula Weight	553.05
Instrument	STOE STADI4
Temperature (K)	200 (2)
Wavelength (Å)	0.71073
Crystal system	Monoclinic, 2/m, 2nd setting
Space group	$P2_1/n$ (no 14), non-conventional $P2_1/c$
Unit cell dimensions	a = 8.904 (3) Å α = 90° b = 16.371 (4) Å β = 94.45 (3)° c = 15.104 (5) Å γ = 90°
Unit cell volume ($Å^3$)	2194.9 (12)
Number of units (Z)	4
Density (calculated) ($Mg\ m^{-3}$)	1.674
Absorption coefficient (mm^{-1})	2.865
F (000)	1088
Crystal size (mm)	0.380 x 0.456 x 0.684
Theta range for data collection (°)	2.49 to 28.16
Index ranges	-11 <=h<= 11, -21 <=k<= 21, -19 <=l<= 19
Reflections collected	18819
Independent reflections	5136 [$R_{(int)}$ = 0.0763]
Absorption correction	None
Max. and min transmission	Not recorded
Refinement method on F^2	Full-matrix least-squares
Data / restraints / parameters	5136 / 0 / 263
G.O.F. on F^2	1.020
Final R indices [I>2sigma(I)]	R1 = 0.0401, wR2 = 0.0830
R indices (all data)	R1 = 0.0649, wR2 = 0.0903
Extinction coefficient	0.0014 (3)
Largest diff. peak and hole	0.713 and - 0.965 $e.Å^{-3}$

B: Atomic coordinates and equivalent isotropic displacement parameters ($Å^2 \times 10^3$) for (**4.46c**)

Atom	x	y	z	U_{eq} [a]
Br	- 0.0177 (1)	0.6281 (1)	0.7370 (1)	29 (1)
C1	- 0.1667 (4)	0.7724 (2)	0.5720 (3)	28 (1)
C10	0.3779 (5)	0.9125 (3)	0.8032 (3)	43 (1)
C11	0.3300 (5)	0.8416 (3)	0.8395 (3)	44 (1)
C12	0.2406 (5)	0.7873 (2)	0.7864 (3)	34 (1)
C13	0.2026 (4)	0.7208 (2)	0.4484 (3)	25 (1)
C14	0.1952 (4)	0.6387 (2)	0.4789 (2)	21 (1)
C15	0.2478 (4)	0.5746 (2)	0.4306 (2)	21 (1)
C16	0.3220 (5)	0.6709 (3)	0.3237 (3)	38 (1)
C17	0.2677 (5)	0.7346 (2)	0.3683 (3)	37 (1)
C18	0.2266 (4)	0.4884 (2)	0.4583 (3)	29 (1)
C19	0.3731 (4)	0.5291 (2)	0.2986 (3)	28 (1)
C2	- 0.1792 (5)	0.8389 (3)	0.5155 (3)	42 (1)
C20	0.3076 (5)	0.5158 (3)	0.2137 (3)	36 (1)
C21	0.3694 (6)	0.4552 (3)	0.1624 (3)	48 (1)
C22	0.4894 (6)	0.4110 (3)	0.1948 (4)	54 (1)
C23	0.5550 (6)	0.4254 (3)	0.2787 (4)	59 (2)
C24	0.4969 (5)	0.4861 (3)	0.3316 (3)	48 (1)
C3	- 0.3193 (6)	0.8710 (3)	0.4881 (3)	60 (2)
C4	- 0.4465 (6)	0.8364 (4)	0.5173 (4)	65 (2)
C5	- 0.4349 (6)	0.7717 (4)	0.5746 (5)	65 (2)
C6	- 0.2959 (5)	0.7386 (3)	0.6020 (4)	43 (1)
C7	0.2001 (4)	0.8051 (2)	0.6988 (3)	25 (1)
C8	0.2470 (5)	0.8776 (2)	0.6631 (3)	41 (1)
C9	0.3370 (6)	0.9308 (3)	0.7168 (3)	49 (1)
N	0.3127 (3)	0.5927 (2)	0.3526 (2)	26 (1)
O1	0.1473 (3)	0.7778 (1)	0.4962 (2)	28 (1)
O2	0.1311 (3)	0.6255 (1)	0.5554 (2)	26 (1)
Sn	0.0542 (1)	0.7290 (1)	0.6149 (1)	20 (1)

[a] Equivalent isotropic U defined as one-third of the trace of the orthogonalised U_{ij} tensor.

C: Hydrogen coordinates and equivalent isotropic displacement parameters ($Å^2 \times 10^3$) for (**4.46c**)

Atom	x	y	z	U_{eq}
H2	- 0.0909 (5)	0.8628 (3)	0.4952 (3)	50
H3	- 0.3269 (6)	0.9168 (3)	0.4493 (3)	72
H4	- 0.5429 (6)	0.8575 (4)	0.4977 (4)	78
H5	- 0.5235 (6)	0.7490 (4)	0.5959 (5)	78
H6	- 0.2892 (5)	0.6931 (3)	0.6411 (4)	52
H8	0.2184 (5)	0.8912 (2)	0.6030 (3)	49
H9	0.3703 (6)	0.9805 (3)	0.6925 (3)	58
H10	0.4399 (5)	0.9492 (3)	0.8384 (3)	52
H11	0.3571 (5)	0.8291 (3)	0.9000 (3)	52
H12	0.2076 (5)	0.7377 (2)	0.8112 (3)	40
H16	0.3683 (5)	0.6812 (3)	0.2702 (3)	46
H17	0.2737 (5)	0.7884 (2)	0.3454 (3)	44
H18A	0.2710 (4)	0.4517 (2)	0.4163 (3)	34
H18B	0.1188 (4)	0.4768 (2)	0.4591 (3)	34
H18C	0.2762 (4)	0.4800 (2)	0.5179 (3)	34
H20	0.2232 (5)	0.5470 (3)	0.1909 (3)	43
H21	0.3263 (6)	0.4449 (3)	0.1039 (3)	58
H22	0.5289 (6)	0.3696 (3)	0.1593 (4)	64
H23	0.6398 (6)	0.3942 (3)	0.3008 (4)	71
H24	0.5424 (5)	0.4973 (3)	0.3893 (3)	57

D: ORTEP diagram

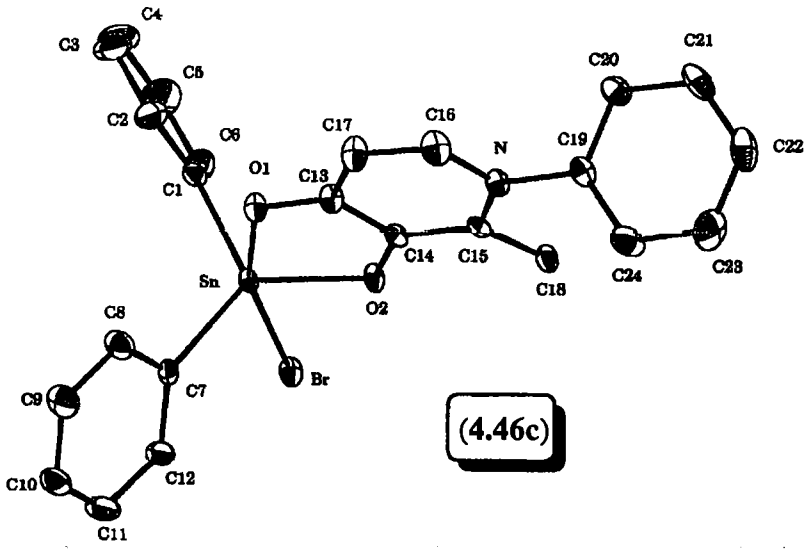

E: Selected bond lengths (Å) and angles (°) for (**4.46c**)

Sn-O(2)	2.060 (2)	C(7)-C(8)	1.381 (5)
Sn-C(7)	2.143 (4)	C(8)-C(9)	1.399 (6)
Sn-C(1)	2.144 (4)	C(9)-C(10)	1.360 (6)
Sn-O(1)	2.184 (3)	C(10)-C(11)	1.366 (6)
Sn-Br	2.5919 (7)	C(11)-C(12)	1.402 (5)
O(1)-C(13)	1.299 (4)	C(13)-C(17)	1.400 (5)
O(2)-C(14)	1.345 (4)	C(13)-C(14)	1.424 (5)
N-C(16)	1.357 (5)	C(14)-C(15)	1.381 (5)
N-C(15)	1.384 (4)	C(15)-C(18)	1.489 (5)
N-C(19)	1.451 (5)	C(16)-C(17)	1.351 (6)
C(1)-C(2)	1.382 (6)	C(19)-C(24)	1.368 (6)
C(1)-C(6)	1.384 (6)	C(19)-C(20)	1.384 (5)
C(2)-C(3)	1.387 (6)	C(20)-C(21)	1.398 (6)
C(3)-C(4)	1.370 (8)	C(21)-C(22)	1.350 (7)
C(4)-C(5)	1.368 (8)	C(22)-C(23)	1.374 (7)
C(5)-C(6)	1.384 (6)	C(23)-C(24)	1.399 (6)
C(7)-C(12)	1.376 (5)		
O(2)-Sn-C(7)	122.0 (1)	C(8)-C(7)-Sn	117.2 (3)
O(2)-Sn-C(1)	118.0 (1)	C(7)-C(8)-C(9)	119.0 (4)
C(7)-Sn-C(1)	119.0 (1)	C(10)-C(9)-C(8)	121.2 (4)
O(2)-Sn-O(1)	77.43 (9)	C(9)-C(10)-C(11)	120.2 (4)
C(7)-Sn-O(1)	91.2 (1)	C(10)-C(11)-C(12)	119.4 (4)
C(1)-Sn-O(1)	91.6 (1)	C(7)-C(12)-C(11)	120.6 (4)
O(2)-Sn-Br	83.99 (7)	O(1)-C(13)-C(17)	124.4 (3)

C(7)-Sn-Br	97.0 (1)	O(1)-C(13)-C(14)	117.9 (3)
C(1)-Sn-Br	98.9 (1)	C(17)-C(13)-C(14)	117.7 (3)
O(1)-Sn-Br	161.32 (7)	O(2)-C(14)-C(15)	121.0 (3)
C(13)-O(1)-Sn	112.2 (2)	O(2)-C(14)-C(13)	117.7 (3)
C(14)-O(2)-Sn	114.8 (2)	C(15)-C(14)-C(13)	121.3 (3)
C(16)-N-C(15)	121.0 (3)	C(14)-C(15)-N	118.0 (3)
C(16)-N-C(19)	117.4 (3)	C(14)-C(15)-C(18)	121.1 (3)
C(15)-N-C(19)	121.6 (3)	N-C(15)-C(18)	120.8 (3)
C(2)-C(1)-C(6)	119.2 (4)	C(17)-C(16)-N	122.3 (4)
C(2)-C(1)-Sn	118.4 (3)	C(16)-C(17)-C(13)	119.6 (4)
C(6)-C(1)-Sn	122.3 (3)	C(24)-C(19)-C(20)	121.7 (4)
C(1)-C(2)-C(3)	120.7 (5)	C(24)-C(19)-N	119.2 (4)
C(4)-C(3)-C(2)	119.6 (5)	C(20)-C(19)-N	119.0 (4)
C(5)-C(4)-C(3)	120.0 (5)	C(19)-C(20)-C(21)	118.0 (4)
C(4)-C(5)-C(6)	120.9 (5)	C(22)-C(21)-C(20)	120.9 (4)
C(1)-C(6)-C(5)	119.5 (5)	C(21)-C(22)-C(23)	120.7 (5)
C(12)-C(7)-C(8)	119.6 (4)	C(22)-C(23)-C(24)	119.9 (5)
C(12)-C(7)-Sn	123.1 (3)	C(19)-C(24)-C(23)	118.8 (4)

Part 13. A : Summary

Compound number	**(4.61)**	
Empirical formula	$C_{18}H_{15}ClO_3Si$	
Formula Weight	342.84	
Instrument	STOE STADI4	
Temperature (K)	293 (2)	
Wavelength (Å)	0.71073	
Crystal system	Monoclinic, 2, 2nd setting	
Space group	$P2_1$ (no 4)	
Unit cell dimensions	a = 10.977 (2) Å	$\alpha = 90°$
	b = 8.950 (2) Å	$\beta = 90.19\ (3)°$
	c = 16.443 (3) Å	$\gamma = 90°$
Unit cell volume ($Å^3$)	1615.4 (6)	
Number of units (Z)	2	
Density (calculated) ($Mg\ m^{-3}$)	1.410	
Absorption coefficient (mm^{-1})	0.322	
F (000)	712	
Crystal size (mm)	0.608 x 0.456 x 0.380	
Theta range for data collection (°)	1.86 to 22.50	
Index ranges	-11 <=h<= 11, 0 <=k<= 9, 0 <=l<= 17	
Reflections collected	2103	
Independent reflections	2103 [$R_{(int)} = 0.000$]	
Absorption correction	None	
Max. and min transmission	Not recorded	
Refinement method on F^2	Full-matrix least-squares	
Data / restraints / parameters	2103 / 0 / 535	
G.O.F. on F^2	1.073	
Final R indices [I>2sigma(I)]	R1 = 0.0229, wR2 = 0.0629	
R indices (all data)	R1 = 0.0237, wR2 = 0.0633	
Absolute structure parameter	0.01 (6)	
Extinction coefficient	None	
Largest diff. peak and hole	0.201 and - 0.170 $e.Å^{-3}$	

B: Atomic coordinates and equivalent isotropic displacement parameters ($Å^2 \times 10^3$) for (**4.61**)

Atom	x	y	z	U_{eq} [a]
C1	0.2607 (3)	- 0.0722 (4)	0.7702 (2)	24 (1)
C10	0.2889 (4)	0.6011 (5)	0.6334 (2)	38 (1)
C11	0.2290 (4)	0.5313 (4)	0.5705 (2)	35 (1)
C12	0.2041 (4)	0.3787 (4)	0.5759 (2)	28 (1)
C13	0.2768 (3)	- 0.0129 (3)	0.5437 (2)	23 (1)
C14	0.1994 (4)	- 0.0912 (4)	0.4910 (2)	29 (1)
C15	0.2437 (4)	- 0.1660 (5)	0.4237 (2)	34 (1)
C16	0.3667 (4)	- 0.1651 (5)	0.4059 (3)	39 (1)
C17	0.4445 (4)	- 0.0872 (5)	0.4558 (2)	39 (1)
C18	0.3990 (4)	- 0.0129 (4)	0.5236 (2)	32 (1)
C19	0.1274 (5)	- 0.2364 (6)	0.8606 (3)	43 (1)
C2	0.2407 (4)	- 0.1658 (4)	0.8340 (2)	28 (1)
C20	- 0.2399 (3)	- 0.3932 (4)	0.7300 (2)	23 (1)
C21	- 0.1232 (3)	- 0.4503 (4)	0.7475 (2)	25 (1)
C22	- 0.0262 (4)	- 0.4148 (5)	0.6951 (2)	32 (1)
C23	- 0.0505 (4)	- 0.3220 (5)	0.6324 (3)	42 (1)
C25	- 0.2588 (4)	- 0.2998 (4)	0.6658 (2)	29 (1)
C26	- 0.3726 (5)	- 0.2302 (6)	0.6395 (3)	43 (1)
C27	- 0.2237 (3)	- 0.4524 (4)	0.9564 (2)	23 (1)
C28	- 0.1003 (4)	- 0.4528 (4)	0.9761 (2)	31 (1)
C29	- 0.0556 (4)	- 0.3782 (5)	0.0446 (2)	39 (1)
C30	- 0.1335 (4)	- 0.3004 (5)	0.0941 (3)	38 (1)
C31	- 0.2563 (4)	- 0.2997 (5)	0.0765 (2)	36 (1)
C32	- 0.3003 (4)	- 0.3741 (4)	0.0088 (2)	28 (1)
C33	- 0.2583 (3)	- 0.7587 (4)	0.8585 (2)	23 (1)
C34	- 0.1970 (4)	- 0.8334 (4)	0.7962 (2)	31 (1)
C35	- 0.1755 (4)	- 0.9859 (5)	0.7995 (3)	36 (1)
C36	- 0.2115 (4)	- 1.0669 (5)	0.8665 (2)	36 (1)
C37	- 0.2710 (4)	- 0.9970 (4)	0.9292 (2)	35 (1)
C38	- 0.2962 (4)	- 0.8447 (4)	0.9246 (2)	29 (1)
C4	0.4489 (4)	- 0.1433 (5)	0.8671 (3)	41 (1)
C5	0.4732 (4)	- 0.0511 (5)	0.8052 (2)	32 (1)
C6	0.3764 (3)	- 0.0160 (4)	0.7528 (2)	24 (1)
C7	0.2413 (3)	0.2932 (4)	0.6415 (2)	24 (1)
C8	0.3030 (4)	0.3677 (4)	0.7040 (2)	31 (1)
C9	0.3245 (4)	0.5209 (4)	0.7006 (3)	36 (1)
Cl1	0.0246 (1)	0.0980 (1)	0.6042 (1)	36 (1)

Cl2	- 0.4754 (1)	- 0.5636 (1)	0.8958 (1)	36 (1)
O1	0.1726 (2)	- 0.0261 (3)	0.7182 (1)	28 (1)
O2	0.3813 (2)	0.0663 (3)	0.6889 (1)	28 (1)
O3	- 0.3275 (2)	- 0.4397 (3)	0.7818 (1)	28 (1)
O4	- 0.1190 (2)	- 0.5317 (3)	0.8112 (1)	29 (1)
O5	0.3384 (3)	- 0.2013 (3)	0.8817 (2)	37 (1)
O6	- 0.1619 (3)	- 0.2643 (3)	0.6186 (2)	37 (1)
Si1	0.2192 (1)	0.0848 (1)	0.6382 (1)	23 (1)
Si2	- 0.2808 (1)	- 0.5504 (1)	0.8618 (1)	23 (1)

[a] Equivalent isotropic U defined as one-third of the trace of the orthogonalised U_{ij} tensor.

C: Hydrogen coordinates and equivalent isotropic displacement parameters ($Å^2$ x 10^3) for **(4.61)**

Atom	x	y	z	U_{eq}
H32	- 0.3841 (34)	- 0.3657 (40)	0.9981 (21)	24 (9)
H14	0.1214 (33)	- 0.0993 (37)	0.5031 (20)	13 (9)
H34	- 0.1649 (35)	- 0.7801 (44)	0.7549 (25)	27 (10)
H37	- 0.2983 (37)	- 1.0591 (49)	0.9776 (25)	38 (10)
H8	0.3391 (34)	0.3117 (43)	0.7468 (25)	28 (10)
H11	0.1962 (41)	0.5895 (54)	0.5258 (28)	51 (12)
H23	0.0041 (42)	- 0.2961 (53)	0.5923 (29)	49 (13)
H9	0.3627 (33)	0.5608 (43)	0.7439 (23)	25 (10)
H16	0.3894 (37)	- 0.2151 (46)	0.3597 (26)	35 (11)
H35	- 0.1378 (35)	- 1.0289 (46)	0.7586 (25)	28 (10)
H29	0.0285 (39)	- 0.3802 (50)	1.0566 (24)	40 (11)
H72	0.1133 (43)	- 0.2249 (50)	0.9214 (33)	55 (14)
H30	- 0.1083 (38)	- 0.2476 (48)	1.1419 (27)	41 (12)
H28	- 0.0443 (33)	- 0.5012 (40)	0.9453 (22)	19 (9)
H38	- 0.3345 (36)	- 0.7967 (46)	0.9676 (26)	32 (10)
H12	0.1695 (34)	0.3362 (45)	0.5380 (25)	25 (10)
H17	0.5262 (48)	- 0.0794 (60)	0.4426 (29)	58 (15)
H262	- 0.3857 (42)	- 0.2393 (49)	0.5845 (33)	51 (13)
H22	0.0554 (38)	- 0.4543 (45)	0.7023 (23)	34 (11)
H18	0.4495 (38)	0.0302 (46)	0.5512 (24)	33 (12)
H4	0.5029 (42)	- 0.1729 (56)	0.9046 (29)	54 (14)
H261	- 0.4420 (50)	- 0.2557 (60)	0.6680 (35)	66 (17)
H15	0.1881 (38)	- 0.2238 (47)	0.3912 (26)	77 (11)
H31	- 0.3177 (38)	- 0.2379 (47)	1.1089 (25)	36 (11)

H5	0.5467 (37)	- 0.0139 (44)	0.7969 (23)	29 (11)
H36	- 0.1956 (41)	- 1.1681 (62)	0.8738 (28)	53 (13)
H71	0.0599 (44)	- 0.2102 (53)	0.8292 (29)	51 (13)
H10	0.3121 (42)	0.7053 (61)	0.6255 (28)	55 (13)
H263	- 0.3714 (51)	- 0.1169 (70)	0.6444 (33)	80 (18)
H73	0.1284 (52)	- 0.3453 (74)	0.8534 (35)	84 (19)

D: ORTEP diagram

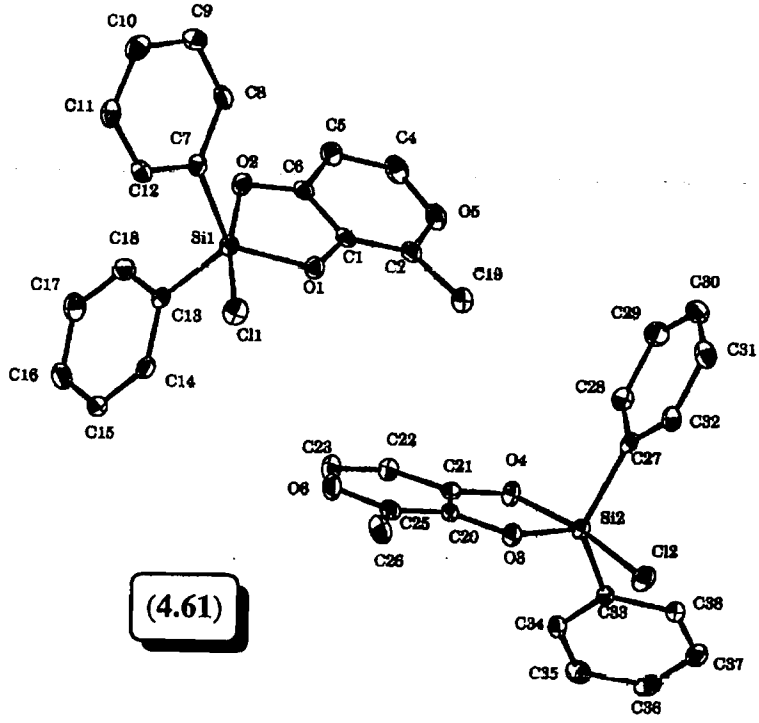

(4.61)

E: Selected bond lengths (Å) and angles (°) for (**4.61**)

Molecule 1:		Molecule 2:	
Si(1)-O(1)	1.726 (2)	Si(2)-O(3)	1.723 (2)
Si(1)-C(7)	1.881 (4)	Si(2)-C(33)	1.881 (4)
Si(1)-C(13)	1.894 (4)	Si(2)-C(27)	1.891 (3)
Si(1)-O(2)	1.969 (2)	Si(2)-O(4)	1.971 (3)
Si(1)-Cl(1)	2.209 (1)	Si(2)-Cl(2)	2.213 (1)
O(1)-C(1)	1.353 (4)	O(3)-C(20)	1.352 (4)
O(2)-C(6)	1.284 (4)	O(4)-C(21)	1.276 (4)
C(1)-C(2)	1.362 (5)	C(20)-C(25)	1.363 (5)
C(1)-C(6)	1.397 (5)	C(20)-C(21)	1.408 (5)
C(2)-O(5)	1.363 (5)	O(6)-C(25)	1.356 (5)
C(2)-C(19)	1.463 (6)	C(25)-C(26)	1.460 (6)
O(5)-C(4)	1.341 (5)	C(23)-O(6)	1.347 (5)

Molecule 1:		Molecule 2:	
C(4)-C(5)	1.337 (6)	C(22)-C(23)	1.349 (6)
C(5)-C(6)	1.402 (5)	C(21)-C(22)	1.409 (5)
C(7)-C(12)	1.383 (5)	C(33)-C(38)	1.396 (5)
C(7)-C(8)	1.398 (5)	C(33)-C(34)	1.398 (6)
C(8)-C(9)	1.392 (6)	C(34)-C(35)	1.386 (6)
C(9)-C(10)	1.373 (6)	C(35)-C(36)	1.379 (6)
C(10)-C(11)	1.375 (6)	C(36)-C(37)	1.374 (6)
C(11)-C(12)	1.396 (6)	C(37)-C(38)	1.393 (6)
C(13)-C(18)	1.383 (6)	C(27)-C(32)	1.394 (5)
C(13)-C(14)	1.401 (5)	C(27)-C(28)	1.391 (5)
C(14)-C(15)	1.382 (6)	C(28)-C(29)	1.398 (5)
C(15)-C(16)	1.382 (6)	C(29)-C(30)	1.373 (7)
C(16)-C(17)	1.372 (6)	C(30)-C(31)	1.378 (6)
C(17) C(18)	1.392 (6)	C(31)-C(32)	1.383 (6)
O(1)-Si(1)-C(7)	125.9 (2)	O(3)-Si(2)-C(33)	125.9 (1)
O(1)-Si(1)-C(13)	117.4 (1)	O(3)-Si(2)-C(27)	117.3 (1)
C(7)-Si(1)-C(13)	116.0 (2)	C(33)-Si(2)-C(27)	116.1 (2)
O(1)-Si(1)-O(2)	84.2 (1)	O(3)-Si(2)-O(4)	84.0 (1)
C(7)-Si(1)-O(2)	87.4 (1)	C(33)-Si(2)-O(4)	87.3 (1)
C(13)-Si(1)-O(2)	90.3 (1)	C(27)-Si(2)-O(4)	90.6 (1)
O(1)-Si(1)-Cl(1)	86.25 (9)	O(3)-Si(2)-Cl(2)	86.48 (9)
C(7)-Si(1)-Cl(1)	94.5 (1)	C(33)-Si(2)-Cl(2)	94.7 (1)
C(13)-Si(1)-Cl(1)	98.2 (1)	C(27)-Si(2)-Cl(2)	97.7 (1)
O(2)-Si(1)-Cl(1)	169.43 (9)	O(4)-Si(2)-Cl(2)	169.47 (9)
C(1)-O(1)-Si(1)	116.3 (2)	C(20)-O(3)-Si(2)	116.6 (2)
C(6)-O(2)-Si(1)	110.7 (2)	C(21)-O(4)-Si(2)	111.3 (2)
O(1)-C(1)-C(2)	123.9 (3)	O(3)-C(20)-C(25)	124.8 (3)
O(1)-C(1)-C(6)	114.2 (3)	O(3)-C(20)-C(21)	114.1 (3)
C(2)-C(1)-C(6)	121.9 (3)	C(25)-C(20)-C(21)	121.1 (3)
C(1)-C(2)-O(5)	117.2 (4)	O(6)-C(25)-C(20)	118.0 (3)
C(1)-C(2)-C(19)	129.4 (4)	C(20)-C(25)-C(26)	128.2 (4)
O(5)-C(2)-C(19)	113.3 (3)	O(6)-C(25)-C(26)	113.7 (3)
C(4)-O(5)-C(2)	121.1 (3)	C(23)-O(6)-C(25)	121.8 (3)
C(5)-C(4)-O(5)	123.9 (4)	O(6)-C(23)-C(22)	122.8 (4)
C(4)-C(5)-C(6)	117.0 (4)	C(23)-C(22)-C(21)	117.3 (4)
O(2)-C(6)-C(1)	114.5 (3)	O(4)-C(21)-C(20)	113.9 (3)
O(2)-C(6)-C(5)	126.7 (4)	O(4)-C(21)-C(22)	127.3 (3)
C(1)-C(6)-C(5)	118.8 (3)	C(20)-C(21)-C(22)	118.8 (3)
C(12)-C(7)-C(8)	116.7 (3)	C(38)-C(33)-C(34)	116.8 (3)

Molecule 1:		Molecule 2:	
C(12)-C(7)-Si(1)	119.2 (3)	C(38)-C(33)-Si(2)	119.0 (3)
C(8)-C(7)-Si(1)	123.8 (3)	C(34)-C(33)-Si(2)	124.0 (3)
C(9)-C(8)-C(7)	121.5 (4)	C(35)-C(34)-C(33)	121.7 (4)
C(10)-C(9)-C(8)	120.0 (4)	C(36)-C(35)-C(34)	120.0 (4)
C(9)-C(10)-C(11)	120.1 (4)	C(37)-C(36)-C(35)	119.9 (4)
C(10)-C(11)-C(12)	119.3 (4)	C(36)-C(37)-C(38)	119.9 (4)
C(7)-C(12)-C(11)	122.3 (4)	C(37)-C(38)-C(33)	121.5 (4)
C(18)-C(13)-C(14)	116.0 (4)	C(28)-C(27)-C(32)	116.5 (3)
C(18)-C(13)-Si(1)	121.6 (3)	C(28)-C(27)-Si(2)	120.6 (3)
C(14)-C(13)-Si(1)	122.4 (3)	C(32)-C(27)-Si(2)	122.8 (3)
C(15)-C(14)-C(13)	121.6 (4)	C(27)-C(28)-C(29)	121.7 (4)
C(16)-C(15)-C(14)	120.8 (4)	C(30)-C(29)-C(28)	120.2 (4)
C(17)-C(16)-C(15)	118.9 (4)	C(29)-C(30)-C(31)	119.3 (4)
C(16)-C(17)-C(18)	119.8 (4)	C(30)-C(31)-C(32)	120.4 (4)
C(13)-C(18)-C(17)	122.9 (4)	C(31)-C(32)-C(27)	122.0 (4)

Part 14. A: Summary

Compound number	**(4.69)**	
Empirical formula	$C_{20}H_{22}Cl_2N_4Sn$	
Formula Weight	508.02	
Instrument	STOE IPDS25	
Temperature (K)	293 (2)	
Wavelength (Å)	0.71073	
Crystal system	Monoclinic	
Space group	$P2_1/n$ (no 14)	
Unit cell dimensions	a = 9.618 (3) Å	α = 90.00 (2)°
	b = 9.515 (4) Å	β = 112.09 (5)°
	c = 12.622 (4) Å	γ = 90.01 (3)°
Unit cell volume ($Å^3$)	1070.3 (6) $Å^3$	
Number of units (Z)	4	
Density (calculated) ($Mg\ m^{-3}$)	1.576	
Absorption coefficient (mm^{-1})	1.455	
F (000)	508	
Crystal size (mm)	0.77 x 0.77 x 0.462	
Theta range for data collection (°)	2.29 to 27.50	
Index ranges	-12 <=h<= 11, 0 <=k<= 12, 0 <=l<= 16	
Reflections collected	2460	
Independent reflections	2460 [$R_{(int)}$ = 0.0000]	
Absorption correction	None	
Max. and min transmission	none and none	
Refinement method on F^2	Full-matrix least-squares	
Data / restraints / parameters	2460 / 0 / 169	
G.O.F. on F^2	1.084	
Final R indices [I>2sigma(I)]	R1 = 0.0308, wR2 = 0.0850	
R indices (all data)	R1 = 0.0321, wR2 = 0.0866	
Extinction coefficient	0.0177 (15)	
Largest diff. peak and hole	0.624 and - 1.203 e.$Å^{-3}$	

B: Atomic coordinates and equivalent isotropic displacement parameters ($Å^2 \times 10^3$) for (**4.69**)

Atom	x	y	z	U_{eq} [a]
Sn	0.5000	0.5000	0.000	38 (1)
Cl	0.7402 (1)	0.5275 (1)	0.1754 (1)	55 (1)
C11	0.6098 (2)	0.5928 (2)	- 0.1041 (2)	44 (1)
C12	0.7585 (3)	0.5624 (3)	- 0.0859 (3)	60 (1)
C13	0.8280 (4)	0.6261 (4)	- 0.1529 (3)	72 (1)
C14	0.7513 (4)	0.7200 (4)	- 0.2369 (1)	69 (1)
C15	0.6038 (4)	0.7501 (3)	- 0.2562 (2)	61 (1)
C16	0.5334 (4)	0.6868 (2)	- 0.1905 (2)	50 (1)
N1	0.4207 (4)	0.7214 (2)	0.0267 (2)	45 (1)
C2	0.5061 (3)	0.8155 (2)	0.1076 (2)	49 (1)
C3	0.4313 (2)	0.9379 (2)	0.0954 (2)	54 (1)
N4	0.2984 (2)	0.9207 (2)	0.0053 (2)	52 (1)
C5	0.2970 (3)	0.7887 (3)	- 0.0332 (2)	52 (1)
C6	0.1813 (5)	1.0258 (5)	- 0.0420 (1)	75 (1)

[a] Equivalent isotropic U defined as one-third of the trace of the orthogonalised U_{ij} tensor.

C: Hydrogen coordinates and equivalent isotropic displacement parameters ($Å^2 \times 10^3$) for (**4.69**)

Atom	x	y	z	U_{eq}
H12	0.8150 (5)	0.5010 (2)	- 0.0230 (4)	52 (11)
H13	0.9320 (4)	0.6090 (4)	- 0.1350 (3)	75 (9)
H14	0.8010 (4)	0.7660 (4)	- 0.2810 (3)	81 (11)
H15	0.5550 (3)	0.8140 (4)	- 0.3100 (3)	65 (8)
H16	0.4330 (3)	0.7060 (3)	- 0.2050 (2)	56 (7)
H2	0.6000 (3)	0.7950 (3)	0.1570 (2)	64 (8)
H3	0.4560 (4)	1.0280 (3)	0.1310 (3)	57 (10)
H5	0.2260 (4)	0.7540 (4)	- 0.0900 (3)	77 (10)
H61	0.1040 (6)	0.9810 (4)	- 0.0810 (4)	78 (15)
H62	0.2070 (6)	1.0900 (6)	- 0.0800 (5)	140 (2)
H63	0.1630 (6)	1.0570 (6)	0.0080 (5)	114 (18)

D: ORTEP diagram

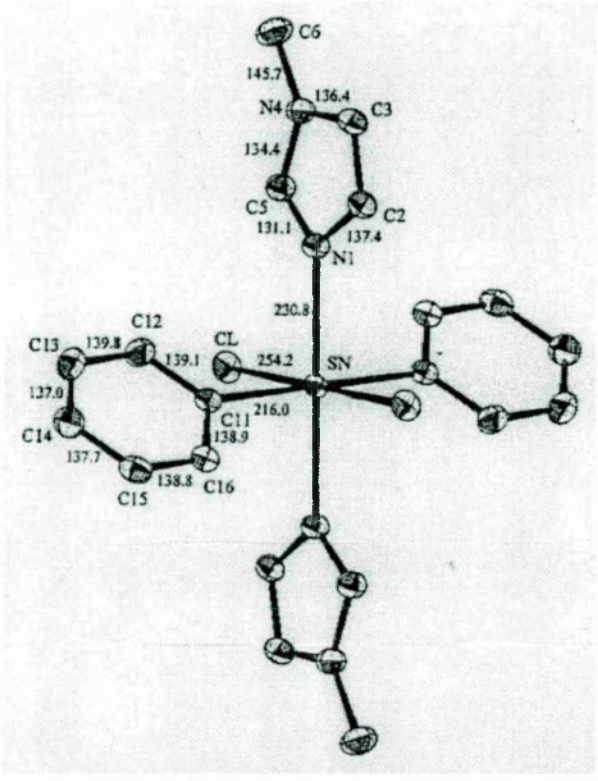

E:	Selected bond lengths (Å) and angles (°) for (**4.69**)		
Sn-C(11)#1	2.160 (2)	C(13)-C(14)	1.370 (5)
Sn-C(11)	2.160 (2)	C(14)-C(15)	1.377 (5)
Sn-N(1)#1	2.308 (2)	C(15)-C(16)	1.388 (4)
Sn-N(1)	2.308 (2)	N(1)-C(5)	1.311 (3)
Sn-Cl#1	2.542 (2)	N(1)-C(2)	1.374 (3)
Sn-Cl	2.542 (2)	C(2)-C(3)	1.347 (4)
C(11)-C(16)	1.389 (3)	C(3)-N(4)	1.364 (4)
C(11)-C(12)	1.391 (3)	N(4)-C(5)	1.344 (3)
C(12)-C(13)	1.398 (4)	N(4)-C(6)	1.457 (4)
C(11)#1-Sn-C(11)	180.0	C(16)-C(11)-Sn	120.4 (2)
C(11)#1-Sn-N(1)	91.17 (8)	C(12)-C(11)-Sn	121.5 (2)
C(11)-Sn-N(1)	88.83 (8)	C(11)-C(12)-C(13)	120.4 (3)
C(11)#1-Sn-N(1)#1	88.83 (8)	C(14)-C(13)-C(12)	120.6 (3)
C(11)-Sn-N(1)#1	91.17 (8)	C(13)-C(14)-C(15)	119.4 (3)
N(1)#1-Sn-N(1)	180.0	C(14)-C(15)-C(16)	120.4 (3)
C(11)#1-Sn-Cl#1	89.74 (7)	C(15)-C(16)-C(11)	121.0 (2)
C(11)-Sn-Cl#1	90.26 (7)	C(5)-N(1)-C(2)	105.6 (2)
N(1)-Sn-Cl#1	88.79 (6)	C(5)-N(1)-Sn	129.8 (2)

N(1)#1-Sn-Cl#1	91.21 (6)	C(2)-N(1)-Sn	124.4 (2)
C(11)#1-Sn-Cl	90.26 (7)	C(3)-C(2)-N(1)	109.5 (2)
C(11)-Sn-Cl	89.74 (7)	C(2)-C(3)-N(4)	106.5 (2)
N(1)-Sn-Cl	91.21 (6)	C(5)-N(4)-C(3)	107.0 (2)
N(1)#1-Sn-Cl	88.79 (6)	C(5)-N(4)-C(6)	126.3 (3)
Cl#1-Sn-Cl	180.0	C(3)-N(4)-C(6)	126.6 (3)
C(16)-C(11)-C(12)	118.1 (2)	N(1)-C(5)-N(4)	111.4 (2)

Symmetry transformations used to generate equivalent atoms

#1: -x+1, -y+1, -z

References

1. J.L. Gay-Lussac, L.J. Thenard; *Mem. Phys. Chem. Soc. Arcueil*; **2**, 317 (1809).

2. W. Dilthey; *Chem. Ber.*; **36**, 923 (1903).

3. S.A. Sullivan, C.H. De Puy, R. Damrauer; *J. Am. Chem. Soc.*; **103**, 480 (1981).

4. I.R. Beattie; *Quart. Rev. Chem. Soc.*; **17**, 382 (1963).

5. (a) K. Hensen, R. Busch; *Z. Naturforsch, B*; **37**, 1174 (1982). (b) H.J. Campbell-Ferguson, E.A.V. Ebsworth; *J. Chem. Soc., (A)*; 1508 (1966).

6. K. Hensen, T. Zengerly, P. Pickel, G. Klebe; *Angew. Chem., Int. Ed. Engl.*; **22**, 725 (1983).

7. A.R. Bassindale, T. Stout; *J. Organomet. Chem.*; **238**, C41 (1982).

8. K. Hensen, T. Zengerly, T. Muller, P. Pickel; *Z. Anorg. Allg. Chem.*; **558**, 21 (1988).

9. J.Y. Corey, R. West; *J. Am. Chem. Soc.*; **85**, 4034 (1963).

10. (a) F. Klanberg, E.L. Muetterties; *Inorg. Chem.*; **7**, 155 (1968). (b) D. Schomburg, R. Krebs; *Inorg. Chem.*; **23**, 1378 (1984).

11. R.K. Marat, A.F. Jansen; *Can. J. Chem.*; **55**, 1167 (1977).

12. (a) H.C. Clark, K.R. Dixon, J.G. Nicolson; *Inorg. Chem.*; **8**, 450 (1969). (b) B.S. Ault; *Inorg. Chem.*; **18**, 3339 (1979).

13. S.A. Sullivan, C.H. DePuy, R. Damrauer; *J. Am. Chem. Soc.*; **103**, 480 (1981).

14. R. Damrauer, S.E. Danahey; *Organometallics*; **5**, 1490 (1986).

15. J.L. Bréfort, R.J.P. Corriu, C. Guérin, B.J.L. Henner, W.W.C. Wong Chi Man; *Organometallics*; **9**, 2080 (1980).

16. (a) R.J.P. Corriu, C. Guérin, B. Henner, Q. Wang; *Organometallics*; **10**, 2297 (1991). (b) B. Becker, R. Corriu, C. Guérin, B. Henner, Q. Wang; *J. Organomet. Chem.*; **359**, C33 (1989).

17. B. Becker, R.J.P. Corriu, C. Guérin, B. Henner, Q. Wang; *J. Organomet. Chem.*; **368**, C25 (1989).

18. R.J.P. Corriu, C. Guérin, B.J.L. Henner, Q. Wang; *Organometallics*; **10**, 3574 (1991).

19. R. Müller, L. Heinrich; *Chem. Ber.*; **94**, 1943 (1961).

20. C.L. Frye; *J. Am. Chem. Soc.*; **92**, 1205 (1970).

21. C.L. Frye; *J. Am. Chem. Soc.*; **86**, 3170 (1964).

22. M. Kira, K. Sato, H. Sakurai; *J. Org. Chem.*; **52**, 948 (1987).

23. R.R. Holmes, R.O. Day, J.S. Payne; *Phosphorus, Sulfur, Silicon*; **42**, 1 (1989).

24. (a) G. Schott, K. Golz; *Z. Anorg. Allg. Chem.*; **383**, 314 (1971). (b) G. Schott, K. Golz; *Z. Anorg. Allg. Chem.*; **399**, 7 (1973).

25. E.L. Muetterties, H. Roesky, C.M. Wright; *J. Am. Chem. Soc..*; **88**, 4856 (1966).

26. C.L. Frye, G.E. Vogel, J.A. Hall; *J. Am. Chem. Soc,* **83**, 996 (1961).

27. A.A. Macharashvili, V.E. Shklover, Yu.T. Struckhov, A. Lapsina, G. Zelchans, E. Lukevics; *J. Organomet. Chem.*; **349**, 23 (1988).

28. (a) J.T.B.H. Jastrzebski, C.T. Knaap, G. van Koten; *J. Organomet. Chem.*; **255**, 287 (1983). (b) R.J.P. Corriu, M. Mazhar, M. Poirier, G. Royo; *J. Organomet. Chem.*; **306**, C5 (1986).

29. G. van Koten, J.G. Noltes; *J. Am. Chem. Soc.*; **98**, 5393 (1976).

30. G. Klebe, M. Nix, K. Hensen; *Chem. Ber.*; **117**, 797 (1984).

31. M.G. Voronkov, Yu.L. Frolov, V.M. D'yakov, N.N. Chipanina, L.I. Gubanova, G.A. Gavrilova, L.V. Klyba, T.N. Aksamentova; *J. Organomet. Chem.*; **201**, 165 (1980).

32. F. Klanberg, E.L. Muetterties; *Inorg. Chem.*; **7**, 155 (1968).

33. (a) S.E. Johnson, J.S. Payne, R.O. Day, J.M. Holmes, R.R. Holmes; *Inorg. Chem.*, **28**, 3190 (1989). (b) S.E. Johnson, R.O. Day, R.R. Holmes; *Inorg. Chem.*; **28**, 3182 (1989). (c) R. Damrauer, B. O'Connell, S.E. Danahey, R. Simon; *Organometallics*; **8**, 1167 (1989).

34. R.J.P. Corriu, G. Royo, A. de Saxcé; *J. Chem. Soc., Chem. Commun.*; 892 (1980).

35. R.J.P. Corriu, C. Guerin; *J. Organomet. Chem.*; **198**, 231 (1980).

36. R.J.P. Corriu, A. Kpoton, M. Poirere, G. Royo, J.Y. Corey; *J. Organomet. Chem.*; **277**, C25 (1984).

37. N.V. Timosheva, T.K. Prakasha, A. Chandrasekaran, R.O. Day, R.R. Holmes; *Inorg. Chem.*; **35**, 3614 (1996).

38. A. Chandrasekaran, R.O. Day, R.R. Holmes; *Organometallics*; **15**, 3189 (1996).

39. I.D. Kalikman, A.I. Albanov, O.B. Bannikova, L.I. Belousova, M.G. Voronkov, V.A. Pestunovich, A.G. Shipov, E.P. Kramarova, Yu.I. Baukov; *J. Organomet. Chem.*; **361**, 147 (1989).

40. D. Kummer, S.C. Chaudhry, J. Seifert, B. Deppisch, G. Mattern; *J. Organomet. Chem.*; **382**, 345 (1990).

41. D. Kummer, S.H. Abdel Halim, W. Kuhs, G. Mattern; *Z. Anorg. Allg. Chem.*; **614**, 73 (1992).

42. (a) S.N. Tandura, M.G. Voronkov, N.V. Alekseev; *Top. Curr. Chem*; **131**, 99 (1989). (b) V.E. Shklover, Yu.T. Struchkov, M.G. Voronkov; *Russ. Chem. Rev.*; **58**, 211 (1989).

43. R.J.P. Corriu, J.C. Young in: *The Chemistry of Organic Silicon Compounds*; S. Patai, Z. Rappoport (eds); John Wiley & Sons; 1241 (1989). (b) C. Chuit, R.J.P. Corriu, C. Reyé, J.C. Young; *Chem. Rev.*; **93**, 1371 (1993).

44. G. Klebe, J.W. Bats, K. Hensen; *J. Chem. Soc. Dalton Trans.*; 1 (1985).

45. G. Klebe, J.W. Bats, K. Hensen; *Z. Naturforsch., B*; **38**, 825 (1983).

46. C. Brelière, F. Carré, R.J.P. Corriu, M. Poirer, G. Royo; *Organometallics*; **5**, 388 (1988).

47. K.D. Onan, A.T. McPhail, C.H. Yoder, R.W. Hillyard Jr.; *J. Chem. Soc., Chem. Commun.*; 209 (1978).

48. C.H. Yoder, C.M. Ryan, G.F. Martin, P.S. Ho; *J. Organomet. Chem.*, **190**, 1 (1980).

49. H.B. Bürgi; *Angew. Chem.*; **27**, 460 (1975).

50. H.B. Bürgi, J.D. Dunitz, E. Shefter; *J. Am. Chem. Soc.*; **95**, 5065 (1973).

51. D. Britton, J.D. Dunitz; *J. Am. Chem. Soc*; **103**, 2971 (1981).

52. H.B. Bürgi, J.D. Dunitz; *Acc. Chem. Res.*; **16**, 153 (1983).

53. M.A. Dvorak, R.S. Ford, R.D. Suenram, F.J. Lovas, K.R. Leopold; *J. Am. Chem. Soc.*; **114**, 108 (1992).

54. M.G. Voronkov, V.M. D'yakov, S.V. Kirpichenko; *J. Organomet. Chem.*; **233**, 1 (1982).

55. M.J. Barrow, E.A.V. Ebsworth, M.M. Harding; *J. Chem. Soc., Dalton Trans.*; 1838 (1980).

56. A.A. Macharashvili, V.E. Shklover, Yu.T. Struchkov, G.I. Oleneva, E.P. Kramarova, A.G. Shipov, Yu.I. Baukov; *J. Chem. Soc., Chem. Commun.*; 683 (1988).

57. V.F. Sidorkin, V.V. Vladimirov, M.G. Voronkov, V.A. Pestunovich; *J. Mol. Struct. (Theochem.);* **228**, 1 (1991).

58. A.R. Bassindale, M. Borbaruah; *J. Chem. Soc., Chem. Commun.*; 1499 (1991).

59. J. Davy; *J. Phil. Trans. Roy. Soc. London*; **102**, 352 (1812).

60. K. Tamao, J. Yoshida, H. Yamamoto, T. Kakui, H. Masumoto, M. Takahashi, A. Kuritua, M. Murata, M. Kumada; *Organometallics*; **1**, 355 (1982).

61. V.A. Bain, R.C.G. Killean, M. Webster; *Acta Crystallogr., Sect. B*; **25**, 156 (1969).

62. (a) U. Wannagat; *Angew. Chem.*; **69**, 516 (1957). (b) U. Wannagat, K. Hensen, P. Petesch, F. Vielberg; *Monatsh. Chem.*; **98**, 1415 (1967).

63. D. Kummer, K.E. Gaisser, T. Seshadri; *Chem. Ber.*; **110**, 1950 (1977).

64. D. Kummer, H. Köster; *Z. Anorg. Allg. Chem.*; **402**, 297 (1973).

65. C. Brelière, F. Carré, R.J.P. Corriu, M. Poirier, G. Royo, J. Zwecker; *Organometallics*; **8**, 1831 (1989).

66. E.L. Muetterties, C.M. Wright; *J. Am. Chem. Soc.*; **86**, 5132 (1964).

67. (a) A. Boudin, G. Cereau, C. Chuit, R.J.P. Corriu, C. Reyé; *Angew. Chem., Int. Ed. Engl.*; **25**, 474 (1986). (b) A. Boudin, G. Cerveau, C. Chuit, R.J.P. Corriu, C. Reyé; *Organometallics*; **7**, 1165 (1988).

68. R.M. Laine; unpublished results.

69. J.A.A. Ketelaar; *Z. Kristallog.*; **92**, 155 (1935).

70. G.Sawitzki, H.G. von Schnering; *Chem. Ber.*; **109**, 3728 (1976).

71. R. Probst, C. Leis, S. Gamper, E. Herdtweck, C. Zybill, N. Auner; *Angew. Chem., Int. Ed. Engl.*; **30**, 1132 (1991).

72. A.G. Davies, P.J. Smith in: *Comprehensive Organometallic Chemistry: The Synthesis, Reactions and Structures of Organometallic Compounds*; G. Wilkinson (ed), Pergamon Press; 519 (1982).

73. K.C. Molloy in: *Chemistry of Tin*; P.G. Harrison (ed), Chapman & Hall; 187 (1989).

74. P.G. Harrison in: *Chemistry of Tin*; P.G. Harrison (ed), Chapman & Hall; 9 (1989).

75. S.S. Al-Juaid, S.M. Dhaher, C. Eaborn, P.B. Hitchcock, J.D. Smith; *J. Organomet. Chem.*; **325**, 117 (1987).

76. H. Preut, H.J. Haupt, F. Huber; *Z. Anorg. Allg. Chem.*; **396**, 81 (1973).

77. L. Smith, Ph.D. Thesis, Univ. London (1972).

78. R. Hoppe, W. Dähne; *Naturwissenschaften*; **49**, 254 (1962).

79. H.C. Clark, R.J. O'Brien, J. Trotter; *J. Chem. Soc.*; 2332 (1964).

80. L.S. Khaikin, A.V. Belyakov, G.S. Koptev, A.V. Golubinskii, L.V. Vilkov, N.V. Girbasova, E.T. Borgoradovskii, V.S. Zavgorodnii; *J. Mol. Struct.*; **66**, 191 (1980).

81. A.G. Davies, S.D. Slater, D.C. Povey, G.W. Smith; unpublished work.

82. N.G. Bokii, G.N. Zakharova, Yu.T. Struchkov; *J. Struct. Chem.*; **11**, 828 (1970).

83. A.G. Davies, H.J. Milledge, D.C. Puxley, P.J. Smith; *J. Chem. Soc., (A)*; 2862 (1970).

84. N.G. Bokii, Yu.T. Struchkov, A.K. Prokof'ev; *J. Struct. Chem.*; **13**, 619 (1972).

85. S.W. Ng; *Acta Cryst.*; C52, 1365 (1996).

86. S.W. Ng, A.J. Kuthubutheen, A. Zainudin, W. Chen, V.G. Kumar Das, B. Schulze, K.C. Molloy, W.-H. Yip, T.C.W. Mak; *J. Organomet. Chem.*; **403**, 101 (1991).

87. S.W. Ng, W. Chen, V.G. Kumar Das; *Acta Crys.*; C48, 2211 (1992).

88. S.W. Ng, C.L. Barnes, M.B. Hossian, D. van der Helm, J.J. Zuckerman, V.G. Kumer Das; *J. Am. Chem. Soc.*; **104**, 5359 (1982).

89. V.G. Kumar Das, L.K. Mun, C. Wei, S.J. Blunden, T.C.W. Mak; *J. Organomet. Chem.*; **322**, 163 (1987).

90. V.G. Kumar Das, L.K. Mun, C. Wei, T.C.W. Mak; *Organometallics*; **6**, 10 (1987).

91. A. Tzschach, K. Jurkschat; *Pure Appl. Chem.*; **58**, 639 (1986).

92. A.G. Davies, L. Smith, P.J. Smith; *J. Organomet. Chem.*; **39**, 279 (1972).

93. J. Wang, X. Yang, J. Cheng, Y. Xu, B. Liu, H. Wang, D. Zhang; *J. Chem. Soc., Dalton Trans.*; 3889 (1996).

94. C.W. Kaufman; U.S. Patent 3,705,943 (1972).

95. A.J. Rein, R.H. Herber; *J. Chem. Phys.*, **63**, 1021 (1975).

96. J.J. Park, D.M. Collins, J.L. Hoard; *J. Am. Chem. Soc.*; **92**, 3636 (1970).

97. G.M. Bancroft, B.W. Davies, N.C. Payne, T.K. Sham; *J. Chem. Soc., Dalton Trans.*; 973 (1975).

98. G.A. Miller, E.O. Schlemper; *Inorg. Chem.*; **12**, 677 (1973).

99. Y. Maeda, R. Okawara; *J. Organomet. Chem.*; **10**, 247 (1967).

100. (a) W.D. Honnick, J.J. Zuckerman; *J. Organomet. Chem.*; **178**, 133 (1979).
(b) D.W. Allen, I. Nowell, J.S. Brooks, R.W. Clarkson; *J. Organomet. Chem.*; **219**, 29 (1981).

101. M. Biesemans, R. Willem, S. Damoun, P. Geerlings, M. Lahcini, P. Jaumier, B. Jousseaume; *Organometallics*; **15**, 2237 (1996).

102. K.C. Molloy, S.J. Blunden, R. Hill; *J. Chem. Soc., Dalton Trans.*; 1259 (1988).

103. G. van Koten, J.G. Noltes; *J. Am. Chem. Soc.*; **98**, 5393 (1976).

104. G. van Koten, J.T.B.H. Jastrzebski, J.G. Noltes, G.J. Verhoeckx, A.L. Speck, J. Kroon; *J. Chem. Soc., Dalton Trans.;* 1352 (1980).

105. D. Dakternieks, H. Zhu; *Organometallics*; **11**, 3820 (1992).

106. R. Cotton, D. Dakternieks; *Inorg. Chim. Acta*; **148**, 31 (1988).

107. P.J. Smith, L. Smith; *Inorg. Chim. Acta Rev.*; **7**, 11 (1973).

108. W. McFarlane, J.C. Maire, M. Delmas; *J. Chem. Soc., Dalton Trans.*; 1862 (1972).

109. L. Verdonck, G.P. van der Kelen; *J. Organomet. Chem.*; **40**, 139 (1972).

110. P.J. Smith, R.F.M. White, L. Smith; *J. Organomet. Chem.*; **40**, 341 (1972).

111. A.C. Chapman, A.G. Davies, P.G. Harrison, W. McFarlane; *J. Chem. Soc., (C)*; 821 (1970).

112. W. McFarlane, R.J. Wood; *J. Organomet. Chem.*; **40**, C17 (1972).

113. D. Dakternieks, H. Zhu, D. Masi, C. Mealli; *Inorg. Chem.*, **31**, 3601 (1992).

114. A.R. Bassindale, M. Borbaruah; *J. Chem. Soc., Chem. Commun.*; 1501 (1991).

115. D. Kummer, S.H. Abdel Halim; *Z. Anorg. Allg. Chem.*; **622**, 57 (1996).

116. V.K. Jain, J. Mason, B.S. Saraswat, R.C. Mehrotra; *Polyhedron*; **4**, 2089 (1985).

117. G. Klebe, K. Hensen, J. Vonjouanne; *J. Organomet. Chem.*; **258**, 137 (1983).

118. V.K. Jain, J. Mason, R.C. Mehrotra; *J. Organomet. Chem.*; **309**, 45 (1986).

119. M. Leeaphon, K. Rohl, R.J. Thomas, P.E. Fanwick, R.A. Walton; *Inorg. Chem.*; **32**, 5562 (1993).

120. A.I. Albanov, V.A. Pestunovich, O.M. Trofimova, N.F. Chernov, M.G. Voronkov; *Z. Obshch. Khim.*; **66**, 1949 (1996).

121. M. Kido, K. Nakagawa; *Chem. Pharm. Bull.*; **30**, 1488 (1982).

122. A.A. Macharashvili, V.E. Shklover, N.Yu. Chernikova, M.Yu. Antipin, Yu.T. Struchkov, Yu.I. Baukov, G.I. Oleneva, E.P. Kramarova, A.G. Shipov; *J. Organomet. Chem.*; **359**, 13 (1989).

123. A.A. Macharashvili, Yu.I. Baukov, E.P. Kramarova, G.I. Oleneva, V.A. Pestunovich, Yu.T. Struchkov, V.E. Shklover; *Zh. Strukt. Khim.*; **28**, 114 (1987).

124. A.A. Macharashvili, Yu.I. Baukov, E.P. Kramarova, G.I. Oleneva, V.A. Pestunovich, Yu.T. Struchkov, V.E. Shklover; *Zh. Strukt. Khim.*; **28**, 107 (1987).

125. Yu.E. Ovchinnikov, A.A. Macharashvili, Yu.T. Struchkov, A.G. Shipov, Yu.I. Baukov; *J. Struct. Chem.*; **35**, 91 (1994).

126. Z. Xie, R. Bau, C.A. Reed; *J. Chem. Soc., Chem. Commun.*; 2519 (1994).

127. H.H. Karsch, F. Bienlein, A. Sladek, M. Heckel, K. Burger; *J. Am. Chem. Soc.*; **117**, 5160 (1995).

128. R.D. Brost, G.C. Bruce, S.R. Stobart; *J. Chem. Soc., Chem. Commun.*; 1580 (1986).

129. S.S. Al-Juaid, C. Eaborn, P.B. Hitchcock, P.D. Lickiss, A. Möhrke, P. Jutzi; *J. Organomet. Chem.*; **384**, 33 (1990).

130. A.H. Buttrus, C. Eaborn, P.B. Hitchcock, P.D. Lickiss; *J. Organomet. Chem.*; **302**, 159 (1986).

131. S.S. Al-Juaid, N.B. Buttrus, R.I. Damja, Y. Derouiche, C. Eaborn, P.B. Hitchcock, P.D. Lickiss; *J. Organomet. Chem.*; **371**, 287 (1989).

132. S.J. Glynn, Ph.D. Thesis, The Open University (1997).

133. A.Padwa, U. Chiacchio, M.K. Venkatramanan; *J. Chem. Soc., Chem. Commun.*; 1108 (1985).

134. M. Mitani, Y. Kobayashi, K. Koyama; *J. Chem. Soc., Dalton Trans. 1*; 653 (1995).

135. B.F. Bonini, G. Mazzanti, P. Zani, G. Maccagnani; *J. Chem. Soc., Perkin Trans. 1*; 1499 (1988).

136. S.G. Rosenfield, H.P. Berends, L. Gelmini, D.W. Stephan, P.K. Mascharak; *Inorg. Chem.*; **26**, 2792, (1987).

137. H. Preut, F. Huber, K. Hengstmann; *Acta. Crys.*; C44, 468 (1988).

138. K. Umakoshi, I. Ichimura, S. Ooi; *Inorg. Chem.*; **26**, 3551 (1987).

139. R. Kumar, V.S. J. de Mel, J.P. Oliver; *Organometallics*; **8**, 2488 (1989).

140. P.A. Pérez-Lourido, J.A. Garcia-Vázquez, J. Romero, M.S. Louro, A. Sousa, Q. Chen, Y. Chang, J. Zubieta; *J. Chem. Soc., Dalton Trans.*; **10**, 2047 (1996).

141. M. Masaki, S. Matsunami, H. Ueda; *Bull. Chem. Soc. Jpn.*; **51**, 3298 (1978)

142. M.D. Couce, G. Faraglia, U. Russo, L. Sindellari, G. Valle; *J. Organomet. Chem.*; **513**, 77 (1996).

143. L. Stefaniak; *Org. Magn. Reson.*; **12**, 379 (1979).

144. Yu.E. Ovchinnikov, M.S. Sorokin, Yu.T. Struchkov, M.G. Voronkov; *Dokl. Akad. Nauk*; **330**, 337 (1993).

145. I.D. Kalikhman, A.I. Albanov, O.B. Bannikova, L.I. Belousova, M.G. Voronkov, V.A. Pestunovich, A.G. Shipov, E.P. Kramarova, Yu.I. Baukov; *J. Organomet. Chem.*; **361**, 149 (1989).

146. Yu.I. Baukov, E.P. Kramarova, A.G. Shipov, G.I. Oleneva, O.B. Artamkina, A.I. Albanov, M.G. Voronkov, V.A. Pestunovich; *Zh. Obshch. Khim.*; **59**, 127 (1989).

147. M.G. Voronkov, A.I. Albanov, A.E. Pestunovich, V.N. Sergeev, S.V. Pestunovich, I.I. Kandror, Yu.I. Baukov; *Metallorgan. Khim.*; **1**, 1435 (1988).

148. A.R. Bassindale, T.B. Posner; *J. Organomet. Chem.*; **175**, 273 (1979).

149. M. Borbaruah, Ph.D. thesis, The Open University (1991).

150. S.D. Brown, J. Burgess, J. Fawcett, S.A. Parsons, D.R. Russel, E. Waltham; *Acta Cryst.*; C51, 1335 (1995).

151. D. Bilodeau, A.L. Beauchamp; *Acta Cryst.*; C52, 2633 (1996).

152. B. Tamhina, M.J. Herak; *Croat. Chem. Acta*; **45**, 603 (1973).

153. B. Tamhina, M.J. Herak; *Mikrochim. Acta I*; 47 (1977).

154. B. Tamhina, M.J. Herak, K. Jakopcic; *J. Less-Common Metals*; **33**, 289 (1973).

155. V. Vojkovic, B. Tamhina, M.J. Herak; *Z. Analyt. Chem.*; **276**, 377 (1975).

156. B. Tamhina, A.G. Ivsic; *Solv. Extr. Ion Exch.*; **5**, 909 (1987).

157. V. Vojkovic, B. Tamhina, M.J. Herak; *Z. Analyt. Chem.*; **285**, 266 (1977).

158. V. Vojkovic, B. Tamhina; *Solv. Extr. Ion Exch.*; **4**, 27 (1986).

159. H. Ishii, S. Numao, T. Odashima; *Bull. Chem. Soc. Jpn.*; **62**, 1817 (1989).

160. M.J. Herak, I. Prpic, B. Tamhina; *Proc. Int. Solvent Extr. Conf.*; 462 (1977).

161. A. Gojmerac, B. Tamhina, M.J. Herak; *J. Inorg. Nucl. Chem.*; **41**, 1475 (1979).

162. B. Schuknecht, E. Uhlemann, G. Wilke; *Z. Chem.*; **15**, 285 (1975).

163. Z. Zhang, S.J. Rettig, C. Orvig; *Inorg. Chem.*; **30**, 509 (1991).

164. M.M. Finnegan, S.J. Rettig, C. Orvig; *J. Am. Chem. Soc.*; **108**, 5033 (1986).

165. M.T. Ahmet, C.S. Frampton, J. Silver; *J. Chem. Soc., Dalton Trans.*; 1159 (1988).

166. S. Alshehri, J. Burgess, K.A. Darcey, M.S. Patel; *Trans. Metal Chem.*; **19**, 119 (1994).

167. J.J. Molenda, M.A. Basinger, T.P. Hanusa, M.M. Jones; *J. Inorg. Biochem.*; **55**, 131 (1994).

168. D.F. Evans, C.Y. Wong; *Polyhedron*; **10**, 1131 (1991).

169. C.I.F. Denekamp, D.F. Evans, J. Parr, J.D. Wollins; *J. Chem. Soc., Dalton Trans.*; 1489 (1993).

170. S. Bhattacharya, N. Seth, V.D. Gupta, H. Nöth, K. Polborn, M. Thomann, H. Schwenk; *Chem. Ber.*; **127**, 10, 1895 (1994).

171. J. Otera, Y. Kawasaki, T. Tanaka; *Inorg. Chim. Acta*; **1**, 294 (1967).

172. J. Burgess, S.A. Parsons; *Polyhedron*; **12**, 1959 (1993).

173. D. Fregona, G. Faraglia, S. Sitran; *J. Coord. Chem.*; **30**, 221 (1993).

174. T.A. Annan, C. Peppe, D.G. Tuck; *Can. J. Chem.*; **68**, 1598 (1990).

175. S.J. Blunden, P.J. Smith; *J. Organomet. Chem.*; **226**, 157 (1982).

176. S.S. Marwaha, J. Kaur, G.S. Sodhi; *J. Inorg. Biochem.*; **54**, 67 (1994).

177. D. Fregona, Z. Guo, G. Faraglia, S. Sitran; *J. Coord. Chem.*; **28**, 73 (1993).

178. J. Usta, D.E. Griffiths; *Biochem. Biophys. Res. Commun.*; **188**, 365 (1992).

179. S.W. Ng, V.G. Kumar Das, G. Yap, A.L. Rheingold; *Acta Cryst.*; C52, 1369 (1996).

180. B.C. Das, G. Biswas, B.B. Maji, K.L. Ghatak, S.N. Ganguly, Y. Iitaka, A. Banerjee; *Acta Cryst.*; C49, 216 (1993).

181. P.G. Harrison, T.J. King, M.A. Healy; *J. Organomet. Chem.*; **182**, 17 (1979).

182. N.G. Bokii, G.N. Zakharova, Yu. T. Struchkov; *J. Struct. Chem.*; **11**, 828 (1970).

183. P.G. Harrison, K. Molloy; *J. Organomet. Chem.*; **152**, 63 (1978).

184. V.G. Kumar Das, Y.C. Keong, N.S. Weng, C. Wei, T.C.W. Mak; *J. Organomet. Chem.*; **311**, 289 (1986).

185. P. Brown, M.F. Mahon, K.C. Molloy; *J. Organomet. Chem.*; **435**, 265 (1992).

186. R.A. Howie, J.-N. Ross, J.L. Wardell; *Acta Cryst.*; C50, 229 (1994).

187. S.M.S.V. Doidge-Harrison, R.A. Howie, J.T.S. Irvine, J.L. Wardell; *Polyhedron*; **11**, 2223 (1992).

188. I.R. Beattie, G.P. McQuillan, L. Rule, M. Webster; *J. Chem. Soc.*; 15 (1963).

189. R.A. Howie, E.S. Paterson, J.L. Wardell; *J. Organomet. Chem.*; **304**, 301 (1986).

190. A.R. Bassindale, M. Borbaruah; *J. Chem. Soc., Chem. Commun.*; 352 (1993).

191. M.F. Mahon, K.C. Molloy, B.A. Omotowa, M.A. Mesubi; *J. Organomet. Chem.*; **511**, 227 (1996).

192. S.J. Blunden, P. Harston, R. Hill, J.L. Wardell; *Appl. Organomet. Chem.*; **4**, 383 (1990).

193. G. Bandoli, A. Dolmella, V. Peruzzo, G. Plazzogna; *J. Organomet. Chem.*; **452**, 47 (1993).

194. J.S. Casas, E.F. Castellano, F.J. García Barros, A. Sánchez, A.S. González, J. Sordo, J. Zuckerman-Schpector; *J. Organomet. Chem.*; **519**, 209 (1996).

195. P.A. Boo, M.D. Couce, E. Freijanes, J.S. Casas, A. Castineiras, A. Sánchez-González, J. Sordo, U. Russo; *J. Organomet. Chem.*; **506**, 253 (1996).

196. C. Orvig, S.J. Rettig, J. Trotter; *Can. J. Chem.*; **65**, 590 (1987).

197. S.J. Rettig, J. Trotter; *Can. J. Chem.*; **60**, 2957 (1982).

198. W. Kliegel, H.-W. Motzkus, S.J. Rettig, J. Trotter; *Can. J. Chem.*; **62**, 838 (1984).

199. K. Undheim, L.A. Riege; *J. Chem. Soc., Perkin Trans. I*; 1493 (1975).

200. D.K. Kennepohl, A.A. Pinkerton, Y.F. Lee, R.G. Cavell; *Inorg. Chem.*; **29**, 5088 (1996).

201. E. Lukevics, I. Segal, I. Birgele, A. Zablotskaya; *Khim. Geterolsikl. Soedin*; **9**, 1255 (1994).

202. W. Pfleiderer, M. Schranner; *Chem. Ber.*; **104**, 1915 (1971).

203. U. Niedbala, H. Vorbrueggen; *J. Org. Chem.*; **39**, 3668 (1974).

204. G. Bastian, M. Hubert-Harat, R. Royer; *C.R. Hebd. Seances Acad. Sci., Ser. C*; **286**, 237 (1978).

205. G.B. Barlin, D.J. Brown, M.D. Fenn; *Aust. J. Chem.*; **37**, 2391 (1984).

206. A.P. Venkov, S.M. Statkova-Abeghe; *Tetrahedron*; **52**, 1451 (1996).

207. S. Santra, S.K. Dogra; *Chem. Phys.*; **207**, 103 (1996).

208. R.K. Chandrasekaran, J.D. Kola; *Inorg. Synth.*; **23**, 21 (1985).

209. R.A. Howie, J.L. Wardell; *Acta Cryst.*; C52, 1424 (1996).

210. K. Blazevic, K. Jakopic, V. Hahn; *Bull. Sci. Cons. Acad. Sci. Arts R.S.F., Yugoslavie, Sect. A*; **14**, 1 (1969).

211. B.E. Fisher, J.E. Hodge; *J. Org. Chem.*; **29**, 776 (1964).

Index of numbered structures

Chapter 1

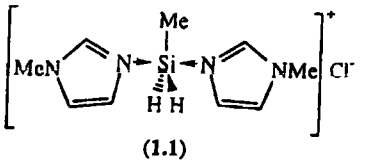

(1.1)

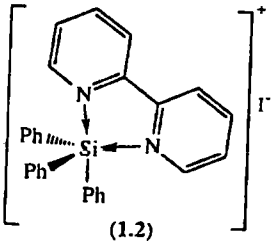

(1.2)

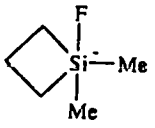

(1.3)

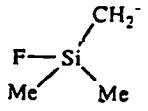

(1.4)

$[Ph_nSi(OMe)_{5-n}]^-$ [K, 18-crown-6]$^+$

(1.5)

$[HSi(OR)_4]^-K^+$

R = Me, ^{n}Bu, ^{s}Bu, ^{i}Pr, Ph.

(1.6)

$[H_2Si(OR)_3]^-K^+$

(1.7)

$[HSi(OR)_4]^-K^+$

(1.8)

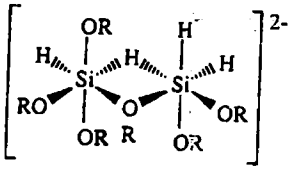

(1.9)

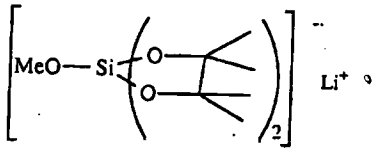

(1.10)

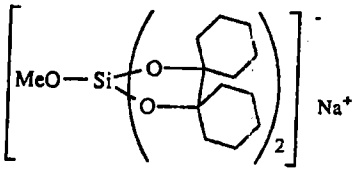

(1.11)

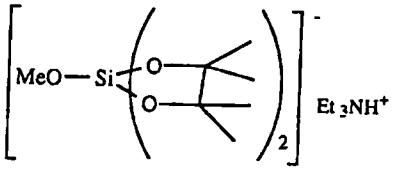

(1.12)

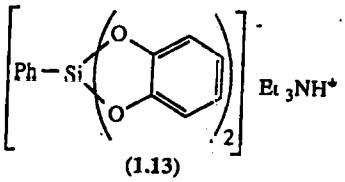

(1.13)

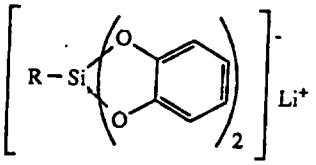

(1.14)

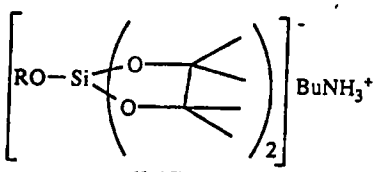

(1.15)

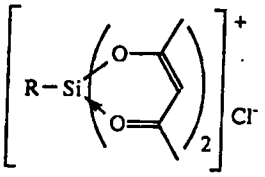

(1.16)

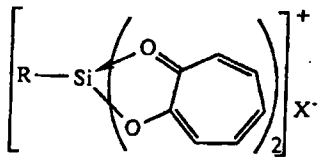

(1.17)

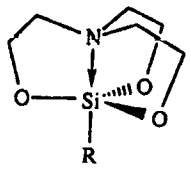

(e.g. R = Me, Cl, Ph)

(1.18)

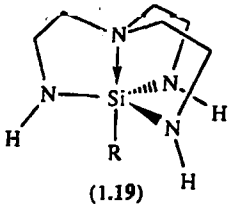

(1.19)

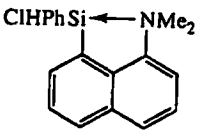

(1.20)

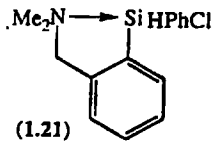

(1.21)

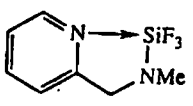

(1.22)

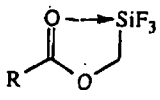

(1.23)

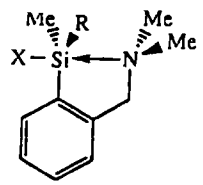

(R = H, α-Np)

(X = F, Cl, Br, OR, SR)

(1.24)

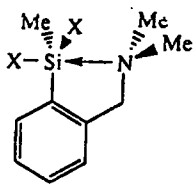

(X = OEt, SEt , F, Cl)

(1.25)

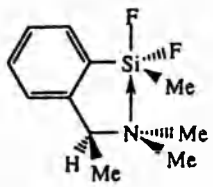

(1.26)

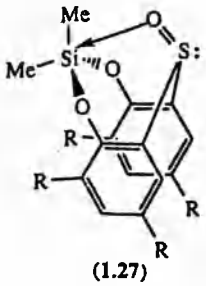

(1.27)
a: R = Me,
b: R = ^{t}Bu

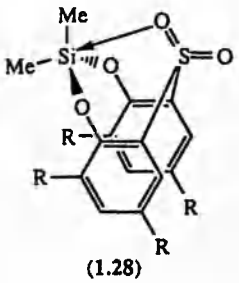

(1.28)
a: R = Me,
b: R = ^{t}Bu

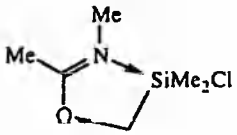

(1.29)

(1.30)

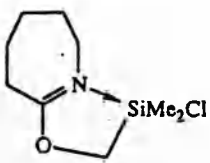

(1.31)

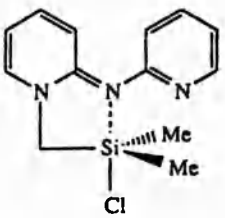

(1.32)

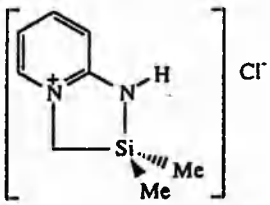

(1.33)

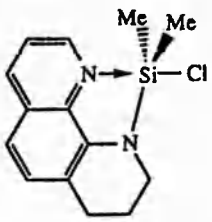

(1.34)

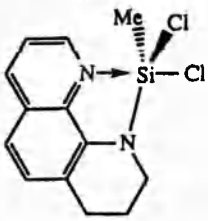

(1.35)

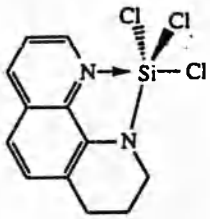

(1.36)

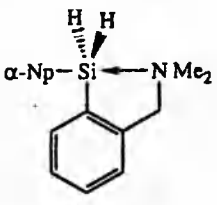

(1.37)

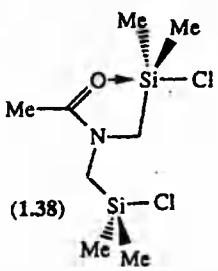

(1.38)

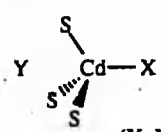

(X, Y = I, S or O)

(1.39a)

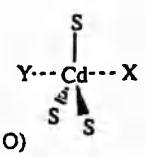

(1.39b)

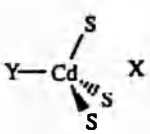

(1.39c)

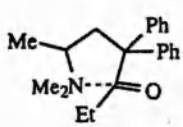

(1.40 A)

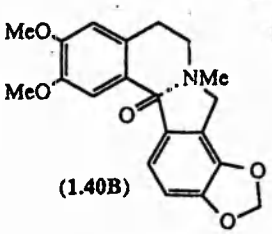

(1.40B)

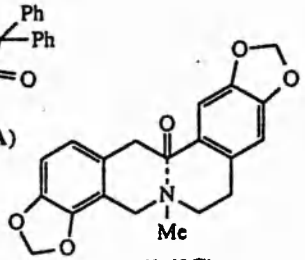

(1.40C)

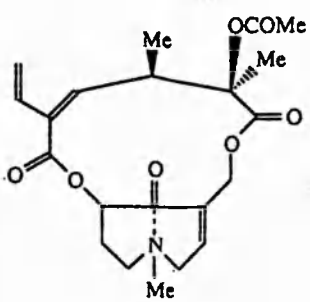

(1.40D)

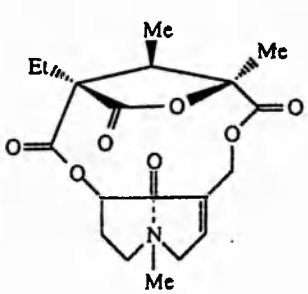

(1.40E)

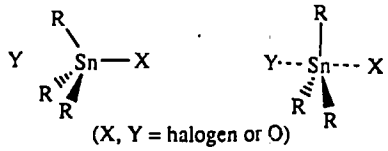

(X, Y = halogen or O)

(1.41a) (1.41b) (1.41c)

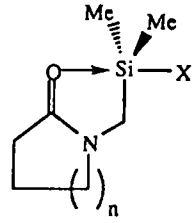

(1.42)

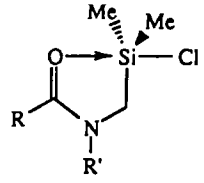

R = Ar, alkyl; R' = NMe_2
R = Me; R' = CH_2SiMe_2Cl
R = $N(alkyl)_2$; R' = NMe_2

(1.43)

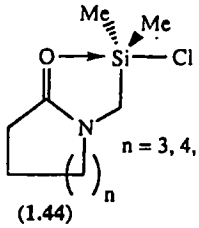

n = 3, 4, 5.

(1.44)

$[RSiF_5]^{2-}$ $2K^+$
(R = long chain alkyl)

(1.45)

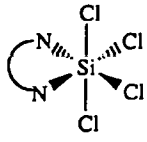

(1.46)

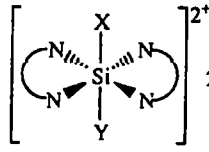

(1.47)

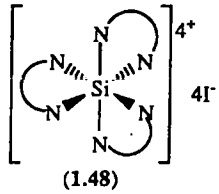

(1.48)

(X, Y = H, CH_3, Ph, OCH_3, Cl)

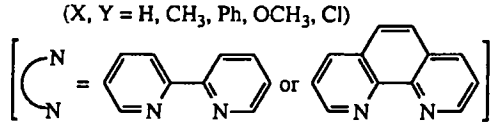

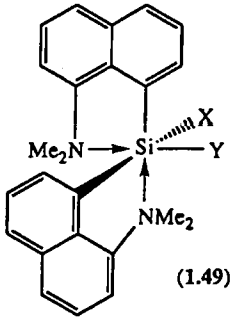

a: X, Y = H
b: X = H, Y = F
c: X, Y = F

(1.49)

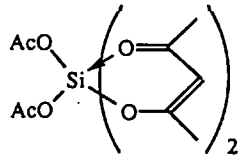

(1.50)

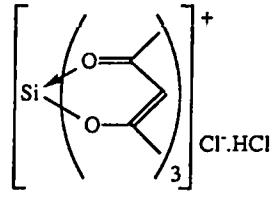

(1.51)

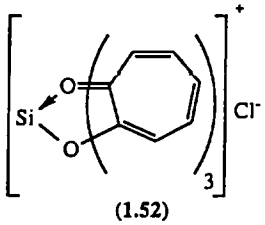

(1.52)

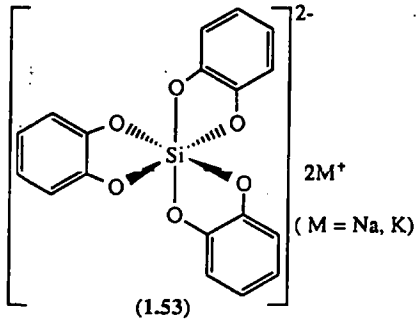

(1.53)

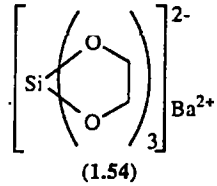

(1.54)

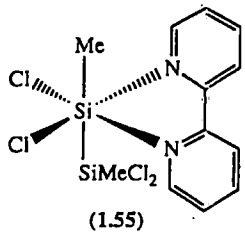

(1.55)

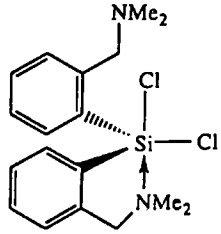

(1.56)

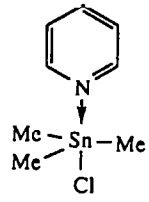

(1.57)

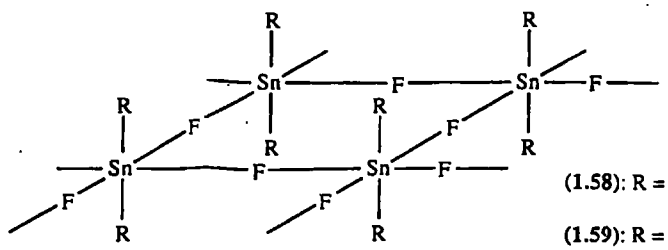

(1.58): R = F

(1.59): R = Me

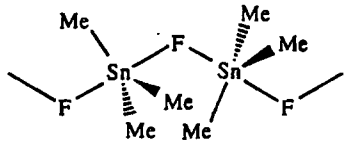

(1.60)

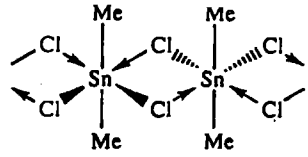

(1.61)

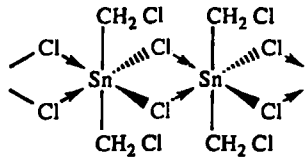

(1.62)

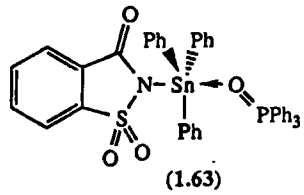

(1.63)

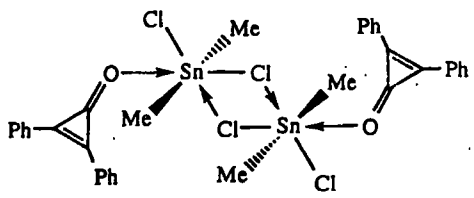

(1.64)

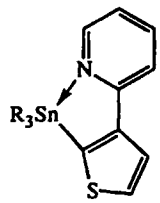

(1.65)

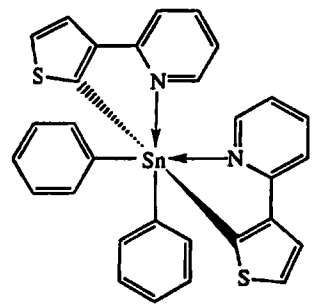

(1.66)

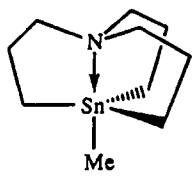

(1.67)

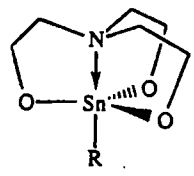

(R = Et, Bu, n-C_8H_{17})

(1.68)

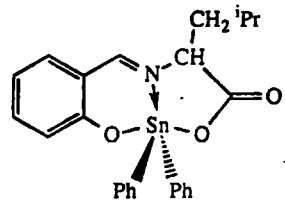

(1.69)

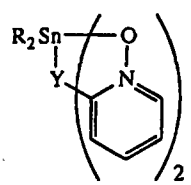

Y = S, O.
R = ^{n}Oct,
= ^{i}Oct,
= ^{n}Hept,
= ^{s}Bu,
= ^{n}Bu,
= Cl.

(1.70)

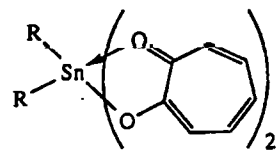

(R = Me, Et, Pr, ^{n}Bu, Ph, benzyl)

(1.71)

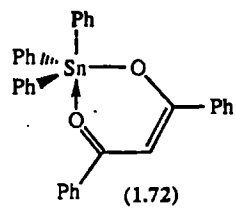

(1.72)

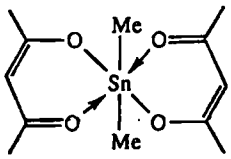

(1.73)

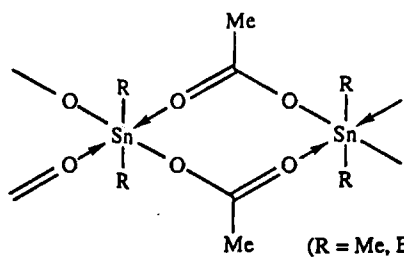

(R = Me, Et, ^{n}Pr, ^{n}Bu)

(1.74a)

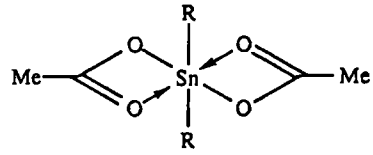

(1.74b)

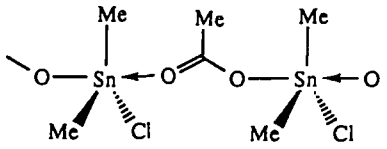

(1.75a)

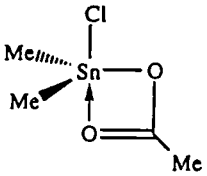

(1.75b)

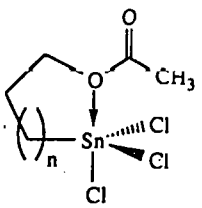

(1.76a)

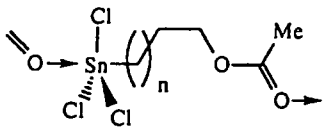

(1.76b)

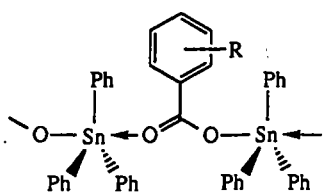

(1.77a)

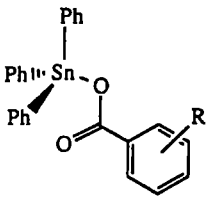

(1.77b)

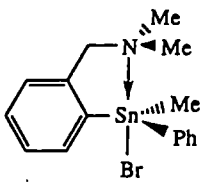

(1.78)

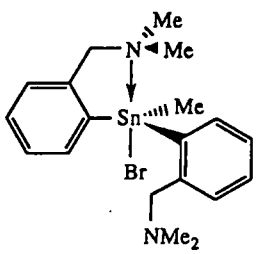

(1.79)

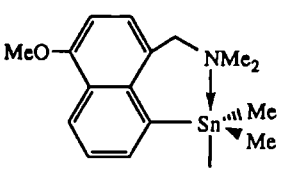

(1.80)

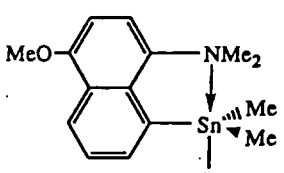

(1.81)

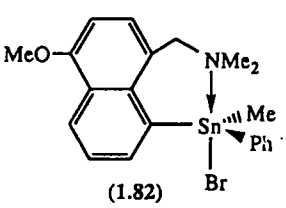

(1.82)

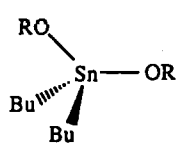

R = Me, ^{i}Bu, ^{t}Bu, ^{i}Pr

(1.83)

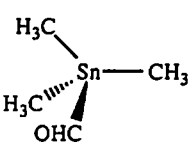

(1.84)

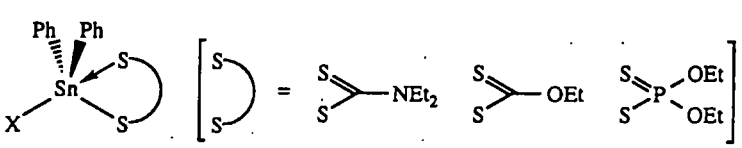

(1.85)

(X = Cl,Br)

(1.85a)

(1.85b)

(1.85c)

Chapter 2

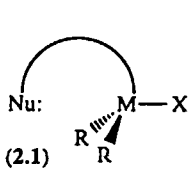
(2.1)

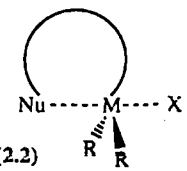
(2.2)

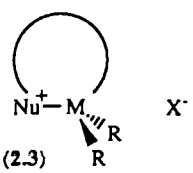
(2.3)

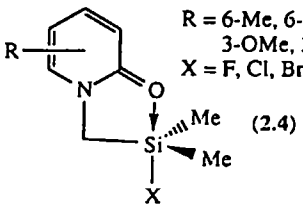
R = 6-Me, 6-Cl, 5-Cl, 3-OMe, 3-NO_2, H.
X = F, Cl, Br, OTf.
(2.4)

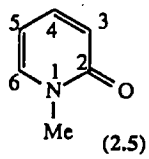
(2.5)

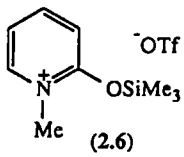
(2.6)

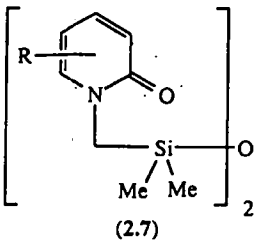
(2.7)

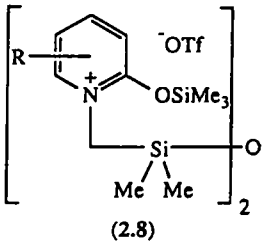
(2.8)

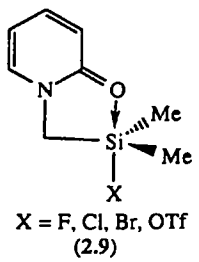
X = F, Cl, Br, OTf
(2.9)

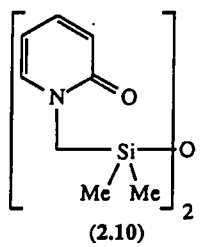
(2.10)

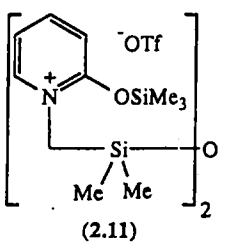
(2.11)

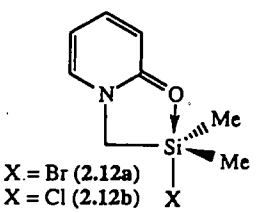
X = Br (2.12a)
X = Cl (2.12b)

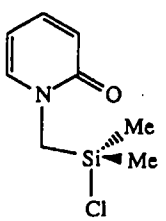
(2.13)

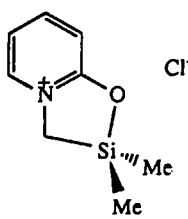
(2.14)

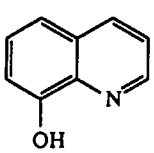
(2.15)

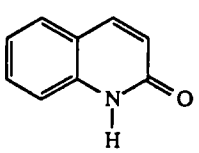
(2.16)

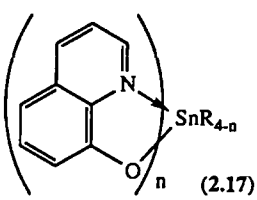
(n = 1, R = Ph_3, Me_3, Et_3, $^nBu_3$
Ph_2Cl, Et_2Cl, $^nOct_2Cl$)
(n = 2, R = Ph, ^{n}Bu, Et, Me)
(2.17)

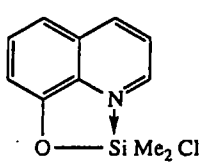
(2.18)

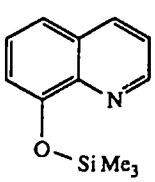
(2.19)

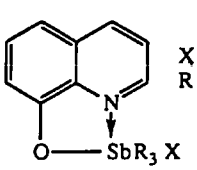
X = Cl, Br.
R = Me, Et, Ph
(2.20)

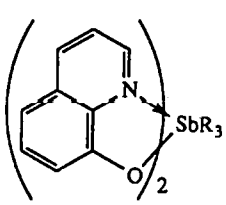
(2.21)

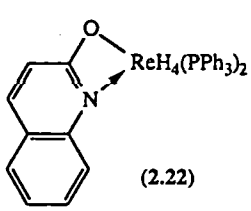
(2.22)

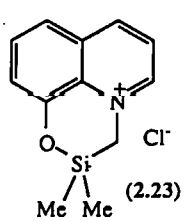
(2.23)

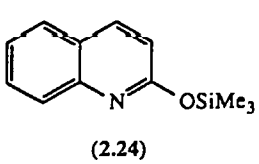
(2.24)

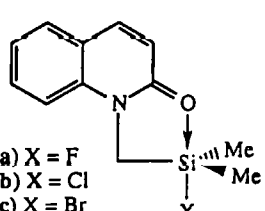
(2.25a) X = F
(2.25b) X = Cl
(2.25c) X = Br
(2.25d) X = OTf

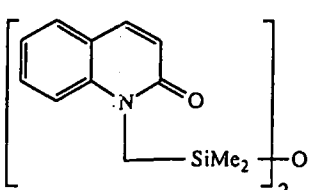
(2.26)

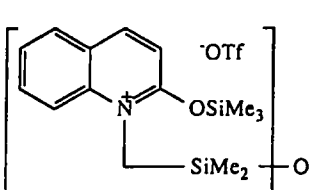
(2.27)

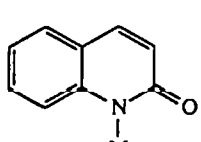
(2.28a)

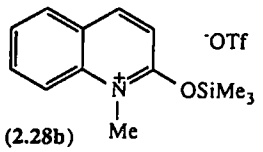

(2.28b)

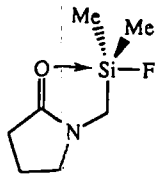

(2.29a)

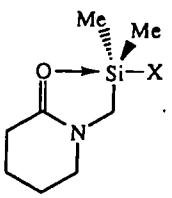

(2.29b) X = Cl
(2.29c) X = Br
(2.29d) X = OTf

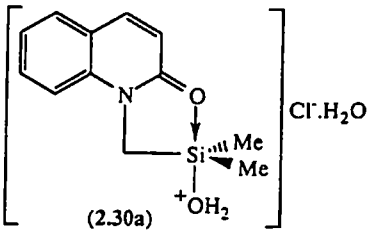

(2.30a)

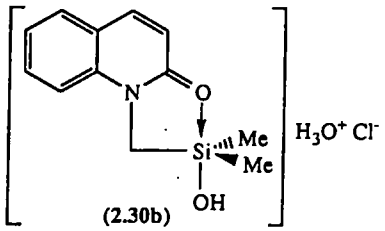

(2.30b)

$[^tBu_3Si(OH_2)]^+ [Br_6CB_{11}H_6]^-$
(2.31)

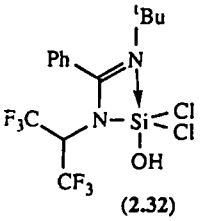

(2.32)

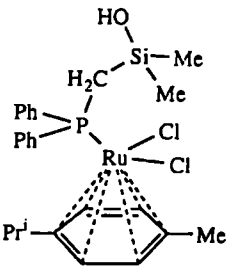

(2.33)

Crystal structures:

$(C_5Me_5)_2Si(OH)_2$
(2.34)

$^iPr_2Si(OH)_2$
(2.35)

$(Me_3Si)_3SiSi(OH)_3$
(2.36)

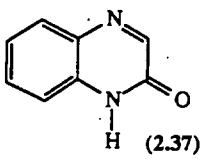

(2.37)

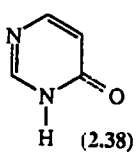

(2.38)

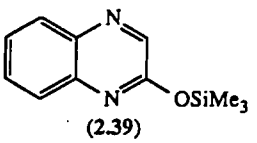

(2.39)

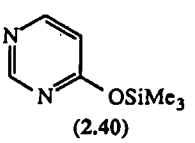

(2.40)

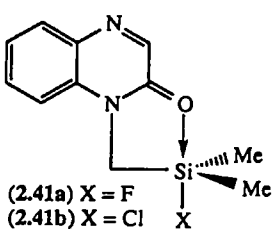

(2.41a) X = F
(2.41b) X = Cl

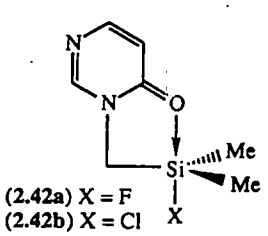

(2.42a) X = F
(2.42b) X = Cl

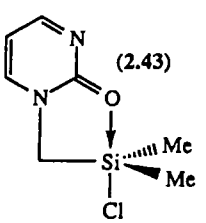

(2.43)

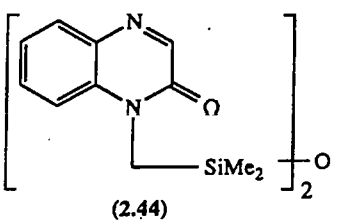

(2.44)

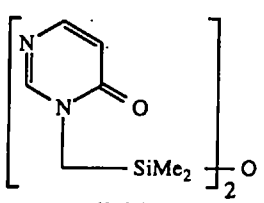

(2.45)

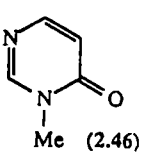

(2.46)

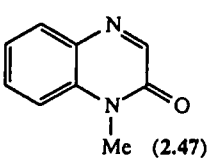

(2.47)

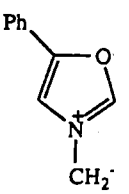

(2.48)

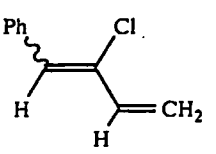

(2.49)

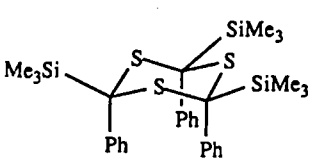

(2.50)

Chapter 3

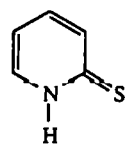

(3.1)

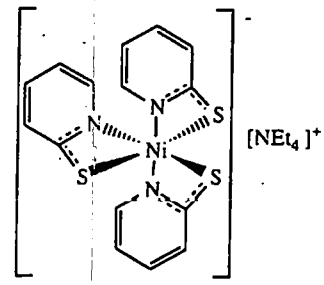

(3.2)

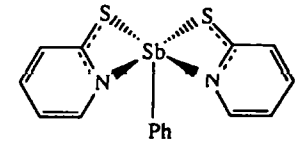

(3.3)

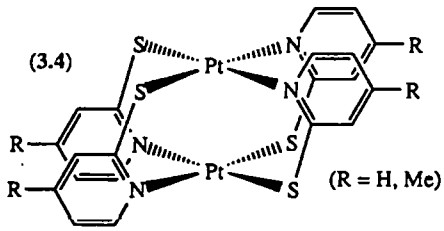

(3.4) (R = H, Me)

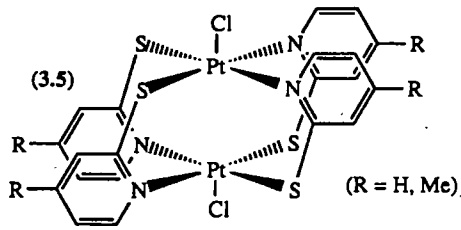

(3.5) (R = H, Me)

(3.7)

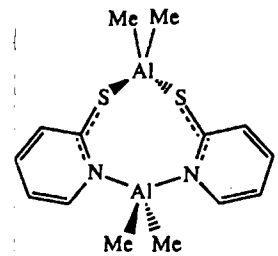

(3.6)

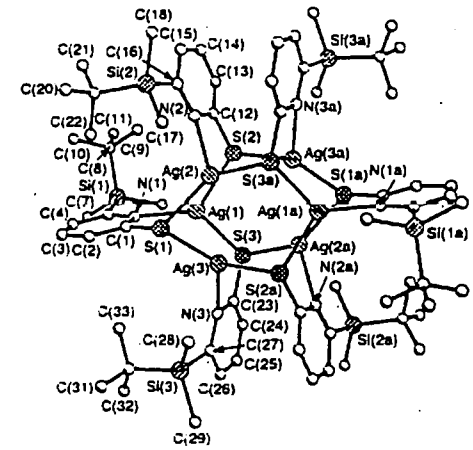

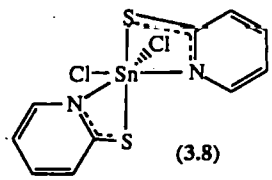

(3.8)

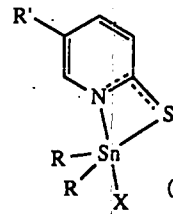

(3.9)

(X = Cl, Br. R = Me, Et, Ph.
R' = CO_2Me, CO_2Et, $CO_2{}^iPr$)

(3.10)

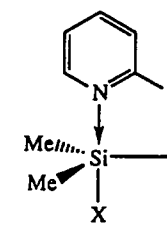

(3.11a) X = F
(3.11b) X = Cl
(3.11c) X = Br
(3.11d) X = OTf

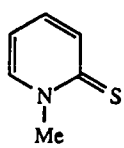

(3.12)

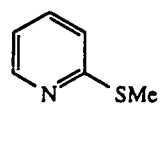

(3.13)

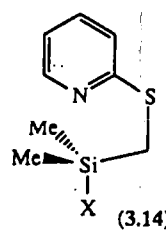

(3.14)

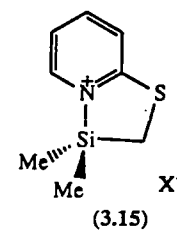

(3.15)

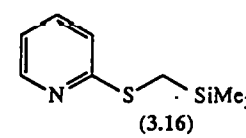

(3.16)

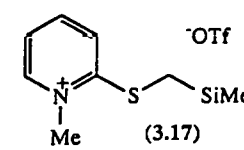

(3.17)

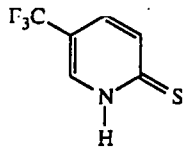

(3.18)

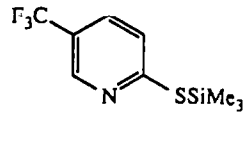

(3.19)

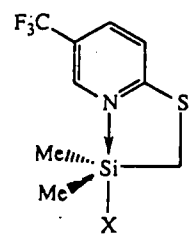

(3.20a) X = F
(3.20b) X = Cl
(3.20c) X = Br
(3.20d) X = OTf

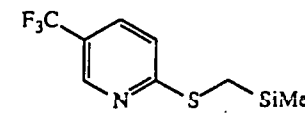

(3.21)

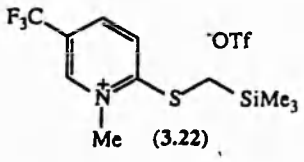

(3.22)

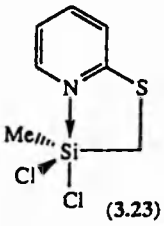

(3.23)

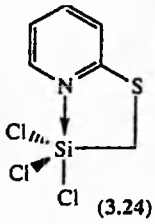

(3.24)

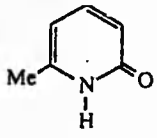

(3.25)

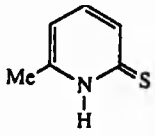

(3.26)

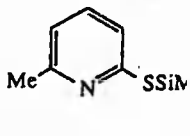

(3.27)

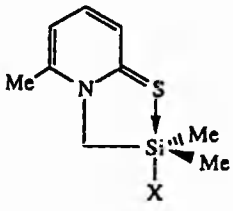

(3.28a) X = F
(3.28b) X = Cl
(3.28c) X = Br
(3.28d) X = OTf

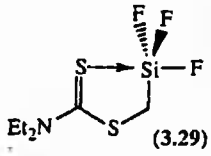

(3.29)

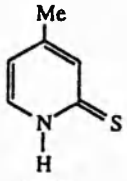

(3.30)

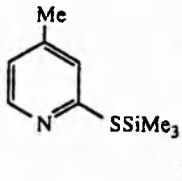

(3.31)

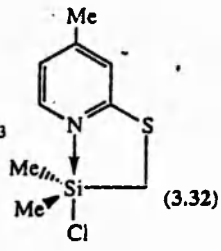

(3.32)

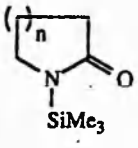

(3.33)

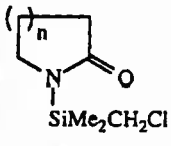

(3.34)

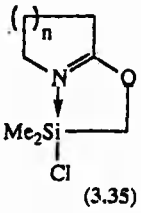

(3.35)

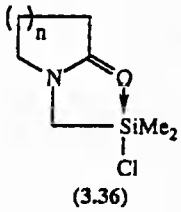

(3.36)

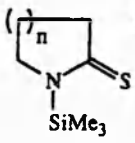

(3.37)

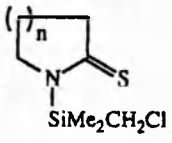

(3.38)

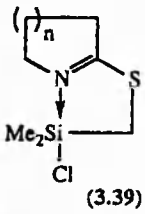

(3.39)

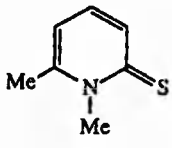

(3.40)

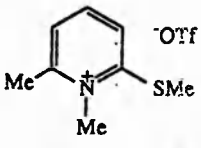

(3.41)

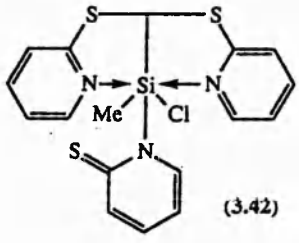

(3.42)

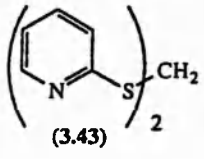

(3.43)

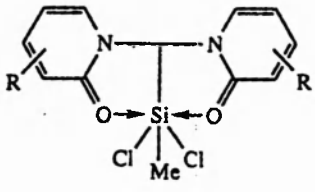

(R = 6-Me, H, 3-OMe)
(3.44)

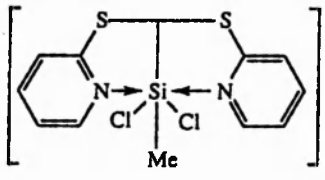

(3.45)

Chapter 4

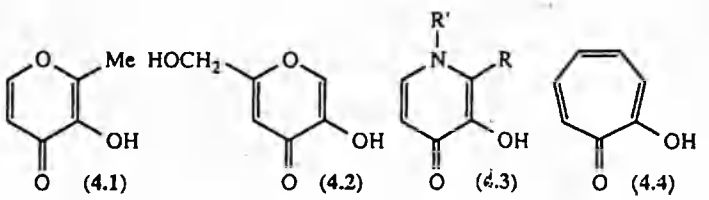

(4.1) (4.2) (4.3) (4.4) (4.5) (4.6) (4.7)

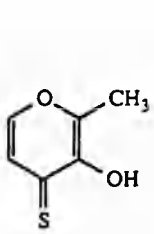

(4.8)

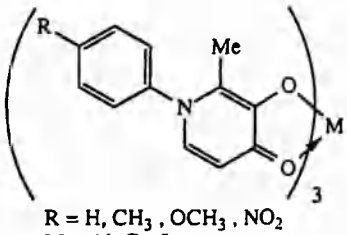

R = H, CH_3, OCH_3, NO_2
M = Al, Ga, In
(4.9)

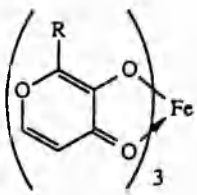

(4.10) R = Me
(4.11) R = Et

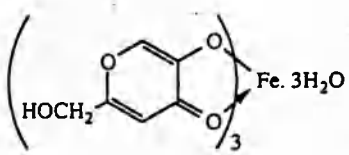

(4.12)

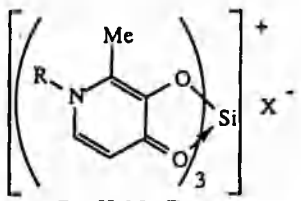

R = H, Me, Et.
X = HSO_4^-, Cl^-, $^-OSO_2CF_3$, $CF_3CO_2^-$
(4.13)

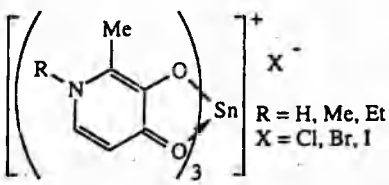

R = H, Me, Et
X = Cl, Br, I
(4.14)

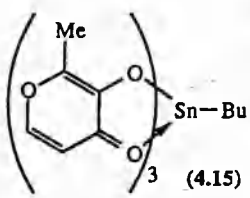

(4.15)

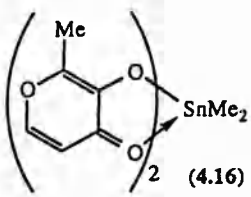

(4.16)

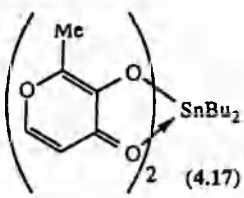

(4.17)

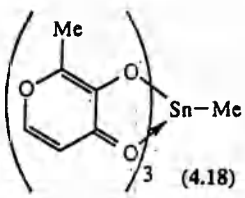

(4.18)

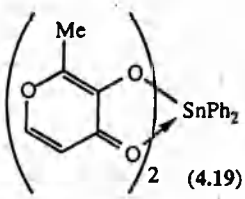

(4.19)

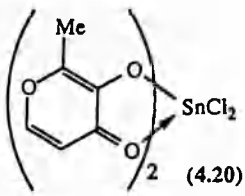

(4.20)

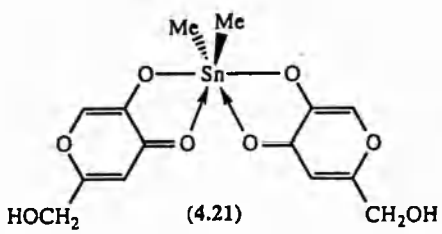

(4.21)

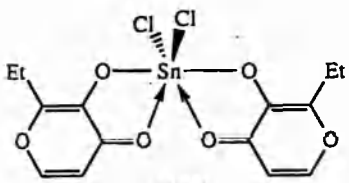

(4.22)

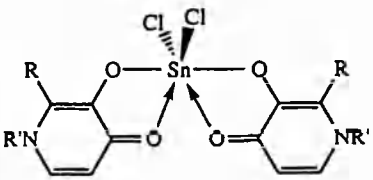

(4.23) R = R' = Me
(4.24) R = Et, R' = Me
(4.25) R = R' = Et

$M(LH)_4 Cl_4$
(4.26)

$M(L)_2 Cl_2$
(4.27)

(M = Sn, Ge; LH = maltol)

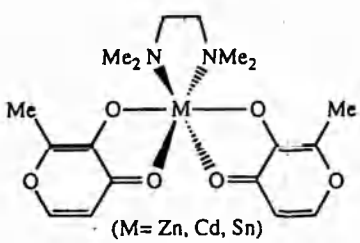

(M= Zn, Cd, Sn)
(4.28)

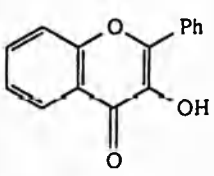

(4.29)

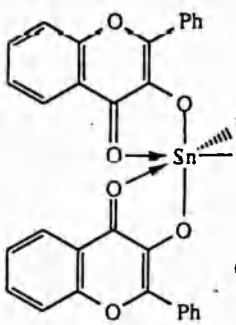

R' = R = Ph, Me, Bu.
R' = Me, R = Cl
(4.30)

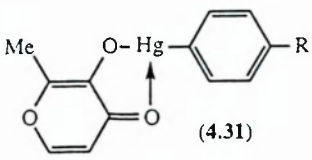

(4.31)

(R = Me, OMe, NO_2)

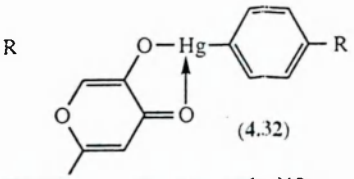

(4.32)

$HOCH_2$ (R = Me, OMe, NO_2)

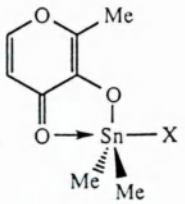

(4.33) (X = Cl, Br)

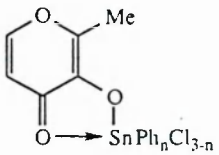

(4.34) (n = 2, 3)

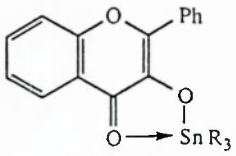

(R = Bu, Ph, c-C_6H_{11} , $PhMe_2CCH_2$)

(4.35)

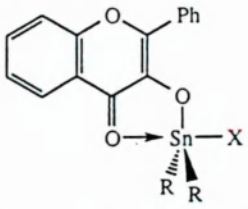

(4.36) R = Me, ^{n}Bu, Et, ^{n}Oct. X = Cl, Br

(4.37) R = Ph, X = Cl

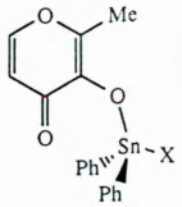

(4.38)

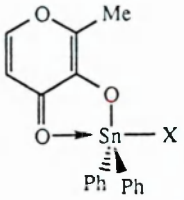

(4.39a) X = Ph
(4.39b) X = Cl
(4.39c) X = Br
(4.39d) X = I

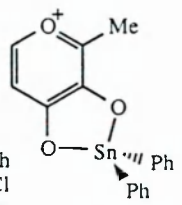

(4.40)

X^-

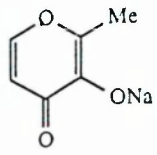

(4.41)

Ph_3SnCl (4.42a)

Ph_2SnCl_2 (4.42b)

Ph_2SnBr_2 (4.42c)

Ph_2SnI_2 (4.42d)

$(Ph_2SnO)_n$ (4.43)

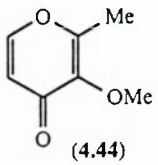

(4.44)

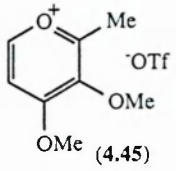

(4.45)

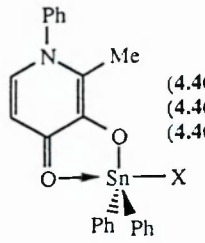

(4.46a) X = Ph
(4.46b) X = Cl
(4.46c) X = Br

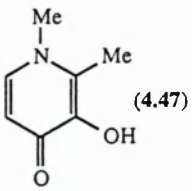

(4.47)

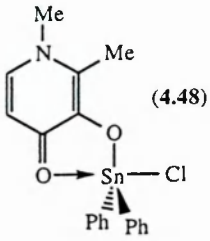

(4.48)

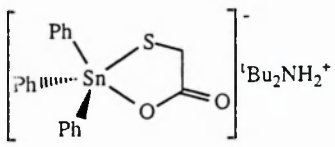

(4.49)

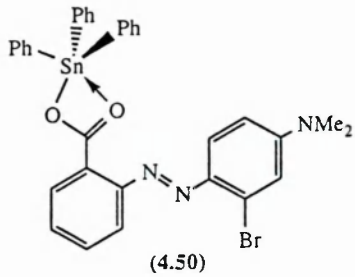

(4.50)

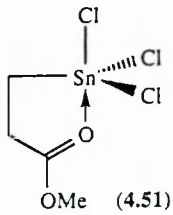

(4.51)

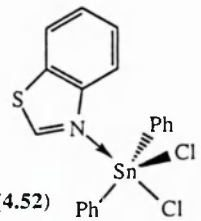

(4.52)

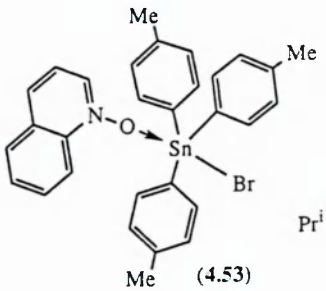

(4.53)

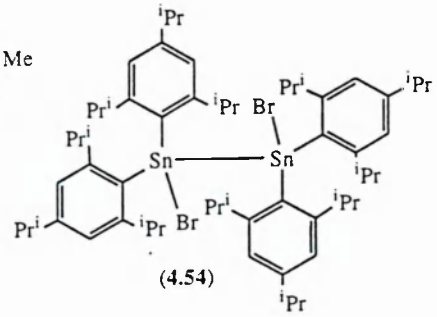

(4.54)

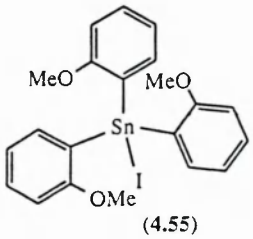

(4.55)

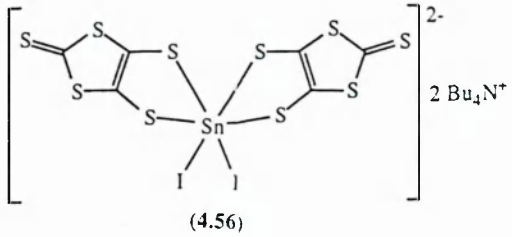

(4.56)

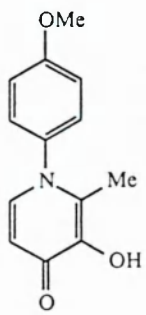

(4.57)

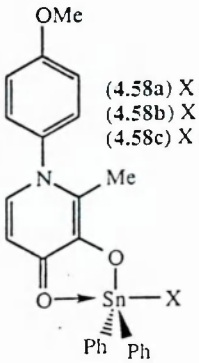

(4.58a) X = Ph
(4.58b) X = Cl
(4.58c) X = Br

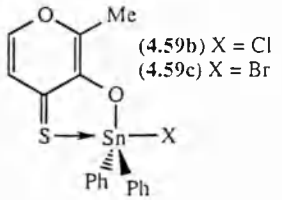

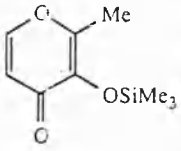

(4.60)

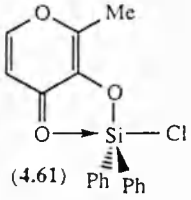

(4.61)

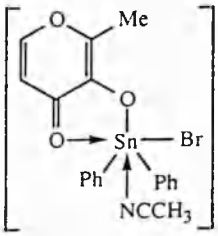

([4.62])

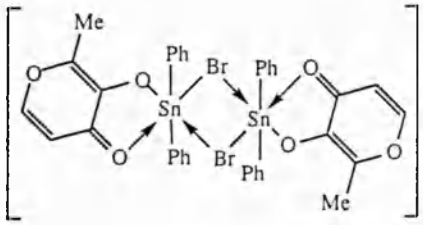

([4.63])

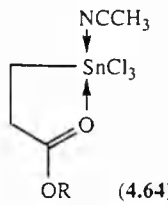

(4.64)

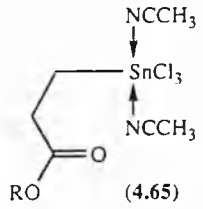

(4.65)

(R = Me, ^{i}Pr, Ar)

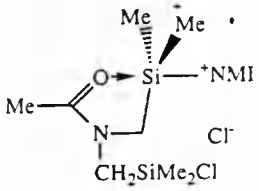

([4.66])

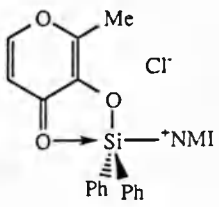

([4.67])

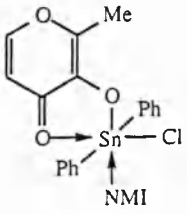

(4.68)

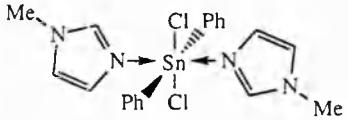

(4.69)

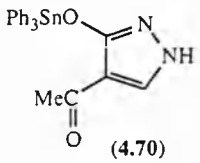

(4.70)

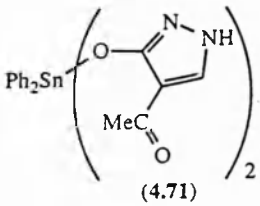

(4.71)

Ph_4Sn

(4.72)

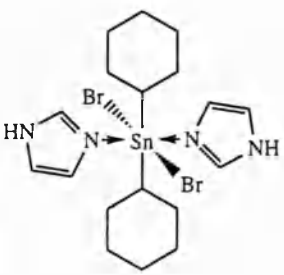

(4.73)

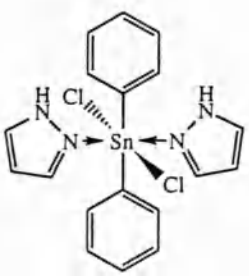

(4.74)

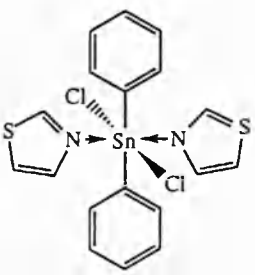

(4.75)

Ph_2BOH

(4.76)

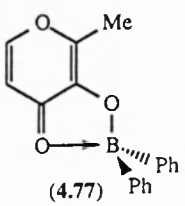

(4.77)

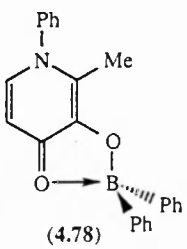

(4.78)

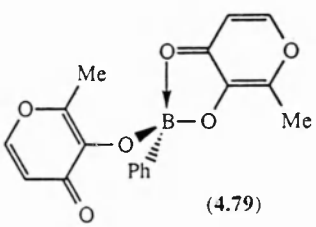

(4.79)

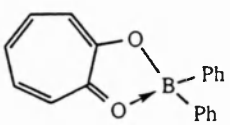

(4.80)

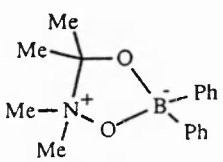

(4.81)

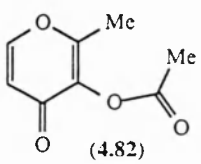

(4.82)